The Mechanistic Modelling and Simulation of Vaccine-Adjuvant Induced Immune Responses



Paul R. Buckley
Brasenose College
University of Oxford

A thesis submitted for the degree of
Doctor of Philosophy in Molecular and Cellular Medicine

Michaelmas 2021

Acknowledgements

- To Prof. Mark Coles and Prof. Jon Timmis, first for having initial faith in me when I interviewed for the project, despite my lack of prior experience. This opportunity has been life changing, and I cannot thank you both enough for that. Second, for your supervision throughout my DPhil and support during resubmission.
- To Prof. Eamonn Gaffney for all of your help during both the initial and re-submission of this thesis. I cannot thank you enough for your guidance and support.
- To Kieran Alden, for your supervision and friendship throughout my DPhil.
- To Margherita Coccia, Arnaud Didierlaurent and Stephane Temmerman, Catherine Collignon, Aurelie Chalon, for your guidance, assistance and openness to sharing your knowledge and data with us. This thesis would not have been possible without you.
- To Dominika Gajdasik, for your friendship, advice, willingness to contribute to this work and for plenty of discussions on AS01's mechanism of action.
- To Prof. David Withers, for discussions regarding AS01 immunology and for providing us with valuable data!
- To Claus Andersen for your supervision throughout the project.
- To Jason Cosgrove, Steph Evans, John Hamp, James Butler, Katrina Reily, Simon Jarret, Emily Taylor, Rita Pinter, for your help and advice over the years.
- To my parents, Robin and Pam, my brother Daniel, my grandparents June and Derek, & wider family, for always supporting me. I could not have done this without you.
- To Prof. Hashem Koohy, for your constant understanding as well as your supervision and guidance in helping me become a better scientist.
- To my friends - Josh S, Tom B, Jon S, Lee C, Danniella S, Eloise J, Emma G, Calum T, Chloe P, Lewis M, Alice S, Tom C, Jess B, Isabelle S, Grace D, Georgia L, Alexia T, Jon D, Alex R, Dori T, Julia T, Raf A, Kunaal O, Holly G, Adam A, Jamie H, Ari M, Jodie B, Rob M, Matt B, Ollie M, Kerraine P and Connor S - for your support & keeping me at my personal level of sanity through the past years of a PhD, and MSc + full-time job.
- To Rosie, for your constant love and support through writing the original thesis and through the re-submission period.

Abstract

Vaccination is one of the most successful public health interventions in human history. A key component of subunit-vaccines are adjuvants; immunostimulants that shape and enhance the immune response to antigens. Despite the importance of adjuvants, the mechanisms of how adjuvants promote immune responses are not fully understood, limiting detailed application of modelling and simulation to determine optimal vaccine formulations, dosing and timings of prime and boost. To rationally accelerate next-generation vaccines while promoting transparency, it is critical to foster a detailed understanding of the mechanism of action of efficacious adjuvants. AS01 is a patented adjuvant used in clinically approved Malaria (RTS,S/AS01) and Herpes-Zoster vaccines (Shingrix). In this thesis, the first detailed theoretical model of AS01's mechanism of action from injection site to generation of antibody response is presented. From this non-executable description of AS01 biology, mathematical models were developed. These mathematical models permitted analysis of the interplay of cytokines (IFNγ, IL12 and IL18) and cells (macrophages, dendritic cells and monocytes) in early events based on data from a murine iliac draining lymph node. Model analysis led to the novel hypothesis that dendritic cells are the predominate cell type responsible for early IL12 production. IL12 is known to synergise with macrophage-derived IL18 to initiate early IFNγ. We provide evidence that AS01-mediated loss of subcapsular macrophages has a role in regulating the duration of IFNγ production acting as an endogenous inhibitory mechanism. Model analysis suggests that this cell loss affects the minimal temporal spacing of AS01-based vaccination required to obtain canonical IFN responses. This mathematical model was extended to capture CD4+ T cell priming dynamics. By analysing two simulations that permit exploring different hypotheses of AS01-mediated CD4+ T cell priming, we observed that our hypothesis of how IFN regulates CD4+ T cell priming was likely to be incomplete, which led to a refined hypothesis for IFNγ's role in this process. We observed that 'inflammation-induced' naïve CD4+ T cell recruitment may be a key factor regulating the magnitude of CD4+ T cell priming. Thus, physiological factors including time of the day and spacing of consecutive jabs may have a key role in AS01 vaccine efficacy.

Contents

1 Introduction **1**

1.1 Introduction to Vaccination 1

1.2 From Intramuscular Injection Site to Tissue Draining Lymph Node Immune Responses 2

1.2.1 Lymph Nodes and Constituents 2

1.3 Early Innate Immune Responses 6

1.3.1 Immune System Recognition 6

1.3.1.1 Toll-like Receptors Initiate Innate Immune Responses . . . 7

1.3.1.2 Nod-like-receptors (NLRs) and Inflammasomes 7

1.3.2 Initiation of an Adjuvant-Mediated Immune Response 8

1.3.3 Immune Cell Migration from Injection Site to Tissue Draining LNs . 9

1.4 Bridging Innate and Adaptive Immunity 9

1.5 Adaptive Immune Responses to Vaccines 10

1.6 Introduction to Adjuvanted Vaccines 11

1.7 Adjuvant System 01 (AS01) 15

1.7.1 Current Understanding of AS01 Mechanism of Action 17

1.7.1.1 Muscle Injection Site Inflammatory Response induced by AS01 17

1.7.1.2 Lymphatic Immune Response Induced by AS01 18

1.7.1.3 The Draining Lymph Node Response induced by AS01 . . 19

1.8 Modelling Biological Systems 21

1.8.1 Mathematical Models in Biology 23

1.8.1.1 Ordinary Differential Equations (ODEs) in Biological Modelling 23

1.8.2 Further Modelling Techniques 25

1.8.3 Mathematical and Computational Modelling in Vaccines and Immunology 25

1.8.3.1 Models of T cell dynamics in lymph nodes 26

1.8.3.2 Models of Cytokines and Cellular Activation 27

1.8.3.3 Application of Mechanistic Modelling in Vaccinology 32
1.9 Model and Simulation Development 36
1.9.1 Simulation Calibration 38
1.9.2 Simulation Validation 39
1.9.3 Sensitivity Analysis Techniques 40
1.10 Thesis Aims and Research Questions 41
1.10.1 Research Questions 42
1.10.2 Thesis Aims 43

2 Materials and Methods 44
2.1 Data Security and Cleaning 44
2.2 Development of a Domain Model for Core AS01 MoA 44
2.2.1 Domain Model Products 44
2.3 Development of Mathematical Models 46
2.3.1 Simulation Development 47
2.4 Simulation Calibration 47
2.5 Simulation Validation 48
2.6 Sensitivity Analysis 49
2.6.1 Local Sensitivity Analysis 49
2.6.2 Global Sensitivity Analysis (eFAST) 50

3 Mapping Experimental Data to Immunological Processes for a Proposal of AS01 Mechanism of Action 51
3.1 Introduction 51
3.2 Results 53
3.2.1 A framework for the application of mechanistic modelling approaches to explore adjuvant MoA 53
3.2.2 A Domain Model for the Core AS01-induced Immune Response . . . 55
3.2.2.1 Research Context 55
3.2.2.2 Experimental Data 57
3.2.2.3 A Core AS01 MoA CellDesigner Diagram to Capture High-Level Biology 61
3.2.3 Extending the CellDesigner Model to Substantiate the Proposal of AS01 MoA 65
3.2.3.1 Defining Expected Behaviours 69
3.2.3.2 State-Machine Diagrams 71
3.2.3.3 Activity Diagrams 75

3.3 Discussion 77

4 Development of a Mathematical Model to Explore Innate IFNγ Production Induced by AS01-adjuvanted Vaccines 79

4.1 Introduction 79
4.2 Results 80
4.2.1 A Domain Model of AS01 induced Innate IFNγ Production 80
4.2.1.1 Research Context 80
4.2.1.2 Gathering Experimental Data 80
4.2.1.3 A CellDesigner Model of Key Components in Early Events of AS01 MoA 81
4.2.1.4 Expected Behaviours Diagram 84
4.2.1.5 Key Observable Phenomena 84
4.2.1.6 Integrating Experimental Insight with Assumptions, Abstractions and Hypotheses 86
4.2.1.7 Activities of Model Entities 87
4.2.1.8 State-Machine-Diagrams 88
4.2.2 A Platform Model of AS01 induced Innate IFNγ Production 92
4.2.2.1 Key Platform Model Refinements, Additions and Simplifications 92
4.2.2.2 Platform Model Diagram Examples 93
4.2.2.3 Ordinary Differential Equations for AS01 induced Innate IFNγ Production 94
4.2.2.4 Equations Prescribing a Variable as a Function of Time . . 96
4.2.3 A Simulation Platform for AS01-induced Innate IFNγ Production . 97
4.2.3.1 Simulation Calibration and Identifiability 97
4.2.3.2 Simulation Validation 99
4.2.3.3 Initial Exploration of Model Parameter Space 104
4.2.3.4 A Non-identifiable Model and Improving Quantitative AS01 Knowledge 107
4.3 Discussion 113

5 Investigating the immunological mechanisms of early cytokine production during AS01 induced immune responses 117

5.1 Introduction 117
5.1.1 Aims 117
5.2 Results 118

5.2.1 eFAST Global Sensitivity Analysis 118
5.2.2 The predicted temporal dynamics of monocytes and DCs on the production of IL12 after AS01 adjuvanted vaccination 119
5.2.3 Determining relationships between cellular production of IL18 and IL12 with the production of IFNγ 120
5.2.4 Exploring the effects of macrophage loss on IFNγ production 126
5.2.4.1 Macrophage Cell Loss May Help to Limit IFNγ production and contribute to its transience 126
5.2.4.2 Predicting the Earliest Time for a Second AS01-based Vaccine Delivery 129
5.2.5 Identification of Parameters with Influence on IFNγ 132
5.3 Discussion 133

6 Mechanistic Models To Explore and Refine Hypotheses Underpinning the CD4+ T cell Response to AS01-adjuvanted Vaccines 139
6.1 Introduction 139
6.2 Results 140
6.2.1 Development of a Domain Model for AS01 CD4+ T cell models . . . 140
6.2.1.1 Research Context 141
6.2.1.2 Curating Experimental Data 141
6.2.1.3 A CellDesigner Model depicting salient events that give rise to CD4+ T cell priming after AS01-adjuvanted vaccination. 148
6.2.1.4 Describing Expected Behaviours 149
6.2.1.5 Integrating Experimental Insight with Assumptions and Further Hypotheses 153
6.2.1.6 Activities of Model Entities 154
6.2.1.7 State-Machine Diagrams and Model Summary 156
6.2.2 A Platform Model for Baseline AS01 CD4+ T cell priming 156
6.2.2.1 A Mathematical Model for AS01-induced CD4+ T cell priming in a murine dLN 163
6.2.3 A Simulation Platform for AS01 induced CD4+ T cell Priming . . . 166
6.2.4 A calibrated 'Baseline' Model of CD4+ T cell priming 167
6.2.5 Simulation Validation 174
6.2.6 Gaps in our understanding of AS01 MoA revealed by model development 175
6.2.6.1 A Refined Hypothesis for monocyte recruitment into the dLN after AS01 175

6.2.6.2 Large variation observed in model output for IFNγ production is consistent with gaps in biological data 177
6.2.7 Negative Regulatory Processes Are Important Components in AS01 MoA 179
6.2.8 Simulation Robustness to Parameter Perturbation to explore CD4+ T cell priming after AS01 181
6.2.8.1 Inflammation-induced naive CD4+ T cell recruitment strongly influences numbers of primed CD4+ T cell 182
6.2.8.2 Early DC activity appears to influence priming of CD4+ T cells after AS01 185
6.2.9 An Alternate Model where IFNγ Considerably Contributes to CD4+ T Priming 186
6.2.9.1 Calibration of the Alternate Model 187
6.2.9.2 Validating the Alternate model 191
6.2.10 Comparing Local Sensitivities for primed CD4+ T cells in the Baseline and Alternate Models 191
6.2.10.1 Key Parameters with similar sensitivities across models . . 191
6.2.10.2 Key Differences between the sensitivities of the 'Alternate' and 'Baseline' Models 194
6.2.11 Exploring the Hypothesis That IFNγ Modulates CD4+ T cell priming through augmenting DC potency 197
6.2.11.1 Employing the Baseline Model to Explore the Extent that IFNγ may enhance CD4+ T cell priming through augmenting DC potency 197
6.2.11.2 Employing the Alternate Model to Explore the Extent that IFNγ may enhance CD4+ Tcell priming through augmenting DC potency 200
6.2.11.3 A New, Refined hypothesis for IFNγ's role in CD4+ T cell responses after AS01 202
6.2.12 Profile-likelihood identifiability analysis for 'Baseline' and 'Alternate' models 204
6.2.12.1 Identifiability of the 'Baseline Model' 204
6.2.12.2 Identifiability of the 'Alternate Model' 206
6.2.13 First steps in ABM Development 207
6.3 Discussion 207

7 Discussion **219**

7.1 Mapping Experimental Data to Known and Hypothetical Mechanistic Function to Produce a Domain Model of the Core AS01 MoA 220

7.2 A Simulator of the Salient Events in Early IFNγ Production After AS01 . . 221

7.3 Analysing the Relative Contribution of Cells and Cytokines During the Early AS01 Response 225

7.4 Exploring Parameters influential in CD4+ T cell priming after AS01 and Hypotheses regarding how IFNγ modulates this Process 231

7.5 Summary of Novel Contributions 235

7.6 Future Directions 237

List of Abbreviations and Glossary **240**

Bibliography **244**

A Appendix A **264**

A.1 Code to solve IFNγ Model ODE 264

A.2 Code to solve CD4+ T cell priming Baseline Model 265

A.3 Code to solve CD4+ T cell priming Alternate Model 266

A.4 Thesis Supplementary 268

A.5 Core AS01 Domain Model 268

B Appendix B **279**

B.1 ABM 279

List of Figures

1.1 **Lymph Node structure and constituents:** Follicles are depicted by orange oval shapes. Afferent lymphatic (AL) vessels drain lymph from peripheral tissues, and transport antigen and antigen-carrying cells into the LN[1, 2, 3]. The bloodstream deposits lymphocytes into the center of the LN via high-endothelial-venules. Cells exit the dLN via the efferent lymphatic vessels. 3

1.2 **A simple overview of diverse adjuvant MoA:** Developing an intimate understanding of adjuvant MoA is vital to rationally tailor subunit vaccines toward combatting known disease pathology. Figure adapted from [4]. . . . 12

1.3 **An overview of the AS01-induced immune response.** Figure adapted with permission from Didierlaurent, Keystone Symposia 2014 [5] 20

1.4 **The CoSMoS Process:** This diagram shows how the various models of the CoSMoS process integrate, with focus placed on the Research Context at the center, informing all products of a CoSMoS project. 38

2.1 **A guide to UML: A description of the adapted version of the UML utilised to develop State-Machine diagrams.** States are represented by rectangular boxes, which may encompass smaller rectangular boxes, indicating parent and sub-states respectively. A black circle indicates the initial state of the object, and the black circle with a surrounding white border indicates the final state. Arrows indicate transitions between the states, and information surrounded by square brackets describe a condition that must be satisfied for the transition to proceed. An expression preceded by a forward slash, indicates further information with respect to a state transition or a state. Finally, dashed lines represent concurrent states and a diamond indicates a decision is to be made, determined by a condition being satisfied. This figure is adapted from [6]. 45

2.2 **A guide to UML: A description of the adapted version of the UML utilised to develop Activity Diagrams.** This figure is adapted from [6]. 46

3.1 **An overview of the Framework for the Application of Mechanistic Modelling Approaches to Exploring Adjuvant Mechanism of Action:** Development of the Domain Model: in this context, development of the domain model began with **(A)** the collection of experimental data from Graphpad Prism and Excel files, and the corresponding experiment metadata (see Methods 2.1). Following this, an automated pipeline was developed to clean, structure, and integrate the experimental results and the corresponding metadata, resulting in machine-readable data. Next, human abstraction, the AS01 data and immunological literature were appropriately integrated **(B)**. The AS01 data informed the development of the model 2-fold, firstly by constituting the available evidence behind the captured processes, but also by informing the rationale underpinning any human abstraction required to inform gaps in understanding. The core MoA model **(C)** was utilized to scope the requirements of the lower-level models describing component function, and so from the core MoA model, State-Machine and Activity Diagrams were developed **(D)**. Furthermore, Domain Model development can inform data collection by permitting the understanding of what data is required to ask the scientific question. Figure and legend adapted from [7] 54

3.2 **GSK generated experimental data showing cell numbers and cytokines after AS01-adjuvanted vaccination 1/2:** A) During an experiment by GSK to determine the cells targeted by QS21, subcapsular macrophages were analysed by flow cytometry 24 hours after stimulation by PBS or QS21 injection and cell numbers quantified in mice [8]. **A)** Subcapsular sinus macrophages after PBS and QS21 stimulation. B-E) To examine cell or cytokine dynamics after AS01 compared with PBS, six to eight week old female C57BL/6 mice were immunised i.m with gE antigen formulated with 1/50th human-dose (HD) AS01b in gastrocnemius muscles, or gE and PBS. Iliac dLN were collected at timepoints between 3 and 48 hours post injection. IFNγ producing cells were assessed by ICS. Cytokines were analysed by MILLIPLEX MAP, a multiplex assay using Luminex technology. For cell detection, fluorescent events were acquired using an LSR2 flow cytometer and analysed by FLOW JO. B-D, F, G) Iliac dLN were collected at timepoints between 6 and 48 hours post injection. **B)** Resident and Migratory DCs at 6, 24, 48 hours following vaccination with AS01 and gE antigen or 24 hours following injection with a PBS control. **C)** Inflammatory monocytes at 6, 24, 48 hours following vaccination with AS01 and gE antigen or 24 hours following injection with a PBS control. **D)** IFNγ+ NK cells at 6 and 24 hours following vaccination with AS01 and gE antigen, or 6 hours following injection with PBS. **E)** IFNγ pg/dLN concentration measured at 3, 6, 24 and 48 hours post-vaccination with AS01 and gE antigen, or 6 hours following injection with PBS. **F)** IFNγ+ CD8+ T cells at 6 and 24 hours following vaccination with AS01 and gE antigen, or 6 hours following injection with PBS. All statistical significance measured by T-test. All data was generated by GSK. 58

3.2 **Experimental data showing cell numbers and cytokines after AS01-adjuvanted vaccination 2/2: G)** IFNγ+ CD4+ T cells at 24 hours following vaccination with AS01 and gE antigen, or 6 hours following injection with PBS. Data were generated by GSK. H) 2W1S+ CD4+ T cells / dLN. Great Smart mice were injected intramuscularly at day 0 with 20 μg 2W1S peptide conjugated to OVA protein and 1/50 Human Dose of AS01. The injection was administered into the gastrocnemius muscle. The response was assesed in the iliac draining lymph nodes at day 5 and day 7. The 2W1S-specific CD4+ T cell response was assesed using MHCII tetramers. The experiments for the data shown in H) were performed by Dominika Gajdasik, University of Birmingham. Different shapes distinguish the experimental stimulation. . 59

3.3 **GSK generated experimental data demonstrating mechanisms underpinning early AS01 MoA:** Boxplots showing 6 hour ICS analysis of **A)** IFNγ+ NK cells / dLN after AS01, with a control PBS injection or anti-IL12p40 antibody, and PBS control. **B)** IFNγ+ NK cells /dLN after immunising C57BL/6 WT or Il18-/- mice with AS01+HBS or PBS. **C)** IFNγ+ NK cells after C57BL/6 mice were treated with 20ul of clodronate liposomes or control liposomes i.m and six days later immunised with AS01 and HBS. **D)** IFNγ+ NK cells / dLN after immunising WT or IL18-/- mice with AS01 and treating with anti-IL12p40 antibody or control antibody. All experiments where AS01 was used, employed Hepatitis B surface antigen formulated with 1/10 HD AS01. 60

3.4 **A core mechanism of action model:** Figure reused from [7] within permissions. **A)** depicts the muscle injection site, where the vaccine components are hypothesised to activate muscle-resident cells, initiating the local immune response resulting in the recruitment of monocytes into the muscle. **B)** depicts the lymphatics where components and cells transport through toward the dLN. **C)** depicts the dLN paracortex. **D)** depicts the dLN follicles. **E)** depicts a Germinal Center. **F)** depicts the blood. **G)** depicts the bone marrow. The colour yellow is used to distinguish elements of a secondary immune response. 62

3.5 **A core mechanism of action model: section A only - the 'Muscle Injection site'.** Vaccine (purple) components are inoculated into the muscle, where the individual components (Antigen, QS21, MPL) activate a muscle-resident cell, which promotes the recruitment and activation of monocytes, and the beginning of maturation for DCs. All three vaccine components freeflow into the lymphatics compartment B, and finally into the dLN (C,D). 64

3.6 **A core mechanism of action model: section C only - the Paracortex.** Monocytes arriving from the lymphatics can secrete IL12, as can arriving activated DCs, and resident DCs that have been activated. This IL12 - along with IL18 - promotes the production of IFNγ from 'IFNγ producing cells'. T cells are activated by Mature DCs in the Paracortex. After activation T cells can proliferate and leave the dLN. 66

3.7 **A core mechanism of action model: sections D and E only - the B cell follicle and Germinal Center.** On the edge of the subcapsular sinus and the B cell follicle, are subcapsular sinus macrophages which can secrete IL18 after activation by QS21. IL18, along with IL12 synergistically promotes the production of IFNγ. SSM can transfer antigen to the B cell follicle. FDCs can also present antigen to B cells such that B cells can be primed. B cells form Germinal Centers (E) where they can become fully activated and differentiate into antibody-secreting-cells and Memory B cells. 67

3.8 **A core mechanism of action model: section F only - the Blood.** Naive T cells that do not experience their cognate antigen re-enter the blood stream. Further, after activation, Effector T Helper and T Memory cells can leave the dLN and circulate in the blood. ASCs and Memory B cells circulate through the blood after dLN activation. 68

3.9 **Defining 'Expected Behaviours':** This diagram describes the research context, based on the exploration of the core AS01 MoA, linking the observable phenomena over the first seven days of the response to AS01 with the hypothesis that is thought to cause these phenomena to manifest. Geometric mean is used for averages. 70

3.10 **A monocyte State-Machine Diagram:** Using UML, the diagram describes the hypothesised function of monocytes after AS01-adjuvanted vaccines. 72

3.11 **A monocyte Activity Diagram:** Activity Diagrams describe actions of model components and their interactions with other components. 76

4.1 **GSK generated experimental data showing cell numbers and cytokines after AS01-adjuvanted vaccination:** A) During an experiment by GSK to determine the cells targeted by QS21, subcapsular macrophages were analysed by flow cytometry 24 hours after PBS or QS21 injection and cell numbers quantified in mice [8]. B-E) To examine cell or cytokine dynamics after AS01 compared with PBS, six to eight week old female C57BL/6 mice were immunised i.m with gE antigen formulated with 1/50th human-dose (HD) AS01b in gastrocnemius muscles, or gE and PBS. Iliac dLN were collected at timepoints between 3 and 48 hours post injection. IFNγ producing cells were assessed by ICS. Cytokines were analysed by MILLIPLEX MAP, a multiplex assay using Luminex technology. For cell detection, flourescent events were acquired using an LSR2 flow cytometer and analysed by FLOW JO. B-D) Iliac dLN were collected at timepoints between 6, 24 and 48 (not shown) hours post injection. Boxplots show A) subcapsular sinus macrophages after PBS and QS21 stimulation. B) Resident and Migratory DCs after AS01 or PBS, C) inflammatory monocytes after AS01 or PBS, D) IFNγ+ NK cells after AS01 or PBS, E) IFNγ after AS01 or PBS. Iliac dLN were collected at timepoints between 3,6,24 and 48 (not shown) hours post injection. All statistical significance measured by T-test. All data was generated by GSK. All 'zero hour' measurements are estimated from PBS controls. 82

4.2 **Scoping cellular interactions:** A CellDesigner Model depicting salient events that give rise to the production of Innate IFNγ. 83

4.3 **Expected Behaviours Diagram:** Linking the phenomena observed from the biological domain to the times in which these are observed, and to the hypotheses for how these phenomena holistically manifest *in vivo*. 85

4.4 **Summarising the underlying biological hypotheses:** A cartoon describing the captured biology. QS21 activates CD169+ macrophages in a caspase-1 dependent manner, resulting in the release of IL18. IL18 can individually promote the production of IFNγ from NK and other IFNγ producers. Furthermore, the model captures the ability for IL12 to individually promote the production of IFNγ by NK and other IFNγ producers. In addition, IL12 and IL18 synergise to promote an augmented production of IFNγ. The source of IL12 is hypothesised to be monocytes and/or DCs, after TLR-4 stimulation by MPL. 87

4.5 **A dendritic cell Activity Diagram.** 89

4.6 **An 'IFNγ Secretor Cell' Activity Diagram.** 90
4.7 **A dendritic cell State-Machine Diagram:** This diagram describes the functionality of DCs as per their hypothesised involvement in early IFNγ production, with respect to our research questions. 91
4.8 **An 'IFNγ Secretor Cell' Activity Diagram.** 92
4.9 **A NK cell Platform Model Diagram.** 93
4.10 **A dendritic cell Platform Model Diagram.** 94
4.11 **A calibrated model of innate IFNγ production after AS01 immune system stimulation:** Time-series graphs showing model fits for **A)** subcapsular macrophages, **B)** dendritic cells, **C)** monocytes, **E)** IL18, **F)** IL12, **G)** IFNγ. Black dots represent the data the model was trained against with corresponding error bars. Red lines represent the mean trajectories, blue shading represents the mean +/- standard deviation for the model outputs, and black lines represent the fit with the lowest objective value. 100

4.12 **Validation of the simulation model:** Boxplots contrasting *in silico* and *in vivo*. All *in vivo* data was generated by GSK and not by the author of this thesis. **A)** Fold changes in IFNγ+ NK cells after respective anti-IL12 depletions. *In vivo* experimentation was performed by treating C57BL/6 WT mice with αIL12p40 or control IgG, and immunized i.m the following day with AS01 and HBsAg. DLNs were collected six hours after immunization and the levels of IFNγ producing NK cells was evaluated by ICS. *In silico*, this experiment was performed by removing any mathematical terms that involve IL12, i.e for NK cell activation and IFNγ production. Simulation is then performed *in silico* for the 'wild type' model and the 'knockout' model. Fold-changes of IFNγ+ NK cells (NKa) at six hours are calculated between the two *in silico* scenarios, and then compared to the corresponding *in vivo* fold-changes. **B)** IFNγ+NK cells after respective IL18R Knockouts. *In vivo* experimentation was performed by immunising i.m C57BL/6 WT or IL18$^{-/-}$ mice with AS01 and Hepatitis B surface antigen (HBsAg). DLNs were collected six hours after immunization and the levels of IFNγ producing NK cells was evaluated by ICS. *In silico*, an IL18R knockout was performed by removing any terms that involve IL18 - i.e NK cell activation and IFNγ production. **C)** IFNγ+ NK cells after respective clodronate-mediated subcapsular macrophage depletions. *In vivo* experimentation was performed by treating C57BL/6 mice with 20ul clodronate liposomes or control liposomes i.m. Six days later mice were immunised with AS01 and HBSag. DLNs are collected and analysed by FACs. *In silico*, this was performed by setting the 'Mo' (CD169+ macrophage) initial condition to zero. **D)** IFNγ+ NK cells after both anti-IL12 and IL18R knockout scenarios *in silico* and *in vivo*. *In vivo* experimentation was performed by treating C57BL/6 WT + control IgG or IL18-/- mice with αIL12p40, and immunized i.m the following day with AS01 and HBsAg. DLNs were collected six hours after immunization and the levels of IFNγ producing NK cells was evaluated by ICS. *In silico* experimentation was performed by removing mathematical terms where both IL12 and/or IL18 are involved. 103

4.13 **Log-transformed parameter space:** showing the distribution of calibrated parameter values. Y-axis is ordered by parameter dimension. Each parameter has been log-transformed to improve readability. 104

4.14 **The importance of VmaxNKaProd1218$_p$ and vMoIL18$_p$ parameters in IFNγ production:** A-B) Simulation results (black dots) at six hours after running the model with different parameter values for *vMoIL18$_p$* (A) and *VmaxNKaProd1218$_p$* (B). By uniformly sampling +/-90% each side of the baseline parameter, 523 parameter sets were sampled and simulated, changing only the parameter of interest. Blue dashed line indicates the calibrated best-fit value of each parameter on the x-axis. The means and error of experimental data for IFNγ at six hours is shown in red. C-D) Parameters *vMoIL18$_p$* (C) and *VmaxNKaProd1218$_p$* (D) were varied over ranges each side of their calibrated best-fit value. Plots show the effect of OAT parameter alterations on simulation measures, assessed by the A-Test. . . 107

4.15 **Profile-likelihood analysis for cell-related parameters:** Plots showing data contribution to the total objective value based on perturbations of parameters. Profile-likelihood analysis was performed using dMod [9]. Confidence interval thresholds are labelled on y-axis. Parameter values are shown on the x-axis. 110

4.16 **Profile-likelihood analysis for cytokine-related parameters:** Plots showing data contribution to the total objective value based on perturbations of parameters. Profile-likelihood analysis was performed using dMod [9]. Confidence interval thresholds are labelled on y-axis. Parameter values are shown on the x-axis. 112

5.1 **Temporal contributions of DCs and monocytes to IL12 production:** Line graphs showing the influence of parameters *vDCIL12$_p$* and *vMonocIL12$_p$* - controlling DC or monocyte production of IL12 respectively - through eFAST global sensitivity analysis. A) shows the first order sensitivity indices. B) shows the total order sensitivity indices. The influence of a dummy parameter which should exhibit no impact on simulation behaviour is also shown. 120

5.2 **The effects of IL18 and IL12 production by each cell type on the resulting IFNγ production:** Boxplots showing the *in silico* production of IFNγ at key timepoints after perturbing four cytokine production parameters, $vMoIL18_p$ controlling macrophage induced IL18, $vDCIL12_p$ controlling DC induced IL12, $vMonocIL12_p$ controlling monocyte induced IL12, and both IL12 production parameters simultaneously (labelled BothIL12). A) shows IFNγ after reducing the parameters 90% from their calibrated baseline. B) shows IFNγ after increasing the parameters 90% from their calibrated baseline. 122

5.3 **Predicted percentage changes in simulated IFNγ after perturbations of cytokine production parameters:** A collection of bar plots showing at key time-points the predicted percentage changes in mean IFNγ after perturbing parameters $vMoIL18_p$ (controlling macrophage IL18 production), $vMonocIL12_p$ and *vDCIl12* (controlling monocyte and DC IL12 production respectively), both $vDCIL12_p$ and $vMonocIL12_p$. Number headings in each subpanel represent an hourly timepoint following simulated AS01 administration. 123

5.4 **Exploring the effects of simulated knockouts on IFNγ production:** Boxplots showing A) A simulated monocyte recruitment knockout and monocyte depletion. This depletion was implemented by setting the monocyte initial condition to zero (monocyte depletion) and the $monocRec_p$ parameter - controlling the rate of monocyte recruitment - to zero (simulating a monocyte-specific-CCR2 knockout). Thus creating a scenario with no monocytes and no monocyte recruitment. B) A simulated DC recruitment and Activation knockout and DC depletion. To implement this depletion we set the parameter controlling DC activation/recruitment ($DC_Afferent_p$) to zero, as well as the DC initial condition. C) Both simulated CCR2 knockout and monocyte depletion and a DC recruitment and Activation knockout and DC depletion. D) A simulated macrophage depletion. 124

5.5 **The temporal effects of IL12 and IL18 production for IFNγ across the first 24 hours:** Line graphs showing the influence of parameters $vDCIL12_p$, $vMoIL18_p$ and $vMonocIL12_p$ on IFNγ through eFAST based global sensitivity. Parameter $VmaxNKaProd1218_p$ controlling the production of IFNγ itself is also shown for comparison. A) First order eFAST sensitivity index. B) Total order sensitivity index. 126

5.6 **Examining the influence of macrophage cell loss on IFNγ production across the first 24 hours of AS01-adjuvanted immune responses:** Plot showing the total and first order eFAST sensitivity indices for the parameter CL_p - controlling the rate of macrophage loss on IFNγ production in the simulation. 127

5.7 **Exploring the effects of zero macrophage cell loss on immune components:** After setting CL_p to zero, time-series plots showing the predicted trajectories of A) macrophages (Mo). B) IL18. C) IFNγ+ NK cells (NKa). D) IFNγ (IFNg). Black dots represent the data the model was trained against with corresponding error bars. Red lines represent the mean trajectories, blue shading represents the mean+/- sd for the model outputs, and black lines represent the predicted trajectory for the originally calibrated 'best fit'. . . 128

5.8 **The 'macrophage cell loss' parameter inhibits IFNγ production:** After doubling the CL_p parameter, time-series plots showing the predicted trajectories of A) macrophages (Mo). B) IL18. C) IFNγ+ NK cells (NKa). D) IFNγ (IFNg). Black dots represent the data the model was trained against with corresponding error bars. Red lines represent the mean trajectories, blue shading represents the mean+/- sd for the model outputs, and blue lines represent the predicted trajectory for the originally calibrated 'best fit'. 129

5.9 **Predicted IFNγ responses after simulating a second AS01 delivery at days 7-28 after initial AS01-based vaccination:** Black data points and error bars show the *in vivo* experimental data for which the original model is calibrated. Model predictions based upon predicted macrophage recovery are visualised. The red line shows the mean IFNg trajectory, while the shaded gray shows the mean +/- the standard deviation. For example, the top-left panel labelled '7' shows the predicted second IFNγ response (red line shows the mean), if one was to perform a second AS01 delivery on day 7 post-injection, with respect to the predicted numbers of available macrophages on day 7. 132

5.10 **Parameters with influence on the simulated IFNγ response after AS01:** Line-graph showing total order sensitivity index values for proportions of variance contributing to simulated IFNγ over the first 24 hours of the simulated immune response. 133

6.1 **Experimental data for model calibration 1/2:** Experimental data used for calibration. A-G, data are colored by whether the measurements were gathered solely from experimental data, or whether a datapoint has been estimated as described in the text. For full descriptions of experiments that led to these data, please see Figure 3.2. From Figure 3.2, the PBS measurements are here used as 'zero hour' timepoints. Remaining timepoints are from experiments with AS01 1/50HD. **A)** The numbers of CD169+ macrophages in the dLN, used as observational data for model macrophages at zero (from PBS measurements) and 24 hour timepoints. **B)** The numbers of CD11c+ MHCII+ DCs in the dLN used as observational data for model DCs, at zero (from PBS measurements), 6, 24, 48 hours. Estimated datapoints are shown for 168 hours. **C)** The numbers of CD11b+ Ly6chi monocytes in the dLN, used as observational data for model monocytes, at zero (from PBS measurements), 6, 24, 48 hours. Estimated datapoints are shown for 168 hours. **D)** The concentration of IFNγ in the dLN, used as observational data for model IFNγ, at zero (from PBS measurements), 3, 6, 24, 48 hours. **E)** The concentration of IFNγ in the dLN, used as observational data for model IFNγ, at zero (from PBS measurements), 3, 6, 24, 48 hours. **E)** The numbers of IFNγ+ NK cells in the dLN, used as observational data for model 'activated NK cells', at zero (from PBS measurements), 6 and 24 hours. Estimated datapoints are shown for 48 hours. **F)** The numbers of IFNγ+ NK cells in the dLN, used as observational data for model 'activated NK cells', at zero (from PBS measurements), 6 and 24 hours. Estimated datapoints are shown for 48 and 72 hours. 144

6.1 **Experimental data for model calibration 2/2:** For full descriptions of experiments that led to these data, please see Figure 3.2. From Figure 3.2, the PBS measurements are here used as 'zero hour' timepoints. Remaining timepoints are from experiments with AS01 1/50 Human Dose. **G)** The estimated numbers of naive CD4+ T cells in the dLN following vaccination with an AS01-adjuvanted vaccine. Zero hour reflects the geometric mean of a PBS control. At hours 120 and 168, these cells are estimated as the difference from geometric means of the total CD4+ T cells and numbers of antigen-specific CD4+ T cells. **H)** The numbers of IFNγ+ CD4+ T cells in the dLN, used as observational data for model primed CD4+ T cells, at zero (from PBS measurements) and 24 hours. **I)** The numbers of 2W1S+ CD4+ T cells in the dlN, measured by Dominika Gajdasik, University of Birmingham. 145

6.2 **Experimental data for model validation:** Colleagues at the university of Birmingham injected C57BL/6 or CD80/80-/- mice with AS01 and 2W1s. At five days post-injection, the numbers of antigen-specific CD4+ T cells were measured. Here, we contrast these two measurements. 148

6.3 **Scoping cellular interactions:** A CellDesigner Model depicting salient events that give rise to CD4+ T cell priming after AS01-adjuvanted vaccination. 150

6.4 **An Expected Behaviours Diagram:** Defining expected behaviours through linking the phenomena observed from the biological data to the times at which these are observed and to the hypotheses for how such phenomena manifest. 151

6.5 **A 'Whole System' Activity Diagram:** showing key activities of different model components and how they interact to produce system wide behaviour. Diagram shows activities for A) Subcapsular sinus macrophages (SCS-Mo), B) QS21, C) monocytes, D) IFNg Producer, E) IFNg, F) resident DCs, G) mature DC, H) naive CD4+ T cells and I) primed CD4 T cells. 155

6.6 **A State-Machine diagram for a CD4+ T cell:** captures both naive and primed states. 157

6.7 **A simplified cartoon of the Domain Model for AS01-induced CD4+ T cell priming.** Describes the captured salient biology. Surrounded by the blue box, is the captured salient biology in the Domain model for innate IFNγ production, as described in Chapter 4. Here, we extend the model (shown in green), to capture canonical priming of CD4+ T cells by DCs, and the ability for IFNγ to enhance this process. 158

6.8 **A Platform Model for AS01 induced CD4+ T cell Priming:** 1/2 . 159

6.8 **A Platform Model for AS01 induced CD4+ T cell Priming:** 2/2. A 'population and interactions' diagram describing the interplay between different model components. The rate 'cognateAct' in the diagram is written in the text and subsequent models as 'cognatePriming', for further clarity. Dotted arrows indicate secretion of a cytokine. Dashed arrows indicate a component acts upon another. 160

6.9 **Calibration of the Baseline AS01 CD4+ T cell Model 1/2:** Caption overleaf. 169

6.9 **Calibration of the Baseline AS01 CD4+ T cell Model 2/2:** Macrophage (A), dendritic cell (B), monocyte (C), IFNγ+ NK cell (D), IL18 (E), IL12 (F), IFNγ (G), Innate IFNγ+ CD8+ T cell (H), Negative Regulatory Processes (I), Adaptive IFNγ+ CD8+ T cell (J), naive CD4+ T cell (K) and primed CD4+ T cell (L) kinetics were fitted using the *dMod* package, employing multi-start trust-region optimisation to minimise the objective value between the model output and observational data. Black dots and error bars show the mean and standard deviation of the biological data upon which the model was calibrated, grey lines represent *in silico* parameterisation outputs, blue shading represents the mean +/- the standard deviation for these *in silico* outputs, red lines represent the mean of the *in silico* outputs, and black lines represent the best fitting (lowest objective value) *in silico* output. . . . 170

6.10 **Validation of the 'Baseline' Model:** Boxplots contrasting *in silico* and *in vivo* **A)** Fold changes in IFNγ+ NK cells after respective anti-IL12 depletions. **B)** IFNγ+NK cells after respective IL18R Knockouts. **C)** IFNγ+ NK cells after respective clodronate-mediated subcapsular macrophage depletions. **D)** IFNγ+ NK cells after both anti-IL12 and IL18R knockout scenarios *in silico* and *in vivo*. 174

6.11 **The AS01 CD4+ T cell priming model is unable to replicate a sharp increase in monocytes between 24 and 48 hours post-injection:** Line-plot showing the distribution of model trajectories for monocytes in the dLN after simulated vaccination with AS01. Two dashed lines show 24 and 48 hours post injection respectively. The central estimates of the *in vivo* experimental data are shown with black points, together with black error bars showing the standard deviation. Grey lines show the trajectories of each model fit, the red line shows the mean of each *in silico* trajectory, the shading represents the mean +/- standard deviation of the trajectories produced by model fits. 176

6.12 **Large variation is observed in *in silico* output for IFNγ production following 48 hours post-simulated-injection:** Line-plot showing the distribution of model trajectories for IFNγ in the Baseline Model. Red dashed line shows the predicted timepoint where the mean of the *in silico* 'innate IFNγ' output peaks. For ease of visualisation, two black dashed lines show the approximate beginning and end of the 'second wave' of IFNγ after AS01. The central estimates of the *in vivo* experimental data are shown with black points, together with black error bars showing the standard deviation. Grey lines show the trajectories of each model fit, the red line shows the mean of each *in silico* trajectory, the shading represents the mean +/- standard deviation of the trajectories produced by model fits. 178

6.13 **Evaluating the role of 'Negative Regulatory Processes' on *in silico* outputs from the 'Baseline' Model:** Simulations were ran under wild-type (model as calibrated, shown in blue) or after the parameter controlling the level of 'Negative Regulatory Processes' was set to zero (shown in red). Line-plots comparing these two scenarios for model entities; Negative Regulatory Processes (A), dendritic cells (B), monocytes (C), IL12 (D), IFNγ (E), Adaptive IFNγ+ CD8+ T cells (F), primed CD4+ T cells (G). The shaded bounds represent the mean +/- the standard deviation of model trajectories produced by the distribution of parameter sets. The line represents the mean of model trajectories. Experimental data upon which the wild-type model was originally calibrated is plotted in black dots and error bars. 180

6.14 **Examining simulation robustness to T cell related parameter alterations on primed CD4+ T cells:** A-D, 100 parameter sets are sampled uniformly across ranges of a factor of 10 each side of the baseline parameter value. Each sampled parameter value is ran 'in place' of the corresponding parameter for every calibrated model fit (n=81). 8100 runs are performed for each parameter, incorporating uncertainty from the model calibration into the analysis. Distribution of simulation responses for primed CD4+ T cells for each parameter, are compared with the simulation responses after running the model with the baseline calibrated 'best fit'. **A-D** show lineplots showing Vargha-Delaney A-Test statistics at different alterations of parameters for those controlling the rates of **A)** primed CD4+ T cell proliferation ($\text{CD4Proliferation}_p$), **B)** B7-mediated cognate CD4+ T cell priming, **C)** T cell dLN exit and anergy (Tcell_ExitAnergy), **D)** inflammation-induced naive CD4+ T cell recruitment. **E)** Boxplot showing the distribution of model trajectories after running the baseline model with values a factor of 3 around the baseline value for '$\text{CD4T0_Inflammatory_Recruitment}_p$'. **F)** Line plot showing the distribution of primed CD4+ T cells after a simulated knockout of inflammation-induced naive CD4+ T cell recruitment. The central coloured lines show the mean for each group, while the shading shows +/- standard deviation of the group. **G)** Boxplots contrasting the distributions of primed CD4+ T cells after the aforementioned simulated knockout at 120 hours and 168 hours post-injection. 184

6.15 **Examining simulation robustness to the parameter controlling DC recruitment into -and activation in- the dLN:** 100 parameter sets were sampled uniformly across ranges of a factor of 10 each side of the baseline parameter value. Each sampled parameter value was ran 'in place' of the corresponding parameter for every calibrated model fit (n=81). Therefore 8100 runs were performed for the parameter, incorporating uncertainty from the model calibration into the analysis. The distribution of simulation responses for primed CD4+ T cells for the parameter, were compared with the simulation responses after running the model with the baseline calibrated 'best fit'. **A)** Lineplot showing Vargha-Delaney A-Test statistics at different alterations and at different timepoints, for the parameter controlling the rates of DC recruitment and dLN activation (DC_Afferent_p). 186

6.16 **Calibrating an Alternate AS01 CD4+ T cell Model 1/2.** continued overleaf. 188

6.16 **Calibrating an Alternate AS01 CD4+ T cell Model 2/2.** This model captures a scenario where IFNγ is hypothesised to play a more prominent role in CD4+ T cell priming. Macrophage (A), dendritic cell (B), monocyte (C), IFNγ+ NK cell (D), IL18 (E), IL12 (F), IFNγ (G), Innate IFNγ+ CD8+ T cell (H), Negative Regulatory Processes (I), Adaptive IFNγ+ CD8+ T cell (J), naive CD4+ T cell (K) and primed CD4+ T cell (L) kinetics were fitted using the *dMod* package, employing multi-start trust-region optimisation to minimise the objective value between the model output and observational data. Black dots and error bars show the mean and standard deviation of the biological data upon which the model was calibrated, grey lines represent *in silico* parameterisation outputs, blue shading represents the mean +/- standard deviation for these *in silico* outputs, red lines represent the mean of the *in silico* outputs, and black lines represent the best fitting (lowest objective value) *in silico* output. 189

6.17 **Validation of the Alternate AS01 CD4+ T cell Model 1:** Boxplots contrasting *in silico* outputs and *in vivo* experimental data **A)** Fold changes in IFNγ+ NK cells after respective anti-IL12 depletions. **B)** IFNγ+NK cells after respective IL18R Knockouts. **C)** IFNγ+ NK cells after respective clodronate-mediated subcapsular macrophage depletions. **D)** IFNγ+ NK cells after both anti-IL12 and IL18R knockout scenarios *in silico* and *in vivo*. 192

6.18 **Local sensitivity analysis for the 'Alternate' model compared with the 'Baseline' Model sensitivities for parameters where the influence is similar in both settings:** A-E, 100 parameter sets are sampled uniformly across ranges of a factor of 10 each side of the baseline parameter value. Each sampled parameter value is ran 'in place' of the corresponding parameter for every calibrated model fit (n=73). Therefore 7300 runs are performed for each parameter, incorporating uncertainty from the model calibration into the analysis. The distribution of simulation responses for primed CD4+ T cells for each parameter, are compared with the simulation responses after running the model with the baseline calibrated 'best fit'. **A-D** show lineplots showing Vargha-Delaney A-Test statistics at different alterations of parameters for those controlling the rates of **A)** primed CD4+ T cell proliferation (CD4Proliferation$_p$), **B)** B7-mediated cognate CD4+ T cell priming, **C)** T cell dLN exit and anergy (Tcell_ExitAnergy), **D)** inflammation-induced naive CD4+ T cell recruitment. 193

6.19 **Local sensitivity analysis for the 'Alternate' model: A-E:** 100 parameter sets are sampled uniformly across ranges of a factor of 10 each side of the baseline parameter value. Each sampled parameter value is ran 'in place' of the corresponding parameter for every calibrated model fit (n=73). Therefore 7300 runs are performed for each parameter, incorporating uncertainty from the model calibration into the analysis. The distribution of simulation responses for primed CD4+ T cells for each parameter, are compared with the simulation responses after running the model with the baseline calibrated 'best fit'. **A-D** show lineplots showing Vargha-Delaney A-Test statistics at different alterations of parameters for those controlling the rates of **A)** recruitment and activation of DCs **B)** Production of IL12 by DCs **C)** Loss of macrophages, **D)** macrophage production of IL18, **E)** IFNγ-dependent CD4+ T cell priming. 196

6.20 **Exploration of DC potency enhanced by IFNγ using the 'Baseline' Model:** A-B) Simulations using the 'baseline' model occurred after the parameter controlling IFNγ enhancement of DC potency (cognateEnhanceIFNg$_p$) was perturbed. The maximum permitted value of this parameter was increased to the calibrated baseline multiplied by 450 (Drastic) or 45 (Mild IFNg Enhance). Parameters within these new ranges were sampled and simulated. A) Line-plot contrasting the model trajectory of primed CD4+ T cells after two scenarios with the 'Baseline' model. For remaining parameters, every local optima was simulated. Shaded intervals show the mean+/- standard deviation of model trajectories. 199

6.21 **Model variants where IFNγ's role is more prominent are qualitatively inconsistent with experimental data:** A) Simulations using the 'Alternate' model occurred after the two parameters controlling rates of DC priming were perturbed within ranges as defined in Table 6.8. Parameters within these new ranges were sampled and simulated. Where values for multiple parameters were changed (Perturb both activation rates), each possible combination of the sampled parameter values was simulated. For remaining parameters, every local optima was simulated. Shaded intervals show the mean+/- standard deviation of model trajectories. 201

6.22 **A simulated 'IFNg' (IFNγ) knockout using the 'Alternate' Model:** A boxplot contrasting the distribution of 'primed CD4+ T cell' model trajectories for each local minima after the 'IFNg knockout' and 'wild-type' scenarios at day 7 post-injection. The simulated IFNγ knockout was implemented by setting the 'IFNg' initial condition to zero, as well as the parameters which produce 'IFNg', $VmaxNKaProd1218_p$, $VmaxNKaProd12_p$, $VmaxNKaProd18_p$, $InnateCD8IFNgProd_p$ and $BasalCD8IFNgProd_p$. The simulation was then run for each local minima. 203

A.1 **A State-Machine diagram for a Muscle-Resident cell.** 268
A.2 **A State-Machine diagram depicting a CD169+ F480 Macrophage.** 269
A.3 **A State-Machine diagram depicting a Dendritic Cell.** 270
A.4 **A State-Machine diagram for a IFNγ Producer cell.** 271
A.5 **A State-Machine diagram for a Naive CD4+ T cell.** 272
A.6 **A State-Machine diagram for a Th1 / Tfh cell.** 273
A.7 **An Activity Diagram diagram depicting a Dendritic Cell.** 274
A.8 **An Activity Diagram diagram depicting a SCS Cell.** 275
A.9 **An Activity Diagram depicting a IFNγ Producer cell.** 276
A.10 **An Activity Diagram depicting a Naive CD4+ T cell.** 277
A.11 **An Activity Diagram depicting a Th1 / Tfh cell.** 278

B.1 **Overview of Hybrid ODE/ABM Platform Model** 279
B.2 **A Platform Model State Machine Diagram for a DC** 280
B.3 **Emergent Detail for DC in the Model** 281
B.4 **Overview of DC Internal Processing** 282

Chapter 1

Introduction

1.1 Introduction to Vaccination

For centuries, smallpox devastated the world. In 1980, the World Health Organisation declared the global eradication of the disease, a remarkable milestone in human history [10]. In 1796, Edward Jenner's seminal discovery that cowpox inoculation (vaccinia virus) protects against inoculated smallpox introduced the concept of modern vaccination [11]. Today, the world rests on the hope that efficacious vaccines will provide long-term, robust protection against COVID-19, the disease caused by the coronavirus SARS-CoV-2 [12]. Indeed, in much of the global north, society is currently transitioning back toward a semblance of normality, in large part due to protection afforded by vaccination. Vaccination has been shown to be one of the most effective routes out of the societal turmoil induced by pandemics, and more broadly is a vital avenue for improving global health.

Adjuvants are immunostimulants that mimic aspects of the innate response and are employed in subunit vaccines to augment, shape, and tailor the immune response to antigens [13, 14, 15, 4, 16, 7]. Despite vaccine successes over the last 200 years, the molecular mechanisms driving the efficacy of many vaccines is not well understood and particularly the mechanism of action (MoA) of adjuvants including chemical (e.g. alum salts) and biological adjuvant effects of virus particles and components are unclear. Providing transparent MoAs for adjuvants and immune priming events will help enable rational design of vaccines formulations, permit identification of improved dosing of vaccine components and timing of delivery to maximise vaccine efficacy and may help combat vaccine hesitancy. Development of the next generation of vaccines with improved transparency and enhanced efficacy is critical in tackling tropical disease and future pandemics. With the exception of the Bacillus Calmette Guerin (BCG) vaccine, all commonly used vaccines are considered to primarily induce protective immunity through humoral (antibody) B cell driven immune responses[17]. However, for some pathogens, antibody responses alone are insufficient to drive pathogen

elimination and thus require effector T cell function through cytokine production or direct cytotoxic T lymphocyte (CTL) activity (e.g. Leishmaniasis) [18]. Thus, although most vaccines induce varying levels of T cell responses, as required to drive high affinity antibody (IgG or IgA) responses, their direct function in vaccine efficacy is incompletely understood. Next generation vaccines will likely require the generation of both robust T cell and neutralising antibody responses. Therefore, a deeper understanding of the mechanisms of how adjuvants might generate robust T cell and antibody-based immunity is required[7].

1.2 From Intramuscular Injection Site to Tissue Draining Lymph Node Immune Responses

Physiology has a key role in regulating the type and timing of an immune response [1]. Therefore, the route of vaccine administration impacts on both the timing, type and efficacy of the generated response. A commonly-used route of vaccine administration is intramuscular (IM) into skeletal muscle, in part due to being an easy, accessible site of administration. Alternative routes include subcutaneous, intradermal, intranasal, oral, genital tract and intravenous. With some exceptions, these routes are less often used in the clinic to vaccinate and in this thesis we will focus on IM-based vaccination. Skeletal muscles are the only voluntary muscle tissue in the human body[19]. It is possible that muscle contraction leads to rapid propagation of vaccine components into local tissue draining lymph nodes (dLNs) after IM administration. Despite its primary role in movement, skeletal muscle contains resident immune cells. During stress e.g. exercise, skeletal muscle cells secrete myokines, modulating localised and systemic immune responses (IL6, IL13) and under pathological conditions (e.g. damage by needle) infiltration by immune cells occurs [20, 21].

Post IM injection, vaccine components diffuse into the interstitial space [15]. From the interstitium, molecules less-than 10nm (∼7Kd) are free to permeate into blood and lymphatic vessels[22], but as blood flow through the blood vasculature is 100-500 times faster than the flow of lymph fluid moving through the lymphatic vessels, small molecules are very rapidly cleared through the blood[22]. In contrast, larger molecules are unable to permeate blood vasculature thus clearance from the injection site occurs through draining lymphatics or through cellular uptake by immune cells that can migrate to dLNs [23]. Different vaccine formulations will modulate rates of clearance and duration of the immune response from the injection site, changing immune responses dynamics.

1.2.1 Lymph Nodes and Constituents

Lymph Nodes (LNs) are kidney-bean-shaped secondary-lymphoid-organs (SLOs) with highly organised structure that filter lymph fluids and act as a meeting site of adaptive and innate

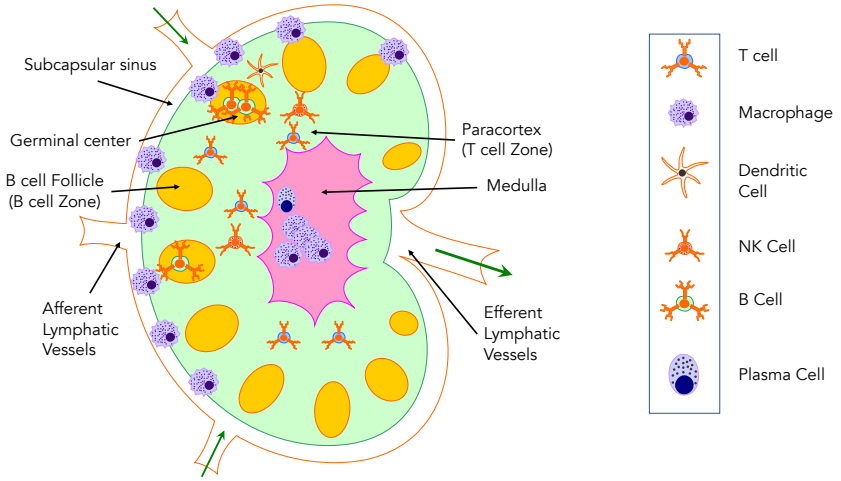


Figure 1.1: **Lymph Node structure and constituents:** Follicles are depicted by orange oval shapes. Afferent lymphatic (AL) vessels drain lymph from peripheral tissues, and transport antigen and antigen-carrying cells into the LN[1, 2, 3]. The bloodstream deposits lymphocytes into the center of the LN via high-endothelial-venules. Cells exit the dLN via the efferent lymphatic vessels.

immune cells (Figure 1.1). LNs are required for the rapid induction of protective immune responses[1, 24]. LNs are anatomically located where lymphatic vessels converge, permitting efficient surveying of extracellular lymph fluid[2]. LNs contain multiple zones including a subcapsular zone, paracortex, cortical and medulla regions with distinct functions during immune responses. The outer area of the cortex (B cell zone) contains organised lymphoid follicles of B cells and stromal fibroblasts [1, 25]. During an immune response, Germinal Centers (GCs) form in the follicles, where B cells can undergo antigen dependent hyper-proliferation (dark zone), mutate their immunoglobulin genes (light zone) and receive T cell help. GCs permit the expansion and development of high affinity memory B cells and B cells that can differentiate into plasma cells which secrete large amounts of high affinity antibody [26].

B cell follicles are comprised primarily of B cells and follicular Dendritic Cells (FDCs)[27] and form lymphoid microarchitectures called FDC networks, which allow B cells to efficiently scan for antigen. FDCs capture antigen-complement complexes. Critically, FDCs secrete a chemokine called 'chemokine (C-X-C motif) ligand 13' (CXCL13) that recruits B cells but also permits optimal B cell scanning [28, 25]. After LN entry through high-endothelial-venules (HEVs), B cells are directed toward CXCL13 gradients in the follicle via their expression of receptor CXCR5[28, 25]. If a B cell becomes activated, it can migrate toward the boundary discriminating the B / T cell zones. Here, they meet T cells which also express CXCR5 [29], and B-T cell interactions here can lead to affinity-maturation and high-affinity B cell responses[26]. It is the choreography of lymphocytes that enables efficient high affinity immune responses. The area between the B cell follicles is the interfollicular

region (IFR) and in recent years is increasingly understood to be a site of importance in immune response generation [30, 31]. The IFR is located adjacent to the subcapsular sinus (SCS) and extends between the lymph node follicles toward the Paracortex. Immediately adjacent to the SCS is populated by NK cells, $\gamma\delta$ T cells, ILCs, 'Innate-like' Memory CD8+ T cells, and NK-T cells[32, 33, 30, 31]. This section of the IFR is increasingly thought to be critical for the initiation of immune responses and interactions that occur here are thought to play a key role in vaccine adjuvant MoA[32].

The Paracortex, (T cell zone) is located deeper into the cortex and is the site of dendritic cell (DC) - T cell interactions, permitting the efficient activation of very rare antigen-specific lymphocytes[1]. DCs are professional 'antigen-presenting-cells' (APCs), and their primary role is to capture and process antigen and present it to T cells. Their phenotype has a key role in determining the type of T cell response through the production of cytokines and co-stimulatory molecules[34]. Therefore, maturation and activation of DCs is a critical event during the initiation of vaccine-induced immune responses [35]. Regulating immune cell entry and exit from LNs is critical in the regulation of immune responses. Entry to LNs from the blood occurs through specialised blood vessels called high-endothelial-venules, which are optimised for lymphoid cell entry from circulation through expression of chemokines and other factors [1]. Cells and lymph fluid exit the LN through the efferent lymphatic vessels in a process regulated by Sphingosine-1-phosphate and its receptors. Inflammation leads to changes in T cell entry and exit[36] through processes that can be modulated by vaccine adjuvants.

The Paracortex houses T cells after they extravasate through HEVs. The Paracortex comprises a fibroblastic-reticular cell network. These cells generate rich gradients of chemokines CCL19 and CCL21, which enable CCR7 expressing cells (the receptor for CCL19/21), e.g., T cells, NK cells and Mature DCs, to converge in the Paracortex[37, 38]. Here mature DCs present antigen to Naive T cells. Mature DCs contact up to 5000 T cells an hour and if there is a cognate interaction, can deliver co-stimulatory molecules to activate T cells [39, 40, 41]. After activation and differentiation, CXCR5 is upregulated by a small subset of T cells, CD4+ T follicular Helper cells (Tfh cells). CXCR5 expression dominates over constitutive CCR7 expression[41], directing Tfh cells into the B cell follicle. Here, they provide survival signals to B cells, which is critical for T-dependent B cell activation[42].

The subcapsular sinus (SCS) is a site of pathogen entry into the LN. The floor of the SCS is lined with CD169+ F4/80- macrophages and lymphatic endothelial cells[3]. These macrophages are strategically positioned in the SCS, enabling them to survey incoming lymph for antigen[43, 44]. Their 'tails' extend into the B cell follicle, permitting capture

of incoming antigen, and its transfer into the follicles for B cell priming [45]. Lymphatic-sinus-dendritic-cells (LS-DCs) can also capture lymph-borne particulate antigens and elicit the early activation of antigen-specific T cells, permitting the generation of rapid T cell responses[30]. This is likely to be a key mechanism involved in IM delivered vaccines as components can rapidly drain into a lymph node draining the injection site[15, 46]. Therefore, LN resident DCs e.g., LS-DCs may have a key role - through the capture of vaccine antigens and stimulation by vaccine adjuvants - thus permitting the rapid induction of T cell responses, before the arrival of migratory DCs from the injection site.

One rare cell type in LNs that has a key role in immune responses both to pathogens and vaccines, are natural killer (NK) cells which are best characterised for a capacity to kill virally-infected cells and tumour cells[47]. Interestingly, recent work suggests reduced number and function of NK cells in patients with severe COVID-19 disesae, leading to reduced clearance of infected cells[48, 49]. NK cells can produce large amounts of cytokines including IFNγ and TNF-α in response to inflammatory signals which can amplify immune responses [50], including to vaccine adjuvants. They have been shown to contribute to immunity against Malaria and other protozoan pathogens [51, 52].

While macrophages are a small percentage of immune cells in the LNs, they have a critical role in the engulfment of foreign substances and cellular debris through phagocytosis[53, 1]. Macrophages are specialised in removal of dead cells and debris, induction and amplification of inflammation and also have a critical roles in the resolution of inflammation and also in adjuvant MoA [1, 46, 8, 54, 55]. There are two anatomically distinct areas of macrophages in the lymph node. First, the SCS, the floor of which is lined with macrophages that survey afferent lymph fluid[3]. This macrophage subset are called subcapsular-sinus (SCS) macrophages (M) and characterised by CD169+ and F4/80- expression. Macrophages are also found in the inner medulla region interacting with medullary fibroblasts and antibody-secreting plasma cells[56]. The inner medulla is rich in lymphocytes and macrophages, which constitute strings known as medullary cords. The inner medulla also contains medullary sinuses that drain into the efferent lymphatics. Lymph fluid, cytokines, antibody and lymphocytes exit the dLN and return to blood circulation or enter a downstream LN in the chain.

All of these specialised compartments in LNs are supported by stromal (fibroblast) networks which permit both structural support and the higher level organisation of immune microenvironments in lymph nodes [57, 58].

1.3 Early Innate Immune Responses

The innate immune response is the first line of defence against threats and is vital during early events in both the injection site and injection-site draining lymph nodes (dLNs)[1, 59]. Following penetration of the skin (physical barrier) and skeletal muscle, tissue-resident innate cells (e.g., macrophages and DCs) produce cytokines, chemokines and other factors, leading to rapid recruitment of inflammatory neutrophils (in mins) and monocytes (in hours) [1, 59, 60]. Neutrophils have short life-spans, are extremely motile and are a 'first responder' at the injection site[61]. They release and respond to inflammatory factors including CXCL8/IL8 and Leukotriene B4[61, 62]. Neutrophils are phagocytic and amplify the initial inflammatory immune response through cytokine production. It has also been shown that neutrophils are capable of capturing antigen[46], although their function as an APC is controversial and despite the recruitment of neutrophils to the injection site and subsequently to dLNs there is little evidence that they have a role in T cell priming or modulating the humoral response to adjuvanted-vaccination.

Monocytes are circulatory white blood cells that extravasate into tissues in response to inflammatory signals and can differentiate into myeloid DCs and monocyte-derived macrophages in response to cytokines and growth factors. While monocytes can also differentiate into tissue repair macrophages, as this thesis is involved with inflammatory events following adjuvanted-vaccination, referral to monocytes in this thesis, unless explicitly stated otherwise, is to murine inflammatory (CX3CR1low Ly6c high, CCR2+, PDL1-) monocytes. Monocytes produce cytokines including IL12, TNF-, and IL-1 in response to stimulation [60, 63, 64, 65, 66, 67, 68]. Unlike neutrophils that home to medullary cords in LNs, monocytes can enter the IFR[69], thus localised cytokine production by infiltrating monocytes from the injection site has the potential to modulate the kinetics of the immune response in dLN.

1.3.1 Immune System Recognition

Innate immune cells express surface receptors, known as Pattern-Recognition-Receptors (PRRs), which recognise 'pathogen-associated-molecular-patterns' (PAMPs) or 'danger-associated-molecular-patterns' (DAMPS)[70]. PRRs can shift cellular transcriptional programming towards an inflammatory architecture, promoting an effective response. There are a broad array of PRRs with various intricacies [71]. Here, we will discuss two subsets of PRRs, Toll-like-receptors (TLRs) and Nod-like-receptors (NLRs), which are involved in (TLR-agonist based) vaccine-induced immune responses and/or the formation of inflammasomes.

1.3.1.1 Toll-like Receptors Initiate Innate Immune Responses

TLRs are a class of transmembrane PRR proteins that are differentially expressed by immune cells including DCs, macrophages, monocytes, NK cells and lymphocytes, and in tissue microenvironments including fibroblasts, skeletal muscle cells and endothelial cells. TLRs, which bind to PAMPS, recognise a broad range of pathogens from bacterial cell walls, flagella proteins to viral RNA, and this property to directly and rapidly initiate immune responses is employed by TLR-agonist vaccine adjuvants [72]. In mice, there are thirteen TLRs compared to ten in humans, with different cell types expressing uniquely different repertoires of TLRs [73]. There are important cross-species differences in expression patterns e.g., TLR4 is highly expressed on mouse B cells but not expressed on human B cells and a similar difference is observed on LN fibroblasts. This variability between species and cell types is important to capture and understand in the translation from pre-clinical models to human vaccines as it likely modifies the MoA.

TLR4 agonists are a common component of current adjuvants, due to the capacity to both enhance immune responses and modulate the type of responses through biasing toward Th1 polarisation. TLR4 interacts with the bacterial endotoxin Lipopolysaccharide (LPS), which is a strongly immunostimulatory endotoxin and can induce septic shock in humans [74, 75]. Thus, although LPS is a potent activator of immune responses, it is too toxic in its native form for use in vaccination and immunotherapies. Thus, modified TLR4 agonists e.g., monophosphoryl lipid A (MPL or MPL A) derived from LPS of *Salmonella Minnesota* and GLA (Glucopyranosyl Lipid A), a synthetic non-toxic analogue of bacterial LPS, are employed to stimulate innate cells post-administration of vaccines [76, 77, 78]. Other TLRs including TLR3 have been employed to stimulate vaccine responses, e.g., use of poly(I:C) in cancer vaccines. The capacity of TLR signalling to not only initiate immune activation but also shape both the inflammatory cell milieu and cytokine profiles, has made TLR stimulation a key component of novel adjuvants.

1.3.1.2 Nod-like-receptors (NLRs) and Inflammasomes

Nucleotide-binding oligomerisation domain-like receptors (NLRs), are intracellular PAMP and DAMP sensors. PAMPs can be taken into cells via phagocytosis [79] and be recognised by NLRs, initiating an innate response. Activation of NLRs drives formation of the inflammasome complex [80, 81, 82, 83]. NLRs detect infectious stimuli (e.g. bacterial metabolites) and cellular danger signals leading to the activation of caspases; proteases which lead to the maturation of key inflammatory cytokines IL1β and IL18 and thus extracellular release of pre-formed protein [84]. Caspase activation can also induce pyroptosis, an inflammatory form of cell death which can stimulate innate immune responses [81]. Each

inflammasome possess a sensor protein, which controls responsiveness to different stimulus [85]. The NLRP3 inflammasome has been the most widely studied[83], and its activation recruits 'apoptosis-associated speck-like protein containing a C-terminal caspase recruitment domain' (ASC), resulting in activation of pro-caspase 1. Activated Caspase-1 can cleave pro-IL-1β and pro-IL18 into bioactive proinflammatory cytokines and activate gasdernmin-d. Active gasdermin-d releases its N-terminal domain which then forms pores in the cell membrane to induce pyroptosis[85]. Pyroptotic cell death leads to the release of antigens and DAMPs including IL1 and high mobility group protein B1 that further amplify the response. Despite the diversity of stimulus that can drive inflammasome formation, the cleavage of pro-IL1β and IL18 is a common output [85]. In contrast to transcription-mediated cytokine production, IL-1β and IL18 are pre-stored in e.g., macrophages and inflammasome activation can result in release of these cytokines [86], thus transcription alone does not regulate the extent and duration of the response. Inflammasome activation can be detrimental to the host however, demonstrated by recent work showing that higher levels of inflammasome-derived products in the sera correlated with COVID-19 disease severity [87]. Indeed, as with all immunological processes, the balance imposed by negative feedback mechanisms is key to regulating the response.

In vaccination, responses may be augmented through pyroptosis-induced cytokine and antigen release. The contribution of inflammasomes to adaptive responses and vaccination is not fully understood, although they are primarily thought to enhance such responses [83]. However, more recent observations indicate in some circumstances, inflammasomes impair adaptive immunity [88, 85], perhaps e.g. through pyroptosis of critical immune cells. Indeed, although inflammasome activation provides initial inflammatory signals, loss of inflammatory cells may restrict the magnitude of the total response. Further work is required to elucidate the role of inflammasome activation and pyroptosis in bridging innate and adaptive immunity to infection and vaccination.

1.3.2 Initiation of an Adjuvant-Mediated Immune Response

PRR stimulation of cells at both the injection site and subsequently in the dLN following vaccine component transport through the lymphatics, not only leads to inflammasome-mediated release of IL1β and IL18 but can lead to large transcriptional changes in gene regulation, resulting in the production of pro-inflammatory cytokines[89, 70, 90]. Inflammatory cytokines and chemokines that are secreted into the ECM can directly and indirectly (via cascades of the cytokine and chemokine network) recruit other immune cells from the blood into the tissue [91, 60, 65, 92, 93, 94, 5]. This influx of cells and production of pro-inflammatory factors augments local inflammation. The inflammatory milieu can

then dictate the nature of the adaptive response[95]. After response initiation, cells e.g., neutrophils, monocytes and DCs infiltrate into the tissue, become activated and secrete cytokines and chemokines which further amplifies local inflammation [61, 96, 97]. Professional APCs express complexes of peptide antigen bound to Major Histocompatability Complex (MHC) molecules on their surface in peptide-MHC (pMHC) complexes. In the lymph node this process is classically performed e.g., by DCs (although other cells do express pMHC after adjuvanted-vaccination [54]) that either migrate from the site of vaccine administration or are resident in dLN and are stimulated by vaccine components (e.g., antigen and adjuvant) in the LN[98]. MHC class II (MHC-II) is constitutively expressed by APCs including DCs, macrophages and B cells and levels can be regulated by pro-inflammatory cytokines e.g., IFNγ [99, 100, 101]. After antigen uptake, DCs and other migratory cells enter tissue draining LNs where they may present pMHC to T cells, promoting adaptive immune responses [18]. However, the same signals that drive pro-inflammatory immune responses may also drive activation of negative regulatory loops e.g., upregulation of microRNAs[102] or induction of cell death, self-regulating the duration of inflammatory cytokine production.

1.3.3 Immune Cell Migration from Injection Site to Tissue Draining LNs

From the site of vaccine administration, innate immune cells e.g. monocytes, dendritic cells and neutrophils migrate to the tissue draining lymph node through the up-regulation of chemokine receptors and changes in adhesion molecule expression [103, 37, 46, 104]. After DCs in tissues efficiently capture antigen, CCR7 is upregulated, which permits response to CCL21 produced by lymphatic endothelial cells, enabling entry into draining lymphatic vessels and recruitment into the lymph node paracortex post lymphatic migration[37]. Other cell types including monocytes and neutrophils are capable of capturing and processing antigen and subsequent migration to dLNs, although their ability to prime T cells is contentious and there is no direct evidence that neutrophils have a role in this process following administration of adjuvants used commonly in the clinic [46, 15, 95, 105]. Nevertheless, neutrophils and monocytes are of critical importance for the production of localised cytokines in the injection site and monocytes can produce inflammatory cytokines in the lymph node microenvironment after vaccination [106, 69]. The relative role of these cell types in vaccines administered by different routes is less clear.

1.4 Bridging Innate and Adaptive Immunity

Migratory DCs can present antigen to T cells following arrival into the dLN. In addition, dLN resident DCs (e.g., lymphatic-sinus DCs) capture free-flowing inoculated antigen (and immunostimulants) from the injection site, and thus can invoke rapid T cell responses [30].

A lining layer of macrophages in the subcapsular sinus can also capture antigenic material and vaccine components, which they transfer directly to B cells in the B cell follicle. Naïve T cells are highly migratory cells that enter the LN paracortex through the HEVs and then migrate on stromal networks in a CCR7 dependent process, and spend about several hours surveying DCs prior to leaving via efferent lymphatics. DCs expressing pMHC on dendritic process provide a large surface area enabling contact with up to 5000 T cells an hour [107]. Due to the small frequency of T cells which can respond to a given pMHC (through cognate TCR recognition), initial DC contact of individual T cells is transient (mins range). If a T cell recognises its cognate pMHC, a longer-lived immunological synapse is formed permitting an organised set of interactions between the APC and T cell [108, 109]. A synapse can last for several hours permitting signal integration leading to a robust T cell activation and IL2 production driving T cell clonal expansion.

1.5 Adaptive Immune Responses to Vaccines

Naïve antigen-specific adaptive immune responses to vaccines and pathogens take multiple days (7-14) to generate due to the very low frequency of responding B and T cells, and the complex temporal multi-stepped process from T and B cell activation to T cell clonal expansion and high affinity plasma cell differentiation. Antigen-C3dg complement complexes bind CD21 expressed on B cells and FDCs, permitting B cell activation. Following activation by cognate antigen complexes, B cells in the dLN follicles can upregulate CCR7 and migrate toward the T / B border [38, 110]. This permits proximity to CXCR5 expressing CD4+ Tfh cells and following cognate interaction between these cells[38], the B cells can undergo two differentiation programmes. First, these cells can differentiate into low affinity short-lived plasmablasts, which secrete IgM to provide a rapid response to antigenic encounter[111]. Second, a Germinal Centre can be established [26, 25] which is a specialised lymphoid microenvironment containing dark and light zones enabling B cells to undergo serial rounds of mutation, affinity maturation (light zone) and proliferation (dark zone), regulated by antigen availability and T cell help. This results in the competitive selection of high affinity class switched B cells that for many clinically approved vaccines provides pathogen protection.

For many diseases, antibodies are insufficient to eliminate disease. In malaria, antibodies alone cannot clear parasitic infection, thus effector T cell responses have a key role in parasite killing through elimination of malaria infected hepatocytes [18]. Thus vaccines that induce robust T cell responses are required [18, 112]. Both CD4+ T Helper subsets (Th cells) and CTLs play vital roles in development, survival, enhancement, regulation, timing, duration and magnitude of the immune response to pathogens and vaccines. Key

functionality of CD4+ T cells includes secretion of pro- and anti-inflammatory cytokines and providing survival signals to B cells [113, 114, 29]. After activation, CD4+ Th cells secrete a specific repertoire of cytokines, dependent on the nature of the stimulation received during activation, which can affect B cell differentiation and class switching [115]. These fates are not necessarily terminal, and there is increasing evidence showing T helper cell plasticity [116]. In contrast, the primary functions of CD8+ T cells are to kill infected cells and secrete cytokines which amplify the response, however there is evidence that they modulate the GC reaction [117, 118, 119, 120, 49]. Vaccines often form relatively poor CTL responses and the reasons for this are unclear. Work is currently ongoing to further CTL responses to vaccination, although 'genetic vaccines' e.g., viral vectors do induce potent CTL responses in humans [121].

In the paracortex, T cells scan pMHC expressed on APCs and following successful activation, can undergo lineage-dependent differentiation into activated CD4+ or CD8+ T cells[108, 122]. T cells require a threshold quantity of cognate antigen (known as signal 1), and co-stimulatory signalling to become fully activated (known as signal 2). If signal one is received, but signal 2 is not, the T cell undergoes anergy - functional inactivation - after a short period of effector activity[123]. For signal 2 to be received, the surface receptor CD28 on the T cell must be ligated by CD80/86 (B7) expressed by an APC. If both signals are satisfactorily received, activation can ensue. Upon second encounter (boost) T and B cell activation is quantitatively and qualitatively different due to a substantial increase in responding T and B cell responding frequency and qualitative changes in memory T cells, leading to more rapid changes in gene expression, thus more rapid effector T cell cytokine production combined with the presence of high affinity class switched B cells.

1.6 Introduction to Adjuvanted Vaccines

Adjuvants are immunostimulants that mimic aspects of the innate response to activate the immune system to prime adaptive immunity. Through enabling more efficacious immune responses, adjuvants reduce the amount of antigen required to elicit an immune response [124, 125]. Due to such qualities, adjuvants are being investigated to combat a wide range of infectious human and veterinary diseases and are being developed as therapeutic vaccines for cancer and Alzheimer's disease [126, 127]. Despite the importance of adjuvants to modern medicine, their mechanisms of action are incompletely understood.

Aluminium salts (alum) were introduced in the 1920s and were the only adjuvant licensed in humans for the following 70 years [125]. In 1997, MF59 was licensed for use against seasonal influenza representing the first new licensed adjuvant since alum [125]. Since then, many adjuvants have been investigated in preclinical models, some of which

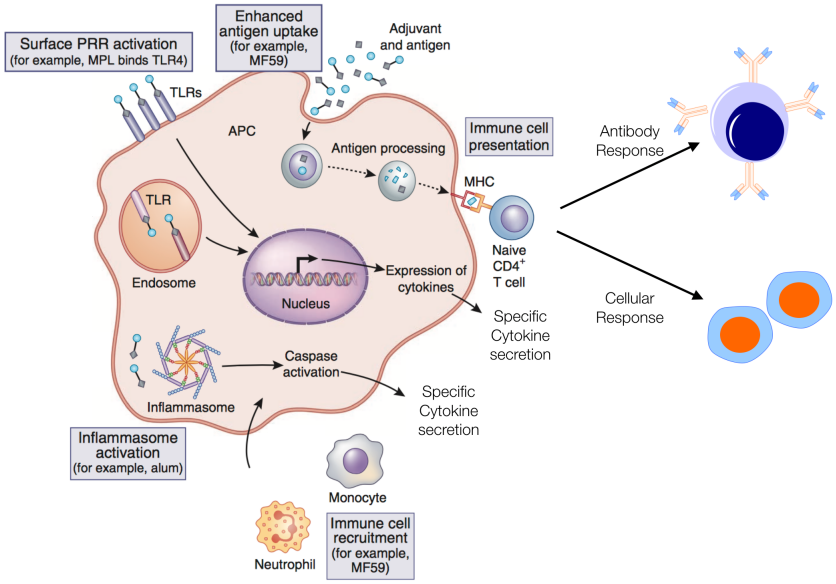


Figure 1.2: **A simple overview of diverse adjuvant MoA:** Developing an intimate understanding of adjuvant MoA is vital to rationally tailor subunit vaccines toward combatting known disease pathology. Figure adapted from [4].

have been trialled in phased clinical trials, although have not been employed in licensed vaccines due to toxicity and efficacy issues. Since MF59's use against seasonal influenza however, four adjuvants have been licensed for use in humans: AS01, AS03, AS04 and cytosine phosphoguanosine (CpG) 1018. Different infectious and non-infectious diseases require different protective mechanisms and different adjuvant formulations can elicit different immune responses, thus providing a rational basis for intelligent vaccine design and engineering, given a pre-requisite understanding of how different adjuvants work. Work to date elucidating adjuvant MoAs using animal models has developed an understanding of the different mechanisms driving adjuvant-induced immune responses and a simple overview is shown in Figure 1.2, adapted from Reed et al [4]. In what follows, we provide an overview of the MoAs of a select few adjuvants, which have some relevance to the work in this thesis.

Adjuvant Systems developed by GSK (AS01, AS03, AS04) are combination adjuvants, comprising multiple different immunostimulants. AS01, a liposome-based adjuvant comprising two immunostimulants (which is discussed in detail in section 1.7) has been shown to enhance the expression of co-stimulatory molecules, augmenting the potency of cells that can prime T cells[32, 15]. AS03 is a squalene-based oil-in-water emulsion widely used in Europe for pandemic and pre-pandemic influenza vaccines [128, 125]. Furthermore, AS03 is under investigation for recombinant spike (surface glycoprotein) COVID-19 vaccines [129] and immunogenicity against SARS-CoV-2 variants of concern [130]. AS03 comprises d1--tocopherol (vitamin E), squalene (derived from shark liver oil), and polysorbate 80 and

induces the recruitment of granulocytes and monocytes [131]. α-tocopherol has been shown to induce IL6, CCL2, CCL3, CCL5 and CSF-3 - cytokines and chemokines which are consistent with increased granulocytes and antigen-bearing monocytes[132]. The resulting immune response generates balanced Th1 and Th2 immune responses, leading to increased protection against flu compared with non-adjuvanted vaccination [131]. In recent years, Howard et al. performed systems biology analysis of the AS03-adjuvanted H5N1 avian influenza vaccine, to examine molecular mechanisms of AS03's enhancement of immune responses to H5N1 antigens[133]. Howard et al. observed that in the adjuvanted group, 90% of subjects exhibited seroprotection with the H5N1-AS03 vaccine, compared with 0% in the non-adjuvanted group. This vaccine led to increased serum IL6 and CXCL10 levels, upregulation of MHC-II-related genes in neutrophils, and upregulation of interferon and antigen presentation and processing genes in DCs, neutrophils and monocytes. Interestingly, the early upregulation of interferon pathways was predictive of antibody titres at 56 days post injection [134], although such correlates have been elusive for many vaccines. Nevertheless, this work showcases the value in understanding how early immune dynamics after adjuvanted-vaccination can lead to protective immunity.

AS04 contains aluminium salts [135] and MPL, a TLR4 agonist, and is used in the hepatitis B and human papillomavirus vaccines (HPV) [136]. AS04 transiently induces NF-κB activity, local cytokine secretion and increased counts of antigen-bearing DCs and monocytes, leading to activation of antigen-specific T cells. CCL2 and CCL3 are observed at the injection site, consistent with the recruitment of DCs and monocytes. It is thought that the presence of Aluminium salts in the vaccine does not synergise with or inhibit MPL, but instead prolongs cytokine production in the injection site. The efficacy of an AS04-adjuvanted vaccine against HPV can reach $\sim$100% almost a decade after primary injection [125, 129]. Alum is the most well characterised and studied adjuvant and generates antibody responses as well as CD4+ T cell responses. Alum was originally thought to promote immune responses through activation of NLRP3, although other research has shown that alum's adjuvant activity is not dependent on NLRP3 [129]. Indeed, the role of NLRP3 in alum's adjuvancy is still under debate. The depot effect is a prolonged release of antigen at the site of injection, to extend the duration of immune system stimulation by a vaccine, leading to augmented responses. Initially, the depot effect was implicated in the adjuvant activity of Alum, although in recent years it has been shown this may not be entirely accurate [98], as it has been observed that using tetanus toxoids adsorbed onto aluminium phosphate, antigen in the injection site was removed within a few hours [90]. The depot effect may e.g., be dependent on formulation and antigen. Cationic liposome-based adjuvant has displayed depot effects at the site of injection in mice [137], whereas MF59, AS03 and

AS01 do not exhibit depot effects [98]. Indeed, AS01 has been shown to drain rapidly from the injection site into draining lymph nodes [5], and 57-73% of AS03's constituent components had drained from the injection site by day three post-injection [138].

MF59 is a squalene based oil-in-water emulsion with a robust safety profile [128]. MF59 is included in vaccines for influenza and has been administered to more than 100 million people [125, 129]. Intramuscular injection of MF59 results in macrophage and DC activation, leading to the production of CCL2, CXCL8, CCL4 etc, which recruits neutrophils, monocytes, DCs etc [139]. Similar to AS01, these cells then capture antigen and migrate through the lymphatics into dLNs, where B and T cells are activated. MF59 enhances cellular uptake through phagocytosis and pinocytosis. Two studies have shown that NLRP3 inflammasome is not required for MF59's adjuvancy, although ASC is critical [140, 98]. Enhanced innate-cell recruitment into a vaccine injection site or dLN and enhanced antigen uptake by APCs by adjuvants such as MF59[65, 4], is thought to increase the efficiency of antigen-processing and presentation, leading to augmented antibody and cellular responses. MF59 induces pro-inflammatory chemokines such as CXCL9 and CXCL10 and is associated with improved cellular recruitment and activation at the injection site [128]. Indeed, data from Lofano et al. show that MF59 affects T-dependent B responses through shaping germinal centres [141]. Many of the mechanistic insights for MF59 have been established in mice. Recently, Alum and MF59 have been made available for COVID-19 vaccine development [126, 129]. Alum for example has been formulated with the SARS-CoV-2 surface glycoprotein (spike), where neutralising antibody production has been suggested to be associated with protection against COVID-19 disease [126]. Technological advancements and the role of adjuvants in the coronavirus pandemic have recently been reviewed by O Hagan et al [129]. Importantly, a recent review has shown that a wide breadth of adjuvants, as well as many novel adjuvants have been provided to help mitigate the SARS-CoV-2 pandemic [142].

Surface or intracellular PRR activation by adjuvants components - including MPL or GLA-SE via TLR4 stimulation - and have a vital role in the initiation of immune responses by adjuvants [18] and their effects are subsequently discussed in more detail in the context of AS01 (section 1.7). NLRs can be activated by adjuvant components, leading to the activation of the inflammasome, which can result in caspase-1 activation[143] and a recent review comprehensively details how different inflammasome-mediated signalling promotes immunogenic adaptive immune responses to a wide-range of vaccine adjuvants [83].

Despite considerable knowledge of adjuvant mechanism-of-action resulting from intense experimental work over the years, there are significant gaps in the understanding of how adjuvants mount immune responses[119, 125]. Recent work has indicated that optimal

vaccination strategies and the effectiveness of subunit vaccines may depend on the effectiveness of antigen-adjuvant-PRR pairings [137, 142]. It has also recently been suggested that understanding adjuvant MoA has been vital for the success of licensed products [129]. Taken together, to tailor antigen-adjuvant-PRR pairings for a medical setting of interest thus embracing the rational design of adjuvanted-vaccines, a deep, detailed knowledge of how adjuvants initiate and maintain immune responses is required. Therefore, to develop the next generation of adjuvants and vaccines, and to improve further the effectiveness of vaccines against pandemic (and wider) disease, it is vital that a holistic mechanistic understanding of adjuvant function is obtained, justified and leveraged in rational adjuvant design. Recently, interdisciplinary approaches have been proposed to accelerate the rational design of novel adjuvants and next-generation adjuvanted-vaccines through systems vaccinology [125]. Indeed, Pulendran et al., argue for hypothesis generation from -omics data insights, which can be tested and validated in animal models. For licensed adjuvants, preclinical experimental data has provided much of the current understanding of adjuvant MoAs. Indeed, through an evaluation of the known-knowns, gaps in understanding, and an examination of the logical implications of integrating insights from *in vivo* experiments, mechanistic modelling can provide a holistic perspective of adjuvant MoAs and extract further insights from available experimental data. In turn, such modelling work can lead to simulations which can be used to explore and analyse mechanisms, to refine hypotheses, and generate novel hypotheses, which can be tested *in vivo*. Therefore, mechanistic modelling has the potential - alongside -omics based hypothesis generation - to extract additional or reinforce insights from available experimental data, therefore improving knowledge of adjuvant MoAs and in turn contributing to the rational design of next-generation adjuvanted-vaccines.

1.7 Adjuvant System 01 (AS01)

The adjuvant AS01 developed by GSK is the focus of this thesis. Development of the Adjuvant System AS01 began more than twenty years ago, and AS01 is today employed in the recently licensed Malaria vaccine RTS,S/AS01, and the licensed herpes-zoster (*shingles*) vaccine Shingrix [144]. AS01 is a liposome-based adjuvant that comprises two immunostimulants: MPL (3-O-desacyl–monophosphoryl lipid A), and QS21, a formulation which has been shown to enhance both antibody and T Helper 1 (Th1) responses to various antigens [32, 15]. Liposomes containing phospholipids can exhibit some adjuvant activity, however due to relatively weak adjuvancy, many liposomal adjuvant formulations comprise immunostimulators [145]. For AS01, no data exist in the literature or from GSK on liposomal contribution to AS01 adjuvancy, although liposomal formulations with considerable similarities to AS01 have been shown to exhibit little or no detectable adjuvant activities

by themselves, while the same liposomes containing MPL exhibited considerable adjuvancy [146]. Despite the current paradigm that the immunostimulatory elements of AS01 are MPL and QS21, further work is required to determine whether there is an adjuvant effect of the AS01-liposome *in vivo* when QS21 and MPL are absent. Liposome and immune system interplay has recently been reviewed in [147].

MPL is a TLR4 agonist and a considerably less toxic derivative of bacterial LPS. MPL has been shown to induce the production of cytokines, and the expression of co-stimulatory molecules in mice [148]. Indeed, TLR4 signalling in hematopoietic cells is critical for AS01 mode-of-action, and AS01-mediated TLR4 signalling is associated with DC activation in the dLN [149]. Recent work has indeed indicated that MPL is the primary driver of DC activation after AS01 [95]. The current understanding suggests MPL directs the immune response towards a polarisation that encompasses the generation of IFNγ^+ antigen-specific T cells, and antibody-isotype switching to IgG2a/c [75]. QS21 is a saponin, derived from the bark of the tree *quillaja saponaria molina, 21.* In 1925, saponins were found to augment antibody responses against diptheria or tetanus [150]. A series of fractions were purified and QS7, QS17, QS18 and QS21 were determined to be potent adjuvants. QS18 was found to be highly toxic in mice, although QS21 and QS7 were substantially less toxic. QS21 was found to be considerably more available. Nevertheless, concerns remained regarding QS21's tolerability when used alone as an adjuvant in humans. As mentioned in AS01, MPL and QS21 are formulated with liposomes. Cholesterol is included in the liposomal membrane which is thought to bind QS21 with the liposome to reduce its toxicity [151]. Indeed, available evidence, as well as discussions with GSK immunologists indicate that with AS01, the liposome serves to co-deliver the two immunostimulants MPL and QS21 to immune populations, whilst also reducing QS21's toxicity [125, 95]. QS21 has been shown to induce antigen-specific antibody responses, CD8+ T cell and polyfunctional CD4+ T cell responses in mice, although primarily CD4+ T cell responses are observed in humans when formulated with MPL as AS01 [8, 15, 152, 153, 154, 155]. After intramuscular injection of fluorescently-labelled QS21 into C57BL/6 mice, Detienne et al. have shown that QS21 co-localised with CD169+ macrophages in the dLN SCS and activated the inflammasome in a caspase-1 dependent manner in these cells, resulting in the release of IL1β and IL18 [8]. Furthermore, *in vitro* experiments demonstrated that QS21 activated the NLRP3 inflammasome in monocytes, also resulting in the secretion of IL-1β and IL18 [153]. Despite this knowledge, QS21's mechanism of action is less understood [156] than MPL's, although both are used as components in multiple vaccine adjuvants.

Classical adjuvants such as alum are used to stimulate humoral responses, although alum is not capable of delivering efficient T cell responses [157]. Experiments from GSK

have demonstrated that utilising QS21 and MPL together, AS01 can elicit potent antibody and robust Th1 responses in mice [15, 32] and humans. Indeed, for some diseases, adjuvants capable of generating robust T Helper, CTL and neutralising antibody responses are required [126]. Despite around 100 years of research toward a Malaria vaccine, RTS,S/AS01, the first commercially licensed vaccine for Malaria, was approved for use by European regulators in 2015 and exhibits limited efficacy [158, 159, 160, 161]. The complex life cycle of the *plasmodium* parasite has hindered vaccine development. Clinical symptoms of Malaria begin after the liver-stage of infection - when malaria-invaded-erythrocytes burst, releasing parasite into the bloodstream [162, 163]. The RTS,S/AS01 vaccine aims to generate immunity against the disease by targeting the pre-erythrocytic stage of infection, as does the Ad-ME.TRAP vaccine, where 11 adjuvants have been assessed and two of which have been shown to enhance vaccine efficacy following a malarious challenge [14]. A vaccine against Malaria should induce both antibody and T cell responses - which RTS,S/AS01 has demonstrated a reasonable ability to do. AS01 is also included in the Shingrix vaccine against Herpes-Zoster, although this disease is rarely fatal. Nevertheless, Herpes-Zoster is associated with severe morbidity in adults over 50 [119]. Shingrix displayed high efficacy results in phase III trials, where two doses result in >90% efficacy against the disease, regardless of age, including in > 70-year-old patients [164]. This demonstrates the ability of AS01 to overcome age-related problems associated with vaccination. The only currently licensed TB vaccine BCG offers protection against disease in children; however, does not offer comprehensive protection against pulmonary tuberculosis in adults. A candidate vaccine formulated with AS01 and the M72 recombinant tuberculosis antigen has demonstrated 54% protection against pulmonary TB in adults [78]. In 2019, it was reported that M72/AS01 reduced the incidence of pulmonary tuberculosis in HIV-negative adults and provided protection for at least 3 years while having an acceptable safety profile [165].

1.7.1 Current Understanding of AS01 Mechanism of Action

Experimental work has elucidated important mechanisms underpinning AS01-induced immunity in mice. Here, we summarise the current understanding of AS01 initiation of innate and adaptive immune response in murine dLNs (Figure 1.3).

1.7.1.1 Muscle Injection Site Inflammatory Response induced by AS01

Fluorescently labelled QS21 and gE antigen are detected in the draining lymph node thirty-minutes post-injection, indicating rapid free-flow of vaccine components from the muscle interstitium through the lymphatics vessels [15]. While QS21 and antigen remain detectable in the muscle 30 minutes after injection, they are almost undetectable by 24 hours [15]. This

rapid clearance of vaccine components suggests the local depot hypothesis is not consistent with AS01 MoA. Cytokine production in the muscle is significantly higher after injection of gE antigen and AS01 than gE alone and cytokines are observed to increase in the muscle over the 3 hours post-injection [15]. Specifically, CXCL1, CCL2, IL6, IL1β and CXCL9 are observed to be rapidly induced at early time-points, declining by 48 hours post-injection (PI) and returning to baseline levels by day 7 PI [15]. Immune cell populations in the injection site and dLN have been quantified by flow cytometry[15]. In the muscle, consistent with the chemokine profile, monocytes (Lin^{-}, CD11b+ Ly6c^{hi}) and neutrophils (SSC^{high}, Ly6G+) were transiently elevated after the injection of gE antigen and AS01, compared to gE antigen alone[15]. This indicates a rapid recruitment of monocytes and neutrophils into the injection site. In contrast, the number of DCs was low, with no significant changes at these time-points [15]. Lymphocyte numbers are relatively low in the muscle during the first seven days PI[15]. Together, these data suggest that resident innate cells are directly activated by AS01 and recruit neutrophils and monocytes into the muscle injection site.

1.7.1.2 Lymphatic Immune Response Induced by AS01

The migration of immune cells from the injection site to the dLN, and those that exit the dLN following AS01-based vaccination was investigated in a sheep cannulation model [46]. Cannulas were used to directly collect both afferent lymphatic (AL) and efferent lymphatic (EL) fluid draining proximal to the dLN, enabling quantification of innate and adaptive immune cell dynamics, entering and exiting the lymph node post either subcutaneous or intramuscular injection of AS01. After demonstrating that AS01 adjuvancy characteristics are conserved in the sheep, the kinetics and trafficking of cells between muscle and dLN was quantified over time. After injection with Hepatitis B Surface Antigen (HBsAg) and AS01, a rapid increase in the number of neutrophils in iliac AL was observed. This increase occurred between 4 and 12 hours after vaccination. Neutrophil numbers in the AL returned to baseline levels prior to 48 hours, indicating transient inflammation. An increase in monocytes in iliac AL was observed between 8-12 hours after IM injection of AS01. Neutrophils were responsible for the majority of cellular transport of HBsAg during the first 28 hours and monocytes were implicated in antigen transport during the first 50 hours. Surprisingly, no significant change in the number of DCs in the AL were observed during the investigation, although between 48h and 72h PI, MHCII^{high} DCs were the predominant cell type transporting antigen [46]. Collectively, this shows that after IM injection of AS01 and HBsAg, antigen is initially predominately transported by neutrophils, followed by monocytes and lastly by DCs however the role of neutrophils in the dLN adaptive immune response is unclear.

1.7.1.3 The Draining Lymph Node Response induced by AS01

Between 6-48 hours in the injection site dLN, the cellularity increases following antigen + AS01 compared to antigen alone [15]. An increase in lymphocytes was observed as early as three hours PI. AS01 also increases the number of MHCII+ DCs in the dLN able to prime T cells, thus activation of this DC population (measured by elevated expression of costimulatory molecules) may contribute directly to T cell priming efficiency [15]. Two different mouse models were utilised to investigate the ability of APC subsets to present antigen to cognate T cells after immunisation with AS01 [5]. First, CD11c- Diptheria-toxin receptor mice were used to mediate DC depletion. Second, the ability of purified APCs to present OVA antigens (from chicken egg-white) was quantified. OVA + AS01 is shown to increase CD4+ T cell and CD8+ T cell responses compared to controls. Overall, T cell responses to immunisation were shown to be dependent on CD11c+ MHCII+ DCs [5]. Monocytes or neutrophils were not observed to present antigen to T cells, thus collectively AS01 enhances the ability of MHCII+ DCs, not monocytes or neutrophils, to present antigen to T cells. While DCs are classically described as the most 'potent' APC, monocytes are the predominate infiltrating cell type in the dLN carrying antigen after AS01, however monocytes express lower levels of MHCII and appear not to be key to antigen presentation. Substantiating these findings, 'classical' DCs have more recently been observed to be superior in priming T cells after AS01 [95].

QS21 and antigen are detected in the dLN within 30 minutes in wild type C57BL/6 mice. Early arrival of antigen is thought to affect the magnitude of the adaptive immune response through activating dLN resident DCs, providing an early signal to cognate T cells before the arrival of migratory DCs from the muscle [15, 30]. QS21 has been shown to activate the inflammasome *in vitro* and co-localise with CD169+ subcapsular sinus macrophages *in vivo*, resulting in caspase-1 mediated release of IL18 from these cells [8]. In recent years, Coccia et al., have shown using transgenic mice and antibody-mediated depletions, that IL12, alongside QS21-mediated IL18 release from subcapsular macrophages synergistically induce IFNγ from NK cells [32]. This rapid, transient and high production of IFNγ peaks approximately six-hours post-injection, returning toward baseline levels by forty-eight hours. 'Optimal' IFNγ requires both MPL and QS21[32]. Serum IFNγ in humans is associated with increased antibody responses and protection from malaria in RTS,S/AS01 challenge studies [166]. Additionally, it has been shown that IFNγ is critical in promoting a functional CD4+ T cell response in mouse models [32], although it is unknown how IFNγ mediates this process. The source of IL12 which promotes IFNγ after AS01 is unknown and difficult to determine *in vivo*. In wider literature, it has been demonstrated that MPL stimulation via TLR4 [32, 89, 167] results in the activation of NF-κB, and downstream transcription

and production of cytokines - including IL12 - that can stimulate APC activity and orchestrate immune responses [168]. Furthermore, DC subsets which are characterised by IL12 expression have been observed in dLNs after AS01 [95], while monocytes produce IL12 after CpG-adjuvanted vaccination [106]. In addition, during responses to oil-emulsion adjuvants, CD4+ T cells have been shown to be in proximity to IL12+ DCs[69], leading to Th1 responses. Overall, current evidence indicates an important role for IL12 not only for the production of IFNγ after adjuvanted-vaccination, but also in directing Th1 polarisation. Furthermore, these data raise the hypothesis that DCs and/or Monocytes could provide IL12 following AS01 administration.

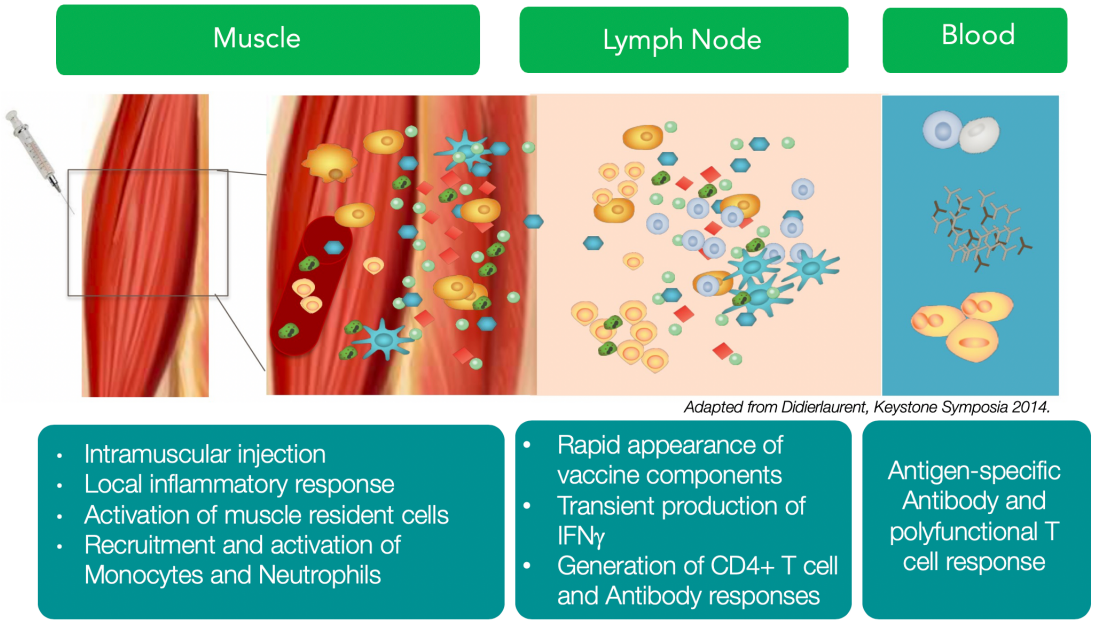


Figure 1.3: **An overview of the AS01-induced immune response.** Figure adapted with permission from Didierlaurent, Keystone Symposia 2014 [5]

Despite this current understanding of how AS01 initiates an immune response in murine dLNs, questions remain regarding AS01's MoA and its application to use quantitative systems pharmacology to dose and formulate adjuvants. It is not completely clear how these experimental insights are integrated to holistically explain how AS01 initiates adaptive immune responses. Questions remain surrounding the transient, high production of IFNγ in the dLN, the source of IL12 which supports IFNγ production and the relationships between IL12, IL18 and IFNγ during the early response. Additionally, it is unclear how IFNγ modulates the CD4+ T cell response to AS01, or what mechanisms are influential in CD4+ T cell priming. **Therefore, one aim of this thesis is to utilise modelling techniques to formalise the current understanding of AS01 MoA and propose an holistic core understanding of AS01 MoA through development of a non-executable model**

and identifying and consolidating knowledge gaps. This would provide the community with an explicit model capturing the insights and assumptions from AS01 experimental data, in conjunction with proposed mechanisms for gaps in understanding. Additionally, such a model would permit an examination of the logical implications of our assumptions of the system, revealed through a holistic perspective of AS01 MoA. Overall, **we aim to employ modelling and simulation to explore key knowledge gaps of this important adjuvant's MoA and propose novel hypotheses, and refine old ones, which can be verified *in vivo*.**

1.8 Modelling Biological Systems

"*Every object that biology studies, is a system of systems*" - Francois Jacob, 1974.

A system is a collection of interconnected, mutually dependent components. Biological systems can exhibit *emergent phenomena* that cannot be observed when considering each component individually [169]. Developing models that capture emergent behaviour of biological processes can thus permit understanding of how complex interactions give rise to emergent biological features, leading to novel insights. Over the years, genetically modified animal models have provided vital insight into animal and human biology. These models have been utilised to determine important mechanisms underpinning immune responses, which has directly impacted on the development of life-saving vaccines and therapeutics, including contributing the current understanding of AS01 MoA. Classically, these preclinical models permit investigation of individual genes and/or proteins, in a reductionist manner, where systems are '*reduced*' to the sum of their components and knowledge is assembled from insights regarding the behaviour of each piece [170]. However, not all mechanistic questions can be addressed in this manner. Indeed, biological systems are more than just the sum of parts, and holistic integration of biological features can permit novel insight.

For decades, models have been used to provide vital insight into human biology, through e.g., animal [171, 172, 173, 174, 32, 119], *in vitro*[175] and also *in silico* approaches [176, 177, 178]. A model is an abstraction that is created to assist an understanding or description of something [179]. A model of a complex system must capture the key structures and components of a system, and how changes of state are governed. Therefore to generate a model, the current understanding of a biological system - or an abstraction of it - is examined and detailed. The model can then be implemented as a simulation and executed on a computer. The process of model development, as well as simulation analyses, can provide novel biological insight by confronting the logical implications of insights from experimental data [180] and by permitting *in silico* routes of experimentation that are infeasible, impractical or unethical to perform *in vivo*. Through simulation analyses, hypotheses underpinning

model structure can be evaluated by determining the extent an hypothesis is consistent with established data [181]. Furthermore, such techniques can provide a quantitative basis for dosing and vaccine delivery schedules [182, 183, 169, 184, 107].

Modelling and simulation can therefore provide a platform for knowledge integration, holistic interpretation of experimental data and hypothesis testing [185]. These techniques are complementary to experimental work, by guiding experimental design through prioritising avenues of *in vivo* exploration [184]. Indeed, formalising an explicit system can produce better science. Modelling forces researchers to think deeply about the domain of interest, and by carefully deciding how to model the data and a system, deeper insight can emerge which was not available *a priori* [180]. Therefore, simulation can be used to propose hypotheses and explore systems, but the art of model design alone can yield novel insight. Thus modelling and simulation possess unique abilities which have the potential to enhance our understanding of biomedical science and clinical medicine, and even to inform the translation of basic science into the clinic.

In silico models in biology can be divided into two broad sections. Top-down approaches / phenomenological models or bottom-up approaches / mechanistic models. Top-down approaches and phenomenological models can be defined as hypothesised relationships between components in a dataset, where the model describes only the relationship between components, and does not seek to describe how these relationships manifest. Thus, mechanistic detail or hypotheses are omitted from the model. These approaches generally aim to discover patterns in and make predictions from, complex multi-variate datasets. Top-down approaches have found significant utility in exploring and extracting information from complex, high-throughput datasets such as microarrays, RNA-seq, epidemiology of disease transmission, and more recently single-cell sequencing [186, 166, 187, 188, 189]. Top-down and machine-learning based approaches have added significant value to medical science, including predicting neoantigen fitness for cancer immunotherapy, highly-accurate predictions of pMHC complexes and models predicting TCR common-specificities [190, 191, 192].

However, top-down, phenomenological approaches can be susceptible to issues with interpreting the data. This may arise from the identification of patterns or correlations with a lack of, or grossly simplified (and potentially inappropriate) understanding of the mechanistic processes that give rise to the observed behaviour. In contrast, bottom-up approaches e.g., mechanistic modelling seek to hypothesise relationships in the data, where the nature of the relationship is described by the biological interactions that are thought to give rise to the phenomena observed in the data. This is performed through the examination and integration of mechanistic insight, producing platforms which can identify knowledge gaps and predict system behaviours [193, 169]. Mechanistic modelling is well-suited to such tasks,

as these techniques permit biological processes to be integrated and represented in relevant detail. Furthermore, the process of understanding and constructing a mechanistic model can reveal logical inconsistencies with hypotheses and knowledge gaps, both of which were not observable *a priori* [169, 180]. Therefore, mechanistic modelling is increasingly being applied to understanding the immune system, including explorations of Tuberculosis, HIV, Granuloma formation, lymph node microenvironments, IBD, Leishmania infection, Sjorgens syndrome, and bacterial infections [194, 195, 196, 197, 198, 199, 200]. The following section describes key modelling techniques that are often employed by mechanistic modelling in the context of improving the understanding of the immune system.

1.8.1 Mathematical Models in Biology

Mathematical modelling has been applied to biological investigation for decades [201]. At the highest level, mathematical models can be classified as deterministic or stochastic. Deterministic mathematical models capture only fixed, non-random effects, resulting in a model that given the same input (i.e., initial conditions and parameter values), will result in the same output. In contrast, stochastic mathematical models capture random fluctuations and probabilistic events. Stochastic processes play a key role in immunity, in contrast to other biological systems that are more deterministic, thus capturing stochasticity can be important in understanding adaptive immune response dynamics.

1.8.1.1 Ordinary Differential Equations (ODEs) in Biological Modelling

ODEs are equations or collections of equations that describe the continuous rates of change of a population, and usually in immunology, with respect to time. ODEs are often described as dynamical systems. These equations capture deterministic dynamics of homogenous populations of elements, where every element of the population undergo activities at the same rate. An individual ODE in a system of ODEs, contains one or more terms involving derivatives of one dependent variable, with respect to another independent variable (e.g. time). Through coupled equations, they are capable of succinctly describing complex interactions between model elements and have been employed to describe biological systems for decades [202]. ODEs are a popular modelling tool due to their simplicity and ability to concisely and appropriately describe large amounts of information. Further, ODE analysis techniques are well established. ODEs need to be supplemented with further conditions, which in the context of biological modelling, are typically initial conditions. An early, fundamental example of the application of ODE modelling to biological investigation is the seminal work of Alan Perelson. Indeed, ODE modelling has been used in HIV research for many years.

The model below is adapted from Perelson's seminal work, and serves as an example to illustrate the fundamentals of an ODE model[203]. This model extends the basic susceptible, infected, recovered model used by epidemiologists to describe the spread of disease:

$$\frac{dT}{dt} = \lambda - d_T T - \beta V T$$
$$\frac{dI}{dt} = \beta V T - \mu I$$
$$\frac{dV}{dt} = \rho I - cV$$

These equations describe the rate of change for three entities, uninfected target cells T, infected cells I and free virus V with respect to time dt. Target cells are produced at a constant rate λ and die at rate d_T. These cells become infected at rate βV controlled by the quantity of free virus. Infected cells I die at rate μ. Infected cells also produce new virus cells at rate p. Virus is removed from the system at rate c. This simple model is able to describe the kinetics of acute infection with HIV. In some biological systems, determining the state of a system at equilibrium is of interest [204]. Steady-states can be found by solving the equations after setting the time derivatives of the ODEs to zero, and linear stability analysis can reveal when steady states are stable, providing insight into the equilibria of the steady states and the behaviour of the dynamical system close to these [205]. Perelson's model has been fundamental in understanding HIV dynamics, and has also been extended to include and predict the effects of anti-retroviral therapy [203, 206].

In biology, many modelled systems are complex and non-linear, and while some simple models are amenable to direct mathematical analysis, often numerical simulation is required. Indeed, when ODEs are used in biological modelling, equations are often solved using numerical integration, resulting in predicted trajectories for each variable in the model. Furthermore, to streamline and increase accessibility of mathematical modelling in biological systems, frameworks such as 'dMod' have been published [9]. Such frameworks provide accessibility to interdisciplinary researchers by providing a framework in common programming languages, not only to define the model variables, parameters, initial conditions and to simulate a model, but often provide optimisation routines to assist fitting of proposed models to observational data. Indeed, in recent years the accessibility of mathematical modelling to biological investigation has been considerably eased by such frameworks. ODEs are capable of modelling a complex system with elegant simplicity, and as they tend to have fewer parameters than more more complex modelling techniques. As analysis techniques for ODEs are well characterised, they are a popular immunological modelling technique. However, the use of ODEs implies several assumptions that may not be appropriate for particular

research questions. Indeed, typically, ODEs do not describe explicit space or capture heterogeneity. For the investigation of some biological questions, further techniques may be required.

1.8.2 Further Modelling Techniques

Partial Differential Equations (PDEs), like ODEs, describe the rate of change involving derivatives, although PDEs contain partial derivatives for two or more independent variables. Typically, spatial variation can be accommodated by the use of partial differential equations. This has led to e.g., the exploration of the proliferation of CD8+ T cells [207], neutrophil trafficking dynamics [208], the spatial distributions of interferons, amongst other biological phenomena. Agent-based models (ABM) are comprised of individual entities called agents. Agents exist in states, which are dictated by attributes and the location at a specific point in time. Transitions between states are governed by a set of rules, which dictate agent behaviour, resulting in autonomous interactions. Aggregating these autonomous interactions lead to the emergence of system-wide behaviour which are not hard-coded, or visible before execution [209]. ABMs can capture explicit space, enabling capture of heterogeneity and space in a single model. These features combined with stochasticity and ability to perform experiments at high granularities, provide an attractive tool for detailed exploration of complex systems, such as the stochastic activation of lymphocytes in dLN microenvironments, or questions involving spatial dynamics [193, 210, 211]. However compared to ODEs, due to their inherent complexity demands ABMs require more data for parameterisation, take larger amounts of time to simulate, and thus large amounts of time and effort to analyse comprehensively.

1.8.3 Mathematical and Computational Modelling in Vaccines and Immunology

For many years, mechanistic models have been employed to provide insight into the immune system in health and disease, however their use in exploring mechanisms induced by vaccines are limited [184, 212]. Their use in exploring adjuvant MoA is even more rare. Generally, the term 'computational vaccinology' refers to top-down approaches to aid vaccine design[184, 198], e.g by predicting target epitopes of interest [213]. A key accomplishment of systems approaches in vaccinology, is 'reverse vaccinology' (RV). Rino Rappuoli pioneered RV [213] which utilises the genome of a pathogen of interest: where top-down, bioinformatic approaches are applied to screen the pathogenic genome to identify genes of interest - i.e. which display potential antigenicity or immunodominance. Once potential genes are identified, they are synthetically developed and tested in animal models. The first vaccine

using RV was developed [214] against Serogroup meningococcus B. RV has been utilised to identify candidate vaccines for leishmaniasis, malaria, schistosomiasis, the cow tick and others [215, 216, 217, 218]. Similarly, systems approaches are commonly used to predict immunogenic epitopes [219] - although accuracy of such approaches have been shown to be suboptimal [220]. Such approaches have been employed to identify potential adjuvants for use in vaccines [221], amongst wider vaccinology work [222].

In this thesis, I describe the development and use of mechanistic models of immune system function following AS01-adjuvanted-vaccination into mice. To our knowledge these are the first mechanistic modelling efforts of AS01's MoA, and additionally such modelling has rarely been applied to adjuvant research. Mechanistic modelling studies into vaccine-induced responses are also limited. However, mechanistic models have been used in immunology for decades [223]. Generally, the investigations in this thesis focus on cellular and cytokine interplay in the dLN, involving e.g CD169+ macrophages, cells which produce IFNγ and also the priming of CD4+ T cells. In what follows, I first highlight some key models of T cell function in dLN, and then review seminal models which characterise cytokine and cellular networks (including IFNγ, macrophages and CD4+ T cell dynamics) in infectious disease and have driven mechanistic insight. Following this, I review a selection of mechanistic modelling studies in vaccinology research.

1.8.3.1 Models of T cell dynamics in lymph nodes

Bogle et al., integrated T cell trafficking and motility with the kinetics of T cell activation, to develop a three-dimensional ABM of T cell activation and proliferation within a dLN paracortex [211]. Subsequently, Bogle et al. explored an on-lattice simulation of T cell response to chemotaxis, capturing the motility dynamics emerging from the large density of T cells in the paracortex [224]. Their ABM is capable of simulating large numbers of T cells at appropriate densities and captures dLN expansion and shrinking during the immune response. The success of their model in producing similar behaviour as observed *in vivo*, therefore consolidates the model as a framework for modelling T cell activation and proliferation in scenarios where questions demand detailed T cell motility, and importantly, appropriate data are available for calibration. Through consolidating and formalising insights from experimental data and subjecting these insights to their logical implications, modelling can reveal gaps in biological understanding. With regard to the system under study, Bogle revealed there are many knowledge gaps, and leveraged their novel insights to propose avenues which would further the knowledge of T cell function within the paracortex.

Another key study took a different approach, aiming to calculate the probability of a T cell response. Indeed, by using realistic parameter values from the mouse, Celli et al.,

[107] quantified the probability of T cell - DC encounters through a combination of flow-cytometry, imaging and computational modelling. Their work exposed a threshold in DC numbers required for initiating a T cell response. Indeed, in mice they estimate that a minimum of 85 DCs are required given a precursor frequency of 10^{-6}. In humans, naive antigen-specific T cells are present in similar frequencies and therefore this threshold likely applies. Their work demonstrated that the probability of a T cell to interact with a DC after being resident in a murine dLN for 24 hours was 8%, 58% and 99% in the presence of 10, 100 and 1000 DCs carrying antigen, respectively. Interestingly, their results suggested that increasing efficiency of DC delivery during DC-based vaccination, may not be critically important, due to the underlying efficiency of T cell recruitment by DCs. Such approaches demonstrate the power of quantitative modelling when applied to immunological problems.

1.8.3.2 Models of Cytokines and Cellular Activation

Cytokine modulation of immune responses has been of interest to modellers for many years. Today, it is common understanding that T Helper differentiation is less terminal than once thought [225, 115]. Broadly, T Helper cells can be divided into subsets of the cytokines they produce, e.g Th1 cells secrete IFNγ, TNF-α and IL2, while Th2 cells secrete IL4, IL13 and IL10. Andrew Yates postulated that the classical model of Th1/2 T Helper dogma offered no explanation for observed changes of the dominant helper subset during the immune response, thus he developed a seminal mathematical model of Th1/Th2 differentiation and regulation under constant antigen stimulation [226]. Here, the rates of change for Th1/2 populations involved two positive terms describing activation and proliferation, and a decay term to incorporate cell death. Activation, proliferation and death terms are modulated by secretion of cytokine by Th1 or Th2 cells. This modulation is modelled by generalising groups of cytokines into variables S_1 and S_2, describing cytokine signals representing e.g IFNγ/IL2 or IL4 and IL10 etc respectively. A captured mechanism could therefore be a consequence of an individual cytokine, captured in the group. Inhibitory effects of cytokines are described using saturating Hill kinetics of the cytokine signal strength. Embedded into their modelling, is the assumption that each cell's cytokine production rates are approximately the same, and different cytokine receptor densities are comparable. Given their system of CD4+ T cells, these were reasonable assumptions. For Th1 cells, the activation term is enhanced by available S_1 cytokines, and similarly S_2 for Th2. Both activation terms are inhibited by the 'type 2 signal' - representing IL10. Th1 growth is augmented by S_1, representing IL2 and inhibited by S_2, while Th2 growth is enhanced by both S_1 and S_2 (IL2 and IL4) but also suppressed by both groups (IFNγ/TGF-β). Their model also describes Fas-mediated activation-induced cell death (AICD).

Many interesting findings emerged from their work. Analysis of their model, in light of experimental observations revealed that homeostatic regulation differed between Th1 and Th2 subsets. Indeed, they proposed that Th1 regulation was dominated by cytokine regulated Fas-mediated AICD control while Th2 regulation occurred through inhibition of activation and proliferation. Additionally, they concluded that low levels of antigenic stimulation tend to favour Th1 responses and higher stimulation favours Th2, suggesting cytokine milieu is not the only mediator of polarisation. Analysis revealed that a critical parameter is the susceptibility of Th2 effectors to AICD and a key conclusion is that Th2 susceptibility to AICD is important for stabilising the polarisation of the T helper response. Lastly from their model it appears that innate immune system signals can bias a response towards one helper subset or switch the type of ongoing response. The authors concluded that asymmetries in T cell response dynamics - which are modulated by cytokines - can contribute to the type of immune response as significantly as the differentiation pathway embarked on at antigen presentation.

An important feature of mechanistic modelling in immunology is the exploration of hypothesis veracity [202], complementing experimental work by excluding, generating or refining concepts and theories. An example of this approach was employed to examine monocyte responses in inflammatory bowel disease (IBD)[227] . Prior to this study, work in mice and humans had suggested a role for IL23-producing mononuclear phagocytes in IBD pathogenesis and early-stage clinical trials were showing that blocking IL23 can induce remission in Crohn's and ulcerative colitis patients. Thus, determining regulators of IL23 during this aberrant inflammation was of importance. Through a combination of wet-lab experiments, single-cell RNA sequencing analysis and mathematical modelling, the authors identified IL10 and IL1 as critical regulators of IL23 production by monocytes and determined patient groups with IBD who may benefit from therapies targeting upstream of IL23. The authors derived a transcriptional signature of hyperinflammatory IL23-producing monocytes which predicted disease and resistance to anti-TNF. As part of their investigation into the regulators of IL23, the authors employed an ODE mathematical model to test whether cytokine production was modulated by other cytokines produced by monocytes. After modelling all feasible network topologies, they concluded that most configurations could be excluded. In turn, they identified an optimal network by ranking models based on their fit to data using Akaike information criterion (AIC). This optimal model supported IL10 signalling as a negative feedback mechanism and IL1β as a positive regulator of IL23 production. In addition, their model suggested that IFNγ may amplify IL1α via inhibition of IL10 while amplifying IL23 independently of its role with IL10. Their work is not only an important application of mechanistic modelling to translational science, it is an example of

how both top-down and bottom-up systems approaches can work in tandem, to complement experimental work in supplying mechanistic insights. Indeed with the recent advances in sophistication of single-cell approaches and machine-learning algorithms, integrating mechanistic modelling into these pipelines provides a powerful approach to complement and add mechanistic context to each other - compounding the benefits these approaches can offer alone. Integrating mechanistic modelling into recent advances in single-cell approaches (scRNAseq, spatial genomics, multiplex imaging, high dimensional cytometry) and machine-learning algorithms provides a powerful approach to complement and add to mechanistic models providing new insights that neither approaches alone can offer

While exploring stability and oscillatory behaviour is a powerful technique to reveal mechanisms underpinning T helper responses, systems analysis methods including sensitivity analysis and *in silico* gene knockouts, can be used to reveal important components underpinning immunological systems. Perturbing calibrated models and determining how changes in entities influence the entire system, can elucidate key mechanisms. Denise Kirschner's laboratory has employed mechanistic modelling to examine the role of cellular and cytokine networks in Tuberculosis (TB) infection. Multiple of these models describe immune environments and components similar to those involved in adjuvanted-vaccination, and earlier publications from this group in TB modelling explored questions pertaining to relationships between immune components. Due to these similarities between our intentions, our work was inspired by the thinking involved in their studies, and here I review a selection of these works.

TB is caused by infection with Mycobacterium tuberculosis (Mtb). In 2017 approximately 1.6 million people died from TB [228] and estimates indicate that one-fourth of the global population has latent infection. TB is characterised by complex host-pathogen dynamics spanning multiple organs, time and length scales. It is therefore unsurprising that TB has been the target of comprehensive mechanistic modelling studies for many years [228]. Modelling the host immune response to TB began by using ODEs, due to the lack of spatial data and has since evolved toward models capable of interrogating spatial function of granulomas. In 2001, Wigginton et al., [196] proposed a system of ODEs capturing dynamics of human TB at the site of infection in the lung, to investigate mechanisms underpinning the development of active or latent TB. Through use of saturable kinetics, the authors characterised the cellular and cytokine networks that occur during TB infection, including the complexities of IL12-enhanced IFNγ production using these kinetics. IFNγ had been shown to be important for effective cell-mediated responses to Mtb. Indeed, this cytokine activates resting macrophages, and is well characterised to augment their ability

to eliminate pathogens and release cytokines. Additionally, IFNγ is involved in Th1 differentiation and can wrestle IL4's opposition to this process. In Wigginton's work, cytokine dynamics are generally modelled using saturable kinetics, with terms which are also in the form of Michaelis-Menten [229] kinetics. For example, IFNγ is given as:

$$\frac{dI_y}{dt} = S_g(\frac{B_T}{B_T + C_{10}})(\frac{I_{12}}{I_{12} + S_7}) + \alpha_5 T_1(\frac{M_A}{M_A + C_{14}}) + \alpha_7(\frac{I_{12}}{I_{12} + f_4 I_1 0 + S_4})(\frac{M_A}{M_A + C_{14}})T_0 - \mu_g I_y$$

where B_T is bacteria antigen concentration, I_{12} represents IL12, T_1 is Th1 cells, M_A are activated macrophages, and T_0 is Th0 - Naive CD4+ T cells. This equation describes IFNγ production by Th1 cells at rate $\alpha 5$ and by Th0 at maximal rate $\alpha 7$, reflecting the *Vmax* parameter from Michaelis-Menten kinetics. This production of IFNγ by both cells, is induced by antigen-presentation from activated macrophages. IFNγ by Th0 is enhanced by IL12 with saturable kinetics and is inhibited by IL10 in the denominator. Therefore, production level is dependent on the relative levels of IL12 and IL10. IFNγ decays at rate μ_g, proportional to available IFNγ. The source S_g term accounts for extra production by cells not included in the system. This is modelled as a function of bacterial concentration B_T and IL12. Their work demonstrates an elegant way to succinctly capture complex cytokine and cellular mechanistic information in simple equations. Parameters were mostly estimated from published research, and their study provides a valuable guide to estimating parameters from experimental data, with a detailed, exoteric explanation of their equations. Using a combination of virtual depletion experiments, examining different disease trajectories and altering parameter values, the authors analysed their model. They concluded that if the immune response is initially skewed toward a Th2 polarisation, then active TB develops, while if the initial response is polarised towards a Th1 associated response, the "result is not definitive" [196]. Their work showed that if latent TB is achieved, this may be at the expense of tissue damage if regulated by a balance of Th1/Th2 responses through production of IFNγ, IL-10 and IL-4. This critical work is an excellent example of how saturable kinetics described by differential equations can be used to succinctly capture and explore complex immunology, and improve mechanistic understanding of immune responses. Indeed, their work provides a framework - given appropriate assumptions - for ODE modelling of cytokine-induced cellular activation.

In 2010, Marino and Kirschner developed a two-compartment model of the immune response to tuberculosis. Alongside development of a novel model fitting procedure, the authors aimed to provide a gateway toward further spatial and mechanistic investigations of TB infection in the dLN and the lung. Indeed their study focused on identifying mechanisms underpinning immune control in these organs. To this end, they propose a large ODE

model, with 32 equations and 210 parameters comprising populations of macrophages, DCs and T cells. This model also captures function of cytokines TNF, IFNγ, IL12 and IL10. Given data availability at the time and that their questions relate to relationships between immune components, ODEs were employed to model T cell priming. Naive CD4+ T cells in dLN are modelled by capturing a constant homeostatic source of cells, inflammation-induced recruitment by mature DCs, differentiation to so-called precursor Th1 - dependent on mature DCs (capturing priming) - and natural death. Here, the natural death rate is given by parameter $\mu N4$ and consequently the constant source of naive CD4+ T cells is a function of the death rate and initial condition: $SN4 = \mu N4 \times N4(0)$, where N4(0) is the number of naive CD4+ T cells at time zero. For primed cells (precursor Th1), the corresponding equation describes differentiation from naive CD4+ T cells and proliferation of these cells. Proliferation is modelled using logistic growth (S-shaped curve, describes growth where resources are limited, where initial growth is followed by a decrease in growth rate as a population size approaches a carrying capacity) and is inhibited by IL10. Additionally, differentiation and migration out of the dLN is captured. Given our research interests, their model provides a framework for succinctly describing CD4+ T cell priming in a dLN in a situation with limited quantitative data, to explore relationships between model components.

To fit their model, the authors sampled the parameter space using Latin hypercube sampling and qualitatively rejected parameter sets which produced trajectories which did not conform to experimental data. The set that most closely fit the data, was used as a starting point for non-linear least squares fitting. This process permits starting optimisation close to a local optimum. After calibration, the model was validated using virtual gene depletions and sensitivity analysis employed to reveal factors controlling immune responses to TB infection. They proposed that TNF plays a major role in recruiting phagocytes to the lung and that IL10 influences the balance of dominant macrophage phenotypes in both modelled organs, suggesting roles for both cytokines in TB immune control.

Marino and Kirschner then reported a multi-organ compartment hybrid model to integrate the temporal dynamics of TB infection with the spatial dynamics of granulomas[230]. Through utilising an ABM for the lung compartment and non-linear ODEs for the lymph node, they sought to study immune-cell activation and priming in the dLN and granuloma formation in the lung during TB infection. Their primary finding from this work was the importance of APC migration into the dLN from the lung, for the generation of immunity against TB. Kirschner's lab recently extended this model through the addition of a blood compartment to capture recirculating T cells [231]. They varied ODE initial conditions for central and effector memory CD4+ and CD8+ T cells to mimic a vaccination scenario

where memory has been generated, and utilised this model to track how the presence of circulating memory cells can affect the granuloma scenarios. They found that increasing the numbers of CD8+ T cells increases the chance of sterilisation, whereas increasing CD4+ memory cells does not influence the outcome of a granuloma. The authors suggested that their work indicates a vaccine for TB could greatly influence the outcome of an infection, and that focus should be afforded toward a vaccine that generates the appropriate numbers and ratios of memory cells. Given the wide immunological applicability of modelling cellular and cytokine networks and kinetics, much of Kirschner's earlier work on modelling TB infection can serve as inspiration for starting to apply such techniques to fields of immunology where mechanistic modelling has rarely been employed, e.g adjuvant MoAs. Their work also demonstrates the power of simple and initial modelling steps to examine the role of cells and cytokines in immunological settings, which can serve as a platform to incrementally develop complex models.

1.8.3.3 Application of Mechanistic Modelling in Vaccinology

Despite the limited application of mechanistic modelling to vaccinology [184, 232], we outline below salient models which have driven insight in vaccinology. T cell based vaccines can provide protection against chronic infection. However, in certain circumstances, expansion of antigen-specific lymphocytes have failed to provide protection, and generated immunopathology after subsequent pathogen exposure. Johnson et al., [233] therefore developed a mathematical model to examine the conditions that expanding T cells leads to protection vs. adverse pathology. At the time, work had observed in murine-based experiments that increasing the number of antigen-specific lymphocytes can lead to increased pathology e.g in lymphocytic choriomeningitis and hepatitis B viruses. One hypothesis at the time was that adverse pathology could be avoided by broadening the immune response. Their mathematical model thus captured the interplay between viral replication, immune exhaustion and escape, to link T cell-based vaccination to pathology developed after infection. Indeed, the authors developed a simple model of virus-host interaction, which is integrated with a framework for quantifying pathology. The model describes uninfected target cells, virus-infected cells and the magnitude of the immune response. An additional variable describes the level of immune exhaustion. Pathology was quantified by the loss of host target cells as well as cytokine secretion by activated immune cells, although their focus in the paper is on target cell loss.

The authors found that immunisation against persistent viral infection can indeed increase adverse events following infection and that this pathology is highest for noncytopathic viruses, occurring at intermediate levels of T cell memory. Their work suggested that a

vaccine that "tips the balance away from immune exhaustion and toward viral clearance may inadvertently increase transient immunopathology even when there is viral clearance". Their model suggested that even with broad immunisation against viral epitopes, adverse reactions could occur. As with many compelling mechanistic modelling studies, their work leads to *in vivo* testable predictions that were not clear *a priori*, thus reducing the avenues of exploration by guiding experimental design. While an important contribution to computational vaccinology, their research context and simplicity of how cytokine and cellular responses to vaccination are modelled does not lend itself to a detailed examination of vaccine MoA.

Cancer immunotherapy relies on activation and expansion of CD8+, and as more recent data shows, CD4+ T cells [234]. Given recent advances e.g determining the immunogenic potential and cancer-specificity of neoantigens[1], efforts have been intensely focused on vaccines for cancer. However, these vaccines have not all been successful. To explore mechanisms that lead to vaccine failure, Brown et al., [183] developed an ABM of CTL activation in a lymph node paracortex, driven by a short-peptide-vaccine. The model predicts cognate antigen off-rate from MHC-I receptors on DCs is a crucial determinant for vaccine design, as variation in this parameter exhibits a sharp transition in CTL activation probability. Their work indicates that for off-rates beyond this transition, there are no appropriate vaccination strategies that would rescue the response to these peptides; however, for slightly slower off-rates the model becomes sensitive to the quantity of DC and T cell interactions after DC infiltration in the dLN. Brown predicts that some peptides used in cancer-vaccines have zero probability of initiating T cell activation. This finding is interesting as it could explain the lack of success of some short-peptide vaccinations, but also suggests that tools predicting epitope immunogenicity could be improved by considering peptide off-rate. This is consistent with the findings from Celli et all., that DC delivery rates into dLNs may be less critical than other parameters. Indeed, Brown's work suggests that it is the timing of DC arrival and the peptide binding off rates that are critical determinants of vaccine success with short peptide vaccines.

ABM has also been utilised to model mammary carcinoma, a corresponding vaccine (Triplex) and immune system competition, together comprising a simulator called 'SimTriplex' [235]. Triplex is a preventative breast cancer vaccine, composed of a target antigen, with MHC-I molecules and IL12 as adjuvants [235]. SimTriplex captures and simulates the behaviour of macrophages, DCs, CTLs, NK cells, 'vaccine cells', 'cancer cells', B cells, T Helper cells, antigens, immunocomplexes, IL12, IFNγ and IL12 in naive and vaccinated mice. To our knowledge, SimTriplex is one of the only simulators to explicitly include adjuvant MoA.

[1] cancer-specific antigens that arise from mutated cancer cell proteins

Their model is fit to *in vivo* data e.g the distribution of nodules, to reproduce metastasis and predicted vaccination strategies that permit the same protection as the canonical strategy but with fewer injections. They show that an initial 'massive' dose followed by a 'few' boosts, could reduce the number of vaccinations by approx 45% and still combat the exponential growth of cancer cells. This simulator has been utilised to optimise the vaccination schedule, achieving the same efficacy while reducing the number of injections of the vaccine [236]. These predictions have been verified *in vivo* - demonstrating the power of mechanistic modelling of vaccination processes.

For differential equation models of vaccine-mechanisms, many of these are applied to cancer scenarios. In 2014, Pappalardo reported an ODE model to determine the frequency and quantity of booster vaccines required to sustain long-lasting and protective memory T cell responses against tumor antigens. They describe a six-equation model of immune populations in mice after a dendritic-cell vaccination. Their system captures populations of DCs, naive and activated CD8 T cells, memory T cells as well as IFNγ. In contrast to Wigginton's work, IFNγ is modelled here more simply: released from activated and memory T cells at a linear rate (proportional to cell number) and is lost from the system at a rate proportional to available IFNγ. In Pappalardo's model, IFNγ does not appear on the right-hand-side of any equation, however is used as a readout to assess activated CD8+ T cells. Their work defined the contribution of model parameters to the quantity of IFNγ, using a Latin-hypercube based sensitivity analysis. In this thesis, we employ sensitivity analysis techniques to examine IFNγ after AS01, adopting a similar approach to Wigginton who modelled cytokine production with saturable kinetics. Pappalardo also predict a time window in which vaccine boosts may be detrimental to the immune response. As the authors recognised, their work is limited by the use of only mouse data for model development. This is a natural first step in the development of vaccinology mechanistic models, however as further data emerges mechanistic models of vaccine-induced immune responses in humans, should become common-place.

One example in a clinical setting, is a mechanistic model of yellow-fever vaccine responses. The yellow-fever vaccine YF-17D is one of the most effective vaccines ever made, and top-down systems-based approaches have yielded insights into gene signatures that predict human immune responses following vaccination [134]. In 2018, Bonin et al., argued for a simulator detailing the human immune response to yellow-fever vaccination, which may shed light on remaining questions e.g the optimal dose to immunise against disease whilst minimising reactogenicity [212]. Bonin therefore presented a 'first step' to simulate the YF vaccine. Their 'qualitatively validated' ODE model of the immune response describes ten immune populations, including APCs, plasma cells, virus and antibodies. Their model did

not capture CD4+ T cells due to lack of experimental data, which likely limited scenarios for which the model could be employed. The authors have since introduced these cells into the model, as they had aimed to simulate the effects of the vaccine in HIV-infected individuals. The authors conclude their model is able to qualitatively reproduce clinical results from the literature, however they imply that further experimental data is required for a comprehensive quantitative validation, a situation that is not rare in modelling vaccine responses. While an important contribution, this study appears to describe only a central estimate of populations using one set of parameters, thus their work could have been enhanced by a range of techniques which permit development of parameter distributions and capture error in biological data. Given that many vaccine modelling efforts capture only antibody and T cell trajectories after vaccination over large time-periods, sometimes with inappropriate descriptions of biological components and/or entire disregard to the mechanisms which produce these high level dynamics, Bonin's work describing detailed immunological function after vaccination is refreshing. Furthermore, modelling human immune responses is a nontrivial endeavour. Not only does this type of work add mechanistic insight, it supplies a detailed understanding of how a vaccine is thought to work [7], thus providing additional transparency. Indeed, through thinking deeply about how a system is to be modelled, further understanding can be extracted from the logical implications of formalising experimental insights [180].

More recently, Bonin et al., [232] supplied further validation of their model, showing that it could quantitatively reproduce behaviour observed in experimental data. The authors predict the lowest dose to establish immunity against yellow-fever is approximately half the reference dose, as well as suggesting waning antibody levels over ten years may require a booster dose to protect against disease. Together, their work demonstrates that mathematical modelling in immune responses can contribute important insights into vaccine-induced immune responses, which may not be possible through wet-lab experiments alone.

Adjuvants MoA involve a limited number of cells and cytokines thus mathematical mechanistic models can provide quantitative insights into the early priming events. Capturing the entirety of the immune response in a singular model would be challenging as the number of cells and processes would be intractable, however modelling individual steps and processes is possible and can provide novel and unexpected insights into components of the system. Despite this selection of studies where mechanistic modelling is employed to explore vaccine-induced immune responses, such techniques have rarely been applied to consolidate, propose or analyse adjuvant MoAs. Gaffney's work [237] applied mathematical models to optimising adjuvant chemotherapy scheduling by use of a tumor growth model which incorporated cell cycle dynamics, however his work was not focused on the adjuvant MoA.

Pappalardo et al., developed a pipeline that predicts the most effective citrus adjuvants for enhancing the immune response to Influenza A infection [238]. Indeed, a PubMed search for the term "(mathematical OR computational OR in silico) AND adjuvant AND mechanism" produced 464 literature matches, none of which report a mechanistic model of an adjuvant's MoA. Therefore, a large gap exists in the literature for mapping adjuvant experimental data to known and hypothetical mechanistic function, to produce a platform for developing simulators to explore adjuvant immune responses. While to our knowledge no model explicitly describes the interplay between cell-types, cytokines and AS01 immunostimulants during the early immune response, given the rich systems biology literature describing immune system function in the dLN, one does not need to start from scratch in this arena. Given the youth of mechanistic modelling in AS01 MoA, it is important to embrace simplicity in the first steps of this work.

1.9 Model and Simulation Development

When a model of a complex biological system is developed, the relationship between simulation implementation and the underlying biology must be carefully described, defined and articulated [239]. Frameworks have been developed to aid principled model development and enforce robust model development.

Overview, Design Concepts and Details Protocol: Overview, Design Concepts and Details Protocol (ODD) is a computational modelling framework from the field of ecology, tailored for the specific design of ABM [240]. The encompassing concept of ODD is to structure information about models in a similar fashion. The ODD protocol is structured around three blocks: Overview, Design Concepts and Details, which comprise seven sub-blocks to promote transparent and replicable design. The overview section comprises submodels called 'purpose', 'State Variables and scales' and 'Process Overview and scheduling'. The overview section aims to outline the purpose of the model and its high-level structure. The Design Concepts block aims to link the description of the underlying design of the model with the general concepts in the system under study. Finally, the Details block comprises three submodels, 'Initialisation', 'Input' and 'Submodels'. This block is an extension of the overview and provides a further description of how the model is implemented, essentially acting as a blueprint of the model.

The Complex Systems Modelling and Simulation (CoSMoS) Process: The CoSMoS Process details a framework for the development of mathematical and computational models of complex systems [241, 242]. While its premise is general, it has often been employed in the exploration of complex biological systems [239, 243, 205, 6]. The work overseen by a CoSMoS project is inherently interdisciplinary, involving collaboration between

scientists and engineers, although the two need not be separate. The CoSMoS process is inherently flexible, which provides an advantage over ODD - which in contrast is focused on ABM development. A model development framework should alleviate bias around the choice of modelling methodology, not introduce it, so appropriate modelling techniques are chosen with respect to the research questions rather than based on pre-assumed approach. If systems-based modelling approaches are to improve our understanding of a biological system, the relationship between the biological understanding and how this knowledge is captured *in-silico* must be understood. Too often, models are developed based on crude, inappropriate or even incorrect biological assumptions and abstractions. In the realms of immunology, previous work in the Coles and Timmis laboratories has evolved CoSMoS: a principled approach for the development of such tools, to generate confidence that a model is fit for its purpose as providing a platform for exploring and contributing to our understanding of a real-world biological system. The CoSMoS process has three key phases. These are distinguished to capture different motivations. These phases are:

- **Discovery Phase:** establishes the scientific basis for the work. The discovery phase identifies and models the system of interest (i.e. the domain), and elucidates the scientific questions. This phase is not concerned with simulation or implementation concepts, but with the science of the system.
- **Development Phase** results in a simulation platform upon which experimentation can be performed. This is informed by the products developed in the Discovery Phase.
- **Exploration Phase** encapsulates the employment of the simulation to explore the scientific questions that were elucidated during the discovery phase.

These three phases oversee the development of a series of models, which undergo iterative modification throughout a CoSMoS project. Through iterative development, the aim of the process is to achieve systematic model development, aid reproducibility and document subsequent model changes. The products which are developed during a CoSMoS project are as follows;

- **Research Context:** articulates what the motivation is for the project. The research context formulates the scientific questions which are to be addressed by the simulation platform.
- **Domain:** a natural system of which modellers aim to simulate.
- **Domain Model:** describes the current and relevant understanding of the domain, extracted from the observable phenomena (e.g experimental data). No simulation

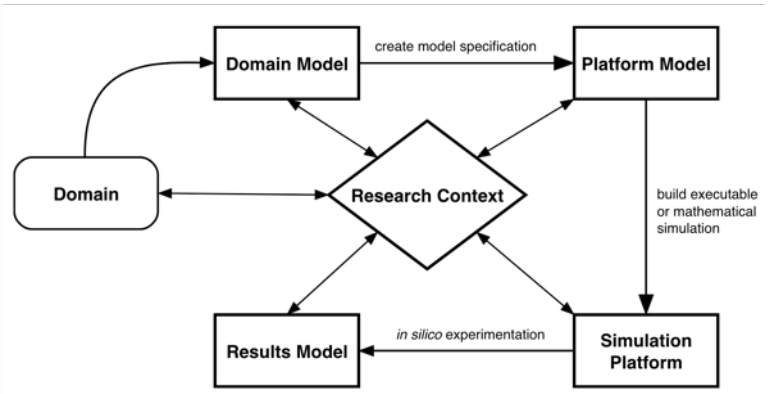


Figure 1.4: **The CoSMoS Process:** This diagram shows how the various models of the CoSMoS process integrate, with focus placed on the Research Context at the center, informing all products of a CoSMoS project.

implementation details are yet considered. Here, it is common to introduce assumptions, abstractions etc, which can reinforce or challenge 'known-knowns' and reveal knowledge gaps.

- **Platform Model:** describes how the domain is to be implemented in the system, and how the questions defined in the research context will be addressed. A process of refinement and simplification is often natural here, due to gaps in understanding, data or challenges related to available computational resources.
- **Simulation Platform:** is the result of encoding the platform model into software. Simulation can be performed upon the simulation platform.
- **Results Model:** encapsulates the understanding that results from the simulation, including answers to the questions postulated in the research context. The results model captures output from the simulation, which may need to be verified *in vivo*.

How these separate models interface is shown in Figure 1.4. Domain and Platform Model decisions can be evidenced using argument notation - a technique inspired from aerospace engineering - to enhance confidence one has in a model. The focus of evidencing these model design decisions and rationale is first to promote transparency and permit more extensive scrutiny of models and second to document decisions formally. Online copy of tools are available on the Kennedy Institute Resources page:
https://www.kennedy.ox.ac.uk/technologies/resources

1.9.1 Simulation Calibration

Once a simulation platform has been developed, the next step is to tweak the simulation to behave like that of real-world data, or hypotheses and intuition in areas lacking data, through assigning values to parameters. Calibration thus aims to ensure the simulation

reflects real-world data. This can be informed by domain-expert intuition, mathematical estimation of parameters through minimising a cost function or developing a probability distribution for the most likely parameter set(s), extracting parameters from the literature, and/or determining parameter values through empirical estimation [244, 245]. Traditional calibration methods in systems biology aim to minimise the error between the simulation output, and observational data, thus incrementally tweaking parameters to arrive at a baseline parameter set [244, 205], while retaining an understanding of the observational error. In this context, data used for calibration is usually cell numbers, protein concentrations, anatomical dimensions, etc. The desired result is a set of values for each model parameter which converge on behaviour that conforms with observational data. This process is also termed 'model fitting'. Bayesian approaches to calibration utilise Bayes' Theorem to to provide a mechanism to account for parameter uncertainty through iteratively updating uncertainty distributions [246]. Bayes' Theorem links prior information - that has intrinsic uncertainty - to posterior information through the likelihood of observed outputs [247]. In contrast to traditional calibration, instead of only minimising the error between the observational data and outputs of a model, Bayesian calibration aims to determine the most likely uncertainties of parameter values, which result in an output where the observational data is most likely.

1.9.2 Simulation Validation

After calibration, the desired product is a simulation platform that adheres to observational data (i.e. the model fits the data). Such a simulation may not yet be useful, as it could describe the data accurately, but may fail to make reliable predictions. This phenomenon, where a model corresponds too closely to the data, is known as 'over-fitting' and is an issue with traditional methods of calibration, where the implication exists that there is no uncertainty in real-world data. An over-fit model contains more parameters than can be justified by the data. Unfortunately, due to the complexity of biological systems and the scarcity of biological data that can be used to identify parameter values uniquely, over-fitting is a common problem for mechanistic models in systems biology [248]. To mitigate the risk of using an overfit model, a process of model validation may occur. In conjunction with model validation, to improve confidence in a model, abstractions and assumptions should be clearly documented to provide transparency and permit scrutiny [249]. To validate a model in systems biology, experimental data can be withheld from calibration. After calibration, *in silico* experiments are performed to replicate the scenarios which produced the withheld dataset, to determine whether the quantitative or qualitative response of the simulation is

consistent with observational data upon which the model was not trained. This provides some confidence in the predictive capacity of a model.

1.9.3 Sensitivity Analysis Techniques

Sensitivity Analysis (SA) comprises a collection of well-established techniques to characterise how a system responds to alterations in input parameter values [250]. SA can be utilised to understand whether a result from *in silico* experimentation could be an artifact of simulation parameterisation or a reflection of the biology underpinning the system. Furthermore, sensitivity analysis is capable of providing novel insight into a biological system through the identification of parameters which are highly influential in producing model output, which in turn can identify roles for novel biological mechanism represented by said parameter [251, 252, 228]. These mechanisms can then be examined and verified experimentally *in vivo* or *in vitro*. Furthermore, sensitivity analysis can be performed to examine important, or all timepoints throughout the duration of a simulation, and provide temporal context which may not be observed through qualitative reasoning from experimental data. Overall, SA can be employed to examine temporal kinetics, and guide experimental design by reducing and prioritising avenues of research.

Local SA can examine the robustness of simulation output, as a result of perturbing the value of a single parameter. This is performed using an 'one-at-a-time' (OAT) approach [181]. Previous work in our labs developed a technique that determines whether altering a parameter value leads to a statistically significant change in simulation behaviour. This utilises the non-parametric Vargha-Delaney 'A-Test' [253] to contrast baseline simulation output, with simulation responses after running the model with altered parameter values. This technique provides a statistical measure of the effect that a parameter perturbation has on simulation output. An A-Test result above 0.71 or below 0.29 indicates that a statistically significant difference between two populations is observed, whereas a result of 0.5 indicates there is no difference. An A-Test score of approximately 0.5 implies that alteration in the values of a parameter of interest produces a negligible impact on simulation responses. In contrast, if an effect is observed, i.e. a simulation result is sensitive to alterations in the value of parameter i, this can suggest that parameter i warrants further examination. Further investigation of such a parameter may (if appropriate) occur through global sensitivity analysis, or perhaps *in vivo* work.

Local SA cannot reveal compound effects which occur when more than one parameter is adjusted simultaneously. Indeed, the effects that one parameter has on simulation output may be dependent on the value of another. To examine compound effects, global sensitivity analysis is required [181]. Multiple approaches can be used to examine global

sensitivity. For example, latin-hypercubes can be used to sample the parameter space, and subsequently simulation is performed for all generated points in parameter space. Partial-rank-correlation-coefficients can be employed to examine whether perturbations in a parameter's value correlates with output of a simulation variable (e.g., cytokine concentration) of interest [254]. Partial-rank-correlation-coefficients account for non-linear relationships in the data, and can correct for effects caused by other parameters. If a strong correlation is revealed through use of a partial-rank-correlation-coefficient, such a relationship can suggest influential biological factors. Another method of performing global sensitivity analysis is through extended Fourier Amplitude Sampling Test (eFAST)[255]. eFAST is a variance decomposition method with similarities to ANOVA, where parameter values are varied and the variation in the simulation output is quantified. This variance is then partitioned, and a fraction of variance is attributed to the alterations of each input parameter. In this context, this suggests how sensitive the simulation and biological system is to a parameter of interest. To partition the variance, parameter values are chosen through a sinusoidal curve at different frequencies for different parameters. Fourier analysis is employed to measure the magnitude of a parameter's frequency in the simulation output, which results in a measure of the sensitivity of the simulation to each parameter called a 'sensitivity index'. Generally, this process is repeated for a 'dummy' parameter across an arbitrary sampling range, although this 'dummy' parameter has no impact on simulation behaviour, permitting comparison of the influence of each parameter, with one that is known to have no influence on simulation behaviour. Throughout this thesis I refer to 'simulation analysis techniques' or similar, which reflects for example sensitivity analysis or *in silico* experimentation, rather than mathematical analysis.

1.10 Thesis Aims and Research Questions

Adjuvant effects induced by chemical adjuvants, RNAs or viral products in vaccines are essential for priming efficacious immune responses. Improving formulation, dosing and timing is an essential tool to enhance vaccination and apply vaccines to both infectious and non-infectious disease. Different adjuvants work by diverse immunological MoAs, therefore to rationally design the next-generation adjuvant-antigen-PRR pairings to diseases of interest, further understanding of adjuvant MoAs is required [142]. *In vivo* experimentation has provided vital insight into adjuvant MoAs. However, key questions remain, and filling such knowledge gaps has the potential to improve next-generation adjuvanted-vaccines. Indeed, the heightened public attention on vaccination and dosing strategies during the pandemic, reiterates the importance of developing a holistic understanding of vaccine MoAs as part of an important public health challenge.

Mechanistic modelling can integrate diverse experimental data types and can substantiate experimental measurements with detailed mechanistic insight, generating a synergistic cycle of modelling and experimentation. A holistic articulation of a biological system can be invaluable in articulating the current state of knowledge and provides a platform to identify knowledge gaps. It additionally can be used to develop simulation models to run virtual experiments. A model based on understanding and assumptions of a system, can be employed to examine the logical implications of knowledge and assumptions, and provide new insights into the underlying mechanisms. Despite these benefits, mechanistic mathematical modelling has rarely been applied to exploring adjuvant MoA.

1.10.1 Research Questions

This thesis first provides a detailed non-executable model of core AS01 MoA, through integrating and mapping experimental data to known and hypothesised mechanistic function underpinning AS01 MoA. We then develop and analyse simulation models to explore AS01 MoA. These explorations first focus on early cytokine production and cellular responses. Following analysis of the early immune response, we then develop multiple models to explore the CD4+ T cell response to AS01 (identifying important mechanisms through sensitivity analysis) and alternating hypotheses for how IFNγ may modulate this process.

The key thesis hypotheses are as follows: In naïve mice immunised with AS01;

- Monocyte and DC derived IL12 supports macrophage derived IL18 in the early synergistic production of IFNγ.
- Macrophage derived IL18 more profoundly contributes to synergistic IFNγ production than IL12 after AS01.
- The loss of subcapsular macrophages after QS21 limits the innate response to avoid toxicity.
- DCs provide vital, early inflammatory signals to initiate the cytokine response.
- A second, primary vaccination too soon after the first could be detrimental to the IFNγ response due to a delay in macrophage recovery.
- Early IFNγ substantially enhances DC maturation which in turn augments the priming of CD4+ T cells in dLNs.

These hypotheses drive the following research questions:

1. In preclinical models, after intramuscular injection of a vaccine adjuvanted with AS01, how does AS01 initiate an immune response? What are the key interactions that give rise to the generation of antigen-specific CD4+ T cell responses and antibody production? How could IFNγ regulate these processes?

2. The source of IL12 post IM AS01 administration is unknown. Given the assumption that monocytes and DCs both produce IL12 at the same rate, what differences do we observe in the temporal dynamics of cellular IL12 production? What hypotheses do these insights generate?
3. What is the relationship between each cell type's respective production of IL18 or IL12 with the production of IFNγ? How does this differ over time? What is the dominant cytokine in initiating early IFNγ?
4. What are the most influential parameters involved in early IFNγ production after AS01?
5. What effects does the loss of macrophages have on the IFNγ production? What would happen to the immune response if no macrophage cell loss occurs? How could this cell loss affect IFNγ responses after a second AS01 delivery?
6. What immune system processes influence the generation of the CD4+ T cell response to AS01?
7. Is the hypothesis that IFNγ modulates the CD4+ T cell response via substantially enhancing DC potency to prime T cells after AS01, consistent with the experimental data?
8. Where does the mechanistic model(s) indicate that our understanding of AS01 MoA is incomplete?

1.10.2 Thesis Aims

Addressing the above questions is encapsulated by the following four aims to:

1. Derive a 'core model' of AS01 MoA - describing in detail how AS01 initiates an efficacious immune responses - by integrating and mapping experimental data to known and hypothetical mechanistic function.

2. Develop a mathematical model using the AS01 'core model' to explore early mechanisms regulating IFNγ production induced by AS01. To constrain any developed simulations using available data for parameterisation and validation.

3. Analyse the relative role of different immune cells and cytokines in the early IFNγ response to AS01-adjuvanted vaccines, to determine parameters influential in interferon-gamma production and the role of macrophages in the induction of immune responses to AS01.

4. Generate simulations to identify influential parameters involved in CD4+ T cell priming and to explore hypotheses regarding how IFNγ modulates the CD4+ T cell response to AS01-adjuvanted vaccines.

Chapter 2

Materials and Methods

2.1 Data Security and Cleaning

Data from GSK and D. Gajdasik (Prof. Wither's group, University of Birmingham) was securely transferred to the University of Oxford. The data was structured and cleaned using Perl scripts and all raw datasets securely returned to GSK. All data in the thesis has been processed and cleaned. Raw datasets are available upon request to GSK. All biological data used in this thesis was generated by either GSK scientific team or by the Wither's group (University of Birmingham); the author of this thesis did not generate any of the biological data. As part of thesis these data were structured, cleaned and linked to associated metadata. These structured data were used in model development and validation.

2.2 Development of a Domain Model for Core AS01 MoA

In Chapter 3, we employed the discovery phase of CoSMoS process to develop a model of 'core' AS01 MoA. After documenting the research context, we developed a CellDesigner model using *CellDesigner 4.4*. In Chapter 3, Systems Biology Graphical Notation (SBGN) was used to describe a complex inter-cellular system that determines tissue-mediated immune response. Domain Model diagrams e.g 'Expected Behaviours', 'Activity Diagrams' and 'State-Machine' diagrams were subsequently developed in Adobe InDesign CC 2017 version 12.1.0.56 and written in an adapted form of UML [256].

2.2.1 Domain Model Products

Previously, 'Expected Behaviours', 'Activity' and 'State-Machine' diagrams have been produced during development of Domain Models of biological systems [181, 243, 239, 6, 205, 257]. Here, we applied a similar approach to vaccine adjuvant MoA, to develop new understanding into temporal behaviours and sensitivity of the MoA to cellular and cytokine dynamics.

Expected behaviours diagrams describe how components identified in the research context contribute to system level behaviour, and how phenomena observed *in vivo* links with the temporal understanding of the system. Hypotheses for how these phenomena are expected to manifest are also described. This diagram therefore links the scope and hypotheses of the model to *in vivo* experimental data. Activity Diagrams describe activities and events in the system that emerge from interactions between cellular components. These diagrams are used to represent work flows and are written in an adapted form of the unified modelling language (UML) [181, 243, 169, 6, 205]. In the current context, they describe interactions between captured biological entities. State-Machine diagrams describe the different states a component (entity) can exist in, and requirements that govern transitions between these states. State-Machine diagrams are also written in an adapted form of UM (Figure 2.2 - Figure 2.3).

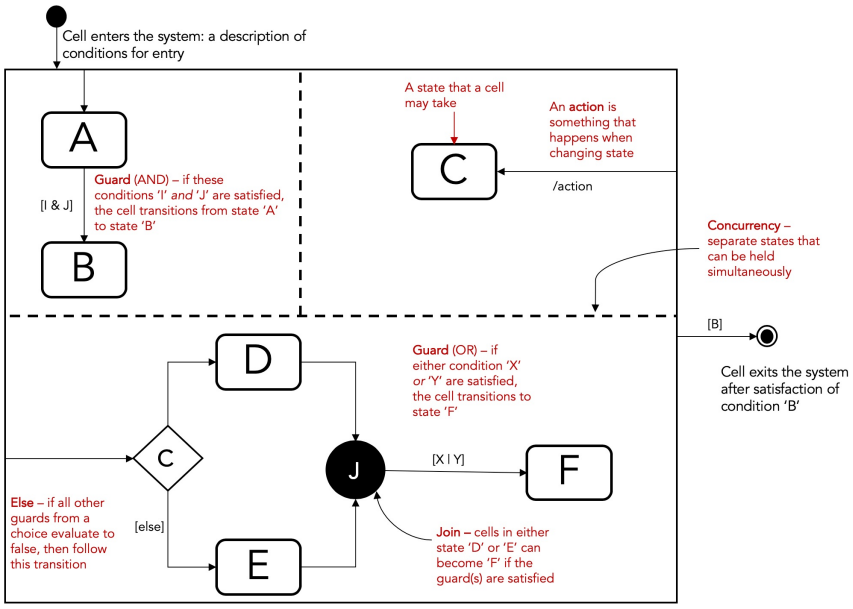


Figure 2.1: **A guide to UML: A description of the adapted version of the UML utilised to develop State-Machine diagrams.** States are represented by rectangular boxes, which may encompass smaller rectangular boxes, indicating parent and sub-states respectively. A black circle indicates the initial state of the object, and the black circle with a surrounding white border indicates the final state. Arrows indicate transitions between the states, and information surrounded by square brackets describe a condition that must be satisfied for the transition to proceed. An expression preceded by a forward slash, indicates further information with respect to a state transition or a state. Finally, dashed lines represent concurrent states and a diamond indicates a decision is to be made, determined by a condition being satisfied. This figure is adapted from [6].

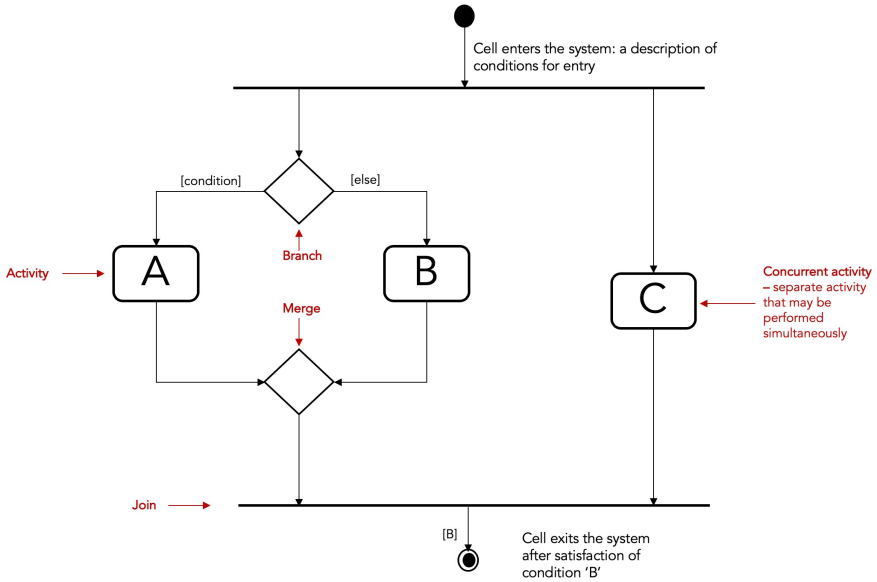


Figure 2.2: **A guide to UML: A description of the adapted version of the UML utilised to develop Activity Diagrams.** This figure is adapted from [6].

2.3 Development of Mathematical Models

For the development of both the 'innate IFNγ AS01' model (Chapter 4) and the 'AS01 CD4+ T cell priming' model(s) (Chapter 6), we proposed and developed collections of ODE by following the CoSMoS process. Here, we articulate the research context preceding computational model development. Following this, we developed a Domain Model. A Domain Model is a representation of the biological system, and products of such a model are not strictly confined, although in this case the Domain Model products are generally diagrams describing system function. The Domain Model describes what is currently known and unknown, integrating insights gleaned from experimental data and domain-expert opinion. To create an appropriate representation of biology and to minimise bias from (potentially) favoured modelling methodologies, implementation details were not considered at the domain modelling stage, therefore a 'Domain Model' describes only the biological system, free of mathematical or computational language. In this thesis, the Domain Model is composed of CellDesigner diagrams for high-level scoping of the system of interest, Expected Behaviours, Activity Diagrams and State-Machine diagrams. Next, we constructed a Platform Model, which reflects how the Domain Model will be implemented, using mathematical and computational language. The Platform Model additionally details the choice of most appropriate modelling methodology for which the simulation will be constructed.

2.3.1 Simulation Development

In this thesis, the Platform Model was implemented by computer code describing the ODEs, in order to create a 'Simulation Platform'. Here, all models were implemented as ODEs in the R package *dMod* [9]. *dMod* is a flexible framework aimed at streamlining the process of developing ODE models, with a focus on biological systems. Advantages of *dMod* include but are not limited to 1) automated *C* code generation for fast simulation of models, 2) parameter-estimation based on trust-region optimisation informed by sensitivity equations, 3) identifiability analysis based on the profile-likelihood method, which has been shown to be more appropriate for cases where models are unidentifiable (common in systems biology contexts). From within *dMod*, we utilised *deSolve*[258] to solve the model via the *lsoda* function. *lsoda* automatically switches between stiff and nonstiff methods which is advantageous as it means the user does not have to determine the stiffness of the problem.

To produce model output, fixed and free parameter values (or multiple sets of parameter values potentially each representing a local optima), including initial conditions (as well as any parameter transformations) were supplied to a function, alongside a vector of times. In the case of the 'AS01 CD4+ T cell priming' models (see Chapter 6), the vector of times were 0-168 hours. For the 'innate IFNγ model', the vector of times were 0-24 hours. Multiple sets of parameter values can be provided; thus, the simulation model is run for each set, generating model output for each set of input parameters. Often, each different set of model parameter values can refer to a local optima found through calibration.

2.4 Simulation Calibration

Observational data for calibration is described throughout the thesis. Unless stated otherwise, the geometric mean and the standard deviation were used as central point estimates and error respectively for model optimisation. The geometric mean was used instead of the arithmetic mean due to outliers in the data. For simulation platforms presented in this thesis, we calibrated all unknown parameter values by adopting an incremental approach. Given the large parameter space to be sampled, the scarcity of the experimental data, and the 'cascading' nature of the models, we isolated sets of model equations where possible, performed optimisation and then incrementally incorporated and optimised portions of the model. For parameter estimation, we used the *dMod* package, which employs weighted least squares estimation. The *dMod* framework was utilised due to its simplicity in implementation, succinctness in model description, ability to deal with noise in the experimental observations and implement models via compiled-code, thus increasing run-time efficiency. To estimate parameters, an objective function is generated and through minimisation, the

model is fit to the data using a trust region optimiser as described in detail in Kaschek et al [9]. Briefly, trust-region optimisation defines a region around a current best solution. This region is adjusted at different iterations and if a reasonable model of the objective function is found, then the region is enlarged and conversely if a worse agreement is found the region is reduced. For ODE models, this optimisation routine less frequently steps into regions of parameter space for which the ODE cannot be solved [9].

To illustrate our calibration approach, we provide an example based on optimising the model presented in Chapter 4. Given the 'cascading' nature of the model, we isolated portions of the model, optimise, and then incrementally incorporate sets of components until the entire model had been optimised. We first isolated macrophage (Mo) and 'IL18' equations and produced a 'best-guess' fit of parameter values by gathering estimates from the literature, which were manually tweaked. These were passed to the trust-region optimiser to minimise the objective function between the model and corresponding experimental data. A 'best fit' set of parameters were developed and retained. Next, the following isolated set of model components are included (DC, monocyte and IL12 equations). The best-fit parameters retained from the previous fitting procedure were employed as starting points for model fitting. For parameters among newly included equations, values from the literature or best guesses were used as starting positions. The model was then optimised. This process is repeated until the entire model was included and a 'best fit' was produced for all parameters.

Once the entire model had been subject to optimisation and a 'best fit' parameter set developed, we next employed a multi-start strategy to further explore the parameter space. Here, we used the 'best fit' set of parameters as a starting point. We then spread the initial positions of optimisation throughout the parameter space and optimised. This resulted in a set (or distribution) of multiple local optima that fit the data with a range of objective values [9]. The 'best fit' set is that which exhibited the lowest objective value. From the collective set of local optima, we yielded a distribution of values for each model parameter. Furthermore from simulating these local optima, we yielded a distribution of simulation trajectories (across timepoints), for each model component, across local optima.

2.5 Simulation Validation

Prior to development of computational models, data were gathered from internal GSK databases and Dominika Gajdasik in Prof. David Withers group at the University of Birmingham. We set aside specific data for the purpose of calibration ***or*** for validation. In no circumstance was any validation data used in model calibration. The aim with these experiments was to confirm that the model is able to predict experimental data for which

it was not calibrated to. This may indicate that the model possesses reliable predictive capacity. For simulation validation, *in silico* models were modified and simulated to replicate a corresponding *in vivo* scenario. Such replications were performed by amending parameter values or setting them to zero, or by removing relevant terms from the model equations. Using the modified model, simulation was performed and the distribution of corresponding model output *in silico* (e.g., IFNγ+ NK cells), was compared with the distribution of *in vivo* readouts (e.g., IFNγ+ NK cells), using a statistical test (usually t-tests or wilcoxon tests or both).

2.6 Sensitivity Analysis

Both local and global sensitivity analysis are used throughout this thesis. For models with very large parameter spaces, local sensitivity analysis was preferred due to the combinatorics involved with appropriately examining large parameter spaces with global sensitivity analysis.

2.6.1 Local Sensitivity Analysis

Local sensitivity analysis determines how alterations in a single input parameter influences simulation behaviour. We employed a 'one-at-a-time (OAT) based technique' to analyse local sensitivity [181, 252]. Therefore, we analysed the variation of simulation output values for a variable of interest across local optima, as each parameter is perturbed individually. Therefore, the output which is analysed for local sensitivity, is the distribution of cell numbers or cytokine levels across local optima, at each timepoint, following the perturbation of a parameter of interest. The output distribution of values after an individual parameter alteration, is contrasted with a 'reference' distribution, which represents the calibrated 'normal' model with no perturbation. The two distributions are compared using the Vargha-Delaney A-test [253], a non-parametric statistical test to measure the effect-size difference between two distributions. The use of a non-parametric test allowed us to avoid the assumption that the sampling distributions are normally distributed [181].

Such analysis can indicate how robust simulation outputs are to the perturbation of a single parameter [259]. The A-Test compares two distributions, A and B. The A-test is a value between 0.0 and 1.0, and indicates the probability that a random sample from distribution A, is larger than one chosen from distribution B [253]. Therefore, this A-test can be used to indicate when statistically significant changes in simulation output have occurred following the perturbation of a parameter value [181].

Parameter values for the perturbation were sampled uniformly across a pre-defined parameter space, with some defined increment [260]. To increase computational efficiency,

parallel processing was employed using both the *foreach* and *doParallel* packages in R. While OAT-based local sensitivity analysis can elucidate the effects of perturbing a single parameter, it cannot reveal non-linear effects that may occur when more than one parameter are adjusted simultaneously. In such a case, global sensitivity analysis is required.

2.6.2 Global Sensitivity Analysis (eFAST)

For global sensitivity analysis, we used the extended Fourier Amplitude Sensitivity Test (eFAST)[255], employing R package *pksensi*[261]. With smaller sample sizes, sensitivity indices can be variable. Therefore, *pksensi* employs a phase-shift approach to undergo replicated sampling from randomised starting points across the parameter space. From these replications, convergence of the sensitivity indices are calculated as described in Hsieh et al [261] which follows the method by Sarrazin et al [262]. This technique evaluates how robust the results are to variation. Simply, a sensitivity index with respect to a parameter and model variable which does not converge, indicates that a larger sample number should be used to reduce variation. An acceptable cutoff of for convergence is considered as 0.1.

In this thesis, a sample size of 150,000 was chosen for each parameter, with 5 replicates. The algorithm was set to uniformly sampl parameter values across pre-defined ranges, which are reported at appropriate sections in the thesis. Two sensitivity indexes are calculated for each parameter, against a simulation variable of interest, termed the eFAST First-Order Sensitivity Index, and the Total-Order Sensitivity Index. The First-Order index suggests the proportion of simulation output variance which can be attributed to a parameter of interest. Total-Order sensitivity index suggests the variance as a result of higher-order, non-linear effects between the parameter of interest and other perturbed parameters. As above, parallel processing was utilised to increase computational efficiency.

Chapter 3

Mapping Experimental Data to Immunological Processes for a Proposal of AS01 Mechanism of Action

Note: parts of this text are adapted or reused from a publication of this work under a CC-BY licence: Buckley et al, Frontiers in Immunology 2019.

3.1 Introduction

The mechanistic understanding of AS01 and other vaccine adjuvant MoAs has been developed using genetically modified pre-clinical mouse models that contain genetic reporters, fixed T and B cell repertoire (TCR and BCR transgenic mouse lines) and deficiency for key cytokine, signaling pathways and cell lineages [32, 15]. However, not all mechanistic questions can be addressed in this manner. Systems biology methodologies can provide a holistic perspective on MoAs through mapping experimental data and insights with known and hypothetical mechanistic function and wider immunological knowledge [184, 263, 264, 134, 252]. Through carefully thinking through how to model a system, experimental insights can be challenged or reinforced, knowledge gaps identified, assumptions articulated and hypotheses produced for inevitable gaps in understanding. Indeed, Paul Nurse has recently argued for such an approach, arguing for modelling molecular and cellular components involved in a biological system in order to permit analysis of system dynamics [265]. In his recent opinion piece, he makes the point that "even writing down equations without seeking their solutions can be helpful, simply because it imposes greater rigour on model building". While equations will not be proposed until Chapter 4, this chapter adopts a similar philosophy, and thus presents the development of a detailed, non-

executable model which seeks to capture and describe in detail the current understanding of AS01 MoA, to serve as a knowledge base from which simulations will be developed.

In many cases, uncertainty exists between experimental mouse data and underlying mechanisms, thus explicitly defining and thinking through how these link, can reveal knowledge gaps and add insight into a system. The resulting product explicitly describes the current understanding of a system. We argue this process of 'Domain Modelling' leads to transparent, rigorous science and a deeper understanding of a system, by forcing analysis and formulation of intuition and insight, as well as an assessment of the resulting logical implications of our ideas, assumptions etc [180]. In turn, these models can guide the design of more targeted experiments. In the current context, these non-executable models also inform the development of simulations [179], permitting exploration of relationships between different components in the biological system. Through hypothesis generation or refinement, these methods can guide and optimise experimental design [236, 266, 193, 184, 267, 268, 239]. Importantly, mechanistic modelling has rarely been applied to exploring adjuvant MoAs, which are extraordinarily complex systems, spanning multiple organs and levels of biological hierarchy [119]. Given the aforementioned reasons, we therefore argue that considerable insight can be extracted from mapping the current experimental results regarding how adjuvants modulate immune responses, with known and hypothetical mechanisms. From there, targeted research questions can be identified, and in the current context, mechanistic modelling can be used to explore such questions.

Therefore, this chapter first presents a framework for applying such concepts to adjuvant research. Guided by this framework, we developed a 'Domain Model', mapping the experimental data to known and hypothetical mechanistic function, to propose the current understanding of AS01 MoA [7] and identify knowledge gaps. We therefore examined AS01 experimental insight and integrated this knowledge with wider immunological literature and novel hypotheses in-place of knowledge gaps. We aimed to supply a transparent and carefully thought through proposal, supported by an evidence-base from biological experiments, for how AS01 generates immune responses. Compounding these benefits, detailed descriptions of how immune-components are thought to interact leading to immune responses after adjuvanted-vaccination, can serve as a foundation for the development of simulations focused on exploring research questions of interest.

Integration of engineering principles with experimental immunology, to accelerate and de-risk vaccine adjuvant development and deployment, involved the use of modelling and simulation, from the description of detailed biological mechanisms to development of iterative mathematical models with the aim to provide insights to guide experiments. This highly interdisciplinary approach must bring a diverse range of expertise from academia and

industry. This international team supporting this project therefore bought together expertise in immunology and vaccinology with systems biology, computer science and software / systems engineering.

We were aware that to enable high quality, highly-interdisciplinary research, we needed to communicate effectively. Indeed, ideas and concepts should be articulated clearly, and one should be confident that they are perceived accurately. For work on highly complex systems such as adjuvant MoAs, this is paramount. Additionally, modelling exercises must also be transparent and open to scrutiny. Therefore, it was decided that a scoping and communication exercise would first occur, to scrutinise the high level understanding of AS01 MoA using highly-visual notation. We therefore employed the model design software *CellDesigner* to produce a visual overview of AS01 MoA understanding and hypotheses, which we then used to inform more complex engineering models [269]. Canonical use of CellDesigner describes intracellular biology through the Systems Biology Graphical Notation (SBGN) [270], permitting capture and abstraction of large amounts of information, to improve team communication and reduce perception issues [271]. This process permits transparency, scrutiny of ideas and provides a platform for knowledge retention. As our system is an organ spanning, intercellular system overseeing many hierarchies of biological detail, SBGN in CellDesigner was adapted for our purposes. Thus, CellDesigner's capacity to translate a non-executable model into an executable simulator is not appropriate for the questions addressed in this thesis

The Domain Model presented in this chapter not only provides a platform to communicate immunological knowledge but also provides a logical basis for simulation development. Overall, we provide a detailed proposal of how AS01 generates immune responses. In addition, we hope that through use of the framework presented here, which reflects many learnt lessons, these concepts could be utilised more generally to consolidate and improve the understanding of other adjuvant MoAs.

3.2 Results

3.2.1 A framework for the application of mechanistic modelling approaches to explore adjuvant MoA

We first designed a framework, describing how we would apply mechanistic modelling approaches to exploring adjuvant MoA (Figure 3.1). This framework serves as an instantiation of the CoSMoS process, and is concerned with the 'Discovery Phase' (section 1.9) of a CoSMoS project. This framework encapsulates the work presented subsequently in this chapter. Overall, the framework provides a guide for Domain Modelling of adjuvant MoAs. We first

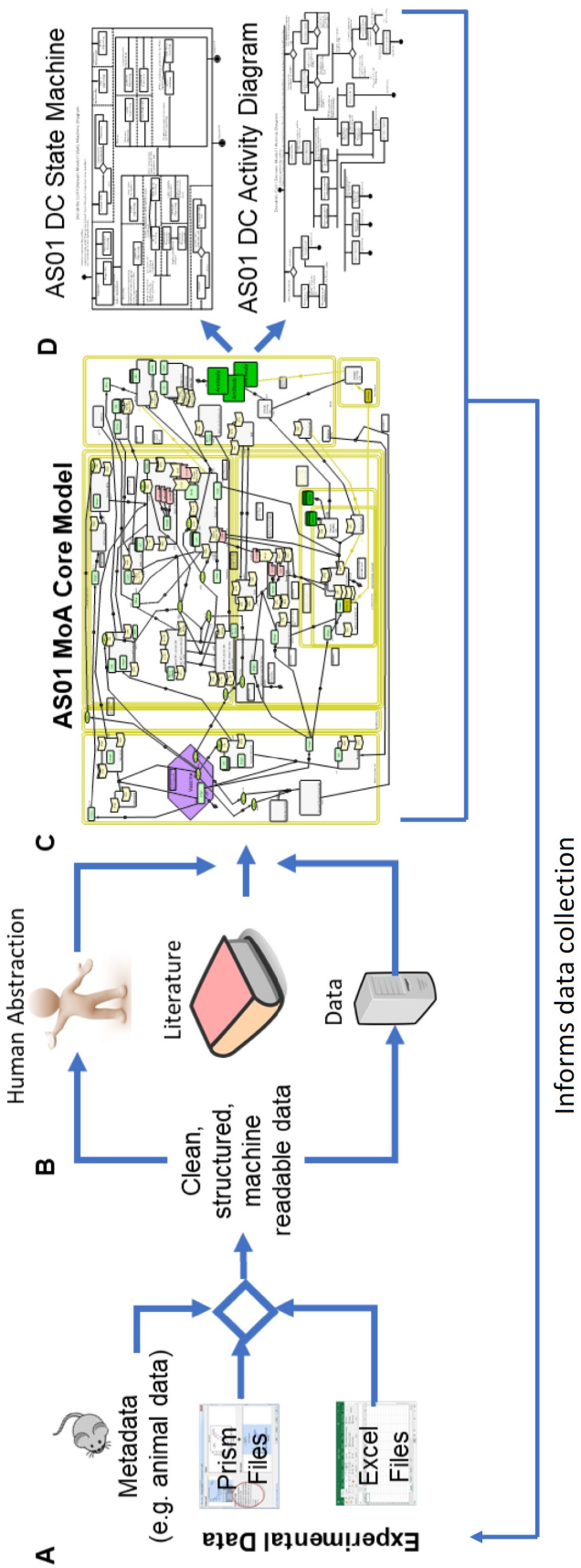


Figure 3.1: **An overview of the Framework for the Application of Mechanistic Modelling Approaches to Exploring Adjuvant Mechanism of Action:** Development of the Domain Model: in this context, development of the domain model began with (**A**) the collection of experimental data from Graphpad Prism and Excel files, and the corresponding experiment metadata (see Methods 2.1). Following this, an automated pipeline was developed to clean, structure, and integrate the experimental results and the corresponding metadata, resulting in machine-readable data. Next, human abstraction, the AS01 data and immunological literature were appropriately integrated (**B**). The AS01 data informed the development of the model 2-fold, firstly by constituting the available evidence behind the captured processes, but also by informing the rationale underpinning any human abstraction required to inform gaps in understanding. The core MoA model (**C**) was utilized to scope the requirements of the lower-level models describing component function, and so from the core MoA model, State-Machine and Activity Diagrams were developed (**D**). Furthermore, Domain Model development can inform data collection by permitting the understanding of what data is required to ask the scientific question. Figure and legend adapted from [7]

gathered and cleaned experimental data, from which we extracted, scrutinised and examined measurements, correlations and the mechanistic insight described in section 1.7. It is not possible or appropriate to develop a model of the entire complex system such as the one under study, thus we next incorporated appropriate abstractions and assumptions to simplify the model. Collectively, this process revealed knowledge gaps,which were recorded and novel hypotheses to fill gaps were generated. All the aforementioned work was integrated, culminating in the 'AS01 MoA Core CellDesigner Model'. We then used this diagram to inform the scope of further diagrams detailing functions of different immunological components in this system. Therefore, the framework guided the development of the 'Core AS01 Domain Model'.

3.2.2 A Domain Model for the Core AS01-induced Immune Response

By following the framework in Figure 3.1, we produced a 'Domain Model' describing in detail the 'core' of AS01 MoA. In what follows, we describe the development of this model. The diagrams presented in this Chapter, were all created by the author of this thesis, although they were developed in collaboration with experimental immunologists at GSK Vaccines. Therefore, the Domain Model that follows, consolidates and builds on insights published by GSK immunologists for a holistic proposal of AS01 MoA.

3.2.2.1 Research Context

We first defined the research context, which sets the scope and purpose of the model, describes the motivation for the study and articulates the research questions to be addressed by modelling exercises and/or the simulation platform. Based on the murine experimental data, the research context can therefore be encapsulated by the following questions (research question 1, section 1.10.1) :

1. **In preclinical models, after intramuscular injection of a vaccine adjuvanted with AS01, how does AS01 initiate an immune response?**
2. **What are the key interactions that give rise to the generation of antigen-specific CD4+ T helper cell responses and antibody production?**
3. **How could IFNγ regulate these different processes?**

The domain of study is the generation of the adaptive response to AS01, primarily in the lymph node draining the muscle injection site. Salient mechanisms in the lymphatics, muscle injection site and blood were also captured. Simple dynamics in the bone marrow were also described to capture the basics of a recall response. The captured cell types, alongside the inclusion and exclusion criteria are in Table 3.1.

Entity	**Included or Excluded**	**Justification**
Muscle-resident cell	Included	We hypothesised that cells resident in the muscle (potentially skeletal muscle, macrophages or endothelial cells) are activated by AS01 upon injection, resulting in the production of chemokines that recruit neutrophils and monocytes. This entity is included to capture this hypothesised initiation of the response.
CD169+ F4/80- sub-capsular sinus macrophages	Included	These macrophages have been shown to release IL18 after QS21 mediated activation of caspase-1 [8]. IL18 contributes to the production of IFNγ by NK cells [32]. In addition, this cell can capture antigen and transfer it into the B cell follicles [272].
IFNγ Secretor Cells	Included	This cell type is an abstraction that encompasses Natural Killer cells, Natural Killer T-cells, innate-like CD8+ T-cells, ILC1s and gamma-delta T-cells in this high-level model. These cells have all shown to secrete IFNγ to a varying degree after innoculation with an AS01-adjuvanted vaccine [32]. Inclusion of this entity is vital as IFNγ has been shown to be critical for promoting CD4+ T cell responses to AS01.
Monocytes	Included	After i.m injection of AS01 and an antigen, it has been demonstrated in an ovine lymphatic cannulation model that monocytess infiltrate the dLN in large numbers [46]. Their function in this context is not yet clear, however we hypothesised that they secrete IL12 [**?**], and we capture their well characterised ability to differentiate into DCs [15].
Dendritic Cells	Included	The enhancement of adaptive immunity by AS01 has been shown to depend on activated dendritic cells and thus DCs are captured [15].
IFNγ	Included	IFNγ is a significant component of the response to AS01. Whilst questions remain on its function in this context, its transient production has been shown to be critical for the generation of cytokine-producing CD4+ T cells after AS01-based vaccination [32].
IL12	Included	IL12 has been shown to synergise with IL18 to promote optimal production of IFNγ after vaccination with AS01 [32].
IL18	Included	IL18 has been shown to synergise with IL12 to promote optimal production of IFNγ after vaccination with AS01 [32].
T Helper Cells	Included	CD4+ T cells are induced after AS01 vaccination and are a critical component of the immune response [32].
Follicular dendritic cells	Included	While their role has not been elucidated through experiments with AS01, fDCs are a key component of the adaptive response. They secrete CXCL13 which organises B cells in the follicles and attracts CXCR5+ T Helper cells towards the T / B border, in order for them to provide survival signals to B cells. Furthermore, fDCs can capture and express antigen.
B cells	Included	There are scant data on B cell responses to AS01, however the synthesis of antibody is captured as it is a critical component of vaccination. Therefore, canonical, high-level B cell dynamics are captured to facilitate the inclusion of events that give rise to the synthesis of antibody.
Antibody-secreting-cells	Included	Antibody-secreting cells are included as they are a critical component of antibody synthesis.
Memory B cells	Included	Memory B cells are included to capture basic dynamics of the secondary immune response.
Memory T cells	Included	Memory T cells are included to capture basic dynamics of the secondary immune response.
IL-6	Excluded	This cytokine is excluded. IL6 is a highly pleiotropic cytokine with both anti and pro-inflammatory function. While IL6 is produced after AS01 vaccination in mice, its role is unclear and thus not included at this stage.
Neutrophils	Excluded	This cell type is excluded, as there is no evidence that neutrophils contribute to early IFNγ production or IFNγ modulation of the adaptive response to AS01. Furthermore, there are conflicting data from other systems on the role of neutrophils during the immune response in the dLN.
CD4+ T Helper 17:	Excluded	This cell type is excluded. IL17-producing CD4+ T cells are observed after M72/AS01E vaccination [273], although there is no evidence that IL17-producing CD4+ T cells contribute to the production of IFNγ or its modulation of the adaptive response to AS01.
Regulatory CD4+ T cells	Excluded	This cell type is excluded. Even if these cells are induced by AS01, we are unsure of their contribution to the research context.
Antigen-complement complexes	Excluded	This entity is excluded. Antigen-C3dg complexes are critical for driving the high-affinity antibody response through binding to of C3dg-antigen complexes to CD21 on FDCs, however because the model is not addressing mechanistic questions on the germinal centre response, which is C3dg dependent, complement has not been included in the model.

Table 3.1: Inclusion and Exclusion Criteria for the Core AS01 MoA CellDesigner Model: describing the rationale underpinning the inclusion and exclusion of various entities, and model abstractions and assumptions.

3.2.2.2 Experimental Data

Experimental data from GSK and other sources were used to develop the Domain Model. The different experimental datasets were stored in different formats, in different locations and thus required a considerable amount of work to develop a curated dataset that could be used in model development. The data from these different sources were curated, cleaned, structured and re-analysed.

Here, we present the curated data which informs much of our current quantitative knowledge of AS01 mechanism-of-action to date (for a detailed description please see section 1.7), with respect to our research questions. The insights and trends that follow in this section, with the exception of the data shown in Figure 3.2G and 3.2H have been previously published, although these *specific* experimental measurements are not published [5, 54]. Unless stated otherwise, experiments were performed by GSK in C57BL/6 mice.

While the muscle-injection site data from e.g., Didierlaurent et al [5] informed Domain Model development, here for brevity we only show the data measured from dLN (Figure 3.2). GSK measured the numbers of CD169+ subcapsular macrophages in the dLN after PBS or QS21 (Figure 3.2A), and observed a clear reduction in the number of cells after QS21 compared with the control. The mechanism causing this reduction in cells is currently unknown however it is thought to be mediated by QS21-induced pyroptosis, although this has not yet been confirmed. Indeed, at the current level of the data, alternate hypotheses e.g., cellular displacement or a reduction of CD169 expression, cannot be excluded. Additionally, the knock-on effects of this cell loss of macrophages is currently known. Next, we show the numbers of CD11c+ MHCII+ DCs in the dLN following vaccination with a model antigen and AS01 (Figure 3.2B). This population of cells encompasses both migratory (CD11c+ MHCII^{high}) and resident DCs (CD11C+ MHCII^{med}). While large variation in the levels of these cells was observed at timepoints 6, 24 and 48hrs there is an increase in the central estimates over the course of the first 48hrs, although this change is not significant. Further published and unpublished data from GSK has also found an increase in this cell types during the first 48hrs post AS01 administation [5]. Next, we show the increase in the numbers of CD11b+ Ly6c^{high} monocytes following AS01 (measured at 6, 24 and 48 hours) post-injection in C57BL mice, compared with PBS (0 hour estimate) (Figure 3.2C).

IFNγ+NK cell levels are increased at six hours post-injection of AS01 compared with after PBS (labelled as hour 0), although this increase is transient as the numbers of these cells return towards baseline levels by 24 hours post-injection (Figure 3.2D). These data indicate that the number of these cells peaks at approximately 6 hours post injection, consistent with Figure 3.2E showing the concentration of IFNγ over time, which peaks at approximately 6 hours post injection. Further sampling frequency would be required to

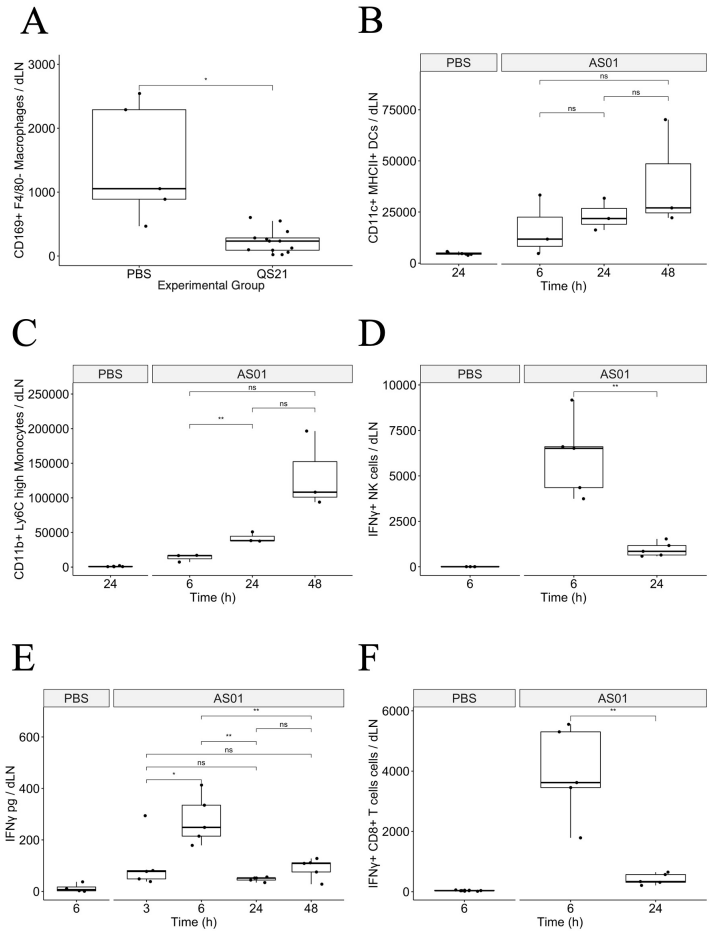


Figure 3.2: **GSK generated experimental data showing cell numbers and cytokines after AS01-adjuvanted vaccination 1/2:** A) During an experiment by GSK to determine the cells targeted by QS21, subcapsular macrophages were analysed by flow cytometry 24 hours after stimulation by PBS or QS21 injection and cell numbers quantified in mice [8]. **A)** Subcapsular sinus macrophages after PBS and QS21 stimulation. B-E) To examine cell or cytokine dynamics after AS01 compared with PBS, six to eight week old female C57BL/6 mice were immunised i.m with gE antigen formulated with 1/50th human-dose (HD) AS01b in gastrocnemius muscles, or gE and PBS. Iliac dLN were collected at timepoints between 3 and 48 hours post injection. IFNγ producing cells were assessed by ICS. Cytokines were analysed by MILLIPLEX MAP, a multiplex assay using Luminex technology. For cell detection, fluorescent events were acquired using an LSR2 flow cytometer and analysed by FLOW JO. B-D, F, G) Iliac dLN were collected at timepoints between 6 and 48 hours post injection. **B)** Resident and Migratory DCs at 6, 24, 48 hours following vaccination with AS01 and gE antigen or 24 hours following injection with a PBS control. **C)** Inflammatory monocytes at 6, 24, 48 hours following vaccination with AS01 and gE antigen or 24 hours following injection with a PBS control. **D)** IFNγ+ NK cells at 6 and 24 hours following vaccination with AS01 and gE antigen, or 6 hours following injection with PBS. **E)** IFNγ pg/dLN concentration measured at 3, 6, 24 and 48 hours post-vaccination with AS01 and gE antigen, or 6 hours following injection with PBS. **F)** IFNγ+ CD8+ T cells at 6 and 24 hours following vaccination with AS01 and gE antigen, or 6 hours following injection with PBS. All statistical significance measured by T-test. All data was generated by GSK.

determine a more precise peak of this so-called innate-IFNγ. As mentioned, much of the available data in their original sources (prior to our curation) were disparate. In this light,

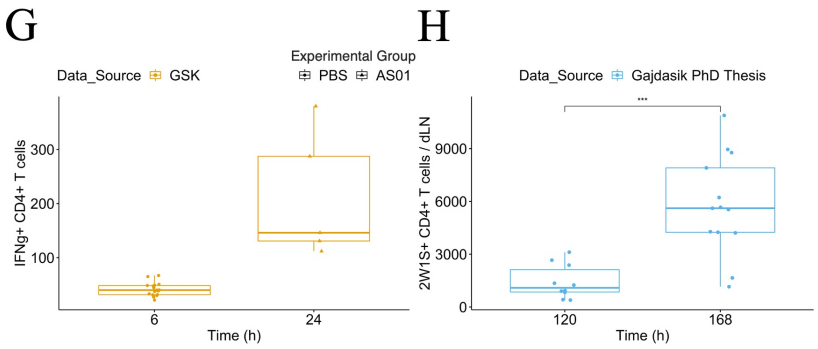


Figure 3.2: **Experimental data showing cell numbers and cytokines after AS01-adjuvanted vaccination 2/2: G)** IFNγ+ CD4+ T cells at 24 hours following vaccination with AS01 and gE antigen, or 6 hours following injection with PBS. Data were generated by GSK. H) 2W1S+ CD4+ T cells / dLN. Great Smart mice were injected intramuscularly at day 0 with 20 μg 2W1S peptide conjugated to OVA protein and 1/50 Human Dose of AS01. The injection was administered into the gastrocnemius muscle. The response was assesed in the iliac draining lymph nodes at day 5 and day 7. The 2W1S-specific CD4+ T cell response was assesed using MHCII tetramers. The experiments for the data shown in H) were performed by Dominika Gajdasik, University of Birmingham. Different shapes distinguish the experimental stimulation.

we were unable to curate a holistic dataset regarding CD4+ T cell numbers after AS01 over the first seven days of the response to AS01. We therefore gathered data from two sources. We were able to gather data from GSK on the numbers of IFNγ+ CD4+ T cells at 24 hours post-injection with AS01, and after PBS injection (Figure 3.2G). IFNγ expression by these cells indicate that these cells are, or are becoming activated, therefore we argue that these data by proxy represent the numbers of 'activated CD4+ T cells' at such timepoints. Unsurprisingly, the numbers of these cells at these timepoints are low.

For antigen-specific CD4+ T cells, we were kindly provided measurements of these cells at 120 and 168 hours post-injection of AS01 by Dominika Gajdasik (University of Birmingham). Gajdasik measured the numbers of these cells after injection with 2W1S (a listeria monocytogenes antigen) and AS01 at the aforementioned timepoints, in accordance with GSK guidelines on experiments with AS01 (Figure 3.2H). Taken together, the IFNγ+ CD4+ T cell data from GSK and Gajdasik's CD4+ T cell data indicate an increase in the number of 'activated CD4+ T cells' over the first seven days of the response to AS01. Using mice deficient for key cytokines and proteins regulating immune vaccine immune responses and using *in vivo* cell depletion systems, murine experimental data collected by GSK and Withers laboratory has been cleaned, structured and are presented. These datasets have provided key insights into underlying mechanisms of AS01 MoA and the role of observed changes in cell numbers and cytokine concentrations.

Figure 3.3A shows a clear reduction in the number of IFNγ+ NK cells in the dLN after C57BL mice were vaccinated with AS01 + HBS and treatment with aIL12p40, compared

to AS01+HBS alone. Figure 3.3B shows almost an elimination of IFNγ+ NK cells in the dLN in IL18-receptor-knockout mice after AS01+HBS compared to a wild-type C57BL6 mice. The conclusion from [32] is that "AS01-induced accumulation of IFNγ+ NK cells was dependent on both IL18 and IL12". Indeed, accumulation of IFNγ+ NK cells is completely eliminated when IL12 and IL18 are targeted (Figure 3.3D)[32]. The relative contributions by IL12 and IL18 to IFNγ production are yet to be elucidated although these data suggest that IL18's role may be more prominent.

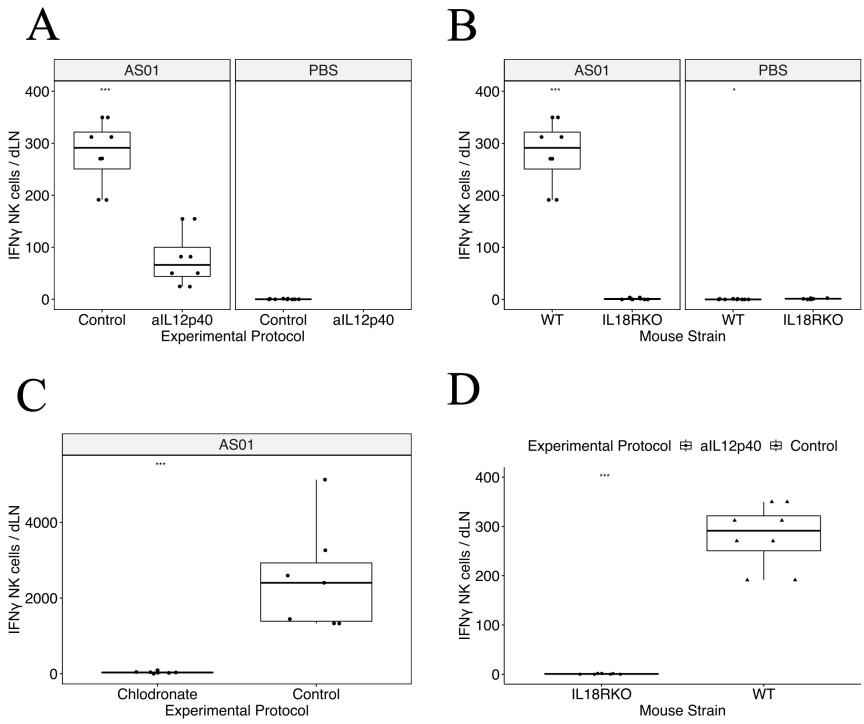


Figure 3.3: **GSK generated experimental data demonstrating mechanisms underpinning early AS01 MoA:** Boxplots showing 6 hour ICS analysis of **A)** IFNγ+ NK cells / dLN after AS01, with a control PBS injection or anti-IL12p40 antibody, and PBS control. **B)** IFNγ+ NK cells /dLN after immunising C57BL/6 WT or Il18-/- mice with AS01+HBS or PBS. **C)** IFNγ+ NK cells after C57BL/6 mice were treated with 20ul of clodronate liposomes or control liposomes i.m and six days later immunised with AS01 and HBS. **D)** IFNγ+ NK cells / dLN after immunising WT or IL18-/- mice with AS01 and treating with anti-IL12p40 antibody or control antibody. All experiments where AS01 was used, employed Hepatitis B surface antigen formulated with 1/10 HD AS01.

GSK additionally determined that the source of IL18 are Subcapsular macrophages, through an experiment where these cells are depleted by clodronate liposomes and the number of IFNγ+ NK cells are assesed. The data are reproduced in Figure 3.3C, showing that depleting SCS-Mo almost entirely blocks the numbers of IFNγ+ NK cells. Any measurements observed following injection with PBS controls, are assumed to represent baseline conditions and - due to the absence of data under naive conditions - are therefore used throughout this thesis as 'zero hour' timepoints.

3.2.2.3 A Core AS01 MoA CellDesigner Diagram to Capture High-Level Biology

Guided by the framework in Figure 3.1, the research context, and the aforementioned experimental data, we began to answer research question 1 (section 1.10.1) - through scoping a joint understanding of high-level AS01 biology between research teams, resulting in one shared model. We defined the derived product describing AS01'a high level MoA, as the Core MoA CellDesigner diagram: *The Core MoA CellDesigner diagram describes only the high-level hypothesis of the interactions underpinning the system, informed by observable phenomena, rational assumption and abstraction. While scoping the high-level interactions, the highly-visual nature of this diagram helps to reduce misunderstandings or miscommunications of the captured biology.*

To create the diagram, we followed a four step process to implement the 'knowledge integration' section in Figure 3.1B:

1. Development of an illustration incorporating current knowledge of how the adjuvant generates an adaptive immune response in a specific (wild-type murine) host.
2. The illustration was used to generate a formal 'CellDesigner' model.
3. An iterative process of 'CellDesigner' model development was followed, to incorporate key team ideas: capturing, refining and extending key aspects of the biology where e.g an insight or idea did not stand up to the logical implications of formalising that idea or insight.
4. The final model was scrutinised, based on team discussions, resulting in a collective understanding agreed by all parties, to generate a single combined model of the adjuvant's MoA.

To develop the AS01 MoA CellDesigner diagram an adapted version of SBGN was utilised, defined in Table 3.2. The table includes only aspects that were changed, so if a symbol is not listed in Table 3.2, it was either unchanged, or not used.

The entire core AS01 MoA CellDesigner diagram (Figure 3.4) illustrates how organ compartments are connected and immune factors interconnect. For legibility, each compartment is presented separately in Figures 3.5-3.8. We set out predominately to capture the detail of the primary response to AS01, although key aspects of a recall response are included. As observed *in vivo*[5], after intramuscular injection of an AS01-adjuvanted vaccine (Figure 3.4A / Figure 3.5) the adjuvant components both activate local cells and drain into the dLN (Figure 3.6 - 3.7) initiating the immune response. In the muscle (Figure 3.4A / Figure 3.5), we propose the abstracted hypothesis that MPL and QS21 activate a 'muscle-resident immune cell', which through chemokine secretion, recruits CCR2+ Ly6C-hi monocytes from

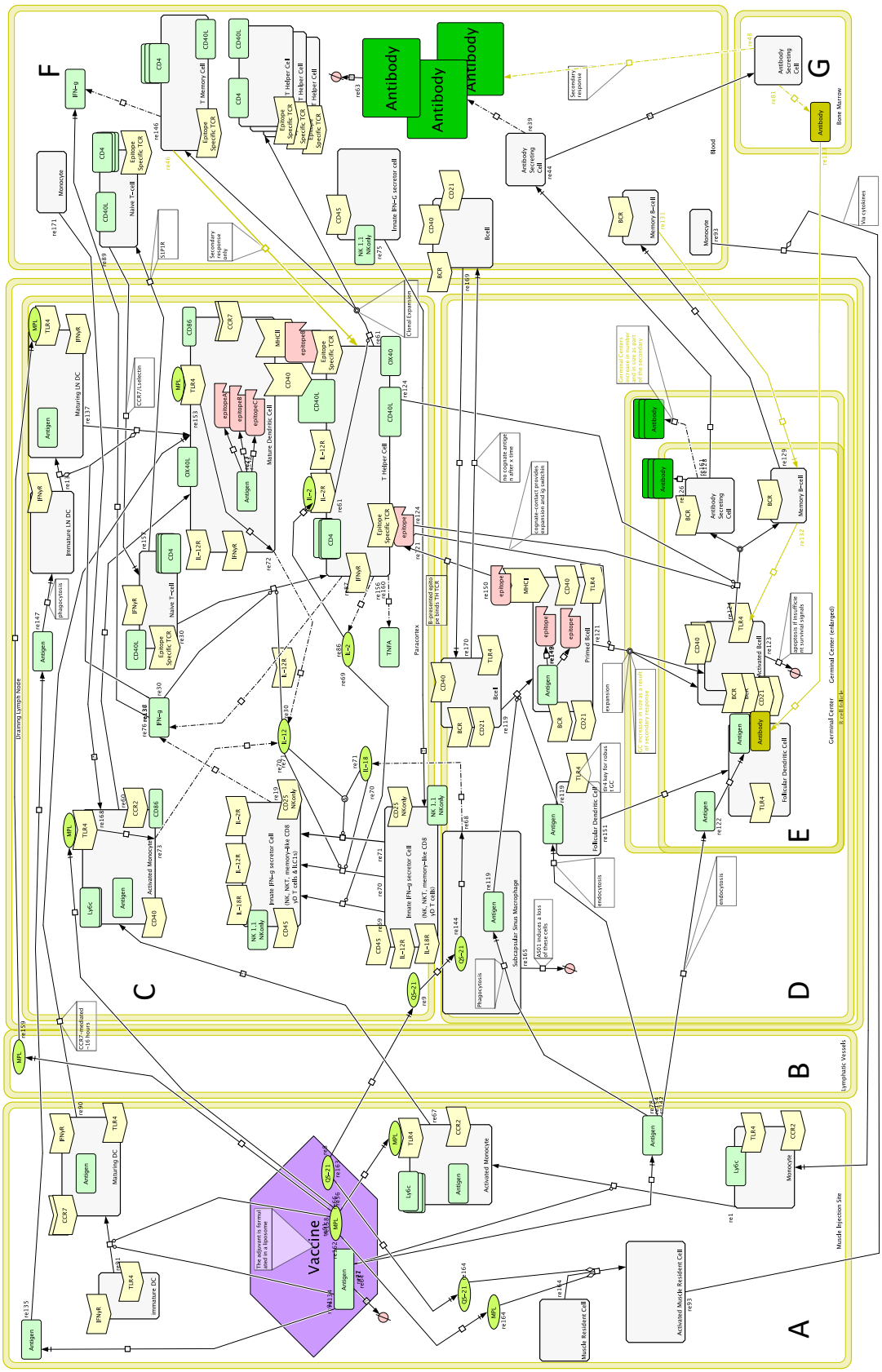


Figure 3.4: **A core mechanism of action model:** Figure reused from [7] within permissions. **A)** depicts the muscle injection site, where the vaccine components are hypothesised to activate muscle-resident cells, initiating the local immune response resulting in the recruitment of monocytes into the muscle. **B)** depicts the lymphatics where components and cells transport through toward the dLN. **C)** depicts the dLN paracortex. **D)** depicts the dLN follicles. **E)** depicts a Germinal Center. **F)** depicts the blood. **G)** depicts the bone marrow. The colour yellow is used to distinguish elements of a secondary immune response.

Symbol Type	**Original Use**	**Adapted Use**
Compartment	Cell membrane	Organ
Complex	Organelles	Cell Types
Protein	Protein	Protein
Transport	Intracellular Transport	Cellular Migration or Protein Diffusion
Cell Receptor	Cell Receptor	Membrane Receptor
Simple Molecule	Simple Molecule	Extracellular Molecule (cytokine or vaccine component)
Catalysis	Reaction Catalyst	Positive inter or intracellular modulation
Unknown Transition	An unknown transition	A transition without direct evidence
Translation	Protein Translation	Cytokine Secretion
Modulation	Modulation	Potentially positive and negative modulation
Boolean logic gate AND	Boolean logic gate AND	Synergy between model entities
State transition	State transition	Cellular differentiation
Truncated Protein	Truncated Protein	Epitopes
Degradation	Degradation	Apoptosis or protein/antigen decay
Dissociation	Dissociation	Clonal Expansion

Table 3.2: Adapting the Systems Biology Graphical Notation for the description of intercellular biology.

the blood into the injection site. We propose that monocytes can be activated by MPL [274]. After MPL stimulation and/or antigen capture monocytes migrate into the dLN. Monocyte migration into dLN has been directly observed using lymphatic cannulation in an ovine (sheep) vaccination model following AS01-adjuvanted vaccination [46]. Although it is hypothetically possible that monocytes can infiltrate injection site draining LNs from HEVs, there is no biological data to indicate that occurs *in vivo* after AS01 and it is improbable that it would impact on kinetics, thus the possibility has not been included in the model.

Muscle-resident DCs (Figure 3.4A / Figure 3.5) can be activated by MPL and/or antigen and subsequently undergo maturation[95]. We distinguish key stages of DC maturation as separate entities: 'immature DC', 'maturing DC' and 'mature DC'. Here, we propose that immature DCs express TLR4 and IFNγ-receptor, and that maturing DCs additionally express CCR7 (which mediates migration from tissue to the LN paracortex[103]) and co-stimulatory molecules (CD80/86), IL12 receptor and vaccine peptide antigen-MHCII (pMHC) complexes.

In addition to the migration of DCs and monocytes into the LN, we captured the observation that AS01 and antigen free-flow from the injection site through the afferent lymphatics (AL) (Figure 3.4B) into the dLN [5]. After arrival in the dLN, it is known that QS21 co-localises with CD169+ SCS-M, (Figure 3.4D/3.7D) and can induce IL18 secretion from these cells [8]. Secreted IL18 delivers an activation signal to 'innate IFNγ secretor cells' (ISC) [32] (Figure 3.4C / Figure 3.6C). This ISC cell type is an abstraction to promote

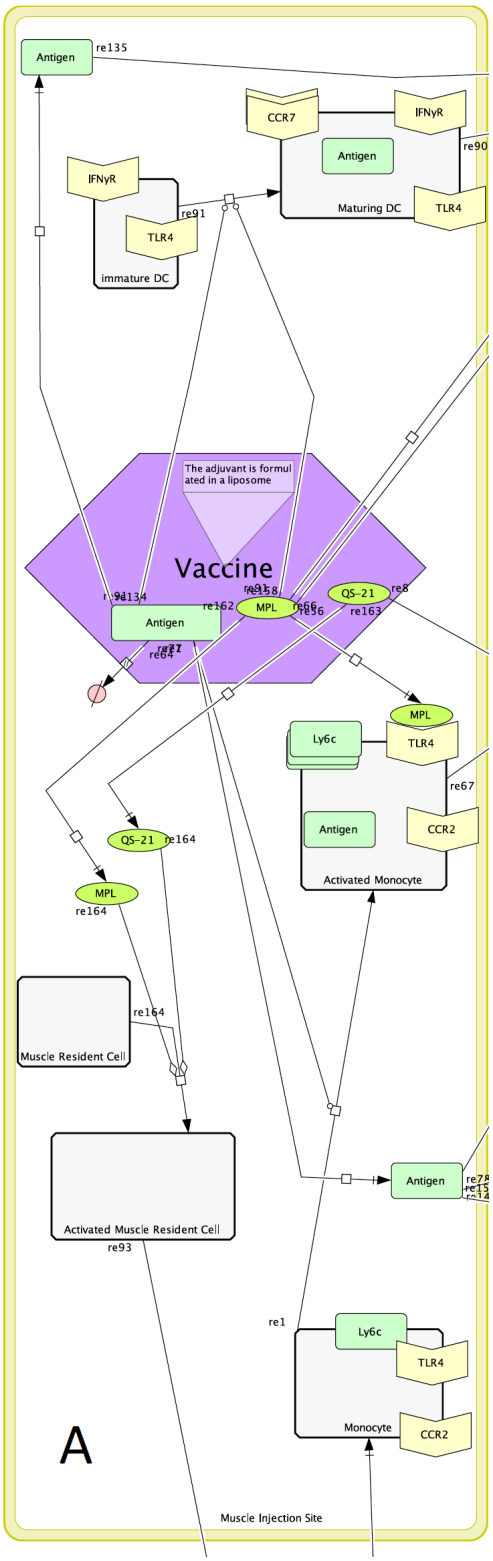


Figure 3.5: **A core mechanism of action model: section A only - the 'Muscle Injection site'.** Vaccine (purple) components are inoculated into the muscle, where the individual components (Antigen, QS21, MPL) activate a muscle-resident cell, which promotes the recruitment and activation of monocytes, and the beginning of maturation for DCs. All three vaccine components freeflow into the lymphatics compartment B, and finally into the dLN (C,D).

simplicity, encompassing cells, primarily NK, which have been shown to contribute to innate production of IFN after AS01 stimulation of the immune system [32]. IL18 stimulation of ISCs is capable of promoting the production of IFN, augmented by IL12 [32]. During a secondary response, we propose that IFNγ initiation may be supplemented by IL2 derived from antigen-specific CD4+ T cells, further promoting synergistic production of IFN.

We propose that SCS-M (along with follicular dendritic cells) can capture free-flowing antigen, and transfer it to B cells in the follicle [272], contributing to their priming (Figure 3.7E). As observed *in vivo* after AS01, the model describes the capacity of activated monocytes to differentiate into DCs [15] (Figure 3.6C). Ourselves and GSK immunologists hypothesised that IL12 is secreted by a pool of DCs (including monocyte-derived-dendritic-cells (MoDCs)) and activated monocytes, which is captured in the model. At early time points, IFNγ and IL12 are thought to promote differentiation of Naïve cognate CD4+ T-cells towards a T Helper 1 (Th1) polarisation [275]. We capture T Helper cells in the model, although an abstraction is made at this level for diagrammatic simplicity. Indeed, the cell is a single entity, where no distinction is made between Th subsets. In the lower-level models, distinctions between phenotype of these cells are captured. Here, the Th cell provides expansion, immunoglobulin switching and survival signals to B cells, or secretes Th1-associated cytokines (TNF-α, IL2, IFNγ). We also captured key stages of antigen-specific B cell priming, activation, and differentiation into 'antibody-secreting-cells' or memory B cells, and the formation of germinal centers (Figure 3.4D/E and Figure 3.7). Additionally in the blood compartment (Figure 3.4F / Figure 3.8) we described the circulation of Th subsets after lymph node egress, and antibody circulation. The remit of the modelling exercise only required the capture of the generation of T cell and antibody responses, and not the quality or functionality of the antibody response, nor the characteristics of the T cell response in peripheral tissues, thus these are not modelled.

The Core AS01 MoA CellDesigner model is a platform to communicate ideas and scopes the broad requirements for remaining Domain Model development. This model can be additionally used for knowledge retention: e.g Ensembl and UniProt ID's were stored in the notes for each entity. Pubmed ID's were also stored to evidence the modelling decisions.

3.2.3 Extending the CellDesigner Model to Substantiate the Proposal of AS01 MoA

The 'Core AS01 MoA CellDesigner Diagram' visualised high-level AS01 MoA and supplied a platform for communication between research teams. This comprises the first product of our Domain Model. However, to form a basis for simulation construction, the Domain Model should additionally detail lower-level behaviours, functions of- and interactions between-

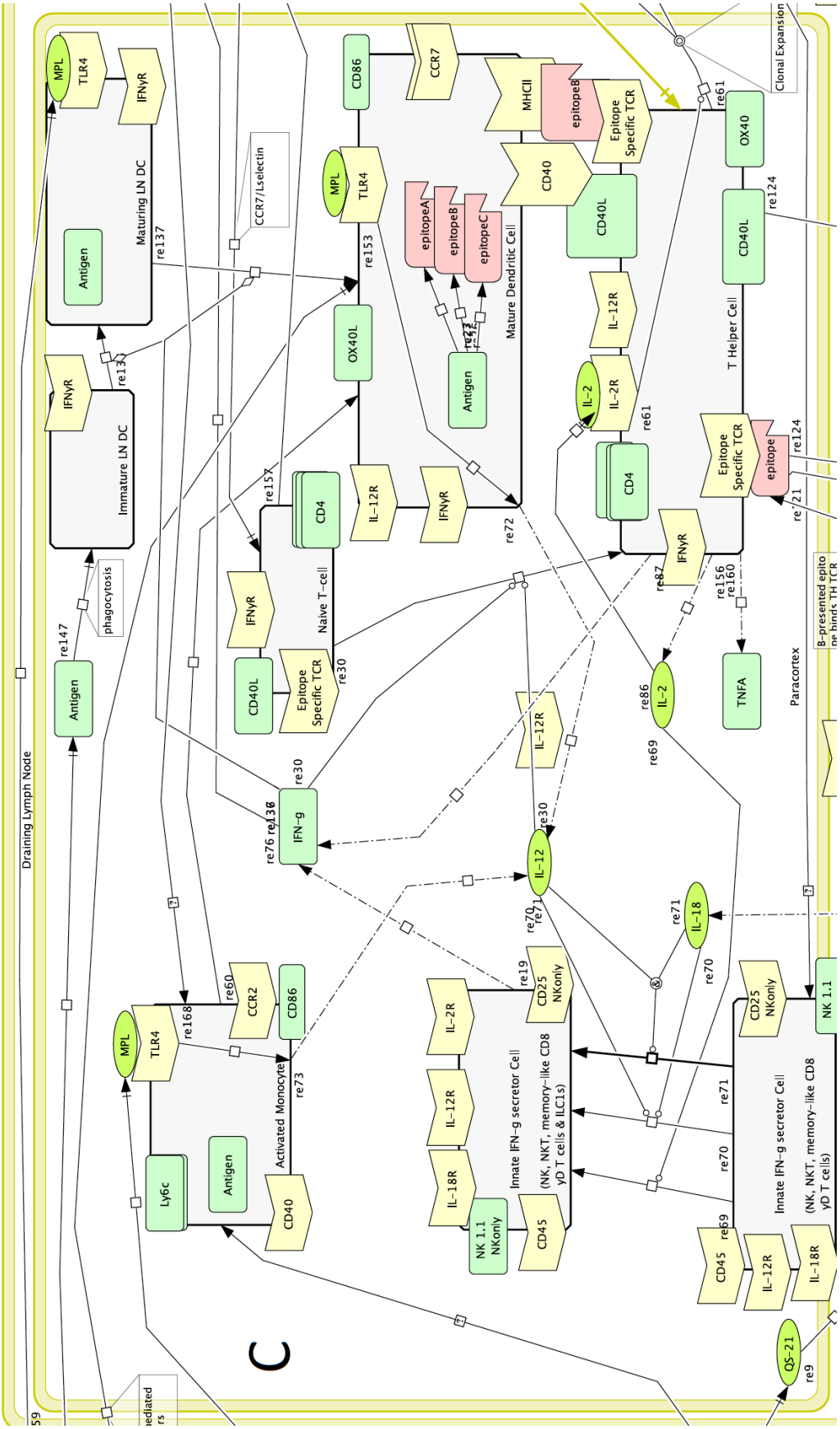


Figure 3.6: **A core mechanism of action model: section C only - the Paracortex.** Monocytes arriving from the lymphatics can secrete IL12, as can arriving activated DCs, and resident DCs that have been activated. This IL12 - along with IL18 - promotes the production of IFNγ from 'IFNγ producing cells'. T cells are activated by Mature DCs in the Paracortex. After activation T cells can proliferate and leave the dLN.

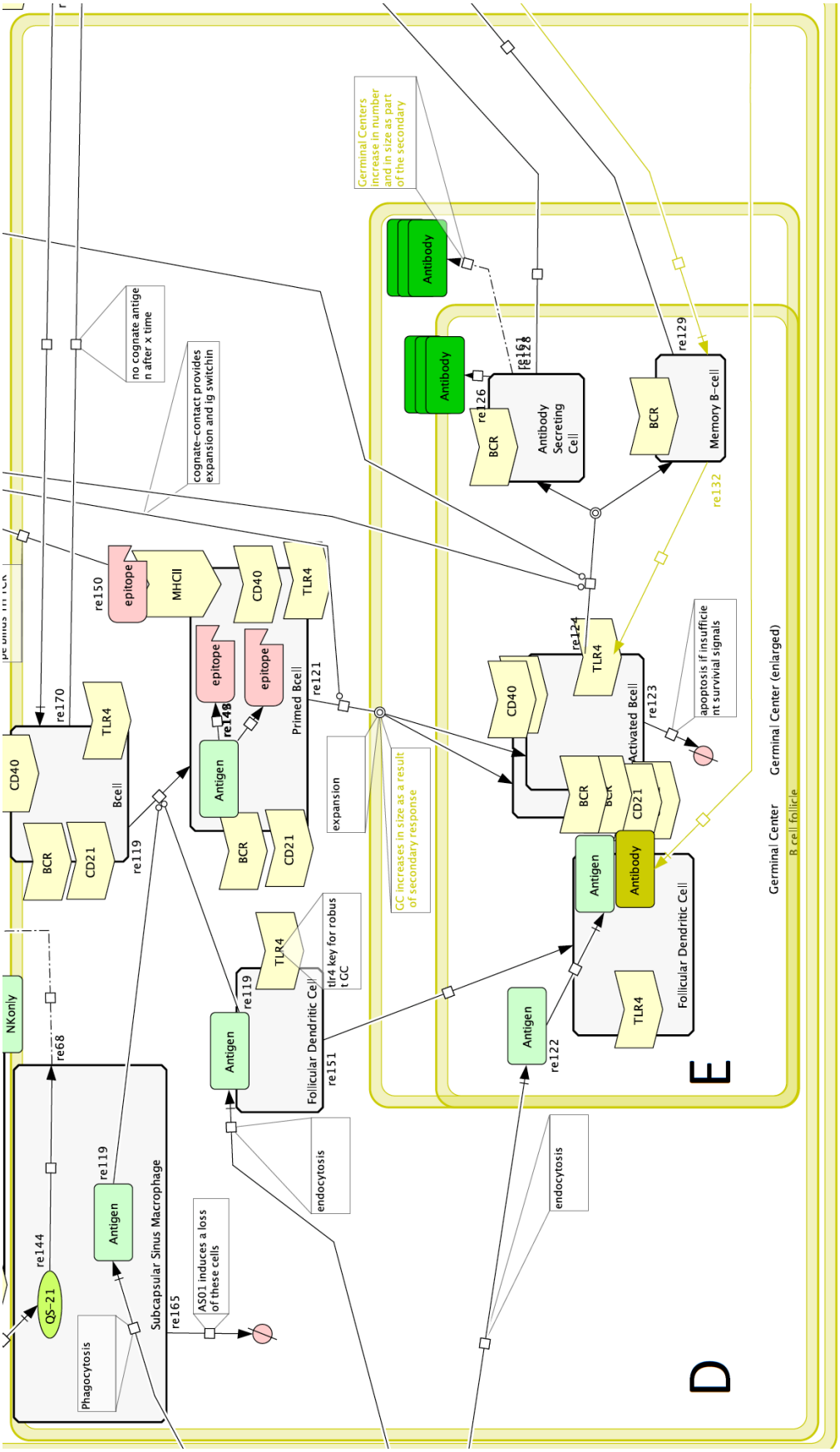


Figure 3.7: **A core mechanism of action model: sections D and E only - the B cell follicle and Germinal Center.** On the edge of the subcapsular sinus and the B cell follicle, are subcapsular sinus macrophages which can secrete IL18 after activation by QS21. IL18, along with IL12 synergistically promotes the production of IFNγ. SSM can transfer antigen to the B cell follicle. FDCs can also present antigen to B cells such that B cells can be primed. B cells form Germinal Centers (E) where they can become fully activated and differentiate into antibody-secreting-cells and Memory B cells.

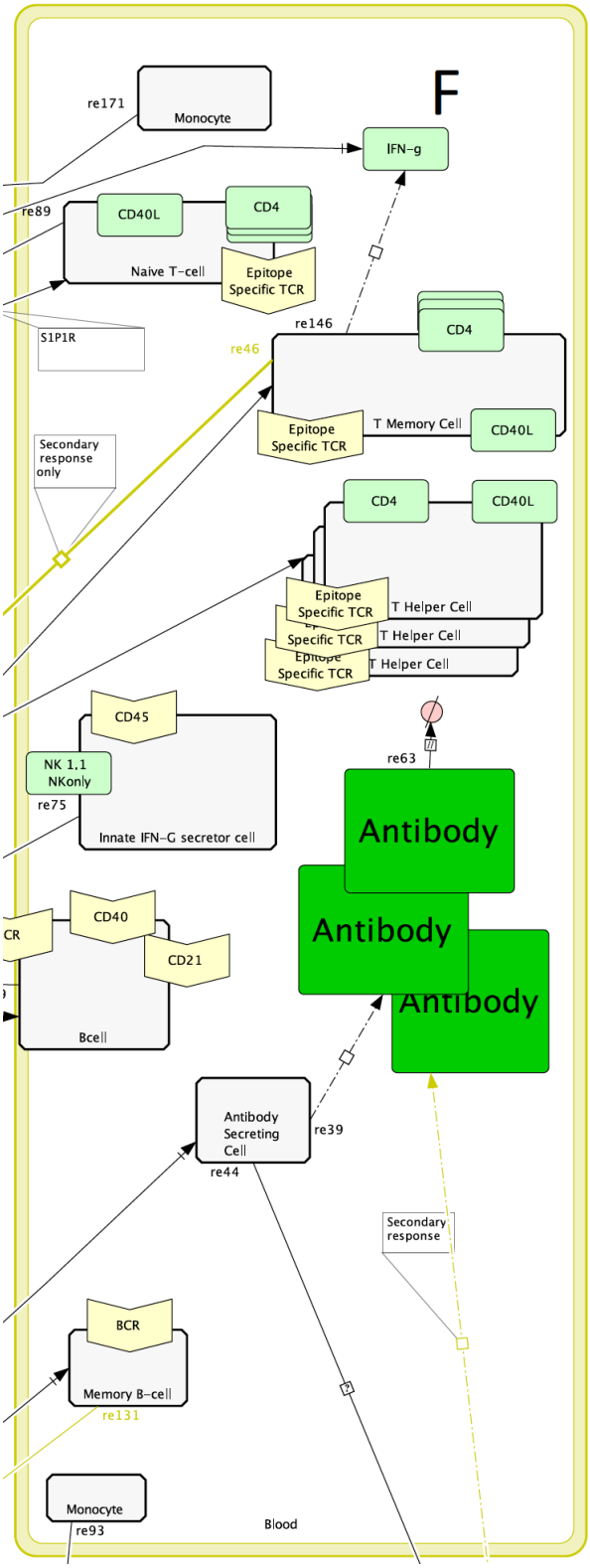


Figure 3.8: **A core mechanism of action model: section F only - the Blood.** Naive T cells that do not experience their cognate antigen re-enter the blood stream. Further, after activation, Effector T Helper and T Memory cells can leave the dLN and circulate in the blood. ASCs and Memory B cells circulate through the blood after dLN activation.

model components. The careful examination of immune function required to develop such models, can also identify logical inconsistencies with the current understanding, as well as reveal further knowledge gaps. Therefore, with our research questions in mind, we substantiated the Domain Model by extending the CellDesigner model, through the development of Expected Behaviours- State-Machine- and Activity-Diagrams. Care must be taken to capture the relevant biology, and where abstractions are made, these were decided to be appropriate and decisions behind inclusion and exclusion of functionality and rationale for abstractions were clearly documented to maintain a trail of the considerations involved. Rigorous documentation enables transparency of the decisions behind model development.

3.2.3.1 Defining Expected Behaviours

The 'Expected Behaviours' diagram (Figure 3.9) builds upon the CellDesigner model presented in Figure 3.4, linking temporal data with proposed mechanistic function (section 2.2). This diagram defines the research context and phenomena that is observed through experimentation, and summarises hypotheses for how these phenomena are thought to manifest. Through aggregation of these individual interactions, system-wide behaviours that are not intuitively understood from the defined interactions alone may begin to emerge. To improve aesthetics, some hypotheses have been simplified for this diagram. Here, we define expected behaviours occurring over the first seven days of the response:

Thirty Minutes Post Injection (Figure 3.9A): it is observed that the majority of QS21 and antigen remains in the muscle interstitium, although QS21 and antigen are detected in the dLN at this timepoint [15]. Thus we hypothesised that firstly, vaccine components - MPL and QS21 - have activated cells resident in the muscle injection site, and secondly, antigen, MPL and QS21 have flowed rapidly through the lymphatics into the dLN.

Three Hours Post Injection (Figure 3.9B): Higher levels of vaccine components are observed in the dLN than at thirty minutes post injection [15]. QS21 has co-localised with CD169+ subcapsular sinus macrophages. IFNγ has risen to approximately 80 pg per dLN, which coincides with an increase in the numbers of IFNγ+ NK cells [32]. Thus we hypothesised that QS21 has been captured by CD169+ SCS macrophages, resulting in the release of IL18, which is synergising with IL12 to promote the production of IFNγ. Additionally we hypothesised that IL12 is produced by DCs[69] and/or monocytes, after stimulation by MPL. Moreover, we capture infiltrating monocytes from the injection site.

Six Hours Post Injection (Figure 3.9C): IFNγ levels in the draining lymph node peak at approximately six hours post injection, as do the numbers of IFNγ+ cells. Monocyte and MHCII+ DC numbers in the dLN are at approximately 12,000 and 13,000 respectively. We therefore hypothesised that monocytes are infiltrating the dLN, resident DCs are becoming

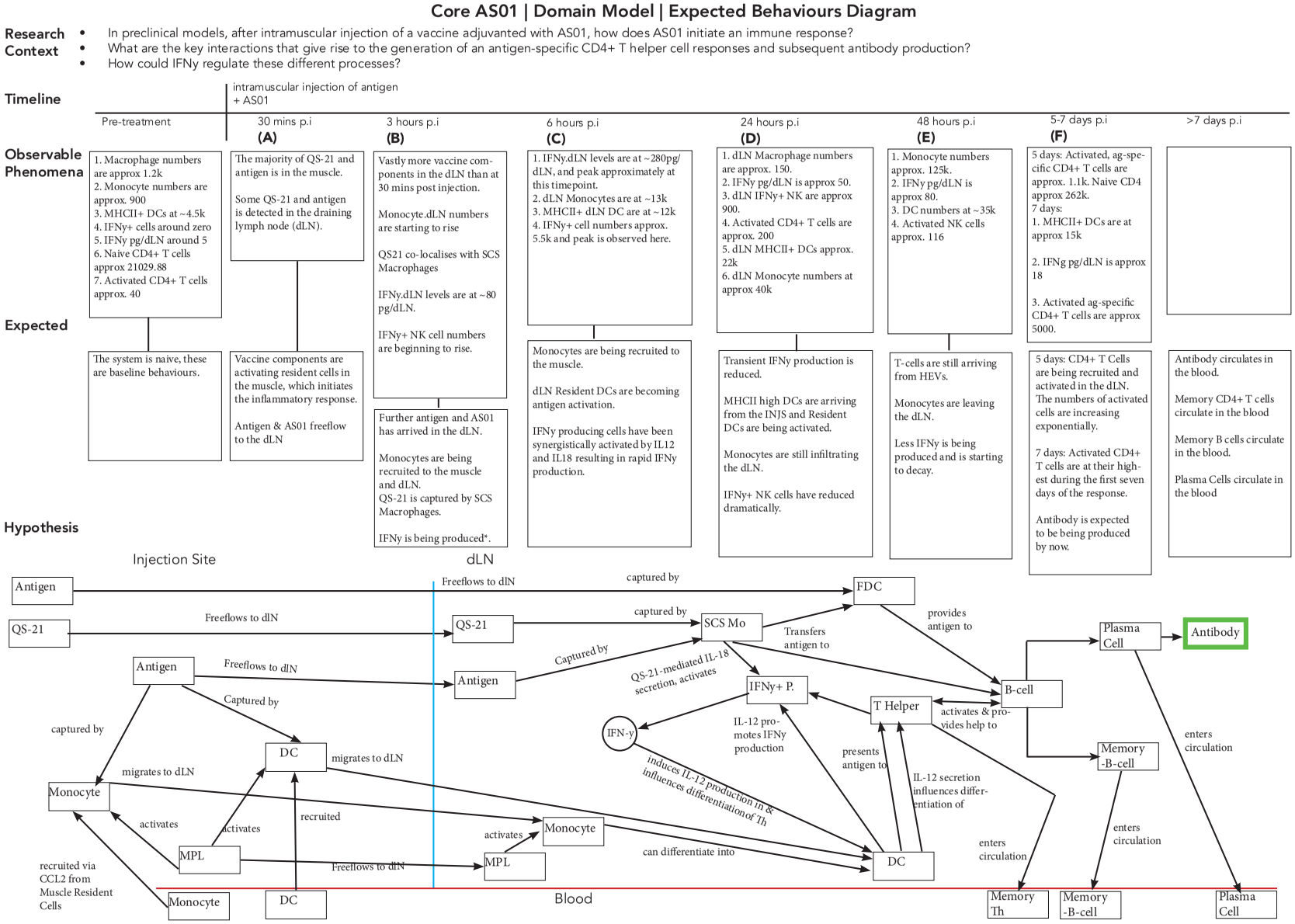


Figure 3.9: **Defining 'Expected Behaviours':** This diagram describes the research context, based on the exploration of the core AS01 MoA, linking the observable phenomena over the first seven days of the response to AS01 with the hypothesis that is thought to cause these phenomena to manifest. Geometric mean is used for averages.

activated and a small quantity of monocytes are differentiating into DCs. As observed *in vivo*, we describe IFNγ production that peaks approximately at this timepoint [32].

Twenty Four Hours Post Injection (Figure 3.9D): Macrophage numbers have dropped dramatically to approximately 150 cells after QS21 inoculation [8]. It is unclear whether these cells downregulate biomarkers or perhaps undergo pyroptosis. To appreciate this ambiguity, we hypothesised that QS21 mediates a 'loss' of these cells. In the dLN, IFNγ is approximately 47 pg/dLN, and levels of IFNγ+ NK cells are approximately 900. We hypothesise that this reduction in IFN is due to a combination of autoinhibition and/or decay [276]. Activated CD4+ T cells are beginning to rise marginally and MHCII+ DCs have increased to approximately 22k. MHCII$^+$ DCs will be arriving from the injection site by this timepoint, as well as resident DCs becoming activated thus augmenting DC numbers. It is expected that in small numbers, Naive CD4+ T cells have been primed by DCs and are undergoing activation by this time point.

Day Five to Day Seven Post Injection (Figure 3.9F): antigen-specific (2W1S+)[1] CD4+ T cell numbers are at approximately 1100 at day 5 *(Gajdasik 2019, unpublished)*. We thus hypothesise that by day 5, Naive CD4+ T cells are being activated and are proliferating. At seven days post injection, antigen-specific CD4+ T cells are approximately 5000 - the highest level during the first seven days of the response *(Gajdasik 2019, unpublished)*.

The expected behaviours diagram therefore integrates phenomena observed from experimental data, temporal context of these observations, insight yielded from the phenomena observed, as well as hypotheses for mechanisms underpinning such insights.

3.2.3.2 State-Machine Diagrams

Following development of an Expected Behaviours diagram, State-Machine diagrams were produced. These diagrams build on experimental insight by integrating known mechanistic function (gleaned from the experimental data) with the above hypotheses regarding functionality captured in the expected behaviours diagram. These descriptions take the form of detailing states for which each model component can exist in, and of interactions which govern transitions between these states. These State-Machine diagrams thus substantiate the Expected-Behaviours diagram as well as the 'core AS01 MoA CellDesigner' diagram. In what follows, I narrate salient elements captured in the diagrams. Select diagrams are presented here through the text, while some remaining diagrams are in Appendix A and referred to here. The entire model - including immune components less pertinent to the subsequent work in the thesis - is described in Supplementary 'AS01 Core Model' (please see Appendix A.4 for the link).

[1] 2W1S is a listeria monocytogenes antigen.

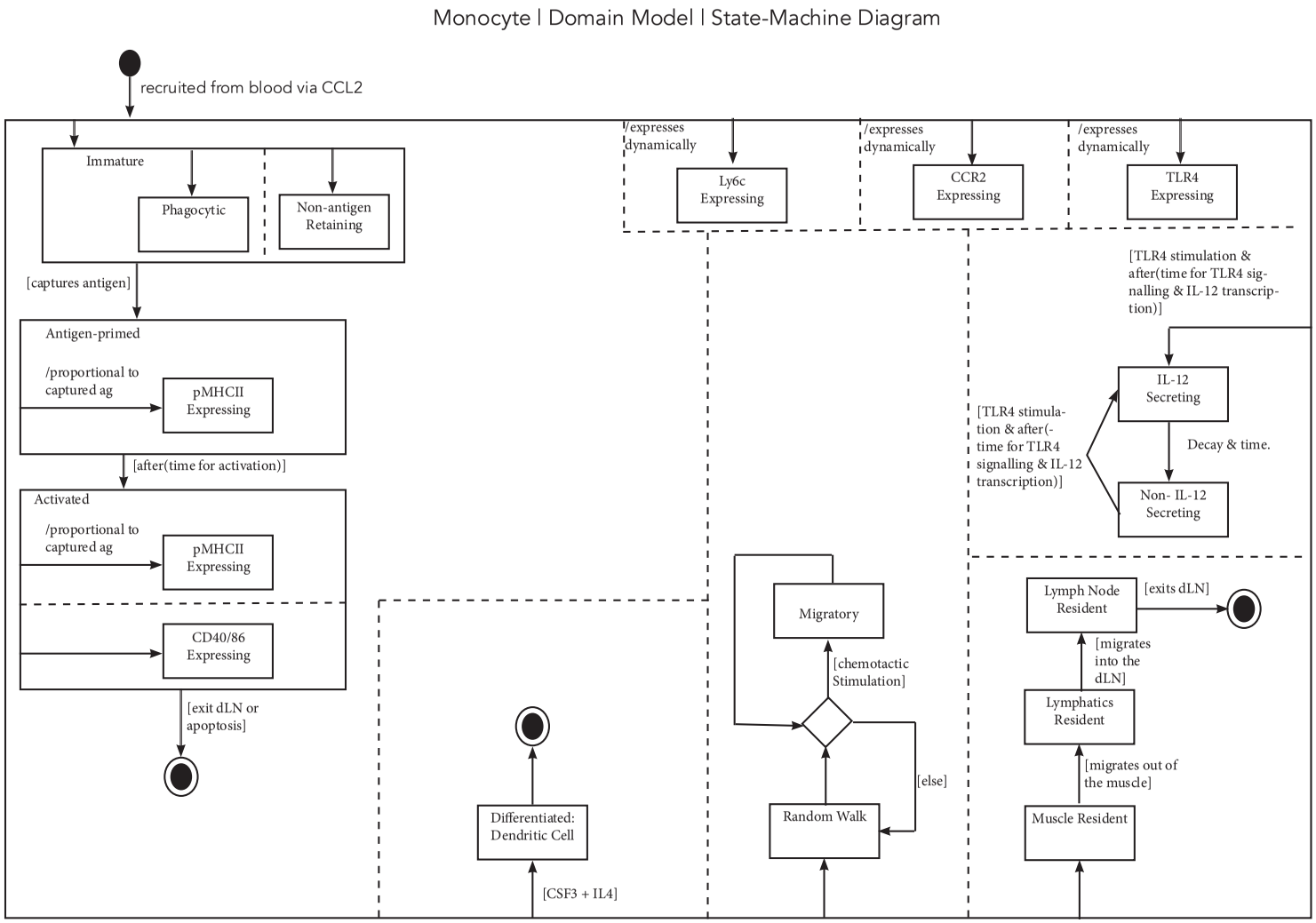


Figure 3.10: **A monocyte State-Machine Diagram:** Using UML, the diagram describes the hypothesised function of monocytes after AS01-adjuvanted vaccines.

The 'muscle-resident cell' entity (Figure A.1) is an abstraction to capture the hypothesis that a cell resident in the muscle - such as macrophages, Skeletal Muscle and/or Endothelial Cells - initiates the immune response through secretion of cell-recruitment factors. The cell is resident in the muscle and is recruited at a rate that maintains equilibrium. Muscle-resident cells are initially in a 'Resting' state. After stimulation from AS01 immunostimulants, they adopt a 'Secreting innate-cell-recruitment factors' state. The innate cell recruitment factors (such as CCL2, CCL3, CXCL8/IL-8 etc) secreted from these cells can recruit neutrophils and subsequently monocytes [277, 278, 97, 60, 46] into the injection site. Muscle-resident cells can return to a 'Resting' state if they receive anti-inflammatory signals or lack sufficient further stimulation.

Monocytes enter the system from the blood and are recruited via CCL2 (Figure 3.10). Monocytes are initially in a 'Immature' parent state, comprising two sub-states: 'Phagocytic' and 'Non-antigen retaining', where the cell can phagocytose antigen, but hasn't captured any yet. Monocytes adopt the 'Antigen-primed' parent state if they capture antigen, whilst also entering the 'pMHCII expressing' [46] state. After the time required for activation, monocytes enter an 'activated' parent state, comprising two sub-states: 'pMHCII expressing', and 'CD40/80 expressing'. Monocytes exit the system if they exit the dLN, or receive signals to undergo apoptosis. Concurrently, a monocyte can undergo differentiation to a DC if the cell receives specific cytokine stimulation [279]. Simultaneously, monocytes are initially in a 'Random Walk' state. However, if they receive chemotactic stimulation, they adopt a 'Migratory' state. This can permit their migration from the muscle injection site, through the lymphatics, into and around the dLN and to exit the dLN [46]. Simultaneously to all prior behaviour, if the monocyte receives TLR4 stimulation, monocytes can begin to secrete IL12 [280, 67]. Monocytes can return to a 'Non-secreting IL12' state if they do not receive further relevant stimulation over time.

For dendritic cells, we capture an abstraction which represents a pool of DC subsets (including MoDCs) (Figure A.3 and [7]). DCs enter the system resident in either the injection site or in the dLN. Initially, the cell is in an 'immature' state, and is therefore in the 'Phagocytic' substate, and the DC doesn't possess antigen [281]. Following antigen capture, and/or stimulation by a TLR4 agonist, the cell adopts the 'maturing' state, where it exhibits varying phagocytic capacity, increased expression of pMHCII complexes and CCR7, CD80/86. Here, as hypothesised, the cell can secrete IL12 [282, 283, 284]. The increased expression of CCR7 allows the cell to chemotactically migrate towards CCL19/21 gradients in both draining lymphatics and dLN paracortex. When a DC is fully mature, it is not phagocytic, expresses high levels of pMHCII complexes, CCR7, CD80/86, and can secrete IL12. During all life stages, this cell dynamically expresses CD11c, and TLR4. Mature DCs

can also present antigen to T cells. The cell exits the system if it undergoes apoptosis. The CD169+ F4/80$^-$ macrophage (Figure A.2) is resident in the dLN subcapsular sinus at time zero. It is in a 'sessile' state and expresses TLR4 at all stages of its captured life cycle. It is initially in an 'Immature' state, which comprises two sub-states: 'Phagocytic' and 'Non-antigen-retaining'. If the cell captures antigen, the cell adopts the 'Antigen-primed' parent state. Whilst the cell is 'Antigen-primed', it is 'Phagocytic' and 'Antigen-expressing'. After the time it takes for full activation, the cell adopts the 'activated' parent state, where it is only 'Antigen Expressing' i.e it has ceased to be phagocytic. Simultaneously, if the cell experiences QS21 stimulation, and caspase-1 activation occurs, IL18 is released from these cells. As a result of AS01 stimulation, there is some probability *p(SSM cell loss)* that this cell enters the 'Cellular Loss' state, in which it subsequently leaves the system. The mechanism underpinning this cell loss remains to be elucidated *in vivo*.

The IFNγ producer cell is an abstraction to capture multiple cell types which have been demonstrated to secrete IFNγ after vaccination with AS01 [32] (Figure A.4). IFNγ producer cells enter the dLN via HEVs, or are resident at time zero in the medulla or paracortex. Initially, they are in a 'Inactive' parent state which comprises two sub-states: 'CXCR3 expressing', and 'CCR7 expressing' [285, 31]. If an IFNγ producer cell receives 'sufficient activation signals', the cell can enter an 'activated' state. The 'activated' state comprises various substates [52], where they additionally express CXCR3 and CCR7. The cell is initially 'Non-proliferative' however if it receives IL15 stimulation, this cell can begin to proliferate [286]. Whilst in an 'activated' state, following stimulation by any combination of IL12 and/or IL18 and/or IL2, this cell can produce IFNγ [32, 287].

Despite the name, this 'Naive CD4+ T cell' entity (Figure A.5) describes states of a CD4+ T cell, from naivety through stages of its activation, until it undergoes differentiation into a fully activated cell, anergy or apoptosis [288, 114, 289, 290, 113]. As well established, we captured that Naive CD4+ T cells enter the dLN via HEVs from the blood. During naivety, the cell expresses IL12R, IFNγR, CD28, its TCR, and CCR7. If its TCR binds a cognate pMHCII, it forms a complex with the APC and the CD4+ T cell enters the 'Partially activated' state. If the cell receives stimulation of CD28 by CD80/86, it can adopt an 'activated' state, else it becomes 'Anergic' and exits the system. After entering the 'activated' state, this cell also enters sub-states 'Proliferative', 'IL2R expressing', and 'In a Complex with APC'. During activation, if the cell is in an 'IL12 and IFNγ' or 'Tfh cytokine' dominated environment, it can transition into a 'Th1/Tfh T Helper cell' (described below). Otherwise, the cell adopts the 'Differentiated: Other T Helper cell' state, and exits the system. 'Th1 / Tfh T Helper' cells enter the system after differentiation from a Naive CD4+ T cell (Figure A.6). Initially, this cell is in a 'Primed' state. If the cell has received

IL12 and IFNγ stimulation, it adopts the 'Th1' parent state thus becoming a Th1 cell, otherwise, if it receives 'sufficient Tfh cytokine stimulation' it enters the 'Tfh' parent state, becoming a Tfh cell [291, 292]. Th1 cells can secrete IFNγ, TNF-α, and IL2. If a Tfh cell interacts with a cognate B cell, it adopts the 'providing signals' state, where it attempts to provide survival signals to the associated B cell. At some rate, both Th1 and Tfh cells become 'Memory Th cells'. Simultaneously to all states, this cell is in a 'Membrane S1PR expressing' state - the expression of which increases throughout time spent in the dLN [293]. Increased expression of SIP1R eventually permits T cell exit from the dLN. Simultaneously to all prior states, this cell is in 'CD40L expressing' and 'IL2R Expressing' states. Further, if IL2 sufficiently binds IL2R expressed on this cell, it enters a 'Proliferative' state. Memory T cell, B cell, FDCs, antibody-secreting cells and Memory B cell state and activity diagrams are described in Supplementary 'AS01 Core Model'.

3.2.3.3 Activity Diagrams

To avoid repetition after description of the State-Machines, salient activities are described briefly.

Monocytes enter the system after being recruited into the injection site via CCL2 (Figure 3.11). Initially, they survey the environment and can become 'antigen primed' if they encounter antigen. Whilst 'antigen-primed', monocytes will continue to phagocytose antigen, express pMHCII on their surface, and express CD40/86. Once the cell has captured 'sufficient' antigen, it ceases to phagocytose antigen. Concurrently, monocytes can begin to secrete IL12 if TLR4 is stimulated by an agonist. Furthermore, monocytes are capable of differentiating into DCs after receiving the appropriate stimulus.

Following exposure to antigen, and/or stimulation by a TLR-4 agonist, a DC can begin maturing, as described in the state-diagrams, and can eventually become fully mature (Figure A.7). SCS macrophages (Figure A.8) can undergo four - potentially concurrent - scenarios, although if a scenario involves a 'stop' - i.e exiting the system - then all concurrent activities are ceased (Figure A.13). **1)** If the cell captures antigen, it can present this antigen on its surface. **2)** If there is QS21 mediated activation of caspase-1, the cell can release prestored IL18. If there is further stimulation it can dynamically secrete IL18. **3)** The cell can receive apoptosis or pyroptosis signals and leave the system. **4)** If the cell receives stimulation by AS01 and some probability *p(SSM cell loss)* is evaluated, the cell can exit the system. The 'IFNγ Producer cell' enters the system via HEVs, or is resident upon vaccination in the medulla or paracortex - expressing CXCR3 and CCR7 (Figure A.9). Initially the cell surveys the environment, and if the cell receives sufficient activation signals, it can begin activation and secrete IFNγ. If a 'Naive CD4+ T cell' receives chemotactic stimulation,

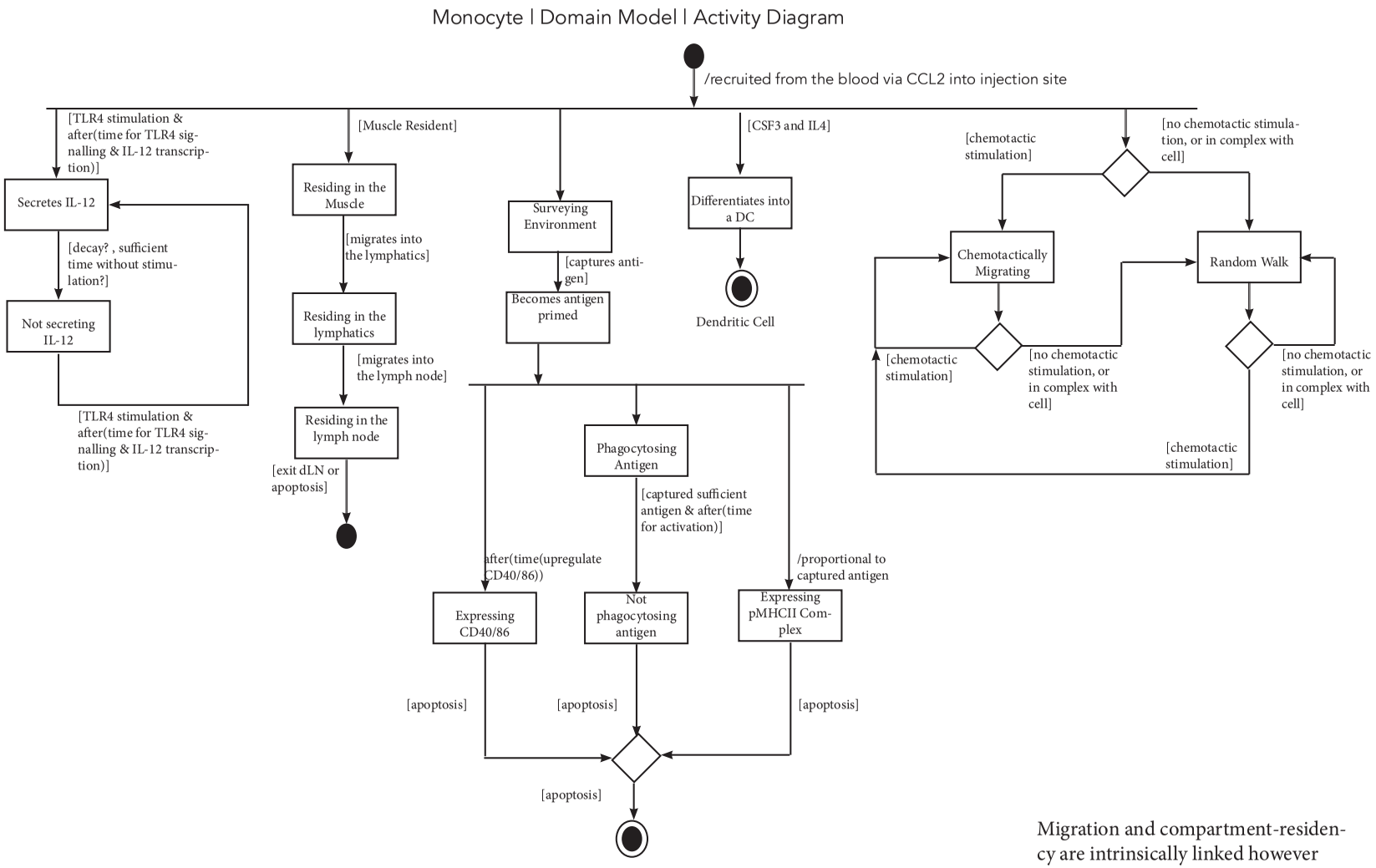


Figure 3.11: **A monocyte Activity Diagram:** Activity Diagrams describe actions of model components and their interactions with other components.

it can begin to chemotactically migrate, otherwise it continues to undergo a random walk (Figure A.10). If the cell comes into contact with a cognate APC, and there is appropriate TCR stimulation by antigen, the Naive CD4+ T cell can become activated, differentiate or become angeric. The 'Th1/Tfh T Helper cell' cell enters the system after differentiation from the Naive CD4+ T cell. If the cell receives, or has received sufficient IL2 stimulation it can begin proliferating (Figure A.11). Here, Tfh activities involve upregulation of CXCR5 and downregulation of CCR7. Dominating CXCR5 expression over CCR7 directs the cell towards the CXCL13 gradients in the B cell follicle, permitting contact with B cells. Here, the B cell can cyclically provide expansion and Ig switching signals to antigen-primed B cells. Additionally, the cell can provide survival signals to B cells in a Germinal Center. Th1 activities involve cytokine secretion, and differentiation into a Memory Th cell. Lastly, both Tfh and Th1 activities depict an ability to exit the dLN.

In summary, a novel Domain Model of AS01 MoA has been formulated to address research question 1 (section 1.10.1), developing a holistic proposal for how AS01 initiates and maintains an immune response. Naturally, the work described in this chapter - asking questions about a domain of interest and proposing a Domain Model - revealed and consolidated knowledge gaps, for which we formulated novel hypotheses. These knowledge gaps and hypotheses are littered throughout the chapter. Select knowledge gaps of interest as identified by this work, and formally represented as thesis research questions 2-8 (shown previously in section 1.10.1).

3.3 Discussion

As scientific problems have become more challenging and technology has become more advanced, collaboration between disciplines has increased dramatically. Today, approximately 90% of science and engineering publications are written by more than two authors and many articles are authored by 6-10 writers from more than one institution [294]. 'Team science' has enabled important scientific breakthroughs, from work which enabled the first black hole image [295, 296], to developing life-saving vaccines against SARS-CoV-2 [297]. However, interdisciplinary research naturally presents challenges surrounding communication and integration of expertise. In the current study, we considered it imperative to evolve a framework to guide and streamline research between groups. We found the rigorous process encapsulated by the framework described here, combined transparency and scrutiny through team science to generate confidence in the Domain Model of AS01 MoA. The development of this model brought together key expertise and focused our efforts on asking appropriate questions, by revealing high priority knowledge gaps - resulting in further, more specific

research questions (section 1.10.1), which are subsequently explored by Chapters 4, 5 and 6 of this thesis.

To our knowledge, this thesis presents the first mechanistic modelling efforts in order to explore AS01 MoA. However, in recent years, top-down systems-based analyses have shed light on adjuvant MoAs. For example, microarray analysis has recently been used to determine differences in transcriptional programming between Alum and MF59 [298]. Additionally, systems analysis has been utilised by GSK Vaccines to explore immune responses in humans receiving three doses of RTS,S/AS01 [299]. Transcriptional signatures were examined, and gene-set-enrichment-analysis exploring blood-transcription-modules (BTMs) aimed to characterise functional pathways altered by vaccination with RTS,SAS01. Collectively, their data indicate that protective immunity observed with RTS/AS01 is developed through accumulation of high levels of anti-circumsprozoite antibodies. Their data show that cell-cycle, plasma cells and B cell BTMs correlate with immunogenicity and protection against Malaria [298]. In comparison to 'top-down' approaches, mechanistic modelling aims not only to integrate and consolidate mechanistic information to identify salient processes underpinning a complex system, but also to predict system behaviours and generate novel hypotheses.

This chapter supplies the community with the most detailed model to-date of AS01's mechanism of action. Insights from experimental data have been integrated with wider immunological literature and detailed hypotheses to fill knowledge gaps, producing the first novel, holistic model of AS01s MoA. This Domain Model provides carefully thought through formulations of immune system function after AS01. This model not only provides a foundation from which to build simulations and test hypotheses, but generated novel hypotheses for the high priority knowledge gaps that were also identified through this work. We believe that these concepts will complement work on AS01 MoA and envision that these 3Rs-based approaches can be applied more generally to improve the understanding of other adjuvant MoAs. As well as supplying a detailed model, collectively, the work in this chapter extends current understanding of AS01 MoA, by unifying experimental insight with hypotheses, assumptions and abstractions to address the question(s) posed (research question 1 section 1.10.1), therefore proposing a novel, integrated current knowledge-base regarding how AS01 initiates and maintains immune responses.

Chapter 4

Development of a Mathematical Model to Explore Innate IFNγ Production Induced by AS01-adjuvanted Vaccines

4.1 Introduction

Vaccines adjuvanted with AS01 generate a rapid and transient innate immune response in animal models [15], resulting in stark production of IFNγ observed to peak at approximately six hours post-injection [32]. Further, IFNγ has been shown to be vital for a functional CD4+ T cell response to AS01-adjuvanted vaccines [32]. Over the past 20 years, experiments in animal models have elucidated vital mechanisms underpinning such responses. [15, 32, 46]. However, through producing an explicit description of the current understanding of AS01 MoA - culminating in the model presented in Chapter 3 - important knowledge gaps and specific research questions regarding the production of innate IFNγ were revealed and consolidated:

1. The source of IL12 post IM AS01 administration is unknown. Given the assumption that monocytes and DCs both produce IL12 at the same rate, what differences do we observe in the temporal dynamics of cellular IL12 production? What hypotheses do these insights generate?
2. What is the relationship between each cell type's respective production of IL18 or IL12 with the production of IFNγ? How does this differ over time? What is the dominant cytokine in initiating early IFNγ?
3. What are the most influential parameters involved in early IFNγ production after AS01?

4. What effects does the loss of macrophages have on the IFNγ production? What would happen to the immune response if no macrophage cell loss occurs? How could this cell loss affect IFNγ responses after a second AS01 delivery?

This chapter therefore addresses thesis Aim 2 (section 1.10.2), by describing work which produced a simulator to answer questions 2-6 (see above). Indeed, this chapter presents the development of a model and simulation to explore early IFNγ production after AS01. The resulting simulation was constrained using available parameterisation and validation data.

4.2 Results

4.2.1 A Domain Model of AS01 induced Innate IFNγ Production

After a literature examination we determined that no suitable simulators exist for exploring early AS01 MoA, although a mechanistic model that explores the lung and dLN immune response during mycobacterium tuberculosis infection had previously described dynamics relevant to our research context. [196]. Indeed, Wigginton's model captures cytokine-mediated cellular activation, leading to the production of further cytokines. Therefore, Wigginton's work served as inspiration for development of the AS01 innate IFNγ simulator presented in this chapter. In turn, an instantiation of the CoSMoS process was implemented and the research context was established.

4.2.1.1 Research Context

The domain of interest is the salient events during the first 24 hours of the innate immune response to AS01-adjuvanted vaccines in a murine iliac dLN. In particular, these salient events are involved in the production of IFNγ. The research context encapsulates the questions presented in section 4.1. Therefore, the entities to be captured in this model are AS01's immunostimulants, QS21 and MPL, monocytes, DCs, CD169+ SCS macrophages, cells which produce IFNγ after AS01 (primarily NK cells), IL12, IL18, and IFNγ.

4.2.1.2 Gathering Experimental Data

We gathered experimental data to inform model conception, calibration and validation. However, as is common in mechanistic system biology projects, experimental data for this system is sparse. Therefore, we carefully partitioned data for use in calibration *or* validation. We next cleaned and structured the entire collection of data. The data generated by GSK and previously shown in Figure 3.2 regarding cell numbers and cytokine concentrations was set aside for calibration and informed Domain Model development. Here we re-present the

data relevant for our current research context, i.e., for captured cell types and cytokines over the first 24 hours of the response to AS01 (Figure 4.1).

We first show data on how cell numbers and cytokines change after AS01. Firstly, Figure 4.1A shows distributions of CD169+ macrophages after PBS or QS21. Compared to the PBS control, a clear reduction in the number of these macrophages is observed after QS21. This loss is thought to be induced by QS21-mediated pyroptosis, although this has not been confirmed and cellular displacement, or a reduction of CD169 expression, may also be responsible. Figure 4.1B shows the distributions of Migratory (CD11C+ MHCII^{high}) and resident DCs (CD11C+ MHCII^{med}) after AS01. While the large variation in the data may reflect that the increase in the central estimates over time is not statistically significant, we suggest that an increase in these cells appears to occur over the first 24 hours to AS01. Figure 4.1C shows the increase in the numbers of CD11b+ Ly6c^{high} monocytes following AS01 (measured at 6 and 24 hours) injection in C57BL mice, compared with PBS (0 hour estimate). Figure 4.1D shows the distribution of IFNγ+ NK cells after PBS (0 hour estimate) or AS01 injection into C57BL mice (6 and 24 hours). These data indicate that the number of these cells peaks at approximately 6 hours post injection, consistent with Figure 4.1E showing the concentration of IFNγ over time, which appears to peak at 6 hours post injection. These specific data are currently unpublished, however these trends are available in Coccia et al[32].

To examine whether any developed simulation represents behaviours of the modelled system, rather than just fits to the data through calibration, we withheld the knockout and depletion data shown previously in Figure 3.3 from calibration, for use in 'model validation'. Insights from these data however conceptually informed development of the 'AS01 innate IFNγ Domain Model'.

4.2.1.3 A CellDesigner Model of Key Components in Early Events of AS01 MoA

Next, we scoped high-level model interactions to generate a CellDesigner model, with respect to research questions 2-6 (Figure 4.2). This scoping process involved a refinement of the core AS01 MoA CellDesigner model presented in Chapter 3, further discussions with GSK Vaccines immunologists, and extracting relevant knowledge from AS01-based publications and wider immunological literature. Here, the CellDesigner model depicts high-level interactions initiated by injection of vaccine components (Antigen, MPL, QS21) which freeflow from the muscle injection site (*left*), into the draining lymph node (*center*). Monocytes can become activated in the injection site and migrate into the dLN, where they secrete IL12. Free-flowing MPL can stimulate dLN resident DCs and/or migratory DCs[95, 69],

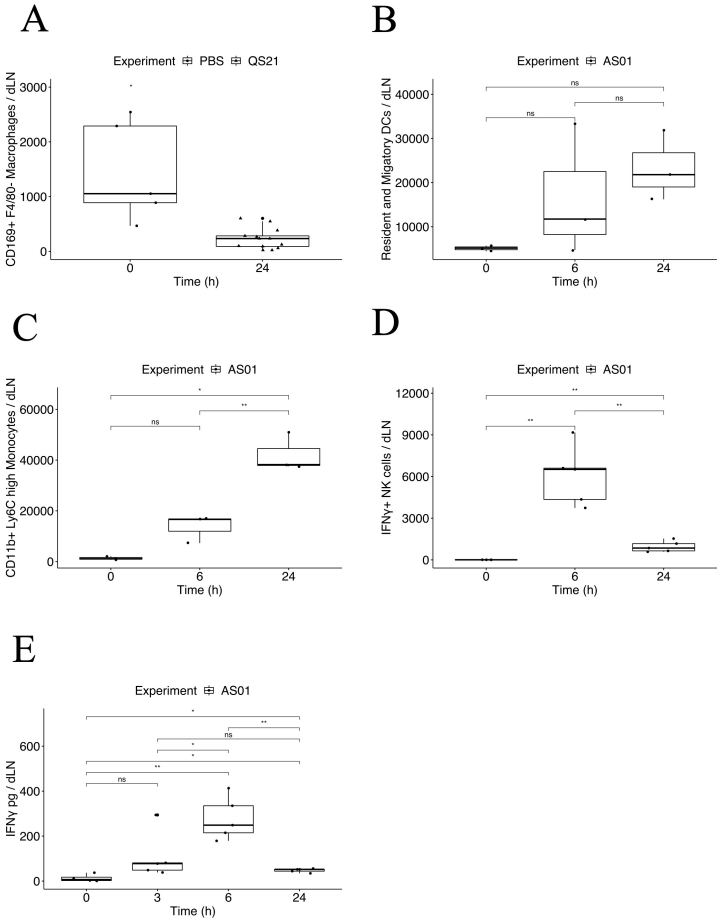


Figure 4.1: **GSK generated experimental data showing cell numbers and cytokines after AS01-adjuvanted vaccination:** A) During an experiment by GSK to determine the cells targeted by QS21, subcapsular macrophages were analysed by flow cytometry 24 hours after PBS or QS21 injection and cell numbers quantified in mice [8]. B-E) To examine cell or cytokine dynamics after AS01 compared with PBS, six to eight week old female C57BL/6 mice were immunised i.m with gE antigen formulated with 1/50th human-dose (HD) AS01b in gastrocnemius muscles, or gE and PBS. Iliac dLN were collected at timepoints between 3 and 48 hours post injection. IFNγ producing cells were assessed by ICS. Cytokines were analysed by MILLIPLEX MAP, a multiplex assay using Luminex technology. For cell detection, flourescent events were acquired using an LSR2 flow cytometer and analysed by FLOW JO. B-D) Iliac dLN were collected at timepoints between 6, 24 and 48 (not shown) hours post injection. Boxplots show A) subcapsular sinus macrophages after PBS and QS21 stimulation. B) Resident and Migratory DCs after AS01 or PBS, C) inflammatory monocytes after AS01 or PBS, D) IFNγ+ NK cells after AS01 or PBS, E) IFNγ after AS01 or PBS. Iliac dLN were collected at timepoints between 3,6,24 and 48 (not shown) hours post injection. All statistical significance measured by T-test. All data was generated by GSK. All 'zero hour' measurements are estimated from PBS controls.

resulting in the secretion of IL12. IL12 from either cell type can promote the production of IFNγ from 'Innate IFNγ Secretor Cells'. In addition, free-flowing QS21 can co-localise with subcapsular sinus macrophages, initiating a release of IL18, which can individually - and synergistically with IL12 - promote IFNγ from 'Innate IFNγ Secretor Cells'.

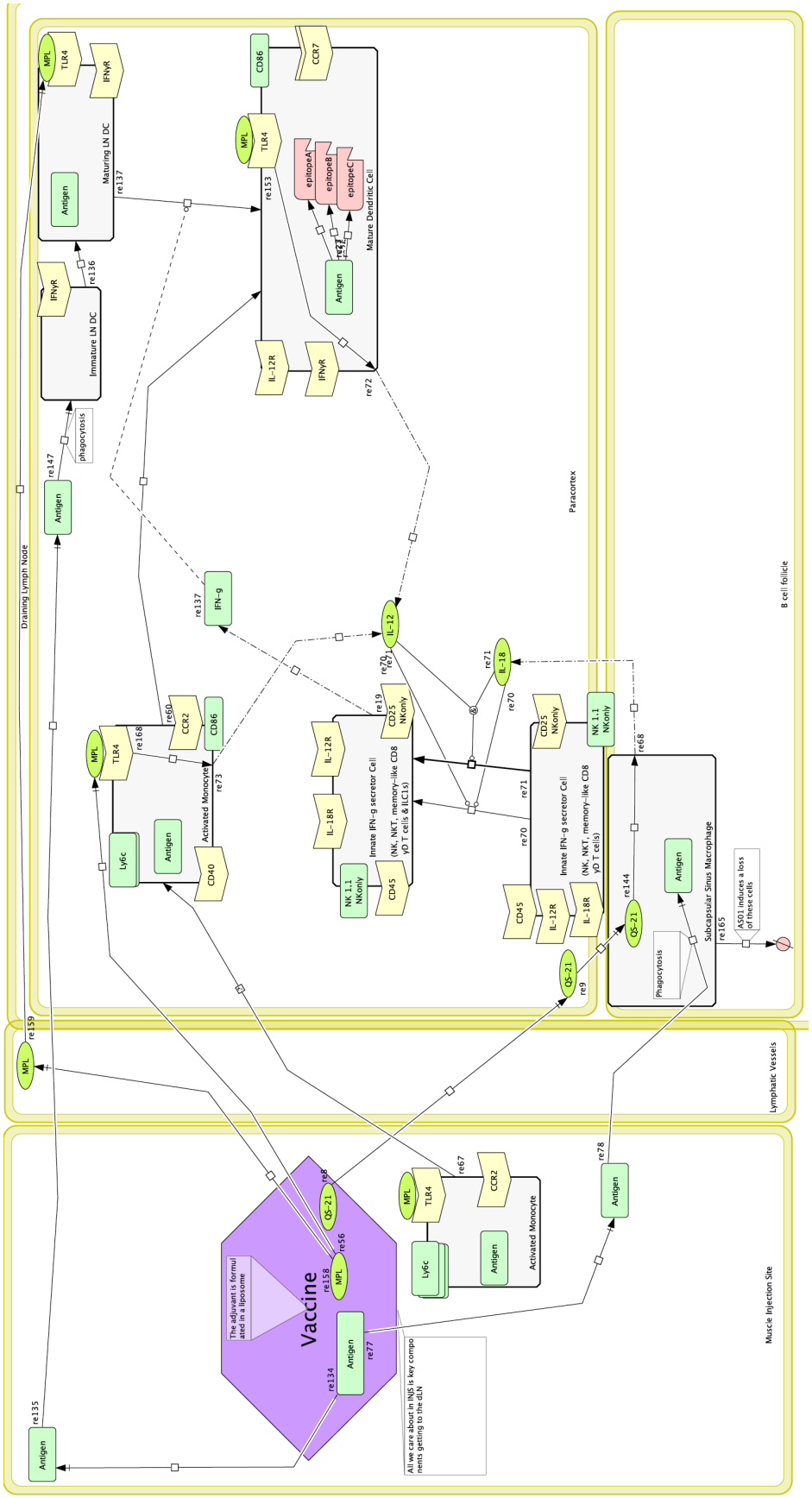


Figure 4.2: **Scoping cellular interactions:** A CellDesigner Model depicting salient events that give rise to the production of Innate IFNγ.

4.2.1.4 Expected Behaviours Diagram

Following high-level scoping, we constructed an Expected Behaviours diagram, to describe how hypothesised mechanisms interact to produce the phenomena observed *in vivo* (Figure 4.3). The following describes the key insights of the Expected Behaviours diagram. References to publications and/or figures are provided as evidence.

4.2.1.5 Key Observable Phenomena

1. **QS21-bodipy, and antigen are observed in the draining lymph node thirty minutes after injection [15].** It is hypothesised that MPL follows similar dynamics, reaching the dLN within thirty minutes to activate cells.
2. **QS21 co-localisation with SCS macrophages results in a considerable loss of these cells (Figure 4.1A) [8].** QS21 co-localises with SCS macrophages and a loss of these cells is observed between 0 and 24 hours post-injection. Indeed, it is hypothesised that QS21 results in the dysfunction or 'loss' of these macrophages, with numbers reducing drastically by 24 hours post injection.
3. **Monocyte levels rise in the draining lymph node over the first 24 hours (Figure 4.1C) [15].** Monocyte infiltration into the draining lymph node is captured. In accordance with immunological literature, this process is mediated by CCR2 expression on monocytes. Using a sheep cannulation model, immunologists at GSK showed that these infiltrating monocytes are predominately inflammatory monocytes and we hypothesise that they secrete IL12.
4. **IFNγ is produced and peaks approximately six hours post-injection, returning close to baseline by 24 hours post-injection (Figure 4.1E) [32].** Experiments in mice have shown that 'optimal' levels of IFNγ are produced when both MPL and QS21 are injected. This production of IFNγ peaks at approximately six hours and returns close to baseline by 24 hours post injection.
5. **Early induction of IFNγ by AS01 is mediated by subcapsular sinus macrophages via IL18, and is supported by IL12 (Figure 3.3) [32].** IL18 and IL12 promote the production of IFNγ by NK cells. IL18 has been shown to be produced by SSM after AS01. The source of the IL12 unknown and is a key question, as is the temporal dynamics of cellular production. It has been observed in wider literature that monocytes and DCs produce IL12. Thus, we hypothesise that the source of IL12 is both monocytes and DCs, after TLR4 stimulation by MPL [69, 168, 63, 67, 68].

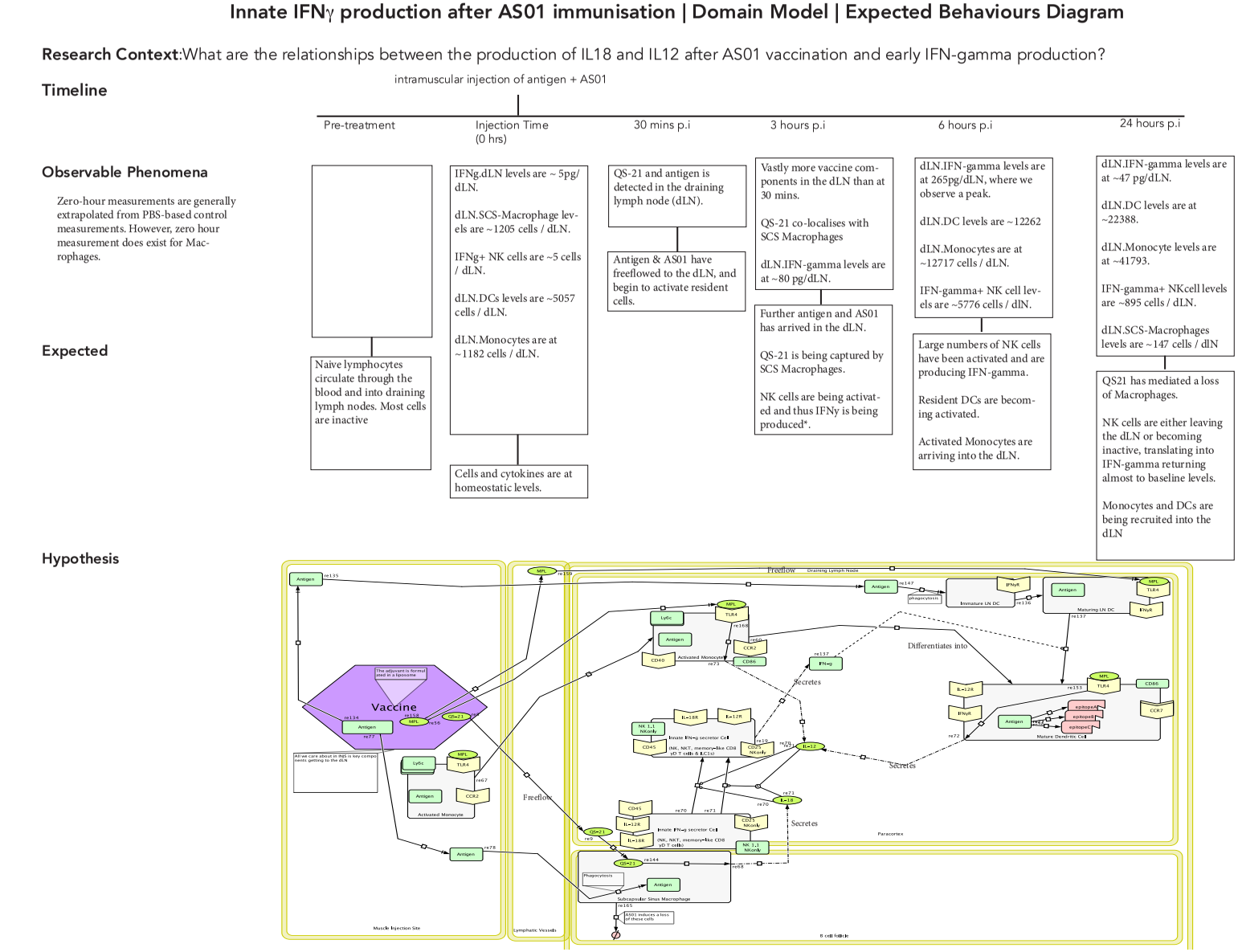


Figure 4.3: **Expected Behaviours Diagram:** Linking the phenomena observed from the biological domain to the times in which these are observed, and to the hypotheses for how these phenomena holistically manifest *in vivo*.

4.2.1.6 Integrating Experimental Insight with Assumptions, Abstractions and Hypotheses

As described in Chapter 3, we next integrated assumptions and further hypotheses into the previously described insights from experimental data. The following describes key *hypotheses*, *abstractions* and *assumptions* that were thus integrated into this Domain Model.

1. **Abstraction: Neutrophils are omitted from the model**. Neutrophils rapidly infiltrate the dLN after injection with an AS01-adjuvanted vaccine, although their functionality is unclear. There are various schools of thought and conflicting data in the literature [300]. There is no evidence that these cells contribute to our research questions, thus at this stage of investigation, neutrophils were omitted from the model.
2. **Hypothesis: Monocytes are activated by MPL.** Neeland et al., observed that monocytes arriving in the dLN are MHC-II^{intermediate} [46]. Inflammatory monocytes (CD14+ LY6C+ CCR2+) have been shown to express TLR4. Thus, we hypothesised that these cells are activated via TLR4 by MPL prior to arrival in the dLN.
3. **Hypothesis: Monocytes secrete IL12 after being activated by MPL**. In other immunological systems, there is evidence that monocytes secrete IL12 after being activated via TLR4 [106].
4. **Hypothesis: activated monocytes possess the ability to differentiate into DCs**.
5. **Hypothesis: dendritic cells can become activated by MPL[95] to secrete IL12**. MPL has been observed to be the primary driver of DC activation in AS01 [95] Furthermore, a subset of DCs which in mice have been shown to be involved in AS01 MoA, are characterised by IL12 expression in other systems [95].
6. **Assumption: Cells that are producing IFNγ are activated**. IFNγ^{+} NK cells in the experimental data are assumed to be activated, and in the model are referred to as 'Activated NK cells'.

Importantly, liposomes are not explicitly modelled in any part of this thesis. As mentioned in section 1.7, in general, due to relatively weak adjuvancy, many liposomal adjuvant formulations comprise immunostimulants alongside the liposome. Indeed, the liposome is considered to serve as a delivery vehicle for AS01's immunostimulants MPL and QS21. For AS01 specifically, to our knowledge there is no evidence that the liposome contributes to AS01's immune-enhancing MoA. Furthermore liposomal formulations with considerable similarities to AS01 have been shown to produce little or no detectable adjuvant effect by themselves, however in the presence of MPL substantial immunostimulatory effects are observed [146]. While not conclusive for AS01, these data are consistent with the current

paradigm that the immunostimulatory components of AS01 are MPL and QS21, although an investigation into the effects of AS01's liposome in the absence of QS21 and MPL would be valuable. Nevertheless, there is no evidence that AS01's liposome directly contributes to the research questions examined in this thesis, beyond acting as a delivery vehicle for AS01's known immunostimulants: MPL and QS21. [95].

Given these reasons, in light of our research questions, we therefore have decided to model the known immunostimulatory effects of AS01, which are mediated via MPL and/or QS21. Indeed, we are forced to abstract any possible lower-level contribution that the liposome may make to AS01 MoA, and assume it is captured in the modelled mechanisms involving QS21 or MPL. This is reasonable, as the experimental data providing insights used to describe mechanisms, or calibrate and validate the model, includes MPL and QS21 as constituents of AS01 - formulated with the liposome. A cartoon summary of the captured model mechanisms and hypotheses is shown in Figure 4.4.

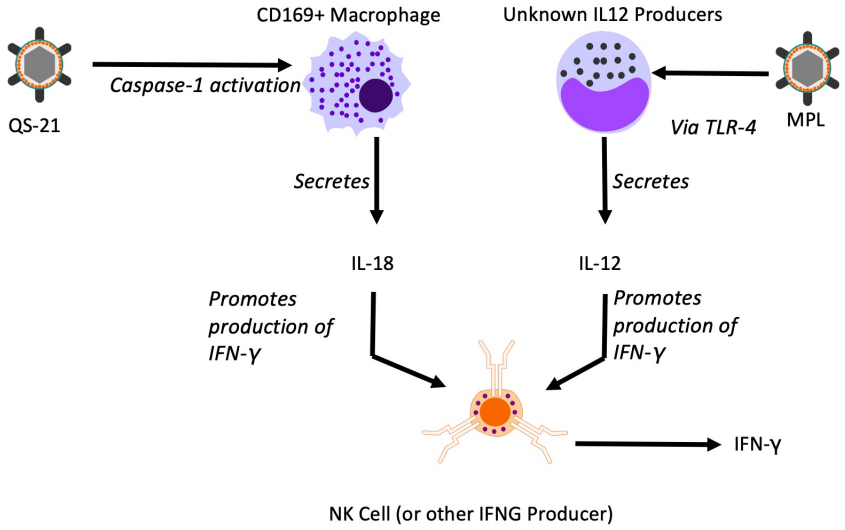


Figure 4.4: **Summarising the underlying biological hypotheses:** A cartoon describing the captured biology. QS21 activates CD169+ macrophages in a caspase-1 dependent manner, resulting in the release of IL18. IL18 can individually promote the production of IFNγ from NK and other IFNγ producers. Furthermore, the model captures the ability for IL12 to individually promote the production of IFNγ by NK and other IFNγ producers. In addition, IL12 and IL18 synergise to promote an augmented production of IFNγ. The source of IL12 is hypothesised to be monocytes and/or DCs, after TLR-4 stimulation by MPL.

4.2.1.7 Activities of Model Entities

Activity Diagrams formalise and substantiate the mechanisms hypothesised to contribute to the production of IFNγ over the first 24 hours post injection of an AS01-adjuvanted vaccine. While the entirety of the model is too large to present all diagrams in a single

thesis chapter, the activities of each cell type in the domain model are described here and salient diagrams are shown. Please see supplementary I-D (**I**FNg Model **D**omain Model, link in Appendix A.2) for the full activity and State-Machine diagrams.

CD169+ subcapsular sinus macrophage Activities (Supplementary I-D Figure 3): This cell type is resident in the lymph node subcapsular sinus at *t0*. Initially, the cell surveys the environment and following stimulation by QS21, it can begin activation. If caspase-1 is activated by QS21, the cell can begin to release IL18. Through provoking 'cellular loss', QS21 activation can also cause the cell to exit the system.

Monocyte Activities (Supplementary I-D Figure 7): Initially, a monocyte is either resident in the dLN or recruited at some rate. The cell becomes activated by TLR4 stimulation. If antigen-primed, the cell carries antigen. If the cell receives TLR4 stimulation, it begins to secrete IL12. This cell can also differentiate into a DC.

DC Activities (Figure 4.5): The DC is either resident in the dLN at *t0* or arrives from the lymphatics. Initially, the DC surveys the environment, where it can capture antigen and/or be stimulated by TLR4 to mature. During the 'maturing' phase, it upregulates B7, CCR7 and expresses pMHCII complexes on its surface pending antigen capture. Following TLR4 stimulation it can secrete IL12. The cell becomes mature over time where it expresses high levels of CCR7, B7 and pMHCII. Due to the upregulation of CCR7, a DC that is not resident in the dLN paracortex will begin migration towards the CCL19/21 gradients there.

IFNγ Secretor Cell Activities (Figure 4.6): This cell type is either resident at *t0* in the paracortex or medulla or enters the system via HEVs (Figure 4.6). Initially, the cell surveys the environment, and can become activated to secrete IFNγ by a combination of IL12 *and* IL18 or IL12 *or* IL18. The cell can stop secreting IFNγ if stimulation wanes. The cell can additionally exit the system if it receives apoptosis signals.

4.2.1.8 State-Machine-Diagrams

State-Machine diagrams were next developed to articulate the different states entities exhibit and to define the cellular and environmental cues that govern transitions between states. All State-Machine diagrams are described, although examples are only shown for DCs and Innate IFNγ Secretor Cells. The full model is available in Supplementary I-D.

Subcapsular CD169+ macrophage states (Supplementary I-D Figure 2): This cell is resident in the dLN SCS at *t0*. Initially, the cell is in an 'immature' state and following QS21 stimulation it can enter the 'activated' state. Here, the cell can enter the 'IL18 secreting' state if caspase-1 is activated. The capacity to not secrete IL18 is also captured. Simultaneously, this cell can exit the system after transition into the 'Cellular Loss' state after QS21 stimulation.

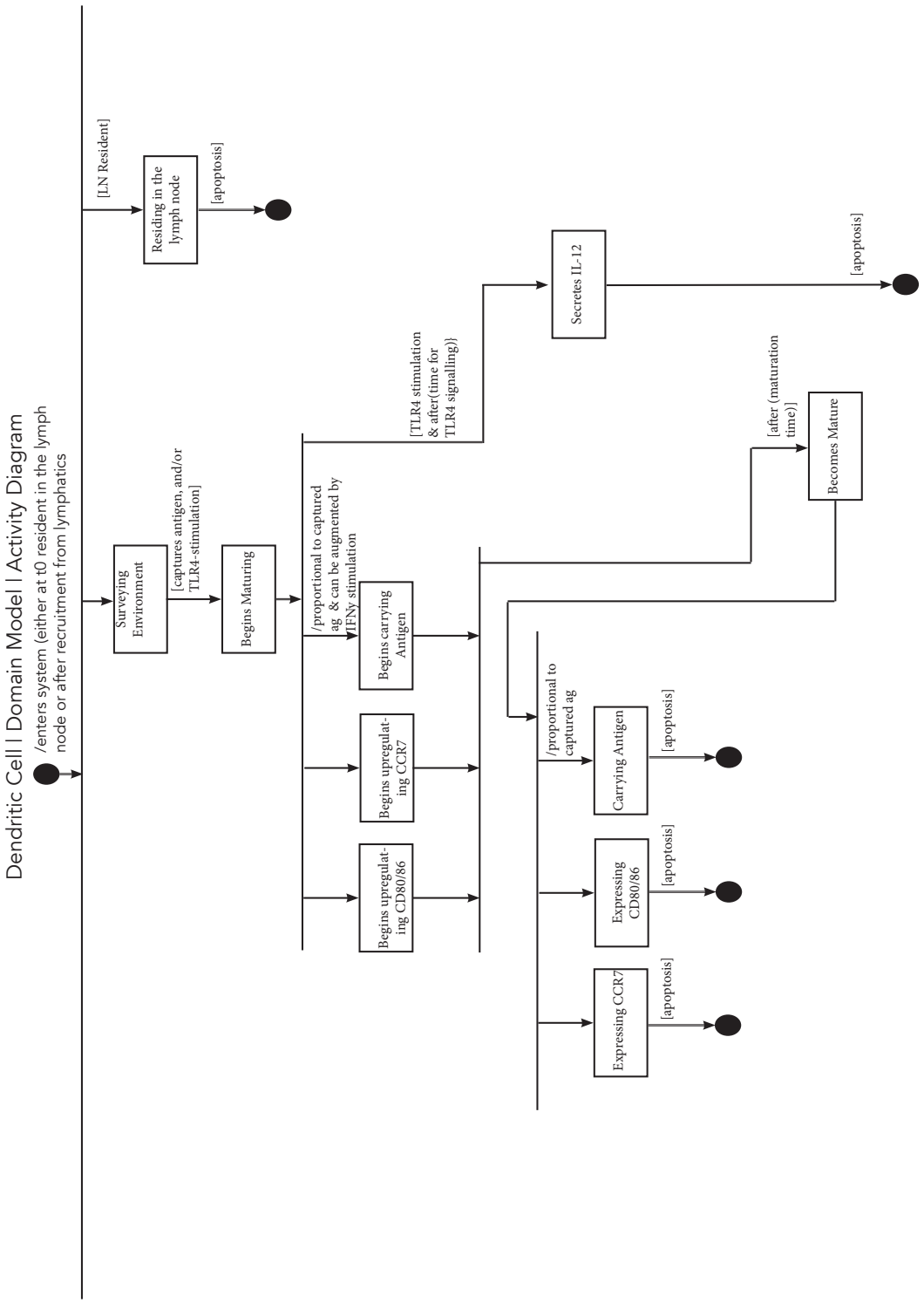


Figure 4.5: **A dendritic cell Activity Diagram.**

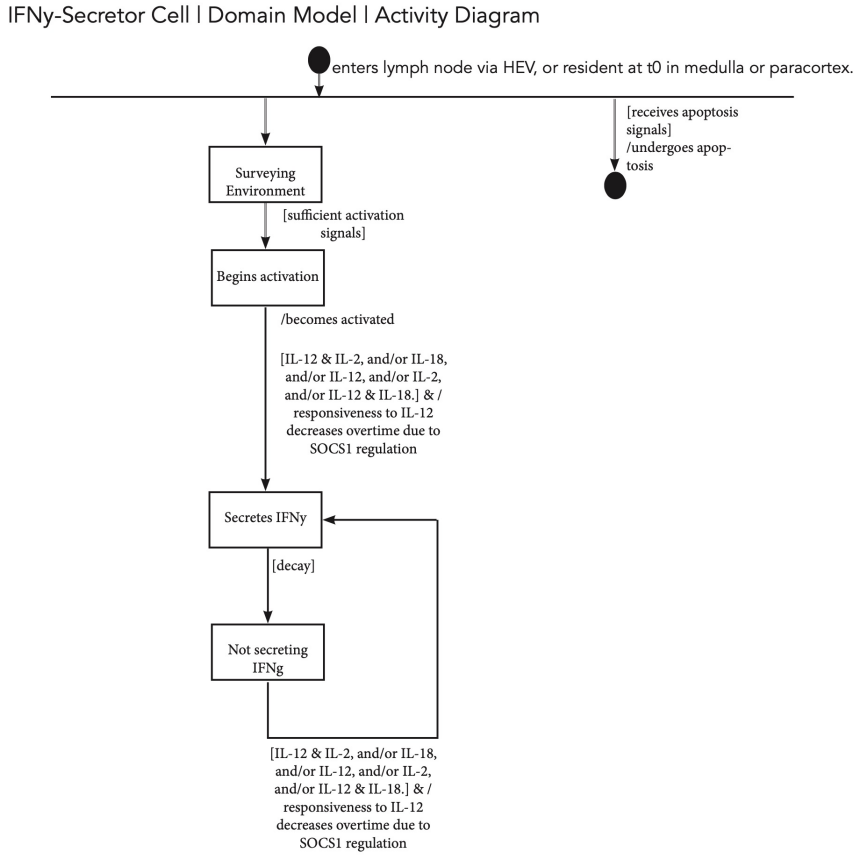


Figure 4.6: **An 'IFNγ Secretor Cell' Activity Diagram.**

Monocyte States (Supplementary I-D Figure 6): This cell type is either resident at *t0* or recruited into the dLN. Initially, it is in an 'immature' state and become activated. If a Monocyte is stimulated by TLR4, it can secrete IL12. The 'activated' parent state comprises sub-states, which oversees differentiation into a DC or a macrophage, secretion of IL12, antigen-carry, and CD40/86 expression.

State-Machine for dendritic cells (Figure 4.7): The DC is initially in an 'immature' state with substates 'phagocytic' and 'non-antigen-retaining'. After stimulation via TLR4 and/or antigen capture, it enters the 'maturing' state. Here, the DC varies its phagocytic capacity depending on the acquired levels of antigen, and increases expression of CCR8, B7 and pMHC complexes. It can also secrete IL12 if stimulated via TLR4. After entering the mature state, the cell exits the phagocytic substate and instead expresses high levels of CCR7, B7, pMHCII. It can also secrete IL12 while mature.

State-Machine for Innate IFNγ Secretor Cell (Figure 4.8): The cell is either resident in the dLN or becomes activated. Initially the cell is 'inactive' and can become 'activated' after sufficient activation signals. If this signals are from IL12 or IL18 the cell can secrete IFNγ. The ability for the cell to stop secreting IFNγ is captured.

Figure 4.7: **A dendritic cell State-Machine Diagram:** This diagram describes the functionality of DCs as per their hypothesised involvement in early IFNγ production, with respect to our research questions.

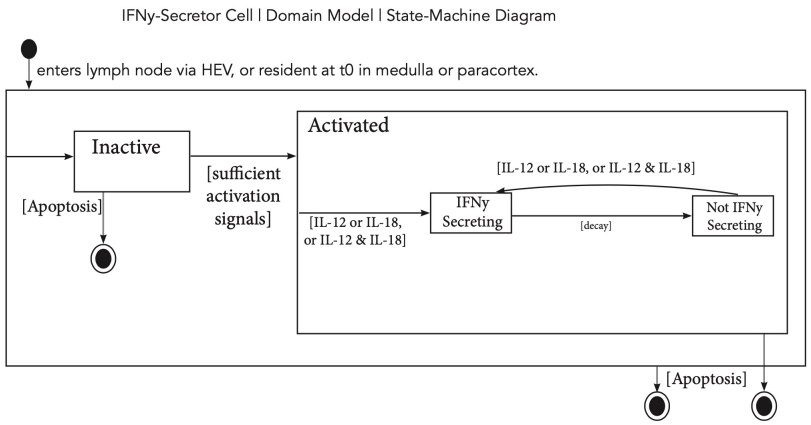


Figure 4.8: **An 'IFNγ Secretor Cell' Activity Diagram.**

4.2.2 A Platform Model of AS01 induced Innate IFNγ Production

Following Domain Modelling, we constructed a Platform Model. Here, we expressed the 'Domain Model' as a mathematical and computational specification. First, we decided on a modelling methodology. Advantages and disadvantages of commonly-used techniques to model biological systems have been described in Chapter 1. Our research questions involved relationships between model components, rather than spatial dynamics or heterogeneity (which typically ask for PDEs/ABMs). Additionally, AS01 experimental data for calibration is sparse and these are the first mechanistic modelling efforts targeted at exploring AS01 MoA. Indeed, no spatial-data are available for AS01-induced immune responses in lymph node microenvironments. Taken together, we decided that ODEs are the most appropriate modelling technique for this work.

4.2.2.1 Key Platform Model Refinements, Additions and Simplifications

Following the choice of modelling methodology, we introduced refinements, additions and simplifications into the Platform Model with an emphasis on enough simplicity as is appropriate.

First, given the focus on dLN kinetics, only the dLN dynamics were modelled and not the muscle injection site or afferent lymphatics. Instead, rates of infiltration into the dLN are used to capture the relevant output from the muscle injection site and/or afferent lymphatic compartments. Secondly, the Domain Model - for simplicity - describes an abstracted cell-type called an 'Innate IFNγ Secretor' cell, composed of cells that produce IFNγ. To embrace simplicity, after discussion with GSK immunologists, only NK cells were modelled in the current work, as unpublished evidence demonstrates that NK cells predominately mediate the innate IFNγ relevant for this model, while CD8+ T cells instead are observed to primarily mediate the second peak of IFN. Antigen and antigen-mediated activation of

cells was also abstracted out of the mode at this stage, as the research context is concerned only with adjuvant-mediated dynamics. Additionally, no evidence exists to suggest that monocytes differentiate into macrophages after AS01, so only monocyte differentiation into DCs is captured [5]. In accordance to recent data, the rate of monocyte differentiation into DCs is assumed to be limited [95]. This differentiation is modelled as a linear rate, omitting any complexity involving CSF3 and IL4 at this stage. Finally, monocytes in the dLN are assumed to be activated, as it is likely their infiltration into the dLN is due to prior activation elsewhere.

4.2.2.2 Platform Model Diagram Examples

Next, the Platform Model interactions were depicted. The following section provides examples of these diagrams, while the full platform model is published in Supplementary I-P (**I**FNg Model **P**latform Model, link in Appendix A.2).

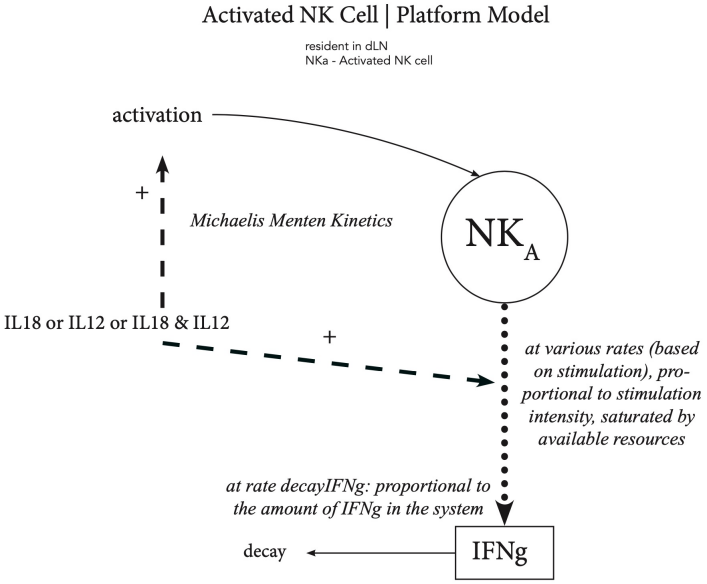


Figure 4.9: **A NK cell Platform Model Diagram.**

Figure 4.9 shows interactions captured in the Platform Model for an activated NK cell (*NKa*). IL18 and IL12 stimulates an increase in the number of these cells (i.e., increases the numbers of activated cells) and promotes the production of IFNγ, at rates which correspond to either synergistic (requiring both IL18 and IL12) or individual (at lower rates, requiring only IL12 or only IL18) activation. Synergistic activation of NK cells to produce cytokine follows saturable kinetics (which are in the form also of Michaelis-Menten), while individual activation is linear. Figure 4.10 describes the interactions captured in the Platform Model for the DC (*DC*). After stimulation by MPL, DCs secrete IL12 at rate $vDCIL12_p$. Monocytes (*Monoc*) can differentiate into DCs at rate $MonocDiffDC_p$.

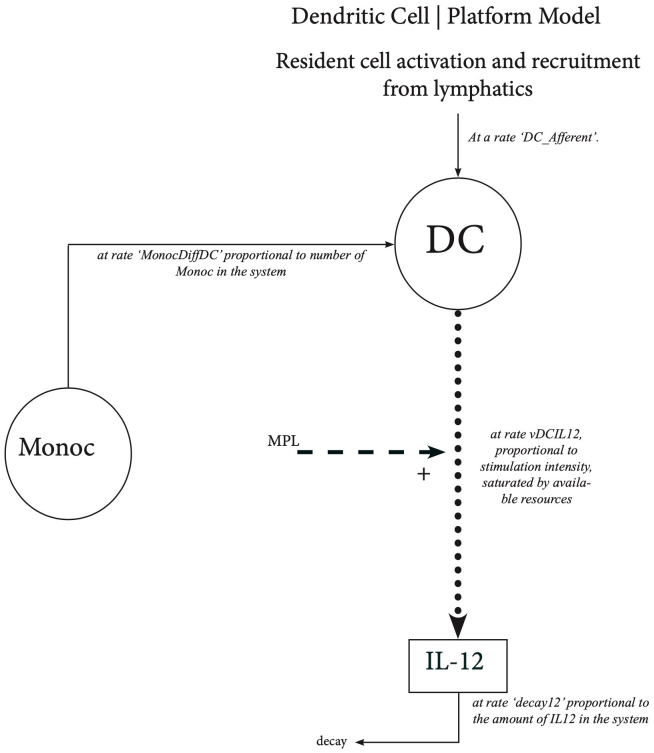


Figure 4.10: **A dendritic cell Platform Model Diagram.**

4.2.2.3 Ordinary Differential Equations for AS01 induced Innate IFNγ Production

Next, we manually derived a set of ODEs from the Platform Model diagrams. Thus, we propose a system of non-linear ordinary differential equations to describe the mechanisms captured in the full Platform Model. Throughout what follows in this thesis, parameters are given the subscript 'p' to distinguish parameters from variables. While for brevity this chapter only presents example Platform Model diagrams, we here describe the ODE model in full details.

$$\frac{dMo}{dt} = -(CL_p \times Mo \times QS21_p) \tag{4.1}$$

Equation 4.1 describes the rate of change of SCS macrophages (Mo). *Mo* reduce as a function of time at a rate proportional to CL_p, controlled by parameter $QS21_p$.

$$\frac{dMonoc}{dt} = (monocRec_p \times MPL_p) - (MonocDiffDC_p \times Monoc) \tag{4.2}$$

Equation 4.2 describes the rate of change of monocytes (*Monoc*), which are recruited into dLN at rate $monocRec_p$, controlled by parameter MPL_p. These cells can differentiate into DCs at rate $MonocDiffDC_p$.

$$\frac{dDC}{dt} = (MonocDiffDC_p \times Monoc) + (DC_Afferent_p \times MPL_p) \tag{4.3}$$

Equation 4.3 describes the rate of change of DCs (DC). The first term describes the rate of monocytes differentiating into DCs. $DC_Afferent_p$ controls the rate at which DCs become activated and are recruited into the dLN during inflammation over the first 24 hours, and this is hypothesised to be controlled by MPL [149, 95].

$$\begin{aligned}\frac{dNKa}{dt} &= +VmaxNKa_{1218p} \times (\frac{IL18}{IL18 + KM_{IL18bp}}) \times (\frac{IL12}{IL12 + KM_{IL12bp}}) \\ &+ VmaxNKa12_p \times IL12) \\ &+ VmaxNKa18_p \times IL18 \\ &- (NKDecay_p \times NKa)\end{aligned} \tag{4.4}$$

Equation 4.4 describes the rate of change of activated NK cells (NKa). The first term describes saturation kinetics, capturing the synergistic activation of NKa as induced by IL12 and IL18, at maximal rate $VmaxNKa1218_p$. The second and third terms describe the individual activation of NK cells by IL12 or IL18 - external to the synergy - at rates $VmaxNKa12_p$ and $VmaxNKa18_p$ respectively. The final term describes the reduction of activated NK cells as observed over time, perhaps due to inactivation or LN exit.

$$\frac{dIL18}{dt} = (vMoIL18_p \times Mo \times QS21_p) - (decay18_p \times IL18) \tag{4.5}$$

Equation 4.5 describes the rate of change for IL18. The first term describes QS21-induced production of IL18 by macrophages (Mo), at rate $vMoIL18_p$. The second term describes IL18 decay, proportional to the amount of IL18 in the system.

$$\begin{aligned}\frac{dIL12}{dt} &= (vMonocIL12_p \times Monoc \times MPL_p) + (vDCIL12_p \times DC \times MPL_p) \\ &- (decay12_p \times IL12)\end{aligned} \tag{4.6}$$

Equation 4.6 describes the rate of change of IL12 in the system. The first and second terms describes the rate of (hypothesised) MPL_p induced production of IL12 by monocytes and DCs respectively. The last term describes IL12 decay, proportional to the amount of IL12 in the system.

$$\begin{aligned}\frac{dIFNg}{dt} &= (VmaxNKaProd_{1218p} \times IL18 \times (\frac{IL12}{IL12 + KMNKa_{IL12b\,p}}) \times NKa) \\ &+ (VmaxNKaProd_{18p} \times IL18 \times NKa) \\ &+ (VmaxNKaProd_{12p} \times IL12 \times NKa) \\ &- (decayIFNg_p \times IFNg)\end{aligned} \tag{4.7}$$

Equation 4.7, describes the rate of change of IFNγ (*IFNg*). The first term describes the 'synergistic' production of *IFNg* by activated NK cells (*NKa*) as induced by *IL18* and *IL12* at maximal rate $VmaxNKaProd1218_p$, and this equation describes saturation kinetics. The first description of this term included a half-saturation constant for IL18, mirroring $KM_NKa_IL12b_p$, however after a sensitivity analysis this parameter was deemed to have no discernible effect on model behaviour and was thus removed. The second and third terms describe the production of *IFNg* by *NKa*, when induced by IL18 or IL12 alone, controlled by rates $VmaxNKaProd18_p$ and $VmaxNKaProd12_p$ respectively. The final term is a decay term which is proportional to the amount of *IFNg* in the system.

4.2.2.4 Equations Prescribing a Variable as a Function of Time

Multiple of the aforementioned equations, exhibit no, or limited non-linearity and can simply be written as functions of time. Solving more complex differential equations analytically is beyond the competency of the author, and therefore these equations were solved using Mathematica and are written below:

Firstly, the equation 4.1 for macrophages (Mo), can be re-written as;

$$Mo = Mo_0\, \mathrm{e}^{-CL_p \times QS21_p \times t} \tag{4.8}$$

The equation 4.2 for monocytes (Monoc) can be re-written as;

$$Monoc = Monoc_0\, \mathrm{e}^{-MonocDiffDC_p \times t} + \frac{monocRec_p \times MPL_p}{-MonocDiffDC_p}(1 - \mathrm{e}^{-MonocDiffDC_p \times t}) \tag{4.9}$$

By substituting in equation 4.9, the equation 4.3 for DCs (DC) can be re-written as;

$$\begin{aligned}DC = DC_0 + (Monoc_0 - \frac{monocRec_p \times MPL_p}{MonocDiffDC_p}(1 - \mathrm{e}^{-MonocDiffDC_p \times t}) \\ +(monocRec_p \times MPL_p + DC_Afferent_p \times MPL_p) \times t\end{aligned} \tag{4.10}$$

Model Entity Name	**Full Entity Name**
Mo	CD169+ F4/80- macrophages
Monoc	CD11b+ Lyc6-high monocytes
DC	Resident and migratory dendritic cells
NKa	activated IFNγ^+ NK cells
IL18	Interleukin 18
IL12	Interleukin 12
IFNg	IFNγ

Table 4.1: Table of Simulation Measures: Defining the shorthand used in the Simulation

Lastly, by substituting in the equation 4.8, the equation 4.5 for IL18 (IL18) can be re-written as;

$$IL18 = \frac{vMoIL18_p \times QS21_p}{decay18_p - CL_p \times QS21_p}(\mathrm{e}^{-CL \times QS21_p} - \mathrm{e}^{-decay18 \times t}) + IL18_0 \, \mathrm{e}^{decay18_p \times t} \quad (4.11)$$

In what follows, these equations for model variables macrophages, monocytes, DCs and IL18 maybe referred to as 'function of time' variables, while the remaining model equations are referred to as 'non-linear' variables. These equations which are written as a function of time will not be integrated, rather the model will be simulated as ODEs. However, these equations are presented for completeness.

4.2.3 A Simulation Platform for AS01-induced Innate IFNγ Production

Following Platform Modelling, we implemented the system of ODEs to develop a simulation platform for AS01-induced innate IFNγ production. We implemented the simulation platform in R, using the *dMod* package for the implementation of deterministic sets of differential equations. *dMod* provides an accessible framework for model implementation, C code automation to improve simulation speed, parameter estimation, and identifiability analysis. The R code used to implement, solve the ODE and plot the prediction is available in Appendix A.1. Table 4.1 presents the shorthand used in the model, which refers to simulation populations.

4.2.3.1 Simulation Calibration and Identifiability

Some parameters cannot be estimated *in vivo*, thus *in vitro* measurements are often used to estimate parameter values. This can add uncertainty if an *in vivo* system is modelled. Furthermore, it is inappropriate and impossible to model an entire complex system, so it is natural to omit components of the biological system from a simulator, in which case model parameter values must be adjusted from their "real" values to compensate for absent components [245]. Taken together, even if parameter values are known, we argue that

calibration should still occur. In the current setting, many of the parameter values are unknown, therefore we performed calibration to fit the model to the observational data. The observational data is summarised in Table 4.2.

Prior to calibration, we expected the model to be non-identifiable, due to the scarcity of the available biological data and the necessary complexity of the model. Indeed, many experiments required to identify parameters e.g cytokine production rates have not been performed in the context of AS01, complicating the calibration problem. This is common in systems biology and we strongly believe that if a careful calibration occurs and confidence in model predictions are generated through model validation, structurally or practically non-identifiable models can still generate hypotheses to be tested *in vivo*; thus the models can be useful [239]. Indeed, Gutenkunst et al.[301] demonstrated that many systems biology models possess many unconstrained parameters, but nevertheless provide important contributions. Thus, they suggested that modellers should focus on predictions from the models rather than precise parameterisation. In the current setting, it was likely that multiple parameter sets may reasonably fit the observational data. Therefore, in what follows, to mitigate the aforementioned issues while capturing uncertainty in the data and parameter estimates, we set generated a distribution (or set) of values for each parameter, through multi-start optimisation. Here, each parameter set corresponds to a local minima. Furthermore, through *in silico* 'model validation' experiments we confirmed that this set of parameters adequately represents the system behaviours, rather than just fits the calibration data.

The *dMod* framework in R was employed for optimisation, which uses weighted least squares estimation to minimise the objective function (see Methods). Due to the complexity of the calibration problem, we employed an incremental calibration approach (see Methods), isolating incremental portions of the model for optimisation. The 'cascading' nature of the captured biology and thus the model permitted this incremental approach. A similar has been employed previously by Hamp in *in silico* modelling of leishmaniais [257]. We therefore began the optimisation process by isolating the macrophage (Mo) equations. Relevant values from the literature were gathered [196, 197, 302, 303, 304, 205], and we then manually adjusted such values to produce reasonable trajectories within an order of magnitude of the corresponding experimental data. We then supplied appropriate ranges for such parameter to the optimisation algorithm. After a best-fit set of parameters (the parameter set with the smallest objective value) for this isolated portion of the model was generated, we incrementally added a model portion as above, in this case the IL18 equations, and optimised. We followed the aforementioned cycle, until we had one 'best-fit' set of parameters for the full

Model Entity Name	**Timepoints**	**Measurements**
Mo (macrophages)	0, 24 hrs	Geo. mean and sd. QS21 stimulation *in vivo*.
DC	0, 6, 24 hrs	Geo. mean and sd. AS01 stimulation *in vivo*.
Monoc (monocytes)	0,6,24 hours	Geo. mean and sd. AS01 stimulation *in vivo*.
NKa (Activated NK cells)	0,6,24 hrs	Geo. mean and sd. AS01 stimulation *in vivo*.
IL18	No data available	No data available.
IL12	No data available	No data available.
IFNg (IFNγ)	0,3,6,24 hrs	Geo. mean and sd. AS01 stimulation *in vivo*.

Table 4.2: Summary of Experimental Data Availability and Measurements for Model Calibration: 'Geo.mean' is shown as shorthand for the 'geometric mean', and 'sd' is shown as shorthand for the 'standard deviation'. All 'zero hour' data was estimated from PBS controls. 'No data available' reflects that no data were available in the relevant context for AS01-adjuvanted vaccination. The experimental data summarised in this table is presented in Figure 4.1. All measurements are following AS01 or QS21 administration into C57BL/6 mice.

model. As mentioned, given the scarcity of the experimental data and the necessary complexity of the model, there are likely multiple parameter sets which fit the data. Therefore, for the full model, we next employed a multi-start trust-region optimiser to further explore the parameter space, by spreading the starting positions for optimisation. This calibration routine therefore yielded 64 parameter sets, i.e., different local minima with respect to the fitting data. These local minima may be referred to throughout this thesis as 'local optima'. After simulating these 64 parameter sets, we visualised the model trajectories (Figure 4.11).

In most cases, the simulation output conforms reasonably to the experimental data. For IL12 and IL18, we have no observational data. Unsurprisingly the variation in model trajectories for IL12 is large. The results from calibration suggest that the production of IL12 increases as a function of time, following the trajectories of the monocytes and DCs, the IL12-producing cells. Interestingly, IL18, for which we have no experimental data, is predicted to rapidly and transiently increase, peaking at approximately three hours post-simulated-injection before decaying. This is likely due to the loss of macrophages over time, and the requirement that *NKa* accumulation and *IFNg* production are both transient (as observed *in vivo*). These data also illustrate that large variation in the experimental data (black points with error bars). The parameter sets derived from calibration are summarised in Table 4.4.

4.2.3.2 Simulation Validation

Following calibration, we performed *in silico* 'model validation' experiments to provide confidence that the model is not over-fit. Over the years, GSK immunologists have performed gene knockout or antibody-mediated protein depletion experiments, where often the read-outs are the number of IFNγ+ NK cells. These data were withheld from calibration for the purpose of simulation validation [32]. These experimental data contrast the levels of

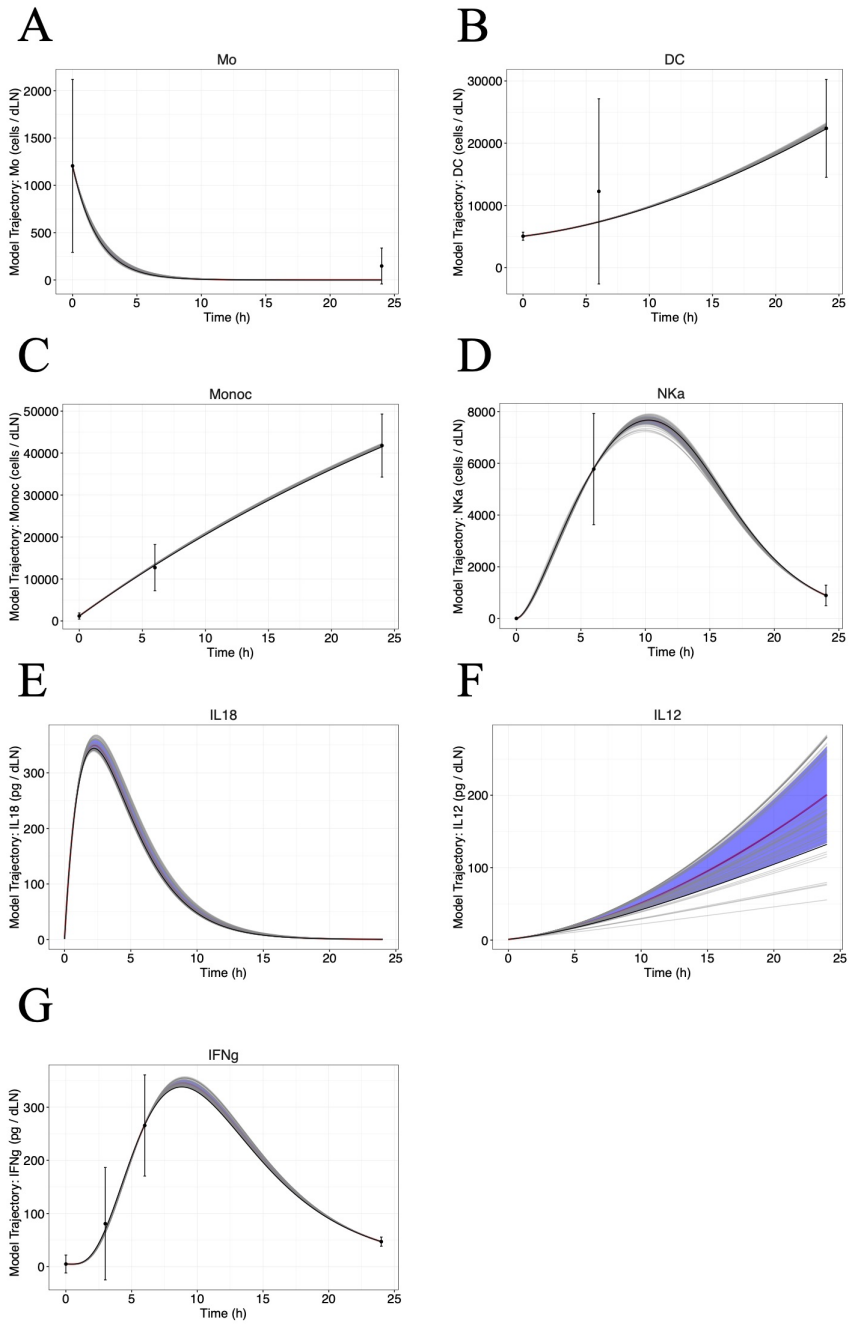


Figure 4.11: **A calibrated model of innate IFNγ production after AS01 immune system stimulation:** Time-series graphs showing model fits for **A)** subcapsular macrophages, **B)** dendritic cells, **C)** monocytes, **E)** IL18, **F)** IL12, **G)** IFNγ. Black dots represent the data the model was trained against with corresponding error bars. Red lines represent the mean trajectories, blue shading represents the mean +/- standard deviation for the model outputs, and black lines represent the fit with the lowest objective value.

IFNγ+ NK cells between wild-type and various knockout settings (Table 4.3). These data were compared to simulation model output, following *in silico* knockout experiments.

For three of the four *in silico* validation experiments, we compared the numbers of IFNγ+ NK cells observed after the particular *in vivo* knockout experiment, with the numbers of 'NKa' cells (representing IFNγ+ NK cells *in silico*) in the model output after an analogous, simulated knockout. For the remaining *in silico* validation experiment (αIL12 knockout), we compared *in vivo* fold-changes of IFNγ+ NK cells between the wild-type and the knockout, with the *in silico* fold-changes of 'NKa' cells between the wild-type and the knockout following an analogous simulated knockout experiment. An incompletely understood phenomenon from AS01 studies *in vivo*, is that different experiments produce measurements for the same cell type or cytokine at different orders of magnitude, perhaps due to technical variation and/or different dosing protocols. In particular, for the αIL12 depletion experiment, set aside for model *validation* (see Table 4.3 and Figure 4.12), we observed that the wild-type numbers of IFNγ+ NK cells were an order of magnitude different than the wild-type number of IFNγ+ NK cells as observed in the data used for model *calibration*. The quantitative observations observed in the data used for model calibration are more consistent with wider experiments into AS01 MoA. Nevertheless, the trend between the numbers of these cells after the αIL12-depletion compared to the WT is useful information for model validation, hence the decision to compare the fold-changes between WT and KO after this *in vivo* experiment, to that which is observed after the analogous experiment *in silico*.

We therefore examined whether the *in silico* model produces statistically significant differences to *in vivo* data, following four *in silico* experiments. In a case where significant differences are observed, the model fits (representing local minima with respect to the fitting data) would have been considered inappropriate. All experiments are assessed at six hours post injection *in vivo* or simulated *in silico* injection. Both *in vivo* and *in silico* experiments are described in detail in the legend for Figure 4.12. In what follows, reference to an *in silico* wild-type scenario, reflects the model output visualised in Figure 4.11, i.e., the calibrated baseline simulation output.

We first examined whether the model produced significantly different fold-change differences in *in silico* IFNγ+ NK cells between *in silico* WT and IL12-knockout scenarios, compared with the analogous experimental data following an IL12 depletion *in vivo*. *In silico*, we removed the effects of IL12 from the model, and simulated each local optima producing a distribution of IFNγ+ NK cells at six hours post-simulated-injection for the IL12-knockout scenarios. Fold-changes were calculated between the (simulated) 'wild type' distribution of IFNγ+ NK cells and the simulated knockout, and contrasted with the *in*

Measured Entity	**Timepoints**	**Experiment**	**Measurement Compared to Model**
IFNγ+ NK cells (NKa in model).	6 hrs	αIL12 depletion + AS01 vaccination.	Fold-change in IFNγ+ NK cells / dLN between WT and KO.
IFNγ+ NK cells (NKa in model).	6 hrs	IL18-receptor KO + AS01 vaccination.	IFNγ+ cells / dLN in the KO mouse.
IFNγ+ NK cells (NKa in model).	6 hrs	clodronate-mediated subcapsular macrophage depletion + AS01 vaccination.	IFNγ+ cells / dLN after the depletion.
IFNγ+ NK cells (NKa in model).	6 hrs	IL18-receptor KO+ αIL12 depletion + AS01 vaccination.	IFNγ+ cells / dLN in the 'double-KO' mouse.

Table 4.3: Summary of Data Withheld from Calibration for use in Model Validation: WT is used as shorthand for 'wild-type', KO is used as shorthand for 'knockout'.

vivo data (Figure 4.12A). Here, we calculated *in vivo* fold-changes between the numbers of IFNγ+ NK cells following injection of AS01 and a model antigen into wild-type C57BL/6 mice, with the numbers of IFNγ+ NK cells following the same vaccination in C57BL/6 mice treated with αIL12p40 (Figure 4.12A). We observed that the *in silico* model produces a distribution of fold-changes which are consistent with the fold-changes observed *in vivo* (*T-test p=0.77, wilcoxon p=0.21*). Despite not replicating the *in vivo* variation, we deemed the result of this validation experiment acceptable. Next, we tested whether the model produced significant differences in *in silico* IFNγ+ NK cell numbers after a simulated IL18 knockout, compared with those observed *in vivo*, after an IL18R knockout experiment (Figure 4.12B). We observed that distribution of IFNγ+ NK cell numbers after the *in silico* knockout is not significantly different to the observed *in vivo* distribution of cells (*T-test p=0.26, wilcoxon p=0.36*). Thus we deemed the result of this validation experiment acceptable. We examined whether the model produced significant differences in the number of IFNγ+ NK cells after an *in silico* CD169+ macrophage depletion, compared with the numbers of IFNγ+ NK cells observed *in vivo* following a clodronate-mediated subcapsular sinus CD169+ macrophage depletion (Figure 4.12C). Again, we did not observe significant differences in the numbers of IFNγ+ NK cells after the *in silico* knockout, compared with the *in vivo* depletion of these cells (*t-test p=0.82*, *wilcoxon p=0.73*, Figure 4.12C). We therefore deemed the result of this validation experiment acceptable.

Lastly, we sought to whether the model produced statistically significant differences in *in silico* IFNγ+ NK cell numbers compared with the *in vivo* data after a 'double knockout' experiment, following αIL12 depletion and IL18RKO (Figure 4.12D). Here, we did observe a statistically significant difference between the *in silico* predictions and *in vivo* observations (*T-Test p=0.023, wilcoxon p<0.05*). However, the differences in the numbers of cells between experimental settings are minuscule with median values ranging around one cell in both settings. Despite minor numerical differences between the distributions of IFNγ+ NK

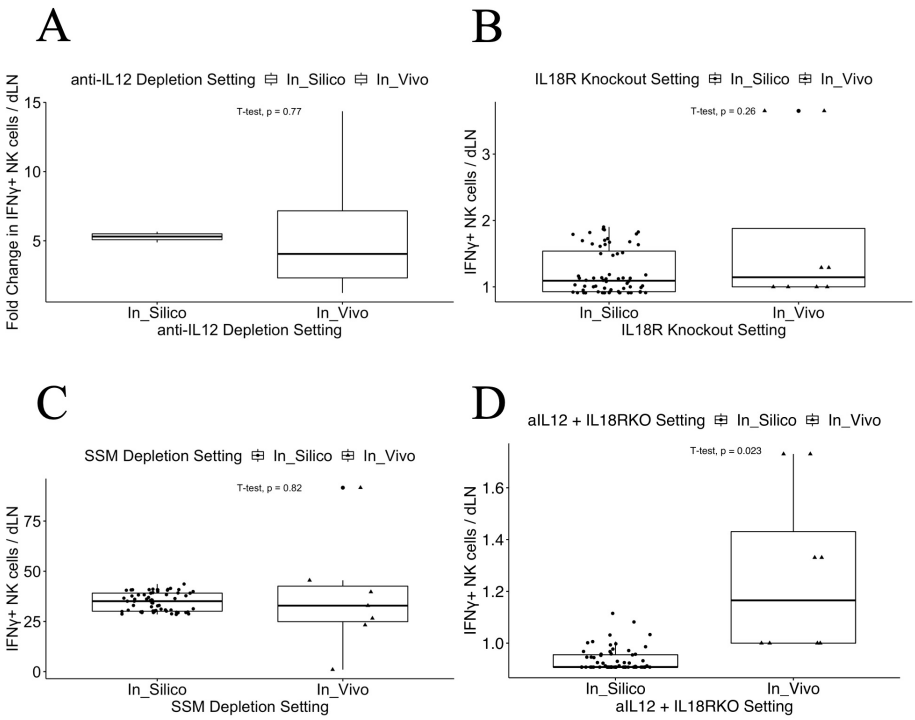


Figure 4.12: **Validation of the simulation model:** Boxplots contrasting *in silico* and *in vivo*. All *in vivo* data was generated by GSK and not by the author of this thesis. **A)** Fold changes in IFNγ+ NK cells after respective anti-IL12 depletions. *In vivo* experimentation was performed by treating C57BL/6 WT mice with αIL12p40 or control IgG, and immunized i.m the following day with AS01 and HBsAg. DLNs were collected six hours after immunization and the levels of IFNγ producing NK cells was evaluated by ICS. *In silico*, this experiment was performed by removing any mathematical terms that involve IL12, i.e for NK cell activation and IFNγ production. Simulation is then performed *in silico* for the 'wild type' model and the 'knockout' model. Fold-changes of IFNγ+ NK cells (*NKa*) at six hours are calculated between the two *in silico* scenarios, and then compared to the corresponding *in vivo* fold-changes. **B)** IFNγ+NK cells after respective IL18R Knockouts. *In vivo* experimentation was performed by immunising i.m C57BL/6 WT or IL18$^{-/-}$ mice with AS01 and Hepatitis B surface antigen (HBsAg). DLNs were collected six hours after immunization and the levels of IFNγ producing NK cells was evaluated by ICS. *In silico*, an IL18R knockout was performed by removing any terms that involve IL18 - i.e NK cell activation and IFNγ production. **C)** IFNγ+ NK cells after respective clodronate-mediated subcapsular macrophage depletions. *In vivo* experimentation was performed by treating C57BL/6 mice with 20ul clodronate liposomes or control liposomes i.m. Six days later mice were immunised with AS01 and HBSag. DLNs are collected and analysed by FACs. *In silico*, this was performed by setting the 'Mo' (CD169+ macrophage) initial condition to zero. **D)** IFNγ+ NK cells after both anti-IL12 and IL18R knockout scenarios *in silico* and *in vivo*. *In vivo* experimentation was performed by treating C57BL/6 WT + control IgG or IL18-/- mice with αIL12p40, and immunized i.m the following day with AS01 and HBsAg. DLNs were collected six hours after immunization and the levels of IFNγ producing NK cells was evaluated by ICS. *In silico* experimentation was performed by removing mathematical terms where both IL12 and/or IL18 are involved.

cells *in vivo* vs. *in silico*, we argue that the model does replicate the dynamics observed *in vivo* - i.e., the numbers of these cells are almost eliminated in the *in silico* double knockout. Taken together, we deemed that the model was fit for purpose.

4.2.3.3 Initial Exploration of Model Parameter Space

Model calibration derived 64 parameter sets each representing a local minima with respect to fitting data, which are summarised in Table 4.4. The following section details the parameter space of the calibrated model, and highlights different possible model behaviours in select regions of the parameter space. Further exploration of model behaviours in different regions of the parameter space, as per our research questions - follow in Chapter 5. Of particular note, we are interested in the transience of the system and the dynamics away from the systems steady states, therefore in what follows, we did not utilise methodology such as stability analysis.

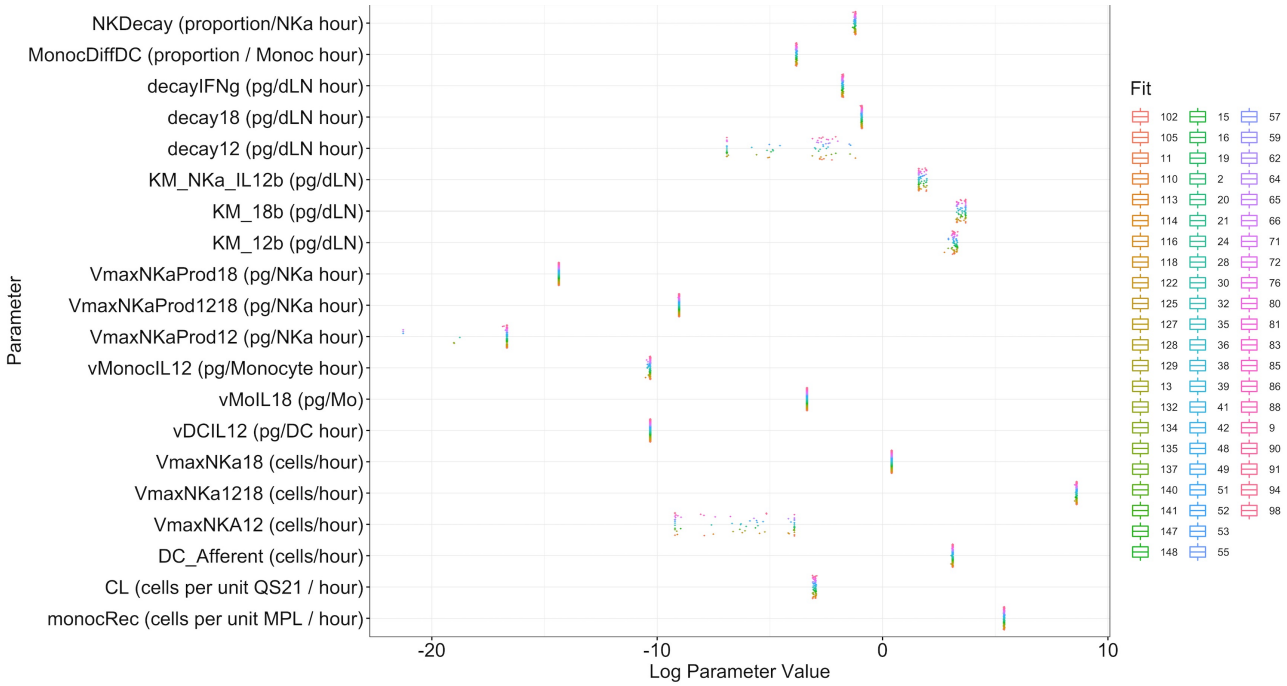


Figure 4.13: **Log-transformed parameter space:** showing the distribution of calibrated parameter values. Y-axis is ordered by parameter dimension. Each parameter has been log-transformed to improve readability.

	Parameter	LowerRange	BestFitValue	UpperRange	LowerRange_Calib	UpperRange_Calib	Mu	Units
1	$monocRec_p$	2.175E+02	217.52468649	2.250E+02	1.000E+01	2.250E+02	2.148E+02	cells per unit MPL / hour
2	$MonocDiffDC_p$	2.142E-02	0.02142500	2.264E-02	1.000E-03	2.000E-01	2.061E-02	proportion / Monoc hour
3	$DC_Afferent_p$	2.088E+01	22.50000000	2.250E+01	1.000E+00	2.250E+01	2.055E+01	cells/hour
4	CL_p	4.475E-02	0.05054920	5.406E-02	1.000E-04	1.000E-01	5.063E-02	cells per unit QS21 / hour
5	$vMoIL18_p$	3.500E-02	0.03500000	3.500E-02	7.000E-03	3.500E-02	2.047E-02	pg/Mo
6	$decay18_p$	3.742E-01	0.40000000	4.000E-01	1.000E-03	4.000E-01	4.000E-01	pg/dLN hour
7	$VmaxNKaProd1218_p$	1.156E-04	0.00012000	1.200E-04	1.136E-05	1.200E-04	1.200E-04	pg/NKa hour
8	$KM_NKa_IL12b_p$	5.000E+00	5.00000000	7.140E+00	5.000E+00	5.000E+01	5.000E+00	pg/dLN
9	$VmaxNKaProd18_p$	5.777E-07	0.00000058	5.777E-07	1.534E-07	5.777E-07	5.777E-07	pg/NKa hour
10	$VmaxNKaProd12_p$	5.777E-10	0.00000006	5.777E-08	5.777E-10	5.777E-08	5.777E-08	pg/NKa hour
11	$decayIFNg_p$	1.652E-01	0.16597714	1.755E-01	1.000E-02	4.000E-01	1.675E-01	pg/dLN hour
12	$vMonocIL12_p$	2.705E-05	0.00003333	3.333E-05	2.000E-05	3.333E-05	3.000E-05	pg/Monocyte hour
13	$vDCIL12_p$	3.333E-05	0.00003333	3.333E-05	2.000E-05	3.333E-05	3.000E-05	pg/DC hour
14	$decay12_p$	1.000E-03	0.10813473	3.000E-01	1.000E-03	3.000E-01	1.094E-01	pg/dLN hour
15	$VmaxNKa1218_p$	5.053E+03	5499.98153413	5.500E+03	1.000E+02	5.500E+03	5.000E+03	cells/hour
16	KM_18b_p	2.622E+01	26.96231749	4.000E+01	5.000E+00	4.000E+01	1.500E+01	pg/dLN
17	KM_12b_p	1.558E+01	22.55488406	2.809E+01	5.000E+00	4.000E+01	1.500E+01	pg/dLN
18	$VmaxNKA12_p$	1.000E-04	0.00010462	2.000E-02	1.000E-04	2.000E-02	2.000E-02	cells/hour
19	$VmaxNKa18_p$	1.500E+00	1.50000000	1.500E+00	1.000E-01	1.500E+00	1.500E+00	cells/hour
20	$NKDecay_p$	2.657E-01	0.30000000	3.000E-01	1.000E-02	3.000E-01	3.000E-01	proportion/NKa hour

Table 4.4: Parameter Values derived from calibration. 64 parameter sets were produced after multi-start fitting to experimental data. 'LowerRange' and 'UpperRange' represent the lower and upper range respectively of the parameter values yielded from the 64 fits. 'BestFitValue' is the value if the parameter from the local optima with the lowest objective value. 'LowerRange_Calib' and 'UpperRange_Calib' reflect the range provided to the multi-start trust-region optimiser following the incremental optimisation process. 'Mu' represents the best fit after incremental optimisation, i.e., the starting point provided to the multi-start trust region algorithm. Given no data on QS21 and MPL, parameters $QS21_p$ and MPL_p are set arbitrarily to a value of '10', hence mechanisms involving these parameters are described e.g 'cells per unit MPL_p'. Parameters 1-6 i.e above the horizontal line, can separated in equations that prescribe a variable as a function of time, while parameters below this line are involved in more complex nonlinear equations.

The calibrated ranges of parameters are visualised in Figure 4.13. For some parameters, their values converge at similar regions, e.g the monocyte recruitment parameter ($monocRec_p$), whereas in contrast some parameters' values are spread across the parameter space e.g the parameter controlling the rate of IL12 decay $decay12_p$ and the parameter controlling the rate of activation of NK cells by IL12 alone *VmaxNKA12*. The latter two parameters unsurprisingly occupy a large range in parameter space, as there is no available IL12 data to constrain these parameters. These data suggest that experimental data regarding IL12 concentrations after AS01 *in vivo* or *in vitro*, may help constrain IL12 related parameters. A global sensitivity analysis - which is detailed further throughout Chapter 5, in particular section 5.2.5 - identified the parameters controlling the rates of a) synergistic production of IFNγ by NK cells $VmaxNKaProd1218_p$ and b) macrophage production of IL18 $vMoIL18_p$, as the most influential parameters in the production of IFNγ over the first six hours after AS01. This is a critical timeframe, corresponding to when the peak of IFNγ is observed *in vivo*.

To explore the behaviour of the simulation in different regions of the parameter space of these two parameters, we uniformly sampled and simulated parameter values across a range of +-90% of the baseline 'best fit' value of each parameter (Figure 4.14A-B). Each parameter was sampled and simulated individually, i.e., in a 'one at a time' manner. We observed strong relationships between each parameter and simulated *IFNg* at six hours post-injection. Additionally, we found that model output in the small region of the best-fit calibrated values conform well to the experimental data. This suggests in the simulation, *IFNg* would not be robust to variation in the assigned best-fit calibrated values of these parameters and thus we likely have a practical identifiability problem.

We next sought to evaluate these two parameters' robustness. We therefore varied $vMoIL18_p$ and $VmaxNKaProd1218_p$ 10% either side of their 'best fit' calibrated value, and used the Vargha-Delaney A-Test to determine the size of the effect on IFNγ after each parameter alteration, compared with the baseline calibrated 'wild-type' model (Figure 4.14C-D). For $vMoIL18_p$, we assigned values within the range of 0.0315 and 0.0385. Small deviation from the calibrated value produced a large effect-size, demonstrating that the simulator is not robust to changes in this parameter's value. For $VmaxNKaProd1218_p$, we assigned values between 1.08e-04 and 1.32e-04. Again, small deviation produced a large effect-size for this parameter. These data demonstrate that simulated IFNγ is not robust to alterations in the values of these parameters. Together, the data in Figure 4.14 may explain why these parameters were assigned tight ranges through calibration (see Table 4.4). Given their importance, further investigation is required to constrain these values, and it is likely that *in vitro* experimentation will be necessary. Indeed, the scarcity of quantified

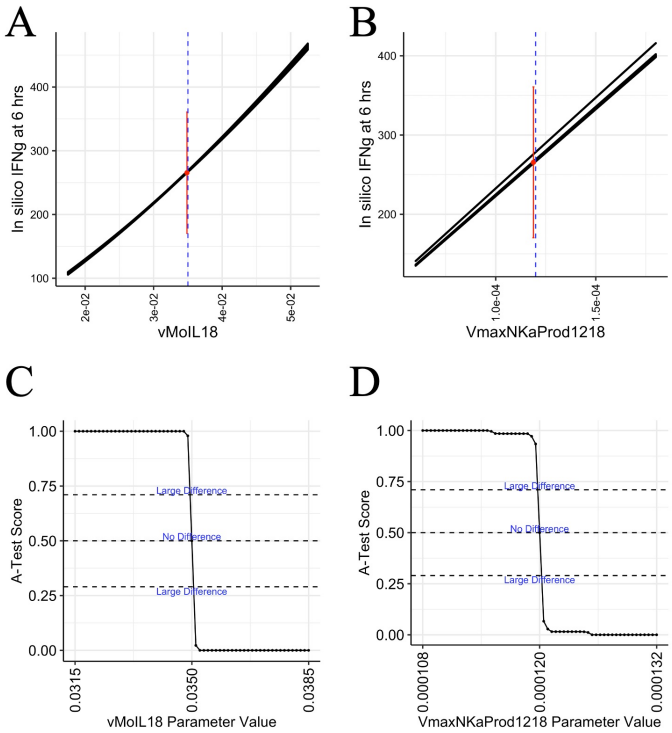


Figure 4.14: **The importance of VmaxNKaProd1218$_p$ and vMoIL18$_p$ parameters in IFNγ production:** A-B) Simulation results (black dots) at six hours after running the model with different parameter values for *vMoIL18$_p$* (A) and *VmaxNKaProd1218$_p$* (B). By uniformly sampling +/-90% each side of the baseline parameter, 523 parameter sets were sampled and simulated, changing only the parameter of interest. Blue dashed line indicates the calibrated best-fit value of each parameter on the x-axis. The means and error of experimental data for IFNγ at six hours is shown in red. C-D) Parameters *vMoIL18$_p$* (C) and *VmaxNKaProd1218$_p$* (D) were varied over ranges each side of their calibrated best-fit value. Plots show the effect of OAT parameter alterations on simulation measures, assessed by the A-Test.

values within the domain appears to lead to a situation where the model is likely to not be identifiable. In what follows, we aimed to leverage such insights to guide experimental design by proposing experiments which may improve the quantitative understanding of the system.

4.2.3.4 A Non-identifiable Model and Improving Quantitative AS01 Knowledge

Model identifiability is concerned with calibration. A model is classified as identifiable if one is able to precisely estimate the true value of the parameters. Often, model identifiability is not explored in mechanistic models. Gutenkunst et al. [305] recognised that due to vast experimental difficulties in estimating *in vivo* parameters and uncertainty produced by fitting to experimental data, that parameter estimation is a major obstacle. Indeed, they evaluated 17 systems biology models and determined that the parameters were not well constrained, a phenomenon they refer to as 'sloppy'. They observe that all models

evaluated were non-identifiable. The authors argue that direct parameter measurements are inefficient at constraining predictions made by sloppy models, and that insistence on tight estimates of the parameters are unnecessary, as they do not enhance model predictions. Gutenkust et al suggest researchers focus "not on the quality of their parameter values but on the quality of their predictions". To embrace this notion in a situation with scant data, we sought to be transparent about the modelling process, systematic and careful in Domain and Platform modelling, and incorporate uncertainty yielded from the data and parameters when making predictions using the model; through generating a distribution of values for each parameter via multi-start optimisation.

Precisely identifying this model's parameters would require *in vivo* data regarding more model components. For vaccination with AS01 adjuvants, experimental data are variable, and in some cases experiments that evaluate the same cell type, produce measurements with order of magnitude differences. The reason for this is not known. Thus, it is likely that models developed in this thesis are likely to be non-identifiable. In such a case, the model is treated as a theoretical construct [239]. Its purpose is to explore whether hypotheses and knowledge gaps that are developed in Chapter 3 are consistent with the phenomena observed *in vivo*, and where possible to refine these hypotheses. This model will also be explored to propose new hypotheses underpinning AS01 MoA, however, model identification and thus precise calibration is likely not possible. In our laboratories, identifiability of models has ranged from minimal exploration into the problem, to a similar scenario as presented in this thesis where the model is deemed non-identifiable *a priori* [239]. Despite this, models were deemed predictive and ultimately contributed to understanding various immunological systems. Indeed, the aforementioned non-identifiable model, considered a theoretical construct similar to the situation here, made predictions which were later confirmed *in vivo* [239].

Nonetheless, we performed identifiability analysis using the profile-likelihood method [9], as proposed by [306]. We postulated that the benefit of this analysis would be two-fold. Firstly, identifiability analysis would enable further insight into the model, and secondly, we could leverage identifiability insights to illuminate the limitations of our quantitative understanding of the system - an opportunity for modelling to guide experimentation which would further our understanding of this important adjuvant. Briefly, through posing a parameter estimation problem using real or simulated data, the profile-likelihood can provide the range of parameter values which are supported by available observational data. Indeed, the profile-likelihood represents the likelihood that values of a single parameter agree with the observational data. For a parameter x, we compute the profile-likelihood by changing the value systematically. Remaining parameters are optimised and the log-likelihood ratio

is assessed. The parameter is therefore profiled step-by-step by scanning along its axis, for each provided value of x. In both directions (i.e increasing or reducing the parameter), the objective value (measurement of agreement of the model and the data) may increase, i.e agreement with the data will reduce. By a certain point, the objective value exceeds a confidence threshold and one can reject values beyond this threshold, which in turn provides the confidence interval. As a result, identifiability can be examined. Non-identifiability can be firstly characterised by a flat profile, where the confidence interval is open. Here, altering the parameter does not alter the log-likelihood enough to pass the confidence threshold in either direction. Non-identifiability can also be characterised by a semi-open confidence interval. Here, in one direction the threshold is passed however in the other direction, it is not possible to constrain the parameter to a confidence interval. In contrast, an identifiable parameter has a closed confidence interval, i.e in both directions, there comes a point where alterations in a parameter's value produces worse fits to the observational data and therefore exceeds the confidence threshold. For the profile-likelihood analysis performed throughout this thesis, we examined the profile-likelihoods by starting from every local optima and confirmed differences were not observed in identifiability across fits. However, for simplicity the profile-likelihoods in Figure 4.15 and 4.16 are generated from examining identifiability starting at the 'best-fit' set of parameters.

Figures 4.15 and 4.16 show the effects on the objective value after perturbing values of parameters of interest. The visualised parameters were selected to highlight a range of different identifiability scenarios arising from this model. Table 4.5 shows the confidence bounds for each parameter as determined by the profile-likelihoods. For the $monocRec_p$ parameter, we found that the 95% confidence interval is closed in both directions, thus the parameter is identifiable (Figure 4.15A). It is important to note however, that it is likely that this parameter is only identifiable in this setting as the parameter 'MPL_p' is fixed. Indeed, in model development due to a lack of MPL or QS21 biodistribution data, we had to arbritrarily fix these parameters. To identify $monocRec_p$ in the context of more accurate, varying MPL concentrations, rich data would likely be required on MPL quantifications in the dLN.

For '$MonocDiffDC_p$' we were able to identify an upper bound for the parameter (Figure 4.15B). Given the observation that monocytes do differentiate into DCs after AS01 albeit at limited rates [5, 95], one can assume that the lower bound of this parameter is at least zero. The small calibrated ranges of this parameter's values are consistent with the very recent observation that monocyte differentiation into DCs occurs, but is limited after AS01 [95]. In future work, additional quantitative data on DC subsets including MoDCs may constrain this parameter further.

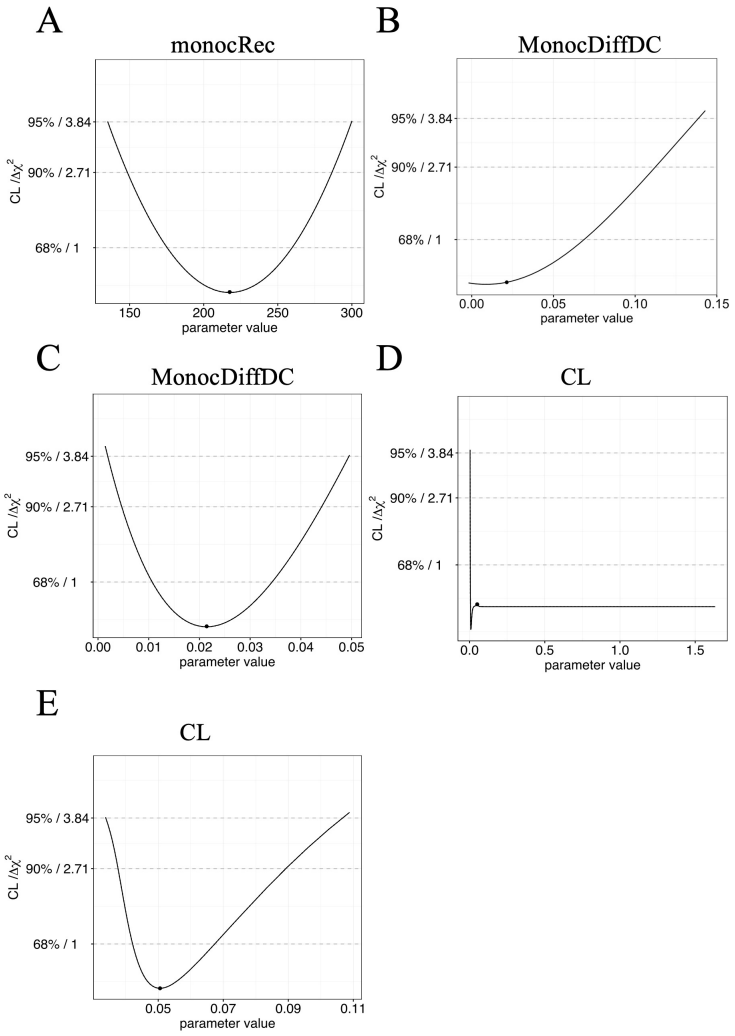


Figure 4.15: **Profile-likelihood analysis for cell-related parameters:** Plots showing data contribution to the total objective value based on perturbations of parameters. Profile-likelihood analysis was performed using dMod [9]. Confidence interval thresholds are labelled on y-axis. Parameter values are shown on the x-axis.

Indeed, through exploring the profile-paths [9], we observed a coupling between $MonocDiffDC_p$ and the parameters $monocRec_p$, $DC_Afferent_p$ and CL_p (data not shown). Indeed, fixing these parameters resulted in a closed confidence interval, thus enabling $MonocDiffDC_p$ to be identified in this context (Figure 4.15C). This insight suggests that identifying the values for parameters controlling rates of monocyte recruitment $monocRec_p$, DC recruitment and activation $DC_Afferent_p$ and macrophage cell loss CL_p may enable the identification of the rate to which monocytes differentiate into DCs after AS01, as would further data on DC subsets. With respect to $DC_Afferent_p$, large variation exist in the available DC data, which perhaps complicates the ability to identify $MonocDiffDC_p$ without fixing parameters. Indeed, $DC_Afferent_p$ itself is not identifiable (Table 4.5). Furthermore, we were only able to compute a lower bound for the CL_p parameter which controls macrophage cell

loss after QS21 stimulation (Figure 4.15D). While it is possible to infer that the parameter should be >0 (as a reduction of these cells is observed in the experimental data), given the current available data we are unable to determine the *rate* at which macrophage cell loss occurs. Indeed, there only exist data at two timepoints for the CD169+ macrophage numbers, each with large variation around the measurements. From the profile-likelihood in Figure 4.15D, we can only infer that the CL_p parameter is small but not zero. The profile-likelihood here is not flat however, indicating that the parameter could be identified given further data. Our findings here suggest that to identify the rate at which macrophage cell loss occurs, we require additional data between zero and 24 hours, to provide an understanding of the shape of macrophage loss. Only by fixing 16 model parameters are we able to constrain the CL_p parameter (Figure 4.15E).

We next evaluated the identifiability of key cytokine production parameters. For the $vMonocIL12_p$ parameter, we were unable to compute an upper or lower bound of the parameter (Figure 4.16A). By fixing 14 of the model parameters, we are able to to close the confidence interval in one direction (Figure 4.16B). However, even after fixing these parameters, zero production of IL12 by monocytes would not produce further disagreement with the data. This is unsurprising as there is no available IL12 data for fitting to constrain the parameter values. Despite this, it is important to retain this parameter as it represents an important hypothesis that we required to capture. Unsurprisingly, a similar situation is observed for $vDCIL12_p$ - the confidence interval is open in both directions (Figure 4.16C). Again, fixing 14 model parameters allows identification of an upper bound for this parameter (Figure 4.16D). Given the lack of data on IL12 concentrations to constrain these values, during profile-likelihood analysis these parameters are likely to be compensated by other parameters, perhaps leading to the flat profiles we observed (although they are not completely flat). Flat profile-likelihoods can suggest that a parameter is not influential, however, sensitivity analysis demonstrated that these two parameter are influential in IFNγ production (presented in Chapter 5). Therefore, despite flat profile-likelihoods, these parameters do not represent subordinate mechanisms. In light of these data, we argue that experimental data on IL12 concentrations after respective cell stimulation would be considerably valuable, and improve the ability to identify these two parameters as this would enable estimations of IL12 related activation and decay parameters. Indeed, our results indicate that examination of respective production of IL12 by these cells after AS01-adjuvanted vaccination *in vitro* would greatly enhance the simulator and our understanding of innate IFNγ after AS01.

Figure 4.16E shows that we are unable to identify the $VmaxNKaProd1218_p$ parameter, which controls the rate of IL12 and IL18 synergistically induced production of IFNγ. Surprisingly, a reasonable amount of experimental data exist for IFNγ production. Fixing all

other parameters closed the 95% confidence interval in the upper direction (Figure 4.16F). During this analysis we observed that leaving '$VmaxNKaProd18_p$' unconstrained detrimentally affects the identifiability of $VmaxNKaProd1218_p$. The $VmaxNKaProd18_p$ parameter represents the production of IFNγ after stimulation of NK cells only by IL18, i.e., in absence of MPL_p induced IL12 and therefore in absence of IL12 and IL18 synergy. This indicates that analysis of the relative contributions of individual IL12 and IL18 after MPL or QS21 alone, to the total IFNγ production and the synergy, following a dose-response study would assist identification of this parameter.

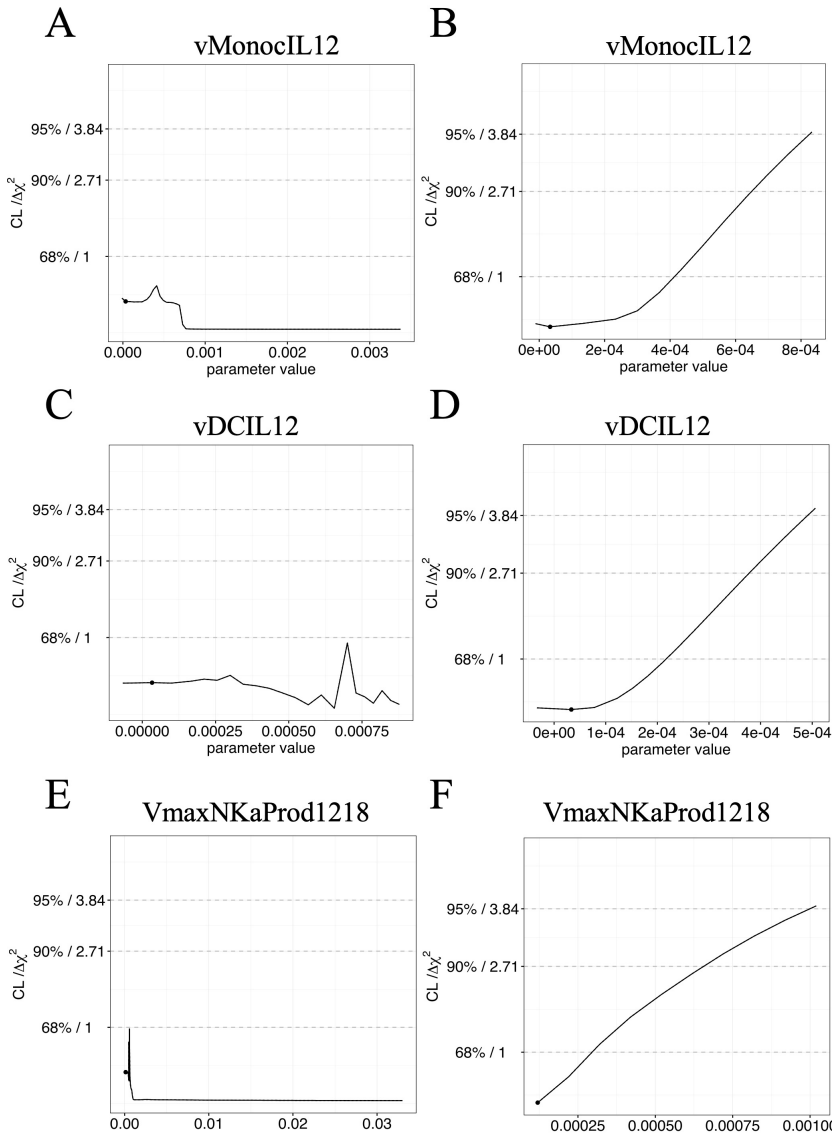


Figure 4.16: **Profile-likelihood analysis for cytokine-related parameters:** Plots showing data contribution to the total objective value based on perturbations of parameters. Profile-likelihood analysis was performed using dMod [9]. Confidence interval thresholds are labelled on y-axis. Parameter values are shown on the x-axis.

Parameter	value	Lower	Upper
$monocRec_p$	2.17525E+02	-1.76878E+01	2.90376E+02
$decay12_p$	1.08135E-01	-Inf	Inf
$decay18_p$	4.00000E-01	-Inf	Inf
$NKDecay_p$	3.00000E-01	-Inf	Inf
KM_18b_p	2.69623E+01	-Inf	Inf
KM_12b_p	2.25549E+01	-Inf	Inf
$MonocDiffDC_p$	2.14250E-02	-Inf	1.38714E-01
$decayIFNg_p$	1.65977E-01	-Inf	Inf
$vMonocIL12_p$	3.33333E-05		Inf
$VmaxNKa1218_p$	5.49998E+03	-Inf	Inf
VmaxNKA12	1.04624E-04	-Inf	Inf
$VmaxNKa18_p$	1.50000E+00	-Inf	Inf
$decay12_p$	1.08135E-01	-Inf	Inf
$vDCIL12_p$	3.33333E-05	-Inf	Inf
CL_p	5.05492E-02	3.28622E-03	Inf
$vMoIL18_p$	3.50000E-02	-Inf	Inf
$DC_Afferent_p$	2.25000E+01	-Inf	2.75513E+02
$KM_NKa_IL12b_p$	5.00000E+00	-Inf	Inf
$VmaxNKaProd18_p$	5.77734E-07		
$VmaxNKaProd1218_p$	1.20000E-04	-Inf	Inf

Table 4.5: Identifiability of IFNγ AS01 Model: All local optima were assesed as starting points for profile-likelihood analysis. The column 'value' here shows the best fit of the parameter as determined by optimisation. 'Lower' and 'Upper' show the lower and upper bounds respectively yielded from profile-likelihood analysis.

In summary, profile-likelihood analysis of this model was unable to determine confidence bounds for many parameters, confirming our anticipation that the model is mostly non-identifiable. We did not explore further model reduction in light of these findings, as we strongly believe that the hypotheses and understanding underpinning the model is captured as simple as possible, so to produce a model appropriate for the exploration of our research questions. In this light, we have shown that the quantitative understanding of the early IFNγ response to AS01 is limited, and leveraged these insights to propose experimental avenues which would improve the model's identifiability and in turn improve the quantitative understanding of the system.

4.3 Discussion

In this chapter, we proposed a mathematical model of the salient events underpinning the innate IFNγ response after AS01-adjuvanted vaccination in the dLN. To satisfy thesis aim 2 - to create, calibrate and validate such a model - we followed the CoSMoS process[242]. Prior to model development, we performed a comprehensive literature search and determined that no suitable models existed, although models e.g., developed by Wigginton et al. [196] captured similar kinetics, and thus could serve as inspiration here. Furthermore, we had determined that while statistical models can be advantageous in many settings, much of the experimental data we had access to for AS01 were based on measurements from small numbers of mice, potentially limiting the statistical power of phenomenological models. Therefore, we focused our efforts on mechanistic modelling rather than the use of statistical

models, as for our research questions, these would not be the most appropriate techniques nor able to provide robust statistical inference.

The work in Chapter 3 resulted in questions pertaining to the early immune response to AS01, and to construct a mathematical model appropriate for exploration of a set of these questions, we refined the key output of Chapter 3, the *Core AS01 Domain Model*, in light of the research questions 2-6 defined in section 4.1. Indeed, for development of the IFNγ model, the 'core' Domain Model from chapter 3 provided insight into the scope necessary to construct the IFNγ model. To develop the IFNγ model, we first gathered experimental data, which we separated for calibration (Figure 4.1) and validation. Subsequently and informed by the work in Chapter 3, we constructed a Domain Model - summarised in Figure 4.4 - which captured the relevant biology with respect to the research questions. Next, we constructed a Platform Model, to express the Domain Model in computational and mathematical language. This specification consisted of detailed diagrams describing implementation details for captured entities. These diagrams led to the proposal of a set of ODEs, which (generally) employ saturation kinetics to capture cellular activation and cytokine production. Saturation kinetics - which follow the form of Michaelis-Menten - have been used previously to describe intercellular interactions, and cellular interactions with cytokines [196, 197]. We therefore took inspiration from such work, resulting in a simple ODE model of immune function pertaining to innate IFNγ production after AS01. Given the simplicity of some model equations, we separated linear equations which can be written as functions of time, from more complex non-linear equations.

A mathematical model to explore IFNγ production after AS01 stimulation: We implemented the ODE model in R using the package *dMod*. We then calibrated the simulation against the data set aside for parameterisation. The model kinetics are of a 'cascading' nature, where generally, one can isolate portions of the model, optimise, and incrementally include 'next-event' portions for calibration. This incremental approach to develop a best-fit set of parameters, serves to reduce the complexity of the calibration problem, and thus allow sufficient sampling of the parameter space by isolating portions of the model. Once the best-fit set of parameters had been generated by this process, multi-start fitting was employed, spreading starting positions of optimisation throughout the parameter space, which yielded multiple parameter sets, each reflecting a local minima (with respect to fitting data). In analysis with this model, each local minima are treated as equally likely, thus are each employed in analysis, producing a distribution of predicted model output for each ODE variable. Following calibration, we performed model validation by comparing output from knockout variants to analogous experimental data for which the model was not calibrated against. After comparing analogous model and *in vivo* entities

after corresponding *in silico* and *in vivo* experimental scenarios, we determined that model validation had been satisfactory and that the model was fit for purpose (Figure 4.12). Therefore, a key output of this chapter, satisfying thesis aim 2, is a simulation of innate IFNγ production after AS01, which fits the experimental data well, and has satisfactorily predicted observational data upon which it was not calibrated.

Practical Identifiability would likely be improved by MPL, QS21 and Cytokine Concentration Data: Next, we enumerated the parameter space of calibrated fits and evaluated model robustness to two important (determined by a sensitivity analysis detailed in Chapter 5) parameters (Table 4.4, Figure 4.13,4.14). We observed that multiple parameters converged on similar values in log-space, while some parameters e.g., $decay12_p$ and *VmaxNKA12* exhibited a wide range of values. Further, we found that simulated IFNγ was not robust to alterations in the values of the parameters controlling macrophage-induced IL18 and synergistic production of IFNγ by NK cells. This suggested we may have a practical identifiability issue. We next utilised the profile-likelihood method to analyse model identifiability and based on these insights, we proposed new experiments which may improve the quantitative understanding of the system (section 4.2.3.4, Table 4.5).

This work implied for example, that model identifiability could be improved through the incorporation of time-series QS21 and/or MPL concentration data. Such data is not available and the two vaccine immunostimulants were therefore captured as parameter values. During calibration, we arbitrarily fixed the values of these parameters to '10', thus the model calibration and resulting parameter values are in the context of these parameters being set to 10. Indeed, parameter units which are affected by MPL or QS21 are generally described e.g., as '*per unit of* MPL_p'. Clearly, quantifications of MPL or QS21 would not be identical throughout the entire simulation and thus a more precise parameterisation is likely, through incorporating MPL and QS21 concentration data, were such data to become available. Further, none of the cytokine production parameters are identifiable with the current available data. We were also unable to locate sufficient data on rates of the captured cells' production of these cytokines in the literature. Therefore we proposed that model identifiability and quantitative understanding of AS01-induced immune responses could also be improved by dose-response assays *in vitro* with AS01, assessing the respective production of IL12, IL18 and IFNγ by key cell types. Notwithstanding, we leveraged the identifiability analysis performed in this chapter to not only reveal the limited quantitative understanding of the system that can be extracted from the experimental data, but to suggest avenues of research which may improve these gaps in understanding. In retrospect, we could have placed more focus on collaborations to generate *in vitro* measurements for areas

of the model where no data exist whatsoever, early in the project. Furthermore, quantifications of cell types after AS01 vary between orders of magnitude and so a meta-analysis of the available experimental data could have been valuable. Further model validation could also have occurred by various cross-validation techniques e.g leave-one-out, however such techniques were not utilised due to high variability in the limited experimental data.

In many research settings, stability analysis can be appropriate and valuable (e.g., Perelson's HIV model, see section 1.8.1.1). Additionally for disease spread models, conclusions (e.g the effects of social distancing interventions) may rest upon the state of the system at equilibrium. Analysis of steady-states and their stability was considered for the model developed in this chapter (and those presented in Chapter 6). However, the focus of the thesis is to produce simulators which fit the dynamics of the available experimental data, and employ these simulators to reveal or propose relationships between different cells and cytokines during early AS01 vaccination, and analyse transient temporal kinetics. Thus, we argue that our interests - or the conclusions in following chapters - do not rest upon the stability of steady-states and therefore this analysis would not yield the insight required to support work within the scope of this thesis at this time.

Summary: The primary result of this chapter is the first calibrated and validated mechanistic model of AS01 MoA, which provides a simulation platform upon which *in silico* experimentation and model analysis can occur to explore the early immune response to AS01. While no data exist for IL18, IL12, MPL and QS21 concentrations, the proposed model can recapitulate the available experimental data and after simulating scenarios for which the model is not trained against, the model produces consistent responses of IFNγ+ cells compared with the *in vivo* data. For the reasons outlined by Gutenkust et al [305], we focused on developing confidence in the simulator through a principled design and model validation. We do propose that confidence in the model could be improved even further, by future generation of data for gaps highlighted in this chapter and incorporating such data into the model. This work provides a model for use in *in silico* experimentation and serves as a useful gateway for further development. This chapter has also highlighted our limited quantitative understanding of early AS01-adjuvanted immune responses and proposes experiments - guided by *in silico* evidence - which may improve the quantitative understanding of early AS01 MoA. This model is utilised to investigate the early cytokine response to AS01 in the following chapter.

Chapter 5

Investigating the immunological mechanisms of early cytokine production during AS01 induced immune responses

5.1 Introduction

In Chapter 3, the current understanding of AS01-induced immune responses was formalised, knowledge gaps were identified and consolidated and research questions were formulated. In Chapter 4, a mathematical model describing salient events that lead to the transient production of IFNγ over the first 24 hours was proposed. In what follows, we employed the simulation developed in Chapter 4 to investigate our research questions. These research questions involve examination of relationships between cells and cytokines following vaccination with MPL and QS21. To elucidate such relationships, we evaluated downstream effects of parameter perturbations and performed sensitivity analyses as well as *in silico* knockout experiments.

5.1.1 Aims

In this chapter, we addressed **aim 3 (section 1.10.2)** by answering research questions 2-6, which are reproduced below. Each question is in the context of AS01 adjuvanted vaccination.

1. The source of IL12 is unknown. Given the assumption that monocytes and DCs both produce IL12 at the same rate, what differences do we observe in the temporal dynamics of potential cellular IL12 production? What hypotheses do these insights generate?

2. What is the relationship between each cell type's respective production of IL18 or IL12 with the production of IFNγ? How does this differ over time? What is the dominant cytokine in initiating early IFNγ?
3. What are the most influential parameters involved in early IFNγ production after AS01?
4. What effects does the loss of macrophages have on the IFNγ production? What would happen to the immune response if no macrophage cell loss occurs? How could this cell loss affect IFNγ responses after a second AS01 delivery?

5.2 Results

5.2.1 eFAST Global Sensitivity Analysis

Throughout this chapter, we employed global sensitivity analysis by use of eFAST (see Methods for full details). eFAST provides a statistical measure regarding the proportion of variance attributed to parameter alteration, therefore evaluating how sensitive the simulation is to that parameter [307]. Here, we describe how eFAST global sensitivity analysis was performed in this Chapter. Each parameter was sampled (unless specified otherwise) 150,000 times within pre-defined ranges (Table 5.1) and analysed using the R package *pksensi* [261]. With the exception of *decayIFNg* on IFNγ at hour 1, all parameters with respect to their influence on assesed model components reached an acceptable level of convergence (<0.1), thus sensitivity indices were deemed acceptably robust across replicates. Given the considerable number of parameters, in order to reduce the required parameter sampling space for eFAST analysis, we fixed parameters where possible and appropriate. All initial conditions were fixed, as they were extracted from control data. Both the parameters $monocRec_p$ and $MonocDiffDC_p$ can be estimated mathematically from the data using Taylor expansion, leading to estimates for $monocRec_p$ of ~ 200 cells per hour and a rate of monocyte differentiation ($MonocDiffDC_p$) of 0.0191. The best fits yielded from model calibration for $monocRec_p$ and $MonoDiffDC$ respecitvely were 217 cells per hour and 0.0214. Given their consistency with mathematical estimates, we fixed these two parameters for eFAST at their 'best fit' values. A profile-likelihood based identifiability analysis placed the $DC_Afferent_p$ parameter within the ranges of 22.5-275. Therefore, this range was used to constrain this parameter for eFAST. The remaining parameters were sampled within the ranges in Table 5.1, leaving 18 model parameters and a dummy (see Methods).

	Parameter	Min	Baseline	Max
1	$VmaxNKaProd1218_p$	2.400E-05	1.200E-04	1.200E-03
2	$KM_NKa_IL12b_p$	1.000E+00	5.000E+00	2.500E+01
3	$VmaxNKaProd18_p$	1.155E-07	5.777E-07	2.889E-06
4	$VmaxNKaProd12_p$	1.155E-08	5.777E-08	2.889E-07
5	$decayIFNg_p$	5.000E-02	1.660E-01	4.000E-01
6	$DC_Afferent_p$	1.000E+00	2.250E+01	2.755E+02
7	$vMonocIL12_p$	3.333E-06	3.333E-05	3.333E-04
8	$vDCIL12_p$	3.333E-06	3.333E-05	3.333E-04
9	$decay12_p$	1.000E-04	1.081E-01	3.500E-01
10	CL_p	3.000E-02	5.055E-02	6.000E-02
11	$vMoIL18_p$	1.000E-02	3.500E-02	5.000E-02
12	$decay18_p$	3.500E-01	4.000E-01	4.500E-01
13	$VmaxNKa1218_p$	2.750E+03	5.500E+03	1.100E+04
14	KM_18b_p	1.348E+01	2.696E+01	5.392E+01
15	KM_12b_p	1.128E+01	2.255E+01	4.511E+01
16	$VmaxNKa12_p$	5.000E-05	1.046E-04	4.000E-02
17	$VmaxNKa18_p$	1.000E+00	1.500E+00	2.000E+00
18	$NKDecay_p$	2.500E-01	3.000E-01	3.000E-01
19	dummy	1.000E-02	NA	1.000E+00
20	$monocRec_p$	Fixed	2.175E+02	Fixed
21	$MonocDiffDC_p$	Fixed	2.142E-02	Fixed

Table 5.1: Ranges of parameters used for eFAST analysis. Baseline shows the calibrated best fit parameter set. A 'Fixed' label shows the parameter is fixed to the best calibrated value.

5.2.2 The predicted temporal dynamics of monocytes and DCs on the production of IL12 after AS01 adjuvanted vaccination

While it is known that synergy between IL12 and macrophage-mediated IL18 promotes the production of early IFNγ following AS01-adjuvanted-vaccination, the source of IL12 and its temporal kinetics are poorly understood. We and colleagues at GSK hypothesised that IL12 is produced by both monocytes and DCs. Due to lack of IL12 data or cellular production rates of IL12 following AS01, during model development, we assumed that these cell types produce IL12 at the same rate. Given these assumptions, we utilised the model to propose temporal dynamics of IL12 production after AS01 and to refine hypotheses, which could be tested experimentally.

DCs may initiate the early IL12 response: We analysed the influence of the parameters - $vMonocIL12_p$ and $vDCIL12_p$, representing rates of production of IL12 by monocytes and DCs respectively - by eFAST global sensitivity analysis (Figure 5.1). Both the first order (Figure 5.1A) and total order sensitivity indexes (Figure 5.1B) suggest that - given the aforementioned assumptions - over the first five hours of the response to AS01, DCs contribute substantially more to simulated IL12 than monocytes. Indeed, the experimental data used for model calibration demonstrates that higher numbers of DCs are located in the dLN at these timepoints, which in turn perhaps explains this result. Through deep consideration of the experimental data, this observation may be reached from qualitative reasoning, however the mechanistic model has helped reveal this finding and its analysis has proposed the temporal kinetics of cellular production of IL12. Furthermore, this insight provides additional confidence that the model has reasonably captured the underlying bi-

ology, given the consistency with qualitative reasoning. Interestingly, despite substantially more monocytes than DCs at later timepoints (see Figure 4.11 B and C), both first and total order sensitivity indexes suggest that simulated monocytes do not become the primary source of IL12 at any period over the first 24 hours to AS01, however the influence of both $vDCIL12_p$ and $vMonocIL12_p$ is similar by approximately 15 hours post-injection. Therefore, given that DCs are more prevalent in the early stages of the response to AS01, model analysis indicates that DC IL12 is dominant at early stages, however, interestingly, the large infiltration of monocytes may not compensate for DC dominance at the latter stages of the simulation.

In summary, we have utilised the innate IFNγ AS01 model to suggest the temporal dynamics of IL12 production after AS01, based on the hypothesis that both monocytes and DCs secrete IL12 after MPL stimulation at similar, if not identical, rates. Our model analysis generates a refined hypothesis, proposing that early in the response, DCs primarily contribute to the production of IL12, although the influence of monocytes and DCs becomes more similar during the latter stages of the simulation. This analysis generates the novel hypothesis that DCs may provide an early IL12 signal to promote innate-IFNγ production.

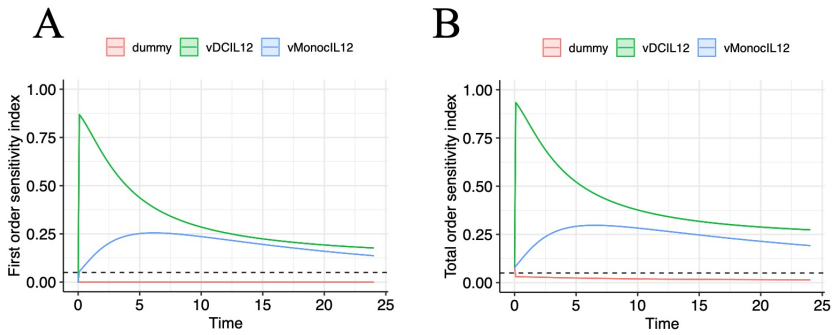


Figure 5.1: **Temporal contributions of DCs and monocytes to IL12 production:** Line graphs showing the influence of parameters $vDCIL12_p$ and $vMonocIL12_p$ - controlling DC or monocyte production of IL12 respectively - through eFAST global sensitivity analysis. A) shows the first order sensitivity indices. B) shows the total order sensitivity indices. The influence of a dummy parameter which should exhibit no impact on simulation behaviour is also shown.

5.2.3 Determining relationships between cellular production of IL18 and IL12 with the production of IFNγ

Parameter Perturbations Suggest a Hierarchy of Influence Over IFNγ Production: We next examined the relationship between the production of IL18 and IL12 by respective cells, with the production of IFNγ. Experimental data generated by GSK shows that after vaccination with HBsAg and AS01 into IL18RKO mice, IFNγ+ NK cells measured by ICS are almost eliminated, compared with HBsAg and AS01 vaccination into

C57BL/6 mice treated with an αIL12 depleting antibody, which instead results in a $\sim$5 fold reduction in these cells (see Figure 3.3A-B) [32]. This suggests that IL18 provokes IFNγ production to a larger extent than IL12 during the synergy required for optimal IFNγ. Through formalising such insights, computational modelling can evaluate such suggestions and help develop a deeper understanding of underlying mechanisms. We utilised the 'AS01 IFNγ model' to examine this insight, as well as to generate novel hypotheses for DC and monocyte roles in IFNγ production. Coccia's experiments analysed the impact of IL18R knockouts and αIL12 depletion on IFNγ+ NK cells, however the simulation developed here allows us to propose the impact of IL18 and IL12 directly on IFNγ itself. We first evaluated the differences in simulated IFNγ at key time-points after perturbing values +/-90% from the baseline (best fit) of parameters 1) $vMoIL18_p$ controlling the rate of IL18 production by macrophages, 2) $vMonocIL12_p$ and 3) $vDCIL12_p$, controlling the rate of IL12 production by monocytes and DCs respectively, and 4) both $vDCIL12_p$ and $vMonocIL12_p$ together. Comparing the effects on simulation output after changing the values of key parameters within the same percentage range from respective baseline values, can indicate which parameters exhibit the largest effects on IFNγ.

We examined simulated IFNγ production after perturbing each of the aforementioned parameters -90% (Figure 5.2A) or +90% (Figure 5.2B). Compared with the baseline values (labelled WT), changes of $vMoIL18_p$ values by +/-90% produced more profound changes in simulated IFNγ at all timepoints than those observed for other assessed parameters, including when both IL12 production parameters $vMonocIL12_p$ and $vDCIL12_p$ were perturbed simultaneously (labelled BothIL12). At one and three hours, perturbing the values of $vDCIL12_p$ produced more profound changes in IFNγ than $vMonocIL12_p$ (Figure 5.2A-B). At eight and sixteen hours the IFNγ levels are similar between $vMonocIL12_p$ and $vDCIL12_p$ changes of +/- 90%. By twenty four hours, $vMonocIL12_p$ adjustments produced marginally larger changes to IFNγ than $vDCIL12_p$. Unsurprisingly by perturbing both IL12 production parameters changes are more profound at all time-points compared with perturbing $vDCIL12_p$ or $vMonocIL12_p$ alone.

By examining barplots displaying the mean percentage change in simulated *IFNg* from baseline after changing each parameter by +/-90% (Figure 5.3), we observed that the largest positive change observed in simulated IFNγ is at 3 hours provoked by $vMoIL18_p$ (approx. 151.01%), while the largest negative change is -96.37% by the same parameter at 24 hours. These data further indicate a hierarchy of influence in IFNγ production, where macrophage-released IL18 is most dominant by six hours post injection, when the peak is observed experimentally. At this stage we cannot exclude second-order effects (see Methods: Global sensitivity analysis) which may add nuance to these observations. Nevertheless, despite a

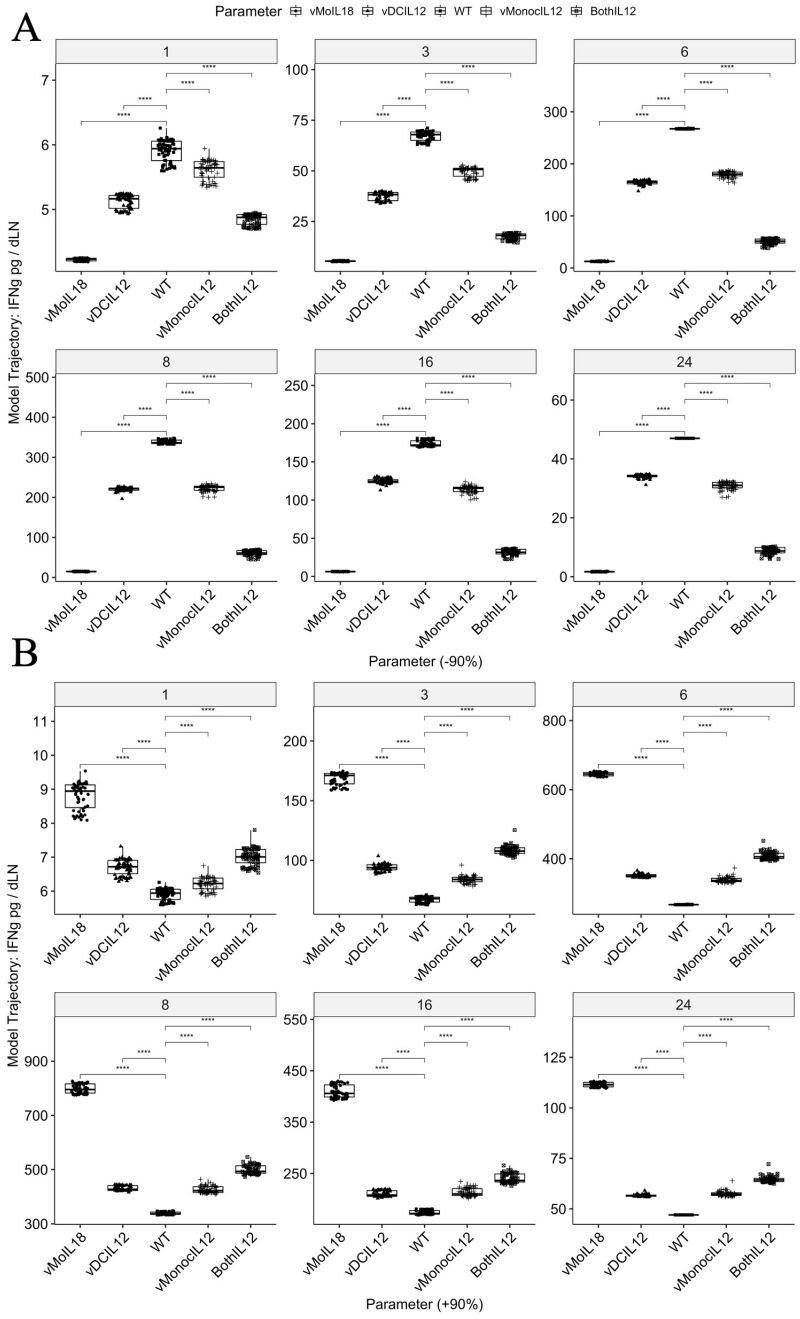


Figure 5.2: **The effects of IL18 and IL12 production by each cell type on the resulting IFNγ production:** Boxplots showing the *in silico* production of IFNγ at key timepoints after perturbing four cytokine production parameters, $vMoIL18_p$ controlling macrophage induced IL18, $vDCIL12_p$ controlling DC induced IL12, $vMonocIL12_p$ controlling monocyte induced IL12, and both IL12 production parameters simultaneously (labelled BothIL12). A) shows IFNγ after reducing the parameters 90% from their calibrated baseline. B) shows IFNγ after increasing the parameters 90% from their calibrated baseline.

much larger population of monocytes than DCs at latter stages, the simulation indicates only small differences in promoting IFNγ production between these two populations of cells during this timeframe. It is worth clarifying at this stage that as we do not know

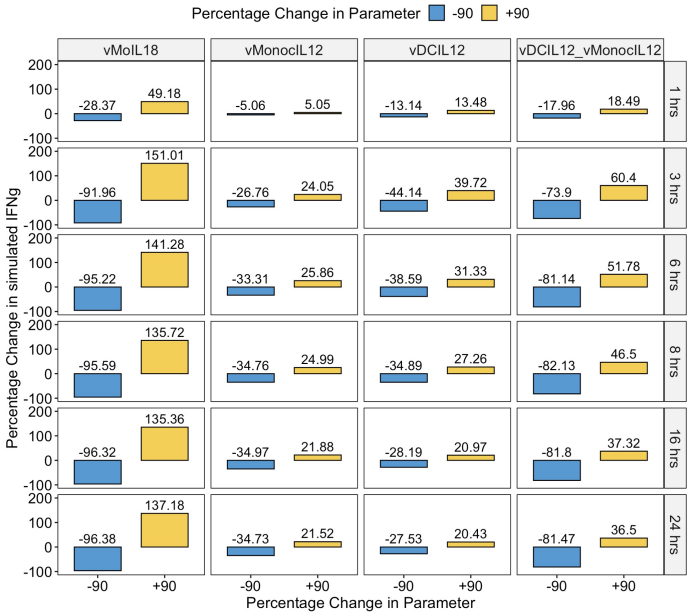


Figure 5.3: **Predicted percentage changes in simulated IFNγ after perturbations of cytokine production parameters:** A collection of bar plots showing at key time-points the predicted percentage changes in mean IFNγ after perturbing parameters $vMoIL18_p$ (controlling macrophage IL18 production), $vMonocIL12_p$ and $vDCIl12$ (controlling monocyte and DC IL12 production respectively), both $vDCIL12_p$ and $vMonocIL12_p$. Number headings in each subpanel represent an hourly timepoint following simulated AS01 administration.

the rate to which monocytes or DCs produce IL12 after AS01, during calibration these cells are assumed to produce IL12 within the same range. Together, our insights add further evidence to the implication that macrophage-released IL18 is most influential in the synergistic production of IFNγ after AS01, and suggest that at early time-points, DCs may provide the primary source of IL12 to support IL18 in initiating the IFNγ response, supported by IL12 from monocytes. Experimental data on IL12 and IL18 production after AS01 will help to quantitatively refine these predictions.

IL18 and DC-IL12 may Primarily Initiate Early IFNγ: Next, we further characterised the hierarchy of cellular cytokine production controlling the IFNγ response. Thus, we performed three *in silico* knockout experiments, each to compare wild type IFNγ and knockout responses. First, we simulated a monocyte-recruitment knockout and monocyte-depletion to evaluate the change in predicted IFNγ compared with the WT simulation (Figure 5.4A). We observed marginal reductions at one hour post-simulated injection in the knockout compared with the WT (-1.059 fold change, Table 5.2). The fold-change differences between the WT and the knockout continues to increase over time and at 24 hours post injection the largest fold-change reduction is observed (-1.781). These data are consistent with previous observations that monocyte influence on IFNγ may increase throughout the duration of the response.

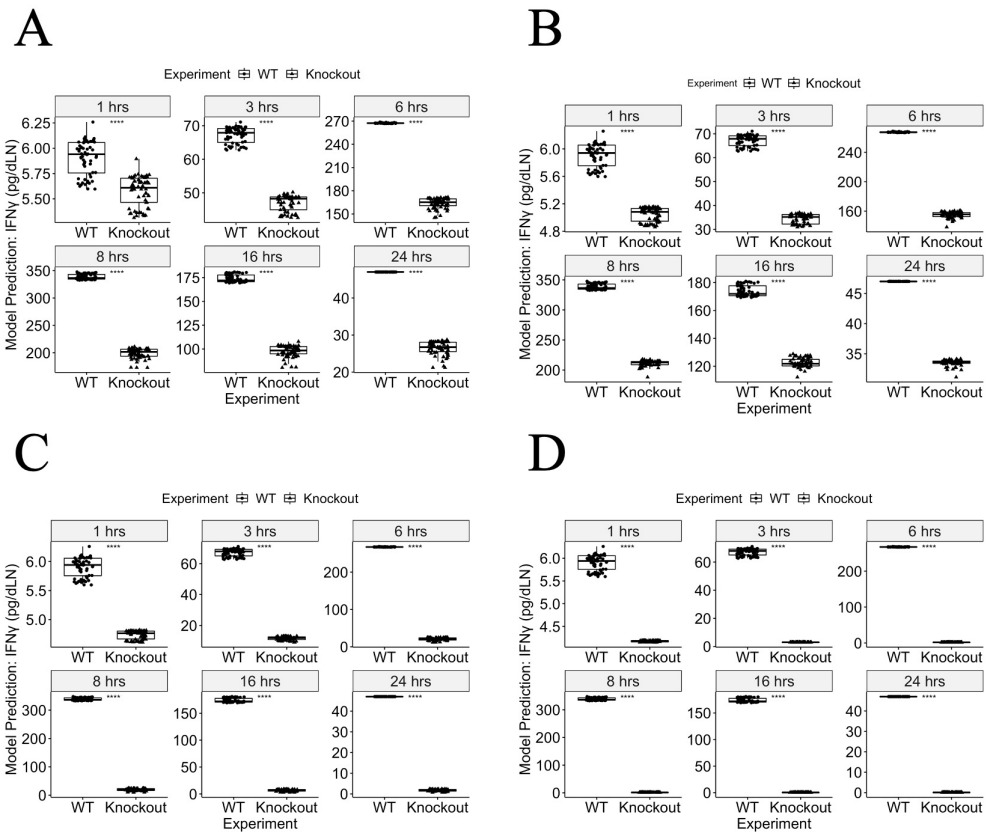


Figure 5.4: **Exploring the effects of simulated knockouts on IFNγ production:** Boxplots showing A) A simulated monocyte recruitment knockout and monocyte depletion. This depletion was implemented by setting the monocyte initial condition to zero (monocyte depletion) and the $monocRec_p$ parameter - controlling the rate of monocyte recruitment - to zero (simulating a monocyte-specific-CCR2 knockout). Thus creating a scenario with no monocytes and no monocyte recruitment. B) A simulated DC recruitment and Activation knockout and DC depletion. To implement this depletion we set the parameter controlling DC activation/recruitment ($DC_Afferent_p$) to zero, as well as the DC initial condition. C) Both simulated CCR2 knockout and monocyte depletion and a DC recruitment and Activation knockout and DC depletion. D) A simulated macrophage depletion.

Next, we simulated a DC depletion and DC activation/DC recruitment knockout and compared changes in IFNγ with the WT simulation (Figure 5.4B). At hours one, three and six, the fold-changes between WT and KO are larger than observed with the monocyte-recruitment knockout and monocyte depletion (Table 5.2), further suggesting DC-produced IL12 could be more influential for early IFNγ than monocyte IL12. After six hours, the fold-change reductions in IFNγ in the DC depletion become smaller incrementally, while fold-changes of IFNγ in the monocyte-recruitment knockout and monocyte depletion increase. Following this, a double knockout was performed, simulating a DC and DC activation/DC recruitment depletion together with a monocyte depletion and monocyte-recruitment knockout (Figure 5.4C). Unsurprisingly, fold-changes in geometric means of IFNγ between the WT and the knockout are all larger than separate DC and monocyte depletions, here peak-

	Time	DC Depletion	Monocyte Depletion	DC& Monocyte Depletion	Macrophage Depletion
1	1 hrs	-1.169	-1.059	-1.246	-1.413
2	3 hrs	-1.950	-1.431	-5.780	-22.553
3	6 hrs	-1.725	-1.632	-13.297	-149.158
4	8 hrs	-1.602	-1.702	-18.038	-264.818
5	16 hrs	-1.419	-1.778	-28.763	-173.765
6	24 hrs	-1.403	-1.781	-29.278	-47.003

Table 5.2: Effects of each simulated knockout experiment on IFNγ production. Measurements are given in fold-changes of geometric mean of *IFNg* distributions between the WT to the knockout scenario.

ing at 29.27 fold-change at 24 hours. Lastly, a macrophage depletion was performed to evaluate the effects a loss of IL18 has on early IFNγ (Figure 5.4D). Fold-changes between the WT and the knockout are larger than any of the DC/monocyte *in silico* knockouts at each time-point except hour one. Indeed, the fold-change in geometric means between WT and macrophage KO IFNγ peaks at 8 hours at -264.818. Together, these data further indicate that macrophage-induced IL18 is the most influential cytokine in promoting the IFNγ response after AS01, supported primarily by DC produced IL12 at early time-points, followed by monocyte IL12.

Next, we sought to consolidate these model findings through a global SA using eFAST (Figure 5.5), assessing the influence of these parameters on simulated IFNγ. Here, we used the methodology described in section 5.2.1, however this time each parameter was sampled 200,000 times. Each parameter, model variable and timepoint combination reached an acceptable level of convergence (<0.1) for the sensitivity indexes, with the exception of $decayIFNg_p$ at hour 1 (not shown). Consistent with previous results presented in this section, for both first order (Figure 5.5A) and total order sensitivity indexes (Figure 5.5B), of the IL12/IL18 production parameters $vMoIL18_p$ exhibits the strongest influence on IFNγ production across the entire simulation, while only the parameter controlling the synergistic production of IFNγ itself exerts a stronger influence. Over the first 10 hours, $vDCIL12_p$ is the second most influential cytokine production parameter for IFNγ. From approximately 10 hours post injection, the influence of $vDCIL12_p$ and $vMonocIL12_p$ begin to converge, and given the confidence intervals it is unclear which parameter is dominant.

The substantial influence of $vMoIL18_p$ on simulation behaviour strongly suggests that macrophage-released IL18 is the dominant cytokine involved in the early production of IFNγ after AS01. Indeed, during model calibration, all model fits capture a sharply transient IL18 curve, and thus a large parameter value to produce the observed rapid, early increase. Furthermore, these insights suggest that DC - rather than monocyte - production of IL12 may be most influential to early innate IFNγ, the peak of which is observed experimentally at six hours post-injection. We suggest that there is confidence in our work, due to the ability of the model to reflect the IL18R knockout and αIL12 depletion data, upon which

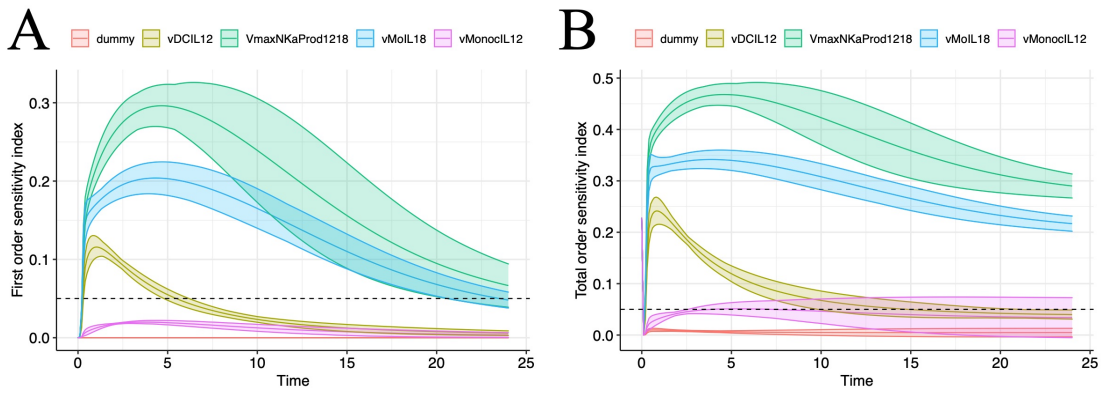


Figure 5.5: **The temporal effects of IL12 and IL18 production for IFNγ across the first 24 hours:** Line graphs showing the influence of parameters $vDCIL12_p$, $vMoIL18_p$ and $vMonocIL12_p$ on IFNγ through eFAST based global sensitivity. Parameter $VmaxNKaProd1218_p$ controlling the production of IFNγ itself is also shown for comparison. A) First order eFAST sensitivity index. B) Total order sensitivity index.

the model was not trained. This work has therefore refined current- and generated novel-hypotheses on the extent of contribution of cells and cytokines to initiating IFNγ after AS01.

5.2.4 Exploring the effects of macrophage loss on IFNγ production

The previous analyses indicated that macrophage-induced IL18 is most dominant in provoking the IFNγ response. This observation combined with minimal understanding of macrophage loss after AS01, raised multiple questions. First, what effect does this loss of macrophages have on the production of IFNγ? To examine this, we quantified the influence of the macrophage cell loss parameter CL_p on the IFNγ levels throughout the simulation, using eFAST. Second, we explored model predictions in the absence of CL_p effects. Finally, we hypothesised that the loss of macrophages after AS01 could be detrimental to IFNγ responses after a second AS01 delivery that occurred too soon after a first vaccination. Indeed, we produced a simple linear model to predict numbers of macrophages that have recovered at time-points between the first injection and 30 days post. We employed macrophage recovery estimates to simulate and predict IFNγ production after a second AS01 vaccination at day x following the first AS01-adjuvanted vaccination. We aim to provide a framework that suggests when subsequent doses of AS01 could be administered without detriment to IFNγ.

5.2.4.1 Macrophage Cell Loss May Help to Limit IFNγ production and contribute to its transience

First, we performed eFAST global sensitivity analysis to determine the influence of macrophage cell loss rate CL_p on IFNγ production during the 24 hours following simulated AS01-based

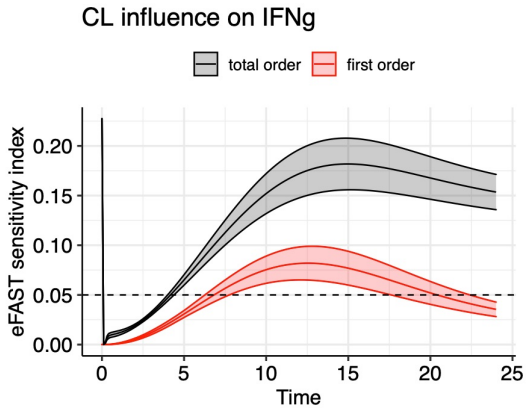


Figure 5.6: **Examining the influence of macrophage cell loss on IFNγ production across the first 24 hours of AS01-adjuvanted immune responses:** Plot showing the total and first order eFAST sensitivity indices for the parameter CL_p - controlling the rate of macrophage loss on IFNγ production in the simulation.

vaccination (Figure 5.6). Here, we used the methodology described in section 5.2.1, however this time each parameter was sampled 200,000 times. We observed modest influence on IFNγ. Given the previously observed dominance of IL18 in initiating simulated IFNγ, CL_p's influence is unsurprising. As this parameter controls the rate of macrophage decay, this model finding suggests the hypothesis that the loss of macrophages may serve as an inhibitory mechanism to limit the production of IFNγ to immunomodulatory but not toxic levels. To explore this further, we performed an experiment where CL_p is set to zero, i.e no macrophage loss occurs while the rate of NK recruitment is kept the same, and analysed model predictions. Clearly, this is an physiologically unreasonable scenario and we thus expect physiologically unreasonable predicted concentrations of cells and cytokines. Rather than claim to quantify cytokine concentrations or cell counts after such an experiment, we instead aimed to assess trends arising from this analysis to generate hypotheses.

As expected, the number of macrophages remains constant over the course of the simulation after setting CL_p to zero (Figure 5.7A). This provokes vast production of simulated IL18, which plateaus from ∼10 hours post injection at >900 pg/dLN (Figure 5.7B). The sustained and enhanced availability of IL18 combined with no adjustments to the maximal NK cell activation parameter, results in an increased number of NKa cells over the entire simulation, which begins to saturate toward latter stages (Figure 5.7C). In turn, this generates an enormous quantity of simulated IFNγ, reaching ∼12.5k pg/dLN by 24 hours (Figure 5.7D).

To confirm that the CL_p parameter inhibits IFNγ production in the model, for each model fit we doubled the rate of the CL_p parameter and compared the resulting model trajectories to the baseline calibrated best fit (Figure 5.8). Here, for each model trajectory,

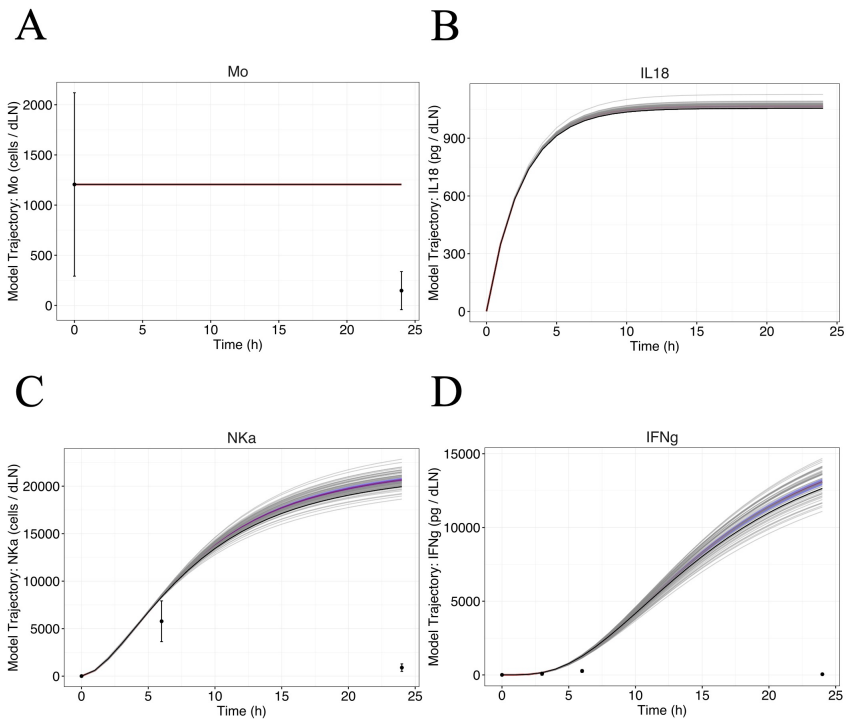


Figure 5.7: **Exploring the effects of zero macrophage cell loss on immune components:** After setting CL_p to zero, time-series plots showing the predicted trajectories of A) macrophages (Mo). B) IL18. C) IFNγ+ NK cells (NKa). D) IFNγ (IFNg). Black dots represent the data the model was trained against with corresponding error bars. Red lines represent the mean trajectories, blue shading represents the mean+/- sd for the model outputs, and black lines represent the predicted trajectory for the originally calibrated 'best fit'.

we observed significant (wilcoxon test) reductions at key timepoints between the predicted trajectories and the calibrated best fit for macrophages (Figure 5.8A, p<2.2e-16 at 2 hours), IL18 (Figure 5.8B, p<2.2e-16 at 3 hours), NK cells (Figure 5.8C, p<2.2e-16 at 6 hours) and IFNγ (Figure 5.8D, p<2.2e-16 at 6 hours). In summary, these model predictions indicate that through limiting the availability of IL18, macrophage cell loss limits the production of IFNγ thus contributing to its transience. For the scenario presented in Figure 5.7 where CD169+ macrophage cell loss was eliminated, we reiterate that these concentrations of cells or cytokines are physiologically unreasonable. This work firstly suggests a novel hypothesis that QS21-induced macrophage cell loss may serve as an endogenous inhibitory mechanism, contributing to the transience of the IFNγ production observed in experimental data. A limitation of this work however is that there are almost certainly other inhibitory mechanisms which are not modelled, which will contribute to this effect and may be in-part be also effectively represented by the CL_p parameter. Nevertheless, we propose that this analysis highlights an underappreciated gap in our understanding of AS01 induced vaccination: that inhibitory mechanisms are less well understood. Transience of the innate immune response is a key characteristic of AS01, but its inhibitory mechanisms are not fully un-

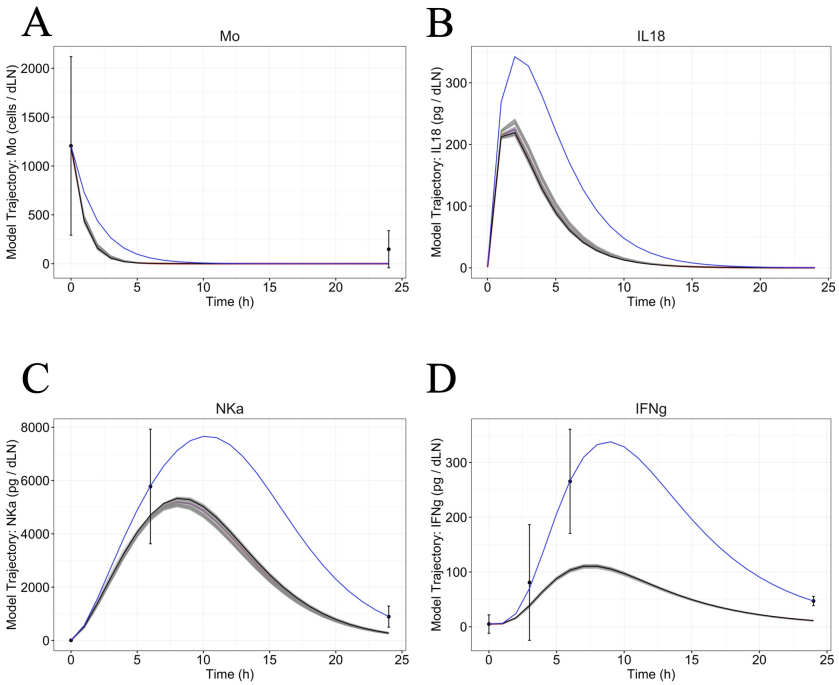


Figure 5.8: **The 'macrophage cell loss' parameter inhibits IFNγ production:** After doubling the CL_p parameter, time-series plots showing the predicted trajectories of A) macrophages (Mo). B) IL18. C) IFNγ+ NK cells (NKa). D) IFNγ (IFNg). Black dots represent the data the model was trained against with corresponding error bars. Red lines represent the mean trajectories, blue shading represents the mean+/- sd for the model outputs, and blue lines represent the predicted trajectory for the originally calibrated 'best fit'.

derstood. Overall, the model findings suggest that alongside other inhibitory mechanisms, QS21-induced macrophage loss may serve as a novel inhibitory mechanism underpinning AS01-adjuvanted vaccination.

5.2.4.2 Predicting the Earliest Time for a Second AS01-based Vaccine Delivery

Particularly given the recent heightened sensitivity to pandemic disease, it is reasonable that multiple vaccines, using different antigens containing AS01 may be used in future vaccination regimens. Furthermore, unpublished data (not able to be shown) suggests there may be negative effects to the response magnitude, if consecutive AS01-based inoculations occur too close to each other, e.g., in a prime-boost scenario. There are multiple hypotheses of why such 'interference' may occur, one of which is that the levels of CD169+ macrophages in the dLN that are required for IL18 production (and in turn 'optimal' IFNγ) may not have recovered from their observed loss in time to supply IL18.

For a second vaccine delivery that occurs close to the first, it is unclear whether the loss of macrophages could be detrimental to IFNγ responses after AS01. The importance of such questions is heightened by recent studies and public debate, regarding the efficacy of vaccines after delayed second- or smaller first-doses. Indeed, Voysey et al [308] observed with

ChAdOx1 nCoV-19 that there is increased efficacy after a reduced first dose and their work suggests that a larger space between doses may improve efficacy [309]. Prior to these recent ChAdOx1 observations, we had reasoned that delayed recovery of full immune function could plausibly impact the effectiveness of a subsequent vaccination. Given the absence of mechanistic understanding for this emerging phenomenon, we explored the hypothesis that delayed CD169+ macrophage recovery (following their loss as observed during AS01-adjuvanted vaccination) could impact AS01 responses following a second vaccine delivery which occurs too soon after the first. Unfortunately, we were unable to directly simulate the booster response to AS01 at this stage, due to data availability. While we are interested in the innate response so recall differences on developing adaptive responses would not be relevant, there are potential relevant differences in prime and boost innate immune responses which would be required to capture for a full examination of the observed 'interference' during recall. For example, antigen-specific IL2 may provide an alternate signal[310] which may provide some stimulation for IFNγ, which is not observed during primary responses. Nevertheless, we are able to simulate the effects that delayed macrophage recovery may have on IFNγ following a second vaccine delivery containing AS01. We reasoned that this analysis would not only suggest whether a refractory period is required following a first vaccination with AS01, but may suggest whether a similar mechanism could plausibly affect prime-boost responses as observed by GSK.

To explore whether a delay in macrophage recovery may affect the IFNγ response after a second AS01 delivery, we estimated the numbers of recovered macrophages at day x following a first AS01 vaccination. Given estimates of macrophage levels at day x, we used these as initial conditions for simulating IFNγ production following a second vaccine delivery - occurring on day x, thus examining the role of delayed macrophage recovery on subsequent IFN. There is very little data available on recovery of macrophages following their loss in dLNs. To our knowledge, there is no available quantified raw data evaluating the loss of these cells and subsequent recapitulation. Gaya et al., witnessed a similar disruption [311] and demonstrate that the layer of SCS macrophages is "re-established" by 28 days post-injection in a different model system. In the current context, after QS21 injection, there is an 87.74% reduction in the geometric means of CD169+ macrophages over 24 hours[8]. Thus, in the model we assume no further loss occurs after 24hrs based on these data and assume the observed loss of subcapsular macrophages by QS21 is restored by 27 days later. These data and assumptions informed a simple linear model, which takes the percentage loss of macrophages by the end of 24 hours of simulating the IFN response to AS01 (compared with t0) using our innate IFNγ model, coupled with the assumption that 87.74% loss can be recapitulated 27 days later, to predict/estimate how

many days it would take for full macrophage recovery, given some percentage loss (i.e., those different percentage losses produced by model fits). Given absence of further data at this stage we assume simple linear recovery, thus estimated recovery times are then used to predict the number of macrophages that have recovered at day x following initial injection. This calculation is used as the initial condition of macrophages for a simulated second AS01 delivery at day x post initial injection, therefore estimating and reflecting the potential conditions with respect to available macrophages, if one were to vaccinate on day x following the first vaccination. Indeed, we simulate to make predictions of IFNγ based on the levels of macrophages recovered (i.e macrophages available at second vaccination). Figure 5.9 shows the simulated IFNγ responses based on the predicted numbers of macrophages present at each assessed day of second AS01 injection, compared with the experimental data for IFNγ pg/dLN over the first 24 hours of the primary AS01-induced immune response. Qualitatively, for the average (mean) predicted responses of IFNγ after the refractory period, we observed that by days 21-22 post the first injection, the mean simulated response is within the error of the experimental data at six hours, suggesting these may be the earliest times where a detriment is not observed, for the average case.

Interestingly, there is considerable uncertainty around these predictions. For model trajectories around the upper region of the response, i.e mean+ one standard deviation, one may be able to vaccinate as early as between 14-18 days following the first dose. In contrast, for the lower region of the response (i.e mean minus one standard deviation), even by day 28 following the first injection, one is not within the error of the experimental data suggesting a detriment is still observed. These model findings imply that applying constraints on scheduling is sensible, whilst a refractory period between consecutive AS01-based vaccinations (especially with different antigens) may benefit the immune response. Our modelling efforts suggests that in the average case, one should avoid vaccinating earlier than 21 days following the first dose. However, this analysis revealed particularly distorted outliers, where in some cases a second vaccination between days 14-18 may lead to no detriment. The model predicted some cases where even waiting 28 days, the resulting IFNγ at six hours would not be within the error of the WT mice.

Taken together, based on our current understanding, available data and model analysis, the hypothesis that macrophage loss could detrimentally affect a second vaccine delivery with AS01 is reasonable, and we provide an initial framework for the range of impact consecutive vaccines containing AS01 within the following month may have on IFNγ responses to AS01.

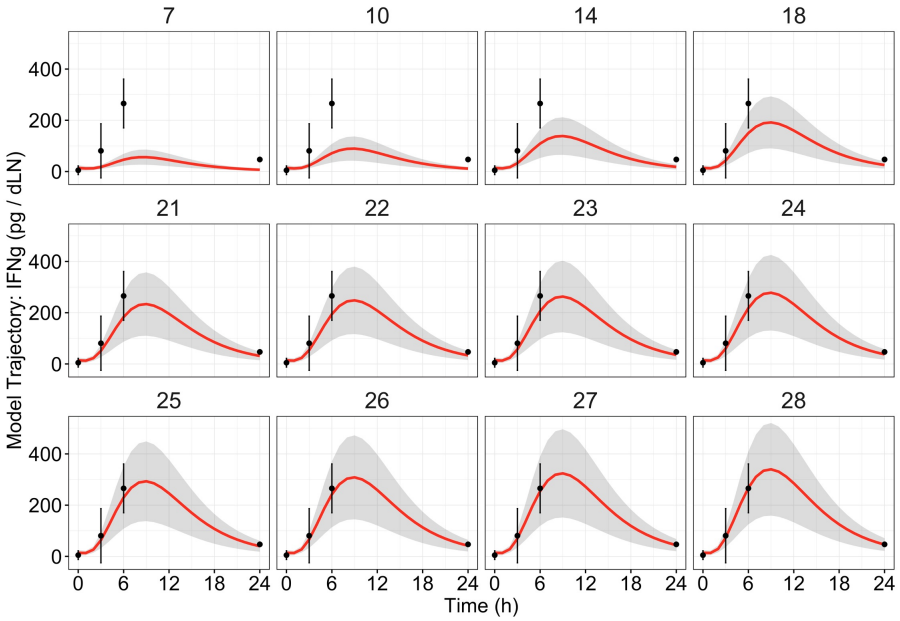


Figure 5.9: **Predicted IFNγ responses after simulating a second AS01 delivery at days 7-28 after initial AS01-based vaccination:** Black data points and error bars show the *in vivo* experimental data for which the original model is calibrated. Model predictions based upon predicted macrophage recovery are visualised. The red line shows the mean IFNg trajectory, while the shaded gray shows the mean +/- the standard deviation. For example, the top-left panel labelled '7' shows the predicted second IFNγ response (red line shows the mean), if one was to perform a second AS01 delivery on day 7 post-injection, with respect to the predicted numbers of available macrophages on day 7.

5.2.5 Identification of Parameters with Influence on IFNγ

Global sensitivity analysis of a mechanistic model can permit examination of parameter contributions to biological mechanisms represented by parameter. An important consideration for developing the next-generation of AS01-like adjuvants, is to determine the most important parameters and immune factors, so to assist preservation of these characteristics when exploring alternate formulations. Therefore, we performed an eFAST based SA following the methodology described in section 5.2.1 and examined the parameters which influence IFNγ over the first 24 hours of the response.

Figure 5.10 shows the total order sensitivities for parameters that exhibit >0.15 total order sensitivity index values for IFNγ at some point over the first 24 hours of the immune response. Indeed, compared to the dummy parameter, each of the visualised parameters exhibit significant affects on IFNγ throughout the simulation. This figure summarises many insights yielded from this chapter. With the exception of *decaayIFNg* at hour 1, unsurprisingly the parameter $VmaxNKaProd1218_p$ controlling the synergistic production of IFNγ exhibits the highest influence over simulated IFNγ. As previously shown and further demonstrated in Figure 5.10, we propose that $vDCIL12_p$ contributes more to the initiation

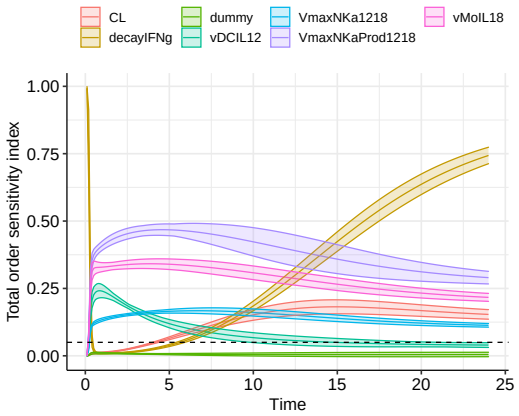


Figure 5.10: **Parameters with influence on the simulated IFNγ response after AS01:** Line-graph showing total order sensitivity index values for proportions of variance contributing to simulated IFNγ over the first 24 hours of the simulated immune response.

of the experimentally observed IFNγ peak at six hours than $vMonocIL12_p$. Furthermore, the parameter CL_p, controlling the rate of QS21-induced macrophage cell loss exhibits a reasonable influence on simulated IFNγ. Qualitative reasoning reveals that this effect would be negative, given that this parameter controls the rate of removal of the IL18 producing component of the system. The parameter controlling the activation of NK cells induced by IL12 and IL18 synergistically exhibits a consistent reasonable influence across the entire first 24 hours post-injection of AS01. After an initial, substantial contribution and reduction in influence, the parameter controlling IFNγ decay, increases its influence steadily toward the end of the simulation. Together we provide a baseline framework for the salient mechanisms underpinning IFNγ production after AS01-adjuvanted vaccination.

5.3 Discussion

We employed the mechanistic model of early AS01-induced IFNγ response, to explore key questions surrounding IL12, IL18 and IFNγ production.

Predicted temporal dynamics of cellular production of IL12: Using the model, we first proposed temporal dynamics of DC and monocyte production of IL12, given the hypothesis that monocytes and DCs produce IL12 at similar if not identical rates after AS01 (section 5.2.2). We performed eFAST-based global sensitivity analysis which proposed that under the aforementioned hypothesis and assumption, DC production of IL12 is substantially more influential during the response to AS01, although by approximately 15 hours post-injection, both cell type's influence becomes similar. Interestingly, model analysis generated the novel hypothesis that DCs may provide an early IL12 signal to promote innate-IFNγ production. This finding rests on the assumption that IL12 is produced at sim-

ilar rates by both cell types, so estimations of these rates *in vitro*, could be integrated into a next iteration of model development, to confirm and/or refine these results. Inflammatory monocytes have been shown to produce IL12 after CpG adjuvanted vaccination [106]. A subset of DCs which are in-part characterised by expression of IL12 have been observed to play a role in dLN responses after AS01 [95] and IL12+ DCs have been implicated in Th1 responses to wider adjuvants [69]. Therefore, it is plausible that these cells secrete IL12 after AS01, although this should be confirmed *in vitro/in vivo*, and the rates of which these separate cell types produce this cytokine would enable refinement of this work. Conversations with colleagues at GSK have highlighted that IL12 concentration is difficult to measure in the dLN in this mouse system, therefore mechanistic modelling can complement experimental work, in efforts to deconvolute the roles and temporal kinetics of cell types during early immune responses to AS01. In this context, we have proposed temporal cellular kinetics of IL12 production and avenues for *in vitro* work, the results of which could be fed back into the modelling cycle to provide further insights into IL12 production after AS01-adjuvanted vaccination.

DCs may provide a key source of IL12 to support IL18 in initiating innate IFNγ: We next explored the relationship between cellular production of IL12 or IL18 and the production of innate IFNγ (section 5.2.3). Each respective cellular cytokine production parameter, as well as both cellular-IL12 parameters simultaneously, were perturbed within a +/- 90% range from the best-fit value and the effects each perturbation had on the resulting IFNγ at key time-points were evaluated. Four *in silico* knockout experiments followed. Collectively, these modelling efforts provided evidence that macrophage-induced IL18 is the most significant contributor to IFNγ at all timepoints, supported early, primarily by DC IL12 and then monocyte IL12 at later timepoints. These results were consolidated through global sensitivity analyses. Coccia et al [32] found that subcapsular macrophage IL18 and an unknown source of IL12 contribute to the innate IFNγ response individually and synergistically. Their results also suggested that IL18 was more influential for 'optimal' IFNγ than IL12, although both cytokines were required. Through use of a formal mathematical model, our work consolidates this insight, demonstrating that IL18 is primarily influential for early IFNγ. Our work is limited by the use of a prediction for IL18 and IL12 trajectories after AS01, based on parameter estimates. Indeed, evaluating whether the parameter values for macrophage production of IL18, as well as DC and monocyte production of IL12 are 'physiologically' reasonable, stems from domain intuition and are constrained to some extent from fitting other parameters to the data. We suggest that these predictions could be quantitatively refined following the generation of *in vitro* data on respective cellular cytokine production after AS01 stimulation. If generated, re-fitting the model to IL18 and

IL12 experimental data to provide more accurate parameter estimations would almost certainly result in quantitative alterations, however we are confident that these insights would stand, as the model is currently able to replicate the available *in vivo* data used for calibration, and also dynamics of IL18RKO and αIL12 depletion experiments, upon which it was not trained.

Coccia's work additionally implied that prepositioned cells in the dLN are targeted by AS01 to promote innate IFNγ. Our work supports this implication, as the biological data used to inform the model demonstrate that DCs are in higher numbers in the dLN at early time-points, and in turn analysis of the model indicates that DCs may be primarily involved in providing IL12 to support IL18 in initiating innate IFNγ over the first six hours. This model finding is based on the reasonable assumption that both DCs and monocytes produce IL12 at similar, if not identical rates after AS01. Thus, the hypotheses that DCs and monocytes produce IL12 after adjuvanted-vaccination are grounded in experimental evidence from wider systems, although *direct in vivo* confirmation that these cells produce IL12 after AS01 has been difficult to generate. To confirm this assumption and provide further confidence in resulting insights, we propose a dose-response *in vitro* experiment assessing IL12 production after AS01 by DCs or monocytes. In addition to adding confidence in our findings, this experiment would enable estimation of respective IL12 production rates and their uncertainties, which could be incorporated into next-iteration research using the model. Therefore, this modelling work has generated hypotheses which can guide experimental design, contributing to an iterative research cycle.

AS01-induced macrophage cell loss may contribute to the transience of innate IFNγ: A global sensitivity analysis showed that macrophage cell loss influences simulated IFNγ production. Through knowledge of the mathematical structure, we deduced that this effect on IFNγ would be negative. Therefore, we reasoned that CL_p may contribute to the transience of the IFNγ response to AS01, through eliminating the cells which produce IL18, in-effect imposing a time-limit on the synergistic production of innate-IFNγ. To explore this further, we simulated a theoretical scenario where the rate of macrophage cell loss was zero and evaluated model trajectories for macrophages, IL18, NKa and IFNγ trajectories (section 5.2.4.1). Unsurprisingly, we observed physiologically unreasonable predictions for these entities and drastic increases in cell numbers / cytokine levels were observed for each entity. While we do not suggest these cellular or cytokine levels are precise quantifications of such a scenario, we proposed that the trend suggests a novel hypothesis: that this loss of macrophages may limit aberrant cytokine production after AS01 vaccination, which may reduce reactogenicity.

Is QS21 pleiotropic? Within the model, QS21-induced IL18 is dominant in promoting IFNγ production during a pro-inflammatory phase of the response. The model behaviour whereby QS21-induced loss of macrophages limits aberrant cytokine production, proposes the novel hypothesis that QS21 is pleiotropic, exerting both pro- and anti-inflammatory roles during the early stages of the immune response to AS01. In turn, this may serve to robustly initiate the immune response whilst also contributing to its transience. Recent work has highlighted that QS21's mechanism of action is not well understood [146, 156]. Here, in the context of AS01 MoA, we propose that through initiating release of IL18 by subcapsular macrophages, QS21 performs a pro-inflammatory function, while simultaneously initiating a loss of these macrophages, it limits the time-period for which IL18 is released. Therefore, we have generated a novel hypothesis for QS21 after AS01-adjuvanted vaccination.

AS01-mediated macrophage cell loss may dictates a requirement for temporal spacing of AS01 based vaccines: Within the era of COVID-19 pandemic, vaccinology concepts e.g., effective dosing strategies are being closely followed by the general public. For multiple vaccines, evidence is emerging that a delay between prime and boost, or a fractional dosing regimen may improve vaccine efficacy [312, 308, 313]. Specifically for AS01, there are currently multiple licensed vaccines against different diseases which employ this adjuvant formulated with disease-relevant antigens. Data we are unable to show, suggests that there could be 'interference' during a recall immune response, if prime-boost with AS01 occurs too close together. We reasoned that this may mean that a refractory period is required between two vaccinations with AS01. In section 5.2.4.2, we explored one hypothesis for why this may occur, that due to prolonged macrophage recovery after cell loss, there may be less IL18 available to stimulate a second IFNγ response to AS01. Gaya et al., published, to our knowledge, the only publicly-available data on macrophage recovery after dLN loss of these cells, although their work did not employ AS01 as a stimulant. Given lack of any other data, we utilised their insights to inform what Macrophage recovery may look like after AS01. We thus employed our model to simulate a second vaccine delivery after AS01, during periods of macrophage recovery (up to one month following the first dose), to explore whether delayed recovery may affect an immune response after a second vaccine delivery. Our model predictions implied that the IFNγ response would be detrimentally affected due to reduced numbers of macrophages and suggested that in the average case, a few weeks may be a sufficient refractory period. However, we observed considerable uncertainty around these predictions. Indeed, if a subject had a poor response, i.e a longer macrophage recovery/less optimal IFNγ production, these data suggest a refractory period of more than 28 days.

Importantly, for AS01-based vaccines, this data collectively suggests that if possible, one should wait a minimum of a month (based on Gaya et al's wider data showing a 30

day recovery period for the macrophages) before vaccinating again in mice for a robust response in most cases. This work also suggests that first, 'interference' could be observed with consecutive vaccinations which did not accommodate a refractory period and that delayed macrophage recovery is a reasonable hypothesis for why this may occur. These insights are consistent with a model that is built on the current understanding of AS01 MoA and available data. Thus, our hypothesis is deemed to be reasonable, and we propose it should be explored for whether (and if so to what extent) delayed macrophage recovery contributes to observed 'interference' during the AS01 secondary recall response. Innate dynamics may differ during the secondary recall response, therefore our data raise questions regarding the extent (during a recall response) antigen-specific IL2 may recapitulate limited IL18 during different stages of macrophage recovery after primary responses to AS01. If IL2 does recapitulate the dynamics, examination of thresholds of IL2 required at different timepoints throughout the refractory period for canonical IFNγ during a booster response would be of interest. Furthermore, it will be interesting to examine the effects of spatial dynamics here, as one would assume that antigen-specific IL2+ cells would need to be in proximity to NK cells to provide this alternate signal to promote IFNγ. We also propose that it should be explored whether vaccination into a different muscle (thus draining to a different LN where macrophages may be available) to a first primary vaccination alleviates these issues. In addition, such incapacitated 'innate pathways', may in-part contribute to the observations in humans that delayed[309] and/or fractional dosing [312, 313], and/or reduced first doses [308] could improve vaccine efficacy. Given that our work is based upon mouse data, the insights presented with respect to consecutive AS01 vaccinations is based upon our understanding in mice. This is a limitation of this work, and translational work is required to examine the mechanisms underpinning any refractory period in humans, however existing observations in humans regarding delayed dosing and its impact on efficacy, suggest that the hypotheses generated here are plausible in humans. Overall, this type of work shows the power of mechanistic modelling in immunology, to generate and refine testable hypotheses which can streamline experimental design by reducing the combinatorial explosion of experiment possibilities.

Key Parameters Required for AS01's Innate IFNγ: To answer question 4 - *what are the most important parameters with influence over IFNγ after AS01?* - an eFAST-based global sensitivity analysis was performed where all parameters were perturbed simultaneously. Any parameters exhibiting a total order sensitivity index $>$ than 0.15 with IFNγ at some point over the first 24 hours post-injection were reported, and our work therefore provides a landscape of the temporal kinetics and influential parameters involved in IFNγ production after AS01 (section 5.2.5). This work extends previous insights from Coccia

[54], who demonstrated that IFNγ is produced primarily by NK cells in the dLN, initiated by QS21-induced IL18 from macrophages with support from IL12, by indicating the temporal landscape upon which these kinetics occur, and consolidating the hierarchy of influence over innate interferon. Through an examination of each parameter captured in the model - given our research context - this work supplies a framework which can serve as a 'baseline comparison' for researchers exploring next-generation AS01-based adjuvants, to ensure that important or desired AS01 characteristics are conserved.

Additional comments: The analysis presented here is made possible through the development of the core AS01 model in Chapter 3, which led to the development of the simulator in Chapter 4, where hypotheses, experimental insight, generated knowledge gaps and rational assumptions are considered for model development. After discussion with AS01 domain experts, it was decided that CD8+ T cells would explicitly be omitted from the model and calibration would proceed using IFNγ+ NK cell data. This is because while CD8+ T cells are observed to produce IFNγ by ICS over the first 24 hours, we are unaware of whether this IFNγ is released by the cells. Indeed, the prevailing insight from GSK experiments is that NK cells mediate the IFNγ production over the first 24 hours and CD8+ T cells mediated the second peak after 24 hours. NK cells in the model serve as a conduit for IFNγ release, where the production and not its source is examined in detail. Thus CD8+ T cells were omitted. Nevertheless, two interesting avenues of research would provide insight into whether CD8+ T cells contribute to the early response. First, *in vivo* CD8+ T cell depletion to determine whether the IFNγ production as assessed by ELISA or Luminex is affected. Second, extension to the model developed in Chapter 4 could be incorporate a range of contribution, if any, is observed *in vivo*. This work utilises the mechanistic model of early AS01 immune response developed in chapter 4. Here, we provided new insights in AS01 MoA and an alternative hypotheses for the determinants driving overall efficacy which can in the future be tested experimentally.

Chapter 6

Mechanistic Models To Explore and Refine Hypotheses Underpinning the CD4+ T cell Response to AS01-adjuvanted Vaccines

6.1 Introduction

The CD4+ T cell response is paramount in conferring protection with AS01-adjuvanted vaccines, and early IFNγ has been observed to control CD4 T cell responses and correlate with protection in humans [32]. However, the mechanism by which early IFNγ controls the CD4+ T cell response to AS01 is unclear, and mechanisms which further influence CD4+ T cell priming after AS01 are yet to be fully established. Following the *in silico* investigation into innate IFNγ production after AS01 in Chapter 5, we explored the CD4+ T cell response to AS01. Here, we set out to establish parameters which influence CD4+ T cell priming and explore how IFNγ may control the CD4+ T cell response to AS01 [32]. Additionally, we aimed to reveal where our understanding of the system is incomplete and leverage these insights to propose refined and novel hypotheses and experiments (*in silico* or *in vivo*), which could add to our understanding of AS01 MoA. Work in this chapter thus extends the IFNγ model developed in Chapter 4, to capture a simple implementation of CD4+ T cell priming by DCs after AS01-adjuvanted vaccination.

Along with GSK vaccines, we hypothesised that IFNγ may control the CD4+ T cell response to AS01 by substantially enhancing DC potency through promoting upregulation of pMHCII complexes and co-stimulatory molecules on the DC, which may in turn augment the numbers of CD4+ T cells that become primed (hereby 'primed CD4+ T cells'). We therefore sought to explore the veracity of such a hypothesis using mechanistic modelling.

Taken together, we sought to address the following research questions (see section 1.10).

- What immune system processes influence the generation of the CD4+ T cell response to AS01?
- Is the hypothesis that IFNγ modulates the CD4+ T cell response via substantially enhancing DC potency to prime T cells after AS01, consistent with the experimental data?
- Where does the mechanistic model(s) indicate that our understanding of AS01 MoA is incomplete?

To answer these questions, we established five aims for this chapter:

1. To extend the IFNγ simulation to capture a simple implementation of CD4+ T cell priming.
2. To utilise the simulation to determine influential model parameters underpinning the priming of CD4+ T cells after AS01-adjuvanted vaccination, thus proposing key mechanisms underpinning this response.
3. To explore the '*IFNγ enhancement*' hypothesis - that IFNγ controls the CD4+ T cell response to AS01-adjuvanted vaccines by substantially enhancing DC potency which in turn augments the priming of CD4+ T cells.
4. To utilise the model(s) developed in this chapter to reveal where our understanding of the system is incomplete, to propose refined and novel hypotheses and experiments which could reduce incompleteness and thus further our understanding of the system.
5. To utilise the insights developed in this chapter to propose directions for the refinement of mechanistic models of CD4+ T cell priming after AS01.

This chapter addresses thesis aim 4 (section 1.10.2).

6.2 Results

6.2.1 Development of a Domain Model for AS01 CD4+ T cell models

After literature examination, we confirmed that no suitable simulations exist to explore the first seven days of the immune response to AS01, although simple models integrating innate immune dynamics with early CD4+ T cell priming have been proposed and utilised e.g., from the Kirschner laboratory [196, 197]. We therefore created a novel model which is presented and analysed in this chapter. The new model was inspired by previous work from Marino et al [197], who model lymph-node CD4+ T cell priming dynamics, in the context of tuberculosis infection.

6.2.1.1 Research Context

Our domain of interest is the immune response over the first seven days in a murine iliac dLN, in response to an AS01-adjuvanted vaccine. We therefore captured the following entities: AS01 immunostimulants QS21 and MPL, inflammatory monocytes, resident and migratory MHCII+ DCs, CD169+ subcapsular macrophages, cells which mediated IFNγ production over the first seven days e.g CD8+ T cells and NK cells, IL12, IL18, IFNγ and CD4+ T cells.

6.2.1.2 Curating Experimental Data

Gathering Data for Model Calibration: Quantitative data at different time points for both cell numbers and cytokine concentrations throughout the primary immune response to AS01 is relatively limited. Complicating the limited amount of data is the large variation in quantitative measurements between different experiments with the same experimental readouts (e.g. FACS data) despite the use of genetically identical mice. There was also large differences in AS01 dosing between sets of experiments making cross-experimental comparisons difficult. Despite these complexities, we curated a dataset to enable development of a simple exploratory model of the first seven days of the immune response to AS01. Here, we present this biological data from different experiments performed by GSK and by Dominika Gajdasik in Prof. David Withers laboratory (University of Birmingham). The choice of data used for calibration or validation has been highlighted. Whilst aiming to maximise the available data, we sought to limit confounding factors that lead to additional uncertainty and lack of confidence in model predictions. Therefore, we kept the number of different experiments from which data were gathered to a minimum. For fitting, we only gathered measurements from experiments using the standard murine dose of AS01: 1/50 of the human dose (1/50HD). Quantitative readouts of cytokine and cellular dynamics can differ substantially between dosing concentrations, and 1/50HD is considered the 'standard' murine dose of AS01 for pre-clinical development.

Although limiting a sufficient set of measurements for key cells and cytokines, the same 1/50HD experiments were used to calibrate the model in Chapter 4. However, for the current work, for some experimental readouts of immune cells, we were only able to locate AS01 datasets at important time-points from older experiments (e.g., non-physiological dosing) or wider experiments (e.g., both different antigens and adjuvant dosing) with slightly different protocols. For these datasets the observed trends are often consistent with the key datasets used to parameterise the models, however e.g., quantifications of cells/cytokines following 1/10HD may be orders of magnitude different than with 1/50HD. Furthermore, for model calibration we were advised by GSK immunologists to use the more recent datasets which

employed 1/50HD as e.g., wider datasets contain other dosing and/or other slight differences in protocol.

Thus, we reasoned it would be inappropriate to mix and match quantitative data from many different experiments. However, for the more recent experiments performed with 1/50HD, there was insufficient datasets for the latter stages of the immune response, thus for calibration we would be missing important information regarding simulation endpoints. For example, for the numbers of CD11c+ MHCII+ DCs measured in the dLN after 1/50HD, we only had available the numbers of these cells at timepoints 0,6,24 and 48 hours post-injection from recommended experiments. These data are appropriate for use in modelling the first 48hrs but of no help in calibrating the model beyond that. However, from a much older experiment, we had data on these DCs at 168 hours post-injection. Therefore, rather than exclude these datasets entirely, we used the trends (e.g., fold-changes between 0 hrs and 168hrs) within these older time-series data, to estimate cell numbers at key time-points where we lacked data from experiments using AS01b 1/50HD, although we aimed to minimise the use of such estimates. These calculations are described in what follows in detail. This is less than ideal when modelling, however we reasoned that it was more appropriate to use estimates informed by wider AS01 data, than to continue with such large gaps in the data available for model fitting. Obviously ideally new datasets would have been collected but this was not possible due to experimental priorities.

After incorporating the estimates into the dataset, we observed consistency with the trends for each cell type, with what was published by GSK [54] [5], improving confidence that these estimates are reasonable. Indeed, by 7 days post-injection of AS01-adjuvanted vaccine, many innate component kinetics were observed to have "returned toward baseline", which provided a level of confidence that our estimates from the wider experiments were not unreasonable. Nevertheless, work in this chapter is limited by data availability, therefore in what follows, we aimed to suggest trends that arise from exploratory analysis of a theoretical model, rather than produce detailed quantitative analyses.

Data for Simulation Calibration: Figure 6.1 shows the data gathered for model calibration. In each panel, any data-points for zero hours represent measurements of the corresponding readout after a PBS control instead of AS01. Estimated datapoints are shown in blue. As presented in Chapter 4, we show data from an experiment by GSK [8] where researchers measured the numbers of CD169+ macrophages at twenty-four hours after injection with QS21 or a PBS control (Fig 6.1A). Next, we show the numbers of CD11c+ MHCII+ migratory and resident DCs in the dLN at 0-168 hours after AS01 (Figure 6.1B). Here, we extend the experimental data shown in Figure 3.2B, by including 48 hours post-injection data-points from the same experiment, observing an increase in DCs after 24

hours. Without estimated data, we are left with a large gap between 48 hours and the end of the desired modelling period at day 7. MHCII+ DCs play a paramount role in CD4+ T cell priming, so we estimated the level of these cells at day 7, by locating an older internal GSK dataset which additionally contained measurements for DC subsets at this timepoint.

To estimate numbers of DCs at the intended simulation endpoint (168 hours post-injection), we gathered data from an earlier GSK experiment with AS01, which contained measurements for CD11c+ MHCII+ DCs (same cell population as those we aim to model) at this timepoint, as well as earlier timepoints throughout the first seven days post-injection. By seven days post-injection, the numbers of these cells have "returned toward baseline levels" [5]. Therefore, using the PBS control measurements from this older experiment as the 'baseline' zero-hour timepoint, we calculated the geometric mean of percentage changes between the PBS measurements (representing time zero), and those at 168 hours-post injection, to provide a reflection of the relationship at 'baseline', and that at 168 hours post-injection. This average percentage change was then applied to each zero-hour PBS measurement in the 'more recent' dataset we set aside for calibration here to estimate the 168 hour datapoints. We estimated that the numbers of DCs reduce between 48 hours and 168 hours post injection towards the baseline levels (Figure 6.1B), which is consistent with the findings in [5], thus allowing a reasonable approximation of the kinetics. In absence of further experimental data, future work will seek to incorporate further uncertainty around these and other estimates, perhaps by bootstrapped sampling of the percentage changes.

Figure 6.1C shows the *in vivo* data at available timepoints across the first seven days post-injection for inflammatory monocytes in the dLN. Again, we estimated levels of these cells at 168 hours post-injection using the same approach described above for DCs. After integrating the experimental observations and those estimated at 168 hours post-injection, we observed a peak at approximately 48 hours post-injection before returning toward baseline by day 7, again consistent with trends observed by Didierlaurent. We witnessed a slight increase in IFNγ between 24 hours and 48 hours post-injection, although this was not significant (Figure 6.1D). This increase is considered to be the initiation of a 'second wave' of IFNγ. The prevailing notion is this is mediated by CD8+ T cells (internal GSK data, not yet published). Unfortunately, due to technical issues and/or differences in dosing between experiments, we were unable to curate or estimate the concentration of IFNγ beyond 48 hours post injection, revealing gaps in understanding regarding the magnitude and peak of this 'second wave' of IFNγ.

Figure 6.1E shows the numbers of IFNγ+ NK cells observed *in vivo* at 0,6, 24 and 48 hours post-injection. Beyond 24 hours, *in vivo* data are limited. Given the importance of these cells in at least the early response to AS01 and our requirements on data curation,

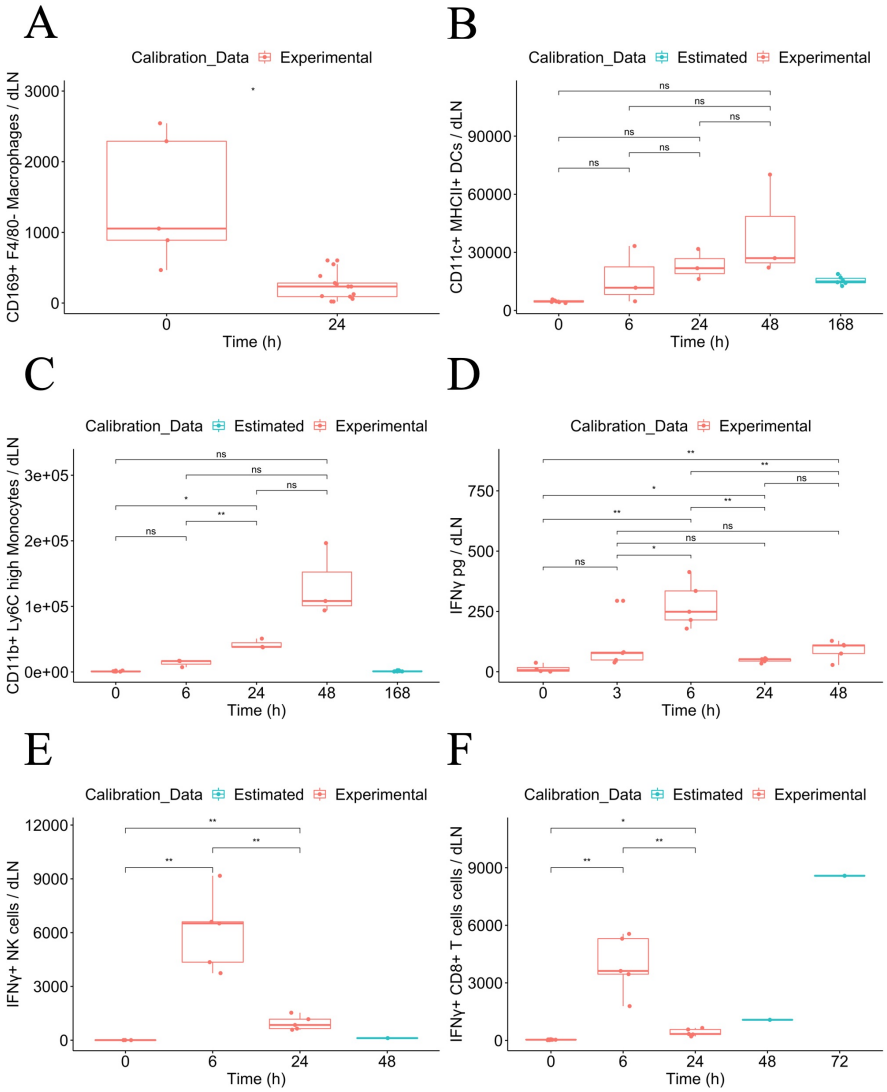


Figure 6.1: **Experimental data for model calibration 1/2:** Experimental data used for calibration. A-G, data are colored by whether the measurements were gathered solely from experimental data, or whether a datapoint has been estimated as described in the text. For full descriptions of experiments that led to these data, please see Figure 3.2. From Figure 3.2, the PBS measurements are here used as 'zero hour' timepoints. Remaining timepoints are from experiments with AS01 1/50HD. **A)** The numbers of CD169+ macrophages in the dLN, used as observational data for model macrophages at zero (from PBS measurements) and 24 hour timepoints. **B)** The numbers of CD11c+ MHCII+ DCs in the dLN used as observational data for model DCs, at zero (from PBS measurements), 6, 24, 48 hours. Estimated datapoints are shown for 168 hours. **C)** The numbers of CD11b+ Ly6chi monocytes in the dLN, used as observational data for model monocytes, at zero (from PBS measurements), 6, 24, 48 hours. Estimated datapoints are shown for 168 hours. **D)** The concentration of IFNγ in the dLN, used as observational data for model IFNγ, at zero (from PBS measurements), 3, 6, 24, 48 hours. **E)** The concentration of IFNγ in the dLN, used as observational data for model IFNγ, at zero (from PBS measurements), 3, 6, 24, 48 hours. **E)** The numbers of IFNγ+ NK cells in the dLN, used as observational data for model 'activated NK cells', at zero (from PBS measurements), 6 and 24 hours. Estimated datapoints are shown for 48 hours. **F)** The numbers of IFNγ+ NK cells in the dLN, used as observational data for model 'activated NK cells', at zero (from PBS measurements), 6 and 24 hours. Estimated datapoints are shown for 48 and 72 hours.

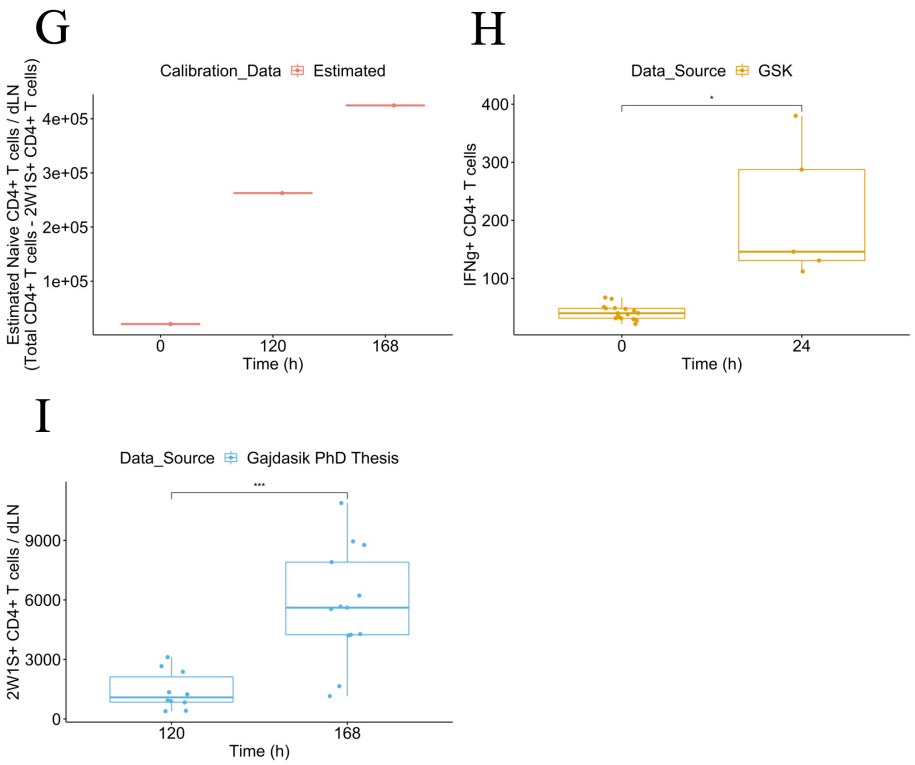


Figure 6.1: **Experimental data for model calibration 2/2:** For full descriptions of experiments that led to these data, please see Figure 3.2. From Figure 3.2, the PBS measurements are here used as 'zero hour' timepoints. Remaining timepoints are from experiments with AS01 1/50 Human Dose. **G)** The estimated numbers of naive CD4+ T cells in the dLN following vaccination with an AS01-adjuvanted vaccine. Zero hour reflects the geometric mean of a PBS control. At hours 120 and 168, these cells are estimated as the difference from geometric means of the total CD4+ T cells and numbers of antigen-specific CD4+ T cells. **H)** The numbers of IFNγ+ CD4+ T cells in the dLN, used as observational data for model primed CD4+ T cells, at zero (from PBS measurements) and 24 hours. **I)** The numbers of 2W1S+ CD4+ T cells in the dlN, measured by Dominika Gajdasik, University of Birmingham.

we decided to estimate the 48 hour data-point. With the data described in Figure 4.1, we had measurements for IFNγ+ NK cells between 0,6,24 hours. To estimate the numbers of these cells at 48 hours post-injection, we gathered data from a separate experiment, which measured the numbers of these cells at both 6 hours post-injection and 48 hours post-injection of 1/10HD of AS01. Although the quantifications of the readouts are inconsistent with the more commonly used 1/50HD data and thus complicate their integration, the trends between different timepoints are consistent across these experiments irrespective of the dose used. Given that in this data the peak of these cells is described at 6 hours post-injection before returning toward baseline by 48 hours [32], we used these additional data to calculate the change in abundance of these cells between the 6 and 48 hour timepoints. We took the geometric mean of the values at these timepoints, and calculated there was a 97.98% reduction in these cells between 6 and 48 hours post-injection with this experiment.

This calculation was then applied to the the numbers of these cells at 6 hours post-injection for the IFNγ+ NK cell measurements shown in Figure 4.1 that we had gathered with the intention of calibration (shown in Figure 4.1), to estimate the 48 hour data point.

Collectively, these data show an increase of IFNγ+ NK cells, peaking at approximately 6 hours post-injection before returning to baseline levels by 48 hours, consistent with observations by Coccia [32]. Some internal GSK experiments have shown a slight increase of these cells after 48 hours, although we were unable to curate these data. The second wave of IFNγ is considered to be mediated by CD8+ T cells and not NK cells, indicating that NK cells are less important for our research questions after 48 hours. Nevertheless, future modelling efforts should aim to incorporate data on these cells at later timepoints and explore effects of these cells beyond 48 hours in detail, when such data is available. However, given that these cells are considered not to be the primary mediator of IFNγ following 48 hours post injection, we were satisfied with estimating only this timepoint. This is a limitation, however given the scarcity of the experimental data, we sought to gather a 'minimal set' of data to calibrate such a model, while minimising how much of it was estimated.

Figure 6.1F shows the numbers of IFNγ+ CD8+ T cells observed *in vivo* in the dLN at 0,6,24,48 and 76 hours post injection. Given our criteria to minimise confounding factors, there are limited data regarding these cells at these time-points over the first seven days. Internal GSK data which is yet to be published, demonstrates that CD8+ IFNγ+ T cells mediate the second wave of IFNγ after approximately 24 hours post-injection. Therefore, beyond 24 hours, the importance of these cells to our research context increases, and we make a central estimate for these cells at 48 and 72 hours post-injection. Similar to estimating measurements for IFNγ+ NK cells described previously, we have measurements of CD8+ IFNγ T cells after experiments using the large dose of AS01b 1/10HD. Given these cells are considered to be the primary mediator of IFNγ after 24 hours post-injection with AS01, we estimated numbers of these cells at both 48 and 72 hours post-injection. Similar to the above with NK cells, we gathered the additional experiment where 1/10HD was used and calculated the change between the geometric means of the measurements of these cells between 24 hours and 48 hours and then 48 hours and 72 hours. These changes were then applied to our 1/50HD data, to generate a central estimate these cells at 48 and 72 hours post-injection. Again, future work will seek to incorporate uncertainty into these estimates, although comprehensive *in vivo* datasets would be more valuable. Here, we observed a transient increase in the cells over the first 24 hours, which will be referred to as the 'innate CD8+ T cell response', and a subsequent increase from estimated data considered to represent 'adaptive CD8 + T cells'.

We next calculated the numbers of naive CD4+ T cells in the dLN after vaccination with AS01 at 0, 120 and 168 hours post-injection (Figure 6.1G). D. Gajdasik from the Withers' lab, supplied us with data after an experiment where C57BL/6 mice were injected with 2W1s *listeria monocytogenes*, administered IM into the gastrocnemius muscle with either 1/50HD AS01 or PBS. Data were not generated for 2W1S antigen and control liposomes. At 120 and 168 hours post-injection, the total, and antigen-specific CD4+ T cell numbers were measured in iliac dLNs, although measurements after PBS are only available at day 5. After PBS+2W1S, negligible antigen-specific 2W1S+ T cells were observed (data not shown), compared with significant increases instead following AS01 administration. Thus, there are very few antigen-specific CD4+ T cells after PBS+2W1s and we therefore assumed the number of total CD4+ T cells after PBS, would provide a reasonable approximation of baseline naive CD4+ T cells. To estimate the number of cells at zero hours, we thus employed the geometric mean of the PBS control measurement for total CD4+ T cells. For hours 120 and 168, we have measurements of total and antigen-specific CD4+ T cells after AS01+2W1s. For these two timepoints, we thus make the assumption that the naive CD4+ T cells are the proportion of total CD4+ T cells, which are not antigen-specific. Therefore for these time-points we calculate central estimates of naive CD4+ T cells as the number of total CD4+ T cells less the 2W1s+ CD4+ cells, after AS01 using geometric means of each population. Again, future work will seek to incorporate the breadth of potential uncertainty into these estimates. Next, we show the distributions of IFNγ+ CD4+ T cells as provided by GSK, at 0 and 24 hours post injection (Figure 6.1H). Given IFN expression, we assume these are primed CD4+ T cells. We observed a slight increase in the number of IFNγ+ CD4+ T cells over the first 24 hours, suggesting low levels of priming. Lastly, as kindly provided by D. Gajdasik, we show distributions of antigen-specific 2W1S+ CD4+ T cells in the dLN, following AS01 vaccination at 120 and 168 hours post-injection.

The use of approximated 'central estimates' are a limitation of this work, and further experimental data incorporating inherent biological variation are required to reinforce the trends observed throughout this chapter. Additionally, future work should seek to incorporate additional uncertainty around these estimates into the curated data, although as a simple 'first step' in this exploratory modelling work to suggest trends, where we needed to make approximations of the kinetics, we sought to gather only central estimates.

Data for Simulation Validation: In addition to the data for simulation validation presented in Figure 3.3, we were kindly provided data from D.Gajdasik, who measured the numbers of 2W1s+ CD4+ T cells in C57BL/6 or CD80 & CD86 deficient mice after injection with 2W1s and AS01b (Figure 6.2). Here, we observed in B7-KO mice that compared to the wild type scenario in C57BL/6 mice, the number of 2W1s+ CD4+ T cells at 120 hours

post injection are almost eliminated after AS01-adjuvanted vaccination, indicating that activation of these cells is mediated by CD80 and CD86. Collectively, the data previously shown in Figure 3.3 (used to validate the innate IFNγ model) and the data shown in Figure 6.2 are set aside for simulation validation for the current work.

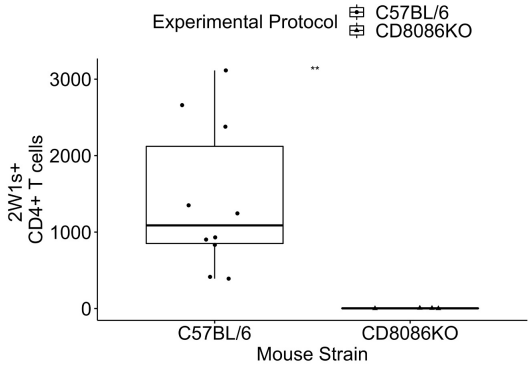


Figure 6.2: **Experimental data for model validation:** Colleagues at the university of Birmingham injected C57BL/6 or CD80/80-/- mice with AS01 and 2W1s. At five days post-injection, the numbers of antigen-specific CD4+ T cells were measured. Here, we contrast these two measurements.

6.2.1.3 A CellDesigner Model depicting salient events that give rise to CD4+ T cell priming after AS01-adjuvanted vaccination.

We next scoped high-level interactions hypothesised to promote the phenomena observed *in vivo* (Figure 6.3). In this CellDesigner diagram, the muscle injection site is labelled as *A)* and the draining lymph node labelled as *B)*. Given the nature of the model, which extends the innate IFNγ model, Figure 6.3 refines and extends the dynamics described in section 4.2.1.3 and in Figure 4.2. Here, we additionally capture the presentation of antigen by Mature DCs (highlighted as MDC B1) to 'T Helper Cells' (highlighted as B2). The 'Mature DC' can express CD80/86 (B7), pMHCII and OX40L. pMHCII expression presents antigen to the 'T Helper Cell'. Expression of pMHCII can be enhanced by IFNγ. OX40L expression on DCs has been shown to be critical for effector Th1 responses (in the case of listeria monocytogenes) and here we hypothesise OX40L is induced by IFNγ [314]. Collectively, we capture IFNγ's potential role in enhancing DC potency, as per our 'IFNγ enhancement hypothesis'.

For space on the diagram, the 'T Helper Cell' represents both 'naive' and 'primed' CD4+ T cells. If a 'naive T Helper' cell comes into contact with a 'Mature DC' expressing their cognate antigen, they can become a 'primed T Helper Cell' and if this cell becomes fully activated it can secrete an array of cytokines. State-diagrams and Activity Diagrams developed later will assist in discriminating between these naive and activated CD4+ T cells. Our research context is only interested in dynamics involved in the generation of

activated or 'primed CD4+ T cells', and thus effector functions of these cells e.g., providing survival signals to B cells are not captured.

6.2.1.4 Describing Expected Behaviours

Following high-level scoping of the system, we constructed an 'Expected Behaviours' diagram (Figure 6.4). This diagram extends the Expected Behaviours diagram presented in section 4.2.14 in Figure 4.3. While some components of the Expected Behaviours diagram presented in Chapter 4 are omitted for diagrammatic space here, the phenomena described in section 4.2.1 apply here unless explicitly described otherwise.

Key Observable Phenomena

Here, we describe the phenomena observed *in vivo* as depicted in Figure 6.4, alongside hypotheses for how these phenomena manifest. What is described below, extends those phenomena in section 4.2.1.5 for the innate IFNγ model. These insights were extracted from the biological data shown in Figure 6.1 and hypotheses for underlying mechanisms were developed in collaboration between ourselves and GSK.

1. **At six hours post injection, MHCII+ CD11c+ DCs numbers have increased from approx. 4,500 to approx. 12000 (Fig 6.1B) :** We hypothesised the cause of this observed rise in DCs at this timepoint is in-part due to limited numbers of monocytes which have differentiated into DCs but primarily, that resident DCs have become activated. Migratory DCs could also contribute to this increase although these cells aren't likely to arrive from the injection site until approximately 16 hours post injection.
2. **At six hours post injection, IFNγ+ CD8+ T cells have increased from approx. 30 cells to approx. 3500 (Fig 6.1F) :** The numbers of (innate) CD8+ T cells are increasing, although these cells are secreting negligible levels of IFNγ [32].
3. **By twenty-four hours post injection, MHCII+ CD11c+ DCs numbers have increased from approx. 12k at six hours to approx. 22,000 cells (Fig 6.2B) :** We hypothesised that DCs are being activated in the dLN and MHCII+ DCs are arriving from the injection site. The previously high production of IFNγ (see 4.2.1.5: peaks at approx. 6 hours) has enhanced OX40L and/or pMHCII expression on some DCs.
4. **At twenty-four hours post injection, IFNγ+ CD8+ T cell numbers have reduced from approx. 3.5k cells at six hours to approx. 400 cells (Fig 6.1F).** Innate IFNγ+ CD8+ T cells have left the dLN or moved into a 'non-IFNγ secreting' state, resulting in the decrease in IFNγ+ cells.

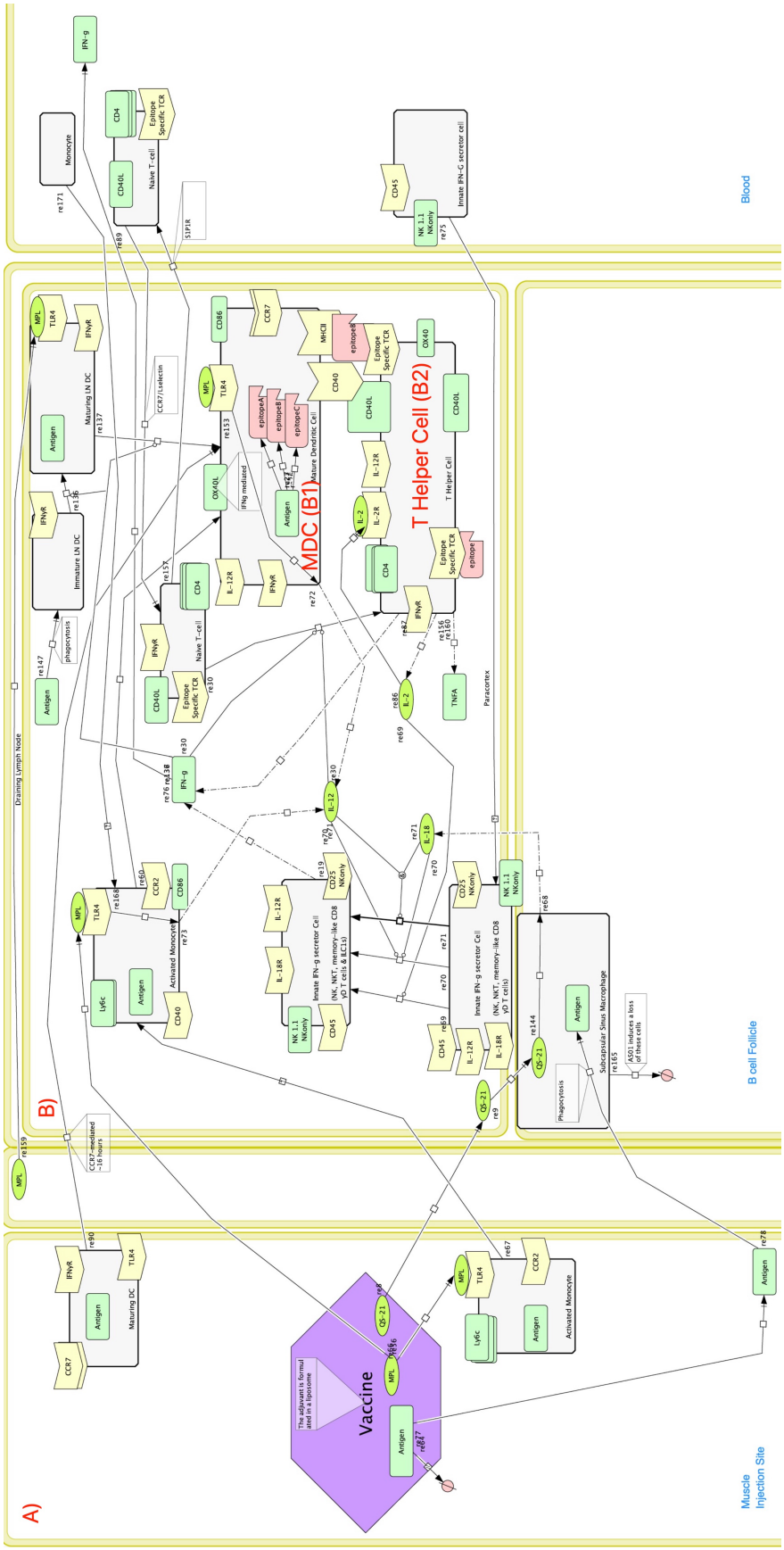


Figure 6.3: **Scoping cellular interactions:** A CellDesigner Model depicting salient events that give rise to CD4+ T cell priming after AS01-adjuvanted vaccination.

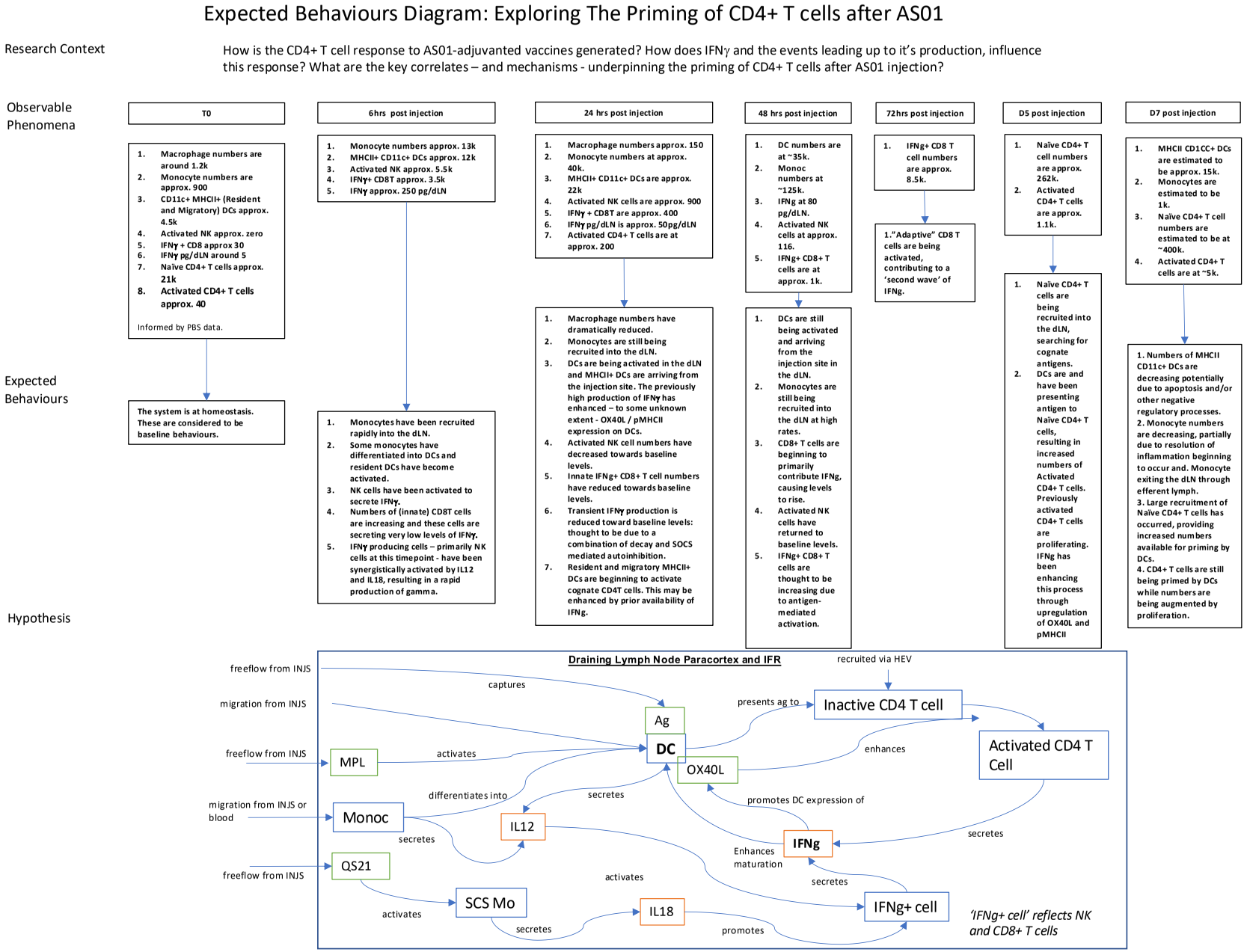


Figure 6.4: **An Expected Behaviours Diagram:** Defining expected behaviours through linking the phenomena observed from the biological data to the times at which these are observed and to the hypotheses for how such phenomena manifest.

5. **At twenty-four hours post injection, Activated (IFNγ+) CD4+ T cells have increased from approx 40 cells at time-zero to 200 (Fig 6.1H):** We thus hypothesised that resident and migratory MHCII+ DCs are beginning to activate CD4+ T cells. This may be enhanced by availability of IFNγ.
6. **At fourty-eight hours post injection, MHCII+ CD11c+ DCs and inflammatory monocyte numbers have increased from respective measurements at six hours to approx. 35,000 and 125,000 respectively (Fig 6.1B and 6.1C):** We hypothesised that DCs are still being activated in the dLN, compounded by those arriving from the injection site, thus augmenting numbers of MHCII-expressing DCs. Secondly, we hypothesised that monocytes are still being recruited into the dLN at high rates.
7. **At fourty-eight hours post injection, IFNγ+ CD8+ T cells have increased to approx. 1000 (Fig 6.1F):** We hypothesised that these cells are increasing in number due to antigen-mediated activation, reflecting an 'adaptive IFNγ+ CD8+ T cell' population.
8. **At fourty-eight hours post injection, IFNγ has increased from the measurement at 24 hours to approximately 80 pg/dLN (Fig 6.1D):** Based on internal GSK data, we hypothesised that CD8+ T cells are beginning to contribute IFNγ, causing levels to rise.
9. **At fourty-eight hours post injection, Activated (IFNγ+) NK cells have reduced from the measurement at 24 hours to approx. 116 cells (Fig 6.1E):** Many NK cells have either left the lymph node or stopped producing IFNγ, resulting in a substantial reduction in the numbers of these cells.
10. **At seventy-two hours post injection, IFNγ+ CD8+ T cells have increased again to approx 8,500 cells (Fig 6.1F):** We hypothesised that 'adaptive CD8+ T cells' are being activated further, contributing to a 'second wave' of IFNγ.
11. **At five-days post injection, naive CD4+ T cell numbers have increased from approx. 21000 cells at time-zero to approx. 262,000 (Fig 6.2G):** We hypothesised that naive CD4+ T cells are being recruited into the dLN in large numbers, searching for cognate antigen.
12. **At five-days post injection, Activated (2W1s+ antigen-specific) CD4+ T cells have increased to approx. 1,100 (Fig 6.1I):** We first hypothesised that DCs are and have been presenting antigen to naive CD4+ T cells - some of which become primed as a result of a successful cognate interaction, leading to increased numbers of antigen-specific CD4+ T cells. Additionally, we hypothesised that 'activated' CD4+ T cells are and have been proliferating, contributing to this increase

in cell number. Lastly, we hypothesise that IFNγ has been enhancing this process through upregulation of pMHCII and OX40L on DCs, augmenting the numbers of activated antigen-specific cells.

13. **At seven-days post injection, MHCII+ CD11c+ DCs are estimated to have reduced to approx. 15,000 (Fig 6.1B):** We hypothesised that the numbers of MHCII+ DCs have decreased toward baseline due to apoptosis and/or other negative regulatory processes.
14. **At seven-days post injection, inflammatory monocytes are estimated to have reduced to approx. 1,000 (Fig 6.1C):** We hypothesised that monocyte numbers are estimated to have decreased toward baseline due to monocyte egress from the dLN [46] and/or other negative regulatory processes.
15. **At seven-days post injection, naive CD4+ T cell numbers have increased from day 5 and are estimated to be approx. 400,000 (Fig 6.1G):** We hypothesised that naive CD4+ T cells have been recruited in large numbers into the dLN.
16. **At seven-days post injection Activated (2W1s+ antigen-specific) CD4+ T cells have increased to approx. 5000 (Fig 6.1 I):** We hypothesised that CD4+ T cells are still being primed by DCs, while levels of these cells are being augmented by proliferation of already-activated cells.

6.2.1.5 Integrating Experimental Insight with Assumptions and Further Hypotheses

In addition to assumptions, hypotheses etc described for the AS01 innate IFNγ Domain Model in section 4.2.1.6 and the expected behaviours just described (section 6.2.1.4) , this section details further assumptions and hypotheses related to our research questions.

1. **Hypothesis: IFNγ promotes OX40L expression on 'Mature DCs' which in turn can enhance DC stimulatory potency.** In infection with Listeria monocytogenes, Gajdasik et al [314] observed that OX40L expression by DCs is regulated by cross-talk with NK cells and IFNγ signalling enhances OX40L. In this system, OX40L by DCs was required for the generation of functional Th1 cells. Further, after transfecting DCs with OX40L mRNA, Dannull et al [315] observed that DC capacity to stimulate CD4+ T cells was increased, as was T cell polarisation.
2. **Assumption: DCs arriving into the dLN are already activated. This may have occurred in the injection site by either antigen uptake or adjuvant components.** It has been well characterised in wider systems that after capturing antigen in the periphery, these cells upregulate CCR7 to migrate into towards

dLN [316]. Furthermore, following vaccination with AS01-adjuvanted vaccines, Didierlaurent et al characterised that arriving DCs are MHCII-high, demonstrating prior capture of antigen. Here, we assume that DCs that arrive into the dLN have already been activated.

3. **Hypothesis: IFNγ can enhance expression of CD80 and CD86 on DCs.** After AS01-adjuvanted vaccination in IFNγR mice there is a considerable reduction of CD80 and CD86 MFI compared to the wild-type in C57BL/6 mice [32]. Taken together with Gajdasik's observations that CD4+ T cell priming is B7-dependent, we therefore hypothesise that IFNγ enhancement of B7 expression on DCs may contribute to CD4+ T cell priming.

6.2.1.6 Activities of Model Entities

Next, Activity Diagrams were developed to extend those described in 4.2.1.7 for the innate IFNγ model, in order to capture an extension of that model to incorporate CD4+ T cell priming. While the entire model is too large to present in a single thesis chapter, we present a 'whole system' Activity Diagram, which describes the key functionality of each model entity, and how each component interacts with each other to produce the whole system behaviour (Figure 6.5). Please see supplementary T-D (**T**cell Model **D**omain Model, link in Appendix A.2) for the full Domain Model diagrams.

Here we describe the Activity Diagram in Figure 6.5. Subcapsular sinus macrophages (**A**, labelled SCS-Mo), enter the system resident in the SCS. If this cell interacts with free-flowing QS21 (**B**), the SCS-Mo can become activated and secrete IL18 [8], which can promote the production of IFNγ. Monocytes (**C**) enter the system activated, after migrating into the dLN. Given appropriate signals, a limited proportion of these cells may differentiate into a mature DC. Arriving monocytes are pMHC-int [46], assumed to be activated and secrete IL12 (stimulated by MPL) as hypothesised in Chapter 4. IL12 can also be produced by 'Mature DCs', which promotes the production of IFNγ. Synergistically IL18, and IL12 augment the IFNγ production by 'IFNg Producer cell'. 'IFNg Producer' cells (**D**) enter the system either resident in the dLN or after recruitment via HEVs. The 'IFNg Producer' entity represents both NK cells and IFNγ+ CD8+ T cells at respective time periods. If this cell is activated by IL12 or IL18, this cell can produce IFNγ. In the event this cell is activated by both IL12 and IL18, synergistic IFNγ production by this cell is observed as described by Coccia et al.

IFNγ (IFNg, **E**) enters the system after being secreted by an 'IFNg Producer'. IFNγ can enhance pMHCII and/or B7 expression on 'Resident DC' (**F**), or 'Mature DC' (**G**). Resident DCs (**F**) enter the system resident in the dLN. If MPL binds TLR4 expressed

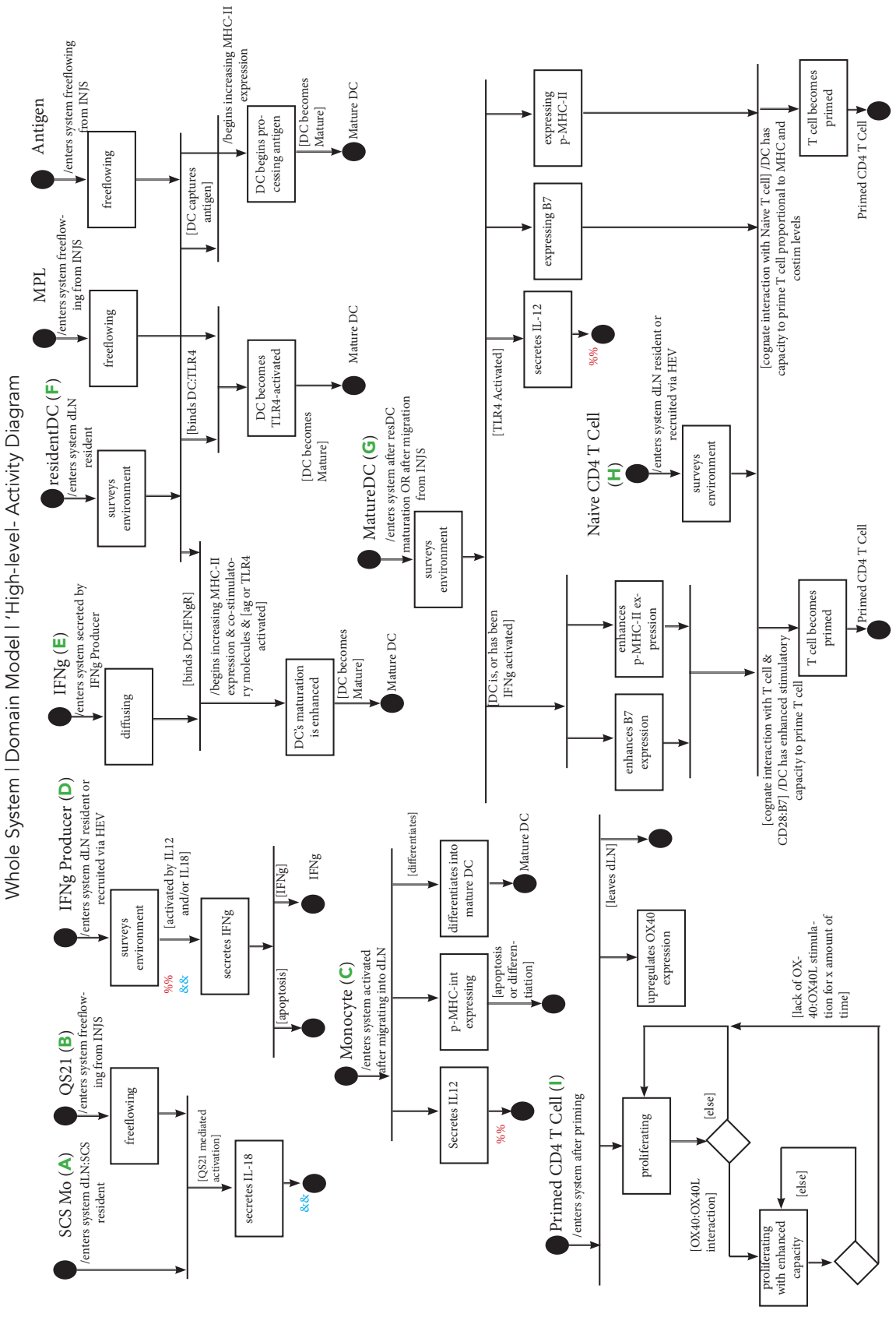


Figure 6.5: **A 'Whole System' Activity Diagram:** showing key activities of different model components and how they interact to produce system wide behaviour. Diagram shows activities for A) Subcapsular sinus macrophages (SCS-Mo), B) QS21, C) monocytes, D) IFNg Producer, E) IFNg, F) resident DCs, G) mature DC, H) naive CD4+ T cells and I) primed CD4 T cells.

on the DC, the cell can become 'TLR-4 activated', which is one avenue that the cell may transition (differentiate) into a 'Mature DC'. Simultaneously, if a Resident DC captures antigen, peptide processing and presentation occurs, leading to expression of pMHCII on the surface of these cells. Antigen processing by a resident DC also leads to the cell transitioning into a 'Mature DC'. Therefore, 'Mature DCs' (**G**) enter the system either, after a resident DC has matured as described or, after migrating into the dLN from the injection site. The former, represents 'MHCII+ resident DCs' and the latter represents 'MHCII+ migratory DCs' [5]. If this cell is - or has been - activated by IFNγ, it can exhibit enhanced expression of pMHCII and/or B7. Indeed, if this cell has been activated by TLR4, it can secrete IL12. Naive CD4+ T cells (**H**) circulate through the lymphatic system, exploring lymph nodes for their cognate antigen. During inflammation, large increases in the numbers of these cells recruited to lymph nodes are observed [317, 318, 314]. This cell enters the system either resident in the dLN at time-zero or by arriving via HEV. If this cell undergoes a cognate interaction with a 'Mature DC', the T cell can become primed. The potency to which DCs can prime CD4+ T cells is hypothesised to be substantially enhanced by IFNγ availability, through mechanisms described previously. 'Primed (CD4+) T cells' (**I**) enter the system after priming by mature DC. This cell proliferates and upregulates OX40 expression. A successful OX40/OX40L interaction may augment proliferative capacity.

6.2.1.7 State-Machine Diagrams and Model Summary

Next, we developed State-Machine diagrams for all model entities. Given the size of the model, only the State-Machine diagram for a CD4+ T cell is shown here, while the remaining Domain Model diagrams are in Supplementary T-D. Figure 6.6 shows a State-Machine diagram for CD4+ T cells. This diagram represents both naive and primed CD4+ T cells, distinguished through state-transitions. Putting everything together, Figure 6.7 summarises the salient biology captured in the Domain Model.

6.2.2 A Platform Model for Baseline AS01 CD4+ T cell priming

Next, we constructed a Platform Model, to express the Domain Model in computational and mathematical language. Similarly as described in section 4.2.2, our questions of interest involve relationships between model components rather than heterogeneity or spatial dynamics. As highlighted previously, the available experimental data for calibration is sparse and we aimed to embrace simplicity. Collectively, we reasoned that ODEs would be the most appropriate modelling technique.

To ease illustration of how the domain model (Figure 6.5) is represented by the computational and mathematical specification in Figure 6.8, we have kept the labelling of entities

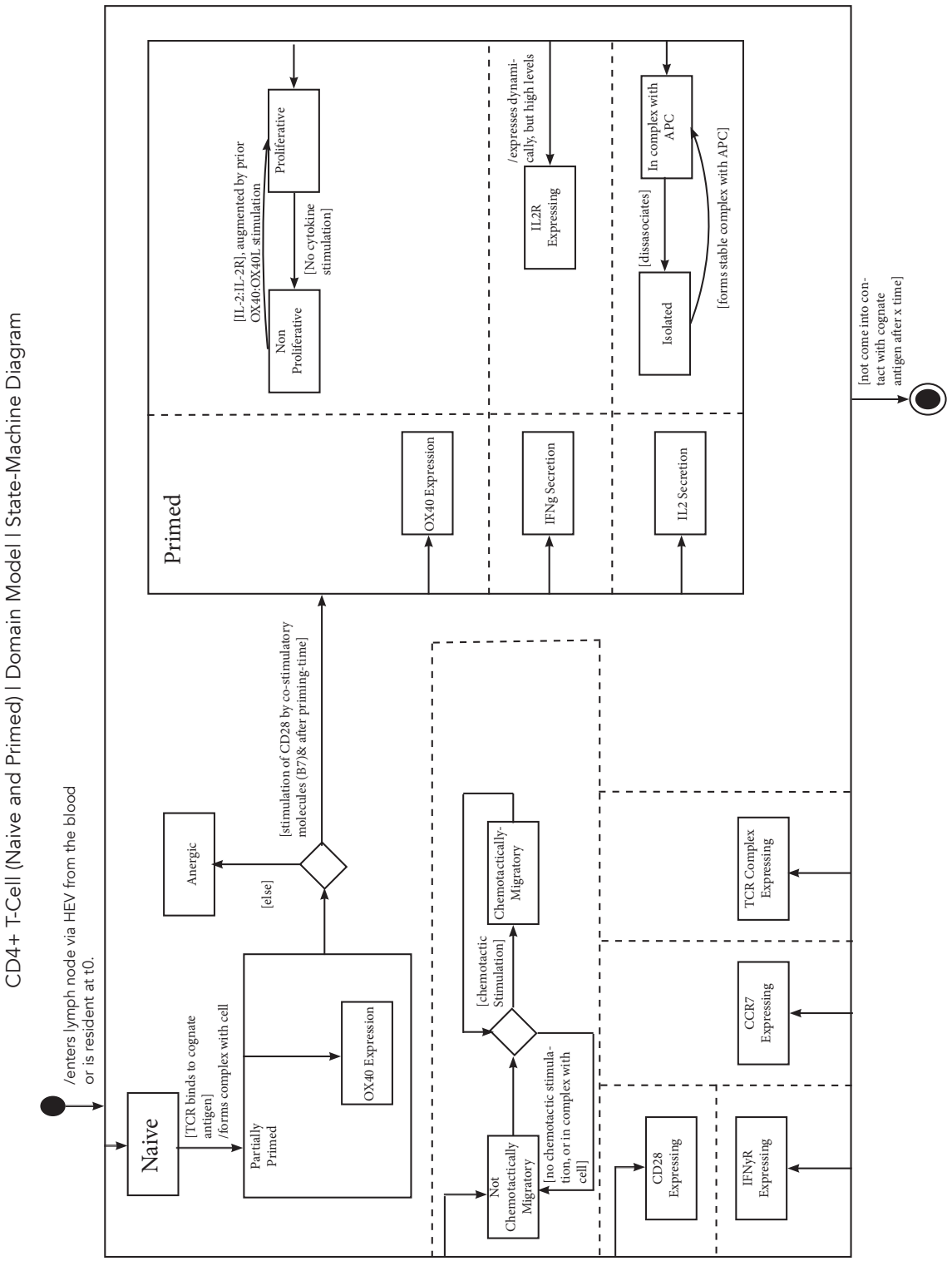


Figure 6.6: **A State-Machine diagram for a CD4+ T cell:** captures both naive and primed states.

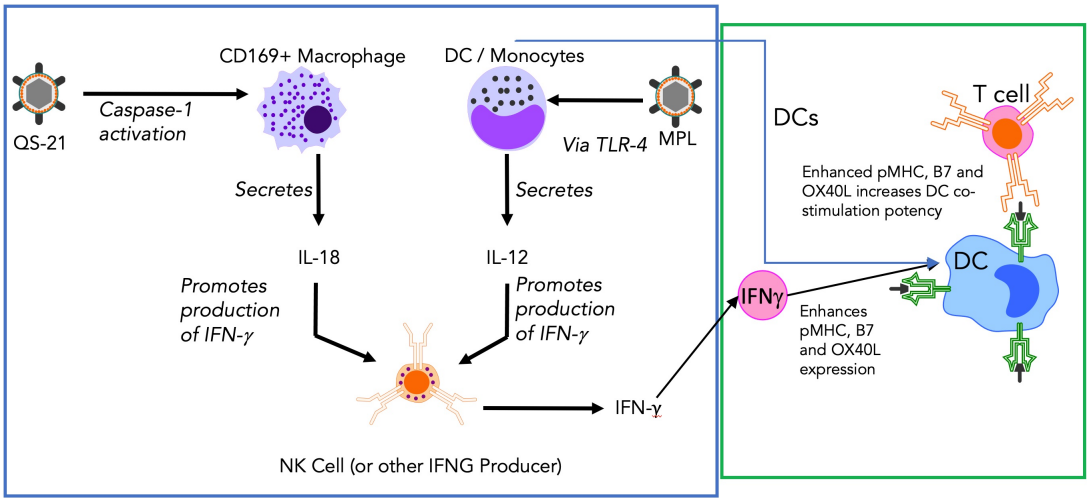


Figure 6.7: **A simplified cartoon of the Domain Model for AS01-induced CD4+ T cell priming.** Describes the captured salient biology. Surrounded by the blue box, is the captured salient biology in the Domain model for innate IFNγ production, as described in Chapter 4. Here, we extend the model (shown in green), to capture canonical priming of CD4+ T cells by DCs, and the ability for IFNγ to enhance this process.

as consistent as possible between these two figures. Here, we describe simplifications, refinements and additions that were made, culminating in the Platform Model. Please see supplementary T-P (**T**cell Model **P**latform Model, link in Appendix A.2) for the full Platform Model diagrams. Figure 6.8 shows a 'Population and Interactions' diagram, describing how the salient components of the Platform Model interact. Indeed, following stimulation with QS21 (B), subcapsular sinus macrophages (A, named 'Mo') are lost as described by Detienne et al., [8] at rate CL_p, and they secrete IL18 at rate $vMoIL18_p$. IL18 can promote the production of IFNγ. Monocytes (C, named 'Monoc') enter the system activated, at rate $monocRec_p$ and can secrete IL12 at rate $vMonocIL12_p$ which is induced by MPL_p. These cells additionally can differentiate into DCs (representing 'Mature DCs') at rate $MonocDiffDC_p$. A decay of these cells occurs at rate $MonocDecay_p$. In the Platform model, monocyte expression of pMHC is not captured as after AS01 these cells are not observed to prime T cells *in vivo*, despite their observed pMHC-int expression [5].

In the Domain Model, 'IFNg Producer' cells were captured, representing NK and CD8+ T cells which produce IFNγ. Here, these cells are separated into three populations of cells. Firstly, IFNγ NK cells (D.1, labelled as 'NKa'). Furthermore, as recommended by GSK immunologists, IFNγ+ CD8+ T cells were separated into two populations of CD8+ T cells to appropriately discriminate their contribution: innate IFNγ+ CD8+ T cells (D.2, labelled as 'InnateCD8') and Adaptive IFNγ CD8+ T cells (D.3, labelled as 'AdaptiveCD8'). IFNγ+ NK cells (D.1) are activated by IL12 and/or IL18 at rates $VmaxNKa1218_p$, $VmaxNKa18_p$, $VmaxNKa12_p$, representing synergistic activation induced by IL12 and IL18, individual acti-

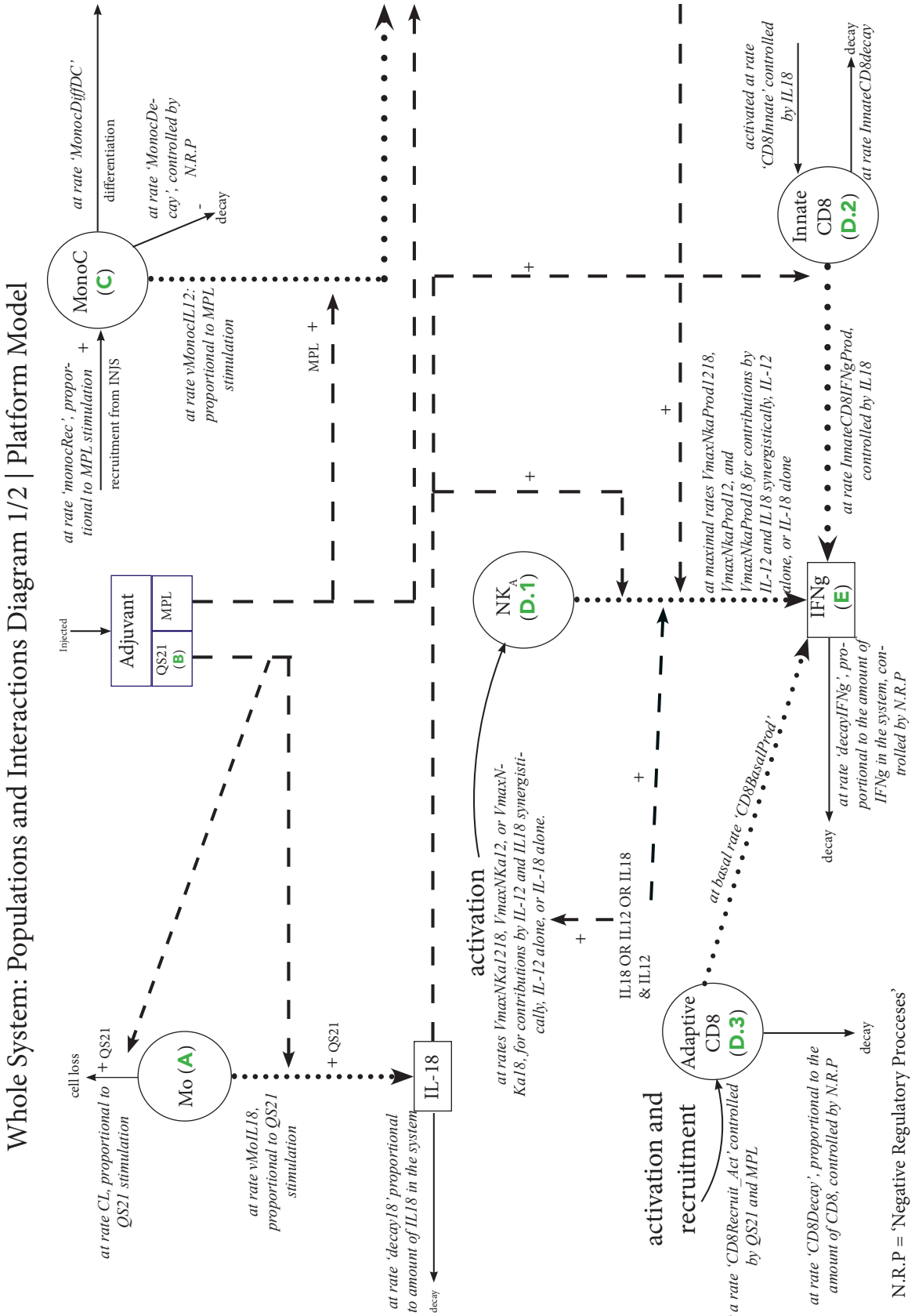


Figure 6.8: **A Platform Model for AS01 induced CD4+ T cell Priming:** 1/2

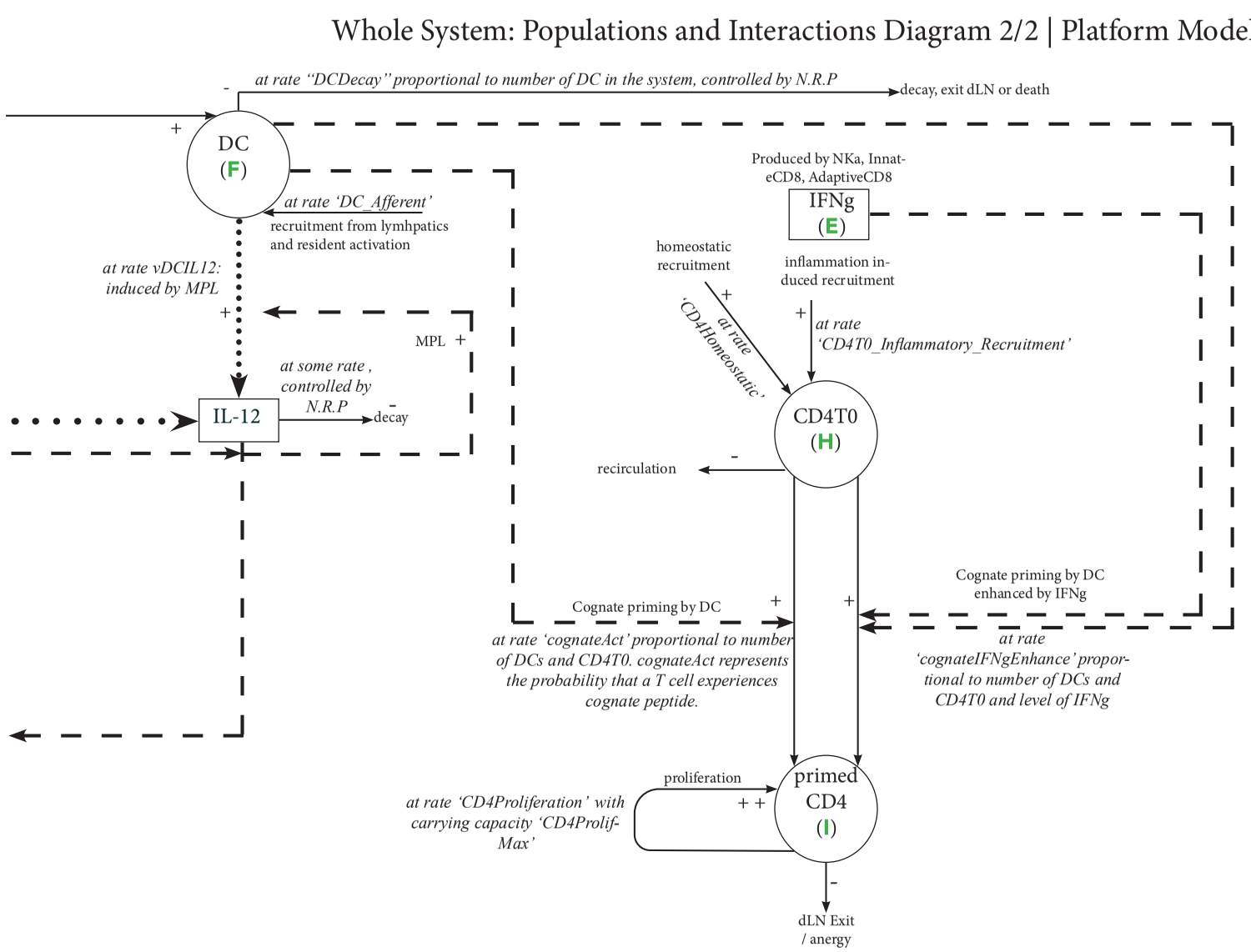


Figure 6.8: **A Platform Model for AS01 induced CD4+ T cell Priming:** 2/2. A 'population and interactions' diagram describing the interplay between different model components. The rate 'cognateAct' in the diagram is written in the text and subsequent models as 'cognatePriming', for further clarity. Dotted arrows indicate secretion of a cytokine. Dashed arrows indicate a component acts upon another.

vation only by IL18, and individual activation only by IL12, respectively, where $VmaxNKa1218_p \geq VmaxNKa18_p \geq VmaxNKa12_p$. These activation rates lead to production of IFNγ at rates $VmaxNKaProd1218_p$, $VmaxNKaProd18_p$ and $VmaxNKaProd12_p$ where $VmaxNKaProd1218_p \geq VmaxNKaProd18_p \geq VmaxNKaProd12_p$. These differences in activation and therefore production rates are represented in this manner as synergistic activation by IL18 and IL12 has been observed to contribute substantially more IFNγ than IL18 or IL12 alone, and additionally the number of IFNγ+ cells are more substantially reduced in IL18R-/- mice compared with αIL12 depletion [32] suggesting that IL18 contributes more to the activation of these cells than IL12.

Innate IFNγ+ CD8+ T cells (D.2) enter the system activated, at rate $CD8Innate_p$, induced by IL18. Evidence for IL18 induction of this process has been observed in unpublished GSK data. Additionally, these cells are hypothesised - given internal GSK data - to secrete very low levels of IFNγ at rate $InnateCD8IFNgProd_p$ and this is also controlled by IL18. It remains to be seen from *in vivo* experimentation using AS01 whether IL12 contributes to this process. A reduction in the number of these cells occurs at rate $InnateCD8decay_p$. Adaptive IFNγ CD8+ T cells (D.3) are recruited and activated at rate $CD8Recruit_Act_p$, which is controlled in the model by QS21 and MPL_p, as we hypothesise that this process is induced by the adjuvant. A reduction in the number of these cells occurs at rate *CD8Decay*. These 'AdaptiveCD8' cells produce IFNγ at a basal rate *CD8BasalProd*.

IFNγ (E, labelled IFNg) enters the system after being secreted by either an NK cell (**D.1**), an innate CD8+ T cell (D.2) or an adaptive CD8+ T cell (**D.3**). In the Domain Model, we describe IFNγ's ability to enhance pMHCII, OX40L and B7 expression on resident and mature DCs. Here, all DCs are assumed to be mature (as they are MHCII+), and the hypothesis that IFNγ can enhance the aforementioned co-stimulatory molecules and pMHCII complexes is modelled as a rate - $cognateEnhanceIFNg_p$ - through which DC numbers able to prime naive CD4+ T cells can be enhanced, leading to increased numbers of primed CD4+ T cells. We aim to create different model variants that capture different magnitudes of IFNg enhancement of CD4+ T cell priming through altering permitted ranges for this parameter during calibration. OX40L and B7 are not modelled directly due to lack of quantitative data after AS01.

We only model mature DCs, therefore we capture dLN resident DCs - which have become activated and express MHCII - as well as migratory DCs which arrive in the dLN expressing MHCII. In the Platform Model, these resident and migratory MHCII+ CD11c+ DCs are represented by the 'DC' entity (**F**, labelled 'DC)'. The parameter $DC_Afferent_p$ represents the rate to which (migratory) DCs infiltrate the dLN, and also to which resident DCs are activated. This process is controlled by MPL [95]. As these cells are mature, the

'DC' secretes IL12, at a rate $vDCIL12_p$ controlled by MPL_p, which as mentioned promotes the production of IFNγ (E). For simplicity, explicit TLR4 signalling is not modelled here although an abstraction is captured, by which MPL controls the secretion of IL12 by DCs (MPL is a TLR4 agonist). A loss of the number of 'DCs' occurs at rate $DCDecay_p$, hypothesised to be caused by apoptosis and/or other negative regulatory processes. By presenting antigen, these DCs can promote priming of naive CD4+ T cells (H, labelled 'CD4T0') at rate *cognatePriming*. This rate represents DC priming of CD4+ T cells - independent of IFNγ-enhancement - mediated by B7:CD28 interactions. Separately, this rate of cognate priming of CD4+ T cells - mediated by B7:CD28 - can be enhanced by IFNγ through rate $cognateEnhanceIFNg_p$ [32]. CD4+ T cells were modelled with inspiration from previous work by Marino et al [197]. Indeed, a constant source of naive CD4+ T cells (H) are recruited at homeostatic rate $CD4Homeostatic_p$. This parameter is calculated as:

$$CD4Homeostatic_p = \text{CD4T0_death_recirculation}_p \times CD4T0(0)$$

where $CD4T0_death_recirculation_p$ represents the death/recirculation rate of naive CD4+ T cells, and *CD4T0(0)* represents the number of naive CD4+ T cells at time-zero. This is a commonly used approach and has been used in prior immunology work [197, 319]. naive CD4+ T cell inflammation-induced recruitment was also captured as inspired by Marino et al. Here, increased recruitment induced by inflammation occurs at rate $CD4T0_Inflammatory_Recruitment_p$ controlled by MPL and QS21 (as a proxy for inflammation). As described previously, upon priming by (mature) DCs (F), these cells can transition into primed CD4+ T cells (I, labelled primedCD4) at rates *cognatePriming* or $cognateEnhanceIFNg_p$. primed CD4+ T cells can proliferate at rate $CD4Proliferation_p$, with a maximal rate of $CD4ProlifMax_p$. Potential anergy of these cells and their exit from the dLN is modelled as rate $TcellExit_Anergy_p$.

An early version of the model described thus far was implemented, although unable to reasonably describe the experimental data in Figure 6.1. We therefore reasoned the model was incomplete. Specifically, we were able to describe increases of cells and cytokines, however through optimisation the model was unable capture the resolution of inflammation, e.g., reductions of DCs and monocytes after 48 hours towards day 7 as observed in Didierlaurent and Coccia's work [5, 32]. We reasoned that this was because we failed to capture what we term 'Negative Regulatory Processes', i.e., negative regulatory pathways which collectively control the temporal dynamics of innate immune responses. Simply, we had only captured the 'on signal' and not processes which may be time-restricted. These include phosphotases, receptor turnover, ubiquitination, upregulation of 'inhibitory proteins', mIRNAs which downregulate early immune genes and a wide range of other factors

[320]. Naturally, these mechanisms serve to limit autoinflammatory disease or aggressive immunopathology. Given this observation, we introduced a component into the model termed *Negative_Regulatory_Processes* which increases in quantity over time, serving to simply represent the onset of negative regulatory control of the immune response. This component is at this stage assumed to have a more prominent role in the later times of the immune response. This component is captured in Figure 6.8, for DC, monocyte, IFNγ and Adaptive CD8+ T cells and is labelled 'N.R.P'.

6.2.2.1 A Mathematical Model for AS01-induced CD4+ T cell priming in a murine dLN

We propose the following ODEs to describe the mechanisms captured in the Platform Model. Equations or terms which extend the mathematical model in Chapter 4 are labelled in blue.

$$\frac{dMo}{dt} = -(CL_p \times Mo \times QS21_p) \tag{6.1}$$

Equation 6.1 describes the rate of change of SCS macrophages (Mo). Mo reduce as a function of time at a rate proportional to CL_p controlled by $QS21_p$. This equation is identical to that presented in Chapter 4 equation 4.1.

$$\frac{dNRP}{dt} = (InhibitionProduction_p \times NRP) \tag{6.2}$$

Equation 6.2 describes the rate of change of the 'Negative Regulatory Procceses' (NRP). The quantity of this component increases as a function of time at rate $InhibitionProduction_p$.

$$\frac{dMonoc}{dt} = (monocRec_p \times MPL_p) - (MonocDiffDC_p \times Monoc) - (MonocDecay_p \times Monoc \times NRP) \tag{6.3}$$

Equation 6.3 describes the rate of change of monocytes (Monoc), which are recruited at rate $monocRec_p$ which is controlled by MPL_p. These cells can differentiate into DCs at rate $MonocDiffDC_p$, causing a removal of these cells. This rate of differentiation is proportional to the number of monocytes in the system. In an extension to the monocyte equation described in Chapter 4 equation 4.2, equation 6.3 describes a decay of monocytes at rate $MonocDecay_p$, which is proportional to the quantity of NRP. As NRP increases over time, this forces the rate of decay to increase over time.

$$\frac{dDC}{dt} = (MonocDiffDC_p \times Monoc) + (DC_Afferent_p \times MPL_p) - (DCDecay_p \times DC \times NRP) \tag{6.4}$$

Equation 6.4 describes the rate of change for MHCII+ CD11c+ DCs in the model (DC). Monocytes differentiate into DCs at rate $MonocDiffDC_p$, resulting in a limited supply of these cells. A further positive source of DCs is due to activation, as well as recruitment from the afferent lymphatics at - for simplicity - rate $DC_Afferent_p$. Extending the DC equation described in Chapter 4 equation 4.4, we here describe the decay of these cells at rate $DCDecay_p$, controlled by NRP.

$$\frac{dIL18}{dt} = (vMoIL18_p \times Mo \times QS21_p) - (decay18_p \times IL18) \tag{6.5}$$

Equation 6.5 describes the rate of change for IL18. The first term describes the rate of $QS21_p$ induced production of IL18 by macrophages (Mo), at rate $vMoIL18_p$. The second term is a decay term, at a rate proportional to the amount of IL18. This equation is identical to Chapter 4 equation 4.5.

$$\frac{dIL12}{dt} = (vMonocIL12_p \times Monoc \times MPL_p) + (vDCIL12_p \times DC \times MPL_p) - (decay12_p \times IL12 \times NRP) \tag{6.6}$$

Equation 6.6 describes the rate of change of IL12 in the system. As proposed in Chapter 4 equation 4.6, the first and second terms describe the rate of MPL_p induced production of IL12 by monocytes and DCs respectively. Here, the decay term at rate $decay12_p$ is additionally controlled by NRP. Through qualitative reasoning, we expect IL12 to increase in trajectory consistent with that of DC and monocyte availability in the system. However the decay term controlled by NRP, should effectively lead to an increase of the decay rate over time, therefore IL12 production should not spiral unphysiologically.

$$\frac{dNKa}{dt} = +VmaxNKa_{1218p} \times \left(\frac{IL18}{IL18 + KM_{IL18bp}}\right) \times \left(\frac{IL12}{IL12 + KM_{IL12bp}}\right) + (VmaxNKa12_p \times IL12) + (VmaxNKa18_p \times IL18 - (NKDecay_p \times NKa) \tag{6.7}$$

Equation 6.7 describes the rate of change of activated NK cells (NKa). This equation is identical to the 'NKa' equation in Chapter 4, equation 4.4.

$$\frac{dInnateCD8IFNg}{dt} = (CD8Innate_p \times IL18) - (InnateCD8decay_p \times InnateCD8IFNg) \tag{6.8}$$

Equation 6.8 describes the rate of change of innate IFNγ+ CD8+ T cells (InnateCD8IFNg). This variable represents the 0-24 hour (hence innate) population of IFNγ+ CD8+ T cells observed in Figure 6.1F. An increase of these cells occurs due to activation and recruitment at rate $CD8Innate_p$, controlled by IL18. These cells are removed from the system by the decay term, at rate $InnateCD8decay_p$, proportional to the number of cells in the system.

$$\begin{aligned}\frac{dAdaptiveCD8IFNg}{dt} &= (CD8RecruitAct_p \times MPL_p \times QS21_p) \\ &\times AdaptiveCD8IFNg) \times (1 - \frac{AdaptiveCD8IFNg}{AdaptiveCD8Max_p}) \\ &-(AdaptiveCD8Decay_p \times AdaptiveCD8IFNg \times NRP)\end{aligned} \tag{6.9}$$

Equation 6.9 describes the rate of change of adaptive IFNγ+ CD8+ T cells (Adaptive CD8IFNg). This variable represents the 48 hour and onwards population of IFNγ+ CD8+ T cells observed in Figure 6.1F, estimated from wider experimental data (see Methods). The observed rapid recruitment and/or activation of these cells is described using logistic growth. Here, the growth rate $CD8RecruitAct_p$ - which is controlled by MPL_p and $QS21_p$ represents recruitment and activation of these cells and the population maximum is described by $AdaptiveCD8Max_p$. The last term describes a decrease of these cells which is assumed to occur towards the latter of the simulation, at rate $AdaptiveCD8Decay_p$ as they are assumed - based on expert domain intuition - to decay toward day 7 post-injection.

$$\begin{aligned}\frac{dIFNg}{dt} &= (VmaxNKaProd_{1218p} \times IL18 \times (\frac{IL12}{IL12 + KMNKa_{IL12bp}}) \times NKa) \\ &+ (VmaxNKaProd_{18p} \times IL18 \times NKa) + (VmaxNKaProd_{12p} \times IL12 \times NKa) \\ &+(InnateCD8IFNgProd_p \times IL18 \times InnateCD8IFNg) \\ &+(BasalCD8IFNgProd_p \times AdaptiveCD8IFNg) - (decayIFNg_p \times IFNg \times NRP)\end{aligned} \tag{6.10}$$

Equation 6.10, describes the rate of change of IFNγ ($IFNg$). The first three terms are identical to those described for the 'IFNg' component of the previous model (see Chapter 4 section 4.2.2.3 equation 4.7). In contrast to the previous innate IFNγ model, we capture the reasoning that innate IFNγ+ CD8+ T cells secrete low level of this cytokine at rate $InnateCD8IFNgProd_p$, induced by IL18. The fifth term describes a basal rate of production

of IFNγ at rate $BasalCD8IFNgProd_p$ by Adaptive CD8+ T cells. Lastly, we capture the decay of this cytokine at rate $decayIFNg_p$, proportional to the quantity of NRP and available IFNγ.

$$\frac{dCD4T0}{dt} = (CD4Homeostatic_p) + (CD4T0_Inflammatory_Recruitment_p \times CD4T0 \times MPL_p \times QS21_p) - (CD4T0_death_recirculation_p \times CD4T0) - (cognatePriming_p \times CD4T0 \times DC) - (cognateEnhanceIFNg_p \times CD4T0 \times DC \times IFNg) \tag{6.11}$$

Equation 6.11 describes the rate of change of naive CD4+ T cells (CD4T0). These cells are described with a constant source term $CD4Homeostatic_p$ and an inflammatory recruitment term at rate $CD4T0_Inflammatory_Recruitment_p$, which depends on MPL_p and $QS21_p$, the adjuvant immunostimulants. The last two terms control cognate priming of these cells by DCs. The first, describes (IFNγ-independent) canonical DC and B7 mediated priming of these cells at rate $cognatePriming_p$. The last term describes an enhancement of this process, representing an upregulation of DC stimulation potency induced by IFNγ (i.e., IFNγ-dependent pathway), whereby more naive CD4+ T cells are primed by DCs.

$$\frac{dprimedCD4}{dt} = (cognatePriming_p \times CD4T0 \times DC) + (cognateEnhanceIFNg_p \times CD4T0 \times DC \times IFNg) + CD4Proliferation_p \times primedCD4 \times (1 - \frac{primedCD4}{CD4ProlifMax_p}) - (TcellExit_Anergy_p \times primedCD4) \tag{6.12}$$

Equation 6.12 describes the rate of change for primed CD4+ T cells (primedCD4). As CD4T0 cells become primed as described in equation 6.11, the first two terms in equation 6.12 represent the positive influx of CD4T0 cells which are primed by DCs, either independent or dependent on IFNγ at rates $cognatePriming_p$ and $cognateEnhanceIFNg_p$ respectively. The third term describes proliferation of these cells, described using logistic growth, controlled by the growth rate $CD4Proliferation_p$ and the population maximum $CD4ProlifMax_p$. The last term describes a loss of these cells via exiting the dLN or anergy, at rate $TcellExit_Anergy_p$.

6.2.3 A Simulation Platform for AS01 induced CD4+ T cell Priming

The ODEs were implemented as described in section 2.3.1. Table 6.1 shows the shorthand used in the text, equations and results model, to refer to model entities.

Model Entity Name	**Full Entity Name**
Mo	CD169+ F4/80- macrophages
NRP	Negative Regulatory Processes
Monoc	CD11b+ Lyc6-high monocytes
DC	Resident and migratory dendritic cells
IL18	Interleukin 18
IL12	Interleukin 12
NKa	activated IFNγ^+ NK cells
InnateCD8IFNg	activated IFNγ+ CD8+ T cells
AdaptiveCD8IFNg	activated adaptive IFNγ+ CD8+ T cells
IFNg	IFNγ
CD4T0	naive CD4+ T cells
primedCD4	primed CD4+ T cells

Table 6.1: Table of Simulation Measures: Defining the shorthand used in the Simulation

6.2.4 A calibrated 'Baseline' Model of CD4+ T cell priming

We next calibrated the model to our experimental data (data is summarised in Table 6.2). Firstly, to embrace simplicity, we sought to calibrate a 'Baseline' model of CD4+ T cell priming after AS01, based on the aforementioned dynamics, however where the IFNγ-dependent pathway of priming exerted negligible impact on priming. This was performed by supplying very small ranges for the parameter *cognateEnhanceIFNg* to the calibration routine (see Table 6.3 for further details). If successful, this calibration would generate a 'baseline' model of CD4+ T cell priming after AS01, allowing the analysis of a model which essentially did not incorporate the 'IFNγ-enhancement' hypothesis. Subsequently, we extend and calibrate a second 'Alternate' model where IFNγ-**dependent** CD4+ T cell priming was allowed to exert influence on simulation behaviour (the extent of which remained to be explored).

For the 'Baseline' model of CD4+ T cell priming, calibration was performed using *dMod* [9] (Methods section 2.4). Given similar challenges as described in section 4.2.3.1 with the AS01 innate IFNγ model complexity of calibration owing to a large parameter space, we followed the same approach to calibration. To control the optimisation, we incrementally isolated small portions of the feed forward, cascading nature of the model, beginning with the macrophage equation, to fit parameter CL_p before incorporating further sections of the model/equations. This process makes the complexity manageable and we believe enabled the calibration of the innate IFNγ model in Chapter 4. For calibration, the data presented in Fig 6.3 H-I will be consolidated for the 'primed CD4+ T cells' entity. The IFNγ+ CD8+ T cell data will be separated into data to calibrate 'innateCD8IFNg' cells (0-24 hrs data), and 'adaptiveCD8IFNg' (48 and 72 hours). Where possible (e.g., rates estimated from related modelling efforts, cytokine half-lives [302, 303, 304] etc) a 'best guess' set of parameters values and ranges, were gathered from multiple sources in the literature [319, 197, 321, 205]. These were used as initial calibration 'starting points'.

Model Entity Name	**Timepoints**	**Measurements**
Mo (macrophages)	0, 24 hrs	Geo. mean and sd. QS21 stimulation *in vivo*.
DC	0, 6, 24, 48, 168 hrs	Geo. mean and sd. AS01 stimulation *in vivo*. 168 hr data were estimated.
Monoc (monocytes)	0,6,24,48, 168 hours	Geo. mean and sd. AS01 stimulation *in vivo*. 168 hr data were estimated.
NKa (Activated NK cells)	0,6,24,48 hrs	Geo. mean and sd. AS01 stimulation *in vivo*. 48 hr data were estimated.
IL18	No data available	No data available.
IL12	No data available	No data available.
IFNg (IFNγ)	0,3,6,24,48 hrs	Geo. mean and sd. AS01 stimulation *in vivo*.
InnateCD8IFNg and AdaptiveCD8IFNg	0,6,24,48,72	Geo. mean and sd. AS01 stimulation *in vivo*. 48 and 72 hrs data were estimated. Hours 0,6,24 are used for 'InnateCD8IFNg' entity while hrs 48 and 72 are used for 'AdaptiveCD8IFNg'.
CD4T0 (naive CD4+ T cells)	0,120, 168	Geo. mean and sd. Data estimated from AS01 stimulation data *in vivo*.
primedCD4 (primed CD4+ T cells)	0, 24, 120, 168 hrs	Geo. mean and sd. All data from AS01 stimulations *in vivo*. Data at 0, 24 hrs were generated by GSK after examining IFNγ+CD4+ T cells after AS01. Data at 120 and 168 hrs were generated by Dominika Gajdasik, University of Birmingham and readouts are of 2W1S+ CD4+ T cells / dLN after AS01-vaccination.

Table 6.2: Summary of Experimental Data Availability and Measurements for Model Calibration: 'Geo.mean' is shown as shorthand for the 'geometric mean', and 'sd' is shown as shorthand for the 'standard deviation'. All 'zero hour' data was estimated from PBS controls. 'No data available' reflects that no data were available in the relevant context for AS01-adjuvanted vaccination. The experimental data summarised in this table is presented in Figure 6.1, along with full experimental information. Estimated data points and their justification are described in the text and Chapter 2 (Materials and Methods). All 'hrs' timepoints are 'post-injection'.

The calibration process resulted in 81 parameter sets (representing local minima with respect to fitting data) and model trajectories are visualised in Figure 6.9. Code to solve the model using the 'best fit' set of parameters is in Appendix A.2. In what follows, each local minima are treated as equally likely, thus are each employed in analysis, producing a distribution of model output for each ODE variable. Generally, the model is reasonably able to describe the data. However, we observed large variation in the model trajectories for e.g, DCs (Figure 6.9B), which is unsurprising given the variation in the experimental data. For monocytes (Figure 6.9C), clearly the model is unable to fully replicate the rapid increase in the infiltration of monocytes between 24 and 48 hours post injection. We propose that this reveals a gap in our understanding of the early AS01 response, reflecting production of e.g., a cytokine, or another factor which promotes an increase in the monocyte infiltration rate. This is discussed further in section 6.2.6. For primed CD4+ T cells (Figure 6.9L), the observational datapoints are consolidated from data shown in Figure 6.1H-I. For this variable, we observed large variation in the model trajectories, and while the model is able to some extent describe the data, it does not fully reflect the breadth of the experimental data, in particular at 168 hours post injection. This suggests that the model and indeed our understanding of the system, is incomplete.

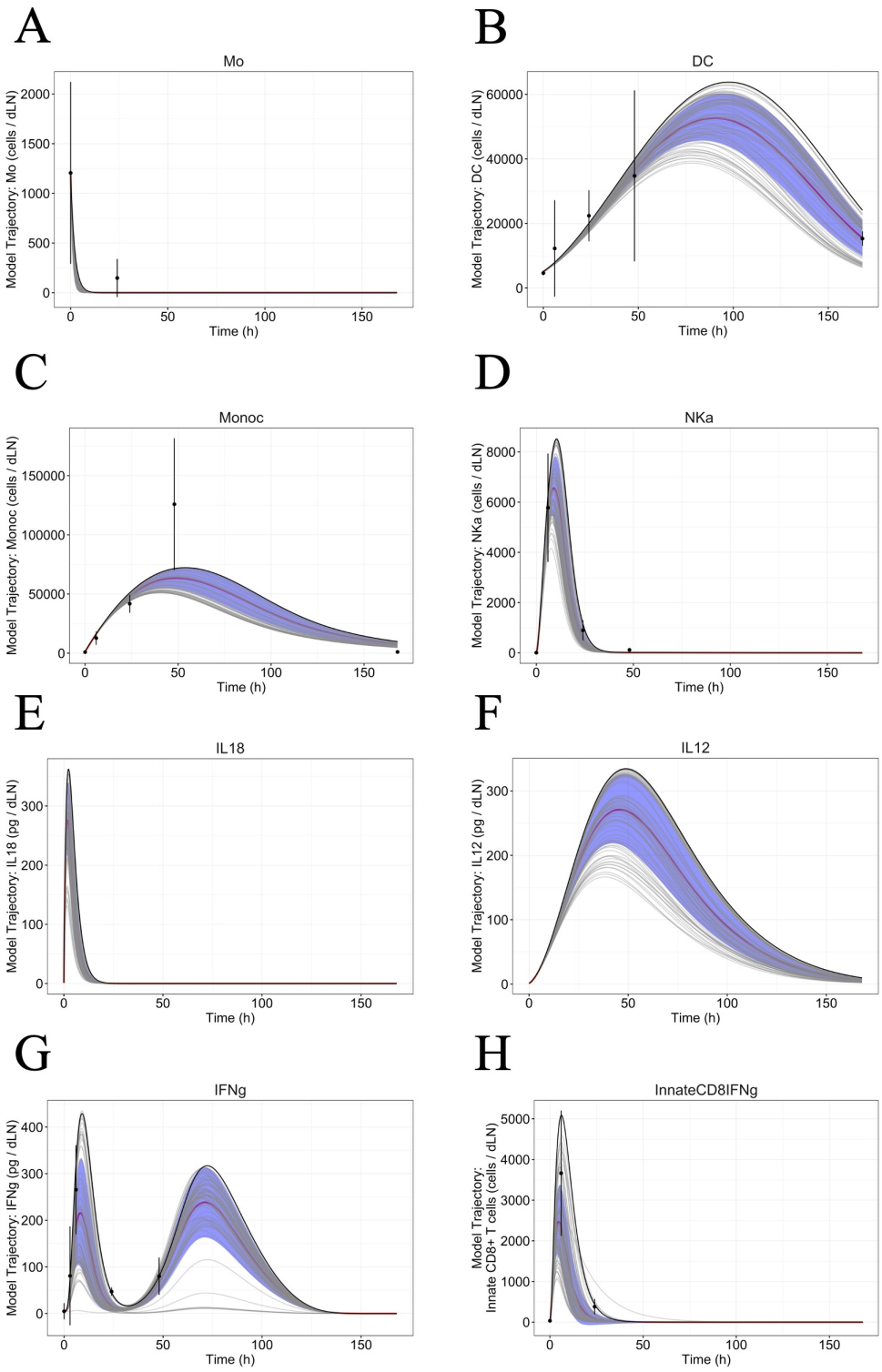


Figure 6.9: **Calibration of the Baseline AS01 CD4+ T cell Model 1/2:** Caption overleaf.

Lastly, we would like to reiterate that in the calibration of this model, the parameter $cognateEnhanceIFNg_p$ - representing IFNγ controlled enhancement of cognate priming of CD4+ T cells - was set with a a mean value of 8.905e-14 across the distribution of parameter

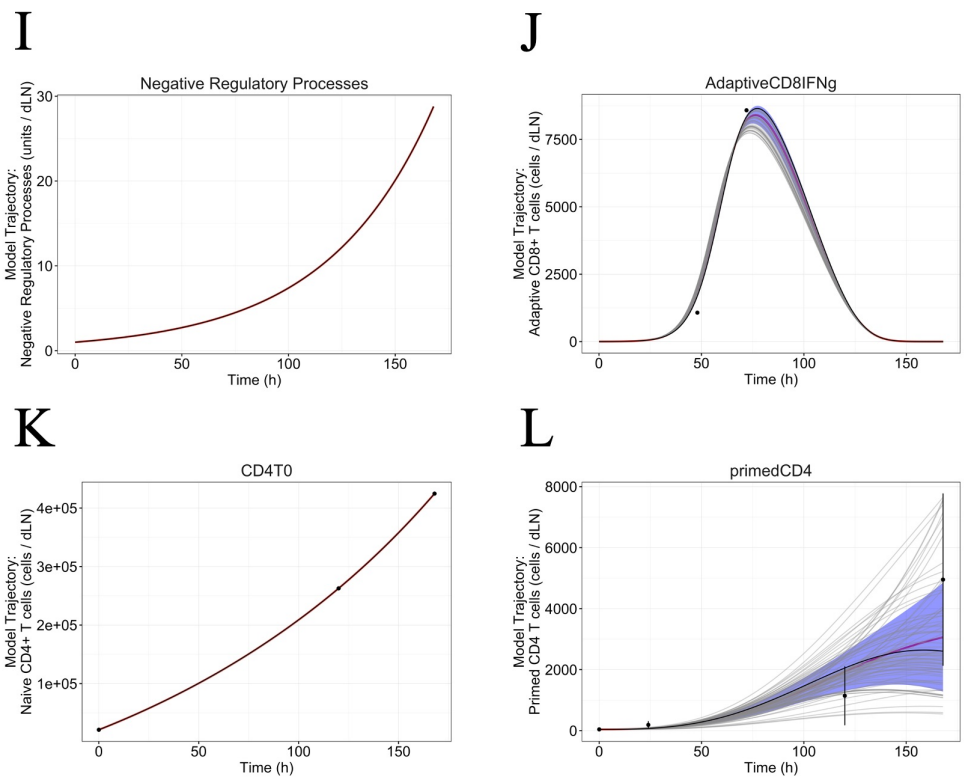


Figure 6.9: **Calibration of the Baseline AS01 CD4+ T cell Model 2/2:** Macrophage (A), dendritic cell (B), monocyte (C), IFNγ+ NK cell (D), IL18 (E), IL12 (F), IFNγ (G), Innate IFNγ+ CD8+ T cell (H), Negative Regulatory Processes (I), Adaptive IFNγ+ CD8+ T cell (J), naive CD4+ T cell (K) and primed CD4+ T cell (L) kinetics were fitted using the *dMod* package, employing multi-start trust-region optimisation to minimise the objective value between the model output and observational data. Black dots and error bars show the mean and standard deviation of the biological data upon which the model was calibrated, grey lines represent *in silico* parameterisation outputs, blue shading represents the mean +/- the standard deviation for these *in silico* outputs, red lines represent the mean of the *in silico* outputs, and black lines represent the best fitting (lowest objective value) *in silico* output.

sets. This is in contrast to $cognatePriming_p$, which was set with a mean value of 3.66e-09 across the distribution of parameter sets. We forced a much lower range of values for $cognateEnhanceIFNg_p$ (hence the lower mean of the distribution), to calibrate a model which reflected a 'Baseline' model of AS01 CD4+ T cell priming, with minimal contribution of the hypothesis that IFNγ enhances CD4+ T cell priming. This was performed so mechanisms could be examined with the 'Baseline' model, separately from this hypothesis, so to identify mechanisms which were robust regardless of the 'IFNγ enhancement' hypothesis.

Values for the parameters and ranges are shown in Table 6.3. A description of each parameter is given in Table 6.4. While this model is able to reasonably describe the data, there are trajectories which cannot reflect the breadth or central estimates of the data. We propose that this reveals gaps in the model. Additionally, this model is constructed on many assumptions and a handful of estimated data points. Thus, given our careful description of

the holistic current understanding of AS01 MoA - working with GSK immunologists who generated vital insights - we additionally propose that the incompleteness of the model also reveals gaps in our understanding of the system. We therefore intend to use this theoretical construct for exploratory analysis, to propose hypotheses underpinning AS01 MoA.

	Parameter	LowerRange	BestFitValue	UpperRange	LowerRange_Calib	UpperRange_Calib	Mu	Units
1	$VmaxNKaProd1218_p$	1.141E-05	1.197E-04	1.200E-04	1.136E-05	1.200E-04	1.200E-04	pg/NKa hour
2	$KM_NKa_IL12b_p$	5.441E+00	5.834E+00	5.834E+00	5.441E+00	5.834E+00	5.487E+00	pg/dLN
3	$VmaxNKaProd18_p$	5.777E-07	5.777E-07	5.777E-07	1.534E-07	5.777E-07	5.777E-07	pg/NKa hour
4	$VmaxNKaProd12_p$	5.777E-08	5.777E-08	5.777E-08	5.777E-10	5.777E-08	5.634E-08	pg/NKa hour
5	$decayIFNg_p$	1.400E-01	1.400E-01	1.750E-01	1.400E-01	1.750E-01	1.500E-01	pg/dLN hour
6	$monocRec_p$	2.698E+02	2.700E+02	2.700E+02	2.100E+02	2.700E+02	2.700E+02	cells per unit MPL / hour
7	$MonocDiffDC_p$	7.006E-03	8.000E-03	8.000E-03	5.000E-03	8.000E-03	8.000E-03	proportion / Monoc hour
8	$DC_Afferent_p$	3.264E+01	4.250E+01	4.250E+01	2.250E+01	4.250E+01	3.254E+01	cells/hour
9	$vMonocIL12_p$	3.297E-05	3.297E-05	3.297E-05	3.227E-05	3.297E-05	3.297E-05	pg/Monocyte hour
10	$vDCIL12_p$	3.333E-05	3.333E-05	3.333E-05	3.227E-05	3.333E-05	3.333E-05	pg/DC hour
11	$decay12_p$	4.178E-02	4.178E-02	7.397E-02	4.178E-02	7.404E-02	4.178E-02	pg/dLN hour
12	CL_p	4.800E-02	4.800E-02	1.000E-01	4.800E-02	1.000E-01	4.887E-02	cells per unit QS21 / hour
13	$vMoIL18_p$	2.000E-02	3.500E-02	3.500E-02	2.000E-02	3.500E-02	3.500E-02	pg/Mo
14	$decay18_p$	3.800E-01	3.800E-01	4.000E-01	3.800E-01	4.000E-01	3.952E-01	pg/dLN hour
15	$VmaxNKa1218_p$	5.489E+03	5.489E+03	5.489E+03	5.442E+03	5.489E+03	5.489E+03	cells/hour
16	KM_18b_p	3.264E+01	3.264E+01	3.526E+01	3.264E+01	3.526E+01	3.264E+01	pg/dLN
17	KM_12b_p	2.370E+01	2.478E+01	2.494E+01	2.369E+01	2.494E+01	2.369E+01	pg/dLN
18	$VmaxNKA12_p$	9.143E-03	9.143E-03	9.143E-03	4.941E-03	9.143E-03	9.143E-03	cells/hour
19	$VmaxNKa18_p$	1.500E+00	1.500E+00	1.500E+00	1.500E+00	1.501E+00	1.500E+00	cells/hour
20	$NKDecay_p$	2.931E-01	2.931E-01	2.970E-01	2.931E-01	2.970E-01	2.931E-01	proportion/NKa hour
21	$DCDecay_p$	1.750E-03	1.751E-03	3.499E-03	1.750E-03	3.500E-03	1.750E-03	proportion of DC per unit N.R.P/hour
22	$MonocDecay_p$	1.000E-02	1.000E-02	2.000E-02	1.000E-02	2.000E-02	1.044E-02	proportion of Monoc per unit N.R.P/hour
23	$CD8Innate_p$	3.124E+00	5.000E+00	5.000E+00	1.000E+00	5.000E+00	3.328E+00	cells / pg IL18 hour
24	$CD8RecruitAct_p$	1.993E-03	1.993E-03	2.061E-03	1.000E-04	3.700E-03	9.060E-04	cells per unit of QS21 and MPL / hour
25	$InnateCD8decay_p$	6.586E-02	1.825E-01	4.000E-01	1.000E-02	4.000E-01	1.601E-01	proportion of InnateCD8 / hour
26	$AdaptiveCD8Decay_p$	2.500E-02	2.500E-02	2.500E-02	2.500E-02	1.100E-01	2.500E-02	proportion of AdaptiveCD8 per unit N.R.P / hour
27	$InnateCD8IFNgProd_p$	1.000E-13	1.000E-13	1.000E-12	1.000E-13	1.000E-12	1.000E-12	pg/InnateCD8 hour
28	$BasalCD8IFNgProd_p$	1.000E-03	2.250E-02	2.250E-02	1.000E-03	2.250E-02	1.243E-02	pg/AdaptiveCD8 hour
29	$InhibitionProduction_p$	2.000E-02	2.000E-02	2.000E-02	2.000E-02	2.250E-02	2.000E-02	unitless
30	$AdaptiveCD8Max_p$	1.636E+04	2.100E+04	2.100E+04	8.580E+03	2.100E+04	1.624E+04	cells/dLN
31	$CD4T0_death_recirculation_p$	5.746E-02	5.767E-02	5.812E-02	1.000E-02	1.500E-01	5.824E-02	proportion of CD4T0/hour
32	$CD4T0_Inflammatory_Recruitment_p$	6.388E-04	6.423E-04	6.454E-04	1.250E-05	9.900E-04	6.467E-04	cells per unit MPL and QS21/hour
33	$cognatePriming_p$	1.375E-09	4.582E-09	4.600E-09	1.375E-09	4.600E-09	2.100E-09	proportion of CD4T0/DC hour
34	$cognateEnhanceIFNg_p$	5.000E-14	1.000E-13	1.000E-13	5.000E-14	1.000E-13	1.000E-13	proportion of CD4T0/DC / pg IFNg hour
35	$CD4Proliferation_p$	7.900E-02	7.900E-02	1.187E-01	7.900E-02	1.400E-01	7.900E-02	cells/hour
36	$CD4ProlifMax_p$	1.260E+07	7.888E+07	1.000E+08	1.000E+04	1.000E+08	1.000E+07	cells/dLN
37	$TcellExit_Anergy_p$	6.750E-02	1.000E-01	1.000E-01	6.750E-02	1.000E-01	8.000E-02	cells/hour

Table 6.3: Parameter Values derived from calibration for the **Baseline CD4+ T cell Priming Model**. 'LowerRange' and 'UpperRange' represent the lower and upper range respectively of the parameter values yielded from all model fits. 'BestFitValue' is the value if the parameter from the local optima with the lowest objective value. 'LowerRange_Calib' and 'UpperRange_Calib' reflect the range provided to the multi-start trust-region optimiser following the incremental optimisation process. 'Mu' represents the best fit after incremental optimisation, i.e., the starting point provided to the multi-start trust region algorithm. Given no data on QS21 and MPL, parameters $QS21_p$ and MPL_p are set arbitrarily to a value of '10', hence mechanisms involving these parameters are described e.g 'cells per unit MPL_p'.

	Parameter	Definition	Units
1	$VmaxNKaProd1218_p$	Maximal rate of synergistic IFNg production by NKa cells	pg/NKa hour
2	$KM_NKa_IL12b_p$	Half-sat constant on synergistic IL12 on production of IFNg by NKa cells	pg/dLN
3	$VmaxNKaProd18_p$	Maximal rate of IFNg production by NKa when induced by IL18 alone	pg/NKa hour
4	$VmaxNKaProd12_p$	Maximal rate of IFNg production by NKa cells when induced by IL12 alone	pg/NKa hour
5	$decayIFNg_p$	Rate of decay / reduction of IFNg	pg/dLN hour
6	$monocRec_p$	Rate of monocyte recruitment	cells per unit MPL_p / hour
7	$MonocDiffDC_p$	Rate of monocyte differentiation into DCs	proportion / Monoc hour
8	$DC_Afferent_p$	Constant controlling DC infiltration from afferent lymphatics	cells per unit MPL_p/hour
9	$vMonocIL12_p$	Maximal rate of IL12 production by Monoc	pg/Monoc hour
10	$vDCIL12_p$	Maximal rate of IL12 production by DCs	pg/DC hour
11	$decay12_p$	Rate of decay / reduction of IL12	pg/dLN hour
12	CL_p	Rate of Mo loss proportional to number of Mo available	cells per unit $QS21_p$ / hour
13	$vMoIL18_p$	Maximal rate of IL18 production by Mos	pg/Mo
14	$decay18_p$	Rate of decay / reduction of IL18	pg/dLN hour
15	$VmaxNKa1218_p$	Maximal rate of synergistic activation of NK cells by IL12 and IL18	cells/hour
16	KM_18b_p	Half-sat constant on synergistic IL18 on NKi to NKa	pg/dLN
17	KM_12b_p	Half-sat constant on synergistic IL12 on NKi to NKa	pg/dLN
18	$VmaxNKa12_p$	Maximal rate of individual activation of NK cells by IL12	cells/hour
19	$VmaxNKa18_p$	Maximal rate of individual activation of NK cells by IL18	cells/hour
20	$NKDecay_p$	Rate of reduction NKa	proportion/NKa hour
21	$DCDecay_p$	Rate of DC dLN exit or death	proportion of DC per unit N.R.P/hour
22	$MonocDecay_p$	Rate of monocyte dLN exit or death	proportion of Monoc per unit N.R.P/hour
23	$CD8Innate_p$	Rate of innate CD8 T cell activation by IL18	cells / pg IL18 hour
24	$CD8RecruitAct_p$	Rate of adaptive CD8 T cell activation by $QS21_p$ and MPL_p	cells per unit of $QS21_p$ and MPL_p / hour
25	$InnateCD8decay_p$	Rate of innate CD8 T cell system exit	proportion of InnateCD8 / hour
26	$AdaptiveCD8Decay_p$	Rate of adaptive CD8 T cell system exit	proportion of AdaptiveCD8 per unit N.R.P / hour
27	$InnateCD8IFNgProd_p$	Rate of IFNg production by innate CD8 T cells	pg/InnateCD8 hour
28	$BasalCD8IFNgProd_p$	Basal rate of IFNg production by adaptive CD8 T cells	pg/AdaptiveCD8 hour
29	$InhibitionProduction_p$	Rate of N.R.P increase	unitless
30	$AdaptiveCD8Max_p$	AdaptiveCD8 carrying capacity	cells/dLN
31	$CD4T0_death_recirculation_p$	Rate of naive CD4 T cell death or egress from dLN	proportion of CD4T0/hour
32	$CD4T0_Inflammatory_Recruitment_p$	Rate of inflammation-induced naive CD4 T cell recruitment	cells per unit MPL_p and $QS21_p$/hour
33	$cognatePriming_p$	Rate of B7 mediated priming of cognate CD4+ T cells by DC	proportion of CD4T0/DC hour
34	$cognateEnhanceIFNg_p$	Rate of B7 mediated & IFNg enhanced priming of cognate CD4 T cells by DC	proportion of CD4T0/DC / pg IFNg hour
35	$CD4Proliferation_p$	primed CD4 T cell proliferation rate	cells/hour
36	$CD4ProlifMax_p$	primed CD4 T cell carrying capacity	cells/dLN
37	$TcellExit_Anergy_p$	primed CD4 T cell dLN egress or anergy rate	cells/hour

Table 6.4: Full Description of the Parameters in the CD4+ T cell Models: 82 parameter sets were derived from calibration. Here, the parameters, their definition and respective units are listed. N.R.P represents 'Negative Regulatory Procceses'. 'AdaptiveCD8' and 'InnateCD8' are used for simplicity instead of 'AdapticveCD8IFNg' and 'InnateCD8IFNg' respectively. In following model variants, '$cognatePriming_p$' and '$cognateEnhanceIFNg_p$' may be referred to as '$cognatePriming_NonIFNgControlled_p$' and '$cognatePriming_p_IFNgControlled_p$' respectively, although this will be clearly outlined.

6.2.5 Simulation Validation

Despite the imperfections in model calibration, we reasoned that the simulation could be sufficient for use in *in silico* experimentation, if it was capable of passing 'simulation validation' criteria. We therefore determined whether the model was capable of predicting data upon which it was not trained. Firstly, we simulated *in silico* SSM depletion (Figure 6.10A), IL18RKO (Figure 6.10B), αIL12 depletion (Figure 6.10C), IL18RKO+αIL12 depletion (Figure 6.10D). These 'model validation' *in silico* experiments were performed and contrasted with *in vivo* data as described previously in section 4.2.4.3. Here, for the SSM depletion, we did not observe a significant difference between the *in silico* and *in vivo* distributions (Figure 6.10A). We reasoned that the result of this validation experiment is acceptable.

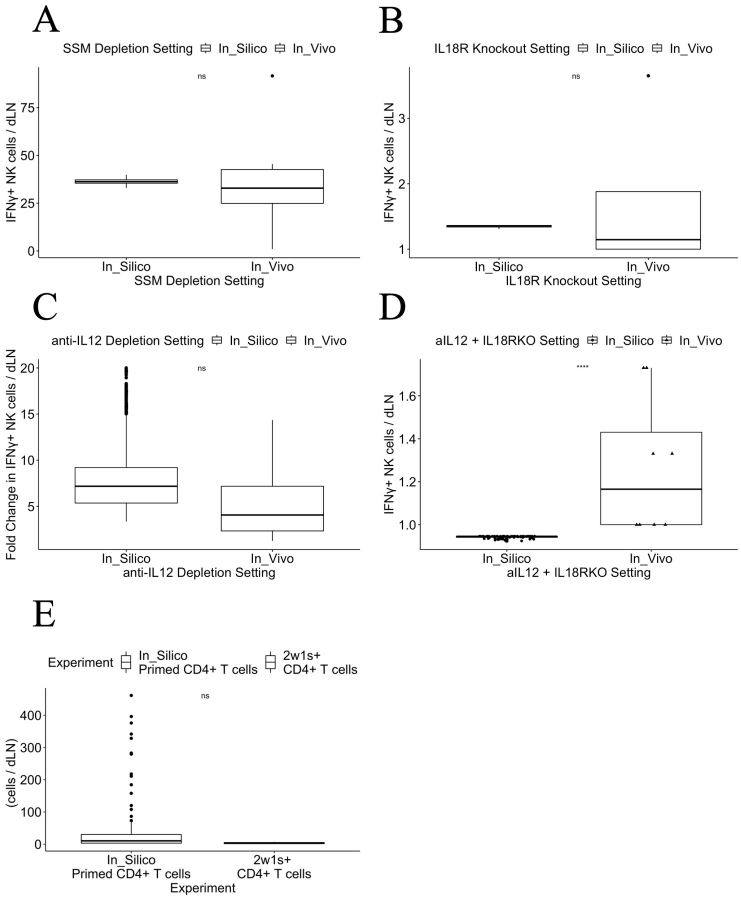


Figure 6.10: **Validation of the 'Baseline' Model:** Boxplots contrasting *in silico* and *in vivo* **A)** Fold changes in IFNγ+ NK cells after respective anti-IL12 depletions. **B)** IFNγ+NK cells after respective IL18R Knockouts. **C)** IFNγ+ NK cells after respective clodronate-mediated subcapsular macrophage depletions. **D)** IFNγ+ NK cells after both anti-IL12 and IL18R knockout scenarios *in silico* and *in vivo*.

For the *in silico* 'IL18R knockout', we did not observe a distinction between the means

of the two distributions and thus the result of this validation experiment is acceptable (Figure 6.10B). Similarly, for the 'αIL12 depletion', we did not observe a significant difference between the two distributions and thus the result of this validation experiment is acceptable (Figure 6.10C). For the αIL12 depletion and IL18R double knockout, we did observe a significant distinction between the two groups (Figure 6.10D, p=3.4e-06). However, we argue that because the distinction between the means is numerically so minor, the model is still able to recapitulate the dynamics observed *in vivo* and thus the result of this validation test is acceptable. Lastly, we compared an *in silico* prediction of the number of 'primedCD4' cells after the parameter that represents CD80/86 priming of CD4+ T cells ($cognatePriming_p$) is set to zero, with the distribution of 2W1S+ CD4+ T cells after AS01 in CD80/86 knockout mice (Figure 6.2E). We found considerably larger variation in the *in silico* distribution of cells compared to the *in vivo* setting, however the trend is not significant (Wilcox Test). Despite differences in variation, we believe that the *in silico* knockout generally recapitulates the dynamics observed *in vivo* (i.e a substantial reduction in the number of cells is observed) and thus the result of this validation test is acceptable. Taken together, while there are differences observed *in silico* when compared with the *in vivo* validation data upon which the model was not trained, we observed that the model is generally capable of recapitulating the dynamics observed *in vivo* and thus the simulator is deemed appropriate for *in silico* exploration.

6.2.6 Gaps in our understanding of AS01 MoA revealed by model development

Through the development of the present model, we have observed gaps in our understanding of AS01 MoA, as well as large quantitative gaps in data availability. Here, we highlight salient examples of these gaps, and propose novel and refined hypotheses for the gaps, as well as avenues to reduce this incompleteness.

6.2.6.1 A Refined Hypothesis for monocyte recruitment into the dLN after AS01

The present model is unable to fully replicate the rapid increase in the infiltration of monocytes into the dLN observed *in vivo* between 24 and 48 hours post-injection (Figure 6.11). Model analysis therefore indicates that our understanding for how monocytes are recruited and infiltrate into the dLN following AS01-adjuvanted vaccination - as proposed in Chapter 3, guided by experimental insight from Neeland et al., [46] - is incomplete. Therefore, we reasoned that this sharp increase in the quantity of these cells could be explained by a combination of two previously overlooked mechanisms and thus in what follows, we propose novel hypotheses for this particular gap in AS01 MoA.

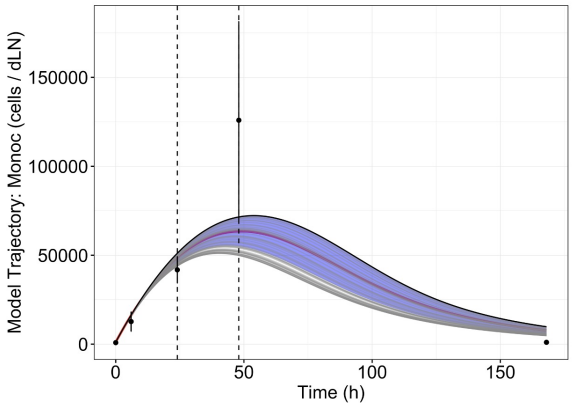


Figure 6.11: **The AS01 CD4+ T cell priming model is unable to replicate a sharp increase in monocytes between 24 and 48 hours post-injection:** Line-plot showing the distribution of model trajectories for monocytes in the dLN after simulated vaccination with AS01. Two dashed lines show 24 and 48 hours post injection respectively. The central estimates of the *in vivo* experimental data are shown with black points, together with black error bars showing the standard deviation. Grey lines show the trajectories of each model fit, the red line shows the mean of each *in silico* trajectory, the shading represents the mean +/- standard deviation of the trajectories produced by model fits.

First, during the development of the 'Core AS01 Domain Model' presented in Chapter 3, after discussions with GSK immunologists and despite a rapid increase in neutrophils into the dLN after AS01, we took a decision not to include these cells into the model [7]. We took this decision because 1) we had no evidence for their contribution to our research questions, 2) we were unsure on their functionality in dLN after AS01, 3) we had a lack of experimental data for these cells in dLN, 4) there are conflicting data on their dLN function in wider literature. For the sake of simplicity, CCL2 - a chemokine involved in recruitment of CCR2+ monocytes - is not explicitly captured in the models presented here. Instead, a fixed rate of monocyte recruitment is captured. Interestingly, using human neutrophils Yoshimura et al [322] observed that these cells produce CCL2 after stimulation with TLR4 or TLR2 in the presence of IFNγ. Indeed as mentioned, neutrophils are known to rapidly infiltrate sheep dLNs prior to monocytes after AS01 [46].

Collectively, these insights lead to a novel hypothesis for how monocytes are recruited into the dLN after AS01. We hypothesise that upon arrival into the dLN early during the response, neutrophils experience an environment with ample IFNγ. In combination with TLR4 stimulation by MPL, we hypothesise that IFNγ may induce a 'profound' level of CCL2 from neutrophils [322], leading to an increased rate of monocyte recruitment between 24 and 48 hours post injection. Such a hypothesis is not explored in this thesis. Future work may seek to capture such mechanisms and an improved agreement of such a model with the biological data could indicate the veracity of such a hypothesis. Furthermore, *in vivo* experiments could be designed to explore such a hypothesis. An additional factor which may

augment this increase in recruitment of monocytes at these time-points, is the expansion of lymph nodes during inflammation. Indeed, we propose that the canonical rate of monocyte influx may also increase potentially proportional to the increased surface area of the dLN, in-part enabling an increase in the rate of monocyte influx. This increased rate of monocyte input may be required to achieve the increase observed *in vivo* between 24 and 48 hours post-injection.

Our observation that the model was unable to entirely replicate the biological data, has therefore refined our understanding of AS01 MoA by identifying an important knowledge gap and proposing a new hypothesis. Indeed, we proposed that a combination of CCL2 production by neutrophils and lymph node expansion may in concert increase the rates of monocyte infiltration into the dLN during inflammation.

6.2.6.2 Large variation observed in model output for IFNγ production is consistent with gaps in biological data

Despite the well characterised importance of IFNγ to the immune response after AS01, large gaps remain in the quantitative knowledge of IFNγ production after AS01 over the first seven days. Such gaps have been identified and reinforced through the development of the model in this chapter. Figure 6.12 shows the model trajectory of IFNγ over the first seven days. Over the first 48 hours of the immune response, the model was able to reasonably describe the data and the breadth of model fits reflect the variation in the biological data. However, it is generally accepted that innate IFNγ production - i.e the 'first wave' - peaks at six hours, returning towards baseline by 24 [32]. In the context of AS01, experimental data rarely includes measurements of IFNγ at 16 hours post injection and to our knowledge IFN concentrations have never been tested between 6-15 hours post injection of AS01. Interestingly, the model - where the trajectory of IFNγ recapitulates *in vivo* dynamics - suggests that the peak of innate IFNγ may not be at six hours, but instead at approximately 8 hours post-injection (Figure 6.12). This suggests that limited sampling frequency may conceal a gap in our understanding of an important aspect of AS01 MoA. Indeed, model analysis suggests that to fully understand when the IFNγ peak occurs after AS01, measuring IFNγ levels at timepoints between 3-16 hours could be valuable. Additional data at these timepoints would not only further our understanding of IFNγ production after AS01, but would also improve the accuracy of model calibration and improve practical identifiability. Indeed, with data points for IFNγ only at 3,6 and 24 hours post-injection, the optimisation may compensate between decay and production rates thus contributing to identifiability issues.

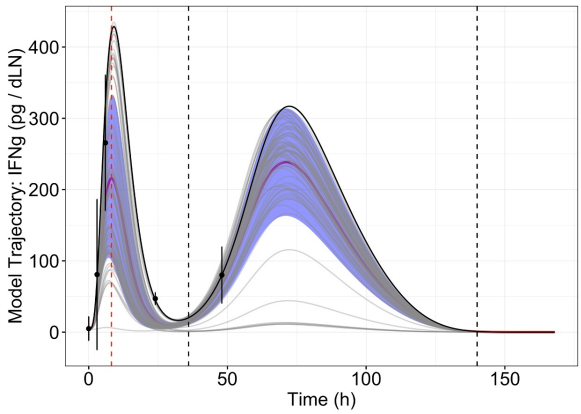


Figure 6.12: **Large variation is observed in *in silico* output for IFNγ production following 48 hours post-simulated-injection:** Line-plot showing the distribution of model trajectories for IFNγ in the Baseline Model. Red dashed line shows the predicted timepoint where the mean of the *in silico* 'innate IFNγ' output peaks. For ease of visualisation, two black dashed lines show the approximate beginning and end of the 'second wave' of IFNγ after AS01. The central estimates of the *in vivo* experimental data are shown with black points, together with black error bars showing the standard deviation. Grey lines show the trajectories of each model fit, the red line shows the mean of each *in silico* trajectory, the shading represents the mean +/- standard deviation of the trajectories produced by model fits.

Secondly, the development of this model has revealed that little is known about the 'second wave' of IFNγ. In Figure 6.12, dashed lines indicate i) approximate times of its initiation ($\sim$36 hours) and ii) end of the second wave ($\sim$140 hours). Unfortunately, for this time period, we were only able to curate a robust datapoint for 48 hours, which through model calibration enables the model to describe what appears to be the initiation of the 'second wave'. However, following 48 hours, we have no information regarding the magnitude of the peak, or when it ends. Illustrated by the range of local optima in Figure 6.12, model analysis reveals a large temporal and quantitative gap in our understanding of IFNγ production after AS01 MoA. Lastly, through model construction we identified a knowledge gap regarding which immune factor induces the second wave of IFNγ. In the mathematical model, the production of IFNγ by adaptive CD8+ T cells is therefore abstracted at a high level to reflect this unknown (see equations 6.8 and 6.9, section 6.2.2.1).

There are two clear hypotheses for induction of 'second wave' IFNγ . Firstly, antigen-dependent activation of CD8+ T cells could produce IFNγ. Secondly, IL18 could initiate IFNγ release from these cells, for which some unpublished evidence exists. However, it appears that our current understanding of AS01 MoA is inconsistent with the latter hypothesis. Indeed, macrophages are the only known source of IL18 after AS01/QS21. Given a lack of AS01/QS21 data for macrophages after 24 hours where many of these cells are lost, and a study by Gaya et al which showed replenishment of SCS Mo takes approx. 28 days [311], it is reasonable that there would be limited macrophages - i.e IL18 producing

cells - during the period where CD8+ T cells are thought to secrete IFNγ thus constituting the 'second wave'. As IL18 production rests on macrophages in our current understanding of this system, the lack of IL18-producing cells appears to be temporally inconsistent with a hypothesis that IL18 induces IFNγ from CD8+ T cells and raises questions e.g, whether there's another source of IL18, or whether macrophages begin to recover by these early timepoints and provide IL18. Nevertheless, such gaps in our quantitative and temporal understanding limit the insight of the MoA of this adjuvant. Overall, the model has helped to shed light on novel AS01 MoA knowledge gaps, and guided us to propose new questions, as well as refined and novel hypotheses which could be explored with further research.

6.2.7 Negative Regulatory Processes Are Important Components in AS01 MoA

Prior to refinement of the mathematical model that is proposed in section 6.2.2.1, we undertook an initial calibration of a model which did not describe the 'negative regulatory processes' (NRP) variable. During this initial calibration, we observed that the model could not describe decays in the observational data and thus trends observed by Didierlaurent and Coccia [5, 32]. We therefore reasoned that we were missing elements of the immune response which increase inhibitory function over time and thus resolve and/or limit inflammation. We therefore incorporated the 'NRP' component, which in-effect increases rates of decay toward the latter stages of simulation. Biologically, the NRP variable reflects an increase in the functionality of negative regulatory pathways in the immune system. Given the importance of this component in model development, coupled with the limited understanding of such mechanisms after AS01, we sought to examine the effect that absence of this component has on model behaviour. Thus, we performed an experiment where across all local optima, we set the parameter *InhibitoryProduction* (which controls the rate of NRP) to zero. This modification effectively 'knocks-out' NRP from the system. We then simulated this scenario, while keeping all other parameters at calibrated values as in Table 6.3 and compared the results to the 'wild-type' model.

First, we confirmed that the *in silico* knockout correctly eliminated the 'Negative Regulatory Processes' variable (Figure 6.13A). In turn, we observed a profound effect on DC numbers, resulting in a consistent increase as a function of time in the absence of decay (Figure 6.13B). In this scenario, the model cannot replicate the estimated decay of these cells in the observational data, suggesting that without the NRP component in the model, the DC levels may never adhere to the observations of Didierlaurent et al., [5] (where DC numbers reduce toward baseline by day 7 post-injection). For monocytes, we observed that in the knockout scenario compared to the wild-type, the monocyte levels increase rapidly as

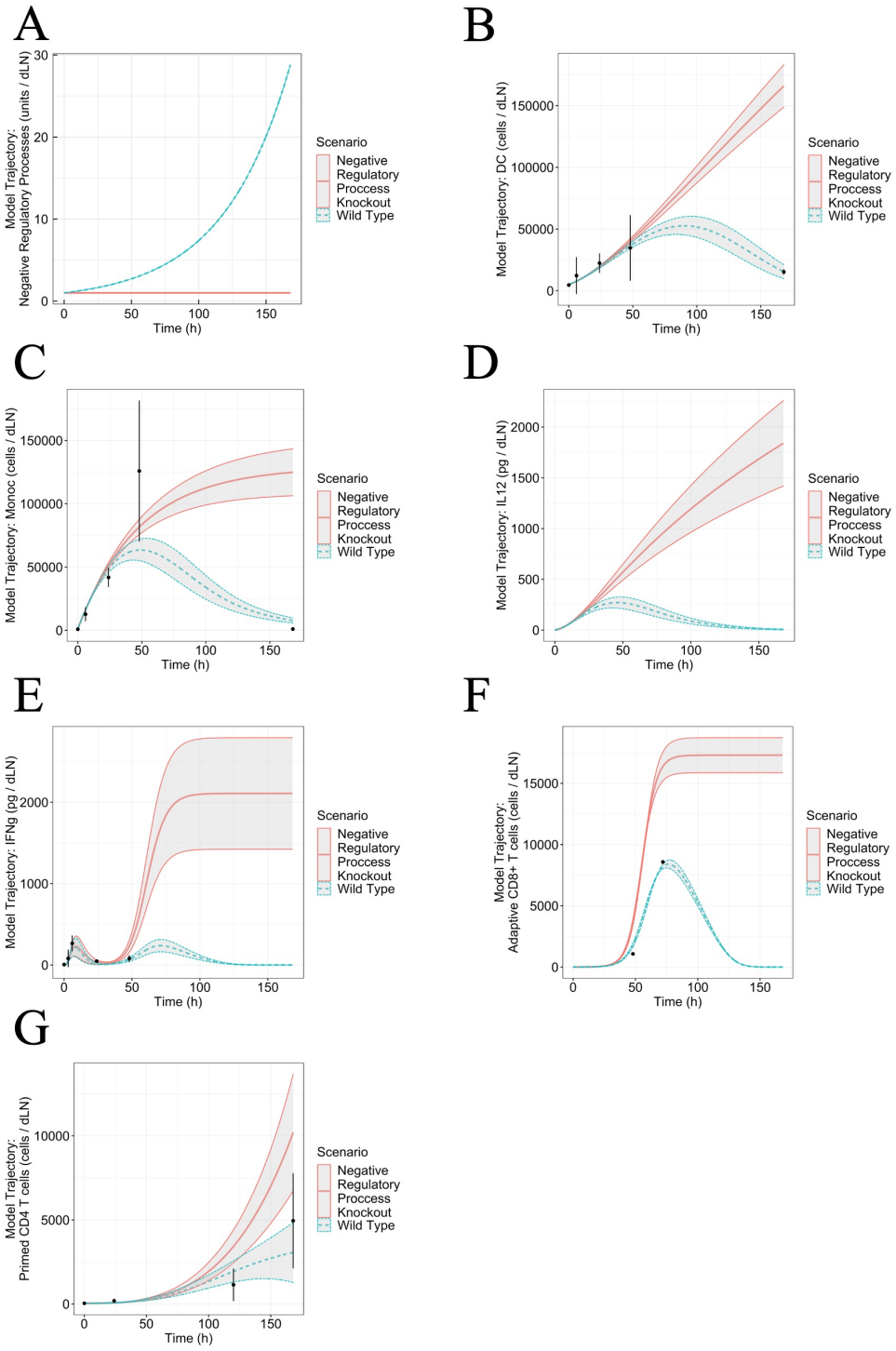


Figure 6.13: **Evaluating the role of 'Negative Regulatory Processes' on *in silico* outputs from the 'Baseline' Model:** Simulations were ran under wild-type (model as calibrated, shown in blue) or after the parameter controlling the level of 'Negative Regulatory Processes' was set to zero (shown in red). Line-plots comparing these two scenarios for model entities; Negative Regulatory Processes (A), dendritic cells (B), monocytes (C), IL12 (D), IFNγ (E), Adaptive IFNγ+ CD8+ T cells (F), primed CD4+ T cells (G). The shaded bounds represent the mean +/- the standard deviation of model trajectories produced by the distribution of parameter sets. The line represents the mean of model trajectories. Experimental data upon which the wild-type model was originally calibrated is plotted in black dots and error bars.

a function of time, before beginning to plateau towards the end of the simulation. Again, in the absence of the negative regulatory processes component, it does not appear that a reduction in the quantity of these cells would occur, such that the model output would be consistent with the observations of Didierlaurent et al., [5]. For IL12, removal of NRP results in *in silico* IL12 production which does not decay (Figure 6.13D). Importantly, removal of NRP causes an enormous disparity with between simulated IFNγ and the wild-type model or the experimental data, in particular after 48 hours post-injection (Figure 6.13E). Given the observed timeframe of this large disparity, we reason this is perhaps due to considerable increases which are observed in in Adaptive CD8+ T cells (Figure 6.13F), although this may potentially also be due to increases in monocytes and DCs (and therefore IL12 which promotes IFNγ). Lastly, after removal of NRP in the knockout scenario, we observed an increase in the number of primed CD4+ T cells which is inconsistent with both the 120 and 168 hour experimental data, although given that the original wild-type model has room for improvement in fits to these observational data, we cannot exclude that the observed effect may be an artifact (Figure 6.13G). Interestingly for primed CD4+ T cells, the NRP knockout scenario changes the shape of the curve toward that which more reflects the experimental data. Future model development may benefit from exploring this effect during calibration. Together, model analysis firstly indicates the importance of this component, which we suggests justifies its inclusion in the model. Secondly, these data suggest that inhibitory mechanisms after AS01 warrant further attention.

6.2.8 Simulation Robustness to Parameter Perturbation to explore CD4+ T cell priming after AS01

Next, we aimed to identify mechanisms involved in CD4+ T cell priming after AS01-adjuvanted vaccination. Unfortunately, owing to the combinatorics required to sufficiently sample the present parameter space, a global sensitivity analysis was not undertaken. Therefore, we employed 'one-at-a-time' analysis [181], of the variation of these cells across all local optima, as each parameter is perturbed individually. This may be considered a local sensitivity analysis, where the output is the distribution of primed CD4+ T cell numbers across all local optima, following perturbation of a parameter. We examined each model parameter in turn and perturbed their values within a range of a factor of 10 in each direction from the calibrated 'best fit' value (see Table 6.3 for the calibrated best-fit value). These ranges were explored to examine local sensitivity around a factor of 10 each side of each parameter to examine different model behaviours in parameter space. To assess robustness to parameter perturbations, we then contrasted the distribution of primed CD4+ T cell response values for each sampled parameter value with a 'reference' distribution of primed

CD4+ T cell responses, and assessed robustness using the non-parametric Vargha-Delaney A-Test (see Methods: Local Sensitivity Analysis)[253].

The 'reference' (or wild-type) distribution reflects at each timepoint, the numbers of primed CD4+ T cells after simulating all local optima that were derived from model optimisation. For the 'reference' distribution, for parameter of interest x, for each local optima, the value of parameter x was set to the calibrated 'best fit value' (value of parameter x from the local optima with the lowest objective value, see Table 6.3) for this particular parameter. The remaining parameters, across all local optima are kept the same as what was yielded from calibration. These sets of parameters (a set of parameters corresponds to one local optima) are simulated, producing at each timepoint t, a distribution of values for primed CD4+ T cells. This distribution of values is termed the 'reference' distribution.

To assess local sensitivity for parameter x at time t, first, a range is uniformly sampled from a factor of 10 each side of the calibrated 'best fit' value of parameter x. For each sampled value i, parameter x is set to i across all local optima, and then simulated. The resulting 'perturbed' distribution of values for primed CD4+ T cells (from all local minima), at time t for value i, was compared with the corresponding 'reference' distribution of primed CD4+ T cells at time t through use of the A-Test. A-Test scores therefore reflect the magnitude of the effect-size between the reference distribution, and one where one-at-a-time parameter perturbation has occurred (the perturbed distribution). For parameter x, the A-Test scores are visualised throughout the range of sampled values i, at time t. Please see Methods for more details on local sensitivity analysis performed in this thesis.

Here, the calibrated 'best fit' value was chosen for parameter of interest x to represent the 'reference' point for comparison, to embrace simplicity in the visualisations. However, for any 'one-at-a-time' 'local sensitivity' analysis that follows in this Chapter, we have confirmed that the trends are consistent when *any* of the calibrated values from the top ten local optima (top 10 best fits, deemed by 10 lowest objective values) are used as the reference point for any of the assesed parameters of interest (x) and reported results.

6.2.8.1 Inflammation-induced naive CD4+ T cell recruitment strongly influences numbers of primed CD4+ T cell

Unsurprisingly, for the parameter controlling CD4+ T cell proliferation ($\text{CD4Proliferation}_p$), we observed that perturbing values of this parameter has a 'large' statistical effect on the numbers of primed CD4+ T cells at all examined timepoints (Figure 6.14A). Again, unsurprisingly, the parameter controlling the rate of B7 mediated priming of naive CD4+ T cells by DCs (cognatePriming_p), has a large effect on the numbers of primed CD4+ T cells (Figure 6.14B). Interestingly, the analysis indicates this effect is strongest between 16 and

72 hours, as smaller parameter perturbations are required to produce the most divergent A-Test scores (i.e compared to say 168 hours where larger values fail to produce A-Test scores of ∼0.). Lower effect-magnitudes observed at higher values of $cognatePriming_p$ at 168 hours compared to 16-72 hours, suggests first, 16-72 hours post-injection could be the dominant period of CD4+ T cells priming in this system, and second, that the magnitude of DC-T cell priming has reduced by 168 hours, which is consistent with Didierlaurent's work showing a reduction in the number of MHCII+ DCs in the dLN at these timepoints [5]. Again, consistent with our qualitative reasoning based on model structure, increasing the parameter controlling CD4+ T cell dLN exit and anergy ($TcellExit_Anergy_p$) resulted in a lower distribution of CD4+ T cells (indicated by A-Test >0.75) compared with the reference distribution (Figure 6.14C). At all timepoints perturbations by a factor of 10 in either direction result in large statistical effects as deemed by the A-Test, on the numbers of primed CD4+ T cells.

Interestingly, with the exception of hour one, increasing the value of the parameter controlling the rate of inflammation-induced naive CD4+ T cell recruitment into the dLN ($CD4T0_Inflammatory_Recruitment_p$) results in large statistical effect sizes with primed CD4+ T cell levels, which are strongest between hours 72-168. Thus, the model predicts the rate of inflammation-induced naive CD4+ T cell recruitment as a vital parameter involved in CD4+ T cell priming (Figure 6.14D). By focusing on the predicted numbers of cells within a range of a factor of three increase or decrease from the 'best fit' parameter and assessing the resulting predicted numbers of primed CD4+ T cells, the extent of the sensitivity of this parameter is revealed (Figure 6.14E). Here, we observed that minor alterations this parameter (controlling *naive* CD4+ T cell numbers during inflammation) produces large variation in *primed* CD4+ T cells. Across all model fits, the parameter is highly constrained, likely due to an estimated central datapoint at each timepoint for naive CD4+ T cells, therefore further data are required to examine the impact of this parameter in detail. Nevertheless, we identify the rate of inflammation-induced naive CD4+ T cell recruitment as an important parameter in AS01-induced immune responses and propose that this parameter's importance warrants further investigation into its variation and effects both *in silico* and *in vivo*.

Despite limited knowledge of this parameter's value and variation, its sensitivity suggests a currently unknown mechanism which controls inflammatory recruitment of naive CD4+ T cells after AS01, is strongly influential in priming CD4+ T cells. The importance of such a parameter is perhaps intuitive, however we had not reasoned this parameter would be so important. This parameter represents a currently unconfirmed mechanism, perhaps CCR7 and/or IFNγ mediated recruitment. To explore the importance of

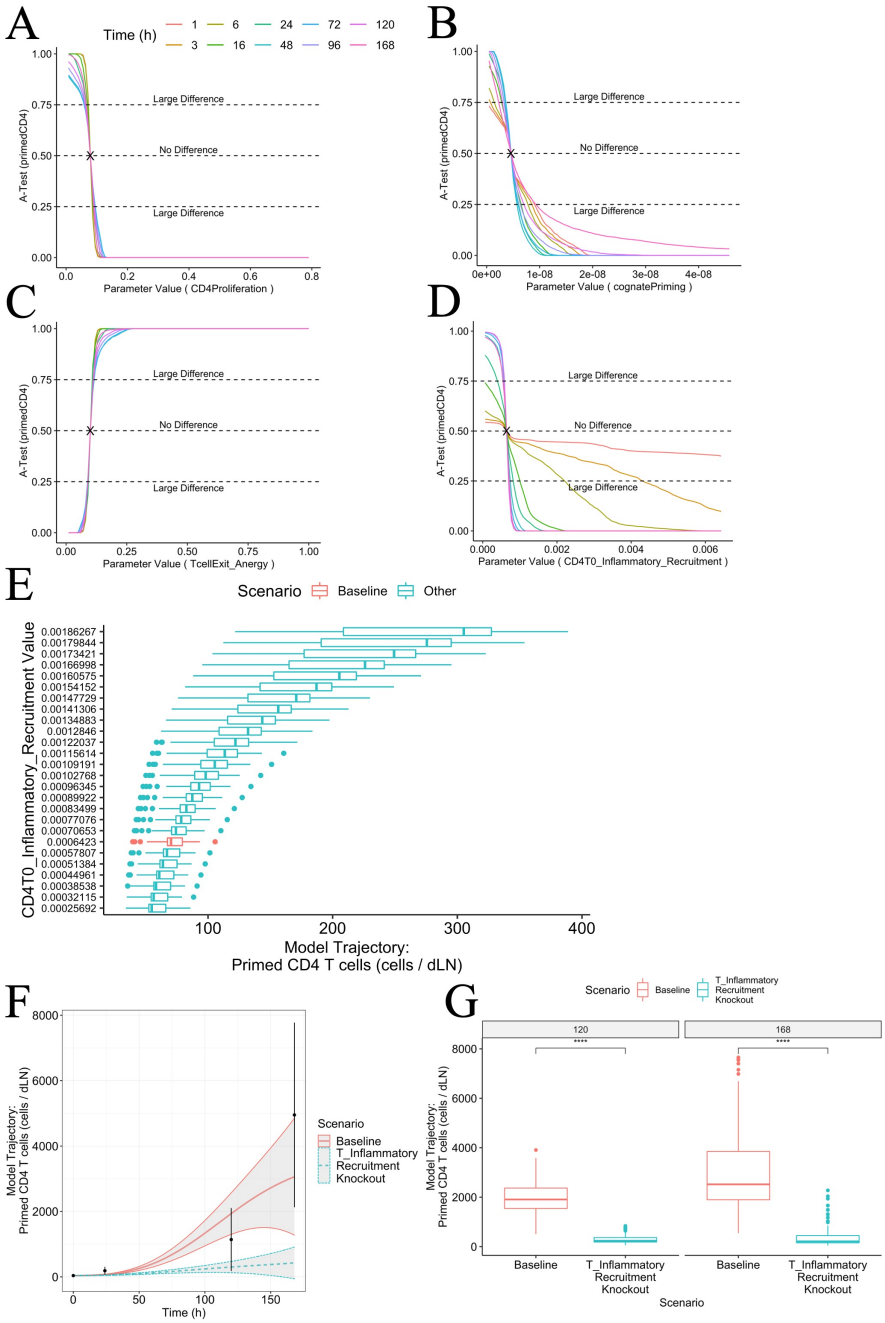


Figure 6.14: **Examining simulation robustness to T cell related parameter alterations on primed CD4+ T cells:** A-D, 100 parameter sets are sampled uniformly across ranges of a factor of 10 each side of the baseline parameter value. Each sampled parameter value is ran 'in place' of the corresponding parameter for every calibrated model fit (n=81). 8100 runs are performed for each parameter, incorporating uncertainty from the model calibration into the analysis. Distribution of simulation responses for primed CD4+ T cells for each parameter, are compared with the simulation responses after running the model with the baseline calibrated 'best fit'. **A-D** show lineplots showing Vargha-Delaney A-Test statistics at different alterations of parameters for those controlling the rates of **A)** primed CD4+ T cell proliferation ($\text{CD4Proliferation}_p$), **B)** B7-mediated cognate CD4+ T cell priming, **C)** T cell dLN exit and anergy (Tcell_ExitAnergy), **D)** inflammation-induced naive CD4+ T cell recruitment. **E)** Boxplot showing the distribution of model trajectories after running the baseline model with values a factor of 3 around the baseline value for '$\text{CD4T0_Inflammatory_Recruitment}_p$'. **F)** Line plot showing the distribution of primed CD4+ T cells after a simulated knockout of inflammation-induced naive CD4+ T cell recruitment. The central coloured lines show the mean for each group, while the shading shows +/- standard deviation of the group. **G)** Boxplots contrasting the distributions of primed CD4+ T cells after the aforementioned simulated knockout at 120 hours and 168 hours post-injection.

the $CD4T0_Inflammatory_Recruitment_p$ parameter further, we simulated its 'knockout' by setting the parameter to zero. We then compared the distribution of knockout responses to the baseline model output from all calibrated fits (local minima). In the knockout, primed CD4+ T cells are almost eliminated (Figure 6.14F). Indeed, at both day 5 (labelled 120 in hrs, p<2.22e-16) and day 7 (labelled 168 in hrs, p<2.22e-16) post-injection, we observe significant reductions in primed CD4+ T cells in the knockout compared with baseline (Figure 6.14G). Together, model analysis suggests that the rate of recruitment of naive CD4+ T cells under inflammatory conditions is a vital parameter controlling CD4+ T cell priming after AS01. Thus, the mechanism underpinning this parameter and the parameter itself warrants more attention to understand what immune factors initiate and maintain this process after AS01, and to determine its values and variation.

Analysis of the model indicates that the sensitivity of this parameter is sufficient that dLN input rates could impact the magnitude of responses to adjuvanted-vaccination. One implication is that deficient input rates of CD4+ T cells perhaps e.g., for people living with HIV, may potentially have a large impact on AS01-induced immune responses. Additionally, Druzd et al [323] observed that circadian rhythm can affect the input rates of lymphocytes into cellular compartments. Taken with our work, it is plausible that vaccinating at different times of day, may impact naive CD4+ T cell recruitment into dLN, which, given the sensitivity of the parameter with CD4+ T cell priming after AS01, could affect the magnitude of the resulting antigen-specific CD4+ T cell response [323, 324]. Our work suggests that understanding the mechanism by which these cells are recruited under inflammatory conditions is a fundamental question for AS01 biology.

6.2.8.2 Early DC activity appears to influence priming of CD4+ T cells after AS01

We next examined the temporal dynamics of how DCs contribute to CD4+ T cell priming. Interestingly, we observed that by three hours post injection, the model predicts that perturbing the $DC_Afferent_p$ parameter - controlling the rate of DC recruitment and activation - generates a large statistical effect size, although this is more of a pronounced effect by six hours (Figure 6.15). Firstly, these data generate the hypothesis that after AS01, early DC activity may elicit rapid priming of CD4+ T cells. This is consistent with observations by Gerner et al [30] in a wider microbial system, who found that lymphatic-sinus DCs rapidly elicit T cell responses to incoming antigens. Furthermore, our data suggest that 16 hours and onwards are critical timepoints where DCs are priming CD4+ T cells, which is perhaps temporally consistent with the arrival of migratory DCs into the dLN. Further model development which discriminates migratory and resident DC subsets, may be able to delineate

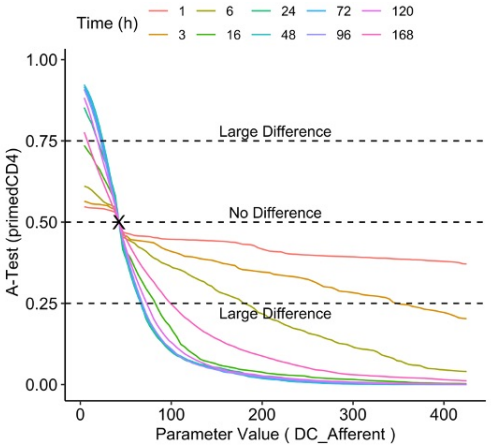


Figure 6.15: **Examining simulation robustness to the parameter controlling DC recruitment into -and activation in- the dLN:** 100 parameter sets were sampled uniformly across ranges of a factor of 10 each side of the baseline parameter value. Each sampled parameter value was ran 'in place' of the corresponding parameter for every calibrated model fit (n=81). Therefore 8100 runs were performed for the parameter, incorporating uncertainty from the model calibration into the analysis. The distribution of simulation responses for primed CD4+ T cells for the parameter, were compared with the simulation responses after running the model with the baseline calibrated 'best fit'. **A)** Lineplot showing Vargha-Delaney A-Test statistics at different alterations and at different timepoints, for the parameter controlling the rates of DC recruitment and dLN activation (DC_Afferent_p).

the extent to which early DC activation contributes to priming of CD4+ T cells after AS01, similarly to what was observed by Gerner et al [30] in a wider microbial system.

6.2.9 An Alternate Model where IFNγ Considerably Contributes to CD4+ T Priming

In section 6.2.4, we explained that the 'Baseline AS01 CD4+ T cell' model was calibrated to minimise influence of the parameter $cognateEnhanceIFNg_p$, which controls IFNγ enhancement of B7-mediated priming of CD4+ T cells by DCs. This was done so that the 'baseline' model could be examined to identify important mechanisms independent of the 'IFNγ enhancement' hypothesis. Later in this chapter, we explore this hypothesis. Here, we describe the calibration of an 'Alternate' model, where IFNγ-dependent and IFNγ-independent avenues of B7 mediated CD4+ T cell priming are permitted to exhibit similar prominence, through allowing similar ranges of the parameters through calibration, if possible. Following calibration and validation of such a model, we compare local sensitivities of the 'Alternate' model with the 'Baseline' model, highlighting key influential parameters which are conserved across models. We then use both models to explore the veracity of the hypothesis that IFNγ contributes to CD4+ T cell priming after AS01 by substantially enhancing DC stimulatory potency.

6.2.9.1 Calibration of the Alternate Model

To accomplish this goal, we re-calibrated the model presented in Figure 6.9 section 6.2.4. Through expanding permitted lower and upper ranges of the $cognateEnhanceIFNg_p$ parameter, we sought to increase its - and therefore IFNγ's - contribution to CD4+ T cell priming. For the 'Alternate' model, to avoid confusion, we define 1) the parameter $cognatePriming_IFNgControlled_p$, which is analagous to *cognateEnhanceIFNg* from the baseline model and represents the rate of IFNγ-dependent CD4+ T cell priming, and 2) the parameter $cognatePriming_NonIFNgControlled_p$ which is analagous to *cognatePriming* and represents the rate of IFNγ-independent priming (see Table 6.6 for details).

Calibration yielded 73 parameters and a higher objective value than the 'Baseline' model, suggesting the 'Alternate' model is a worse fit to data. Code to solve the model using the 'best fit' set of parameters is in Appendix A.3. The values and ranges of parameters which are different after calibration of the 'Alternate' model compared with the 'Baseline' model are shown in Table 6.5. The model trajectories produced by this distribution of parameters are shown in Figure 6.16. Many variable trajectories are similar to those observed in Figure 6.9. Notably, the DC trajectory in Figure 6.16B appears to have a worse agreement with the data than in Figure 6.9B. This is also the case for Figure 6.16H for innate CD8+ T cells, compared with 6.9H. In particular, primed CD4+ T cell model trajectories from the 'Alternate' model (Figure 6.16L) are qualitatively less consistent with the observation data, compared with the 'baseline' model (see Figure 6.9L). Furthermore, during calibration we were unable to further increase the upper range of the parameter controlling IFNγ-dependent CD4+ T cell priming ($cognatePriming_IFNgControlled_p$), without generating substantial discrepancies with the observational data (see Table 6.5 for the permitted and final parameter ranges). Together, the additional inconsistencies with this alternate model and the biological data suggests, that the hypothesis that IFNγ controls the CD4+ T cell response to AS01 [32] through up-regulation of accessory molecules which in turn substantially increases DC stimulatory capacity, is incomplete.

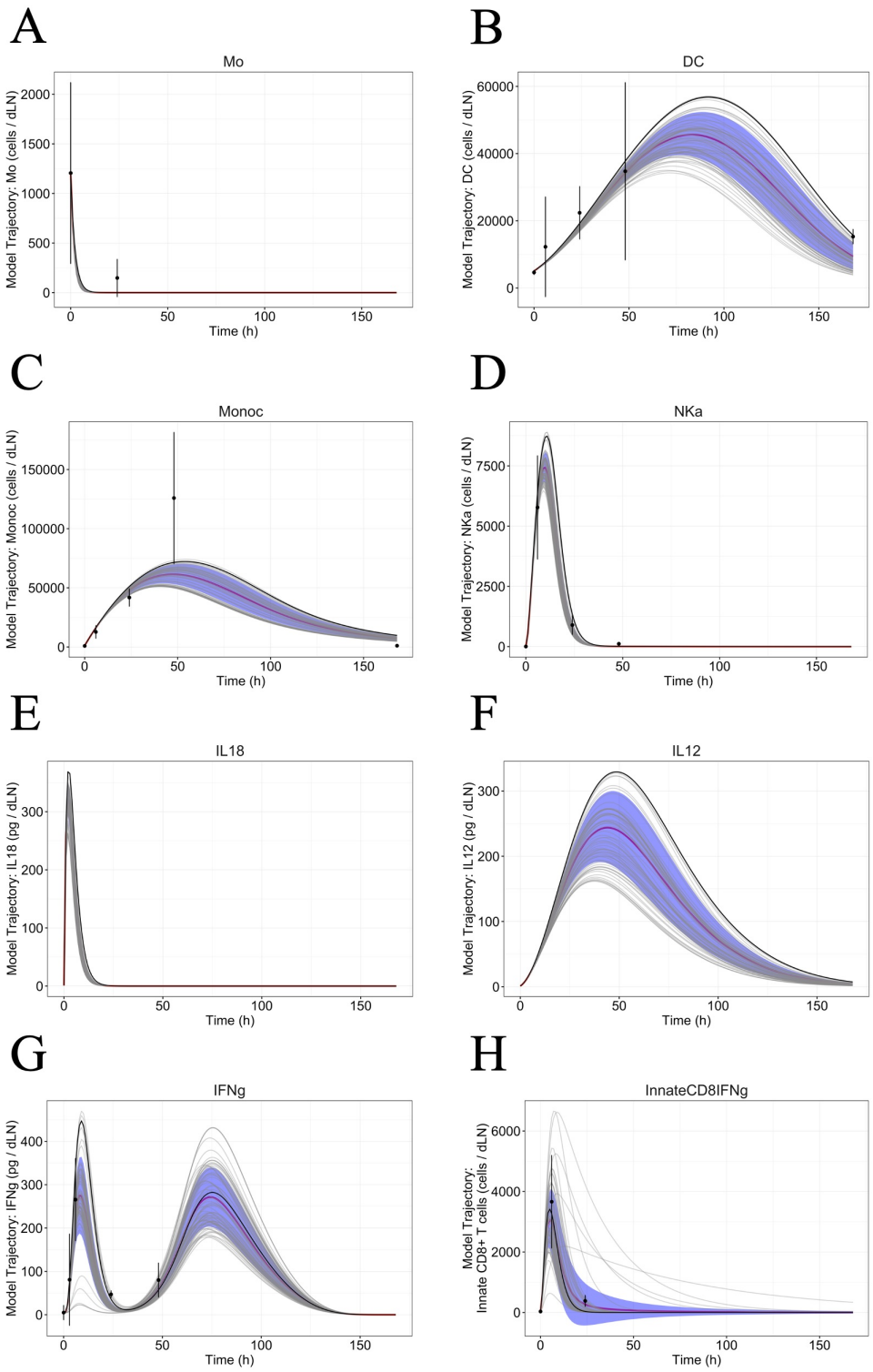


Figure 6.16: **Calibrating an Alternate AS01 CD4+ T cell Model 1/2.** continued overleaf.

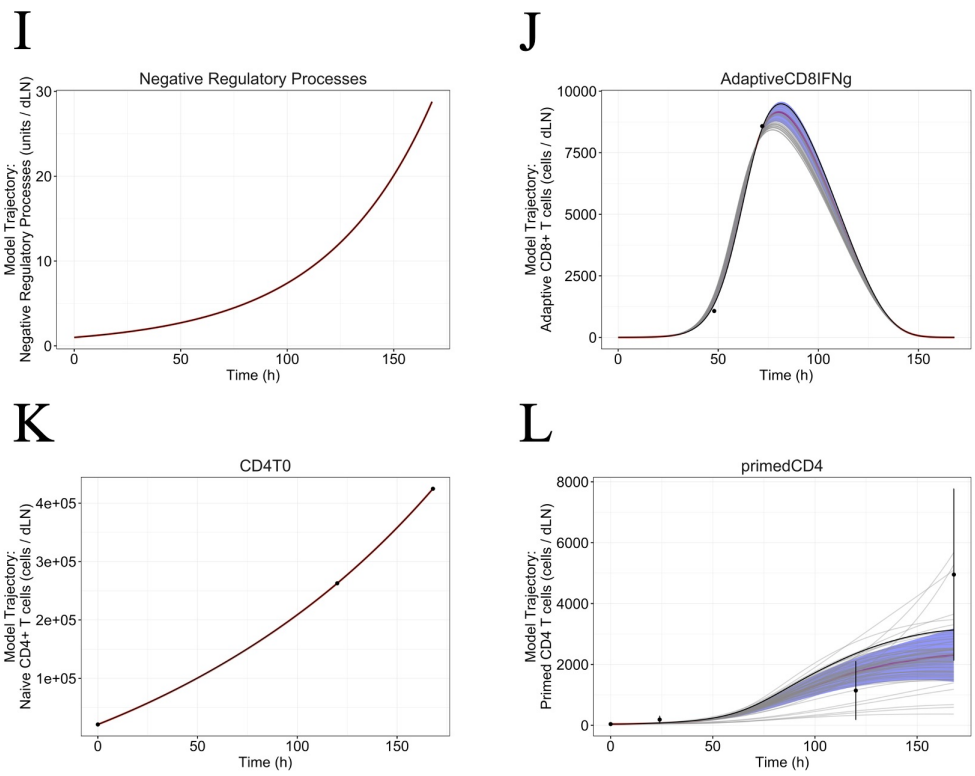


Figure 6.16: **Calibrating an Alternate AS01 CD4+ T cell Model 2/2.** This model captures a scenario where IFNγ is hypothesised to play a more prominent role in CD4+ T cell priming. Macrophage (A), dendritic cell (B), monocyte (C), IFNγ+ NK cell (D), IL18 (E), IL12 (F), IFNγ (G), Innate IFNγ+ CD8+ T cell (H), Negative Regulatory Processes (I), Adaptive IFNγ+ CD8+ T cell (J), naive CD4+ T cell (K) and primed CD4+ T cell (L) kinetics were fitted using the *dMod* package, employing multi-start trust-region optimisation to minimise the objective value between the model output and observational data. Black dots and error bars show the mean and standard deviation of the biological data upon which the model was calibrated, grey lines represent *in silico* parameterisation outputs, blue shading represents the mean +/- standard deviation for these *in silico* outputs, red lines represent the mean of the *in silico* outputs, and black lines represent the best fitting (lowest objective value) *in silico* output.

	Parameter	LowerRange	BestFitValue	UpperRange	LowerRangeCalib	UpperRangeCalib	Mu	Units
1	KM_NKa_IL12b$_p$	5.441E+00	5.44113777	5.834E+00	5.441E+00	5.834E+00	5.487E+00	pg/dLN
2	decayIFNg$_p$	1.400E-01	0.15958440	1.700E-01	1.400E-01	1.700E-01	1.500E-01	pg/dLN hour
3	monocRec$_p$	2.700E+02	270.00000000	2.700E+02	2.100E+02	2.774E+02	2.774E+02	cells per unit MPL / hour
4	DC_Afferent$_p$	3.263E+01	39.64897884	4.000E+01	2.250E+01	4.000E+01	3.254E+01	cells/hour
5	decay12$_p$	4.178E-02	0.04178255	7.404E-02	4.178E-02	7.404E-02	4.178E-02	pg/dLN hour
6	CL$_p$	4.500E-02	0.04500000	6.250E-02	4.500E-02	6.250E-02	4.887E-02	cells per unit QS21 / hour
7	vMoIL18$_p$	3.000E-02	0.03500000	3.500E-02	3.000E-02	3.500E-02	3.500E-02	pg/Mo
8	decay18$_p$	3.800E-01	0.38000000	4.000E-01	3.800E-01	4.000E-01	3.952E-01	pg/dLN hour
9	VmaxNKa1218$_p$	5.488E+03	5489.13342311	5.489E+03	5.442E+03	5.489E+03	5.489E+03	cells/hour
10	KM_18b$_p$	3.264E+01	32.70883175	3.526E+01	3.264E+01	3.526E+01	3.264E+01	pg/dLN
11	KM_12b$_p$	2.369E+01	24.94455965	2.494E+01	2.369E+01	2.494E+01	2.369E+01	pg/dLN
12	VmaxNKa18$_p$	1.500E+00	1.50000000	1.500E+00	1.500E+00	1.500E+00	1.500E+00	cells/hour
13	DCDecay$_p$	2.250E-03	0.00225000	4.920E-03	2.250E-03	6.500E-03	2.250E-03	proportion of DC per unit N.R.P/hour
14	MonocDecay$_p$	1.000E-02	0.01000000	2.000E-02	1.000E-02	2.000E-02	1.044E-02	proportion of Monoc per unit N.R.P/hour
15	CD8Innate$_p$	1.000E+00	5.00000000	5.000E+00	1.000E+00	5.000E+00	3.328E+00	cells / pg IL18 hour
16	CD8RecruitAct$_p$	1.856E-03	0.00185577	1.927E-03	1.750E-03	2.000E-03	1.750E-03	cells per unit of QS21$_p$ and MPL$_p$ / hour
17	InnateCD8decay$_p$	1.232E-02	0.39936158	4.000E-01	1.000E-02	4.000E-01	1.601E-01	proportion of InnateCD8 / hour
18	AdaptiveCD8Decay$_p$	2.000E-02	0.02000000	2.000E-02	2.000E-02	3.500E-02	2.0E-02	proportion AdaptiveCD8/unit N.R.P/hour
19	BasalCD8IFNgProd$_p$	1.500E-02	0.02232430	3.000E-02	1.500E-02	3.000E-02	1.500E-02	pg/AdaptiveCD8 hour
20	AdaptiveCD8Max$_p$	1.635E+04	2.1e+04	2.100E+04	8.580E+03	2.100E+04	1.624E+04	cells/dLN
21	CD4T0_death _recirculation$_p$	5.745E-02	0.05803962	5.825E-02	1.000E-02	1.000E-01	5.824E-02	proportion of CD4T0/hour
22	cognatePriming _IFNgControlled$_p$	5.000E-13	7.25E-12	7.250E-12	5.000E-13	7.250E-12	7.250E-12	proportion of CD4T0/DC hour
23	CD4Proliferation$_p$	4.600E-02	0.04600000	6.809E-02	4.600E-02	8.500E-02	4.600E-02	cells/hour
24	CD4ProlifMax$_p$	1.137E+07	3.687847e+07	1.000E+08	1.000E+04	1.000E+08	1.000E+07	cells/dLN
25	TcellExit_Anergy$_p$	3.713E-02	0.05000000	5.000E-02	5.940E-03	5.000E-02	5.000E-02	cells/hour
26	cognatePriming _NonIFNgControlled$_p$	7.000E-10	2.60E-09	2.600E-09	7.000E-10	2.600E-09	7.000E-10	proportion of CD4T0/DC hour

Table 6.5: Parameter values for the 'Alternate Model'. Only parameters with different values yielded from calibration, compared to the 'Baseline' values in Table 6.3, are shown here. 'LowerRange' and 'UpperRange' represent the lower and upper range respectively of the parameter values yielded from all model fits. 'BestFitValue' is the value if the parameter from the local optima with the lowest objective value. 'LowerRange_Calib' and 'UpperRange_Calib' reflect the range provided to the multi-start trust-region optimiser following the incremental optimisation process. 'Mu' represents the best fit after incremental optimisation, i.e., the starting point provided to the multi-start trust region algorithm. Given no concentration data on QS21 and MPL *in vivo*, parameters QS21$_p$ and MPL$_p$ are set arbitrarily to a value of '10', hence mechanisms involving these parameters are described e.g 'cells per unit MPL$_p$'.

Parameter	Definition
cognatePriming_IFNgControlled$_p$	This parameter is analogous to the 'Baseline' model parameter 'cognateEnhanceIFNg$_p$' and similarly, represents the rate at which IFNg controls B7 mediated priming of cognate CD4 T cells by DC. Here, however the name has been changed for this parameter to reflect IFNg's control rather than enhancement.
cognatePriming_NonIFNgControlled$_p$	This parameter is identical to the 'Baseline' model parameter 'cognatePriming$_p$' and therefore represents the rate of B7 mediated priming of cognate CD4+ T cells by DC.

Table 6.6: Differences in parameter names and definitions for the 'Alternate' model in comparison to the 'Baseline' model. The mathematical structure underpinning these model variants has not changed.

6.2.9.2 Validating the Alternate model

To confirm the alternate model could be reasonably used for our aims, we performed model validation (Figure 6.17) as described previously for the 'Baseline' model (see section 6.2.4). Figure 6.17A-D show results consistent with those in Figure 6.10A-D, whereby validation tests are successfully passed. In contrast to Figure 6.10E for the 'baseline' model, we here observed a significant difference between the *in silico* distribution of cells / dLN compared with the 2W1s+ CD4+ T cell distribution measured *in vivo* (p=0.00084, Wilcoxon Test) (Figure 6.17E). Therefore, this final validation test is not passed for the 'Alternate' model. Nevertheless, we employ this less-appropriate model to support following analyses in comparing the two models and also to explore the veracity of the IFNγ mediated CD4+ T cell priming hypothesis.

6.2.10 Comparing Local Sensitivities for primed CD4+ T cells in the Baseline and Alternate Models

6.2.10.1 Key Parameters with similar sensitivities across models

Next, we examined model behaviours in different regions of parameter space, through assessing 'local sensitivities' of model parameters with primed CD4+ T cells in the 'Alternate' model and comparing insights with those from the 'Baseline'. For the 'Alternate' model, local sensitivity was examined in the manner as described previously in section 6.2.8. Here, we aimed to identify conserved parameters which are important for the numbers of primed CD4+ T cells across both models, irrespective of differences in the prominence of the IFNγ-enhanced priming mechanism. Conserved mechanisms in spite of nuances in model structure provide a level of confidence that such mechanisms are important for CD4+ T cell priming after AS01. Furthermore, we aimed to delineate important parameters underpinning the 'IFNγ enhancement' hypothesis captured in the 'Alternate' model.

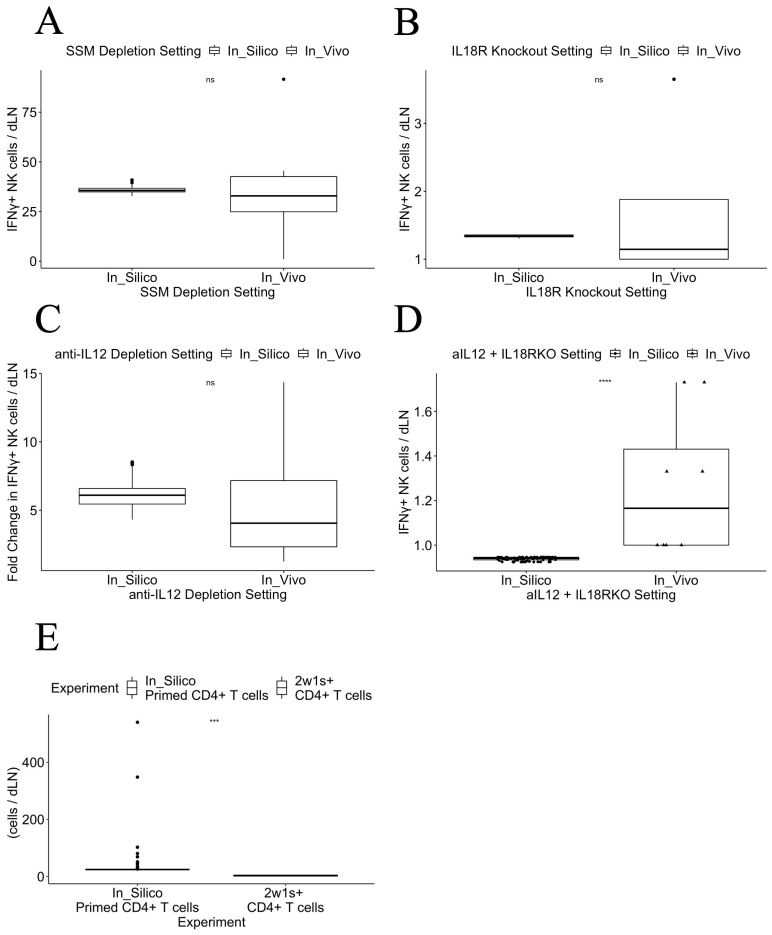


Figure 6.17: **Validation of the Alternate AS01 CD4+ T cell Model 1:** Boxplots contrasting *in silico* outputs and *in vivo* experimental data **A)** Fold changes in IFNγ+ NK cells after respective anti-IL12 depletions. **B)** IFNγ+NK cells after respective IL18R Knockouts. **C)** IFNγ+ NK cells after respective clodronate-mediated subcapsular macrophage depletions. **D)** IFNγ+ NK cells after both anti-IL12 and IL18R knockout scenarios *in silico* and *in vivo*.

It should be noted that we are comparing parameters from two separate calibrations, firstly the 'Baseline' model and secondly the 'Alternate'. In some cases, the reference value (referring to the best fit value from each model variant) for the same or analogous parameter between models may vary. In both local sensitivity analyses, we simulated the parameter within a range of a factor of 10 each side of the value from the calibrated best fit. Therefore, it is appropriate to compare trends between models, however we are not comparing quantitative A-Test results as in some cases parameter values between models may vary by an order of magnitude. Indeed, future global sensitivity analyses of both models, which at this stage is less feasible due to the enormous parameter space, may be able to provide a more quantitative comparison.

For the parameter controlling primed CD4+ T cell proliferation (CD4Proliferation$_p$), we observed similar behaviour between models, where at all assesed timepoints, primed

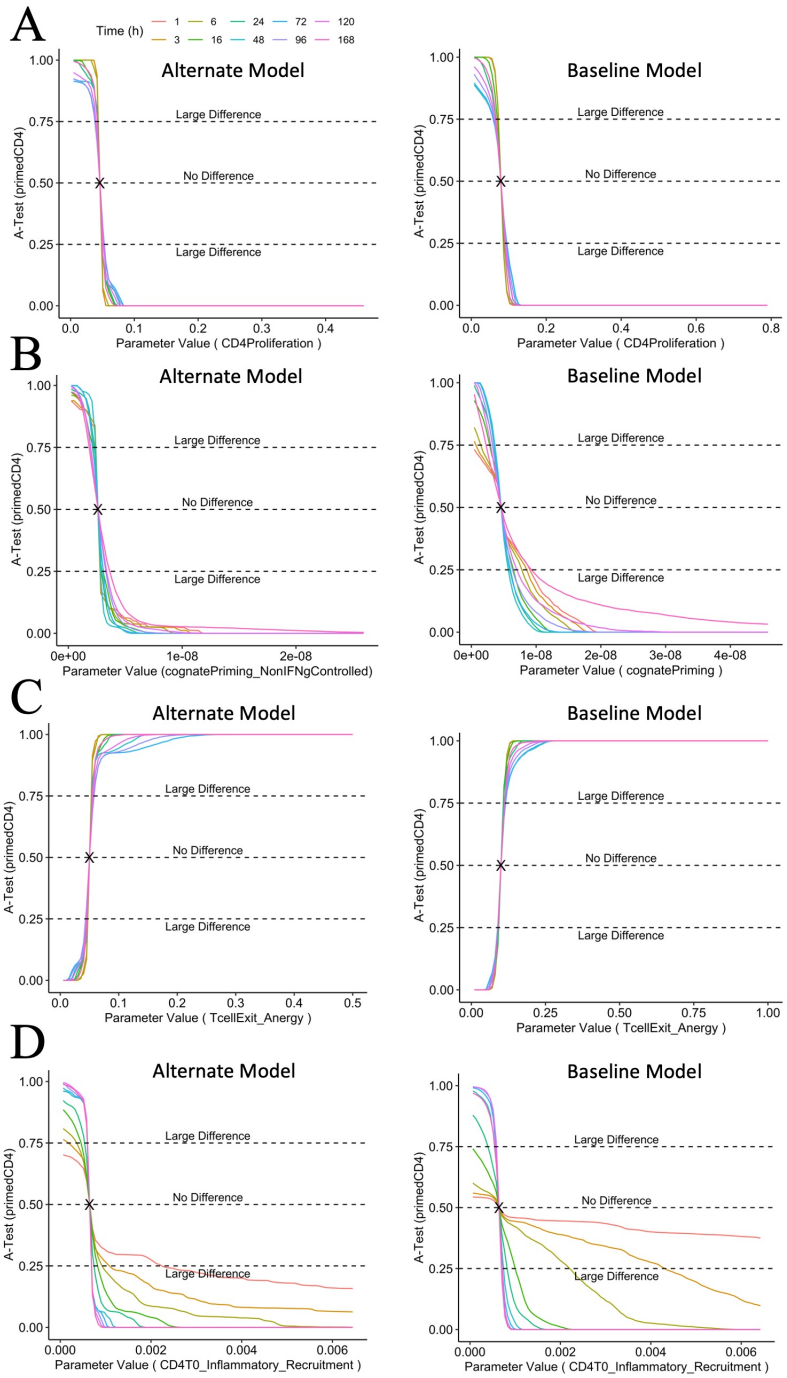


Figure 6.18: **Local sensitivity analysis for the 'Alternate' model compared with the 'Baseline' Model sensitivities for parameters where the influence is similar in both settings:** A-E, 100 parameter sets are sampled uniformly across ranges of a factor of 10 each side of the baseline parameter value. Each sampled parameter value is ran 'in place' of the corresponding parameter for every calibrated model fit (n=73). Therefore 7300 runs are performed for each parameter, incorporating uncertainty from the model calibration into the analysis. The distribution of simulation responses for primed CD4+ T cells for each parameter, are compared with the simulation responses after running the model with the baseline calibrated 'best fit'. **A-D** show lineplots showing Vargha-Delaney A-Test statistics at different alterations of parameters for those controlling the rates of **A)** primed CD4+ T cell proliferation ($\text{CD4Proliferation}_p$), **B)** B7-mediated cognate CD4+ T cell priming, **C)** T cell dLN exit and anergy (Tcell_ExitAnergy), **D)** inflammation-induced naive CD4+ T cell recruitment.

CD4+ T cells are not robust to minor alterations in this parameter (Figure 6.18A). With the 'Baseline' model, the primary mechanism of DC priming of naive CD4+ T cells, controlled by parameter $cognatePriming_p$, is IFNγ-independent. For the 'Alternate' model, perturbations of the analogous parameter ($cognatePriming_NonIFNgControlled_p$, see Table 6.6) produce a 'large' statistical effect size, as observed with the 'Baseline' model (Figure 6.18B). For the parameter controlling T cell dLN exit and anergy, the trends are consistent between the 'Alternate' model (Figure 6.18C) and the 'Baseline' model, whereby the numbers of primed CD4+ T cells are not robust to small alterations in this parameter. For the parameter controlling inflammation-induced naive CD4+ T cell recruitment, the distribution of parameter values between 'Baseline' and 'Alternate' model fits (i.e., those yielded from calibration) are similar. Interestingly, for the 'Alternate' model we observed that at all timepoints, alterations in this parameter produced 'large' statistical effect sizes (Figure 6.18D), while in comparison, the 'Baseline' model between hours 1-6 the model appears to be less sensitive. Nevertheless, this parameter exerts high influence in primed CD4+ T cell levels in both model variants, adding further evidence of its importance in AS01 biology.

6.2.10.2 Key Differences between the sensitivities of the 'Alternate' and 'Baseline' Models

For the parameter controlling the rate of DC recruitment and dLN-resident DC activation ($DC_Afferent_p$), the best fit values are similar between model variants. Interestingly, we observed some differences in sensitivities, where for 'Alternate' model primed CD4+ T cells appear to be more sensitive to $DC_Afferent_p$ than the 'Baseline' model ('Alternate': Figure 6.19A, vs. 'Baseline': Figure 6.15A). Given the model finding in Chapter 5, that based on our hypothesis of DCs producing IL12, DCs may provide an early IL12 signal for innate IFNγ production (see Figure 5.5), it is plausible this explains the increased sensitivity of parameter $DC_Afferent_p$ in the 'Alternate' model where IFNγ-dependent priming has increased prominence compared with the 'Baseline' model. Indeed, we observed that for the 'Alternate' model, between 3-24 hours, perturbing the parameter *vDCIL12* controlling DC IL12 production produces large statistical effect sizes (Figure 6.19B). For the 'Baseline' model, *vDCIL12* exhibits negligible effects on the numbers of primed CD4+ T cells (data not shown), demonstrating that this is an IFNγ-dependent pathway-specific parameter sensitivity.

With the 'Alternate' model, we observed that perturbing values of the parameter controlling macrophage loss rate (CL_p) has a moderate effect on the number of primed CD4+ T cells at 3 and 48 hours, and a large effect at 6,16 and 24 hours post-injection (Figure 6.19C). This suggests that under the current hypothesis that IFNγ enhances DC-CD4+

T cell priming, loss of macrophages may serve as a limiting factor. Indeed, we have observed that macrophage-released IL18 is dominant in promoting innate IFNγ (section 5.2.3), therefore under the IFNγ-enhancement hypothesis, we can reason that altering the loss of macrophages would impact CD4+ T cell priming. Collectively, this suggests that in a scenario where IFNγ enhances the priming of CD4+ T cells after AS01 - the veracity of which remains to be determined - this would be initiated by QS21-mediated IL18-induced IFNγ but at the same time limited by a potential inhibitory mechanism of QS21 through causing a loss of IL18 producing macrophages. This effect is not observed with the 'Baseline' model (data not shown), likely because IFNγ - and transitively IL18 and macrophages - do not influence priming in this model. Interestingly, the parameter which controls IL18 production by macrophages ($vMoIL18_p$) - induced by QS21 - we observed that between 3-72 hours, exhibits large effects on primed CD4+ T cell levels (Figure 6.19D). In Chapter 5, we proposed the novel hypothesis that QS21 may perform both pro- and anti-inflammatory functions during AS01-induced immune responses. If the 'IFNγ enhancement' hypothesis is accepted, one can extend our proposal in Chapter 5, by reasoning that QS21's pro- and anti-inflammatory influence extends to the CD4+ T cell response. Lastly, we examined the local sensitivity of the parameter controlling the rate of IFNγ-dependent CD4+ T cell priming, and observe that at all timepoints this parameter exerts a large statistical effect on the numbers of primed CD4+ T cells (Figure 6.19E).

By comparing the local sensitivity analyses of the 'Baseline' and 'Alternate' models, we propose inflammation-induced naive CD4+ T cell recruitment as a mechanism which requires further attention in AS01 MoA. Indeed, the substantial influence of this parameter with CD4+ T cell priming is conserved across models, despite variations in the hypotheses underpinning calibration. While qualitative reasoning can deduce that perturbing the rate of naive CD4+ T cells into the dLN would affect priming, the extent to which this parameter was important was not obvious to us *a priori*. It is therefore key to quantify the distribution of this parameter which leads to canonical immune responses, and to elucidate which immune mediators are involved in this process. If this mechanism's importance is confirmed, it is plausible that one may be able to improve generated immune responses by exploring different dosing schedules or times of day, given the insight that circadian rhythm can modulate cell infiltration rates [323]. Lastly, dependent on the veracity of the IFNγ enhancement hypotheses and/or the magnitude of role of IFNγ in this process, these findings, alongside the findings of Chapter 5, suggest that if IFNγ does enhance DC ability to prime CD4+ T cells, this would be mediated by IL18 early in the response, supported by IL12, augmented later by the arrival of adaptive CD8+ T cells producing IFNγ and negatively regulated in-part by the loss of subcapsular macrophages.

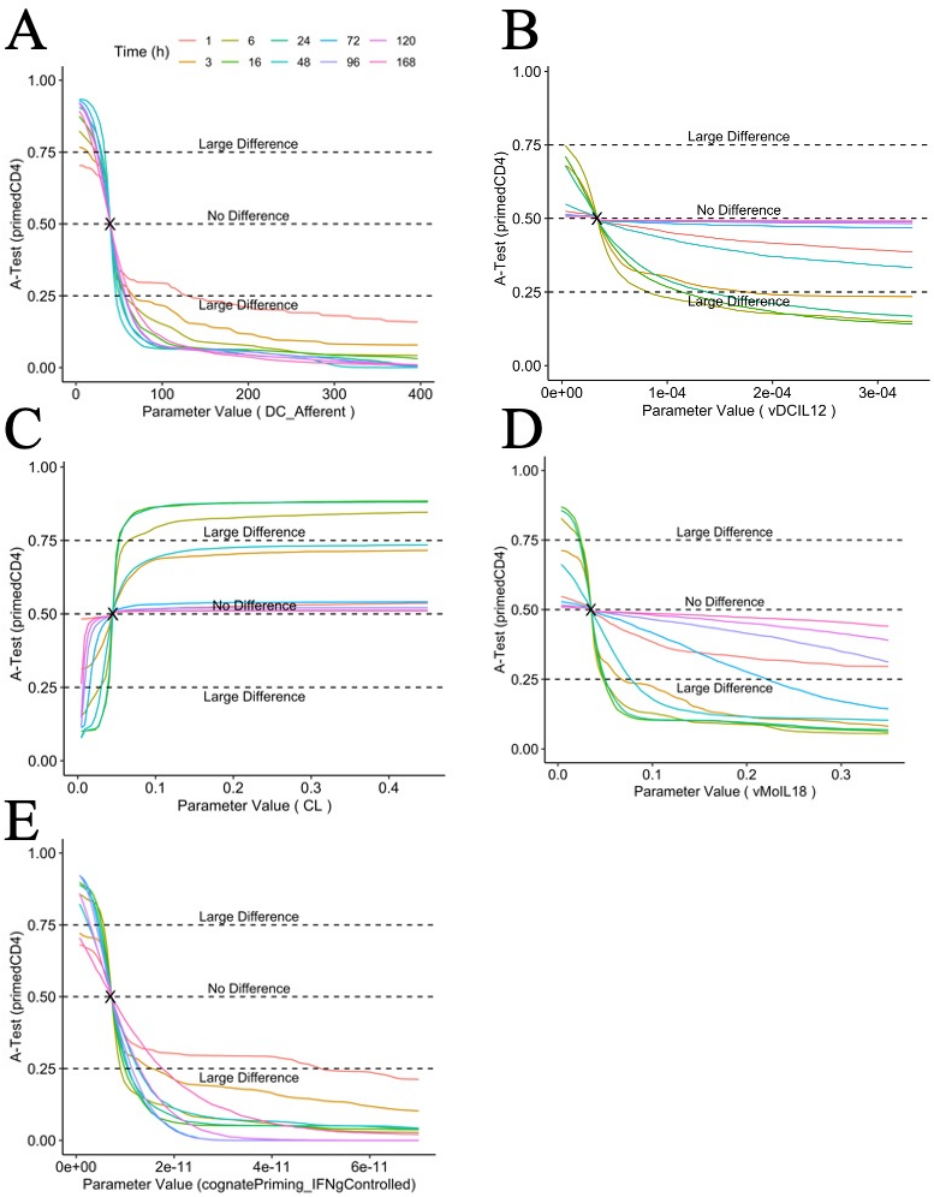


Figure 6.19: **Local sensitivity analysis for the 'Alternate' model: A-E:** 100 parameter sets are sampled uniformly across ranges of a factor of 10 each side of the baseline parameter value. Each sampled parameter value is ran 'in place' of the corresponding parameter for every calibrated model fit (n=73). Therefore 7300 runs are performed for each parameter, incorporating uncertainty from the model calibration into the analysis. The distribution of simulation responses for primed CD4+ T cells for each parameter, are compared with the simulation responses after running the model with the baseline calibrated 'best fit'. **A-D** show lineplots showing Vargha-Delaney A-Test statistics at different alterations of parameters for those controlling the rates of **A)** recruitment and activation of DCs **B)** Production of IL12 by DCs **C)** Loss of macrophages, **D)** macrophage production of IL18, **E)** IFNγ-dependent CD4+ T cell priming.

6.2.11 Exploring the Hypothesis That IFNγ Modulates CD4+ T cell priming through augmenting DC potency

Coccia et al [32] observed that IFNγ controls the CD4+ T cell response to AS01. After a prime-boost regimen comparing the numbers of HBsAg-responsive CD4+ T cells at day 21 post-injection in wild-type and IFNγR knockout mice, Coccia observed an $\sim$80% reduction in the number of CD4+ T cells in the knockout compared to the wild type. However, the mechanism underpinning IFNγ's control of CD4+ T cell priming remains elusive. In what follows, we explore the theoretical feasibility of one hypothesis for how IFNγ controls this process. IFNγ's role in upregulating MHC machinery and co-stimulatory molecules in wider systems is well characterised [314]. Furthermore, after AS01-adjuvanted vaccination into IFNγR deficient mice, a considerable reduction of CD80/86 MFI is observed compared with the wild-type mouse [32]. Together, ourselves and GSK immunologists hypothesised that IFNγ may modulate CD4+ T cell priming through *substantially* or *drastically* **enhancing** the priming potency of DCs (via upregulation of MHC machinery and co-stimulatory molecules), which in turn may augment the numbers of primed CD4+ T cells. Here, we explored this hypothesis through simulation, and then used the resulting information to refine our hypothesis. We therefore leveraged both previously described model variants, the 'Baseline' and 'Alternate' models. Given limits of AS01 experimental data, we expected there is not statistical power to reject a hypothesis, rather we aimed to propose an avenue which is qualitatively more consistent with experimental data. Therefore, we varied parameters controlling IFNγ modulation of CD4+ T cell priming within both models, to explore the extent to which different levels of enhancement of DC potency and thus CD4+ T cell priming are qualitatively consistent with *in vivo* data. We found that our original hypothesis is likely to be incomplete and thus propose refinements based on evidence.

6.2.11.1 Employing the Baseline Model to Explore the Extent that IFNγ may enhance CD4+ T cell priming through augmenting DC potency

To explore our hypothesis, we began with our 'Baseline' model - where as calibrated, IFNγ has negligible impact on the priming of CD4+ T cells, represented by minuscule values for parameter $cognateEnhanceIFNg_p$. Here, under multiple scenarios, we increased the permitted maximum range of this parameter and uniformly sampled values within the new range, to tune the overall magnitude to which IFNγ modulates this process. After simulating these new parameters, we explored the extent that IFNγ can enhance DC potency of CD4+ T cell priming in the model and be qualitatively consistent with the biological data. The ranges of explored parameters and the corresponding (*in silico*) experimental scenarios are shown in Table 6.7. Each newly sampled value of $cognateEnhanceIFNg_p$ were employed

amongst the entire distribution (i.e. for every local minima) of the remaining parameter's calibrated values (those summarised in Table 6.3).

Scenario	**Parameter**	**Original Range**	**New Range**	**Reference Parameter Value**
Baseline (as calibrated)	cognateEnhanceIFNg$_p$	5.0e-14 - 1.0e-13	No change	1e-13
Drastic	cognateEnhanceIFNg$_p$	5.0e-14 - 1.0e-13	5.0e-14 - *4.5e-11*	1e-13
Mild IFNg Enhance	cognateEnhanceIFNg$_p$	5.0e-14 - 1.0e-13	5.0e-14 - *4.0e-12*	1e-13

Table 6.7: **Changes to Parameter Ranges to explore hypothesis that IFNγ substantially enhances CD4+ T cell priming through augmenting DC potency:** Parameter ranges were altered as described in Table 6.7. Values for altered parameters were sampled at increments through the new parameter space, to create model variants and then simulated to explore a corresponding model scenario. The 'Baseline' scenario represents no change from the baseline calibrated model, and uses the parameter sets described in Table 6.3. The 'Drastic' scenario, represents a model variant where IFNγ substantially enhances CD4+ T cell priming. This is achieved through increasing the maximum permitted value of the *cognateEnhanceIFNg$_p$* parameter, in turn increasing its potential influence. The 'Mild IFNg Enhance' scenario represents a model variant where IFNγ mildly enhances CD4+ T cell priming. Other variants were explored but not shown, including where *cognateEnhanceIFN$_p$* and *CD4Proliferation$_p$* were altered simultaneously. Italics indicates where a range has been changed from the original. The dashed-line shows the time of the approximate peak of the 'second wave' of IFNγ.

We first simulated a so-called 'drastic' increase in the maximum allowed value of *cognateEnhanceIFNg$_p$*, which controls IFNγ enhancement of DC priming potency and thus the numbers of primed CD4+ T cells. This 'drastic' increase served to represent a scenario under our hypothesis where IFNγ *substantially* enhances CD4+ T cell priming. Here, the maximum permitted value was set to 450 times larger than the calibrated value for the 'Baseline' (see Table 6.7 for the full parameter ranges explored for each scenario). Indeed, this level of IFNγ enhancement provokes a substantial rise in primed CD4+ T cells, the mean of which reaches a trajectory within the standard error of the experimental data at day 7, but not at day 5 (Figure 6.20). This sharp increase is qualitatively consistent with the peak of the 'second wave' of IFNγ at approx. 71 hours post injection (represented by the dashed line). Furthermore, the standard error of the model trajectory under the 'drastic' scenario is wider than the error of the corresponding observational data, together suggesting that a milder range of IFNγ enhancement is more suitable for further exploration. While qualitatively, the 'drastic' scenario appears to be inconsistent with the experimental data - in particular with the sharp rise at approx. 71 hours - we cannot reject this hypothesis at this level of the data. We next explored a 'Mild IFNg Enhancement' scenario (see Table 6.7), where instead we set the maximum range of the *cognateEnhanceIFNg$_p$* value to *4.0e-12*. This range represents a smaller increase in the maximum permitted value of this parameter than previously: 40 times larger than the baseline value. Compared with

the baseline scenario, the mean of the trajectory after the 'Mild IFNg Enhance' scenario is marginally closer than the 'Baseline' model to the central estimate of the experimental data, with similar standard error (Figure 6.20). The mean of the 'mild' scenario passes through the standard error at both day 5 and day 7, while the 'drastic' scenario does not.

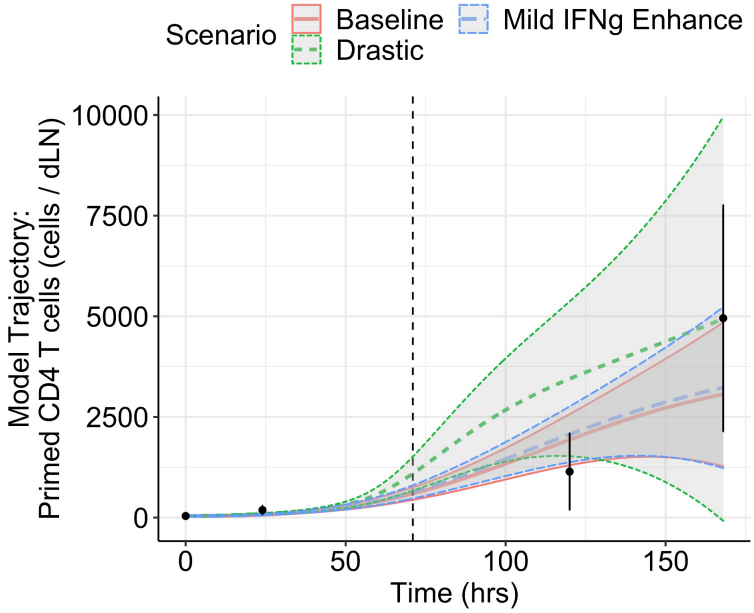


Figure 6.20: **Exploration of DC potency enhanced by IFNγ using the 'Baseline' Model:** A-B) Simulations using the 'baseline' model occurred after the parameter controlling IFNγ enhancement of DC potency (cognateEnhanceIFNg$_p$) was perturbed. The maximum permitted value of this parameter was increased to the calibrated baseline multiplied by 450 (Drastic) or 45 (Mild IFNg Enhance). Parameters within these new ranges were sampled and simulated. A) Line-plot contrasting the model trajectory of primed CD4+ T cells after two scenarios with the 'Baseline' model. For remaining parameters, every local optima was simulated. Shaded intervals show the mean+/- standard deviation of model trajectories.

Given these observations that both a 'drastic' and 'mild' level of enhancement were not completely inconsistent with experimental data, we sought to calibrate such models which reflect these scenarios, by (for *cognateEnhanceIFNg$_p$*) providing the optimiser the ranges as shown for the scenarios in Table 6.7. We reasoned that it was plausible these models may offer better fits to data than the 'Alternate' and/or 'Baseline' models. Unfortunately, we were unable to calibrate such models, as the resulting primed CD4+ T cell trajectories were not consistent with the experimental data. We observed that - consistent with Figure 6.20 for the 'drastic' and 'mild' variants - when trying to calibrate a model with such ranges of *cognateEnhanceIFNg$_p$*, too sharp increases were generated for the numbers of primed CD4+ T cells by approximately 71 hours post simulated injection for the resulting model fits to adhere to the day 5 timepoint of the experimental data. Temporally, this sharp rise is consistent with the predicted peak of the 'second wave' of IFNγ in the model (dashed

line in Figure. 6.20), which suggests that without some form of delay for IFNγ's effects implemented into the mathematical model, a direct enhancement by IFNγ is temporally inconsistent with the experimental data. In turn, this suggests that incorporating a delay into the underlying hypothesis of the biology and thus the model, may improve the fits to experimental data. This may be realised through use of a delay-differential-equation, or a multi-compartment model which captures a waiting time delay for IFNγ's production to its enhancement of DC potency. Biologically, such a feature would describe delays surrounding signalling within the DCs. Additionally, an ABM may be helpful here although the granularity of data required to fit such a model is not yet available. Overall, our results thus far suggest that the current 'IFNγ enhancement' hypothesis is incomplete.

6.2.11.2 Employing the Alternate Model to Explore the Extent that IFNγ may enhance CD4+ Tcell priming through augmenting DC potency

Although we were unable to calibrate a model with 'mild' or 'drastic' levels of IFNγ enhancement of DC potency, we could calibrate a model where the influence of IFNγ-*dependent* and -*independent* B7-mediated priming of CD4+ T cells by DCs is more balanced: the 'Alternate' model (see Figures 6.18B and 6.19E). However, compared with the 'Baseline' model, the 'Alternate' model has a higher objective value, suggesting that it is a poorer fit to data. During calibration of the 'Alternate' model, we were unable to further increase the maximum permitted range of the parameter controlling IFNγ-dependent mediated priming of CD4+ T cells by DCs, which together with the results in the previous section, suggests that our hypothesis for IFNγ enhancement of this process is incomplete.

Using the 'Alternate' model we explored whether alterations to the relative magnitude of IFNγ-dependent vs. -independent priming may enable a better consistency with experimental data, or whether a refinement of the underlying hypothesis is required. We therefore employed the 'Alternate' model to explore varying ratios of influence between both the IFNγ-independent and -dependent avenues of DC priming of CD4+ T cells. This model has been purposely calibrated to capture a scenario where the influence of the two aforementioned 'avenues' of CD4+ T cell priming is more balanced, thus serving as a reasonable platform to alternate these ratios.

To clarify, with the 'Alternate' model, the parameter $cognatePriming_IFNgControlled_p$ represents the avenue where IFNγ enhances CD4+ T cell priming, while the parameter $cognatePriming_NonIFNgControlled_p$ represents IFNγ-independent priming (see Table 6.6). We designed an array of scenarios where ranges of one or both of the aforementioned parameters are altered within newly defined ranges, and a selection of resulting model trajectories are shown here (see Table 6.8 for the parameter ranges and alterations). We simulated

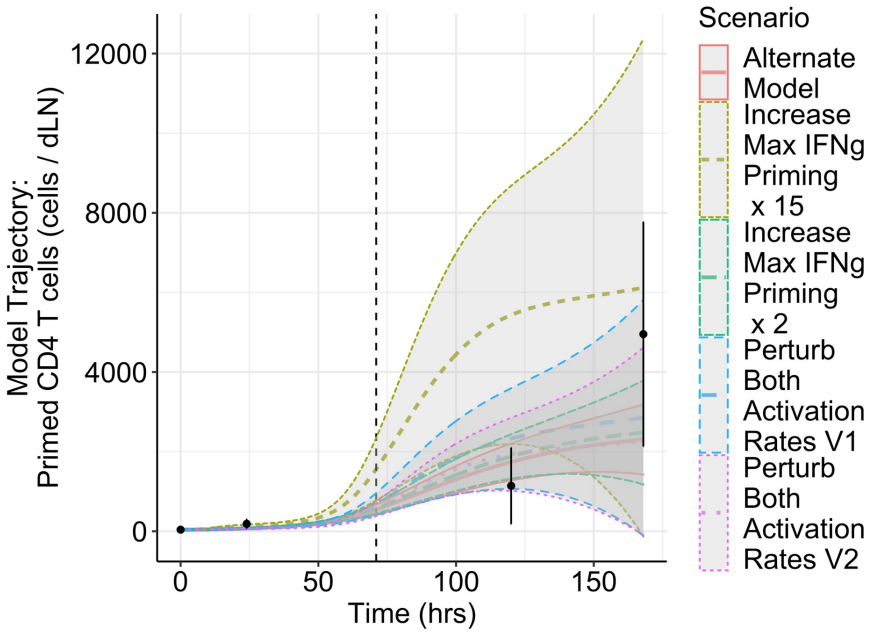


Figure 6.21: **Model variants where IFNγ's role is more prominent are qualitatively inconsistent with experimental data:** A) Simulations using the 'Alternate' model occurred after the two parameters controlling rates of DC priming were perturbed within ranges as defined in Table 6.8. Parameters within these new ranges were sampled and simulated. Where values for multiple parameters were changed (Perturb both activation rates), each possible combination of the sampled parameter values was simulated. For remaining parameters, every local optima was simulated. Shaded intervals show the mean+/- standard deviation of model trajectories.

each scenario and the predicted trajectories are compared in Figure 6.21. We found that by using the 'Alternate' model and increasing the maximum range of this parameter to 15 times larger than the reference value of the $cognatePriming_IFNgControlled_p$ parameter, the resulting number of primed CD4+ T cells were qualitatively inconsistent with the biological data (Figure 6.21). None of the permutations explored with this model improved visual conformity with the biological data. Each scenario where the IFNγ-dependent pathway is given more prominence than with the calibrated 'Alternate' model, even when considerably reducing the parameter controlling IFNγ-independent priming, qualitatively we observed too sharp an increase in primed CD4+ T cells, corresponding with the second peak of IFNγ (Figure 6.21, see dashed line), which does not conform with experimental data at day 5.

In turn, we were unable to calibrate a variant of the 'Alternate' model, where IFNγ-dependent priming was given more prominence, at the expense of IFNγ-independent priming. Indeed, we provided the optimiser the ranges of parameters in Table 6.8, corresponding to each scenario, as well as further variations (and also much looser constraints on ranges). In each case, too sharp an increase in the numbers of primed CD4+ T cells was generated and the models were not appropriately fit to data. In our experience, the 'Alternate' model may represent approximately the highest value(s) of the parameter controlling IFNγ-

dependent priming given the current mathematical structure, where the model was able to be fit to data. Taken together with the results in the previous section, our analyses indicate that our hypothesis for how IFNγ controls the CD4+ T cell response is incomplete, to the extent that we cannot distinguish varying hypotheses for IFNγ's role in CD4+ T cell priming. Overall, model analysis suggests that a delay in IFNγ's effect on DC potency, may improve the fit of a 'CD4+ T cell priming after AS01' model to experimental data.

Scenario	**Parameter**	**Original Range**	**New Range**	**Reference Parameter Value**
Alternate Model	cognatePriming_IFNgControlled$_p$	5.00e-13 - 7.25e-12	No change	7.25e-12
Increase Max IFNg Priming 15 Times	cognatePriming_IFNgControlled$_p$	5.00e-13 - 7.25e-12	5.0e-13 - *1.088e-10*	7.25e-12
Increase Max IFNg Priming 2 Times	cognatePriming_IFNgControlled$_p$	5.00e-13 - 7.25e-12	5.0e-13 - *1.45e-11*	7.25e-12
Perturb Both Activation Rates V1	cognatePriming_IFNgControlled$_p$	5.00e-13 - 7.25e-12	5.0e-13 - *3.625e-11*	7.25e-12
	cognatePriming_ NonIFNgControlled$_p$	7.0E-10 - 2.60e-09	*1.04e-09 - 2.08e-09*	2.60e-09
Perturb Both Activation Rates V2	cognatePriming_IFNgControlled$_p$	5.00e-13 - 7.25e-12	*7.25e-12 - 2.76e-11*	7.25e-12
	cognatePriming_ NonIFNgControlled$_p$	7.0E-10 - 2.6e-09	*5.19e-10 - 1.30e-09*	2.60e-09

Table 6.8: **Changes to Parameter Ranges when the 'Alternate' model was employed to explore IFNγ's role in CD4+ T cell priming:** Parameter ranges were altered as described in the table. Values for altered parameters were sampled at increments through the new parameter space, to create model variants and then simulated to explore a corresponding model scenario. Italics indicates where a range has been changed from the original. Further ranges were explored which are not shown, where the influence of parameter controlling IFNγ-independent priming (cognatePriming_ NonIFNgControlled$_p$) is reduced considerably while increasing the prominence of the IFNγ-dependent pathway (cognatePriming_IFNgControlled$_p$), and in no cases did we improve visual conformity with the experimental data as compared to the 'Alternate' model.

6.2.11.3 A New, Refined hypothesis for IFNγ's role in CD4+ T cell responses after AS01

To explore the incompleteness of our 'IFNγ enhancement' hypothesis further, we performed an *in silico* IFNγ knockout using the 'Alternate' model, which was compared to the wild-type 'Alternate' model as calibrated. We then compared the levels of primed CD4+ T cells at day 7 post-simulated-injection between simulated scenarios, and observed a significant reduction in the number of primed CD4+ T cells (reduction of 19.05% in the means) after the knockout compared with the wild-type (Figure 6.22). After performing an IFNγR knockout *in vivo* and following a day 0 prime, day 14 boost regimen with HBsAg and

AS01, where the number of HBsAg-responsive CD4+ T cells were measured at day 21 post-primary injection, Coccia et. al. observed approximately an 80% reduction in this cell type compared with the same vaccination into C57BL/6 mice [32]. While ours and Coccia's are not analogous experiments thus not permitting a direct comparison, our observed reduction of 19.05% in our simulated IFNγ knockout, compared with Coccia's 80% reduction after an IFNγRKO *in vivo*, suggests that the AS01 CD4+ T cell priming 'Alternate' model is built upon an incomplete understanding and hypothesis of how IFNγ modulates the CD4+ T cell response to AS01.

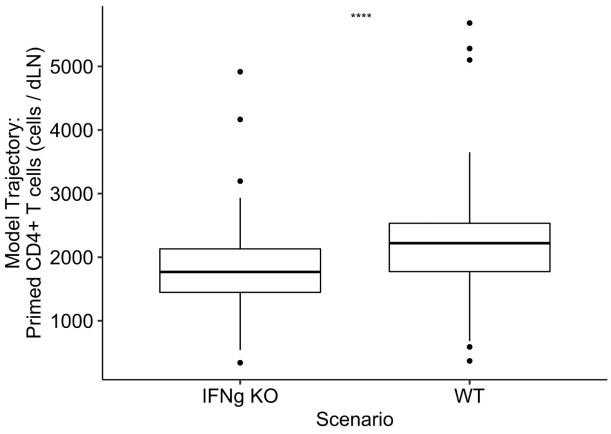


Figure 6.22: **A simulated 'IFNg' (IFNγ) knockout using the 'Alternate' Model:** A boxplot contrasting the distribution of 'primed CD4+ T cell' model trajectories for each local minima after the 'IFNg knockout' and 'wild-type' scenarios at day 7 post-injection. The simulated IFNγ knockout was implemented by setting the 'IFNg' initial condition to zero, as well as the parameters which produce 'IFNg', $VmaxNKaProd1218_p$, $VmaxNKaProd12_p$, $VmaxNKaProd18_p$, $InnateCD8IFNgProd_p$ and $BasalCD8IFNgProd_p$. The simulation was then run for each local minima.

While naturally increasing the parameter controlling the rate of IFNγ-dependent priming ($cognatePriming_IFNgControlled_p$), may induce a larger drop of primed CD4+ T cells in the *in silico* IFNγ knockout that is consistent with Coccia's insight, we have demonstrated that further increases in this parameter induces too high numbers of primed CD4+ T cells to be consistent with the day 5 timepoint of the experimental data (examples shown in Figure 6.21). As mentioned we have tried to calibrate models where $cognatePriming_IFNgControlled_p$ exerts more influence, but were unable to at this level of system understanding. Given Coccia's insight and our work, we have mutually-exclusive data, which indicates our current understanding of the system - upon which our mechanistic model(s) are built - is incomplete. While, we cannot completely exclude that comparing Coccia's IFNγRKO and our simulated IFNγ knockout is misleading as the experiments are performed under different conditions, one would expect more consistency between these scenarios regarding the effect IFNγ has on CD4+ T cells. The insights presented here and in

preceding sections therefore guided a new, refined hypothesis for how IFNγ may modulate DC potency and thus enhance CD4+ T cell priming. Inspection of the effects of increasing the $cognatePriming_IFNgControlled_p$ parameter in Figures 6.21 and 6.20, suggest that a delay in IFNγ's effects on DC potency coupled with considerable enhancement by IFNγ, could provide a better fit to the data, bringing the model more in line with experimental data. Through this refined hypothesis, a considerable enhancement by IFNγ may also be consistent with Coccia's insights.

Additionally, we have used data on the numbers of 2W1S+ CD4+ T cell after AS01, to calibrate the model's 'primed CD4+ T cells'. This 'primed CD4+ T cell' entity, does not capture Th1 differentiation dynamics, which is modulated by cytokines including IFNγ and IL12. Therefore, an additional facet of our refined hypothesis given our insights that the understanding of the system is incomplete, is that IFNγ's control of functional CD4+ T cell responses is in-part mediated through promoting Th1 differentiation. This refined, detailed hypothesis has emerged as a direct result of exploratory mechanistic modelling - integrating hypotheses, assumptions, experimental insights and data, showcasing the ability of such approaches to complement experimental work.

6.2.12 Profile-likelihood identifiability analysis for 'Baseline' and 'Alternate' models

Lastly, we computed profile-likelihoods of both the 'Baseline' and 'Alternate' model parameters, to examine the identifiability of each model. The non-identifiability of certain model parameters can provide insight where future work could seek to improve calibration through further data generation and gathering and/or model reduction [9].

6.2.12.1 Identifiability of the 'Baseline Model'

Table 6.9 shows the confidence intervals with respect to the identifiability of model parameters for the 'Baseline' model, computed from the profile-likelihoods of each parameter. Interestingly, each parameter involved in the production of IFNγ is non-identifiable ($InnateCD8IFNgProd_p$,$BasalCD8IFNgProd_p$, $VmaxNKaProd12_p$, $VmaxNKaProd1218_p$, $VmaxNKaProd18_p$). This may be due to the granularity placed on IFNγ production in the model, where four separate mechanisms corresponding to four parameters are fit to the limited IFNγ experimental data. Here, we have no information on individual contributions with respect to each parameter, however typically during calibration, ranges based on domain intuition of the biological mechanisms were supplied to the optimiser in order to provide constraints regarding which parameter contributes more to the production of IFNγ (e.g., we know that $VmaxNKaProd1218_p > VmaxNKaProd18_p > VmaxNKaProd12_p$). However,

	Parameter	Best Fit	LowerCI	UpperCI	Units
1	$AdaptiveCD8Decay_p$	2.50E-02	2.48E-02	2.52E-02	proportion AdaptiveCD8 per unit NRP / hour
2	$AdaptiveCD8Max_p$	2.10E+04	2.10E+04	2.10E+04	cells/dLN
3	$BasalCD8IFNgProd_p$	2.25E-02			pg/AdaptiveCD8 hour
4	$CD4T0_death_recirculation_p$	5.77E-02	5.64E-02		proportion CD4T0/hour
5	$CD4T0_Inflammatory_Recruitment_p$	6.42E-04		7.44E-04	cells per unit MPL_p and $QS21_p$/hour
6	$CD8Innate_p$	5.00E+00	5.00E+00	5.00E+00	cells / pg IL18 hour
7	$CD8RecruitAct_p$	1.99E-03	1.92E-03		cells per unit of $QS21_p$ and MPL_p / hour
8	CL_p	4.80E-02		4.86E-02	cells per unit $QS21_p$ / hour
9	$DC_Afferent_p$	4.25E+01	4.25E+01	4.25E+01	cells/hour
10	$DCDecay_p$	1.75E-03	1.45E-03	1.85E-03	proportion DC per unit NRP/hour
11	$decay12_p$	4.18E-02	4.12E-02		pg/dLN hour
12	$decay18_p$	3.80E-01	3.79E-01	3.80E-01	pg/dLN hour
13	$decayIFNg_p$	1.40E-01			pg/dLN hour
14	$InhibitionProduction_p$	2.00E-02	1.89E-02		unitless
15	$InnateCD8decay_p$	1.83E-01	1.81E-01	1.83E-01	proportion of InnateCD8 / hour
16	$InnateCD8IFNgProd_p$	1.00E-13			pg/InnateCD8 hour
17	KM_12b_p	2.48E+01	2.48E+01		pg/dLN
18	KM_18b_p	3.26E+01	3.26E+01		pg/dLN
19	$KM_NKa_IL12b_p$	5.83E+00	5.83E+00	5.83E+00	pg/dLN
20	$MonocDecay_p$	1.00E-02	8.97E-03	1.01E-02	proportion of Monoc per unit NRP/hour
21	$MonocDiffDC_p$	8.00E-03	7.46E-03		proportion / Monoc hour
22	$monocRec_p$	2.70E+02	2.70E+02	2.70E+02	cells per unit MPL_p / hour
23	$NKDecay_p$	2.93E-01	2.93E-01	2.94E-01	proportion/NKa hour
24	$vDCIL12_p$	3.33E-05			pg/DC hour
25	$VmaxNKa12_p$	9.14E-03	8.00E-03	1.04E-02	cells/hour
26	$VmaxNKa1218_p$	5.49E+03	5.49E+03	5.49E+03	cells/hour
27	$VmaxNKa18_p$	1.50E+00	1.50E+00	1.50E+00	cells/hour
28	$VmaxNKaProd12_p$	5.78E-08			pg/NKa hour
29	$VmaxNKaProd1218_p$	1.20E-04			pg/NKa hour
30	$VmaxNKaProd18_p$	5.78E-07			pg/NKa hour
31	$vMoIL18_p$	3.50E-02	3.48E-02	3.55E-02	pg/Mo
32	$vMonocIL12_p$	3.30E-05		2.34E-04	pg/Monoc hour
33	$CD4Proliferation_p$	7.90E-02	7.88E-02		cells/hour
34	$CD4ProlifMax_p$	7.89E+07	7.89E+07	7.89E+07	cells/dLN
35	$TcellExit_Anergy_p$	1.00E-01	9.98E-02	1.00E-01	cells/hour
36	$cognatePriming_p$	4.58E-09			proportion of CD4T0/DC hour
37	$cognateEnhanceIFNg_p$	1.00E-13			proportion of CD4T0/DC / pg IFNg hour

Table 6.9: Profile-likelihood based confidence intervals on the identifiability of parameters for the 'Baseline' AS01 CD4+ T cell priming model.

given that constraints on these parameters do not arise from experimental data, rather from ranges of values provided from the literature and/or domain intuition, it is plausible this leads to non-identifiable parameters. Following this insight, we propose that an *in vivo* or *in vitro* exploration into the contributions made by innate vs Adaptive CD8+ T cells (for $InnateCD8IFNgProd_p$ *and* $BasalCD8IFNgProd_p$), the synergistic component ($VmaxNKaProd1218_p$), QS21 and thus IL18 ($VmaxNKaProd18_p$) and MPL and thus IL12 ($VmaxNKaProd12_p$), to the production of IFNγ, may improve the identifiability of these parameters and thus our quantitative understanding of AS01 MoA. If warranted by future research interests, one could fit a considerably simplified version of the IFNγ model in Chapter 4, to the IFNγ kinetics data as well as the IL18R knockout and αIL12 depletion data, which may provide an indication of these parameters' values.

Similarly, the parameters involved in IL12 production are not identifiable, although an upper bound is computed for the parameter controlling the rate of monocyte IL12 production $vMonocIL12_p$. As discussed in Chapter 4, this non-identifiability is unsurprising given there are no data - without technical issues hindering the experiments - on IL12 concentrations after AS01. Experimental immunologists at GSK have informed us this is due to difficulties in measuring IL12 in dLNs *in vivo*. We propose that experiments focused on measuring IL12 production in DC and monocyte cell lines separately *in vitro* would provide valuable data in a first step in aiming to identify these parameters. Interestingly, with

this model we are able to identify an upper bound for the parameter controlling the loss of macrophages (CL_p). Previously in Chapter 4, using the 'Innate IFNγ AS01 model', we were unable to identify an upper bound for this parameter.

6.2.12.2 Identifiability of the 'Alternate Model'

Table 6.10 shows the confidence intervals with respect to the identifiability of model parameters for the 'Alternate' model, computed from the profile-likelihoods of each parameter. Similarly to the 'Baseline' model, we are unable to identify many of the cytokine production rates. Interestingly here, we are able to identify an upper bound for the rate of synergistic production of IFNγ induced by IL12 and IL18 ($VmaxNKaProd1218_p$). Given that in this model, IFNγ subsequently influences the numbers of primed CD4+ T cells, this may provide additional constraints which allows an upper bound of this parameter to be defined. In summary, we have performed profile-likelihood based identifiability analysis for both the 'Baseline' and 'Alternate' models. Given the scarcity of experimental data, it is unsurprising that both simulators are partially-identifiable models. We have shed light on parameters which are not identifiable, and through these insights, in important cases we have suggested *in vivo*, *in vitro* and potentially *in silico* experiments which may shed light on the values of these parameters.

	Parameter	Best Fit	LowerCI	UpperCI	Units
1	$AdaptiveCD8Decay_p$	2.00E-02		2.01E-02	proportion AdaptiveCD8 per unit NRP / hour
2	$AdaptiveCD8Max_p$	2.10E+04	2.10E+04	2.10E+04	cells/dLN
3	$BasalCD8IFNgProd_p$	2.23E-02		2.26E-02	pg/AdaptiveCD8 hour
4	$CD4T0_death_recirculation_p$	5.80E-02	5.79E-02	5.81E-02	proportion CD4T0/hour
5	$CD4T0_Inflammatory_Recruitment_p$	6.45E-04			cells per unit MPL_p and $QS21_p$/hour
6	$CD8Innate_p$	5.00E+00	5.00E+00	5.00E+00	cells / pg IL18 hour
7	$CD8RecruitAct_p$	1.86E-03			cells per unit of $QS21_p$ and MPL_p / hour
8	CL_p	4.50E-02		4.52E-02	cells per unit $QS21_p$ / hour
9	$DC_Afferent_p$	3.96E+01		3.96E+01	cells/hour
10	$DCDecay_p$	2.25E-03			proportion of DC per unit NRP/hour
11	$decay12_p$	4.18E-02	4.17E-02	4.22E-02	pg/dLN hour
12	$decay18_p$	3.80E-01		3.80E-01	pg/dLN hour
13	$decayIFNg_p$	1.60E-01	1.59E-01		pg/dLN hour
14	$InhibitionProduction_p$	2.00E-02	1.93E-02		unitless
15	$InnateCD8decay_p$	3.99E-01	3.99E-01		proportion of InnateCD8 / hour
16	$InnateCD8IFNgProd_p$	1.00E-13			pg/InnateCD8 hour
17	KM_12b_p	2.49E+01	2.49E+01	2.49E+01	pg/dLN
18	KM_18b_p	3.27E+01		3.27E+01	pg/dLN
19	$KM_NKa_IL12b_p$	5.44E+00		5.44E+00	pg/dLN
20	$MonocDecay_p$	1.00E-02	9.80E-03		proportion of Monoc per unit NRP/hour
21	$MonocDiffDC_p$	8.00E-03	7.87E-03		proportion / Monoc hour
22	$monocRec_p$	2.70E+02		2.70E+02	cells per unit MPL_p / hour
23	$NKDecay_p$	2.93E-01	2.93E-01	2.94E-01	proportion/NKa hour
24	$vDCIL12_p$	3.33E-05		1.33E-04	pg/DC hour
25	$VmaxNKa12_p$	9.14E-03		9.30E-03	cells/hour
26	$VmaxNKa1218_p$	5.49E+03		5.49E+03	cells/hour
27	$VmaxNKa18_p$	1.50E+00	1.50E+00	1.50E+00	cells/hour
28	$VmaxNKaProd12_p$	5.78E-08			pg/NKa hour
29	$VmaxNKaProd1218_p$	1.20E-04		1.87E-04	pg/NKa hour
30	$VmaxNKaProd18_p$	5.78E-07			pg/NKa hour
31	$vMoIL18_p$	3.50E-02		3.52E-02	pg/Mo
32	$vMonocIL12_p$	3.30E-05			pg/Monoc hour
33	$CD4ProlifMax_p$	3.69E+07			cells/dLN
34	$TcellExit_Anergy_p$	5.00E-02	4.97E-02	5.03E-02	cells/hour
35	$CD4Proliferation_p$	4.60E-02		4.62E-02	cells/hour
36	$cognatePriming_p$	7.25E-12			proportion of CD4T0/DC / pg IFNg hour
37	cognateNonIFNgControlled	2.60E-09			proportion of CD4T0/DC hour

Table 6.10: Profile-likelihood based confidence intervals on the identifiability of parameters for the 'Alternate' AS01 CD4+ T cell priming model.

6.2.13 First steps in ABM Development

We had aimed to build on analysis of our ODE models, by developing and analysing an ABM. We had hoped to compare results from the ABM with results from ODE models, and to explore questions surrounding the spatial contributions of cells and cytokines, including but not limited to the stochastic generation of CD4+ T cells after AS01. Additionally, an ABM would be able to describe a delay between IFNγ production and its enhancement of DC potency, which the work in this chapter suggests would improve model fits to data. Furthermore, such a model may be able to explore any DC priming enhancement by IFNγ in further detail, by capturing explicit surface expression enhancement by IFNγ on individual cells.

However, following initial stages of ABM development, we determined that the small quantity of available experimental data would not enable an appropriate implementation of an agent-based model. For example, we realised we would have to calculate cytokine and cell number estimates not only for whole-organ data-points, but also for spatial niches in the dLN, for every model entity. Indeed, after AS01, no spatial data was available to us, as well as data on dosing. Furthermore, the parameter estimation problem was already complex with ODE models, and an ABM increases this complexity to a level which - given available observational data - was likely to be unfeasible. Given this and other problems with the scarcity of experimental data, we decided to halt development of this model, embrace simplicity and focus on analysing our ODE models. Despite this, we hope that the initial stages of the ABM that were developed and the captured thinking, could be useful in future work for AS01 modelling, if further data were generated. Therefore, we present a selection of the diagrams for this ABM, in Appendix B1-B4.

6.3 Discussion

The aims of Chapter 6 were to expand on the insights in Chapters 4 and 5, by developing multiple models to identify influential parameters underpinning CD4+ T cell priming after AS01-adjuvanted vaccination. We additionally aimed to explore and refine the hypothesis that IFNγ may substantially enhance the T cell priming potency of DCs. Further, we aimed to use the simulations to reveal where our understanding of the system is incomplete and utilise this information to propose refined and novel hypotheses of AS01 mechanism of action (MoA), and experiments which could thus improve our understanding of AS01 MoA.

Gathering Experimental Data for Model Development: Available data for fitting mathematical models of AS01 MoA is sparse, in particular whilst aiming to use datasets which minimise confounding factors. Despite these challenges, we have sought to make use

of available data. We therefore gathered available and appropriate datasets that adhered to our criteria (e.g., those using the most appropriate murine dose of 1/50HD AS01) which could be used for fitting (section 6.2.1.2). Here, we found that we had very little data for latter stages of the first seven days of the response to AS01. Given the nature of our research questions, we took the decision to use the trends between timepoints from wider AS01 datasets - i.e., those with different doses such as 1/10HD - to approximate some key missing central estimates. For example, we had available to us the numbers of CD11c+ MHCII+ DCs in the dLN, after 1/50HD of AS01, at timepoints 0,6,24, 48. This data was recommended by GSK for fitting. However, we were missing data beyond 48 hours for this cell type, and for a more appropriate calibration, we decided that an estimate of the numbers of these cells at 168 hours - to provide a reflection of the kinetics - would be more suitable than no estimate. We thus found data from wider AS01 experiments, where important missing timepoints were available. Thus the trends in such data, were used to approximate a few central estimates to provide a reflection of missing kinetics for exploratory modelling.

Clearly, this is a less than ideal scenario and a limitation of this chapter, however we reasoned that such estimates would be an improvement on a complete lack of data. Nevertheless, in light of each estimated timepoint, we confirmed that the time-series trends were consistent with trends observed by Didierlaurent et al [119, 5] and Coccia et al [54]. Observations and insights in this chapter to some extent rest on these estimates, thus we aimed to focus on potential trends through exploratory modelling, rather than quantitative predictions. Future and ongoing work will seek to incorporate the additional uncertainty around these estimates into the curated data. However for simplicity, as a 'first step' in exploratory modelling we sought to only use central estimates. Further experimental data using consistent and appropriate dosing concentrations of AS01 would be required to refine such predictions. Naturally such data would be used to refine the calibration of the CD4+ T cell priming models, and we would expect some minor quantitative alterations in the predictions and perhaps wider variation. However, given the consistency between Didierlaurent and Coccia's observations regarding endpoint kinetics for captured cell types and the estimated kinetics in the present study, we would expect the observations, insights and trends to be consistent with that which is presented here, and therefore for the conclusions of this chapter to hold.

A simple 'Baseline' AS01 CD4+ T cell priming model: To capture a simple implementation of CD4+ T cell priming after AS01 for use in exploratory analysis, we extended the innate IFNγ model proposed in Chapter 4. We therefore developed a Domain Model (section 6.2.1, Figures 6.3-6.6) and a Platform Model (section 6.2.2, Figure 6.8). Next, we manually derived ODEs from the Platform model diagrams, (section 6.2.2.1, equations

6.1-6.12), which were implemented to generate a simulation platform (section 6.2.3). We designed the mathematical model with simplicity in mind, as this is a first step in capturing AS01 CD4+ T cell priming. Indeed, our model was inspired by work from the Kirschner lab where naive CD4+ T cells are primed after exposure to Mycobacterium tuberculosis [197]. Our mathematical model also captured the hypothesis that IFNγ can enhance DC priming potency (IFNγ-dependent priming). For simplicity within the first steps of analysis however, to develop a 'Baseline' model, the values for the parameter $cognateEnhanceIFNg_p$ that were permitted for calibration were very small, purposely designed so that this parameter would exhibit negligible effects on the model. Thus, the 'Baseline' model reflected a setting where CD4+ T cell priming by DCs was IFNγ-independent.

By use of multi-start trust-region optimisation (Methods section 2.4), we incrementally calibrated portions of the model to the experimental data. For the full model, calibration yielded 81 different local minima (Table 6.2), all of which exhibited a reasonable fit to experimental data (Figure 6.9). After comparing the model output to data for which the model had not been trained, we deemed the simulation platform as appropriate for use in *in silico* experimentation (section 6.2.5, Figure 6.10).

Refined Hypotheses for monocyte dLN Recruitment: As mentioned, an aim of this chapter was to utilise the developed simulations to further elucidate where AS01 MoA is incomplete and thus propose refined and novel hypotheses and/or experimentation which could reduce these gaps in understanding and therefore improve our knowledge of AS01 mechanism-of-action. We revealed large quantitative gaps in the biological data, as well as missing mechanisms from the model and therefore our understanding of AS01 (section 6.2.6). Specifically, we highlighted gaps in our understanding of monocyte infiltration into the dLN after AS01, in particular between 24 and 48 hours post injection (Figure 6.11), where a sharp increase in the number of cells observed in the experimental data (not estimated) is not replicated by our models. This gap in mechanistic understanding revealed by model development, led us to re-evaluate our hypotheses for monocyte recruitment, indicating a missing model component. To this end, we proposed a refined hypothesis that early IFNγ induces a substantial level of CCL2 by neutrophils which in turn increases the rates of monocyte infiltration into the dLN between 24 and 48 hours. We additionally proposed that monocyte recruitment rates may be augmented by lymph node expansion.

Refined Questions Surrounding 'Adaptive' IFNγ: Through model development we revealed that considerable gaps remain in the quantitative understanding of IFNγ production over the first seven days of the immune response to AS01 (section 6.2.6.2). First, we found that while our model can describe the IFNγ experimental data, it predicts a peak of innate IFNγ at eight hours post-injection, rather than at the current understanding of six

hours. Importantly, there is an 18 hour gap between the experimentally observed peak at six hours and the next measurement. Thus, the model suggests there is an insufficient sampling frequency, and that the peak of innate IFNγ may not be at six hours post-injection. In turn, we proposed that measuring the concentration of IFNγ after AS01 at additional timepoints between 6 and 24 hours post-injection would address this question. Secondly, we demonstrated that the 'second wave' of IFNγ is poorly understood, as following 48 hours post-injection up to day 7, we have no usable information using 1/50HD regarding the magnitude to this wave, when it peaks, or when it ends. Lastly, model development revealed that gaps and inconsistencies remain in the knowledge of the initiation of this 'second wave' of IFNγ, which is thought to be mediated by CD8+ T cells. Improving the understanding of- and parameters underpinning- successful adjuvants is paramount, in order to provide sufficient constraints for the design of next-generation adjuvants. Therefore, to enhance the design of future adjuvants, it is indeed vital to understand how current adjuvants work. To this end, we have proposed gaps in the understanding of AS01 MoA revealed by model development. Furthermore, we have suggested experiments to fill such gaps. In concert, additional data would feed back into the modelling process to potentially improve the practical identifiability of the model and thus enable another iteration of model development, which could then provide further insight than is yielded from the proposed experiments alone.

In summary, this analysis demonstrates how model development can reveal gaps in understanding which may not have been realised otherwise. Confronting experimental insights and our hypotheses with simulation calibration to experimental data, forces an evaluation of our assumptions and their logical implications. Here, such analysis has added to our knowledge of the system through novel, refined and extended hypotheses for AS01 mechanism of action.

Inhibitory Mechanisms in AS01 MoA: Next, we illustrated the importance for so-called 'Negative Regulatory Processes' in the model. Indeed, we were unable to calibrate the so-called 'Baseline' model without the inclusion of a component which in-effect increases the rates of decay for cell types e.g DCs and monocytes, toward the latter timepoints of the simulation. Clearly, so-called 'negative regulatory pathways' are an important factor in AS01 MoA, and we proposed that these mechanisms warrant further exploration for the underlying molecular biology to be determined. This will likely require further *in vivo* experiments.

An 'Alternate' model of CD4+ T cell priming after AS01: To explore hypotheses surrounding IFNγ's role in CD4+ T cell priming after AS01, we calibrated a variant of the 'Baseline' model, which instead captures more of a balance between IFNγ-dependent

and -independent pathways of CD4+ T cell priming. This model possessed the same mathematical structure as the 'Baseline' model, however represents a variant hypothesis. Indeed, during calibration larger ranges were permitted for the parameter controlling the rate of IFNγ-dependent CD4+ T cell priming ($cognatePriming_IFNgControlled_p$), compared with the 'Baseline'. We observed that this model was perhaps less-able to describe the data than the 'Baseline' model (Figure 6.16). Furthermore, during calibration we observed that we were unable to increase the maximum range of the $cognatePriming_IFNgControlled_p$ parameter further without creating large discrepancies with the experimental data. These discrepancies appeared to be due to the 'second wave' of IFNγ - peaking at approximately 72 hours post simulated injection - perhaps causing sharp increases in the numbers of primed CD4+ T cells which was inconsistent with the slower increase of these cells as observed in the experimental data. Nevertheless, an 'Alternate' model was developed for exploration and analysis.

Comparison of Local sensitivities of the 'Baseline' and 'Alternate' models: We compared local sensitivities of the 'Baseline' and 'Alternate' models to indicate important mechanisms which are conserved despite varying underlying hypotheses. Firstly, we observed that the parameters controlling primed CD4+ T cell proliferation, IFNγ-independent cognate priming, T cell dLN exit and anergy and naive CD4+ T cell recruitment under inflammatory conditions were conserved sensitive parameters with the numbers of primed CD4+ T cells across both model variants. We next provided a framework for influential mechanisms that appear to be specific to the IFNγ enhancement hypothesis by highlighting key differences between the parameter sensitivities of the 'Alternate' and 'Baseline' models. In both settings, we were limited by the inability to perform a global sensitivity analysis due to the large number of free parameters and the resulting combinatorial explosion required to sample the parameter space. The use of local sensitivity analysis here is a limitation, which cannot account for compound effects of parameters[254, 260], although can provide some insight into influential model parameters.

By examining differences between the sensitivities of the 'Alternate' and 'Baseline' models, we found that under the 'Alternate' model, primed CD4+ T cell numbers sensitive to variations in the rate of IL12 production by DCs between 3 and 24 hours. Interestingly, this parameter induces negligible effects on the numbers of primed CD4+ T cells with the 'Baseline' model, indicating that under the hypothesis where IFNγ in-part contributes to CD4+ T cell priming, DC IL12 may play a role. It should be noted that after AS01, there is not yet definitive evidence of DC production of IL12, although ourselves and colleagues at GSK hypothesise that it is likely DCs are a source of IL12, due to reasons outlined in Chapter 3 and 4. Additionally, under the 'IFNγ enhancement' hypothesis we observed that

the parameter controlling the rate of macrophage cell loss (CL_p) exhibits moderate-large effects on the numbers of primed CD4+ T cells between 3 and 48 hours post-injection - which is not observed with the 'Baseline' model - indicating a further IFNγ-dependent pathway-specific sensitivity. These findings were expected and consistent with qualitative reasoning, however the temporal insights identified through examining model sensitivities extend that which can be extracted by human reasoning.

Under the 'IFNγ enhancement' hypothesis, QS21 may perform both anti- and pro-inflammatory function for CD4+ T cell priming: As previously mentioned, using the 'Alternate' model, in Figure 6.19C-D, we showed the influence of the CL_p and $vMoIL18_p$ parameters on the numbers of primed CD4+ T cells through a local sensitivity analysis. Interestingly, we observed contrasting effects. Perturbing the parameter controlling QS21-mediated IL18 production by subcapsular macrophages $vMoIL18_p$ exerts a large effect size on the numbers of primed CD4+ T cells, as determined by the Vargha Delaney A-Test, between 3 and 72 hours post simulated injection. In contrast for the parameter controlling the exponential decay rate by which QS21 induces a loss of these subcapsular macrophages (CL_p), we observed a large effect after perturbing the value between 6 and 24 hours post simulated injection. Intuitively, we can reason that via IL18-induced IFNγ, the effects of $vMoIL18_p$ on primed CD4+ T cell numbers would be positive, while the effects of CL_p would be negative (through loss of macrophage-induced IL18). In Chapter 5, we proposed that QS21 may be pleiotropic, exerting both anti- and pro-inflammatory roles during the early stages of the immune response to AS01. Taken together with work in this chapter, these data extend this hypothesis, suggesting that if the 'IFNγ enhancement' hypothesis is accepted, QS21's potential pleiotropy may influence not only IFNγ production, but also contribute to effective CD4+ T cell responses.

Efficiency of naive CD4+ T cell recruitment may have a significant impact on T cell priming after AS01-adjuvanted vaccination: One aim of this chapter was to utilise any developed simulators to examine cellular and cytokine influence on the priming of CD4+ T cells to suggest mechanisms maximising T cell responses, with the overarching aim of increasing vaccine efficacy. The goal of vaccinology to develop correlates of protection and vaccine efficacy has been realised for yellow-fever vaccine among others [325, 134, 326] however for many vaccines this remains elusive, while being key to understanding responses e.g. to SARS-CoV2 variants [327]. While the scope of this model and available experimental data would not permit examination of correlates of vaccine efficacy, it does provide a basis for using model-driven-experimentation to explore the potential role of naïve T cell recruitment in AS01 vaccine efficacy and develop novel approaches to increase adjuvant efficacy without increasing adverse events.

Elucidating immune processes which influence the generation of primed CD4+ T cells after AS01-adjuvanted vaccination is thus an important question, as these cells contribute to protection induced by this adjuvant [32]. Local sensitivity analysis of both the 'Baseline' and 'Alternate' models (sections 6.28 and 6.2.10) demonstrated that the numbers of primed CD4+ T cells are sensitive to minor alterations in rates controlling a) inflammation-induced naive CD4+ T cell recruitment, b) their proliferation and c) cognate priming of primed CD4+ T cells. The consistent sensitivity across both models which capture varying hypotheses, suggests confidence that despite alterations in hypotheses underpinning model calibrations, and the finding that our hypothesis for how IFNγ controls CD4+ T cell priming is incomplete, these factors are influential during the generation of CD4+ T cell priming after AS01. For proliferation and cognate priming rates, these observations were in line with our expectations. Interestingly, we had not expected such sensitivity for the parameter controlling the rate of inflammation-induced naive CD4+ T cell recruitment into the tissue dLN. The large influence of this parameter on model behaviour, suggests firstly, that the number of naive CD4+ T cells that make it into the dLN during inflammation could be a significant factor in the initiation of efficient immune responses to AS01. This finding extends the insight by Didierlaurent et al [5], who suggested that rapid recruitment of naive T cells was likely to have a key role in AS01-based immune responses. Furthermore, this work suggests that physiological differences between 'T cell infiltration rates' in humans may contribute to large variation in individual responses. Thus, defective rates of CD4+ T cell influx in individuals living with HIV or cancer may impact on the efficacy of CD4+ T cell responses in AS01-adjuvanted vaccines, although this would require testing.

The sensitivity of the parameter controlling naive CD4+ T cell entry under inflammatory conditions indicates a role for regulation of T cell entry and exit in resulting T cell response magnitude. This process may be mediated through changes to chemokine expression, inhibition of S1P receptors and addition of rapid changes to the HEV network providing a mechanism to rapidly change inputs by increase in surface area. High levels of CXCL9/CXCL10 induced by AS01[5] might be consistent with a CXCR3-mediated process, however the murine CD4+ T cell response to AS01 is CXCR3-independent (GSK internal, unpublished data). There is considerable redundancy in inflammatory chemokine responses, thus it is likely that multiple chemokines synergise with other mechanisms. Unpublished data in the Coles group is consistent with rapid changes to HEV network being the primary mechanism driving rapid changes to naive T cell entry, although the mechanism of how early cytokines may drive this in response to AS01 is unclear. However, for infections and the related adjuvant GLA/SE, rapid changes to the HEV surface area occur through vascular dilation, up regulation of Meca79 expression on post capillary venous endothelium

and angiogenesis. Thus, further investigation into the mechanisms underpinning inflammation induced changes to the HEV network is warranted with respect to AS01. Therefore, differences between individuals in both blood flows and naive T cell numbers may have a considerable contribution to 'optimal' CD4 +T cell priming.

In the experimental data used to calibrate models in this chapter, there is considerable uncertainty surrounding the numbers of primed CD4+ T cells, which is captured to some extent in both simulation's trajectories for this specific cell type. Furthermore, due to a generally limited set of data and use of central estimates to calibrate the numbers of *naive* CD4+ T cells, the 'true' distribution of values for the parameter which controls the 'inflammation-induced' influx of naive CD4+ T cells is not yet known. Therefore, while the simulation structure (based on our understanding of the biology) indicates a trend that this parameter is highly influential in the numbers of primed CD4+ T cells, further quantitative work is required to determine the extent of values and variation in this parameter in mice, which can then be used to explore its impact in more detail. Indeed, it will be interesting to further explore the effects of this parameter and its variation (perhaps through bootstrapped sampling to estimate data) on the numbers of primed CD4+ T cells. A limitation of this work is that at this stage, we cannot exclude that the use of estimated data and lack of identifiability in this parameter could perhaps to some extent overstate this parameter's observed influence. In addition, due to the simplicity of the model, this is a population level parameter estimated from fitting data. While the parameter represents a biologically plausible level of priming, there is a large range for priming levels *in vivo*. To confirm this insight does not rest on a specific level of priming, we have confirmed with a model capturing lower cognate priming frequencies that this insight still stands (data not shown). Overall, our current evidence based on the structure of the model, combined with the substantial influence observed on the numbers of primed CD4+ T cells given minor alterations of the parameter, point to a prominent role for the $CD4T0_Inflammatory_Recruitment_p$ parameter, despite the current lack of understanding of its variation.

This exploratory modelling work has thus proposed that the numbers of naive CD4+ T cells capable of entering the dLN during the first seven days of the immune response to AS01, may be vital in the resulting magnitude of CD4+ T cell priming. Interestingly, Moon et al. employed a technique using pMHCII tetramers and magnetic beads to explore rare CD4+ T cells in C57BL/6 mice. [328]. Their work demonstrated that larger naive population size was associated with an increased magnitude of the primary T cell response. Interestingly, they proposed that "variation in naive T cell frequency likely explains why immune responses to some peptides are stronger than others." Further, Jenkins et al. [329] proposed that larger numbers of naive CD4+ T cells are advantageous to the host because

generation of effector cells can occur more quickly, and in the elderly larger populations may be important as smaller populations may be susceptible to extinction. Our model findings are consistent with these results and together we propose that larger naive populations which can be recruited via inflammation may result in an increased magnitude of CD4+ T cell priming after AS01. Furthermore, these findings may have implications for AS01 vaccination strategies. Druzd et al. [323] have demonstrated that circadian rhythm regulates lymphocyte migration throughout lymph nodes and that immunisation timing was critical for the magnitude of the adaptive response. Interestingly, they determined that lymphocyte egress and homing is dependent on oscillatory SIP1R and CCR7 expression. Placing our results in the context of these works and given the potential importance of inflammation-induced naive CD4+ T cell recruitment rates in CD4+ T cell priming after AS01, we suggest the time of day of immunisation be analysed for its effects on CD4+ T cell priming, to determine whether one can improve dosing strategies for AS01-based vaccination.

Exploration and refinement of the hypothesis that IFNγ may enhance DC potency in priming CD4+ T cells: Another aim of this chapter was to explore the hypothesis that IFNγ controls the CD4+ T cell response to AS01-adjuvanted vaccines by *substantially* enhancing DC potency through upregulation of accessory molecules, in turn augmenting the priming of CD4+ T cells. In section 6.2.11, we used both the 'Baseline' and 'Alternate' models to explore the extent to which IFNγ modulates CD4+ T cell priming. We found that while we were unable to reject any hypotheses, many of the explored variants of either model described qualitatively sharp increases which occurred close to the peak of the second 'wave' of IFNγ at around 72 hours post-injection. This sharp increase was in many cases qualitatively inconsistent with the 2W1S+ CD4+ T cell experimental observations at day 5 post-injection of AS01 and antigen. Interestingly, the shape of the inconsistent increase we observed here, was qualitatively similar to the increase observed with the experimental data, however the inconsistency stemmed from the increase occurring too early in the response. Furthermore, we tried to calibrate models with more weight on the IFNγ-dependent priming pathway than is achieved with the 'Alternate' model, however we were unable to produce reasonable fits to the data, consistent with our prior observations. Collectively, these insights implied that our current hypothesis is incomplete. Given the observation that the (qualitatively) inconsistent increase in CD4+ T cells was occurring too early under the above conditions, we proposed that incorporating a delay into the model, between the availability of IFNγ and its enhancement of DC potency, may result in a model that is more in line with the biological data. Immunologically, such a delay would represent

the time it takes for IFNγ-mediated signalling to occur within the DC, so that the cell can upregulate e.g., MHC machinery and co-stimulatory molecules.

Through an *in silico* knockout using the 'Alternate' model, we compared the level of contribution of IFNγ to primed CD4+ T cell numbers, with Coccia's [54] observation of an 80% reduction in the number of Hepatitis B surface antigen (HbsAg)+ CD4+ T cells after an IFNγR-KO *in vivo*. We found that with our model, only a $\sim$19% reduction was observed, clearly substantially lower than observed by Coccia. While the conditions of the experiment *in vivo* differ to those captured by our simulation (Coccia's measurement was at day 7 post a 'day 14 booster', ours at simulated day 7 after primary injection), one would expect more consistency with this experimental data, if the simulation accurately represented the biology underpinning IFNγ's control of CD4+ T cell priming. Furthermore, while increasing the calibrated values of the parameter $cognatePriming_IFNgControlled_p$ would clearly induce a larger drop in the simulated knockout, we found this induces too high numbers of CD4+ T cells to be consistent with CD4+ T cell experimental data used for calibration. Therefore, these mutually exclusive observations led us to conclude that our hypothesis underpinning IFNγ's control of CD4+ T cell priming is incomplete, revealing a gap for an evidence-led refinement to this hypothesis. Indeed, we reasoned that a delay in IFNγ's role on DC potency, coupled with considerable enhancement by IFNγ may bring the model more in line with the experimental data used for calibration, as well as Coccia's observations. An additional facet of this refined hypothesis, is a role for IFNγ in Th1 differentiation, which may also contribute to Coccia's observation. In future work, it would be interesting to explore - using statistical approaches - whether models can be calibrated that more effectively describe the experimental data, capturing different or all facets of this refined hypothesis.

A first step in modelling adaptive responses after AS01: Given the scarcity of relevant experimental data we sought to model simple T cell priming dynamics after AS01. This simplicity is a limitation of this work, and interesting questions surrounding immune correlates and stochasticity of the CD4+ T cell response, more detailed models of CD4+ T cell activation and the effects of varying doses, would be vital to explore in future iterations of modelling. Indeed, we were interested in such questions at the onset of the research project, however we learnt that the current availability of data would not permit such work. We have therefore aimed to extract insight from available data, which can be leveraged to propose valuable *in vivo* and *in vitro* experiments, as well as novel and refined hypotheses. An additional limitation to this work, is the approximate central estimates used for calibration, and in particular the absence of reliable data between 48-168 hours for IFNγ+ NK cells (for which we had no data available to even estimate for these

timepoints). We reasoned that the use of such estimates would permit a reasonable first step in exploratory modelling aimed at generating hypotheses, and is an improvement on an absence of such data altogether. Nevertheless, future work should seek to incorporate further uncertainty around these estimates. Further, while it is generally accepted in the community that IFNγ+ NK cells do not control the second wave of IFNγ, we cannot exclude the possibility that their contribution may be understated. We believe their exclusion beyond 48 hours here is justified at this stage of exploratory research to generate hypotheses, although given further data it would be important to evaluate their potential contribution at these timepoints. Indeed, we have aimed to do the best we can with available data, however more robust experimental data on important cell types, at key timepoints over the first seven days of the immune response to AS01 would be invaluable to future AS01 mechanistic modelling.

Summary: The aims of Chapter 6 (section 1.10) were to develop model(s) and analyse simulation(s) to identify potentially important parameters and mechanisms underpinning the CD4+ T cell response to AS01 adjuvanted vaccines, and also to explore and refine the hypothesis that IFNγ may substantially enhance the T cell priming potency of DCs. Additionally, we aimed to use the simulations to reveal where our understanding of the system is incomplete, and leverage this information to propose refined and novel hypotheses which could thus improve our understanding of AS01 MoA. Through development of multiple models based on available AS01 data, we have been able to pose questions to the domain of interest, identify gaps in understanding, generate and propose novel hypotheses and experiments to fill these gaps. For example, we have observed that gaps exist in our quantitative understanding of IFNγ responses following 48 hours after AS01, as well as generated an hypothesis for why our model cannot fit the monocyte data at 48 hours post-injection. We have refined and produced proposals for important parameters involved with AS01 MoA, thus suggesting key mechanisms which underpin the generation of CD4+ T cell priming after AS01. Notably, we observed that dLN input rates of naive CD4+ T cells may be a significant factor in CD4+ T cell priming after AS01, which provokes questions on whether this process could be enhanced, or whether variation of this parameter in humans may have significant effects on the ability to generate robust immune responses to AS01. Further investigation into this parameter is thus warranted. We have additionally proposed parameters which both models in this chapter are sensitive too, as well as those which are only influential under the 'IFNγ enhancement' hypothesis. Furthermore, the work in this chapter has refined our hypotheses and proposed a new direction regarding the role that IFNγ plays during the generation of an immune response to AS01. In future

work, model calibration could be improved by determining an identifiable subset of parameters, or explore whether the model could be reduced to become identifiable. Furthermore, recent advances in the field which speed-up accurate parameter confidence interval estimation through profile-likelihood estimation e.g., Julia implementation CICO [330], could be employed to assist with the identifiability problem. Looking to the future, the proposed simulation platforms serve as a useful beginning to explore more rich modelling of AS01-induced immune responses, including but not limited to further work on the identifiability problem. Through development and analysis of these models, we have generated hypotheses and further research questions which should be explored and answered with further experimental and/or *in silico* work.

Chapter 7

Discussion

In this thesis, we aimed to use modelling and simulation to compile, integrate, interrogate, analyse and extend the current understanding of AS01 MoA. Indeed, using models and simulations, we aimed to explore and generate new hypotheses - as well as refine old ones - for immune processes underpinning AS01 MoA. As described in section 1.10.2, our specific aims were:

1. Derive a 'core model' of AS01 MoA - describing in detail how AS01 initiates an efficacious immune responses - by integrating and mapping experimental data to known and hypothetical mechanistic function.
2. Develop a mathematical model using the AS01 'core model' to explore early mechanisms regulating IFNγ production induced by AS01. To constrain any developed simulations using available data for parameterisation and validation.
3. Analyse the relative role of different immune cells and cytokines in the early IFNγ response to AS01-adjuvanted vaccines, to determine parameters influential in interferon-gamma production and the role of macrophages in the induction of immune responses to AS01.
4. Generate simulations to identify influential parameters involved in CD4+ T cell priming and to explore hypotheses regarding how IFNγ modulates the CD4+ T cell response to AS01-adjuvanted vaccines.

In this chapter, we reflect upon how these aims and the underlying research questions were addressed, highlighting the contributions made by this thesis to the field of AS01 mechanism of action. We additionally highlight the limitations of this thesis and in turn propose further work and future directions. Throughout this reflection, we propose updates to AS01 MoA as contributed by this thesis.

7.1 Mapping Experimental Data to Known and Hypothetical Mechanistic Function to Produce a Domain Model of the Core AS01 MoA

Prior to the work of this thesis, different elements of AS01's complex MoA were understood, but these had not yet been integrated. The process of integrating current understanding, can not only consolidate 'known knowns' and reveal knowledge gaps, but permits greater rigour on the scientific process by confronting the logical implications of our assumptions and insights[180, 265]. Therefore as our first thesis aim, we set out to develop a 'Domain Model' of the core of AS01 MoA.

We first developed a framework to guide this complex integration of expertise across multiple countries and institutions (Chapter 3, Figure 3.1, [7]). This framework enabled the development of complex models of AS01 MoA and eased communication between researchers with wide-ranging and varied expertise. The framework was applied to the development of the first Domain Model of core AS01-induced immune response, through collective collaboration amongst ourselves and colleagues at GSK (Chapter 3). This model was developed to address question 1 (section 1.10.1):

1. In preclinical models, after intramuscular injection of a vaccine adjuvanted with AS01, how does AS01 initiate an immune response? What are the key interactions that give rise to the generation of antigen-specific CD4+ T cell responses and antibody production? How does IFNγ regulate these processes?

This question was addressed by development of the Core AS01 MoA model presented in Chapter 3, which details our current understanding with respect to the question. Through detailing our current understanding, this process revealed knowledge gaps in AS01 MoA. To our knowledge, this work presents the first detailed theoretical model of an adjuvant's MoA. We propose that our framework could guide and streamline development of Domain Models of other adjuvant MoA, which could not only enable analysis of- and comparison between-adjuvant MoAs, but permit improved transparency of how vaccines work [331]. Further, polls for public opinion on the use of animals in research is predicated on the principles of the 3Rs (replacement, refinement, reduction) being implemented [1]. Modelling provides an ethical way to extract further insight from animal research while adhering to 3Rs principles, and can enable transparency in scientific understanding. Here, the resulting product is a model that integrates AS01 literature, wider immunology knowledge, appropriate hypotheses and abstractions. Development of such a model can produce a platform upon which

[1] NC3RS: Public attitudes toward animal research: https://www.nc3rs.org.uk/news/public-attitudes-towards-animal-research-look-poll

ideas can be generated/shared, or simulations can be built [252]. This process is not simply a repackaging of experimental data. Importantly, through thinking deeply about what one is going to model and how to represent the experimental data, additional knowledge is gained into the consequences of our ideas and experimental insights [180, 265]. Indeed, through forcing explicit representation of experimental insight, the modelling process alone can identify knowledge gaps and logical inconsistencies, which were not known *a priori* and ultimately refine hypotheses, thus contributing knowledge to the biological system. For example, the work in this chapter led to the research questions defined in section 1.10.1.

In this light, this work has provided the first detailed non-executable description of how AS01 is thought to generate immune responses. This model provides additional context to experimental insights, and supplies a platform of extensive diagrams upon which models and simulations can be developed, targeted at specific research questions. Further, the identified knowledge gaps can guide mechanistic modelling and animal experiments. Development of this 'Domain Model' was guided by the framework we developed, which we propose can assist in research into wider adjuvant MoAs.

7.2 A Simulator of the Salient Events in Early IFNγ Production After AS01

The work in Chapter 3 revealed knowledge gaps with respect to AS01 MoA, which were translated into research questions and thesis aims. Therefore, our second aim was to model salient events underpinning the early response to AS01-adjuvanted vaccines, to address our third aim: *explore key questions surrounding IL12, IL18 and the events that give rise to IFNγ production after AS01.* Thus, in Chapter 4, we developed a mechanistic model and simulation to explore the following research questions:

1. The source of IL12 post IM AS01 administration is unknown. Given the assumption that monocytes and DCs both produce IL12 at the same rate, what differences do we observe in the temporal dynamics of cellular IL12 production? What hypotheses do these insights generate?
2. What is the relationship between each cell type's respective production of IL18 or IL12 with the production of IFNγ? How does this differ over time? What is the dominant cytokine in initiating early IFNγ?
3. What are the most influential parameters involved in early IFNγ production after AS01?

4. What effects does the loss of macrophages have on the IFNγ production? What would happen to the immune response if no macrophage cell loss occurs? How could this cell loss affect subsequent primary responses of IFNγ?

While we were aware that it was unlikely that any models of AS01 MoA existed, we first searched the literature for existing models which may have been appropriate. Models that include similar components, i.e IL12 and IFNγ (in the context of Th1 differentiation) do exist in the literature, for example by Puniya et al, [116]. However, we ultimately developed a novel simulation platform as no models matched the planned scope of our modelling exercise. In a wider immunological context, we found a model by Wigginton et al[196], from which we were inspired by the simplicity and success of their approach. Wigginton's model described immune processes similar (e.g cellular activation by cytokines etc) - but by no means identical to - those we had intended to model. Their questions were also related to temporal kinetics and relationships between components etc., albeit for a different immunological system. Therefore, we absorbed their approach to modelling and used the underlying mathematical concepts as inspiration for developing our own.

We employed the CoSMoS process, which facilitated the development of an ODE-based simulation (sections 4.21 - 4.23), whereby the existing experimental data can be traced to the captured biology which in turn can be followed directly through to implementation in computer code, increasing confidence in model construction [242, 256, 252, 257]. We began model development from the core AS01 Domain Model presented in Chapter 3. This model was refined and simplified by considering the relevant processes with respect to the research questions outlined above, resulting in an 'innate IFNγ Domain Model'. Next, the Domain Model was represented in a mathematical and computational specification (Platform Model), from which a set of ODEs were manually derived. The ODEs described the loss of subcapsular macrophages and their production of IL18, inflammatory monocytes and DCs and their separate production of IL12, and how both of these cytokines individually and synergistically stimulate the production of IFNγ from NK cells. As mentioned, mathematical formulations for cytokine-induced cell activation etc, were informed by the model proposed by [196]. After implementation of the ODE model, this system was calibrated to the available experimental data provided by GSK Vaccines (section 4.2.3.1). After *in silico* knockout experiments, we determined that the model was able to describe the validation data, which was withheld from model calibration (section 4.2.3.2).

As several of the model equations exhibit no or limited non-linearity and can simply be written as functions of time, analytical reductions of these equations were solved using Mathematica (section 4.2.2.4). The focus of our efforts was on the behaviour of the model

rather than the underlying mathematical structure, hence the focus has been on simulation rather than analytical mathematical explorations. Parameters involved in such equations were separated from those which are involved in more complex nonlinear equations (Table 4.4). Despite this mathematical work, the model was implemented as a set of ODEs and solved numerically although future implementation of the analytical reductions may simplify numerical simulation. Collectively, the result of this work was a simulation platform that offers a direct mapping back to the biological system, increasing confidence that the simulator is an adequate representation of the underlying biology [205, 243, 257, 239]. Indeed, through validation, the ability to predict *in vivo* outcomes for data upon which the model had not been trained, added confidence that the model was suitable as a platform for *in silico* experimentation. Calibration of this model resulted in 64 parameter sets, each representing a local minima with respect to fitting data. Satisfying our aim, the model fit calibration data well and satisfied our validation criteria. Following calibration and validation, the parameter space was enumerated (Table 4.4) and explored (section 4.2.3.3). Indeed, we visualised the log-transformed parameter space, and for two key parameters involved in the production of IFNγ we visualised different possible model behaviours in different regions of the parameter space (Figure 4.13). This work indicated potential issues with identifiability, as the quantity of IFNγ was considerably sensitive to minor alterations in the values of parameters *vMoIL18* and *VmaxNKaProd1218* (representing macrophage IL18 production and synergistic production of IFNγ induced by IL12 and IL18, respectively).

We had anticipated *a priori* that the model was likely to be non- or only partially-identifiable due to the number of parameters the model contained, in the context of sparse experimental data. Before proposing the final set of ODEs, we performed some model reduction informed by sensitivity analysis, in an attempt to mitigate this issue. Through this process, we removed multiple non-influential parameters (data not shown), which ultimately led to the mathematical model proposed in Chapter 4. Here, we had reached a situation where the mechanism underpinning the model was as simple as possible in order to answer our research questions. Identifiability of mechanistic models is a considerable problem, and it has been proposed that many systems biology models are unidentifiable [301]. In past work in our laboratories, the extent of identifiability analysis has ranged from little consideration, to a scenario with work from Butler [239] where an unidentifiable model was used to generate therapeutic and mechanistic insights which were validated *in vivo*. Given Butler's success and similarities with our situation, we followed a similar framework, where given the potential of non-identifiability, we considered the derived model as a theoretical construct upon which we could identify important mechanisms and eliminate subordinate ones, and explore model behaviours through removing/altering model components, in order

to generate novel hypotheses (and refine old ones) and expand insight regarding AS01 MoA. Guided by Butler's success and Gutenkunst et al's., insights [305], we sought to focus on the capacity of the model to make predictions, rather than to identify precise parameter values. Therefore, we focused on developing confidence in the simulator through a principled design process and robust model validation (section 4.2.3).

Given the importance of identifiability, we did analyse the extent that model parameters could be identified (section 4.2.3.4), which in turn we used to suggest experiments which may improve parameter estimation [9]. Through computing parameter profile-likelihoods, we illustrated that many model parameters are indeed unidentifiable and in turn, that the quantitative understanding of the innate IFNγ response to AS01 is limited (Figures 4.18 and 4.19). We leveraged this analysis and proposed experiments and provided insight which could improve the identifiability of the model and therefore our quantitative understanding of AS01 MoA. In particular, this led us suggest that model identifiability could be greatly improved by the acquisition and inclusion of time-series data for the concentrations of QS21 and/or MPL. These components are modelled as fixed-parameters, therefore a more precise parameterisation of the model and the resulting dynamics may be enabled if information on their rates of change were available. Furthermore, such data could enable *in silico* explorations into potential improvements for dosing strategies, which is increasingly important given the current public attention regarding vaccination. We additionally observed evidence that the parameters controlling IL12 production could be identified given further data. Indeed, we argued that examining concentrations of IL12 *in vitro* may provide significant insight into our understanding of the system and may help constrain key parameter values. Furthermore, for the two parameters controlling IL12 production, *vMonocIL12* and *vDCIL12*, we observed almost-flat profile-likelihoods which generally suggests subordinate mechanisms captured by the parameters. However, in Chapter 5, sensitivity analysis revealed that these two parameters are influential for the concentration of IFNγ throughout the duration of the simulation, given our hypotheses underpinning the model and with respect to captured biology. Therefore, despite a flat profile likelihood, the parameters are worth examining in further detail. In summary, we have satisfied aim 2 by deriving - to our knowledge - the first mechanistic model and simulation of AS01-adjuvanted vaccine MoA, for the exploration of key research questions surrounding the production of innate IFNγ after AS01-adjuvanted vaccines. Further, we explored the identifiability of the model, which shed light on our limited quantitative understanding of early AS01-induced immune responses and in turn we have leveraged these insights to guide experiments which could reduce the gaps in quantitative understanding.

7.3 Analysing the Relative Contribution of Cells and Cytokines During the Early AS01 Response

Throughout this thesis we have not systematically considered the entire parameter space for any model as this was not required in order to answer our research questions. Instead, we have examined different model behaviours in different regions of the parameter space, with respect to our questions of interest. For the analysis of the IFNγ model however, we employed eFAST to systematically address perturbations with relevance to our research questions. In this section I will discuss how we addressed aim 3. Here, we utilised the model developed in Chapter 4, to explore the relative roles of cells and cytokines during the IFNγ response to AS01. Additionally to satisfy this aim, we identified influential parameters in IFNγ production, and explored the role of macrophages during early AS01 immune responses. First, we explored the question:

The source of IL12 post IM AS01 administration is unknown. Given the assumption that monocytes and DCs both produce IL12 at the same rate, what differences do we observe in the temporal dynamics of cellular IL12 production? What hypotheses do these insights generate? This question was explored in section 5.2.2. We employed eFAST global sensitivity analysis to examine, based on our hypothesis that DCs and monocytes produce IL12 and the assumption that both cell types produce IL12 at similar if not identical rates, the resulting temporal dynamics of cellular IL12 production. Indeed, we computed the total and first order sensitivities, and we found that DCs are the dominant IL12-producing cell early during the simulated response to AS01, although by approximately 15 hours post-injection monocyte and DC influence becomes similar. Interestingly, the time-scale of early DC dominance with IL12 production, suggests that DCs in the dLN early during the response, may provide an important early IL12 signal to promote IFNγ production after AS01.

We suggest that this work highlights the power of integrating computational modelling with experimental work. Indeed, the use of a computational technique to explore this question was particularly attractive as following discussions with GSK immunologists, we learnt that it is difficult to reliably measure the concentration of IL12 in dLNs *in vivo*. It is well-characterised that DCs produce IL12 [332, 69] and it has been demonstrated that monocytes produce IL12 *in vivo* and *in vitro* and indeed are in some cases the primary source [67, 333, 66, 332]. Indeed, monocytes have been shown to produce IL12 after CpG adjuvanted protein vaccination, while a subset of DCs which are known to express IL12 have been observed in dLNs after AS01 [106, 95]. Therefore, through capturing these immunologically reasonable hypotheses and utilising modelling and simulation techniques, we

have refined the hypothesis for how IL12 is produced after AS01-adjuvanted vaccination. To confirm or refute this new hypothesis, lineage-specific IL12 knockout mice could evaluate the individual contributions of monocytes and DCs to IL12 after AS01-adjuvanted vaccination. Not only could this provide added confidence in the simulator, confirmation of IL12 production by these cells *in vivo* or even *in vitro*, would add further weight to the the predicted temporal kinetics of cellular IL12 production by our model, overseen by a process of model-driven-experimentation [169]. At this stage, our model finding suggested that through an early signal of IL12, DCs may play a key role in initiating IFNγ production after AS01-adjuvanted vaccination, extending and building on our hypothesis in Chapter 3 and Chapter 4, that both DCs and monocytes produce IL12. If experimental evidence is obtained for our observations, we propose that individual variation in input rates of DCs into dLNs during inflammation may in-part contribute to the variation observed in human vaccine responses. Indeed, such variation in humans may be compounded by regulatory processes e.g., circadian rhythm [323], where recruitment rates of cells e.g., DCs change throughout the day. Given the current COVID-19 crisis, further work to evaluate the effects of dosing and time of day of vaccination are ongoing and it is plausible that our findings here - albeit from mouse data - may reflect some of the variations observed in human vaccine responses.

What is the relationship between each cell type's respective production of IL18 or IL12 with the production of IFNγ? How does this differ over time? What is the dominant cytokine in initiating early IFNγ? To elucidate relationships between cellular production of IL18, IL12 and subsequent IFNγ, we examined the effects of perturbing parameters of interest, performed *in silico* knockout experiments and eFAST-based global sensitivity analysis. Indeed, we sought to deconvolute the impact of each cytokine-production parameter on IFNγ production (section 5.2.3, Figures 5.6-5.9). Within the model, macrophage-induced IL18 is substantially more influential than either, or both of the IL12 production parameters combined, with regard to the production of IFNγ. This builds on evidence by Coccia et al. [32], who found that IL18 promotes IFNγ production, supported in synergy by IL12. Indeed, Coccia et al observed that IFNγ+ NK cells were affected more in IL18R$^{-/-}$ mice, compared with αIL12 depletion in C57BL-6 mice. Coccia's findings informed the conceptual development of our model, although the quantitative data was reserved as model validation data. Indeed, through model validation, we observed that the model could describe Coccia's data after simulated knockouts. Not only is the model able to describe Coccia's data upon which it was not calibrated, it is able to extend the insights extracted from the data.

It is difficult to measure IL12 and IL18 concentrations *in vivo* and thus we have no measurements for these cytokines. Therefore, this modelling work adds to our understanding of AS01 MoA by giving us an idea of the scales of influence of IL18 vs. IL12 in initiating IFNγ, allowing us to understand the impact of each cytokine. Indeed, the model itself has provided a viewpoint to how each cytokine is behaving in the system, which could not be deduced solely from the experimental data. This work therefore extends our current understanding of AS01 MoA which we proposed in Chapter 3, by furthering evidence for a quantitative hierarchy in influence of the cytokines involved in initiating IFNγ after AS01. This work additionally generated the novel hypothesis that DCs are the primary contributor of IL12 to the peak of IFNγ observed at six hours. Coccia implied that pre-positioned cells in the dLN are targeted by AS01, which then promote innate IFNγ. Our insights here are consistent with Coccia's suggestion. The biological data used to fit the model showed higher numbers of DCs in the dLN at early time points than monocytes, and in turn the mechanistic model indicates that DCs may not only provide this early signal of IL12, but be dominant in its production over the first 15 hours. It would therefore be interesting to examine the effects on early IFNγ production after depletion of DCs into AS01-adjuvanted mice, which may indicate whether these cells are indeed the primary contributor of IL12 to early IFNγ after AS01.

Interestingly it appears that during latter stages of simulation, dominating numbers of infiltrating monocytes cannot compensate for the IL12 influence by DCs. Migratory DCs take some time (between 8 and potentially 16 hours [30]) to arrive in the dLN, therefore we suggest that our insights are consistent with dLN resident DCs providing this early IL12 signal. We were not able to test this directly however, as for simplicity, none of our modelling distinguished DC subsets. This particular insight rests upon the reasonable hypothesis that both DCs and monocytes produce IL12 after AS01. If we carry over the understanding from other systems that DCs and monocytes are capable of producing IL12 [69, 106, 95] - which we used as a working hypothesis - the implications are that the model indicates DCs primarily provide an early IL12 signal to promote IFNγ after AS01, alongside macrophage-induced IL18. Dose-response experiments *in vitro* assessing DC and monocyte production of IL12 after AS01 would additionally enable identification of respective cytokine production parameters, thus permitting a further iteration of model-driven-experimentation [334] and the potential to extract further insights from available biological data.

What effects does the loss of macrophages have on the IFNγ production? What would happen to the immune response if no macrophage cell loss occurs? How could this cell loss affect IFNγ responses after a second AS01 delivery? In light of the previous model finding that macrophage-released IL18 is dominant in promoting

IFNγ production after AS01, we examined the role of macrophages in the early simulated IFN response. We observed that rates of macrophage cell loss CL_p influenced the IFNγ production, and qualitative reasoning argues this effect would be negative.

Innate-IFNγ availability after AS01-adjuvanted vacccination is transient, peaking at approximately 6 hours post-injection before returning almost to baseline levels by 24 hours post-injection. Given that macrophages are the only known IL18-producing cell in this system and CL_p contributes to their loss, this insight suggested that a downstream effect of QS21-induced macrophage cell loss is a contribution to the transience of IFNγ by limiting available IL18. Indeed, we observed that without this cell loss, the simulation predicted substantial amounts of IFNγ would be produced (section 5.2.4.1). The concentrations of cytokines and numbers of cell-types predicted by this particular analysis were unphysiological and we are clear that we are not aiming to quantify these concentrations in such a scenario. Rather, as our model structure is grounded in available experimental data and given the logical implications of these trends, collectively our observations strongly suggest that QS21-induced loss of macrophages could serve as a negative regulator contributing to the transience of IFNγ production. At first glance, the suggestion that QS21 performs both pro and anti-inflammatory functionality may appear contradictory, however these seemingly antithetical functions of QS21 occur on different timescales. Indeed, release of IL18 is predicted to occur rapidly over the first hours of the response to AS01, whilst model analysis indicates that QS21's antagonistic effects play a more prominent role after this (Figure 5.6).

Two recent works have highlighted that QS21's immunological MoA is incompletely understood [156, 146]. Adding to this gap, the findings in this thesis propose a novel hypothesis for QS21 during immune responses. Prior to the work in this thesis, it was known that QS21 performed pro-inflammatory functionality via stimulating IL18 from macrophages which promoted IFNγ[32]. Additionally, it was known that QS21 induces a loss of these cells[8] although the mechanism for which remains unclear, but is hypothesised to be by pyroptosis. These insights were modelled in Chapter 3 as part of our 'Core AS01 MoA model'. The model findings in Chapter 5 extend the previous understanding by indicating that as well as performing pro-inflammatory functionality, QS21-induced cell loss may negatively regulate the production of IFNγ. This work therefore extends our current understanding of AS01 MoA that is proposed in Chapter 3. Taken together with the model finding that IL18 is the dominant cytokine in initiating IFNγ production after AS01-adjuvanted vaccination (section 5.2.3), our work substantiates the importance of QS21-induced IL18, and suggests a role for QS21 in limiting IFNγ availability.

We next explored the hypothesis that delayed macrophage recovery could 'interfere' with a second vaccine delivery of AS01 that occurred within a month of the first injection.

Indeed, with data we are unable to show, GSK have observed possible interference in the immune response if multiple AS01-based vaccinations occur too close to each other. These observations were made in the context of a prime-boost regimen and questions have also been raised regarding whether interference may be observed with two innoculations containing AS01 but different antigens, were to occur too close to each other. To explore such questions, we simulated IFNγ responses to two consecutive (with a gap of x days) vaccinations with AS01. The modelling indicated that the absence of macrophages would be detrimental to the IFN response following second vaccine delivery. Importantly, our results suggest that a refractory period exists following AS01-induced responses. Indeed, the model predicted that the IFNγ response would be detrimentally affected in a situation where there is a reduction in available macrophages. In the average case, our work suggested that a few weeks may be a sufficient refractory period although we observed considerable uncertainty around these predictions. 'Macrophage cell loss' following vaccination is a reasonably recent experimental finding [8, 311] and there is very limited data available on this effect. Indeed, previous observations in a wider system demonstrates that there is approximately a full recovery of the macrophage layer after 28 days, which informed a linear model to predict numbers of recovered macrophages at day x following the first injection, which in turn fed the analysis in section 5.2.4.2. This work is limited by the use of a single observation for macrophage recovery to inform such predictions and these efforts could be refined by further data on macrophage recovery, which to our knowledge is not publicly available. Furthermore, we were limited by the assumption of linear recovery and the uncertainty around such predictions may be reduced using a different model of macrophage recovery, informed by further data on the numbers of macrophages at timepoints during the refractory period.

Our insights are based on simulations emulating a second AS01 delivery. However, under a recall response we cannot exclude the possibility that antigen-specific IL2 production may be able to recapitulate IFNγ production [310] amongst limited IL18-producing macrophages. Therefore, it will be interesting to examine the interplay between IL12, IL2 and limited IL18 during recall responses to AS01, potential refractory periods, required thresholds of cytokines for canonical IFNγ as well as the spatial dynamics of cellular production (see Discussion Chapter 5 for more detail). We were unable to explore the effects of interference in a prime-boost scenario due to data availability. In light of such data, the simulations presented in this thesis could be extended to explore such questions as well as improvements to prime-boost dosing strategies for AS01-adjuvanted vaccines. The work in this thesis is based on mouse data, and therefore mechanistic models of murine immune responses are developed. This is a limitation of the thesis and naturally, translational work is required to

further these insights, and in this context to improve dose scheduling by accommodating a potential refractory period in humans.

With respect to human vaccination, the insights here generate the hypothesis that similar mechanisms may in-part explain e.g., observations that the efficacy of the ChAdOx1 nCoV-19 vaccine was increased in participants who received a low dose followed by a standard dose (90% efficacy), compared with those who received two standard doses (62.1% efficacy)[308]. ChAdOx1 nCoV-19 and vaccines containing AS01 employ different mechanisms to promote protection. However it is reasonable to speculate, given our findings in the context of available data, that a similar mechanism could be at play, whereby a refractory period - induced by the required recovery of immune component(s) - must be accommodated in order to promote the most effective immune responses to vaccination. This effect may not be realised by the same mechanism with other vaccines (i.e cell loss of macrophages), although we speculate this may occur through accommodating other negative regulatory pathways. To mitigate detrimental effects, we propose two hypotheses to study. First, one should examine the effects of waiting set times before administering the second dose. The most effective refractory periods therefore remain to be elucidated and are likely vaccine-formulation specific. Second, the first dose could be lowered, initiating an immune response perhaps avoiding an intense incapacitation of innate cell activation, which may in-part explain the increased efficacy observed by Voysey et al.

Our findings may have important consequences for the timing and dosing of vaccination regimens. Indeed, we advocate that the potential interference with IFNγ production following a second vaccine delivery, during delayed macrophage recovery is important and given recent consistent observations with other vaccines, including ChAdOx nCoV-19 and RTS,S/AS01 where a delayed fractional dose improves protection[335], we propose that this phenomenon warrants further attention and study. While we additionally advocate further detailed investigations into these effects in humans, we aim to begin such work by examining how many mice would be required to explore these questions and provide statistical power. Overall, model analysis indicates a refractory period following AS01-based vaccinations due to delayed macrophage recovery, and suggests this must be accommodated to generate effective second AS01-based vaccinations. Further, we suggest such mechanisms may provoke the observed 'interference' after a prime-boost vaccination with AS01, although such a mechanism remains to be elucidated and could be suggested through further *in silico* work provided appropriate data. Lastly, our work suggests that perhaps in humans, observed improvements in efficacy after delayed and/or fractional dosing [312, 308, 335] are plausibly mediated through accommodation of refractory periods, which may be caused by similar

mechanisms. In light of our findings, we suggest such effects should be studied as an aspect of perhaps related observations in human vaccines.

7.4 Exploring Parameters influential in CD4+ T cell priming after AS01 and Hypotheses regarding how IFNγ modulates this Process

To address aim 4 and investigate mechanisms underpinning priming of CD4+ T cells after AS01-adjuvanted vaccination and explore hypotheses for how IFNγ controls this process, an extension of the model developed in Chapter 4 was required. We first determined that no suitable models were available and initiated the CoSMoS process, resulting in the 'Baseline AS01 CD4+ T cell' model (sections 6.2.1 - 6.2.3). We calibrated and validated 'Baseline' and 'Alternate' models, representing variants of the hypothesis for the extent that IFNγ controls CD4+ T cell priming. These models both exhibited room for improvement in calibration. Models where calibration has room for improvement, have provided significant contributions to fields of immunology, [257] and partially-identifiable models such as those presented in this thesis, have also provided mechanistic and therapeutic insight [169]. To add value to our understanding of AS01 MoA, we leveraged the inconsistencies between our Baseline model and the experimental data (section 6.2.6), to reveal where our understanding of AS01 MoA is lacking. For example, we observed that despite its importance in the AS01-induced immune response, large gaps remain in our quantitative understanding of IFNγ production, in particular following 48 hours post-injection (section 6.2.6.2). While multiple published works on AS01 MoA describe IFNγ kinetics over time after AS01[5, 54], we proposed that by increasing the sampling frequency at key timepoints, we would likely gain a deeper understanding of the two 'waves' of IFNγ during an immune response to AS01. To improve the design of next-generation vaccines, it is paramount to understand current clinically efficacious adjuvants. Therefore, insights provided by the mechanistic models developed in Chapter 6, led us to propose novel hypotheses (and refine old ones) and targeted research questions which could be explored *in vivo* or *in silico* to reduce the quantitative uncertainty of such an important characteristic of AS01's immune response.

Work in Chapter 6 was limited by data availability, thus we aimed to do the best with the data that we had. This naturally led to limitations with this chapter, in particular we were limited to suggesting trends based on models that capture our current understanding of the biological system. We therefore propose that comprehensive *in vivo* datasets, measuring longitudinal, canonical AS01-induced dynamics of different cell types and cytokines after consistent experimental protocols, would be valuable and would enable one to expand and substantiate the insights generated in particular in Chapter 6.

To identify parameters which the numbers of primed CD4+ T cells are not robust to in both the 'Alternate' and 'Baseline' models, we performed local sensitivity analysis examining different model behaviours at different regions of the parameter space (sections 6.2.8 and 6.2.10). Interestingly, we observed that the parameter controlling naive CD4+ T cell recruitment was of particular importance in both models, suggesting an important unknown mechanism underpinning CD4+ T cell responses after AS01. Furthermore, we utilised local sensitivities to identify parameters which were sensitive in the 'Alternate' model and not the 'Baseline', indicating those which would be important under the hypothesis that IFNγ influences CD4+ T cell priming via enhancing DC potency. Examining parameters that are influential in simulated numbers of primed CD4+ T cells, is not only vital for revealing key mechanisms underpinning a successful adjuvant, but such insights may also be used to improve the next generation of adjuvants. While multiple interesting temporal observations were reported through the local sensitivity analysis of these two models, we focus here on two findings. First, extending the finding in Chapter 5 that QS21 both negatively and positively regulates and influence IFNγ, we observed that under the 'IFNγ enhancement hypothesis' these pleiotropic roles of QS21 would negatively and positively influence simulated numbers of primed CD4+ T cells. Despite long-standing knowledge of QS21's immunostimulatory capabilities, recent work has highlighted that QS21's MoA is not well understood [146, 156]. Our work in Chapter 5 then adds to this gap in understanding by proposing QS21 negatively and positively influences IFNγ production. Chapter 6 then extends this hypothesis by suggesting that if the 'IFNγ enhancement hypothesis' is accepted, QS21 may negatively and positively influence the priming of CD4+ T cells.

Our second key model finding regarding influential parameters and mechanisms underpinning simulated primed CD4+ T cells after AS01, was the observation that the numbers of these cells were not robust to minor alterations in the parameter controlling naive CD4+ T cell recruitment (section 6.2.10). As discussed previously in further detail, understanding the immune processes which influence the generation of primed CD4+ T cells during adjuvanted-vaccination is an important question, firstly to provide a baseline of understanding of how a successful adjuvant works, but also to consider ideas for improving the next generation of adjuvants. Given the substantial influence of the mechanism captured by this parameter, we propose this warrants *in vivo* and *in silico* investigations into the unknown factor(s) controlling naive CD4+ T cell recruitment into the dLN after AS01 and whether different factors are influential at different timepoints during the response etc. For example, models developed in this thesis could be extended to incorporate naive CD4+ T cell recruitment in more detail. Furthermore, if data are generated describing QS21 and MPL concentrations in the dLN over time, dosing strategies at simulated times of day could

be also explored. Due to limitations in the experimental data and our use of single-point estimates to incorporate further data for calibration, our quantitative understanding of this parameter and its variation is limited. This is a limitation of this work, however the magnitude of the observed sensitivity of this parameter and the potential implications, warrant a further exploration into this parameter, its variation, as well as its effects *in vivo*. We intend to perform further *in silico* work to examine this parameter in further detail.

Our work suggests that it may be possible to increase the magnitude of CD4+ T cell priming after AS01 by exploring vaccination at different times of day. Additionally, given the inherent large variation in the human population these data suggests that there is the potential for deficits in the mechanisms that this parameter captures to contribute to suboptimal CD4+ T cell responses after adjuvanted-vaccination. Taken together, we proposed an investigation into the effects on the magnitude of the CD4+ T cell response after AS01-adjuvanted vaccination through alternating the time of day and examining whether significant effects are observed. A growing body of literature demonstrates oscillations in immune function throughout the day associated with circadian clock [336, 337, 338, 339, 340, 341, 342]. Indeed, Long et al.[342] observed that morning vaccination enhances antibody response over afternoon vaccination, whilst Charlotte et al. [343] observed superior cytokine production in individuals vaccinated with BCG in the morning compared to the evening. Indeed for AS01 and other adjuvanted-vaccinations, in light of our results and the body of literature indicating differential immune responses throughout the day, we proposed experiments comparing the magnitude of antigen-specific, polyfunctional CD4+ T cell responses in the morning, afternoon and evening. If time of day is shown to affect the magnitude of the immune response to adjuvanted-vaccination, this could provide an important way to improve protection with limited cost.

Both the 'Alternate' and 'Baseline' models were employed with the aim of exploring whether one could indicate the extent that IFNγ may modulate the CD4+ T cell response by enhancing DC priming potency (section 6.2.1.1). Unfortunately, given the analysis performed we were unable to distinguish any of the hypotheses at this level of the data. To examine, reject or accept any of our hypotheses, a detailed statistical analysis will be required. Notwithstanding, our exploratory work in this remit guided a refinement of the hypotheses we made upon beginning this work. Our exploratory analysis indicated that our hypotheses under the model were incomplete and thus required refinement. In section 6.2.11.3, we argued that a delay between IFNγ availability and any enhancement of DC potency, perhaps coupled with considerable enhancement of DC priming by IFNγ may result in a model that conforms better to the experimental data used for calibration, as well as Coccia's observations [54]. Furthermore, we reasoned that another missing component

may be Th1 differentiation which is modulated by IFNγ and IL12 [344], which may add to how IFNγ might control the numbers of polyfunctional CD4+ T cells. Therefore, exploratory mechanistic modelling has guided the refinement of our hypotheses underpinning AS01 MoA. Despite our efforts, the role of IFNγ remains unclear, although the work in Chapter 6 has refined current understanding, by subjecting a hypothesis to analysis which was subsequently modified in light of new evidence that suggests the original hypothesis was incomplete. Future modelling iterations could seek to extend the models developed here to capture the above refined hypothesis, and employ a rigorous statistical examination to reject or accept different facets of the hypotheses proposed here. Model variants capturing different strands of the above hypothesis could then be compared using Akaike's information criterion [345], which attempts to quantify the ability of a model fit to observational data. Such techniques have provided insight into immunological systems [199].

In this thesis, we have argued that our research interests and the resulting conclusions do not rest upon the stability of steady-states, thus we opted not to focus on this analysis. Indeed, our questions were related to relationships between components and temporal dynamics, not whether steady states are stable. Nonetheless, stability analysis is often valuable, e.g providing insight into macrophage crosstalk with tissue microenvironments by revealing that a negative regulatory loop on their growth factors is required for a stable number of macrophages and fibroblasts [204]. A future vision of the author, pending further development and data generation, is for these AS01 mathematical models to be refined and extended to explore how effective vaccine priming can control subsequent Malaria infection, and examine characteristics where control occurs and where immunity wanes. Indeed, an interesting role for stability analysis would be to determine stable steady-states where there are no Malaria-infected-erythrocytes in RTS/AS01 vaccinated individuals who (after vaccination) were infected with Malaria, perhaps suggesting mechanisms involved in vaccine-protection.

In summary, Chapter 6 provides the first mathematical models and computer simulations of CD4+ T cell priming after AS01 adjuvanted-vaccination. These models were employed for exploratory analysis, to reveal 1) where our quantitative understanding of the system is limited and to guide experiments which could help fill these gaps, 2) to propose important mechanisms underpinning the CD4+ T cell response to this adjuvant, as well as an experimental avenue which may improve the magnitude of this response in next-generation adjuvants, and 3) to propose a refined hypothesis for how IFNγ may control CD4+ T cell responses after AS01.

7.5 Summary of Novel Contributions

The work I have presented in this thesis represents the 'model-driven' portion of model-driven-experimentation. The analyses throughout Chapters 4-6 of this thesis have been made possible through the integration of experimental data, mechanistic hypotheses and immunological understanding underpinning AS01 MoA (see Chapter 3). In summary, I have satisfied the aims of the thesis, while highlighting limitations of our work and proposed future directions, some of which we intend to soon start. I have developed new theoretical models describing AS01 mechanism-of-action, and analysed these models to provide novel insights into AS01 MoA. I have supplied the first Domain Model of Core AS01 MoA [7], integrating and mapping experimental insight to detailed, hypothesised mechanistic function. This Domain Model captures how AS01 is thought to generate both antibody and CD4+ T cell responses, based on carefully thinking through hypotheses surrounding AS01 MoA. Indeed, such work not only provided the first detailed description of AS01 mechanism-of-action, but through subjecting experimental insights to the logical implications of holistically integrating such knowledge, we identified knowledge gaps and important research questions. Indeed, such work demonstrates the consistency of the experimental data, and furthermore this work is an example of the insight that developing mechanistic models can provide to immunology.

The core AS01 MoA model informed the development of the first mechanistic simulations of AS01 MoA. Through developing and analysing a simulation of the salient events leading to IFNγ production, I have provided insights into AS01 MoA via predictions and refined and novel hypotheses that can be tested experimentally. Examples of these insights include but are not limited to predictions regarding the temporal dynamics of cellular IL12 production and substantial evidence that IL18 dominates over IL12 in initiating innate IFNγ. Furthermore, I provided evidence for the novel hypothesis that in the case of AS01, failure to accommodate a refractory period between consecutive AS01 vaccinations could lead to detrimental immune responses, due to a delayed recovery of IL18-producing macrophages. Given recent wider observations regarding increased efficacy after increased spacing between doses in humans, we proposed hypotheses underpinning such effects. Additionally, our modelling provided evidence that QS21 is both a negative and positive regulator during AS01-induced immune responses, which adds a hypothesis to the gap of understanding in QS21's role during immune responses. I extended the 'innate IFNγ model' to capture simple 'Baseline' and 'Alternate' implementations of CD4+ T cell priming, capturing varying hypotheses to explore how IFNγ may modulate the CD4+ T cell response to AS01, and to identify key contributors to these cell's priming. Through model development, I found that

our quantitative and mechanistic understanding as dictated by available data is limited and in places unable to conform as well as hoped to experimental data. I therefore presented refined hypotheses in light of these findings which could be tested experimentally and could provide further data for modelling.

My analysis of the AS01 CD4+ T cell priming models suggested that the rate of recruitment of naive CD4+ T cells into the dLN under inflammatory conditions could be vital for the levels of primed CD4+ T cells observed in the experimental data, which in turn suggests one may be able to increase the magnitude of CD4+ T cell responses to AS01 by exploring different times of day for vaccination. I therefore proposed an avenue of research which may prove fruitful in the design of next-generation adjuvants. Furthermore, this work led to the refinement of our hypothesis for how IFNγ controls CD4+ T cell responses to AS01. Indeed, after being confronted by evidence from our analysis that our model was incomplete, I proposed the refined hypothesis that after IFNγ production occurs, there is a delay where DCs process available IFNγ which results in enhanced DC potency, and therefore considerably enhanced CD4+ T cell priming. Furthermore, IFNγ is also likely to control CD4+ T cell responses to AS01 by (alongside IL12) dictating Th1 polarisation.

Collectively, this thesis therefore provides a substantial first step in mechanistic modelling of AS01 MoA, supplying models, novel and refined hypotheses of AS01 MoA and novel insights and knowledge that can be tested experimentally, thus supporting knowledge generation. Prof. Sir. Paul Nurse recently argued that ideas, as well as data should be generated in order to extend biological knowledge [265]. Of note, he argued for modelling molecular and cellular components of a biological phenomena, as well as writing down equations to impose greater rigour on model building. While Nurse's comments are very recent, such philosophy has been an overarching aim of this thesis throughout my study. Indeed, we have aimed to take the available experimental data, carefully develop mechanistic models, and use these models to refine and extend current understanding of AS01's MoA, and where possible generate new hypotheses and ideas. Given further data, some insights from this thesis will likely be refined. As Nurse argues"it's important to get the facts right, but new ideas are useful, as long as they are based on reasonable evidence and are amenable to correction".

Given that modelling had not previously been applied to AS01 MoA, we employed simple model development and analyses to explore the immune response to a successful adjuvant. In turn, we have articulated for the first time the the current holistic understanding of its MoA and proposed novel insights surrounding its MoA which can be tested experimentally, e.g., a refractory period of AS01 as well as the suggestion that CD4+ T cell responses to AS01 may be enhanced by exploring different time of day for vaccination. Many problems regarding

AS01 MoA remain unsolved, however this thesis has provided a gateway in mechanistic modelling of AS01 MoA. By development of mechanistic models for AS01 mode-of-action and developing refined and proposing novel hypotheses which can be tested *in vivo*, we have provided a significant foundation upon which future research can build. We believe that the techniques employed in this thesis could be applied in a wider setting to improve the understanding of other adjuvant's mechanism-of-action.

7.6 Future Directions

It is our opinion that the most fruitful next step in this work would be to perform *in vitro* and *in vivo* experiments proposed throughout this thesis to increase data availability and confirm or reject findings and propositions from the thesis. New data can then be fed back into the modelling process to develop more sophisticated models and explore further complex research questions.

At the beginning of this project, we first set out to answer complex questions e.g., exploring improvements to vaccination dosing strategies, stochasticity and its role in T cell responses induced by AS01, as well as potentially to suggest correlates of immunity and/or protection. However, after an extensive process of gathering disparate, available experimental data housed across three European countries, we quickly learnt that the data was quite scant and we thus scaled back our ambitions to that which could be afforded by the data. Therefore, throughout this study and the work in this thesis, we have proposed avenues of research targeted not only at improving the understanding of AS01 MoA, but which would permit further computational exploration thus enhancing the insights which could be extracted from the data. Throughout the thesis we have therefore proposed avenues of research which would not only improve the understanding of AS01 MoA, but permit further computational exploration. In particular, generated data describing the concentrations of QS21 and MPL in the dLN over the first few days after AS01-based vaccination could plausibly permit exploratory analysis of dosing strategies with respect to key endpoints e.g., IFNγ production and/or primed CD4+ T cells. Given the partial-identifiability of each model developed here, *in vitro* experiments which aid the identification of cytokine production and cell activation rates etc would also be extremely valuable in attempts to analyse practical identifiability. *In vivo* quantifications of vaccine component concentrations would further enhance this work. Alternate approaches for model calibration could further explore the parameter space to potentially capture more detail from the wide uncertainty in the biological data. This may be achieved using a Bayesian approach [247] where e.g., Markov-chain-Monte-Carlo approaches could be used to estimate the posterior distributions of model parameters [346]. Bayesian approaches are reliant on conditional probability, which

is not the case with Frequentist approaches. For more complex distributions, the posteriors can provide significant value. For example, if two peaks are observed, estimating only the mean and standard deviation is suboptimal, rather the posterior distribution may be able to supply the diversity of behaviour. Frequentist approaches were adopted here, for simplicity in the first steps of modelling AS01 MoA. Further, future work should seek to incorporate further uncertainty around the single-point estimates used to calibrate the CD4+ T cell priming models. Indeed, bootstrap sampling should be able to permit the incorporation of further uncertainty in such estimates, into the modelling work. Such work is currently ongoing.

Furthermore, recent and exciting computational language advances such as 'Julia' [347] may permit analysis with complex mathematical models which is current infeasible. Indeed, solving complex mathematical models takes time. For example, to perform global sensitivity analysis on a model with large numbers of free parameters (such as those presented in Chapter 6 of this thesis), one must sufficiently sample the parameter space and simulate the results. This combinatorial explosion in the search space results in enormous time and resources required to simulate the ordinary differential equations by using programming languages such as R or even C. Indeed, we deemed this problem currently too complex, hence the lack of a *global* sensitivity analysis in Chapter 6. With Julia, Roesch et al. report simulation of biological models can be 50-400 times faster than in R or Python. It would be interesting to examine whether such a performance improvement would be observed through implementing the models presented in Chapter 6, and whether this may permit a thorough global sensitivity analysis. Such advances in computational efficiency has the potential to revolutionise and streamline workflows by integrating mechanistic modelling into experimental medicine pipelines.

Animal models are widely used to model human disease and test the efficacy of vaccines and therapeutics [348]. Such models have provided significant insight into the mechanisms underpinning health and disease. However, in recent years there has been growing appreciation for the fundamental differences between mouse models and human biology, and the impacts on translational research [349, 350, 351]. Through describing known immunological, physiological, genetic etc differences between species such as those used in animal models e.g., mice we propose that it may be possible to take an *in silico* mouse model and make predictions about kinetics in another species e.g., humans. We propose that an important, initial avenue of future research in this direction, pending data availability, would be to use e.g., the murine innate IFNγ model developed here, one could aim to predict the corresponding data describing the dynamics in non-human-primates. We hypothesise that this could be realised by developing a platform capturing known relevant immunological,

physiological and genetic differences between these species, which could be leveraged to make such predictions. It is our strong belief that work such as this - which has strong '3Rs application - has the capacity to radically enhance experimental medicine efforts, and streamline the drug and vaccine development process - which would prove invaluable in combating pandemic and endemic disease.

Finally, Chapter 3 of this thesis presented the first holistic and detailed model of the current knowledge of AS01 MoA, including hypotheses for gaps in understanding. Alongside the aim of Chapter 3 to develop a knowledge-base from which mechanistic models and simulations could be constructed -through detailed further analysis of the insights from experimental data and the logical implications of the holistic perspective of these insights - an overarching implicit aim and philosophy of this thesis was to provide further transparency into AS01-adjuvanted vaccine MoA. Transparency of this information is important, not only to communicate expert thinking to the wider research community for scrutiny, but to provide a basis for further communication of expert understanding of vaccines and how they work[331]. Compounding this benefit of transparency, is that holistic and detailed non-executable models of complex adjuvant MoAs can provide a platform for further mechanistic modelling and/or statistical analysis. We therefore propose that the application of such efforts in understanding wider adjuvant MoA could be powerful, and has the potential to extract further mechanistic insight from currently available experimental data, while adhering to the principles of the 3Rs. Such work can take place within a cycle of model-driven-experimentation, thus guiding experimental design through proposing fruitful avenues of research, with the ultimate aim of improving the understanding of current adjuvant MoAs, in order to enhance the effectiveness of the next-generation of adjuvanted-vaccines.

List of Abbreviations and Glossary

ABM – agent-based model: A modelling approach where each individual entity is explicitly represented. Agent behaviour is governed by a set of pre-defined rules.

AIC - Akaike information criterion: an estimation of prediction error. It is a score which can be used to evaluate which of multiple models is likely to be the best model at describing a dataset.

AICD – activation-induced cell death: a programmed cell death as a result of Fas:FasL interactions.

AL – afferent lymphatics: a lymphatic vessel which enters and/or brings lymph to a lymph node.

APC – antigen-presenting cells: cells that process antigen into peptides and present it in complex with MHC on the cell surface.

AS01 – Adjuvant System 01: a liposome-based adjuvant containing two immunostimulants: QS21 and MPL.

AS03 – Adjuvant System 03: a squaline-based adjuvant.

AS04 – Adjuvant System 04: an aluminium salt and TLR4 agonist-based adjuvant. Contains alum and MPL.

ASC - apoptosis-associated speck-like protein containing a C-terminal caspase recruitment domain: a vital adaptor molecule which bridges the NLRP proteins e.g., NLRP3 with procaspase-1 within an inflammasome, leading to the ativation of caspase-1 and the release of IL1β and IL18.

B7 – a term to collectively describe the co-stimulatory molecules CD80 and CD86.

CoSMoS - The Complex Systems Modelling and Simulation Process: a principled modelling framework, aimed at providing a flexible approach to support modelling and analysis of complex systems.

CTL – cytotoxic T lymphocyte: also known as killer T cells, these are a white-blood cell which expresses glycoprotein CD8, and are vital in killing e.g., cancer cells and infected cells.

DAMPS – Damage-associated-molecular-patterns: also known as danger-associated-molecular-patterns, are intracellular molecules which are discharged from dying or damaged cells.

DC – Dendritic Cells: a professional APC.

dLN – draining lymph node: a lymph node which filters lymph from a particular region or organ. In this thesis, this generally refers to 'muscle-injection-site draining lymph nodes'.

eFAST – extended Fourier Amplitude Sensitivity Test: a variance-decomposition based global sensitivity analysis method.

HBsAg – Hepatitis B surface antigen.

HD – human dose: generally refers to the fraction of a 'human dose' of an adjuvant e.g., AS01 which is used in mice.

HEVs – high endothelial venules: blood vessels which are adapted for lymphocyte trafficking. HEVs are found in secondary lymphoid organs e.g., lymph nodes and Peyer's patches.

IFR – Interfollicular region: in a lymph node, this is the area between B cell follicles.

IM - intramuscular, referring to an intramuscular injection.

IBD - Inflammatory bowel disease.

ISC Innate-IFNg-secretor-cell: a term we use to collectively describe innate cells that secrete IFNγ in the lymph node.

LS-DCs – lymphatic-sinus dendritic cells: these DCs have been shown to capture lymph-borne antigens and subsequently elicit early activation of T cells.

MHC – major histocompatibility complex: refers to a set of substantially polymorphic genes which code for surface proteins which present peptides to the immune system.

MoA – mechanism of action: the way in which a therapeutic agent performs its function, in this case the way that an adjuvant generates and enhances an immune response.

MoDCs – monocyte-derived-dendritic-cells: Dendritic cells which are derived from Monocytes through differentiation.

MPL - 3-O-desacyl–monophosphoryl lipid A: a derivative of bacterial lipopolysaccharides, known to induce a strong Th1 response.

Mtb – Mycobacterium tuberculosis: a species of pathogenic bacteria which is the causative agent of tuberculosis disease.

NHP – non-human-primates: primates such as rhesus macaques which are used as a model of humans in pre-clinical experimental medicine.

NK cells – Natural killer cells: a cytotoxic lymphocyte primarily involved in innate immune function. Known to secrete IFNγ and are classically involved in eliminating cells which are missing 'self' markers of MHC class I.

NKa – activated IFNγ+ NK cell: used throughout this thesis to represent NK cells which are IFNγ+, used as a proxy for activation.

NLRs – Nod-like-receptors: intracellular sensors of PAMPS or DAMPS.

OAT – one-at-a-time. Refers to perturbing parameters individually for local sensitivity

analysis.

ODD - Overview, Design Concepts and Details Protocol: a design framework for developing agent-based models.

ODE – ordinary differential equations: equations or collections of equations that describe the continuous rates of change of a population, and in immunology, usually with respect to time.

PAMPS – pathogen-associated-molecular-patterns: molecular motifs conserved in pathogens. PAMPs trigger pattern-recognition-receptors such as TLRs.

PI – post-injection. Generally refers to a timepoint 'post-injection', i.e., following injection of a substance.

pMHC – peptide and major histocompatibility complex: a peptide which is bound to some MHC protein.

PRRs – Pattern recognition receptor: Proteins which are expressed by immune system cells, which detect PAMPs and DAMPS. Several types of PRRs exist, including Toll-like-receptors and NOD-like-receptors.

QS21 – QS21: an immunostimulatory component derived from the Chilean soap bark tree Quillaja Saponaria.

RV – reverse-vaccinology: a bioinformatic-led approach pioneered by Rino Rappuoli, where a pathogenic genome is screened to find antigenic components of genes, which may be desirable vaccine targets.

SA – sensitivity analysis: application of statistical techniques to assess how a model and/or simulation responds to perturbation of input parameter values.

SCS – subcapsular sinus: in a lymph node, the space which is between the capsule and the cortex. This area receives afferent lymphatic vessels.

SLO – secondary lymphoid organs: these organs such as Spleen, lymph nodes, Peyer's patches and mucosal associated Lymphoid Tissue are sites for interactions of lymphocytes with antigen.

SSM/SCS-Mo – subcapsular sinus Macrophages: Macrophages found in the subcapsular sinus which express an adhesion molecule CD169.

SBGN - Systems Biology Graphical Notation: a standardised graphical language to describe biological systems.

Tfh cells – T follicular helper cells: a subset of CD4+ T cells which provide help to B cells in producing antibody.

Th1 – T Helper 1: a subset of CD4+ T cells which express IFNγ, TNF and IL2. These cells amplify the cell-mediated response to an offending antigen.

TLRs – Toll-like-receptors: PRRs which are expressed on cells such as DCs and Macrophages,

which are critical for the proper function of the immune system. Humans have 10 TLRs while mouse have 13.

UML – unified modelling language: a modelling language used commonly in software engineering to describe system dynamics.

Bibliography

[1] C A Janeway, P Travers, M Walport, and M Shlomchik. Immunobiology: the immune system in health and disease, 1996.

[2] Gwendalyn J Randolph, Stoyan Ivanov, Bernd H Zinselmeyer, and Joshua P Scallan. The Lymphatic System: Integral Roles in Immunity. *doi.org*, 35(1):31–52, 2017.

[3] Dante Alexander Patrick Louie and Shan Liao. Lymph Node Subcapsular Sinus Macrophages as the Frontline of Lymphatic Immune Defense. *Frontiers in Immunology*, 10:347, 2019.

[4] Steven G Reed, Mark T Orr, and Christopher B Fox. Key roles of adjuvants in modern vaccines. *Nature Medicine*, 19(12):1597–1608, 2013.

[5] Arnaud Didierlaurent. Early NK cell activation controls the adjuvant effect induced by AS01 Antigen. *unpublished*, 2014.

[6] Jason Cosgrove. *The Spatial Distribution and Dynamics of CXCL13 in Lymphoid Tissues.* PhD thesis, University of York, 2017.

[7] Paul R Buckley, Kieran Alden, Margherita Coccia, Aurélie Chalon, Catherine Collignon, Stéphane T Temmerman, Arnaud M Didierlaurent, Robbert Van Der Most, Jon Timmis, Claus A Andersen, and Mark C Coles. Application of Modeling Approaches to Explore Vaccine Adjuvant Mode-of-Action. *Frontiers in Immunology*, 10:114, 2019.

[8] Sophie Detienne, Iain Welsby, Catherine Collignon, Sandrine Wouters, Margherita Coccia, Sophie Delhaye, Laurye Van Maele, Séverine Thomas, Maëlle Swertvaegher, Aurélie Detavernier, Abdelatif Elouahabi, Stanislas Goriely, and Arnaud M Didierlaurent. Central Role of CD169+ Lymph Node Resident Macrophages in the Adjuvanticity of the QS-21 Component of AS01. *Scientific Reports*, 6(1):1597, 2016.

[9] Daniel Kaschek, Wolfgang Mader, Mirjam Fehling Kaschek, Marcus Rosenblatt, and Jens Timmer. Dynamic modeling, parameter estimation, and uncertainty analysis in R. *Journal of Statistical Software*, 88(1), 2019.

[10] M A Strassburg. The global eradication of smallpox. *American journal of infection control*, 10(2):53–59, 1982.

[11] Edward Jenner. On the Origin of the Vaccine Inoculation. *The Medical and physical journal*, 5(28):505–508, 1801.

[12] Pedro M. Folegatti, Katie J. Ewer, Parvinder K. Aley, Brian Angus, Stephan Becker, Sandra Belij-Rammerstorfer, Duncan Bellamy, Sagida Bibi, Mustapha Bittaye, Elizabeth A. Clutterbuck, Christina Dold, Saul N. Faust, Adam Finn, Amy L. Flaxman, Bassam Hallis, Paul Heath, Daniel Jenkin, Rajeka Lazarus, Rebecca Makinson, Angela M. Minassian, Katrina M. Pollock, Maheshi Ramasamy, Hannah Robinson, Matthew Snape, Richard Tarrant, Merryn Voysey, Catherine Green, Alexander D. Douglas, Adrian V.S. Hill, Teresa Lambe, Sarah C. Gilbert, Andrew J. Pollard, Jeremy Aboagye, Kelly Adams, Aabidah Ali, Elizabeth Allen, Jennifer L. Allison, Rachel Anslow, Edward H. Arbe-Barnes, Gavin Babbage, Kenneth Baillie, Megan Baker, Philip Baker, Ioana Baleanu, Juliana Ballaminut, Eleanor Barnes, Jordan Barrett, Louise Bates, Alexander Batten, Kirsten Beadon, Rebecca Beckley, Eleanor Berrie, Lisa Berry, Amy Beveridge, Kevin R. Bewley, Else Margreet Bijker, Tracey Bingham, Luke Blackwell, Caitlin L. Blundell, Emma Bolam, Elena Boland, Nicola Borthwick, Thomas Bower, Amy Boyd, Tanja Brenner, Philip D. Bright, Charlie Brown-O'Sullivan, Emily Brunt, Jamie Burbage, Sharon Burge, Karen R. Buttigieg, Nicholas Byard, Ingrid Cabera Puig, Anna Calvert, Susana Camara, Michelangelo Cao, Federica Cappuccini, Melanie Carr, Miles W. Carroll, Victoria Carter, Katrina Cathie, Ruth J. Challis, Irina Chelysheva, Jee Sun Cho, Paola Cicconi, Liliana Cifuentes, Helen Clark, Elizabeth Clark, Tom Cole, Rachel Colin-Jones, Christopher P. Conlon, Aislinn Cook, Naomi S. Coombes, Rachel Cooper, Catherine A. Cosgrove, Karen Coy, Wendy E.M. Crocker, Christina J. Cunningham, Brad E. Damratoski, Lynne Dando, Mehreen S. Datoo, Hannah Davies, Hans De Graaf, Tesfaye Demissie, Claudio Di Maso, Isabelle Dietrich, Tao Dong, Francesca R. Donnellan, Naomi Douglas, Charlotte Downing, Jonathan Drake, Rachael Drake-Brockman, Ruth Elizabeth Drury, Susanna Jane Dunachie, Nick J. Edwards,

Frances D.L. Edwards, Chris J. Edwards, Sean C. Elias, Michael J. Elmore, Katherine R.W. Emary, Marcus Rex English, Susanne Fagerbrink, Sally Felle, Shuo Feng, Samantha Field, Carine Fixmer, Clare Fletcher, Karen J. Ford, Jamie Fowler, Polly Fox, Emma Francis, John Frater, Julie Furze, Michelle Fuskova, Eva Galiza, Diane Gbesemete, Ciaran Gilbride, Giacomo Gorini, Lyndsey Goulston, Caroline Grabau, Lara Gracie, Zoe Gray, Lucy Belle Guthrie, Mark Hackett, Sandro Halwe, Elizabeth Hamilton, Joseph Hamlyn, Brama Hanumunthadu, Irasha Harding, Stephanie A. Harris, Andrew Harris, Daisy Harrison, Clare Harrison, Thomas C. Hart, Louise Haskell, Sophia Hawkins, Ian Head, John Aaron Henry, Jennifer Hill, Susanne H.C. Hodgson, Mimi M. Hou, Elizabeth Howe, Nicola Howell, Cecilia Hutlin, Sabina Ikram, Catherine Isitt, Poppy Iveson, Susan Jackson, Frederic Jackson, Sir William James, Megan Jenkins, Elizabeth Jones, Kathryn Jones, Christine E. Jones, Bryony Jones, Reshma Kailath, Konstantinos Karampatsas, Jade Keen, Sarah Kelly, Dearbhla Kelly, David Kerr, Simon Kerridge, Liaquat Khan, Uzma Khan, Annabel Killen, Jasmin Kinch, Thomas B. King, Lloyd King, Jade King, Lucy Kingham-Page, Paul Klenerman, Francesca Knapper, Julian C. Knight, Stanislava Koleva, Alexandra Kupke, Colin W. Larkworthy, Jessica P.J. Larwood, Anna Laskey, Alison M. Lawrie, Arlene Lee, Kim Yee Ngan Lee, Emily A. Lee, Helen Legge, Alice Lelliott, Nana Marie Lemm, Amelia M. Lias, Aline Linder, Samuel Lipworth, Xinxue Liu, Shuchang Liu, Raquel Lopez Ramon, May Lwin, Francesca Mabesa, Meera Madhavan, Gary Mallett, Kushal Mansatta, Inēs Marcal, Spyridoula Marinou, Emma Marlow, Julia L. Marshall, Jane Martin, Joanne McEwan, Gretchen Meddaugh, Alexander J. Mentzer, Neginsadat Mirtorabi, Maria Moore, Edward Moran, Ella Morey, Victoria Morgan, Susan Jane Morris, Hazel Morrison, Gertraud Morshead, Richard Morter, Yama F. Mujadidi, Jilly Muller, Tatiana Munera-Huertas, Claire Munro, Alasdair Munro, Sarah Murphy, Vincent J. Muster, Philomena Mweu, Andrés Noé, Fay L. Nugent, Elizabeth Nugent, Katie O'Brien, Daniel O'Connor, Blanché Oguti, Jennifer L. Oliver, Catarina Oliveira, Peter John O'Reilly, Mairead Osborn, Piper Osborne, Cathy Owen, Daniel Owens, Nelly Owino, Mihaela Pacurar, Kaye Parker, Helena Parracho, Maia Patrick-Smith, Victoria Payne, Jennifer Pearce, Yanchun Peng, Marco Polo Peralta Alvarez, James Perring, Katja Pfafferott, Dimitra Pipini, Emma Plested, Helen Pluess-Hall, Katrina Pollock, Ian Poulton, Laura Presland, Samuel Provstgaard-Morys, David Pulido, Kajal Radia, Fernando Ramos Lopez, Jade Rand, Helen Ratcliffe, Thomas Rawlinson, Sarah Rhead, Amy Riddell, Adam John Ritchie, Hannah Roberts, Joanna Robson, Sophie Roche, Cornelius Rohde, Christine S. Rollier, Rosanna Romani, Indra Rudiansyah, Stephen Saich, Sara Sajjad, Stephannie Salvador, Lidia Sanchez Riera, Helen Sanders, Katherine Sanders, Shari Sapaun, Chloe Sayce, Ella Schofield, Gavin Screaton, Beatrice Selby, Calum Semple, Hannah R. Sharpe, Adam Shea, Holly Shelton, Sarah Silk, Laura Silva-Reyes, Donal T. Skelly, Heather Smee, Catherine C. Smith, David J. Smith, Rinn Song, Alexandra J. Spencer, Elizabeth Stafford, Amy Steele, Elena Stefanova, Lisa Stockdale, Anna Szigeti, Abdessamad Tahiri-Alaoui, Moira Tait, Helen Talbot, Rachel Tanner, Iona Jennifer Taylor, Victoria Taylor, Rebecca Te Water Naude, Nazia Thakur, Yrene Themistocleous, Andreas Themistocleous, Merin Thomas, Tonia M. Thomas, Amber Thompson, Samantha Thomson-Hill, Jennifer Tomlins, Susan Tonks, James Towner, Nguyen Tran, Julia A. Tree, Adam Truby, Kate Turkentine, Cheryl Turner, Nicola Turner, Sally Turner, Toby Tuthill, Marta Ulaszewska, Rachel Varughese, Neeltje Van Doremalen, Kristin Veighey, Marije K. Verheul, Iason Vichos, Elia Vitale, Laura Walker, Marion E.E. Watson, Benjamin Welham, Julie Wheat, Caroline White, Rachel White, Andrew T. Worth, Danny Wright, Suzie Wright, Xin Li Yao, and Yasmine Yau. Safety and immunogenicity of the ChAdOx1 nCoV-19 vaccine against SARS-CoV-2: a preliminary report of a phase 1/2, single-blind, randomised controlled trial. *The Lancet*, 396(10249):467–478, 8 2020.

[13] Ennio De Gregorio, Elena Caproni, and Jeffrey B Ulmer. Vaccine adjuvants: mode of action. *Frontiers in Immunology*, 4:214, 2013.

[14] Anita Milicic, Christine S Rollier, Choon Kit Tang, Rhea Longley, Adrian V S Hill, and Arturo Reyes-Sandoval. Adjuvanting a viral vectored vaccine against pre-erythrocytic malaria. *Scientific Reports*, 7(1):1–12, 2017.

[15] A M Didierlaurent, Arnaud M Didierlaurent, Catherine Collignon, C Collignon, Patricia Bourguignon, P Bourguignon, S Wouters, Sandrine Wouters, Kaat Fierens, K Fierens, M Fochesato, Michel Fochesato, Najoua Dendouga, N Dendouga, Christelle Langlet, C Langlet, B Malissen, Bernard Malissen, Bart N Lambrecht, B N Lambrecht, N Garcon, Nathalie Garçon, Marcelle Van Mechelen, M Van Mechelen, Sandra Morel, and S Morel. Enhancement of Adaptive Immunity by the Human Vaccine Adjuvant AS01 Depends on Activated Dendritic Cells. *The Journal of Immunology*, 193(4):1920–1930, 2014.

[16] Annalisa Ciabattini, Elena Pettini, Fabio Fiorino, Gabiria Pastore, Peter Andersen, Gianni Pozzi, and Donata Medaglini. Modulation of Primary Immune Response by Different Vaccine Adjuvants. *Frontiers in Immunology*, 7(Suppl 2):2312–2363, 2016.

[17] Andrew J. Pollard and Else M. Bijker. A guide to vaccinology: from basic principles to new developments, 12 2020.

[18] Arnaud M. Didierlaurent, Béatrice Laupèze, Alberta Di Pasquale, Nadia Hergli, Catherine Collignon, and Nathalie Garçon. Adjuvant system AS01: helping to overcome the challenges of modern vaccines. *Expert Review of Vaccines*, 16(1):55–63, 2017.

[19] Walter R Frontera and Julien Ochala. Skeletal Muscle: A Brief Review of Structure and Function. *Calcified Tissue International*, 96(3):183–195, 2014.

[20] Nicolas J Pillon, N J Pillon, Philip J Bilan, P J Bilan, L N Fink, Lisbeth N Fink, Amira Klip, and A Klip. Cross-talk between skeletal muscle and immune cells: muscle-derived mediators and metabolic implications. *American journal of physiology. Endocrinology and metabolism*, 304(5):E453–65, 2013.

[21] Christer Malm. Exercise immunology: a skeletal muscle perspective. *Exercise immunology review*, 8:116–167, 2002.

[22] Natalie L Trevaskis, Lisa M Kaminskas, and Christopher J H Porter. From sewer to saviour - targeting the lymphatic system to promote drug exposure and activity. *Nature Reviews Drug Discovery*, 14(11):781–803, 2015.

[23] Ki-Wook Kim and Joo-Hye Song. Emerging Roles of Lymphatic Vasculature in Immunity. *Immune Network*, 17(1):68–76, 2017.

[24] Ulrich H Von Andrian and Thorsten R Mempel. Homing and cellular traffic in lymph nodes. *Nature Reviews Immunology*, 3(11):867–878, 2003.

[25] Jason Cosgrove, Mario Novkovic, Stefan Albrecht, Natalia B. Pikor, Zhaoukun Zhou, Lucas Onder, Urs Mörbe, Jovana Cupovic, Helen Miller, Kieran Alden, Anne Thuery, Peter O'Toole, Rita Pinter, Simon Jarrett, Emily Taylor, Daniel Venetz, Manfred Heller, Mariagrazia Uguccioni, Daniel F. Legler, Charles J. Lacey, Andrew Coatesworth, Wojciech G. Polak, Tom Cupedo, Bénedicte Manoury, Marcus Thelen, Jens V. Stein, Marlene Wolf, Mark C. Leake, Jon Timmis, Burkhard Ludewig, and Mark C. Coles. B cell zone reticular cell microenvironments shape CXCL13 gradient formation. *Nature Communications*, 11(1):1–15, 12 2020.

[26] Michael Meyer-Hermann, Elodie Mohr, Nadége Pelletier, Yang Zhang, Gabriel D Victora, and Kai-Michael Toellner. A theory of germinal center B cell selection, division, and exit. *Cell Reports*, 2(1):162–174, 2012.

[27] Jan Kranich and Nike Julia Krautler. How Follicular Dendritic Cells Shape the B-Cell Antigenome. *Frontiers in Immunology*, 7(1):225, 2016.

[28] Helen Miller, Jason Cosgrove, Adam J M Wollman, Emily Taylor, Zhaokun Zhou, Peter J O'Toole, Mark C Coles, and Mark C Leake. High-Speed Single-Molecule Tracking of CXCL13 in the B-Follicle. *Frontiers in Immunology*, 9:1073, 2018.

[29] Shane Crotty. A brief history of T cell help to B cells. *Nature Reviews Immunology*, 15(3):185–189, 2015.

[30] Michael Y Gerner, Parizad Torabi-Parizi, and Ronald N Germain. Strategically localized dendritic cells promote rapid T cell responses to lymph-borne particulate antigens. *Immunity*, 42(1):172–185, 2015.

[31] Wolfgang Kastenmüller, Marlene Brandes, Ze Wang, Jasmin Herz, Jackson G Egen, and Ronald N Germain. Peripheral prepositioning and local CXCL9 chemokine-mediated guidance orchestrate rapid memory CD8+ T cell responses in the lymph node. *Immunity*, 38(3):502–513, 2013.

[32] Margherita Coccia, Catherine Collignon, Caroline Hervé, Aurélie Chalon, Iain Welsby, Sophie Detienne, Mary J. Van Helden, Sheetij Dutta, Christopher J. Genito, Norman C. Waters, Katrijn Van Deun, Age K. Smilde, Robert A. Van Den Berg, David Franco, Patricia Bourguignon, Sandra Morel, Nathalie Garçon, Bart N. Lambrecht, Stanislas Goriely, Robbert Van Der Most, and Arnaud M. Didierlaurent. Cellular and molecular synergy in AS01-adjuvanted vaccines results in an early IFNγ response promoting vaccine immunogenicity. *npj Vaccines*, 2(1):1–13, 2017.

[33] Zacarias Garcia, Fabrice Lemaitre, Nico van Rooijen, Matthew L Albert, Yves Levy, Olivier Schwartz, and Philippe Bousso. Subcapsular sinus macrophages promote NK cell accumulation and activation in response to lymph-borne viral particles. *Blood*, 120(24):4744–4750, 2012.

[34] Jacques Banchereau, Francine Briere, Christophe Caux, Jean Davoust, Serge Lebecque, Yong-Jun Liu, Bali Pulendran, and Karolina Palucka. Immunobiology of Dendritic Cells. *dx.doi.org*, 18(1):767–811, 2003.

[35] Stéphanie Hugues. Dynamics of dendritic cell-T cell interactions: A role in T cell outcome. *Seminars in Immunopathology*, 32(3):227–238, 2010.

[36] Jean-Philippe Girard, Christine Moussion, and Reinhold Förster. HEVs, lymphatics and homeostatic immune cell trafficking in lymph nodes. *Nature Reviews Immunology*, 12(11):762–773, 2012.

[37] Alfonso Mart\textbackslash'\textbackslashin-Fontecha, Silvia Sebastiani, Uta E Höpken, Mariagrazia Uguccioni, Martin Lipp, Antonio Lanzavecchia, and Federica Sallusto. Regulation of dendritic cell migration to the draining lymph node: impact on T lymphocyte traffic and priming. *The Journal of Experimental Medicine*, 198(4):615–621, 2003.

[38] Jeffrey Lian and Andrew D Luster. Chemokine-guided cell positioning in the lymph node orchestrates the generation of adaptive immune responses. *Current Opinion in Cell Biology*, 36:1–6, 2015.

[39] Michael D Cahalan and Ian Parker. Choreography of cell motility and interaction dynamics imaged by two-photon microscopy in lymphoid organs. *Annual Review of Immunology*, 26(1):585–626, 2008.

[40] Lois L Cavanagh and Wolfgang Weninger. Dendritic cell behaviour in vivo: lessons learned from intravital two-photon microscopy. *Immunology and Cell Biology*, 86(5):428–438, 2008.

[41] Joanna R Groom. Moving to the suburbs: T-cell positioning within lymph nodes during activation and memory. *Immunology and Cell Biology*, 93(4):330–336, 2015.

[42] André Ballesteros-Tato and Troy D Randall. Priming of T follicular helper cells by dendritic cells. *Immunology and Cell Biology*, 92(1):22–27, 2014.

[43] Imogen Moran, Abigail K Grootveld, Akira Nguyen, and Tri Giang Phan. Subcapsular Sinus Macrophages: The Seat of Innate and Adaptive Memory in Murine Lymph Nodes. *Trends in Immunology*, 40(1):35–48, 2019.

[44] Mirela Kuka and Matteo Iannacone. The role of lymph node sinus macrophages in host defense. *Annals of the New York Academy of Sciences*, 1319(1):38–46, 2014.

[45] Tobias Junt, E Ashley Moseman, Matteo Iannacone, Steffen Massberg, Philipp A Lang, Marianne Boes, Katja Fink, Sarah E Henrickson, Dmitry M Shayakhmetov, Nelson C Di Paolo, Nico van Rooijen, Thorsten R Mempel, Sean P Whelan, and Ulrich H Von Andrian. Subcapsular sinus macrophages in lymph nodes clear lymph-borne viruses and present them to antiviral B cells. *Nature*, 450(7166):110–114, 2007.

[46] Melanie R Neeland, Arnaud M Didierlaurent, Wei Shi, Catherine Collignon, Arnaud M Didierlaurent, Nadine Taubenheim, Els N T Meeusen, Arnaud M Didierlaurent, and Michael J De Veer. The Lymphatic Immune Response Induced by the Adjuvant AS01: A Comparison of Intramuscular and Subcutaneous Immunization Routes. *The Journal of Immunology*, 197(7):2704–2714, 2016.

[47] Noriko Shimasaki, Amit Jain, and Dario Campana. NK cells for cancer immunotherapy, 3 2020.

[48] Charmaine van Eeden, Lamia Khan, Mohammed S. Osman, and Jan Willem Cohen Tervaert. Natural killer cell dysfunction and its role in covid-19. *International Journal of Molecular Sciences*, 21(17):1–17, 2020.

[49] Madhumita Shrotri, May C.I. van Schalkwyk, Nathan Post, Danielle Eddy, Catherine Huntley, David Leeman, Samuel Rigby, Sarah V. Williams, William H. Bermingham, Paul Kellam, John Maher, Adrian M. Shields, Gayatri Amirthalingam, Sharon J. Peacock, and Sharif A. Ismail. T cell response to SARS-cov-2 infection in humans: A systematic review, 1 2021.

[50] Bice Perussia and B Perussia. The Cytokine Profile of Resting and Activated NK Cells. *Methods*, 9(2):370–378, 1996.

[51] Alex M Abel, Chao Yang, Monica S Thakar, and Subramaniam Malarkannan. Natural Killer Cells: Development, Maturation, and Clinical Utilization. *Frontiers in Immunology*, 9:1869, 2018.

[52] Kirsty C Newman and Eleanor M Riley. Whatever turns you on: accessory-cell-dependent activation of NK cells by pathogens. *Nature Reviews Immunology*, 7(4):279–291, 2007.

[53] J Magarian Blander and Ruslan Medzhitov. On regulation of phagosome maturation and antigen presentation. *Nature Immunology*, 7(10):1029–1035, 2006.

[54] Margherita Coccia, Catherine Collignon, Caroline Hervé, Aurélie Chalon, Iain Welsby, Sophie Detienne, Mary J van Helden, Sheetij Dutta, Christopher J Genito, Norman C Waters, Katrijn Van Deun, Age K Smilde, Robert A van den Berg, David Franco, Patricia Bourguignon, Sandra Morel, Nathalie Garçon, Bart N Lambrecht, Stanislas Goriely, Robbert Van Der Most, and Arnaud M Didierlaurent. Cellular and molecular synergy in AS01-adjuvanted vaccines results in an early IFN${$\gamma$}$ response promoting vaccine immunogenicity. *npj Vaccines*, pages 1–13, 2017.

[55] Anthony L Desbien, Natasha Dubois Cauwelaert, Steven J Reed, Hilton R Bailor, Hong Liang, Darrick Carter, Malcolm S Duthie, Christopher B Fox, Steven G Reed, and Mark T Orr. IL-18 and Subcapsular Lymph Node Macrophages are Essential for Enhanced B Cell Responses with TLR4 Agonist Adjuvants. *Journal of immunology (Baltimore, Md. : 1950)*, 197(11):4351–4359, 2016.

[56] Laleh Khodadadi, Qingyu Cheng, Andreas Radbruch, and Falk Hiepe. The Maintenance of Memory Plasma Cells. *Frontiers in Immunology*, 10:721, 2019.

[57] Jonathan E Chang and Shannon J Turley. Stromal infrastructure of the lymph node and coordination of immunity. *Trends in Immunology*, 36(1):30–39, 2015.

[58] Lucas Onder, Mark Coles, Priyanka Narang, Elke Scandella, Qian Chai, Maria Iolyeva, Kerim Hoorweg, Cornelia Halin, Ellen Richie, Paul Kaye, Tom Cupedo, and Burkhard Ludewig. Plenary paper IL-7 {{\textbackslash}textendash} producing stromal cells are critical for lymph node remodeling. *Blood*, 120(24):4675–4683, 2012.

[59] 120273. *Physiology and Pathology of Innate Immune Response Against Pathogens*. IntechOpen, 2017.

[60] Chao Shi and Eric G Pamer. Monocyte recruitment during infection and inflammation. *Nature Reviews Immunology*, 11(11):762–774, 2011.

[61] Carlos Rosales. Neutrophil: A Cell with Many Roles in Inflammation or Several Cell Types? *Frontiers in Physiology*, 9:274, 2018.

[62] M A Mawhin, P Tilly, G Zirka, A L Charles Cardiovascular, and 2018. Neutrophils recruited by leukotriene B4 induce features of plaque destabilization during endotoxaemia. *academic.oup.com*.

[63] Scott A Fulton, Jill M Johnsen, Stanley F Wolf, Derek S Sieburth, and W Henry Boom. Interleukin-12 production by human monocytes infected with Mycobacterium tuberculosis: Role of phagocytosis. *Infection and Immunity*, 1996.

[64] M Rossol, Manuela Rossol, H Heine, Holger Heine, U Meusch, Undine Meusch, D Quandt, Dagmar Quandt, Carina Klein, C Klein, M J Sweet, Matthew J Sweet, S Hauschildt, and Sunna Hauschildt. LPS-induced cytokine production in human monocytes and macrophages. *Critical reviews in immunology*, 31(5):379–446, 2011.

[65] Derek T O Hagan, Samuele Calabro, Marco Tortoli, Barbara C Baudner, Alessandra Pacitto, Mario Cortese, Derek T O'Hagan, Ennio De Gregorio, Anja Seubert, and Andreas Wack. Vaccine adjuvants alum and MF59 induce rapid recruitment of neutrophils and monocytes that participate in antigen transport to draining lymph nodes. *Vaccine*, 29(9):1812–1823, 2011.

[66] G. P. SACKS, C. W. G. REDMAN, and I. L. SARGENT. Monocytes are primed to produce the Th1 type cytokine IL-12 in normal human pregnancy: an intracellular flow cytometric analysis of peripheral blood mononuclear cells. *Clinical & Experimental Immunology*, 131(3):490–497, 3 2003.

[67] S. De Koker, L. Van Hoecke, A. De Beuckelaer, K. Roose, K. Deswarte, M. A. Willart, P. Bogaert, T. Naessens, B. G. De Geest, X. Saelens, B. N. Lambrecht, and J. Grooten. Inflammatory monocytes regulate Th1 oriented immunity to CpG adjuvanted protein vaccines through production of IL-12. *Scientific Reports*, 7(1):1–14, 2017.

[68] Aline Guilmot, Julie Bosse, Yves Carlier, and Carine Truyens. Monocytes Play an IL-12-Dependent Crucial Role in Driving Cord Blood NK Cells to Produce IFN-g in Response to Trypanosoma cruzi. *PLoS Neglected Tropical Diseases*, 2013.

[69] Jeffrey Lian, Aleksandra J. Ozga, Caroline L. Sokol, and Andrew D. Luster. Targeting Lymph Node Niches Enhances Type 1 Immune Responses to Immunization. *Cell Reports*, 31(8), 5 2020.

[70] Shizuo Akira, Satoshi Uematsu, and Osamu Takeuchi. Pathogen Recognition and Innate Immunity. *Cell*, 124(4):783–801, 2006.

[71] Osamu Takeuchi and Shizuo Akira. Pattern Recognition Receptors and Inflammation. *Cell*, 140(6):805–820, 2010.

[72] Minou Adib-conquy, Daniel Scott-algara, Jean-marc Cavaillon, and Fernando Souza-fonseca guimaraes. TLR-mediated activation of NK cells and their role in bacterial/viral immune responses in mammals. *Immunology and Cell Biology*, 92(3):256–262, 2013.

[73] Shizuo Akira and Kiyoshi Takeda. Toll-like receptor signalling. *Nature Reviews Immunology*, 4(7):499–511, 2004.

[74] Beom Seok Park and Jie-Oh Lee. Recognition of lipopolysaccharide pattern by TLR4 complexes. *Experimental & Molecular Medicine*, 45(12):e66–e66, 2013.

[75] C R Casella and T C Mitchell. Putting endotoxin to work for us: monophosphoryl lipid A as a safe and effective vaccine adjuvant. *Cellular and Molecular Life Sciences*, 65(20):3231–3240, 2008.

[76] Mark R Alderson, Patrick McGowan, Jory R Baldridge, and Peter Probst. TLR4 agonists as immunomodulatory agents. *Journal of Endotoxin Research*, 12(5):313–319, 2006.

[77] Nina Bhardwaj, Sacha Gnjatic, and Nikhil B Sawhney. TLR AGONISTS: Are They Good Adjuvants? *Cancer journal (Sudbury, Mass.)*, 16(4):382–391, 2010.

[78] Olivier Van Der Meeren, Mark Hatherill, Videlis Nduba, Robert J Wilkinson, Monde Muyoyeta, Elana Van Brakel, Helen M Ayles, German Henostroza, Friedrich Thienemann, Thomas J Scriba, Andreas Diacon, Gretta L Blatner, Marie-Ange Demoitié, Michele Tameris, Mookho Malahleha, James C Innes, Elizabeth Hellström, Neil Martinson, Tina Singh, Elaine J Akite, Aisha Khatoon Azam, Anne Bollaerts, Ann M Ginsberg, Thomas G Evans, Paul Gillard, and Dereck R Tait. Phase 2b Controlled Trial of M72/AS01 EVaccine to Prevent Tuberculosis. *New England Journal of Medicine*, 379(17):1621–1634, 2018.

[79] Jaye M Platnich and Daniel A Muruve. NOD-like receptors and inflammasomes: A review of their canonical and non-canonical signaling pathways. *Archives of Biochemistry and Biophysics*, 670:4–14, 2019.

[80] Vijay A K Rathinam and Katherine A Fitzgerald. Inflammasome Complexes: Emerging Mechanisms and Effector Functions. *Cell*, 165(4):792–800, 2016.

[81] Xiaowei Guo, Xupin Jiang, Xi Ren, Huanbo Sun, Dongxia Zhang, Qiong Zhang, Jiaping Zhang, and Yuesheng Huang. The Galvanotactic Migration of Keratinocytes is Enhanced by Hypoxic Preconditioning. *Scientific Reports*, 5:10289, 2015.

[82] Eun-Kyeong Jo, Jin Kyung Kim, Dong-Min Shin, and Chihiro Sasakawa. Molecular mechanisms regulating NLRP3 inflammasome activation. *Cellular and Molecular Immunology*, 13(2):148–159, 2016.

[83] Sören Reinke, Aneesh Thakur, Cillian Gartlan, Jelena S. Bezbradica, and Anita Milicic. Inflammasome-Mediated Immunogenicity of Clinical and Experimental Vaccine Adjuvants. *Vaccines*, 8(3):554, 9 2020.

[84] Eun Kyeong Jo, Jin Kyung Kim, Dong Min Shin, and Chihiro Sasakawa. Molecular mechanisms regulating NLRP3 inflammasome activation. *Cellular and Molecular Immunology*, 13(2):148–159, 2016.

[85] Katherine A. Deets and Russell E. Vance. Inflammasomes and adaptive immune responses. *Nature Immunology*, pages 1–11, 2 2021.

[86] Wolfgang Kastenmüller, Parizad Torabi-Parizi, Naeha Subramanian, Tim Lämmermann, and Ronald N Germain. A spatially-organized multicellular innate immune response in lymph nodes limits systemic pathogen spread. *Cell*, 150(6):1235–1248, 2012.

[87] Tamara S. Rodrigues, Keyla S.G. de Sá, Adriene Y. Ishimoto, Amanda Becerra, Samuel Oliveira, Leticia Almeida, Augusto V. Gonçalves, Debora B. Perucello, Warrison A. Andrade, Ricardo Castro, Flavio P. Veras, Juliana E. Toller-Kawahisa, Daniele C. Nascimento, Mikhael H.F. de Lima, Camila M.S. Silva, Diego B. Caetite, Ronaldo B. Martins, Italo A. Castro, Marjorie C. Pontelli, Fabio C. de Barros, Natália B. do Amaral, Marcela C. Giannini, Letícia P. Bonjorno, Maria Isabel F. Lopes, Rodrigo C. Santana, Fernando C. Vilar, Maria Auxiliadora-Martins, Rodrigo Luppino-Assad, Sergio C.L. de Almeida, Fabiola R. de Oliveira, Sabrina S. Batah, Li Siyuan, Maira N. Benatti, Thiago M. Cunha, José C. Alves-Filho, Fernando Q. Cunha, Larissa D. Cunha, Fabiani G. Frantz, Tiana Kohlsdorf, Alexandre T. Fabro, Eurico Arruda, Renê D.R. de Oliveira, Paulo Louzada-Junior, and Dario S. Zamboni. Inflammasomes are activated in response to SARS-cov-2 infection and are associated with COVID-19 severity in patients. *Journal of Experimental Medicine*, 218(3), 3 2020.

[88] Erin Theisen and John Demian Sauer. Listeria monocytogenes-induced cell death inhibits the generation of cell- mediated immunity. *Infection and Immunity*, 85(1), 1 2017.

[89] Alice Gutjahr, Gérard Tiraby, Eric Perouzel, Bernard Verrier, and Stéphane Paul. Triggering Intracellular Receptors for Vaccine Adjuvantation. *Trends in Immunology*, 37(9):573–587, 2016.

[90] Shuting Shi, Haoru Zhu, Xinyu Xia, Zhihui Liang, Xuehu Ma, and Bingbing Sun. Vaccine adjuvants: Understanding the structure and mechanism of adjuvanticity, 5 2019.

[91] Katia De Filippo, Anne Dudeck, Mike Hasenberg, Emma Nye, Nico van Rooijen, Karin Hartmann, Matthias Gunzer, Axel Roers, and Nancy Hogg. Mast cell and macrophage chemokines CXCL1/CXCL2 control the early stage of neutrophil recruitment during tissue inflammation. *Blood*, 121(24):4930–4937, 2013.

[92] Tim Lämmermann, Philippe V Afonso, Bastian R Angermann, Ji Ming Wang, Wolfgang Kastenmüller, Carole a Parent, and Ronald N Germain. Neutrophil swarms require LTB4 and integrins at sites of cell death in vivo. *Nature*, 498(7454):371–375, 2013.

[93] Maria Romano, M Romano, M Sironi, Marina Sironi, Carlo Toniatti, C Toniatti, N Polentarutti, Nadia Polentarutti, P Fruscella, Paolo Fruscella, P Ghezzi, R Faggioni, Raffaella Faggioni, W Luini, Walter Luini, Victor Van Hinsbergh, V van Hinsbergh, Silvano Sozzani, S Sozzani, F Bussolino, V Poli, G Ciliberto, Alberto Mantovani, and A Mantovani. Role of IL-6 and its soluble receptor in induction of chemokines and leukocyte recruitment. *Immunity*, 6(3):315–325, 1997.

[94] Mieke Metzemaekers, Vincent Vanheule, Rik Janssens, Sofie Struyf, and Paul Proost. Overview of the mechanisms that may contribute to the non-redundant activities of interferon-inducible CXC chemokine receptor 3 ligands. *Frontiers in Immunology*, 8(JAN), 2018.

[95] Cedric Bosteels, Kaat Fierens, Sofie De Prijck, Justine Van Moorleghem, Manon Vanheerswynghels, Caroline De Wolf, Aurélie Chalon, Catherine Collignon, Hamida Hammad, Arnaud M. Didierlaurent, and Bart N. Lambrecht. CCR2- and Flt3-Dependent Inflammatory Conventional Type 2 Dendritic Cells Are Necessary for the Induction of Adaptive Immunity by the Human Vaccine Adjuvant System AS01. *Frontiers in Immunology*, 11(January):1–12, 2021.

[96] V Kumar and A Sharma. Neutrophils: Cinderella of innate immune system. *International Immunopharmacology*, 10(11):1325–1334, 2010.

[97] Elzbieta Kolaczkowska and Paul Kubes. Neutrophil recruitment and function in health and inflammation. *Nature Reviews Immunology*, 13(3):159–175, 2013.

[98] Sunita Awate, Lorne A Babiuk, and George Mutwiri. Mechanisms of action of adjuvants. *Frontiers in Immunology*, 4(MAY):110–114, 2013.

[99] Rupert Abele and Robert Tampe. Function of the transport complex TAP in cellular immune recognition. *Biochimica et Biophysica Acta (BBA) - Biomembranes*, 1461(2):405–419, 1999.

[100] Marek Wieczorek, Esam T Abualrous, Jana Sticht, Miguel Álvaro-Benito, Sebastian Stolzenberg, Frank Noé, and Christian Freund. Major histocompatibility complex (MHC) class I and MHC class II proteins: Conformational plasticity in antigen presentation, 2017.

[101] M T Falta and A P Fontenot. Antigen Processing and Presentation. In *Comprehensive Toxicology, Second Edition*. 2010.

[102] Alireza Tahamtan, Majid Teymoori-Rad, Britt Nakstad, and Vahid Salimi. Anti-inflammatory MicroRNAs and their potential for inflammatory diseases treatment, 6 2018.

[103] R Förster, A Schubel, D Breitfeld, E Kremmer, I Renner-Müller, E Wolf, and M Lipp. CCR7 coordinates the primary immune response by establishing functional microenvironments in secondary lymphoid organs. *Cell*, 99(1):23–33, 1999.

[104] Céline Beauvillain, Pierre Cunin, Andrea Doni, Mari Scotet, Sébastien Jaillon, Marie Line Loiry, Giovanni Magistrelli, Krzysztof Masternak, Alain Chevailler, Yves Delneste, and Pascale Jeannin. CCR7 is involved in the migration of neutrophils to lymph nodes. *Blood*, 117(4):1196–1204, 2011.

[105] Leah a Mitchell, Angela J Henderson, and Steven W Dow. Suppression of vaccine immunity by inflammatory monocytes. *Journal of immunology (Baltimore, Md. : 1950)*, 189(12):5612–5621, 2012.

[106] S De Koker, L Van Hoecke, A De Beuckelaer, K Roose, K Deswarte, M A Willart, P Bogaert, T Naessens, B G De Geest, X Saelens, B N Lambrecht, and J Grooten. Inflammatory monocytes regulate Th1 oriented immunity to CpG adjuvanted protein vaccines through production of IL-12. *Scientific Reports*, 2017.

[107] Susanna Celli, Mark Day, Andreas J. Müller, Carmen Molina-Paris, Grant Lythe, and Philippe Bousso. How many dendritic cells are required to initiate a T-cell response? *Blood*, 120(19):3945–3948, 2012.

[108] Jennifer E Smith-Garvin, Gary A Koretzky, and Martha S Jordan. T Cell Activation. *dx.doi.org*, 27(1):591–619, 2009.

[109] Peter A Bretscher. A two-step, two-signal model for the primary activation of precursor helper T cells. *Proceedings of the National Academy of Sciences*, 96(1):185–190, 1999.

[110] J P Pereira, L M Kelly, J G Cyster International immunology, and 2010. Finding the right niche: B-cell migration in the early phases of T-dependent antibody responses. *academic.oup.com*.

[111] Julie Tellier and Stephen L Nutt. Plasma cells: The programming of an antibody-secreting machine, 2019.

[112] Sarah Gilbert. T-cell-inducing vaccines-what's the future. *Immunology*, 2011.

[113] Jinfang Zhu and William E Paul. CD4 T cells: fates, functions, and faults. *Blood*, 112(5):1557–1569, 2008.

[114] Jinfang Zhu, Hidehiro Yamane, and William E Paul. Differentiation of Effector CD4 T Cell Populations. *Annual Review of Immunology*, 28(1):445–489, 2010.

[115] Jasper J.P. van Beek, Maria Rescigno, and Enrico Lugli. A fresh look at the T helper subset dogma. *Nature Immunology*, 22(2):104–105, 2 2021.

[116] Bhanwar Lal Puniya, Robert G Todd, Akram Mohammed, Deborah M Brown, Matteo Barberis, and Tomáš Helikar. A mechanistic computational model reveals that plasticity of CD4+ T cell differentiation is a function of cytokine composition and dosage. *Frontiers in Physiology*, 2018.

[117] Nu Zhang and Michael J Bevan. CD8+ T Cells: Foot Soldiers of the Immune System. *Immunity*, 35(2):161–168, 2011.

[118] Stephen Christopher Jameson and Sara Hamilton. CD8 T cell memory: it takes all kinds. *Frontiers in Immunology*, 3, 2012.

[119] Arnaud M Didierlaurent, Béatrice Laupèze, Alberta Di Pasquale, Nadia Hergli, Catherine Collignon, and Nathalie Garçon. Adjuvant system AS01: helping to overcome the challenges of modern vaccines. *Expert Review of Vaccines*, 16(1):55–63, 2016.

[120] Anastasia Gangaev and Pia Kvistborg. 863 Identification and characterization of an immunodominant SARS-CoV-2-specific CD8 T cell response. *Journal for ImmunoTherapy of Cancer*, 8(Suppl 3):A916–A916, 2020.

[121] Emanuele Sasso, Anna Morena D'Alise, Nicola Zambrano, Elisa Scarselli, Antonella Folgori, and Alfredo Nicosia. New viral vectors for infectious diseases and cancer, 8 2020.

[122] Philippe Bousso. T-cell activation by dendritic cells in the lymph node: lessons from the movies. *Nature Reviews Immunology*, 8(9):675–684, 2008.

[123] Daniel L. Mueller. Mechanisms maintaining peripheral tolerance. *Nature Immunology*, 11(1):21–27, 2010.

[124] Carl W. Davis, Katherine J. L. Jackson, Megan M. McCausland, Jaime Darce, Cathy Chang, Susanne L. Linderman, Chakravarthy Chennareddy, Rebecca Gerkin, Shantoria J. Brown, Jens Wrammert, Aneesh K. Mehta, Wan Cheung Cheung, Scott D. Boyd, Edmund K. Waller, and Rafi Ahmed. Influenza vaccine–induced human bone marrow plasma cells decline within a year after vaccination. *Science*, page eaaz8432, 8 2020.

[125] Bali Pulendran, Prabhu S. Arunachalam, and Derek T. O'Hagan. Emerging concepts in the science of vaccine adjuvants. *Nature Reviews Drug Discovery*, 20(6):454–475, 2021.

[126] Zhihui Liang, Haoru Zhu, Xin Wang, Bo Jing, Zifan Li, Xinyu Xia, Hongwu Sun, Yun Yang, Weiting Zhang, Li Shi, Hao Zeng, and Bingbing Sun. Adjuvants for Coronavirus Vaccines, 11 2020.

[127] Hong-Guo Hu and Yan-Mei Li. Emerging Adjuvants for Cancer Immunotherapy. *Frontiers in Chemistry*, 8:601, 7 2020.

[128] Amanda L. Wilkins, Dmitri Kazmin, Giorgio Napolitani, Elizabeth A. Clutterbuck, Bali Pulendran, Claire Anne Siegrist, and Andrew J. Pollard. AS03- and MF59-adjuvanted influenza vaccines in children, 12 2017.

[129] Derek T. O'Hagan, Rushit N. Lodaya, and Giuseppe Lofano. The continued advance of vaccine adjuvants – 'we can work it out'. *Seminars in Immunology*, 50:101426, 11 2020.

[130] Vincent Pavot, Catherine Berry, Michael Kishko, Natalie G Anosova, Dean Huang, Tim Tibbitts, Alice Raillard, Sylviane Gautheron, Cindy Gutzeit, Marguerite Koutsoukos, Roman M Chicz, and Valerie Lecouturier. SARS-CoV-2 preS dTM vaccine booster candidates increase functional antibody responses and cross-neutralization against SARS-CoV-2 variants of concern in non-human primates. *bioRxiv*, 2:2021.09.20.461023, 2021.

[131] Nathalie Garçon, David W. Vaughn, and Arnaud M. Didierlaurent. Development and evaluation of AS03, an Adjuvant System containing α-tocopherol and squalene in an oil-in-water emulsion. *Expert Review of Vaccines*, 11(3):349–366, 2012.

[132] Sandra Morel, Sandra Morel, Arnaud Didierlaurent, Arnaud Didierlaurent, Patricia Bourguignon, Patricia Bourguignon, Sophie Delhaye, Benoˆ Baras, Valérie Jacob, Camille Planty, Abdelatif Elouahabi, Pol Harvengt, Harald Carlsen, Anders Kielland, Patrick Chomez, Nathalie Garc, and Marcelle Van Mechelen. Adjuvant System AS03 containing ${$\alpha$}$-tocopherol modulates innate immune response and leads to improved adaptive immunity. *Vaccine*, 29(13):2461–2473, 2011.

[133] Leigh M. Howard, Kristen L. Hoek, Johannes B. Goll, Parimal Samir, Allison Galassie, Tara M. Allos, Xinnan Niu, Laura E. Gordy, C. Buddy Creech, Nripesh Prasad, Travis L. Jensen, Heather Hill, Shawn E. Levy, Sebastian Joyce, Andrew J. Link, and Kathryn M. Edwards. *Cell-based systems biology analysis of human AS03-adjuvanted H5N1 avian influenza vaccine responses: A phase i randomized controlled trial*, volume 12. 2017.

[134] Troy D Querec, Rama S Akondy, Eva K Lee, Weiping Cao, Helder I Nakaya, Dirk Teuwen, Ali Pirani, Kim Gernert, Jiusheng Deng, Bruz Marzolf, Kathleen Kennedy, Haiyan Wu, Soumaya Bennouna, Herold Oluoch, Joseph Miller, Ricardo Z Vencio, Mark Mulligan, Alan Aderem, Rafi Ahmed, and Bali Pulendran. Systems biology approach predicts immunogenicity of the yellow fever vaccine in humans. *Nature Immunology*, 10(1):116–125, 2009.

[135] Ravi Danielsson and Håkan Eriksson. Aluminium adjuvants in vaccines – A way to modulate the immune response. *Seminars in Cell & Developmental Biology*, 1 2021.

[136] A M Didierlaurent, Arnaud M Didierlaurent, Sandra Morel, S Morel, L Lockman, Laurence Lockman, S L Giannini, Sandra L Giannini, Michel Bisteau, M Bisteau, H Carlsen, Harald Carlsen, A Kielland, Olivier Vosters, O Vosters, Nathalie Vanderheyde, N Vanderheyde, Daniel Larocque, F Schiavetti, Marcelle Van Mechelen, D Larocque, Nathalie Garçon, Arnaud M Didierlaurent, M Van Mechelen, Sandra Morel, N Garcon, Laurence Lockman, Sandra L Giannini, Michel Bisteau, Harald Carlsen, Anders Kielland, Olivier Vosters, Nathalie Vanderheyde, Francesca Schiavetti, Daniel Larocque, Marcelle Van Mechelen, and Nathalie Garc. AS04, an Aluminum Salt- and TLR4 Agonist-Based Adjuvant System, Induces a Transient Localized Innate Immune Response Leading to Enhanced Adaptive Immunity. *The Journal of Immunology*, 183(10):6186–6197, 2009.

[137] Gabriel Kristian Pedersen, Katharina Wørzner, Peter Andersen, and Dennis Christensen. Vaccine Adjuvants Differentially Affect Kinetics of Antibody and Germinal Center Responses. *Frontiers in Immunology*, 11:579761, 9 2020.

[138] Lawrence Segal, Sandrine Wouters, Danielle Morelle, Gaëlle Gautier, Julien Le Gal, Thomas Martin, Frieke Kuper, Eric Destexhe, Arnaud M. Didierlaurent, and Nathalie Garçon. Non-clinical safety and biodistribution of AS03-adjuvanted inactivated pandemic influenza vaccines. *Journal of Applied Toxicology*, 35(12):1564–1576, 12 2015.

[139] D. T. O'Hagan, G. S. Ott, E. De Gregorio, and A. Seubert. The mechanism of action of MF59 - An innately attractive adjuvant formulation. *Vaccine*, 30(29):4341–4348, 2012.

[140] Ali H. Ellebedy, Christopher Lupfer, Hazem E. Ghoneim, Jennifer DeBeauchamp, Thirumala Devi Kanneganti, and Richard J. Webby. Inflammasome-independent role of the apoptosis-associated speck-like protein containing CARD (ASC) in the adjuvant effect of MF59. *Proceedings of the National Academy of Sciences of the United States of America*, 108(7):2927–2932, 2 2011.

[141] Giuseppe Lofano, Francesca Mancini, Giulia Salvatore, Rocco Cantisani, Elisabetta Monaci, Corrado Carrisi, Simona Tavarini, Chiara Sammicheli, Silvia Rossi Paccani, Elisabetta Soldaini, Donatello Laera, Oretta Finco, Sandra Nuti, Rino Rappuoli, Ennio De Gregorio, Fabio Bagnoli, and Sylvie Bertholet. Oil-in-Water Emulsion MF59 Increases Germinal Center B Cell Differentiation and Persistence in Response to Vaccination. *The Journal of Immunology*, 195(4):1617–1627, 8 2015.

[142] Daniel Mekonnen, Hylemariam Mihiretie Mengist, and Tengchuan Jin. SARS-CoV-2 subunit vaccine adjuvants and their signaling pathways. *Expert Review of Vaccines*, 00(00):1–13, 2021.

[143] Haitao Guo, Justin B Callaway, and Jenny P-Y Ting. Inflammasomes: mechanism of action, role in disease, and therapeutics. *Nature Medicine*, 21(7):677–687, 2015.

[144] Arnaud M. Didierlaurent, Béatrice Laupèze, Alberta Di Pasquale, Nadia Hergli, Catherine Collignon, and Nathalie Garçon. Adjuvant system AS01: helping to overcome the challenges of modern vaccines. *Expert Review of Vaccines*, 16(1):55–63, 2017.

[145] Carl R Alving, Zoltan Beck, Gary R Matyas, and Mangala Rao. Liposomal adjuvants for human vaccines. *Expert Opinion on Drug Delivery*, 5247(February):1–10, 2016.

[146] Carl R. Alving, Kristina K. Peachman, Gary R. Matyas, Mangala Rao, and Zoltan Beck. Army Liposome Formulation (ALF) family of vaccine adjuvants. *Expert Review of Vaccines*, 19(3):279–292, 2020.

[147] Fahimeh Zahednezhad, Maryam Saadat, Hadi Valizadeh, Parvin Zakeri-Milani, and Behzad Baradaran. Liposome and immune system interplay: Challenges and potentials. *Journal of Controlled Release*, 305(April):194–209, 2019.

[148] G De Becker, V Moulin, B Pajak, C Bruck, M Francotte, C Thiriart, J Urbain, and M Moser. The adjuvant monophosphoryl lipid A increases the function of antigen-presenting cells. *International Immunology*, 12(6):807–815, 2000.

[149] Laurye Van Maele, Delphine Fougeron, Delphine Cayet, Aurélie Chalon, Diego Piccioli, Catherine Collignon, Jean-Claude Sirard, and Arnaud M Didierlaurent. Toll-like receptor 4 signaling in hematopoietic-lineage cells contributes to the enhanced activity of the human vaccine adjuvant AS01. *European Journal of Immunology*, 49(12):2134–2145, 12 2019.

[150] Govind Ragupathi, Jeffrey R. Gardner, Philip O. Livingston, and David Y. Gin. Natural and synthetic saponin adjuvant QS-21 for vaccines against cancer, 4 2011.

[151] Harvinder Singh, Gill Richard, and W Compans Editors. Current Topics in Microbiology and Immunology: Nanoparticles for Rational Vaccine Design. Technical report, 2020.

[152] Geert Leroux-Roels, Pascale Van Belle, Pierre Vandepapeliere, Yves Horsmans, Michel Janssens, Isabelle Carletti, Nathalie Garçon, Martine Wettendorff, and Marcelle Van Mechelen. Vaccine Adjuvant Systems containing monophosphoryl lipid A and QS-21 induce strong humoral and cellular immune responses against hepatitis B surface antigen which persist for at least 4 years after vaccination. *Vaccine*, 33(8):1084–1091, 2015.

[153] R Marty-Roix, Robyn Marty-Roix, Gregory I Vladimer, G I Vladimer, K Pouliot, Kimberly Pouliot, D Weng, Dan Weng, R Buglione-Corbett, Rachel Buglione-Corbett, Kim West, K West, John D MacMicking, J D MacMicking, Jonathan D Chee, J D Chee, S Wang, Shixia Wang, S Lu, Shan Lu, E Lien, and Egil Lien. Identification of QS-21 as an Inflammasome-activating Molecular Component of Saponin Adjuvants. *Journal of Biological Chemistry*, 291(3):1123–1136, 2016.

[154] M J Newman, J Y Wu, B H Gardner, C A Anderson, C R Kensil, J Recchia, R T Coughlin, and M F Powell. Induction of cross-reactive cytotoxic T-lymphocyte responses specific for HIV-1 gp120 using saponin adjuvant (QS-21) supplemented subunit vaccine formulations. *Vaccine*, 15(9):1001–1007, 1997.

[155] Oscar Kashala, Roberto Amador, Maria V Valero, Alberto Moreno, Arnoldo Barbosa, Beatrice Nickel, Claudia A Daubenberger, Fanny Guzman, Gerd Pluschke, and Manuel E Patarroyo. Safety, tolerability and immunogenicity of new formulations of the Plasmodium falciparum malaria peptide vaccine SPf66 combined with the immunological adjuvant QS-21. *Vaccine*, 20(17-18):2263–2277, 2002.

[156] Marie Aleth Lacaille-Dubois. Updated insights into the mechanism of action and clinical profile of the immunoadjuvant QS-21: A review. *Phytomedicine*, 60, 2019.

[157] M Kool, K Fierens, and B N Lambrecht. Alum adjuvant: some of the tricks of the oldest adjuvant. *Journal of Medical Microbiology*, 61(Pt_7):927–934, 2012.

[158] Philippe Moris, Erik Jongert, and Robbert G van der Most. Characterization of T-cell immune responses in clinical trials of the candidate RTS,S malaria vaccine. *Human Vaccines & Immunotherapeutics*, 6:0, 2017.

[159] Sofia Casares, Teodor Doru Brumeanu, and Thomas L Richie. The RTS,S malaria vaccine. *Vaccine*, 28(31):4880–4894, 2010.

[160] Geert Leroux-Roels, Isabel Leroux-Roels, Frédéric Clement, Opokua Ofori-Anyinam, Marc Lievens, Erik Jongert, Philippe Moris, W Ripley Ballou, and Joe Cohen. Evaluation of the immune response to RTS,S/AS01 and RTS,S/AS02 adjuvanted vaccines: randomized, double-blind study in malariana{{\textbackslash}"{\textbackslash}i}ve adults. *Human Vaccines & Immunotherapeutics*, 10(8):2211–2219, 2014.

[161] S Clinical Trials Partnership and The RTS,S Clinical Trials Partnership. A Phase 3 Trial of RTS,S/AS01 Malaria Vaccine in African Infants. *New England Journal of Medicine*, 367(24):2284–2295, 2012.

[162] Nicholas J White, Sasithon Pukrittayakamee, Tran Tinh Hien, M Abul Faiz, Olugbenga A Mokuolu, and Arjen M Dondorp. Malaria. *The Lancet*, 383(9918):723–735, 2014.

[163] Ian A Cockburn and Robert A Seder. Malaria prevention: from immunological concepts to effective vaccines and protective antibodies. *Nature Immunology*, pages 1–13, 2018.

[164] Anthony L Cunningham, Himal Lal, Martina Kovac, Roman Chlibek, Shinn-Jang Hwang, Javier D\textbackslash'\textbackslashiez-Domingo, Olivier Godeaux, Myron J Levin, Janet E McElhaney, Joan Puig-Barberà, Carline Vanden Abeele, Timo Vesikari, Daisuke Watanabe, Toufik Zahaf, Anitta Ahonen, Eugene Athan, Jose F Barba-Gomez, Laura Campora, Ferdinandus de Looze, H Jackson Downey, Wayne Ghesquiere, Iris Gorfinkel, Tiina Korhonen, Edward Leung, Shelly A McNeil, Lidia Oostvogels, Lars Rombo, Jan Smetana, Lily Weckx, Wilfred Yeo, and Thomas C Heineman. Efficacy of the Herpes Zoster Subunit Vaccine in Adults 70 Years of Age or Older. *doi.org*, 375(11):1019–1032, 2016.

[165] Dereck R. Tait, Mark Hatherill, Olivier Van Der Meeren, Ann M. Ginsberg, Elana Van Brakel, Bruno Salaun, Thomas J. Scriba, Elaine J. Akite, Helen M. Ayles, Anne Bollaerts, Marie-Ange Demoitié, Andreas Diacon, Thomas G. Evans, Paul Gillard, Elizabeth Hellström, James C. Innes, Maria Lempicki, Mookho Malahleha, Neil Martinson, Doris Mesia Vela, Monde Muyoyeta, Videlis Nduba, Thierry G. Pascal, Michele Tameris, Friedrich Thienemann, Robert J. Wilkinson, and François Roman. Final Analysis of a Trial of M72/AS01 ¡sub¿E¡/sub¿ Vaccine to Prevent Tuberculosis. *New England Journal of Medicine*, 381(25):2429–2439, 12 2019.

[166] Robert A van den Berg, Margherita Coccia, W Ripley Ballou, Kent E Kester, Christian F Ockenhouse, Johan Vekemans, Erik Jongert, Arnaud M Didierlaurent, and Robbert G van der Most. Predicting RTS,S Vaccine-Mediated Protection from Transcriptomes in a Malaria-Challenge Clinical Trial. *Frontiers in Immunology*, 8:1013–1021, 2017.

[167] Verónica Mata-Haro, Caglar Cekic, Michael Martin, Paula M Chilton, Carolyn R Casella, and Thomas C Mitchell. The vaccine adjuvant monophosphoryl lipid A as a TRIF-biased agonist of TLR4. *Science*, 316(5831):1628–1632, 2007.

[168] Sonja T H M Kolanowski, Miranda C Dieker, Suzanne N Lissenberg-Thunnissen, Gijs M W van Schijndel, S Marieke van Ham, and Anja ten Brinke. TLR4-mediated pro-inflammatory dendritic cell differentiation in humans requires the combined action of MyD88 and TRIF. *Innate Immunity*, 20(4):423–430, 2014.

[169] James A Butler, Jason Cosgrove, Kieran Alden, Jon Timmis, and Mark Christopher Coles. Model-Driven Experimentation: A New Approach to Understand Mechanisms of Tertiary Lymphoid Tissue Formation, Function, and Therapeutic Resolution. *Frontiers in Immunology*, 7(6):764–767, 2017.

[170] Anthony Trewavas. A brief history of systems biology. "Every object that biology studies is a system of systems." Francois Jacob (1974). *THE PLANT CELL ONLINE*, 18(10):2420–2430, 2006.

[171] Claudia Monaco, Jagdeep Nanchahal, Peter Taylor, and Marc Feldmann. Anti-TNF therapy: past, present and future. *International Immunology*, 27(1):55–62, 2015.

[172] Robert L Coffman. Origins of the T H 1-T H 2 model: a personal perspective. *Nature Immunology*, 7(6):539–541, 2006.

[173] T R Mosmann, R L Coffman Annual review of immunology, and 1989. TH1 and TH2 cells: different patterns of lymphokine secretion lead to different functional properties. *annualreviews.org*.

[174] Natasha Whibley, Andrea Tucci, and Fiona Powrie. Regulatory T cell adaptation in the intestine and skin. *Nature Immunology*, 20(4):386–396, 2019.

[175] Martin H. Johnson. Robert Edwards: The path to IVF. *Reproductive BioMedicine Online*, 23(2):245–262, 8 2011.

[176] A M Turing. The chemical basis of morphogenesis. *Bulletin of Mathematical Biology*, 52(1-2):153–197, 1990.

[177] David D Ho, Avidan U Neumann, Alan S Perelson, Wen Chen, John M Leonard, and Martin Markowitz. Rapid turnover of plasma virions and CD4 lymphocytes in HIV-1 infection. *Nature*, 373(6510):123–126, 1995.

[178] W O Kermack and A G McKendrick. A Contribution to the Mathematical Theory of Epidemics. *Proceedings of the Royal Society A: Mathematical, Physical and Engineering Sciences*, 115(772):700–721, 1927.

[179] Fiona A C Polack. Choosing and adapting design notations in the principled development of complex systems simulations for research. In *the Modelling of the Physical World Workshop*, pages 1–6, New York, New York, USA, 2012. ACM Press.

[180] Olivia Guest and Andrea Martin. How computational modeling can force theory building in psychological science. 2020.

[181] Mark Read. Statistical and Modelling Techniques to Build Confidence in the Investigation of Immunology through Agent-Based Simulation. *PhD Thesis, Department of Computer Science, University of York*, (September), 2011.

[182] F Pappalardo, S Motta, P L Lollini, and E Mastriani. Analysis of vaccine{{\textbackslash}textquoteright}s schedules using models. *Cellular Immunology*, 244(2):137–140, 2006.

[183] Liam V Brown, Eamonn A Gaffney, Jonathan Wagg, and Mark C Coles. An in silico model of cytotoxic T-lymphocyte activation in the lymph node following short peptide vaccination. *Journal of the Royal Society Interface*, 2018.

[184] Francesco Pappalardo, Darren Flower, Giulia Russo, Marzio Pennisi, and Santo Motta. Computational modelling approaches to vaccinology. *Pharmacological Research*, 92:40–45, 2015.

[185] J. Cosgrove, J. Butler, K. Alden, M. Read, V. Kumar, L. Cucurull-Sanchez, J. Timmis, and M. Coles. Agent-based modeling in systems pharmacology. *CPT: Pharmacometrics and Systems Pharmacology*, 4(11):615–629, 2015.

[186] Daniel E Zak, Vincent C Tam, and Alan Aderem. Systems-Level Analysis of Innate Immunity. *Annual Review of Immunology*, 32(1):547–577, 2014.

[187] Bali Pulendran. Learning immunology from the yellow fever vaccine: innate immunity to systems vaccinology. *Nature Reviews Immunology*, 9(10):741–747, 2009.

[188] Shuzhao Li, Andrei Todor, and Ruiyan Luo. Blood transcriptomics and metabolomics for personalized medicine. *Computational and Structural Biotechnology Journal*, 14:1–7, 2016.

[189] Martin J Fraunholz. Systems biology in malaria research. *Trends in Parasitology*, 21(9):393–395, 2005.

[190] Marta Luksza, Nadeem Riaz, Vladimir Makarov, Vinod P. Balachandran, Matthew D. Hellmann, Alexander Solovyov, Naiyer A. Rizvi, Taha Merghoub, Arnold J. Levine, Timothy A. Chan, Jedd D. Wolchok, and Benjamin D. Greenbaum. A neoantigen fitness model predicts tumour response to checkpoint blockade immunotherapy. *Nature*, 551(7681):517–520, 2017.

[191] Birkir Reynisson, Bruno Alvarez, Sinu Paul, Bjoern Peters, and Morten Nielsen. NetMHCpan-4.1 and NetMHCIIpan-4.0: improved predictions of MHC antigen presentation by concurrent motif deconvolution and integration of MS MHC eluted ligand data. *Nucleic acids research*, 48(W1):W449–W454, 7 2020.

[192] Huang Huang, Chunlin Wang, Florian Rubelt, Thomas J. Scriba, and Mark M. Davis. Analyzing the Mycobacterium tuberculosis immune response by T-cell receptor clustering with GLIPH2 and genome-wide antigen screening. *Nature Biotechnology*, 38(10):1194–1202, 2020.

[193] Ronald N Germain, Martin Meier-Schellersheim, Aleksandra Nita-Lazar, and Iain D C Fraser. Systems biology in immunology: a computational modeling perspective. *Annual Review of Immunology*, 29(1):527–585, 2011.

[194] John W J Moore, Daniel Moyo, Lynette Beattie, Paul S Andrews, Jon Timmis, and Paul M Kaye. Functional complexity of the Leishmania granuloma and the potential of in silico modeling. *Frontiers in Immunology*, 4:35, 2013.

[195] Luca Albergante, Jon Timmis, Lynette Beattie, and Paul M Kaye. A Petri Net Model of Granulomatous Inflammation: Implications for IL-10 Mediated Control of Leishmania donovani Infection. *PLoS Computational Biology*, 9(11):e1003334–13, 2013.

[196] J E Wigginton and D Kirschner. A model to predict cell-mediated immune regulatory mechanisms during human infection with Mycobacterium tuberculosis. *The Journal of Immunology*, 166(3):1951–1967, 2001.

[197] Simeone Marino, Amy Myers, JoAnne L Flynn, and Denise E Kirschner. TNF and IL-10 are major factors in modulation of the phagocytic cell environment in lung and lymph node in tuberculosis: A next-generation two-compartmental model. *Journal of Theoretical Biology*, 265(4):586–598, 2010.

[198] Thomas Hagan, Helder I Nakaya, Shankar Subramaniam, and Bali Pulendran. Systems vaccinology: Enabling rational vaccine design with systems biological approaches. *Vaccine*, 33(40):5294–5301, 2015.

[199] Andreas Handel, Nicole L. La Gruta, and Paul G. Thomas. Simulation modelling for immunologists, 3 2020.

[200] Jonathan Carruthers, Grant Lythe, Martín López-García, Joseph Gillard, Thomas R. Laws, Roman Lukaszewski, and Carmen Molina-París. Stochastic dynamics of francisella tularensis infection and replication. *PLoS Computational Biology*, 16(6), 2020.

[201] National Research Council (US) Committee on Frontiers at the Interface of Computing and Biology, John C Wooley, and Herbert S Lin. Catalyzing Inquiry at the Interface of Computing and Biology. 2005.

[202] Andreas Handel, Nicole L. La Gruta, and Paul G. Thomas. Simulation modelling for immunologists. *Nature Reviews Immunology*, 20(3):186–195, 2020.

[203] Alan S Perelson and Ruy M Ribeiro. Modeling the within-host dynamics of HIV infection. *BMC Biology*, 11(1):10–96, 2013.

[204] Joanneke E. Jansen, Eamonn A. Gaffney, Jonathan Wagg, and Mark C. Coles. Combining mathematical models with experimentation to drive novel mechanistic insights into macrophage function. *Frontiers in Immunology*, 10(JUN):1–9, 2019.

[205] Stephanie Evans. *A Computational Approach to Studying the Inflammatory Processes Active During Helicobacter hepaticus-Induced Intestinal Inflammation.* PhD thesis, University of York, 2016.

[206] Nargesalsadat Dorratoltaj, Ryan Nikin-Beers, Stanca M. Ciupe, Stephen G. Eubank, and Kaja M. Abbas. Multiscale immunoepidemiological modeling of within-host and betweenhost HIV dynamics: Systematic review of mathematical models. *PeerJ*, 2017(9), 2017.

[207] Rustom Antia, Carl T Bergstrom, Sergei S Pilyugin, Susan M Kaech, and Rafi Ahmed. Models of CD8+ responses: 1. What is the antigen-independent proliferation program. *Journal of Theoretical Biology*, 221(4):585–598, 2003.

[208] Matthew Onsum and Christopher V Rao. A mathematical model for neutrophil gradient sensing and polarization. *PLoS Computational Biology*, 3(3):e36–0450, 2007.

[209] Amy L Bauer, Catherine A A Beauchemin, and Alan S Perelson. Agent-based modeling of host{{\textbackslash}textendash}pathogen systems: The successes and challenges. *Information Sciences*, 179(10):1379–1389, 2009.

[210] Jason Cosgrove, J Cosgrove, Jon Timmis, Kieran Alden, James Butler, J Butler, K Alden, Mark Read, M Read, V Kumar, Vipin Kumar, Lourdes Cucurull-Sanchez, L Cucurull-Sanchez, J Timmis, Mark Coles, and M Coles. Agent-Based Modeling in Systems Pharmacology. *CPT: Pharmacometrics & Systems Pharmacology*, 4(11):615–629, 2015.

[211] Gib Bogle and P Rod Dunbar. Agent-based simulation of T-cell activation and proliferation within a lymph node. *Immunology and Cell Biology*, 88(2):172–179, 2010.

[212] Carla R.B. Bonin, Guilherme C. Fernandes, Rodrigo W. dos Santos, and Marcelo Lobosco. A qualitatively validated mathematical-computational model of the immune response to the yellow fever vaccine. *BMC Immunology*, 19(1):15, 5 2018.

[213] Rino Rappuoli. Reverse vaccinology, a genome-based approach to vaccine development. *Vaccine*, 19(17-19):2688–2691, 2001.

[214] Dominic F Kelly and Rino Rappuoli. Reverse Vaccinology and Vaccines for Serogroup B ¡Emphasis Type="Italic"¿Neisseria meningitidis¡/Emphasis¿. In *Hot Topics in Infection and Immunity in Children II*, pages 217–223. Springer, Boston, MA, Boston, MA, 2005.

[215] Lijo John, Georrge J John, and Trupti Kholia. A reverse vaccinology approach for the identification of potential vaccine candidates from leishmania spp. In *Applied Biochemistry and Biotechnology*, 2012.

[216] A E Lew-Tabor and M Rodriguez Valle. A review of reverse vaccinology approaches for the development of vaccines against ticks and tick borne diseases, 2016.

[217] Rino Rappuoli, Rino Rappuoli, Ennio De Gregorio, Matthew J Bottomley, Matthew J Bottomley, Ugo D\textbackslashtextquoterightOro, Ugo D\textbackslashtextquoterightOro, Oretta Finco, and Oretta Finco. Reverse vaccinology 2.0: Human immunology instructs vaccine antigen design. *The Journal of Experimental Medicine*, 213(4):469–481, 2016.

[218] Manisha Pritam, Garima Singh, Suchit Swaroop, Akhilesh Kumar Singh, and Satarudra Prakash Singh. Exploitation of reverse vaccinology and immunoinformatics as promising platform for genome-wide screening of new effective vaccine candidates against Plasmodium falciparum. *BMC Bioinformatics*, 2019.

[219] Kamilla Kjærgaard Jensen, Massimo Andreatta, Paolo Marcatili, Søren Buus, Jason A Greenbaum, Zhen Yan, Alessandro Sette, Bjoern Peters, and Morten Nielsen. Improved methods for predicting peptide binding affinity to MHC class II molecules. *Immunology*, 2018.

[220] Paul R Buckley, Ruichong Ma, Chloe H Lee, Isaac Woodhouse, Jeongmin Woo, Vasily O Tsvetkov, Dmitrii S Shcherbinin, Agne Antanaviciute, Mikhail Shugay, Margarida Rei, Alison Simmons, and Hashem Koohy. Evaluating performance of existing computational models in predicting CD8+ T cell pathogenic epitopes and cancer neoantigens. *bioRxiv*, page 2020.12.25.424183, 12 2020.

[221] Yongqun He. Vaccine adjuvant informatics: From data integration and analysis to rational vaccine adjuvant design, 2014.

[222] H I Nakaya and B Pulendran. Vaccinology in the era of high-throughput biology. *Philosophical Transactions of the Royal Society B: Biological Sciences*, 370(1671):20140146, 2015.

[223] Mario Castro, Grant Lythe, Carmen Molina-París, and Ruy M. Ribeiro. Mathematics in modern immunology. *Interface Focus*, 0 2016.

[224] Gib Bogle and P Rod Dunbar. On-Lattice Simulation of T Cell Motility, Chemotaxis, and Trafficking in the Lymph Node Paracortex. *PLoS ONE*, 2012.

[225] Jens Geginat, Moira Paroni, Stefano Maglie, Johanna Sophie Alfen, Ilko Kastirr, Paola Gruarin, Marco de Simone, Massimiliano Pagani, and Sergio Abrignani. Plasticity of human CD4 T cell subsets, 2014.

[226] Andrew Yates, Claudia Bergmann, J. Leo Van Hemmen, Jaroslav Stark, and Robin Callard. Cytokine-modulated regulation of helper T cell populations. *Journal of Theoretical Biology*, 206(4):539–560, 2000.

[227] Dominik Aschenbrenner, Maria Quaranta, Soumya Banerjee, Nicholas Ilott, Joanneke Jansen, Boyd Steere, Yin Huai Chen, Stephen Ho, Karen Cox, Carolina V. Arancibia-Cárcamo, Mark Coles, Eamonn Gaffney, Simon P.L. Travis, Lee Denson, Subra Kugathasan, Jochen Schmitz, Fiona Powrie, Stephen N. Sansom, and Holm H. Uhlig. Deconvolution of monocyte responses in inflammatory bowel disease reveals an IL-1 cytokine network that regulates IL-23 in genetic and acquired IL-10 resistance, 2020.

[228] Denise Kirschner, Elsje Pienaar, Simeone Marino, and Jennifer J Linderman. A review of computational and mathematical modeling contributions to our understanding of Mycobacterium tuberculosis within-host infection and treatment. *Current Opinion in Systems Biology*, 3:170–185, 2017.

[229] L Michaelis, Maud L Menten, Roger S Goody, and Kenneth A Johnson. Die Kinetik der Invertinwirkung/ The kinetics of invertase action. *Biochemistry*, 1913.

[230] Simeone Marino, Mohammed El-Kebir, and Denise Kirschner. A hybrid multi-compartment model of granuloma formation and T cell priming in Tuberculosis. *Journal of Theoretical Biology*, 280(1):50–62, 7 2011.

[231] Denise Kirschner, Elsje Pienaar, Simeone Marino, and Jennifer J. Linderman. A review of computational and mathematical modeling contributions to our understanding of Mycobacterium tuberculosis within-host infection and treatment. *Current Opinion in Systems Biology*, 3:170–185, 2017.

[232] Carla Rezende Barbosa Bonin, Guilherme Côrtes Fernandes, Reinaldo de Menezes Martins, Luiz Antonio Bastos Camacho, Andréa Teixeira-Carvalho, Licia Maria Henrique da Mota, Sheila Maria Barbosa de Lima, Ana Carolina Campi-Azevedo, Olindo Assis Martins-Filho, Rodrigo Weber dos Santos, and Marcelo Lobosco. Validation of a yellow fever vaccine model using data from primary vaccination in children and adults, re-vaccination and dose-response in adults and studies with immunocompromised individuals. *BMC Bioinformatics*, 21(Suppl 17), 12 2020.

[233] P. L. F. Johnson, B. F. Kochin, M. S. McAfee, I. M. Stromnes, R. R. Regoes, R. Ahmed, J. N. Blattman, and R. Antia. Vaccination Alters the Balance between Protective Immunity, Exhaustion, Escape, and Death in Chronic Infections. *Journal of Virology*, 85(11):5565–5570, 6 2011.

[234] Elise Alspach, Danielle M Lussier, Alexander P Miceli, Ilya Kizhvatov, Michel Dupage, Adrienne M Luoma, Wei Meng, Cheryl F Lichti, Ekaterina Esaulova, Anthony N Vomund, Daniele Runci, Jeffrey P Ward, Matthew M Gubin, Ruan F V Medrano, Cora D Arthur, J Michael White, Kathleen C F Sheehan, Alex Chen, Kai W Wucherpfennig, Tyler Jacks, Emil R Unanue, Maxim N Artyomov, and Robert D Schreiber. MHC-II neoantigens shape tumour immunity and response to immunotherapy. *Nature*, (February), 2019.

[235] Marzio Pennisi, Francesco Pappalardo, Ariannna Palladini, Giordano Nicoletti, Patrizia Nanni, Pier Luigi Lollini, and Santo Motta. Modeling the competition between lung metastases and the immune system using agents. *BMC Bioinformatics*, 2010.

[236] Marzio Pennisi, Roberto Catanuto, Francesco Pappalardo, and Santo Motta. Optimal vaccination schedules using simulated annealing. *Bioinformatics*, 2008.

[237] E. A. Gaffney. The application of mathematical modelling to aspects of adjuvant chemotherapy scheduling. *Journal of Mathematical Biology*, 48(4):375–422, 4 2004.

[238] Francesco Pappalardo, Epifanio Fichera, Nicoletta Paparone, Alessandro Lombardo, Marzio Pennisi, Giulia Russo, Marco Leotta, Alessandro Pedretti, Francesco De Fiore, and Santo Motta. A computational model to predict the immune system activation by citrus-derived vaccine adjuvants. *Bioinformatics*, 2016.

[239] James A Butler. *Model Hybridisation and Visualisation Techniques for the Investigation of Complex Disease Processes*. PhD thesis, University of York, 2016.

[240] Volker Grimm, Uta Berger, Donald L DeAngelis, J Gary Polhill, Jarl Giske, and Steven F Railsback. The ODD protocol: A review and first update. *Ecological Modelling*, 2010.

[241] Fiona A C Polack, Tim Hoverd, Adam T Sampson, Susan Stepney, and Jon Timmis. Complex systems models: Engineering simulations. In *Artificial Life XI: Proceedings of the 11th International Conference on the Simulation and Synthesis of Living Systems, ALIFE 2008*, 2008.

[242] Paul S Andrews, Fiona A C Polack, Adam T Sampson, S Stepney, and J Timmis. The CoSMoS Process, Version 0.1: A Process for the Modelling and Simulation of Complex Systems. *University of York Technical Report, YCS-2010-453, Department of Computer Science, University of York*, (March):1–40, 2010.

[243] Kieran Alden. *Simulation and Statistical Techniques to Explore Lymphoid Tissue Organogenesis.* PhD thesis, University of York, 2012.

[244] Mark N. Read, Kieran Alden, Louis M. Rose, and Jon Timmis. Automated multi-objective calibration of biological agent-based simulations. *Journal of the Royal Society Interface*, 13(122), 2016.

[245] Mark N Read, Kieran Alden, Jon Timmis, and Paul S Andrews. Strategies for calibrating models of biology. *Briefings in Bioinformatics*, 2018.

[246] Marc C Kennedy and Anthony O'Hagan. Bayesian calibration of computer models. *Journal of the Royal Statistical Society: Series B (Statistical Methodology)*, 2001.

[247] Thomas Bayes and Richard Price. An Essay towards Solving a Problem in the Doctrine of Chances By the Late Rev. Mr. Bayes. *Philosophical Transactions (1683-1775)*, 1763.

[248] Gabriele Lillacci and Mustafa Khammash. Parameter estimation and model selection in computational biology. *PLoS Computational Biology*, 2010.

[249] Kieran Alden, Paul S Andrews, Fiona A C Polack, Henrique Veiga-fernandes, Mark C Coles, and Jon Timmis. Using argument notation to engineer biological simulations with increased confidence. *Journal of The Royal Society Interface*, 12(104):20141059, 2015.

[250] Simeone Marino, Ian B Hogue, Christian J Ray, and Denise E Kirschner. A methodology for performing global uncertainty and sensitivity analysis in systems biology. *Journal of Theoretical Biology*, 254(1):178–196, 2008.

[251] Kieran Alden, Jon Timmis, Paul S Andrews, Henrique Veiga-fernandes, and Mark Coles. Extending and Applying Spartan to Perform Temporal Sensitivity Analyses for Predicting Changes in Influential Biological Pathways in Computational Models. *IEEE/ACM Transactions on Computational Biology and Bioinformatics*, 14(2):431–442, 2017.

[252] Kieran Alden, Jon Timmis, Paul S Andrews, Henrique Veiga-fernandes, and Mark C Coles. Pairing experimentation and computational modeling to understand the role of tissue inducer cells in the development of lymphoid organs. *Frontiers in Immunology*, 3(July):120–172, 2012.

[253] András Vargha and Harold D Delaney. A critique and improvement of the CL common language effect size statistics of McGraw and Wong. *Journal of Educational and Behavioral Statistics*, 2000.

[254] Simeone Marino, Ian B Hogue, Christian J Ray, and Denise E Kirschner. *A methodology for perfoming gloabl*, volume 254. 2009.

[255] Andrea Saltelli and Ricardo Bolado. An alternative way to compute Fourier amplitude sensitivity test (FAST). *Computational Statistics and Data Analysis*, 26(4):445–460, 1998.

[256] M Read, Mark Read, P S Andrews, Paul S Andrews, J Timmis, Jon Timmis, V Kumar, and Vipin Kumar. Modelling biological behaviours with the unified modelling language: an immunological case study and critique. *Journal of The Royal Society Interface*, 11(99):10.1098–rsif.2014.0704, 2014.

[257] Jonathan David Hamp. An Interdisciplinary Approach to Investigating Drug Distribution During Experimental Visceral Leishmaniasis. (September), 2018.

[258] Karline Soetaert, Thomas Petzoldt, and R Woodrow Setzer. Solving differential equations in R: Package deSolve. *Journal of Statistical Software*, 2010.

[259] Simeone Marino, Ian B. Hogue, Christian J. Ray, and Denise E. Kirschner. A methodology for performing global uncertainty and sensitivity analysis in systems biology, 9 2008.

[260] Kieran Alden, Mark Read, Jon Timmis, Paul S Andrews, Henrique Veiga-Fernandes, and Mark Coles. Spartan: A Comprehensive Tool for Understanding Uncertainty in Simulations of Biological Systems. *PLoS Computational Biology*, 2013.

[261] Nan Hung Hsieh, Brad Reisfeld, and Weihsueh A. Chiu. pksensi: An R package to apply global sensitivity analysis in physiologically based kinetic modeling. *SoftwareX*, 12:100609, 2020.

[262] Fanny Sarrazin, Francesca Pianosi, and Thorsten Wagener. Global Sensitivity Analysis of environmental models: Convergence and validation. *Environmental Modelling and Software*, 79:135–152, 2016.

[263] C T H Baker, G A Bocharov, J M Ford, P M Lumb, S J Norton, C A H Paul, T Junt, P Krebs, and B Ludewig. Computational approaches to parameter estimation and model selection in immunology. *Journal of Computational and Applied Mathematics*, 2005.

[264] Henry Philip Mirsky, Mark J Miller, and Jennifer J Linderman. Systems biology approaches for understanding cellular mechanisms of immunity in lymph nodes during infection. (734):160–170, 2015.

[265] Paul Nurse. Biology must generate ideas as well as data. *Nature*, 597:305, 2021.

[266] Raimond L Winslow, R L Winslow, N Trayanova, Natalia Trayanova, D Geman, Donald Geman, Michael I Miller, and M I Miller. Computational medicine: translating models to clinical care. *Science Translational Medicine*, 4(158):158rv11–158rv11, 2012.

[267] Juilee Thakar, Ashutosh K Pathak, Lisa Murphy, Réka Albert, and Isabella M Cattadori. Network Model of Immune Responses Reveals Key Effectors to Single and Co-infection Dynamics by a Respiratory Bacterium and a Gastrointestinal Helminth. *PLoS Computational Biology*, 8(1):e1002345–19, 2012.

[268] Brian J Schmidt, Jason a Papin, and Cynthia J Musante. Mechanistic systems modeling to guide drug discovery and development. *Drug Discovery Today*, 18(3-4):116–127, 2013.

[269] Akira Funahashi, Yukiko Matsuoka, Akiya Jouraku, Hiroaki Kitano, and Norihiro Kikuchi. Celldesigner: A modeling tool for biochemical networks. In *Proceedings - Winter Simulation Conference*, 2006.

[270] Nicolas Le Novere, Michael Hucka, Huaiyu Mi, Stuart Moodie, Falk Schreiber, Anatoly Sorokin, Emek Demir, Katja Wegner, Mirit I Aladjem, Sarala M Wimalaratne, Frank T Bergman, Ralph Gauges, Peter Ghazal, Hideya Kawaji, Lu Li, Yukiko Matsuoka, Alice Villeger, Sarah E Boyd, Laurence Calzone, Melanie Courtot, Ugur Dogrusoz, Tom C Freeman, Akira Funahashi, Samik Ghosh, Akiya Jouraku, Sohyoung Kim, Fedor Kolpakov, Augustin Luna, Sven Sahle, Esther Schmidt, Steven Watterson, Guanming Wu, Igor Goryanin, Douglas B Kell, Chris Sander, Herbert Sauro, Jacky L Snoep, and Kurt Kohn Hiroaki Kitano. The systems biology graphical notation. pages 1–8, 2009.

[271] Astrid Junker, Hendrik Rohn, Tobias Czauderna, Christian Klukas, Anja Hartmann, and Falk Schreiber. Creating interactive, web-based and data-enriched maps with the Systems Biology Graphical Notation. *Nature Protocols*, 2012.

[272] Tri Giang Phan, Jesse A Green, Elizabeth E Gray, Ying Xu, and Jason G Cyster. Immune complex relay by subcapsular sinus macrophages and noncognate B cells drives antibody affinity maturation. *Nature Immunology*, 10(7):786–793, 2009.

[273] Adam Penn-Nicholson, Hennie Geldenhuys, Wivine Burny, Robbert van der Most, Cheryl L Day, Erik Jongert, Philippe Moris, Mark Hatherill, Opokua Ofori-Anyinam, Willem Hanekom, Anne Bollaerts, Marie Ange Demoitie, Angelique Kany Kany Luabeya, Evi De Ruymaeker, Michele Tameris, Didier Lapierre, and Thomas J Scriba. Safety and immunogenicity of candidate vaccine M72/AS01 E in adolescents in a TB endemic setting. *Vaccine*, 2015.

[274] Jean-Philippe Michaud, Maxime Hallé, Antoine Lampron, Peter Thériault, Paul Préfontaine, Mohammed Filali, Pascale Tribout-Jover, Anne-Marie Lanteigne, Rachel Jodoin, Christopher Cluff, Vincent Brichard, Rémi Palmantier, Anthony Pilorget, Daniel Larocque, and Serge Rivest. Toll-like receptor 4 stimulation with the detoxified ligand monophosphoryl lipid A improves Alzheimer's disease-related pathology. *Proceedings of the National Academy of Sciences of the United States of America*, 110(5):1941–1946, 2013.

[275] Ichiro Taniuchi. CD4 Helper and CD8 Cytotoxic T Cell Differentiation. *doi.org*, 36(1):579–601, 2018.

[276] Yitzhak Ben-Asouli, Yona Banai, Yehuda Pel-Or, Alexei Shir, and Raymond Kaempfer. Human interferon-gamma mRNA autoregulates its translation through a pseudoknot that activates the interferon-inducible protein kinase PKR. *Cell*, 108(2):221–232, 2002.

[277] Robert B Henderson, Nancy Hogg, Meg Mathies, and Josie A R Hobbs. Rapid recruitment of inflammatory monocytes is independent of neutrophil migration. 102(1):328–335, 2003.

[278] Borko Amulic, Christel Cazalet, Garret L Hayes, Kathleen D Metzler, and Arturo Zychlinsky. Neutrophil function: from mechanisms to disease. *Annual Review of Immunology*, 30(1):459–489, 2012.

[279] Masahiro Hiasa, Masahiro Abe, Ayako Nakano, Asuka Oda, Hiroe Amou, Shinsuke Kido, Kyoko Takeuchi, Kumiko Kagawa, Kenichiro Yata, Toshihiro Hashimoto, Shuji Ozaki, Kenzo Asaoka, Eiji Tanaka, Keiji Moriyama, and Toshio Matsumoto. GM-CSF and IL-4 induce dendritic cell differentiation and disrupt osteoclastogenesis through M-CSF receptor shedding by up-regulation of TNF-{$α$} converting enzyme (TACE). *Blood*, 2009.

[280] Isabelle Bekeredjian-Ding, Susanne Ilona Roth, Stefanie Gilles, Thomas Giese, Andrea Ablasser, Veit Hornung, Stefan Endres, and Gunther Hartmann. T Cell-Independent, TLR-Induced IL-12p70 Production in Primary Human Monocytes. *The Journal of Immunology*, 2006.

[281] Mary F Lipscomb and Barbara J Masten. Dendritic cells: Immune regulators in health and disease, 2002.

[282] Francesca Granucci, Francesca Granucci, Elisabetta Ferrero, Maria Foti, Diego Aggujaro, and Katuscia Vettoretto. Early events in dendritic cell maturation induced by LPS. pages 1079–1084, 1999.

[283] S E Macatonia, N a Hosken, M Litton, P Vieira, C S Hsieh, J a Culpepper, M Wysocka, G Trinchieri, K M Murphy, and a O'Garra. Dendritic cells produce IL-12 and direct the development of Th1 cells from naive CD4+ T cells. *The Journal of Immunology*, 154(10):5071–5079, 1995.

[284] A Snijders, P Kalinski, C M Hilkens, and M L Kapsenberg. High-level IL-12 production by human dendritic cells requires two signals. *International Immunology*, 10(11):1593–1598, 1998.

[285] Alfonso Mart\textbackslash'\textbackslashin-Fontecha, Lindy L Thomsen, Sara Brett, Craig Gerard, Martin Lipp, Antonio Lanzavecchia, and Federica Sallusto. Induced recruitment of NK cells to lymph nodes provides IFN-${$γ$}$ for TH1 priming. *Nature Immunology*, 5(12):1260–1265, 2004.

[286] Guido Ferlazzo, G Ferlazzo, Maggi Pack, M Pack, Dolca Thomas, D Thomas, Casper Paludan, C Paludan, D Schmid, Dorothee Schmid, T Strowig, Till Strowig, Gwenola Bougras, G Bougras, W a Muller, William A Muller, L Moretta, Lorenzo Moretta, C Munz, and Christian Münz. Distinct roles of IL-12 and IL-15 in human natural killer cell activation by dendritic cells from secondary lymphoid organs. *Proceedings of the National Academy of Sciences*, 101(47):16606–16611, 2004.

[287] Eleanor M Riley, A Horowitz, Amir Horowitz, Ron H Behrens, R H Behrens, Lucy Okell, L Okell, A R Fooks, R Anthony, E M Riley, Ron H Behrens, Lucy Okell, and Anthony R Fooks. NK Cells as Effectors of Acquired Immune Responses: Effector CD4+ T Cell-Dependent Activation of NK Cells Following Vaccination. *The Journal of Immunology*, 185(5):2808–2818, 2010.

[288] Andrea A Itano and Marc K Jenkins. Antigen presentation to naive CD4 T cells in the lymph node. *Nature Immunology*, 4(8):733–739, 2003.

[289] Christian R Engwerda, Susanna S Ng, and Patrick T Bunn. The Regulation of CD4(+) T Cell Responses during Protozoan Infections. *Frontiers in Immunology*, 5(OCT):498–499, 2014.

[290] Jennifer J Linderman, Denise E Kirschner, J J Linderman, Mark Miller, Jennifer J Linderman, T Riggs, M Pande, Jennifer J Linderman, Thomas Riggs, M Miller, Manjusha Pande, S Marino, D E Kirschner, and Simeone Marino. Characterizing the Dynamics of CD4+ T Cell Priming within a Lymph Node. *The Journal of Immunology*, 184(6):2873–2885, 2010.

[291] a Berger. Th1 and Th2 responses: what are they? *BMJ*, 321(7258):424, 2000.

[292] Andrew Cope, Gaelle Le Friec, John Cardone, and Claudia Kemper. The Th1 life cycle: molecular control of IFN-${$γ$}$ to IL-10 switching. *Trends in Immunology*, 32(6):278–286, 2011.

[293] Audrey Baeyens, Victoria Fang, Cynthia Chen, and Susan R Schwab. Exit Strategies: S1P Signaling and T Cell Migration, 2015.

[294] National Research Council; Division of Behavioral, Social Sciences, on Behavioral Cognitive, Sensory Sciences; Committee on the Science of Team Science; Nancy J. Cooke, and Editors Margaret L. Hilton. *Enhancing the Effectiveness of Team Science*. 2015.

[295] Katherine L Bouman. Extreme Imaging via Physical Model Inversion : Seeing Around Corners and Imaging Black Holes by. *Doctor Thesis*, 2017.

[296] S Issaoun, M D Johnson, L Blackburn, C D Brinkerink, M Mościbrodzka, A Chael, C Goddi, I Martí-Vidal, J Wagner, S S Doeleman, H Falcke, T P Krichbaum, K Akiyama, U Bach, K L Bouman, G C Bower, A Broderick, I Cho, G Crew, J Dexter, V Fish, R Gold, J L Gómez, K Hada, A Hernández-Gómez, M Janßen, M Kino, M Kramer, L Loinard, R.-S. Lu, S Markoff, D P Marrone, L D Matthews, J M Moran, C Müller, F Roelofs, E Ros, H Rottmann, S Sanchez, R P J Tilanus, P de Vicente, M Wielgus, J A Zensus, and G.-Y. Zhao. The Size, Shape, and Scattering of Sagittarius A* at 86 GHz: First VLBI with ALMA. *The Astrophysical Journal*, 2019.

[297] Florian Krammer. SARS-CoV-2 vaccines in development. *Nature*, pages 1–16, 2020.

[298] Ali M Harandi. Systems analysis of human vaccine adjuvants, 2018.

[299] Dmitri Kazmin, Helder I Nakaya, Eva K Lee, Matthew J Johnson, Robbert Van Der Most, Robert A Van Den Berg, W Ripley Ballou, Erik Jongert, Ulrike Wille-Reece, Christian Ockenhouse, Alan Aderem, Daniel E Zak, Jerald Sadoff, Jenny Hendriks, Jens Wrammert, Rafi Ahmed, and Bali Pulendran. Systems analysis of protective immune responses to RTS,S malaria vaccination in humans. *Proceedings of the National Academy of Sciences of the United States of America*, 2017.

[300] Henry R Hampton, Tatyana Chtanova, and Tatyana Chtanova. The lymph node neutrophil. *Seminars in Immunology*, 28(2):129–136, 2016.

[301] Ryan N. Gutenkunst, Joshua J. Waterfall, Fergal P. Casey, Kevin S. Brown, Christopher R. Myers, and James P. Sethna. Universally sloppy parameter sensitivities in systems biology models. *PLoS Computational Biology*, 3(10):1871–1878, 2007.

[302] Katsushi Hosohara, Haruyasu Ueda, Shin Ichiro Kashiwamura, Takako Yano, Takeharu Ogura, Seishiro Marukawa, and Haruki Okamura. Interleukin-18 induces acute biphasic reduction in the levels of circulating leukocytes in mice. *Clinical and Diagnostic Laboratory Immunology*, 9(4):777–783, 2002.

[303] Claudia L. Hofstra, Ark Van Ingrid, Gerard Hofman, Frans P. Nijkamp, Paula M. Jardieu, and Antoon J.M. Van Oosterhout. Differential effects of endogenous and exogenous interferon-γ on immunoglobulin E, cellular infiltration, and airway responsiveness in a murine model of allergic asthma. *American Journal of Respiratory Cell and Molecular Biology*, 19(5):826–835, 11 1998.

[304] Mitsuru Ando, Yuki Takahashi, Takuma Yamashita, Mai Fujimoto, Makiya Nishikawa, Yoshihiko Watanabe, and Yoshinobu Takakura. Prevention of adverse events of interferon γ gene therapy by gene delivery of interferon γ-heparin-binding domain fusion protein in mice. *Molecular Therapy - Methods and Clinical Development*, 1:14023, 1 2014.

[305] Ryan N Gutenkunst, Joshua J Waterfall, Fergal P Casey, Kevin S Brown, Christopher R Myers, and James P Sethna. Universally Sloppy Parameter Sensitivities in Systems Biology Models. *PLoS Computational Biology*, 3(10):e189–8, 2007.

[306] A. Raue, C. Kreutz, T. Maiwald, J. Bachmann, M. Schilling, U. Klingmüller, and J. Timmer. Structural and practical identifiability analysis of partially observed dynamical models by exploiting the profile likelihood. *Bioinformatics*, 25(15):1923–1929, 8 2009.

[307] Kieran Alden, Mark Read, Jon Timmis, Paul S Andrews, Henrique Veiga-fernandes, and Mark Coles. Spartan: a comprehensive tool for understanding uncertainty in simulations of biological systems. *PLoS Computational Biology*, 9(2):e1002916, 2013.

[308] Merryn Voysey, Sue Ann Costa Clemens, Shabir A Madhi, Lily Y Weckx, Pedro M Folegatti, Parvinder K Aley, Brian Angus, Vicky L Baillie, Shaun L Barnabas, Qasim E Bhorat, Sagida Bibi, Carmen Briner, Paola Cicconi, Andrea M Collins, Rachel Colin-Jones, Clare L Cutland, Thomas C Darton, Keertan Dheda, Christopher J A Duncan, Katherine R W Emary, Katie J Ewer, Lee Fairlie, Saul N Faust, Shuo Feng, Daniela M Ferreira, Adam Finn, Anna L Goodman, Catherine M Green, Christopher A Green, Paul T Heath, Catherine Hill, Helen Hill, Ian Hirsch, Susanne H C Hodgson, Alane Izu, Susan Jackson, Daniel Jenkin, Carina C D Joe, Simon Kerridge, Anthonet Koen, Gaurav Kwatra, Rajeka Lazarus, Alison M Lawrie, Alice Lelliott, Vincenzo Libri, Patrick J Lillie, Raburn Mallory, Ana V A Mendes, Eveline P Milan, Angela M Minassian, Alastair McGregor, Hazel Morrison, Yama F Mujadidi, Anusha Nana, Peter J O'Reilly, Sherman D Padayachee, Ana Pittella, Emma Plested, Katrina M Pollock, Maheshi N Ramasamy, Sarah Rhead, Alexandre V Schwarzbold, Nisha Singh, Andrew Smith, Rinn Song, Matthew D Snape, Eduardo Sprinz, Rebecca K Sutherland, Richard Tarrant, Emma C Thomson, M Estée Török, Mark Toshner, David P J Turner, Johan Vekemans, Tonya L Villafana, Marion E E Watson, Christopher J Williams, Alexander D Douglas, Adrian V S Hill, Teresa Lambe, Sarah C Gilbert, Andrew J Pollard, and Oxford COVID Vaccine Trial Group. Safety and efficacy of the ChAdOx1 nCoV-19 vaccine (AZD1222) against SARS-CoV-2: an interim analysis of four randomised controlled trials in Brazil, South Africa, and the UK. *Lancet (London, England)*, 0(0), 12 2020.

[309] Merryn Voysey, Sue Ann Costa Clemens, Shabir A. Madhi, Lily Yin Weckx, Pedro M. Folegatti, Parvinder K. Aley, Brian John Angus, Vicky Baillie, Shaun L. Barnabas, Qasim E. Bhorat, Sagida Bibi, Carmen Briner, Paola Cicconi, Elizabeth Clutterbuck, Andrea M. Collins, Clare Cutland, Thomas Darton, Keertan Dheda, Alexander D. Douglas, Christopher J. A. Duncan, Katherine R. W. Emary, Katie Ewer, Amy Flaxman, Lee Fairlie, Saul N. Faust, Shuo Feng, Daniela M. Ferreira, Adam Finn, Eva Galiza, Anna L. Goodman, Catherine M. Green, Christopher A. Green, Melanie Greenland, Catherine Hill, Helen C. Hill, Ian Hirsch, Alane Izu, Daniel Jenkin, Simon Kerridge, Anthonet Koen, Gaurav Kwatra, Rajeka Lazarus, Vincenzo Libri, Patrick J. Lillie, Natalie G. Marchevsky, Richard P. Marshall, Ana Verena Almeida Mendes, Eveline P. Milan, Angela M. Minassian, Alastair C. McGregor, Yama Farooq Mujadidi, Anusha Nana, Sherman D. Payadachee, Daniel J. Phillips, Ana Pittella, Emma Plested, Katrina M. Pollock, Maheshi N. Ramasamy, Hannah Robinson, Alexandre V. Schwarzbold, Andrew Smith, Rinn Song, Matthew D. Snape, Eduardo Sprinz, Rebecca K. Sutherland, Emma C. Thomson, Mili Torok, Mark Toshner, David P. J. Turner, Johan Vekemans, Tonya L. Villafana, Thomas White, Christopher J. Williams, Adrian V. S. Hill, Teresa Lambe, Sarah C. Gilbert, Andrew Pollard, and Oxford COVID Vaccine Trial Group. Single Dose Administration, And The Influence Of The Timing Of The Booster Dose On Immunogenicity and Efficacy Of ChAdOx1 nCoV-19 (AZD1222) Vaccine.

[310] Amir Horowitz, Julius C R Hafalla, Elizabeth King, John Lusingu, Denise Dekker, Amanda Leach, Philippe Moris, Joe Cohen, Johan Vekemans, Tonya Villafana, Patrick H Corran, Philip Bejon, Chris J Drakeley, Lorenz von Seidlein, and Eleanor M Riley. Antigen-specific IL-2 secretion correlates with NK cell responses after immunization of Tanzanian children with the RTS,S/AS01 malaria vaccine. *Journal of immunology (Baltimore, Md. : 1950)*, 188(10):5054–5062, 2012.

[311] Mauro Gaya, Angelo Castello, Beatriz Montaner, Neil Rogers, Caetano Reis E Sousa, Andreas Bruckbauer, and Facundo D Batista. Inflammation-induced disruption of SCS macrophages impairs B cell responses to secondary infection. *Science*, 2015.

[312] Jason A Regules, Jason W Bennett, Erik Jongert, Joe Cohen, Marc Lievens, Sheetij Dutta, Marc Lievens, W Ripley Ballou, Susan B Cicatelli, Kristopher M Paolino, Patrick S Twomey, James E Moon, April K Kathcart, Kevin D Hauns, Jack L Komisar, Aziz N Qabar, Silas A Davidson, Matthew E Griffith, Charles D Magee, Mariusz Wojnarski, Jeffrey R Livezey, Adrian T Kress, Paige E Waterman, Ulrike Wille-Reece, Wayne Volkmuth, Daniel Emerling, William H Robinson, Danielle Morelle, Bebi Yassin-Rajkumar, Cynthia K Lee, Richard Weltzin, Robert M Paris, Norman C Waters, Ashley J Birkett, David C Kaslow, W Ripley Ballou, Christian F Ockenhouse, and Johan Vekemans. Fractional Third and Fourth Dose of RTS,S/AS01 Malaria Candidate Vaccine: A Phase 2a Controlled Human Malaria Parasite Infection and Immunogenicity Study. *Journal of Infectious Diseases*, 214(5):762–771, 2016.

[313] Jishnu Das, Jonathan K Fallon, Timothy C Yu, and Erik Jongert. Delayed fractional dosing with RTS,S/AS01 improves humoral immunity to malaria via a balance of polyfunctional NANP6- and Pf16-specific antibodies. 2021.

[314] Dominika W. Gajdasik, Fabrina Gaspal, Emily E. Halford, Remi Fiancette, Emma E. Dutton, Claire Willis, Timo Rückert, Chiara Romagnani, Audrey Gerard, Sarah L. Bevington, Andrew S. MacDonald, Marina Botto, Timothy Vyse, and David R. Withers. Th1 responses in vivo require cell-specific provision of OX40L dictated by environmental cues. *Nature Communications*, 11(1):1–15, 12 2020.

[315] Jens Dannull, Smita Nair, Zhen Su, David Boczkowski, Christian DeBeck, Benjamin Yang, Eli Gilboa, and Johannes Vieweg. Enhancing the immunostimulatory function of dendritic cells by transfection with mRNA encoding OX40 ligand. *Blood*, 2005.

[316] Leopoldo Flores-Romo. In vivo maturation and migration of dendritic cells, 2001.

[317] Morgan C. Hunter, Alvaro Teijeira, and Cornelia Halin. T cell trafficking through lymphatic vessels, 12 2016.

[318] Sarah Johnson, Jennifer Frattolin, Lowell Edgar, Mohammad Jafarnejad, and James Moore. Modelling the effects of lymph node swelling on T-cell response. *bioRxiv*, page 2020.06.19.161232, 6 2020.

[319] Janis E. Wigginton and Denise Kirschner. A Model to Predict Cell-Mediated Immune Regulatory Mechanisms During Human Infection with Mycobacterium tuberculosis . *The Journal of Immunology*, 166(3):1951–1967, 2001.

[320] Michelle A. Sugimoto, Lirlândia P. Sousa, Vanessa Pinho, Mauro Perretti, and Mauro M. Teixeira. Resolution of inflammation: What controls its onset?, 4 2016.

[321] Judith N. Mandl, Rachel Liou, Frederick Klauschen, Nienke Vrisekoop, João P. Monteiro, Andrew J. Yates, Alex Y. Huang, and Ronald N. Germain. Quantification of lymph node transit times reveals differences in antigen surveillance strategies of naïve CD4+ and CD8+ T cells. *Proceedings of the National Academy of Sciences of the United States of America*, 109(44):18036–18041, 10 2012.

[322] Teizo Yoshimura and Munehisa Takahashi. IFN-γ-Mediated Survival Enables Human Neutrophils to Produce MCP-1/CCL2 in Response to Activation by TLR Ligands. *The Journal of Immunology*, 179(3):1942–1949, 2007.

[323] David Druzd, Olga Matveeva, Louise Ince, Ute Harrison, Wenyan He, Christoph Schmal, Hanspeter Herzel, Anthony H Tsang, Naoto Kawakami, Alexei Leliavski, Olaf Uhl, Ling Yao, Leif Erik Sander, Chien Sin Chen, Kerstin Kraus, Alba de Juan, Sophia Martina Hergenhan, Marc Ehlers, Berthold Koletzko, Rainer Haas, Werner Solbach, Henrik Oster, and Christoph Scheiermann. Lymphocyte Circadian Clocks Control Lymph Node Trafficking and Adaptive Immune Responses. *Immunity*, 2017.

[324] Hui Zhuang. Time of day influences immune response to an inactivated vaccine against SARS-CoV-2. *Nature Cell Research*, pages 4–6, 2021.

[325] Justin G Julander, Dennis W Trent, and Thomas P Monath. Immune correlates of protection against yellow fever determined by passive immunization and challenge in the hamster model. *Vaccine*, 2011.

[326] Stanley A. Plotkin. Updates on immunologic correlates of vaccine-induced protection. *Vaccine*, 38(9):2250–2257, 2019.

[327] Susanne H. Hodgson, Kushal Mansatta, Garry Mallett, Victoria Harris, Katherine R.W. Emary, and Andrew J. Pollard. What defines an efficacious COVID-19 vaccine? A review of the challenges assessing the clinical efficacy of vaccines against SARS-CoV-2, 2020.

[328] James J Moon, H Hamlet Chu, Marion Pepper, Stephen J McSorley, Stephen C Jameson, Ross M M Kedl, and Marc K Jenkins. Naive CD4+ T Cell Frequency Varies for Different Epitopes and Predicts Repertoire Diversity and Response Magnitude. *Immunity*, 2007.

[329] Marc K Jenkins and James J Moon. Response to Comment on "The Role of Naive T Cell Precursor Frequency and Recruitment in Dictating Immune Response Magnitude". *The Journal of Immunology*, 2013.

[330] Ivan Borisov and Evgeny Metelkin. Confidence intervals by constrained optimization—An algorithm and software package for practical identifiability analysis in systems biology. *PLOS Computational Biology*, 16(12):e1008495, 12 2020.

[331] Editorial. COVID vaccine confidence requires radical transparency, 2020.

[332] Alles Snijders, Pawel Kalinski, Catharien M.U. Hilkens, and Martien L. Kapsenberg. High-level IL-12 production by human dendritic cells requires two signals. *International Immunology*, 10(11):1593–1598, 11 1998.

[333] Lucia Pitzurra, Robert Cherniak, Monica Giammarioli, Stefano Perito, Francesco Bistoni, and Anna Vecchiarelli. Early induction of interleukin-12 by human monocytes exposed to Cryptococcus neoformans mannoproteins. *Infection and Immunity*, 68(2):558–563, 2 2000.

[334] James A. Butler, Jason Cosgrove, Kieran Alden, Jon Timmis, and Mark Christopher Coles. Model-driven experimentation: A new approach to understand mechanisms of tertiary lymphoid tissue formation, function, and therapeutic resolution. *Frontiers in Immunology*, 8(APR):1–7, 2017.

[335] Suresh Pallikkuth, Sidhartha Chaudhury, Pinyi Lu, Li Pan, Erik Jongert, Ulrike Wille-Reece, and Savita Pahwa. A delayed fractionated dose RTS,S AS01 vaccine regimen mediates protection via improved T follicular helper and B cell responses. *eLife*, 9:1–25, 2020.

[336] Diane B. Boivin, Francine O. James, Aibin Wu, Park F. Cho-Park, Huabao Xiong, and Zhong S. Sun. Circadian clock genes oscillate in human peripheral blood mononuclear cells. *Blood*, 102(12):4143–4145, 2003.

[337] José M. Adrover, Carlos del Fresno, Georgiana Crainiciuc, Maria Isabel Cuartero, María Casanova-Acebes, Linnea A. Weiss, Hector Huerga-Encabo, Carlos Silvestre-Roig, Jan Rossaint, Itziar Cossío, Ana V. Lechuga-Vieco, Jaime García-Prieto, Mónica Gómez-Parrizas, Juan A. Quintana, Ivan Ballesteros, Sandra Martin-Salamanca, Alejandra Aroca-Crevillen, Shu Zhen Chong, Maximilien Evrard, Karl Balabanian, Jorge López, Kiril Bidzhekov, Françoise Bachelerie, Francisco Abad-Santos, Cecilia Muñoz-Calleja, Alexander Zarbock, Oliver Soehnlein, Christian Weber, Lai Guan Ng, Cristina Lopez-Rodriguez, David Sancho, María A. Moro, Borja Ibáñez, and Andrés Hidalgo. A Neutrophil Timer Coordinates Immune Defense and Vascular Protection. *Immunity*, 50(2):390–402, 2019.

[338] Maren Keller, Jeannine Mazuch, Ute Abraham, Gina D. Eom, Erik D. Herzog, Hans Dieter Volk, Achim Kramer, and Bert Maier. A circadian clock in macrophages controls inflammatory immune responses. *Proceedings of the National Academy of Sciences of the United States of America*, 106(50):21407–21412, 2009.

[339] Anne M. Curtis, Marina M. Bellet, Paolo Sassone-Corsi, and Luke A.J. O'Neill. Circadian Clock Proteins and Immunity. *Immunity*, 40(2):178–186, 2014.

[340] Christoph Scheiermann, Yuya Kunisaki, and Paul S. Frenette. Circadian control of the immune system. *Nature Reviews Immunology*, 13(3):190–198, 2013.

[341] Nathalie Labrecque and Nicolas Cermakian. Circadian clocks in the immune system. *Journal of Biological Rhythms*, 30(4):277–290, 2015.

[342] Joanna E. Long, Mark T. Drayson, Angela E. Taylor, Kai M. Toellner, Janet M. Lord, and Anna C. Phillips. Morning vaccination enhances antibody response over afternoon vaccination: A cluster-randomised trial. *Vaccine*, 34(24):2679–2685, 2016.

[343] L. Charlotte, Vera P. Mourits, Valerie A.C.M. Koeken, Simone J.C.F.M. Moorlag, Robine Janssen, Lukas Folkman, Daniele Barreca, Thomas Krausgruber, Victoria Fife-Gernedl, Boris Novakovic, Rob J.W. Arts, Helga Dijkstra, Heidi Lemmers, Christoph Bock, Leo A.B. Joosten, Reinout van Crevel, Christine S. Benn, and Mihai G. Netea. Circadian rhythm influences induction of trained immunity by BCG vaccination. *Journal of Clinical Investigation*, 130(10):5603–5617, 2020.

[344] Jinfang Zhu, Hidehiro Yamane, and William E. Paul. Differentiation of Effector CD4 T Cell Populations. *Annual Review of Immunology*, 28(1):445–489, 2010.

[345] Paul Beier, Kenneth P. Burnham, and David R. Anderson. *Model Selection and Inference: A Practical Information-Theoretic Approach*, volume 65. 2001.

[346] Gloria I. Valderrama-Bahamóndez and Holger Fröhlich. MCMC Techniques for Parameter Estimation of ODE Based Models in Systems Biology. *Frontiers in Applied Mathematics and Statistics*, 5(November):1–10, 2019.

[347] Elisabeth Roesch, Joe G. Greener, Adam L. MacLean, Huda Nassar, Christopher Rackauckas, Timothy E. Holy, and Michael P. H. Stumpf. Julia for Biologists. *arxiv*, 2021.

[348] David Masopust, Christine P Sivula, and Stephen C Jameson. Of Mice, Dirty Mice, and Men: Using Mice To Understand Human Immunology. *The Journal of Immunology*, 2017.

[349] Cassandra Willyard. Squeaky clean mice could be ruining research. *Nature*, 2018.

[350] Stephen Abolins, Elizabeth C King, Luke Lazarou, Laura Weldon, Louise Hughes, Paul Drescher, John G Raynes, Julius C R Hafalla, Mark E Viney, and Eleanor M Rile. The comparative immunology of wild and laboratory mice, Mus musculus domesticus. *Nature Communications*, 2017.

[351] Amanda M Burkhardt and Albert Zlotnik. Translating translational research: Mouse models of human disease, 2013.

Appendix A

Appendix A

A.1 Code to solve IFNγ Model ODE

```
library(dplyr)
library(dMod)
library(data.table)

# Define the model in dMod
dMod_equations_IFNg_24_hr =  eqnvec(
  c(Mo =" - (CL * Mo * QS21) "),
  IL18 = "(vMoIL18 * Mo * QS21) - (decay18 * IL18)",
  Monoc = "+ (monocRec * MPL) - (MonocDiffDC * Monoc)",
  DC = "+ (MonocDiffDC * Monoc) + (DC_Afferent*MPL )",
    IL12 = "(vMonocIL12 * Monoc * MPL) + (vDCIL12 * DC * MPL)
    - (decay12 * IL12)",
  NKa="+ (VmaxNKa1218 * (IL18/(IL18+KM_18b)) * (IL12/(IL12+KM_12b)))
  + (VmaxNKA12 * IL12) + (VmaxNKa18 * IL18) - NKDecay*NKa",
  IFNg = "(VmaxNKaProd1218 * IL18 * (IL12/(IL12+(KM_NKa_IL12b))) * NKa)
  + (VmaxNKaProd18 * IL18 * NKa) + (VmaxNKaProd12 * IL12 * NKa)
  - (decayIFNg * IFNg)")
dMod_MODEL_IFNg_24hr = odemodel(dMod_equations_IFNg_24_hr,solver = "deSolve",
verbose=T,modelname = "IFNg24hr")
predictionFunction = Xs(dMod_MODEL_IFNg_24hr,condition = "fitting")
# Initial conditions and fixed parameters
 fixed_ICs = c(
    Mo = 1205.8197,
    IL18=1,
     Monoc = 1182.3669,
    DC = 5057.8043,
    IL12=1,
    NKa=5.490,
    IFNg = 4.946119,
    MPL=10,
    QS21=10
  )
 # Parameter values
 Parameters = c(
   VmaxNKaProd1218=0.00012,
   KM_NKa_IL12b=5,
   VmaxNKaProd18=5.777339e-07,
   VmaxNKaProd12=5.777339e-08,
   decayIFNg=0.1659771,
   monocRec=217.5247,
   MonocDiffDC=0.021425,
   DC_Afferent=22.5,
   vMonocIL12=3.333333e-05,
   vDCIL12=3.333333e-05,
   decay12=0.1081347,
   vMoIL18=0.035,
```

```
  CL=0.0505492,
  decay18=0.4,
  VmaxNKa1218=5499.982,
  KM_18b=26.96232,
  KM_12b=22.55488,
  VmaxNKA12=0.0001046237,
  VmaxNKa18=1.5,
  NKDecay=0.3
)
times = seq(0,24,by=0.1)
plot((predictionFunction)(times, Parameters,fixed=fixed_ICs)) +
xlab("Time (h)") + ylab("Model Trajectory")
```

A.2 Code to solve CD4+ T cell priming Baseline Model

```
library(dplyr)
library(dMod)
library(data.table)
# Define the model in dMod
dMod_equations_Tcell_Baseline =  eqnvec(
 c(Mo =" - (CL * Mo * QS21) "),
  IL18 = "(vMoIL18 * Mo * QS21) - (decay18 * IL18)",
   Monoc = "+ (monocRec * MPL) - (MonocDiffDC * Monoc) - (MonocDecay * Monoc * NRP) ",
  DC = "+ (MonocDiffDC * Monoc) + (DC_Afferent * MPL) - (DCDecay * DC * NRP) ",
  IL12 = "(vMonocIL12 * Monoc * MPL) + (vDCIL12 * DC * MPL) - (decay12 * IL12 * NRP)",
  NKa="+ (VmaxNKa1218 * (IL18/(IL18+KM_18b)) * (IL12/(IL12+KM_12b))) + (VmaxNKA12 * IL12)
  + (VmaxNKa18 * IL18) - NKDecay*NKa",
  IFNg = "(VmaxNKaProd1218 * IL18 * (IL12/(IL12+(KM_NKa_IL12b))) * NKa)
  + (VmaxNKaProd18 * IL18 * NKa) + (VmaxNKaProd12 * IL12 * NKa)
  + (InnateCD8IFNgProd * IL18 * InnateCD8IFNg) + (BasalCD8IFNgProd * AdaptiveCD8IFNg)
  - (decayIFNg * IFNg * NRP)",
  InnateCD8IFNg = " (CD8Innate * IL18)  - (InnateCD8decay * InnateCD8IFNg)",
  AdaptiveCD8IFNg = "+ (((CD8RecruitAct  * MPL * QS21) * AdaptiveCD8IFNg) * (1-(AdaptiveCD8IFNg/AdaptiveCD8Max)))
  - (AdaptiveCD8Decay * AdaptiveCD8IFNg * NRP) ",
  NRP = "(InhibitionProduction * NRP)",
  CD4T0 = "+(CD4Homeostatic) + (CD4T0_Inflammatory_Recruitment * CD4T0 * MPL * QS21)
  - (CD4T0_death_recirculation * CD4T0) - (cognatePriming * CD4T0 * DC)
  - (cognateEnhanceIFNg * CD4T0 * DC * IFNg) ",
  primedCD4 = " +(cognatePriming * CD4T0 * DC) + (cognateEnhanceIFNg * CD4T0 * DC * IFNg)
  + (CD4Proliferation * primedCD4 * (1-(primedCD4/CD4ProlifMax)))
  - (TcellExit_Anergy * primedCD4) ")

dMod_MODEL_Tcell_Baseline = odemodel(dMod_equations_Tcell_Baseline,solver = "deSolve",verbose=T,
modelname = "BASELINE")

predictionFunction = Xs(dMod_MODEL_Tcell_Baseline,condition = "fitting")

    # Initial conditions and fixed parameters
 fixed_ICs = c(
   Mo = 1205.8197, #Macrophages
   IL18=1,
   Monoc = 1182.3669, #Monocytes
   DC = 5057.8043, #Dendritic Cells
   IL12=1,
   NKa=5.490,
   IFNg = 4.946119, #IFNG
   MPL=10,
   QS21=10,
   InnateCD8IFNg=33.59252,
   AdaptiveCD8IFNg=1,
   NRP=1,
   CD4T0=2.102988e+04,
   primedCD4=3.971233e+01
  )

 Parameters = c(
```

```
  VmaxNKaProd1218=1.197267E-4,
  KM_NKa_IL12b=5.83435,
  VmaxNKaProd18=5.777339E-7,
  VmaxNKaProd12=5.777339E-8,
  decayIFNg=0.14,
  monocRec=270.9,
  MonocDiffDC=0.008,
  DC_Afferent=42.5,
  vMonocIL12=3.29690E-5,
  vDCIL12=3.333333e-05,
  decay12=0.041782,
  CL=0.048,
  vMoIL18=0.035,
  decay18=0.38,
  VmaxNKa1218=5489.13342,
  KM_18b=32.63954,
  KM_12b=24.77689,
  VmaxNKA12=0.0091429,
  VmaxNKa18=1.5,
  NKDecay=0.2931158,
  DCDecay=0.0017509,
  MonocDecay=0.01,
  CD8Innate=4.999,
  CD8RecruitAct=0.0019930,
  InnateCD8decay=0.1825396,
  AdaptiveCD8Decay=0.025,
  InnateCD8IFNgProd=1.0E-13,
  BasalCD8IFNgProd=0.0255,
  InhibitionProduction = 0.02,
  AdaptiveCD8Max=21000,
  CD4T0_death_recirculation=0.0576743006618724,
  CD4T0_Inflammatory_Recruitment=6.42267431978048E-4,
  cognatePriming = 4.58221463375731E-9, #non ifng controlled for baseline
  cognateEnhanceIFNg = 1.0E-13,
  CD4Proliferation=0.079,
  CD4ProlifMax=7.88813071704971E7,
  TcellExit_Anergy=0.1,
  CD4Homeostatic = 1212.8836220031
)

times = seq(0,168,by=0.1)



plot((predictionFunction)(times, Parameters,fixed=fixed_ICs)) + xlab("Time (h)") + ylab("Model Trajectory")
```

A.3 Code to solve CD4+ T cell priming Alternate Model

```
library(dplyr)
library(dMod)
library(data.table)
library(ggplot2)

# Define the model in dMod
dMod_equations_Tcell_Alternate =  eqnvec(
  c(Mo =" - (CL * Mo * QS21) "),
  IL18 = "(vMoIL18 * Mo * QS21) - (decay18 * IL18)",
   Monoc = "+ (monocRec * MPL) - (MonocDiffDC * Monoc) - (MonocDecay * Monoc * NRP) ",
  DC = "+ (MonocDiffDC * Monoc) + (DC_Afferent * MPL) - (DCDecay * DC * NRP) ",
    IL12 = "(vMonocIL12 * Monoc * MPL) + (vDCIL12 * DC * MPL) - (decay12 * IL12 * NRP)",
  NKa="+ (VmaxNKa1218 * (IL18/(IL18+KM_18b)) * (IL12/(IL12+KM_12b))) + (VmaxNKA12 * IL12)
  + (VmaxNKa18 * IL18) - NKDecay*NKa",
  IFNg = "(VmaxNKaProd1218 * IL18 * (IL12/(IL12+(KM_NKa_IL12b))) * NKa)
  + (VmaxNKaProd18 * IL18 * NKa) + (VmaxNKaProd12 * IL12 * NKa)
  + (InnateCD8IFNgProd * IL18 * InnateCD8IFNg) + (BasalCD8IFNgProd * AdaptiveCD8IFNg)
  - (decayIFNg * IFNg * NRP)",
```

```
  InnateCD8IFNg = " (CD8Innate * IL18)  - (InnateCD8decay * InnateCD8IFNg)",
  AdaptiveCD8IFNg = "+ (((CD8RecruitAct  * MPL * QS21) * AdaptiveCD8IFNg) * (1-AdaptiveCD8IFNg/AdaptiveCD8Max))
  - (AdaptiveCD8Decay * AdaptiveCD8IFNg * NRP) ",
  NRP = "(InhibitionProduction * NRP)",
  CD4T0 = "+(CD4Homeostatic ) + (CD4T0_Inflammatory_Recruitment * CD4T0 * MPL * QS21)
  - (CD4T0_death_recirculation * CD4T0) - (cognatePrimingIFNgControlled * CD4T0 * DC * IFNg)
  - (cognateNonIFNgControlled * CD4T0 * DC ) ",
  primedCD4 = " +(cognatePrimingIFNgControlled * CD4T0 * DC * IFNg) + (cognateNonIFNgControlled * CD4T0 * DC)
  + (CD4Proliferation * primedCD4 * (1-(primedCD4/CD4ProlifMax)))
  - (TcellExit_Anergy * primedCD4) ")
dMod_MODEL_Tcell_Alternate = odemodel(dMod_equations_Tcell_Alternate,solver = "deSolve",verbose=T,
modelname = "ALTERNATE")

predictionFunction = Xs(dMod_MODEL_Tcell_Alternate,condition = "fitting")

    # Initial conditions and fixed parameters
 fixed_ICs = c(
   Mo = 1205.8197, #Macrophages
   IL18=1,
   Monoc = 1182.3669, #Monocytes
   DC = 5057.8043, #Dendritic Cells
   IL12=1,
   NKa=5.490,
   IFNg = 4.946119, #IFNG
   MPL=10,
   QS21=10,
   InnateCD8IFNg=33.59252,
   AdaptiveCD8IFNg=1,
   NRP=1, #NRP
   CD4T0=2.102988e+04,
   primedCD4=3.971233e+01
  )

 Parameters = c(
   VmaxNKaProd1218=1.2E-4,
   KM_NKa_IL12b=5.441137,
   VmaxNKaProd18=5.777339E-7,
   VmaxNKaProd12=5.777339E-8,
   decayIFNg=0.15958,
   monocRec=270.0,
   MonocDiffDC=0.008,
   DC_Afferent=39.6489,
   vMonocIL12=3.29690E-5,
   vDCIL12=3.333333e-05,
   decay12=0.041782,
   CL=0.045,
   vMoIL18=0.035,
   decay18=0.38,
   VmaxNKa1218=5489.13342,
   KM_18b=32.70883,
   KM_12b=24.94455,
   VmaxNKA12=0.0091429,
   VmaxNKa18=1.5,
   NKDecay=0.2931158,
   DCDecay=0.00225,
   MonocDecay=0.01,
   CD8Innate=5,
   CD8RecruitAct=0.00186,
   InnateCD8decay=0.399361,
   AdaptiveCD8Decay=0.02,
   InnateCD8IFNgProd=1.0E-13,
   BasalCD8IFNgProd=0.0223243,
   InhibitionProduction = 0.02,
   AdaptiveCD8Max=21000,
   CD4T0_death_recirculation=0.0580396169911887,
   CD4T0_Inflammatory_Recruitment=6.44615603228501E-4,
   cognatePrimingIFNgControlled = 7.25E-12,
   cognateNonIFNgControlled = 2.5950650098947E-9,
```

```
  CD4Proliferation=0.046,
  CD4ProlifMax=3.68784666726818E7,
  TcellExit_Anergy=0.05,
  CD4Homeostatic = 1220.56618057066
)

times = seq(0,168,by=0.1)


plot((predictionFunction)(times, Parameters,fixed=fixed_ICs)) + xlab("Time (h)") + ylab("Model Trajectory")
```

A.4 Thesis Supplementary

For thesis supplementary click the following : link to supplementary

A.5 Core AS01 Domain Model

What follows presents the full Core AS01 Domain Model diagrams.

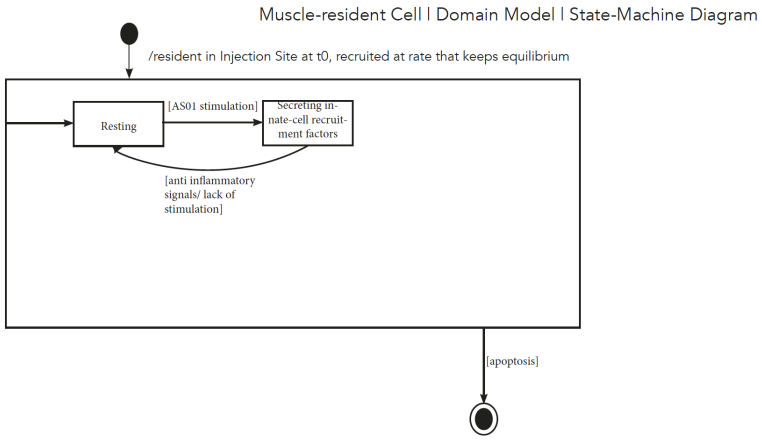


Figure A.1: **A State-Machine diagram for a Muscle-Resident cell.**

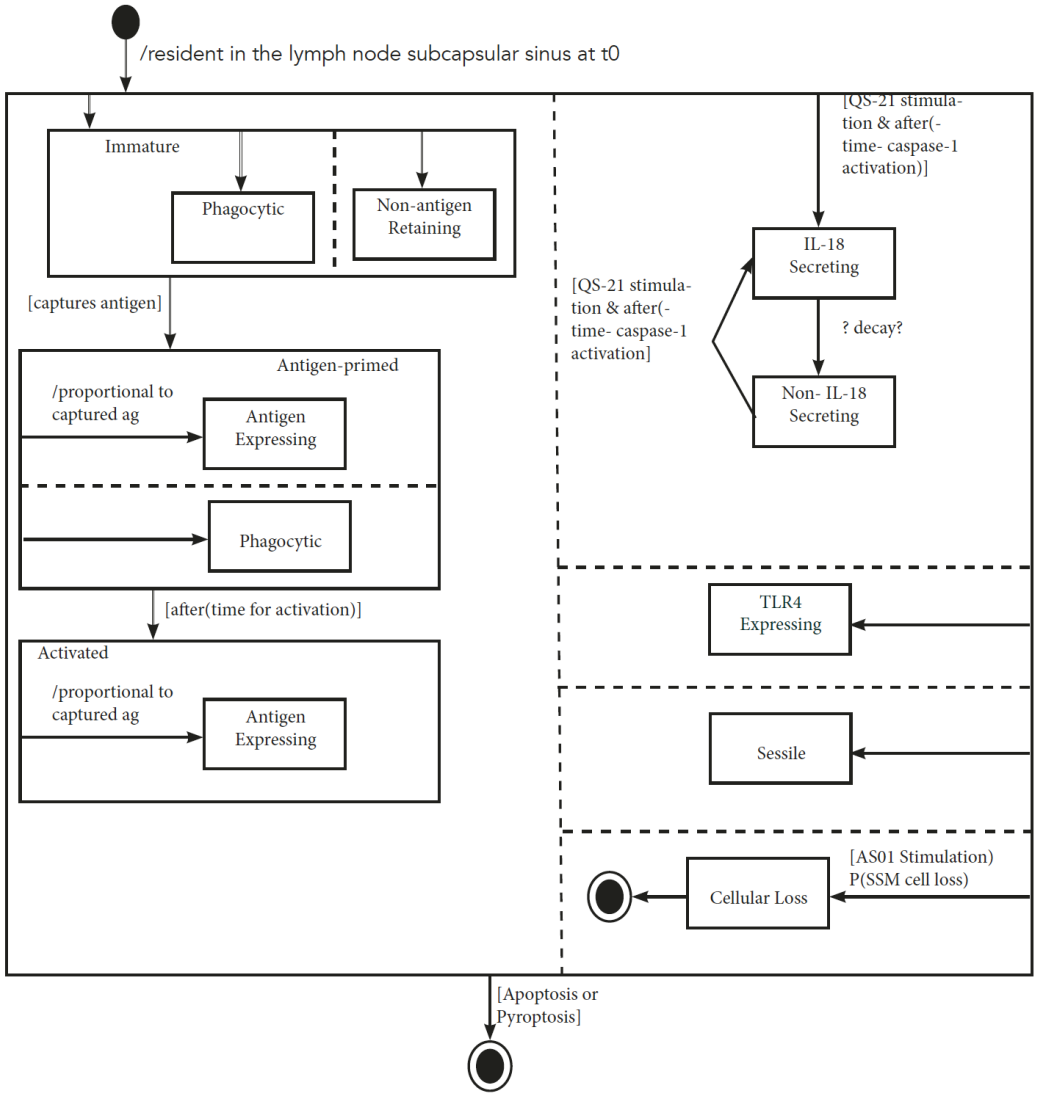


Figure A.2: **A State-Machine diagram depicting a CD169+ F480 Macrophage.**

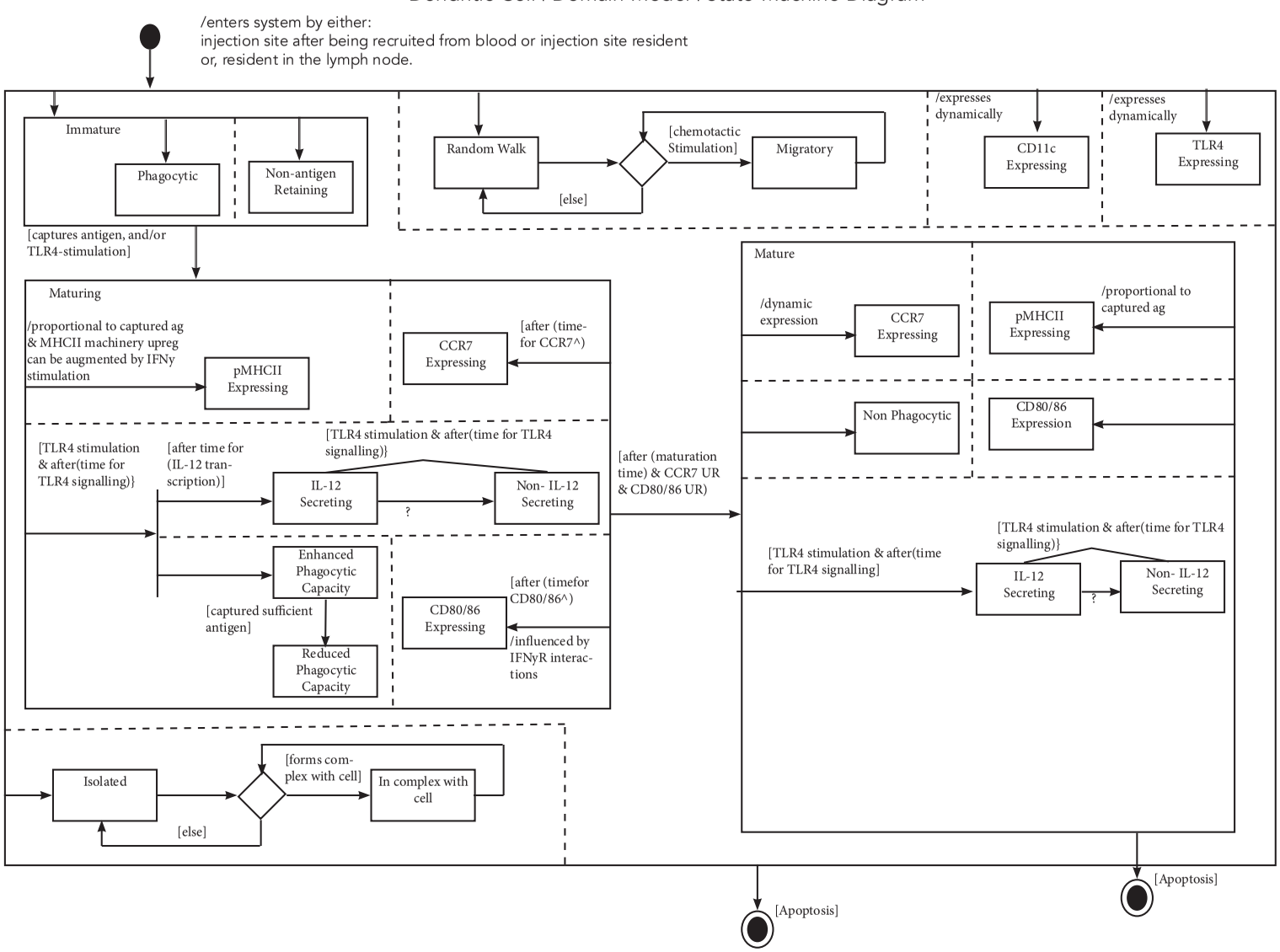


Figure A.3: **A State-Machine diagram depicting a Dendritic Cell.**

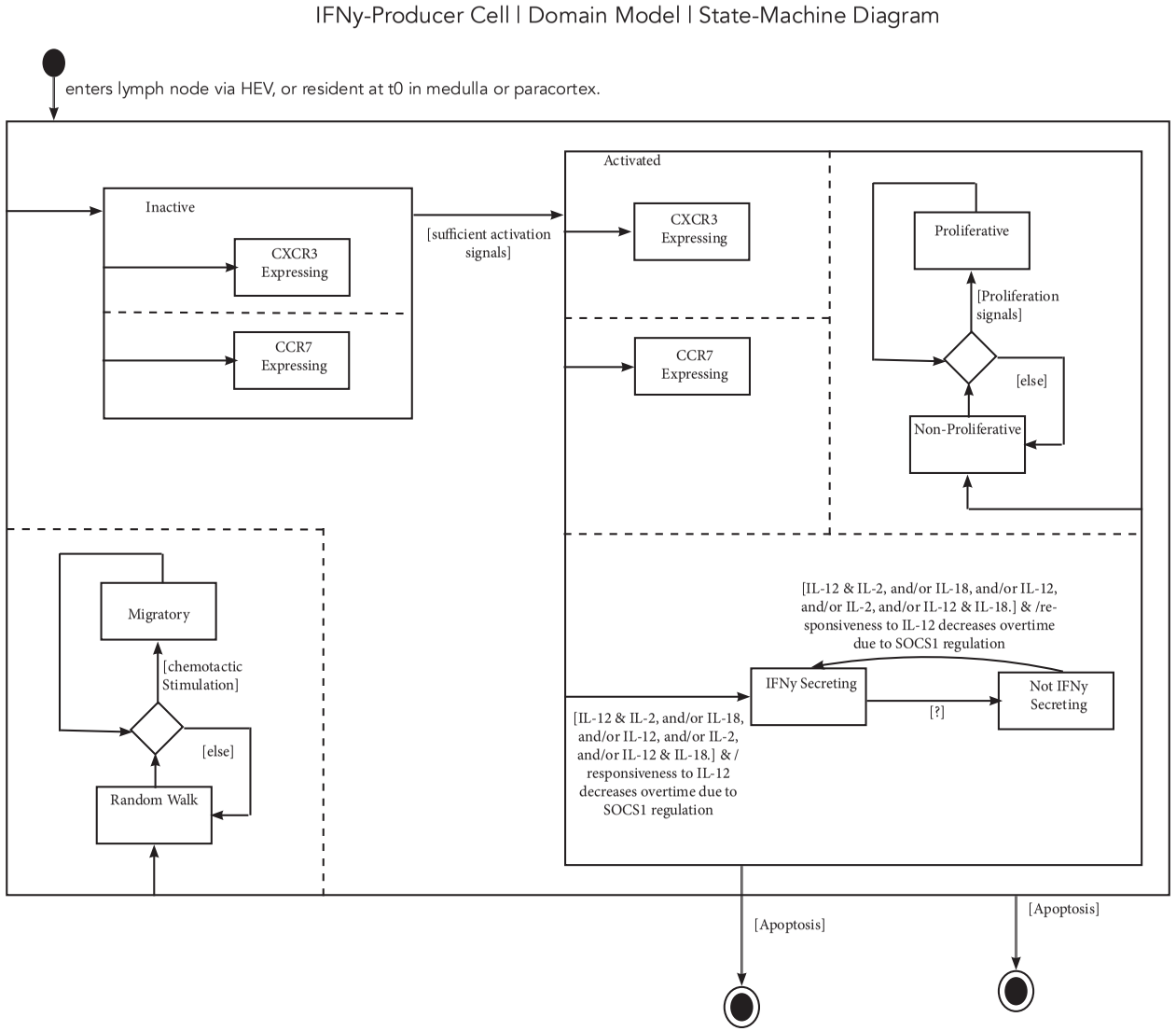


Figure A.4: **A State-Machine diagram for a IFNγ Producer cell.**

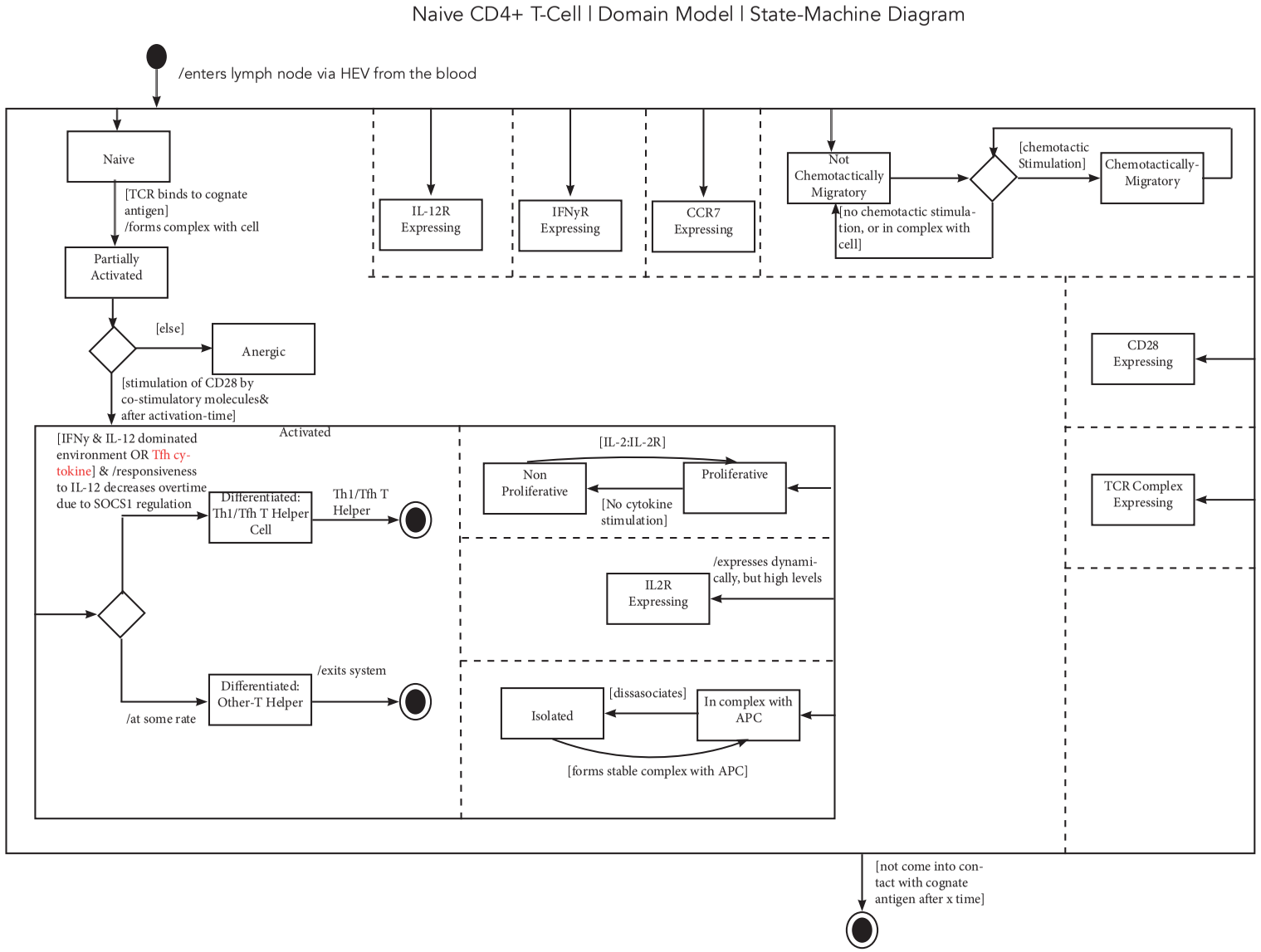


Figure A.5: **A State-Machine diagram for a Naive CD4+ T cell.**

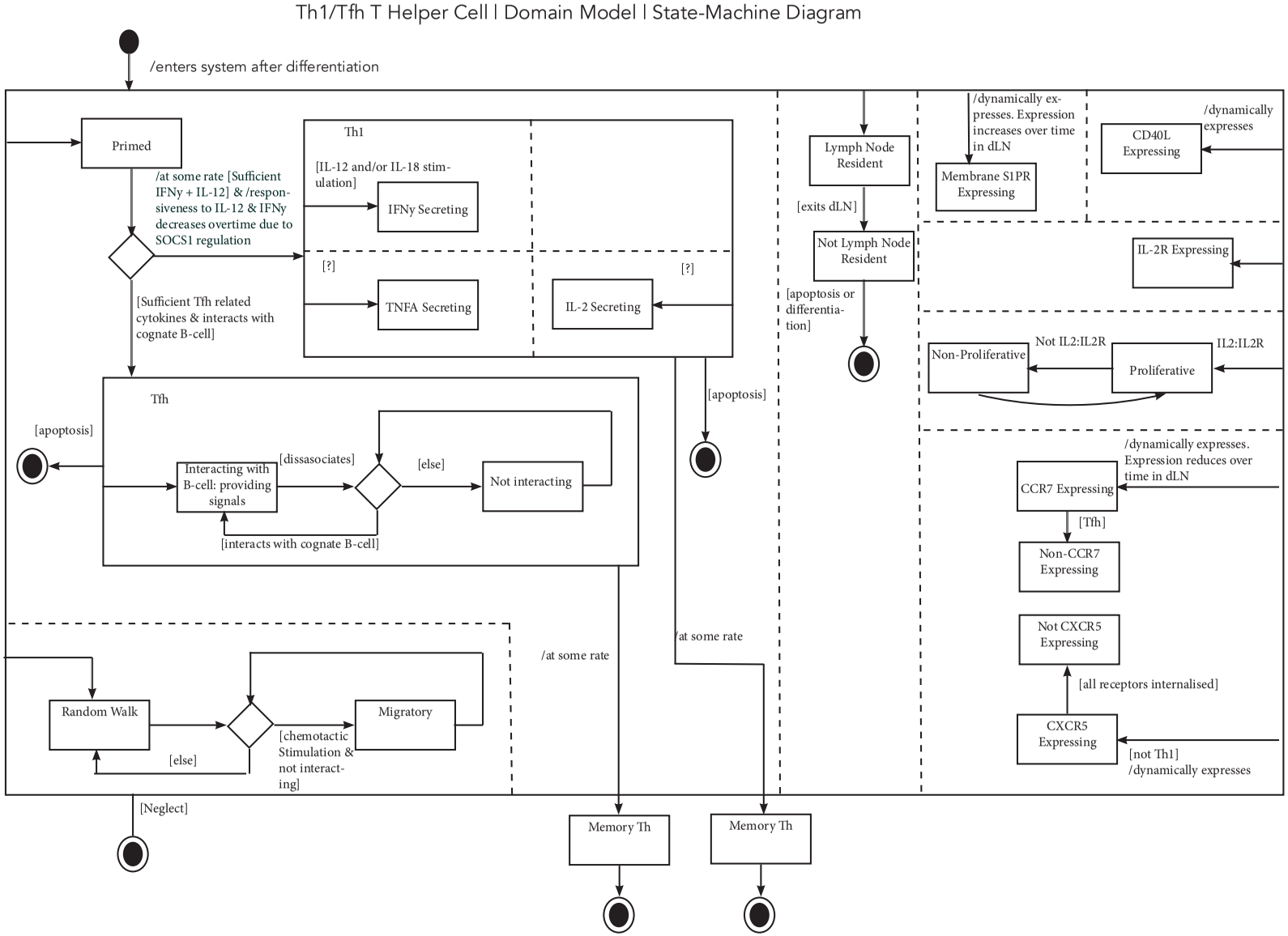


Figure A.6: **A State-Machine diagram for a Th1 / Tfh cell.**

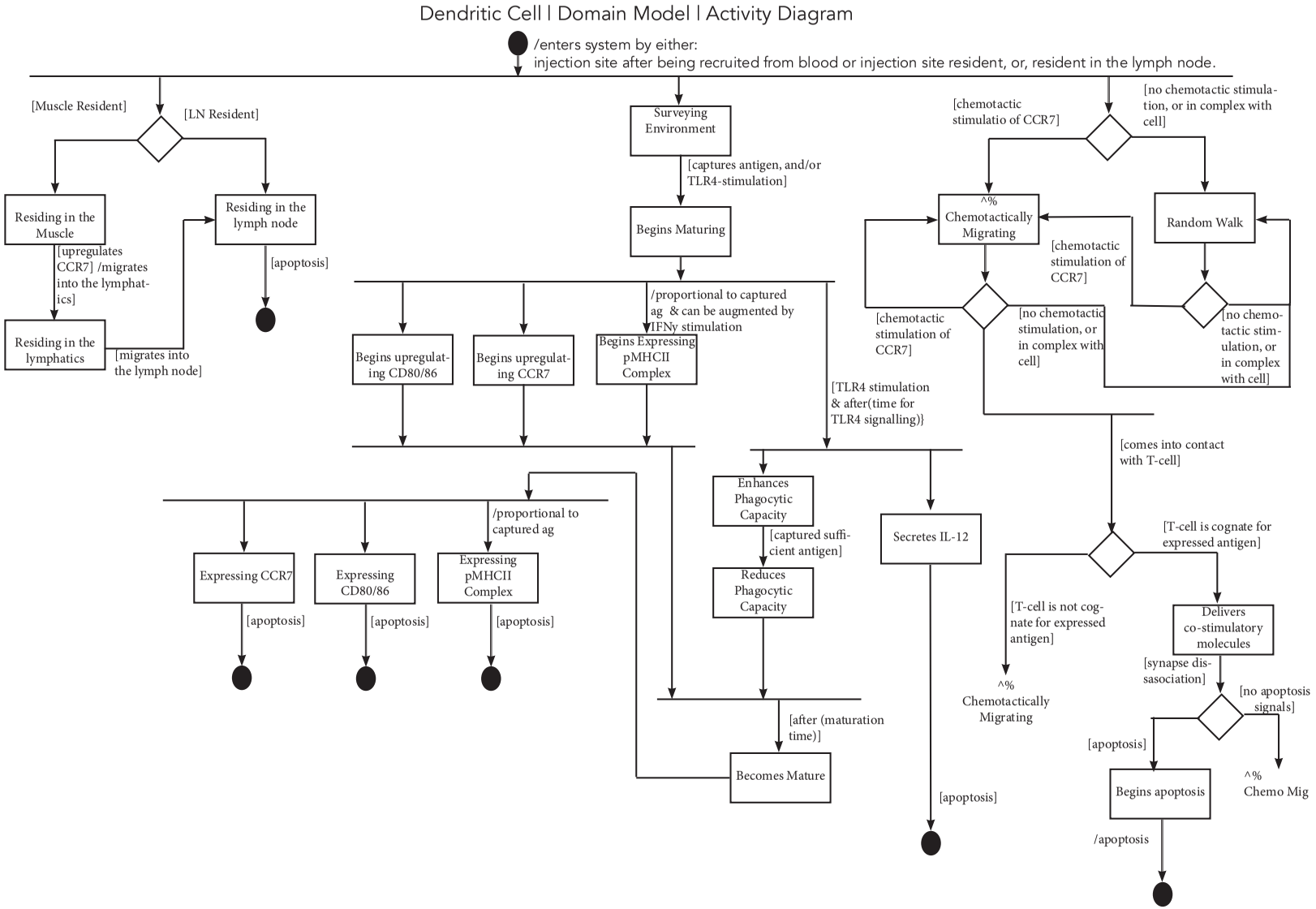


Figure A.7: **An Activity Diagram diagram depicting a Dendritic Cell.**

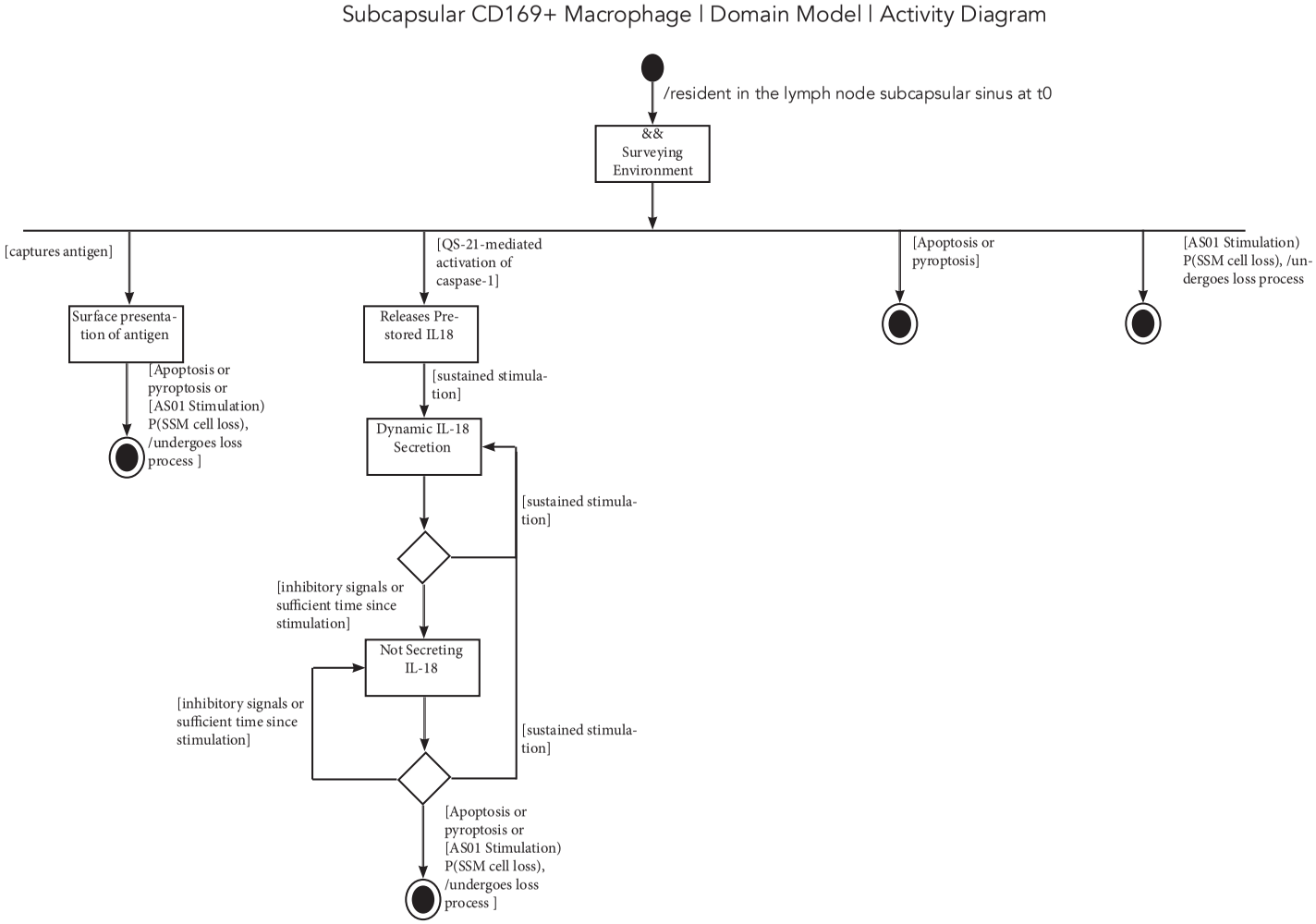


Figure A.8: **An Activity Diagram diagram depicting a SCS Cell.**

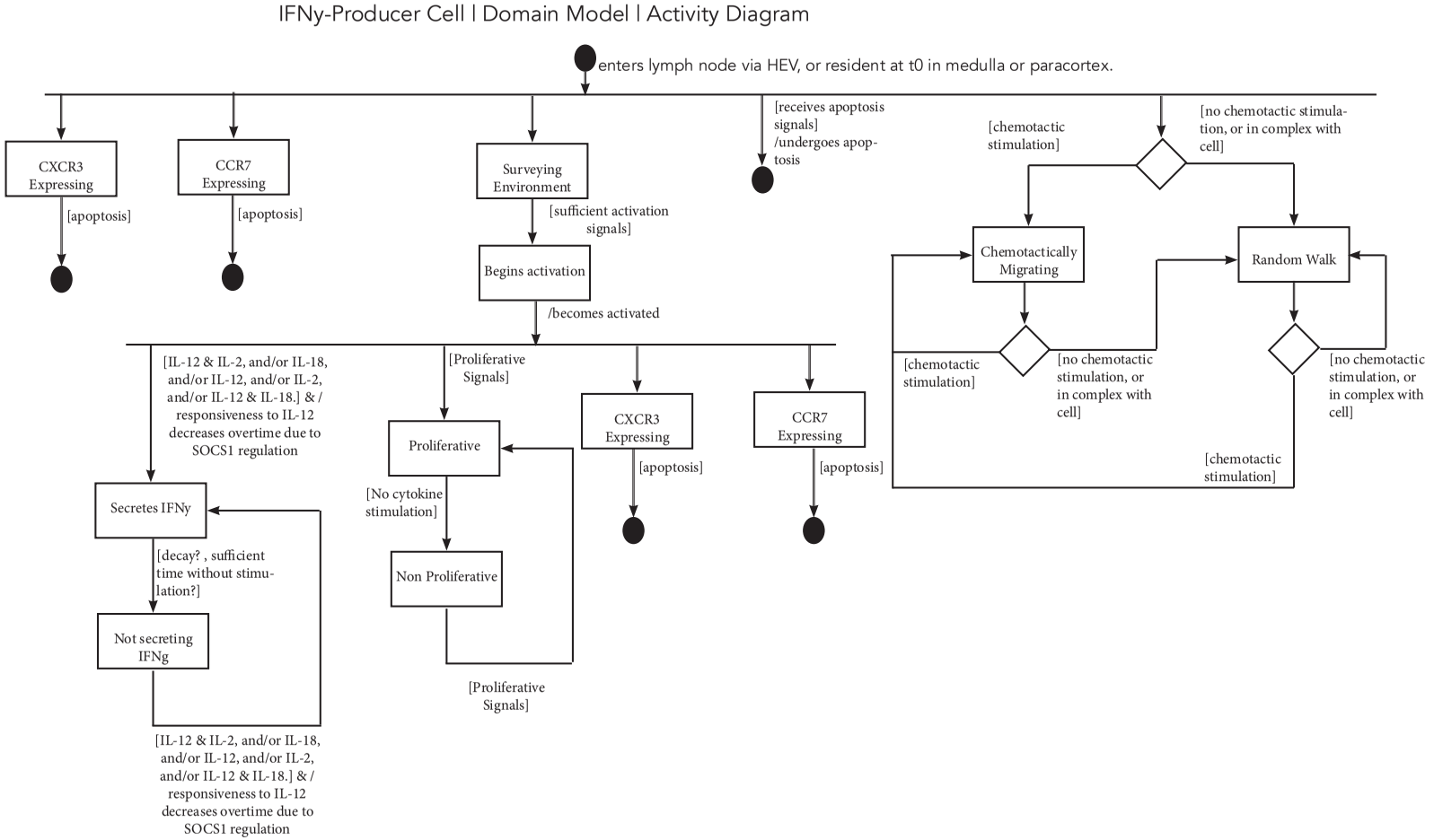


Figure A.9: **An Activity Diagram depicting a IFNγ Producer cell.**

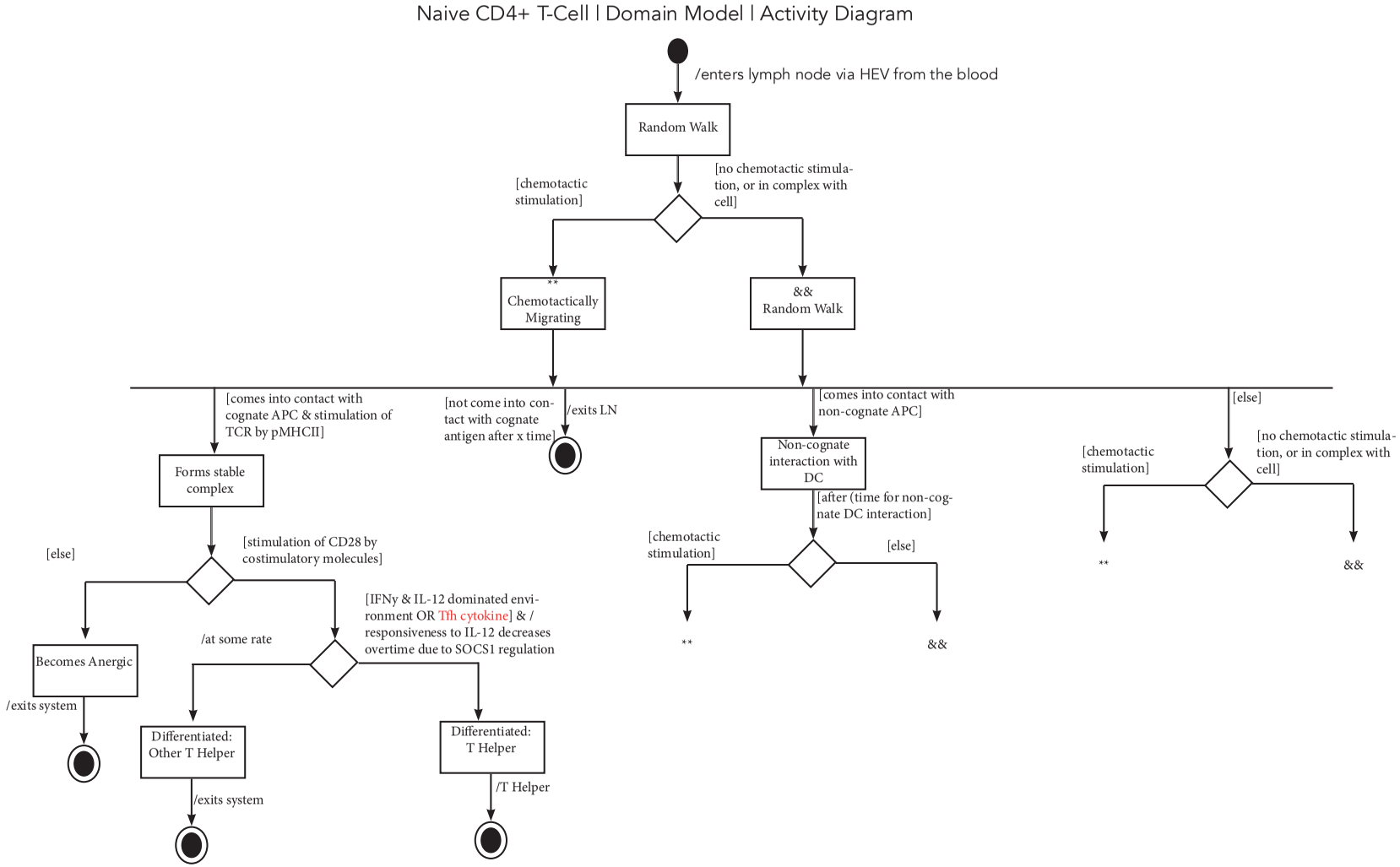


Figure A.10: **An Activity Diagram depicting a Naive CD4+ T cell.**

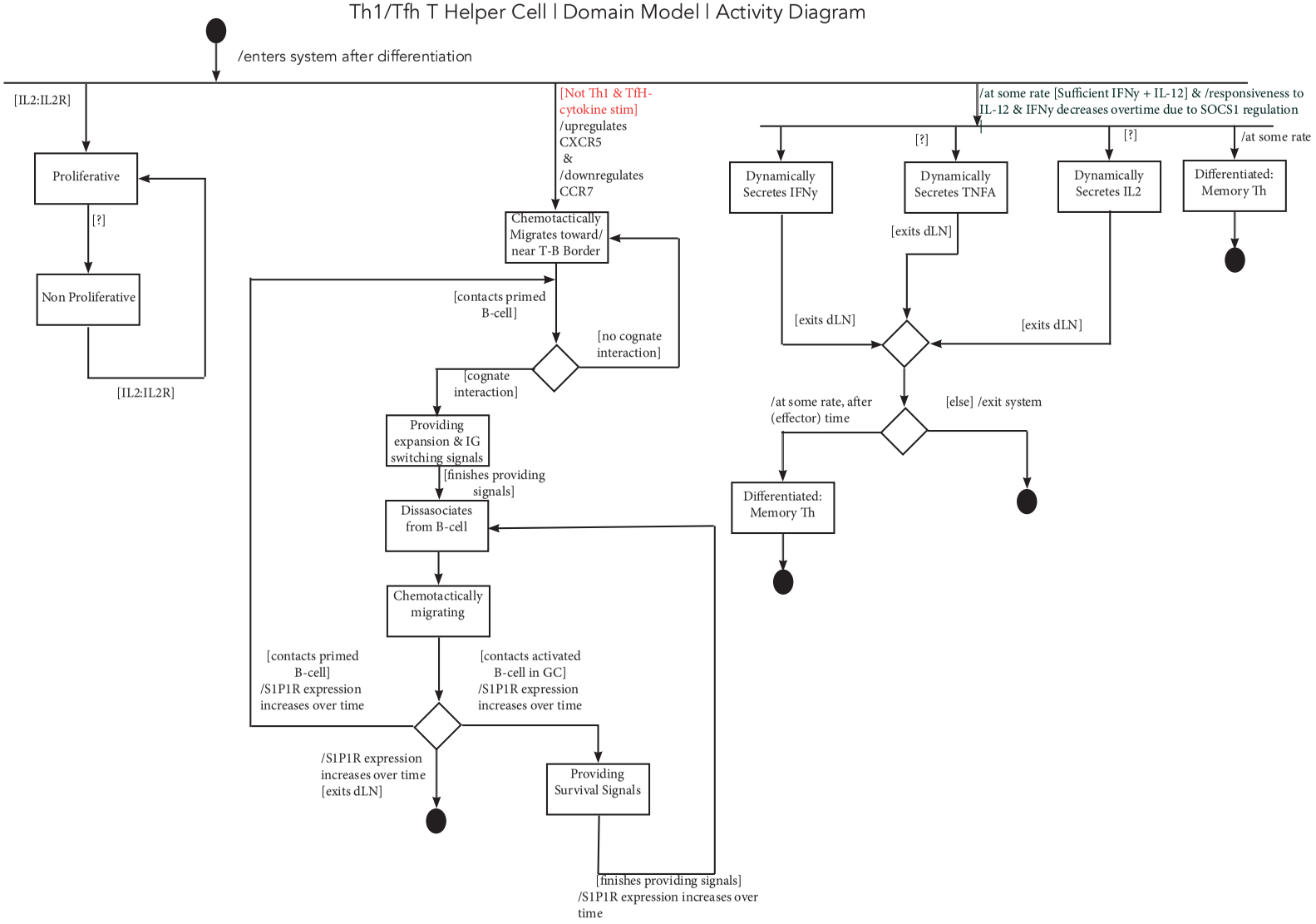


Figure A.11: **An Activity Diagram depicting a Th1 / Tfh cell.**

Appendix B

Appendix B

B.1 ABM

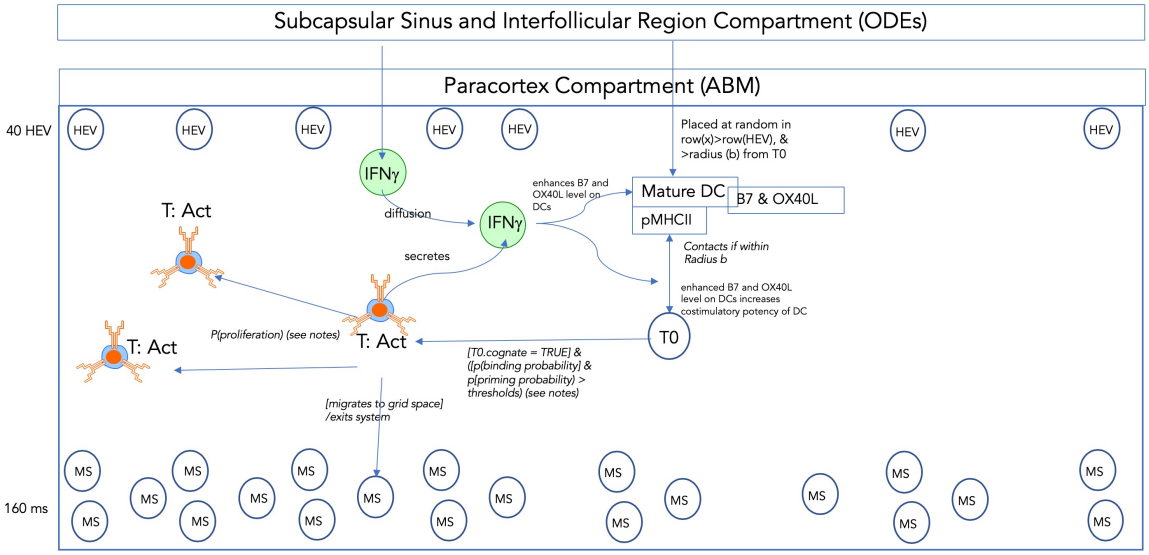


Figure B.1: **Overview of Hybrid ODE/ABM Platform Model**

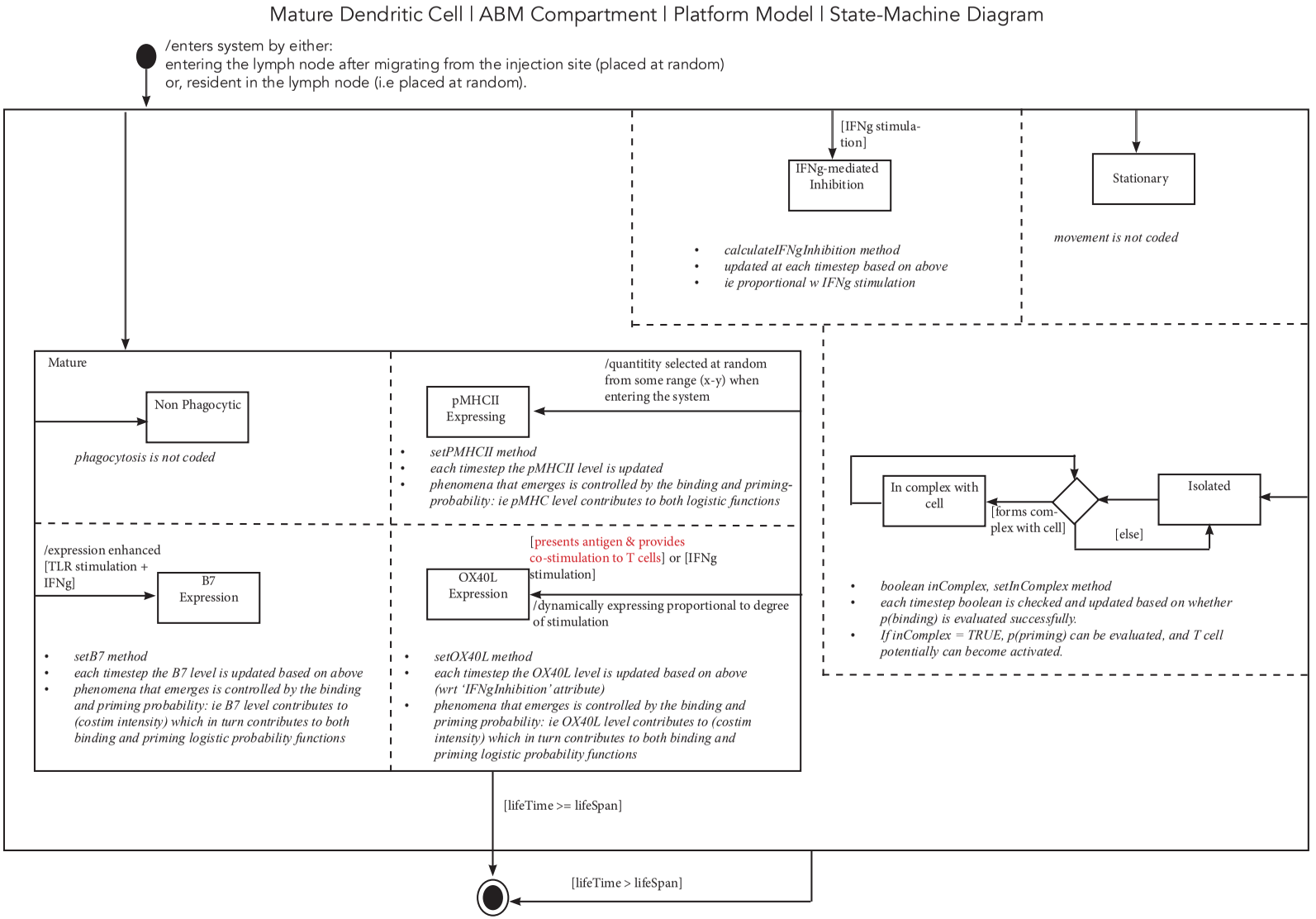


Figure B.2: **A Platform Model State Machine Diagram for a DC**

DC Emergent Life cycle | ABM Compartment | Platform Model

Assumptions:

- All DCs in the ABM compartment are mature
- DCs are stationary in the paracortex, after they have been placed at random

Life cycle

- A number of DCs are entered at random into the system at t0. At t(x) x>0, DCs enter from the SCS/IFR compartment and are placed at random in a grid space, that satisfie the inequality; row(x) > row(HEV) where row(HEV) = 1 & (distanceFromTcell > DC_radius_b). DCs are then stationary.
- Upon entry, DCs are assigned a pMHCII level, a B7 level, and an OX40L level. Please see the notes for how these values are assigned.
- Each timestep a DC scans moores neighbourhood for IFNg, and then 'IFNgEffect' is calculated (see modelling ifng page for function). The B7 level and OX40L levels are then enhanced accordingly see overleaf).
- DCs can contact up to 5000 T cells an hour. If a T cell is within radius m (ie distanceFromTCell <= DC_radius_m), then the two cells are in contact.
- If this inequality is satisfied, binding probability is now calculated, as a logistic function;

$$p(\text{binding}) = \frac{1}{1 + e^{-\frac{x-a}{b}}}$$

where, a=binding threshold, b = curve shape

x = (pMHC_level * otherSynapseFactors)

- pMHC_level is a number with range (0,400).
- otherSynapseFactors is essentially a boolean = (0 | 1) to capture that there are other factors that are implicitly involved, described by some probability.

- if this is satisfied (random number is drawn based on binding probability) AND T0.cognate=TRUE, , then there is a time delay (as in vivo). Over the interaction, the average expression of pMHCII by the DC is recorded, and the primingIndex is calculated as (pMHCIILevel x boundDuration x costimulationIntensity). T cells now are released based on the following criteria; 1) the primingIndex > threshold for activation 2) DC_pMHCII_Level < threshold. 3) T cell is bound for maximum binding period. 4) DC dies.

$$p(\text{priming}) = \frac{1}{1 + e^{-\frac{x-a}{b}}}$$

where, a=priming threshold, b = curve shape

x = (pMHC_level * B7 * OX40L * boundDuration)

- B7 is a number with a range (0,44k) - see overleaf for how this is calculated
- OX40L is a number with a range (0,0.1) - see overleaf for how this is calculated
- boundDuration is a number with range (0,7) - which is the time in hours the cells have been bound
- if this results in priming = TRUE, then the T cell is activated.

Attributes (DC only)

- pMHCII level - The amount of pMHCII on the surface of the DC, which represents the quantity of antigen the DC is carrying. Antigen loaded onto MHCII molecules and presented on the surface of mature DCs, extends the half-life of antigen to approx the lifespan of the cell.
- Co-stimulation intensity level - needs refinement, but could be a value with range (0-1). Maybe the priming probability is then multiplied by this. else, it can be a function that shifts the logistic curve rightwards or leftwards, based on strong or weak intensity respectively.
- OX40L level - this is assumed to initially be proportional to the level of IFNg stimulation the DC has received, and enhanced when DC presents antigen.
- B7 level - this level is constitutive to mature DCs, although the expression level varies. This could be drawn from some distribution, i think we have data on this.
- IFNg responsiveness - this reduces over time based on SOCS regulation. Inverse relationship with SOCS expression
- DC_activation_degree - this is essentially x in the logstic functions above.

Figure B.3: **Emergent Detail for DC in the Model**

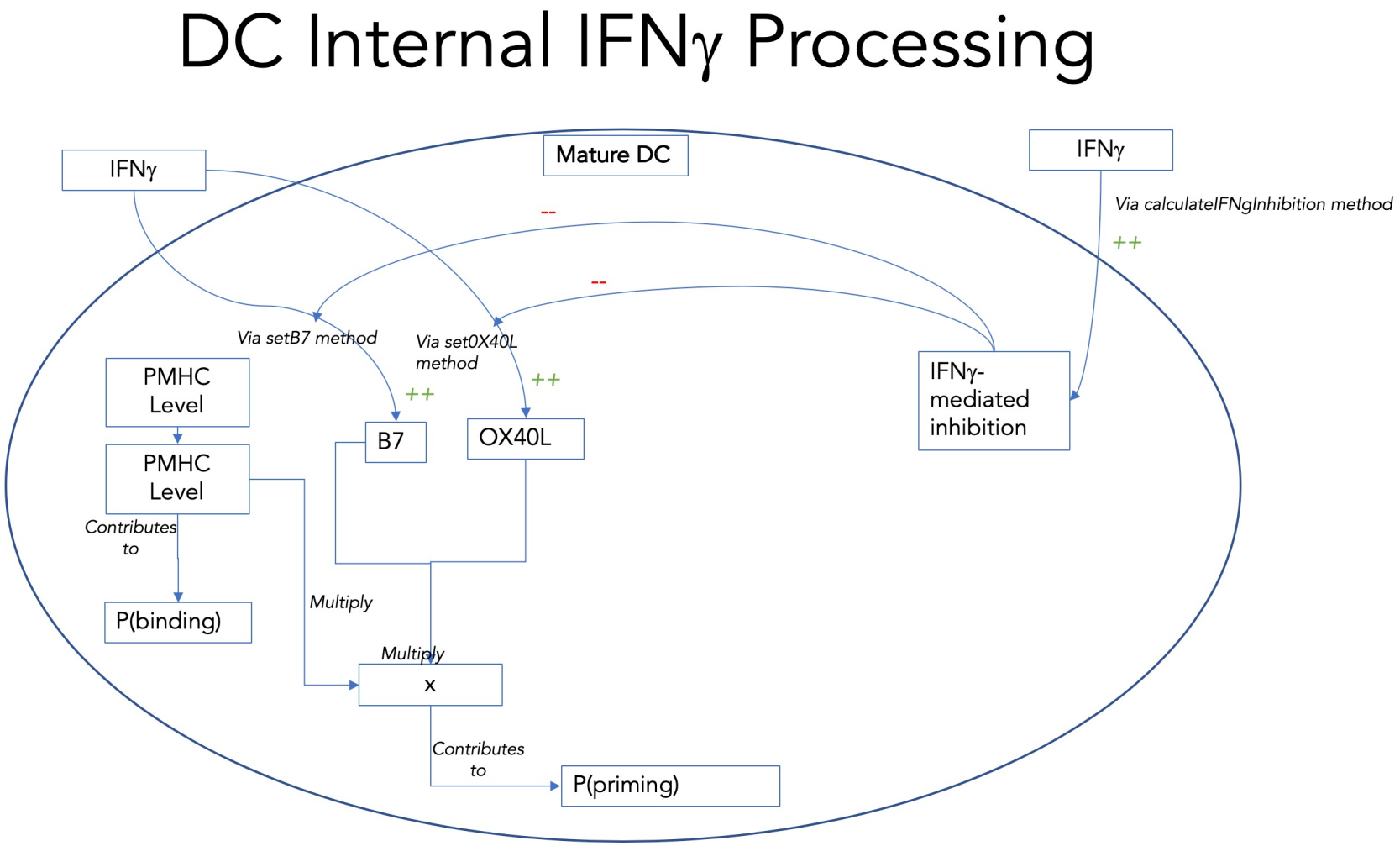


Figure B.4: **Overview of DC Internal Processing**